

Countermeasures to Protect Bridge Abutments from Scour

DETAILS

220 pages | | PAPERBACK

ISBN 978-0-309-42164-5 | DOI 10.17226/17620

AUTHORS

Robert Ettema; Brian D Barkdoll; Bruce W Melville; Transportation Research Board

BUY THIS BOOK

FIND RELATED TITLES

Visit the National Academies Press at NAP.edu and login or register to get:

- Access to free PDF downloads of thousands of scientific reports
- 10% off the price of print titles
- Email or social media notifications of new titles related to your interests
- Special offers and discounts



Distribution, posting, or copying of this PDF is strictly prohibited without written permission of the National Academies Press. (Request Permission) Unless otherwise indicated, all materials in this PDF are copyrighted by the National Academy of Sciences.

NCHRP REPORT 587

**Countermeasures to Protect
Bridge Abutments from Scour**

Brian D. Barkdoll

MICHIGAN TECHNOLOGICAL UNIVERSITY
Houghton, MI

Robert Ettema

UNIVERSITY OF IOWA
Iowa City, IA

Bruce W. Melville

UNIVERSITY OF AUCKLAND
Auckland, New Zealand

Subject Areas

Design • Materials, Construction, and Maintenance

Research sponsored by the American Association of State Highway and Transportation Officials
in cooperation with the Federal Highway Administration

TRANSPORTATION RESEARCH BOARD

WASHINGTON, D.C.

2007

www.TRB.org

NATIONAL COOPERATIVE HIGHWAY RESEARCH PROGRAM

Systematic, well-designed research provides the most effective approach to the solution of many problems facing highway administrators and engineers. Often, highway problems are of local interest and can best be studied by highway departments individually or in cooperation with their state universities and others. However, the accelerating growth of highway transportation develops increasingly complex problems of wide interest to highway authorities. These problems are best studied through a coordinated program of cooperative research.

In recognition of these needs, the highway administrators of the American Association of State Highway and Transportation Officials initiated in 1962 an objective national highway research program employing modern scientific techniques. This program is supported on a continuing basis by funds from participating member states of the Association and it receives the full cooperation and support of the Federal Highway Administration, United States Department of Transportation.

The Transportation Research Board of the National Academies was requested by the Association to administer the research program because of the Board's recognized objectivity and understanding of modern research practices. The Board is uniquely suited for this purpose as it maintains an extensive committee structure from which authorities on any highway transportation subject may be drawn; it possesses avenues of communications and cooperation with federal, state and local governmental agencies, universities, and industry; its relationship to the National Research Council is an insurance of objectivity; it maintains a full-time research correlation staff of specialists in highway transportation matters to bring the findings of research directly to those who are in a position to use them.

The program is developed on the basis of research needs identified by chief administrators of the highway and transportation departments and by committees of AASHTO. Each year, specific areas of research needs to be included in the program are proposed to the National Research Council and the Board by the American Association of State Highway and Transportation Officials. Research projects to fulfill these needs are defined by the Board, and qualified research agencies are selected from those that have submitted proposals. Administration and surveillance of research contracts are the responsibilities of the National Research Council and the Transportation Research Board.

The needs for highway research are many, and the National Cooperative Highway Research Program can make significant contributions to the solution of highway transportation problems of mutual concern to many responsible groups. The program, however, is intended to complement rather than to substitute for or duplicate other highway research programs.

NCHRP REPORT 587

Project 24-18A
ISSN 0077-5614
ISBN: 978-0-309-09895-3
Library of Congress Control Number 2007932422

© 2007 Transportation Research Board

COPYRIGHT PERMISSION

Authors herein are responsible for the authenticity of their materials and for obtaining written permissions from publishers or persons who own the copyright to any previously published or copyrighted material used herein.

Cooperative Research Programs (CRP) grants permission to reproduce material in this publication for classroom and not-for-profit purposes. Permission is given with the understanding that none of the material will be used to imply TRB, AASHTO, FAA, FHWA, FMCSA, FTA, or Transit Development Corporation endorsement of a particular product, method, or practice. It is expected that those reproducing the material in this document for educational and not-for-profit uses will give appropriate acknowledgment of the source of any reprinted or reproduced material. For other uses of the material, request permission from CRP.

NOTICE

The project that is the subject of this report was a part of the National Cooperative Highway Research Program conducted by the Transportation Research Board with the approval of the Governing Board of the National Research Council. Such approval reflects the Governing Board's judgment that the program concerned is of national importance and appropriate with respect to both the purposes and resources of the National Research Council.

The members of the technical committee selected to monitor this project and to review this report were chosen for recognized scholarly competence and with due consideration for the balance of disciplines appropriate to the project. The opinions and conclusions expressed or implied are those of the research agency that performed the research, and, while they have been accepted as appropriate by the technical committee, they are not necessarily those of the Transportation Research Board, the National Research Council, the American Association of State Highway and Transportation Officials, or the Federal Highway Administration, U.S. Department of Transportation.

Each report is reviewed and accepted for publication by the technical committee according to procedures established and monitored by the Transportation Research Board Executive Committee and the Governing Board of the National Research Council.

The Transportation Research Board of the National Academies, the National Research Council, the Federal Highway Administration, the American Association of State Highway and Transportation Officials, and the individual states participating in the National Cooperative Highway Research Program do not endorse products or manufacturers. Trade or manufacturers' names appear herein solely because they are considered essential to the object of this report.

Published reports of the

NATIONAL COOPERATIVE HIGHWAY RESEARCH PROGRAM

are available from:

Transportation Research Board
Business Office
500 Fifth Street, NW
Washington, DC 20001

and can be ordered through the Internet at:

<http://www.national-academies.org/trb/bookstore>

Printed in the United States of America

THE NATIONAL ACADEMIES

Advisers to the Nation on Science, Engineering, and Medicine

The **National Academy of Sciences** is a private, nonprofit, self-perpetuating society of distinguished scholars engaged in scientific and engineering research, dedicated to the furtherance of science and technology and to their use for the general welfare. On the authority of the charter granted to it by the Congress in 1863, the Academy has a mandate that requires it to advise the federal government on scientific and technical matters. Dr. Ralph J. Cicerone is president of the National Academy of Sciences.

The **National Academy of Engineering** was established in 1964, under the charter of the National Academy of Sciences, as a parallel organization of outstanding engineers. It is autonomous in its administration and in the selection of its members, sharing with the National Academy of Sciences the responsibility for advising the federal government. The National Academy of Engineering also sponsors engineering programs aimed at meeting national needs, encourages education and research, and recognizes the superior achievements of engineers. Dr. Charles M. Vest is president of the National Academy of Engineering.

The **Institute of Medicine** was established in 1970 by the National Academy of Sciences to secure the services of eminent members of appropriate professions in the examination of policy matters pertaining to the health of the public. The Institute acts under the responsibility given to the National Academy of Sciences by its congressional charter to be an adviser to the federal government and, on its own initiative, to identify issues of medical care, research, and education. Dr. Harvey V. Fineberg is president of the Institute of Medicine.

The **National Research Council** was organized by the National Academy of Sciences in 1916 to associate the broad community of science and technology with the Academy's purposes of furthering knowledge and advising the federal government. Functioning in accordance with general policies determined by the Academy, the Council has become the principal operating agency of both the National Academy of Sciences and the National Academy of Engineering in providing services to the government, the public, and the scientific and engineering communities. The Council is administered jointly by both the Academies and the Institute of Medicine. Dr. Ralph J. Cicerone and Dr. Charles M. Vest are chair and vice chair, respectively, of the National Research Council.

The **Transportation Research Board** is a division of the National Research Council, which serves the National Academy of Sciences and the National Academy of Engineering. The Board's mission is to promote innovation and progress in transportation through research. In an objective and interdisciplinary setting, the Board facilitates the sharing of information on transportation practice and policy by researchers and practitioners; stimulates research and offers research management services that promote technical excellence; provides expert advice on transportation policy and programs; and disseminates research results broadly and encourages their implementation. The Board's varied activities annually engage more than 5,000 engineers, scientists, and other transportation researchers and practitioners from the public and private sectors and academia, all of whom contribute their expertise in the public interest. The program is supported by state transportation departments, federal agencies including the component administrations of the U.S. Department of Transportation, and other organizations and individuals interested in the development of transportation. www.TRB.org

www.national-academies.org

COOPERATIVE RESEARCH PROGRAMS

CRP STAFF FOR NCHRP REPORT 587

Christopher W. Jenks, *Director, Cooperative Research Programs*
Crawford F. Jencks, *Deputy Director, Cooperative Research Programs*
Robert E. David, *Senior Program Officer*
Eileen P. Delaney, *Director of Publications*
Beth Hatch, *Editor*

NCHRP PROJECT 24-18A PANEL **Area of Soils and Geology—Field of Mechanics and Foundations**

Harry A. Capers, Jr., *Arora and Associates, P.C., Lawrenceville, NJ* (Chair)
Daniel G. Ghore, *Federal Highway Administration*
Jon E. Bischoff, *Utah DOT*
Rebecca S. Burns, *Pennsylvania DOT*
J. Sterling Jones, *Annandale, VA*
Jorge E. Pagán-Ortiz, *Federal Highway Administration*
Patricia Schriener, *St. Johns, MI*
Paul Sharp, *Federal Highway Administration*
David B. Thompson, *Texas Tech University, Lubbock, TX*
Kornel Kerenyi, *FHWA Liaison*
G.P. Jayaprakash, *TRB Liaison*

AUTHOR ACKNOWLEDGMENTS

The authors would like to thank the others who worked laboriously on the project: Roger Kuhnle and Carlos Alonso from the USDA-ARS National Sedimentation Laboratory, who, along with Brian Barkdoll, guided doctoral student Hua Li in the experiments on parallel rock walls, spur dikes, and abutment collars; University of Iowa graduate students Recep Korkut, who worked on geobag and riprap apron at wing-wall abutments, Emelio Martinez, who worked on countermeasure concepts for wing-wall abutments, and Reinaldo Morales, who performed experiments on large-scale apron performance at a spill-through abutment; Art Parola of Riverine, Inc., who performed the 2D modeling; and Sjoerd van Balle-gooy, who performed the work on riprap and cable-tied blocks at both wing-wall and spill-through abutments. In addition, the authors would like to thank Timothy Hess, the Project Manager for NCHRP on this project, and the Review Panel. Thanks also to the staff at all the institutions who also contributed to the organization and facilitation of the work.

FOREWORD

By Robert E. David

Staff Officer

Transportation Research Board

NCHRP Report 587: Countermeasures to Protect Bridge Abutments from Scour will be of interest to transportation departments that are responsible for constructing and maintaining bridges that span waterways. This report provides selection criteria and guidelines for the design and construction of countermeasures to protect bridge abutments and approach embankments from scour damage.

Typical approaches for protecting bridge abutments from scour are to mechanically stabilize the abutment slopes or realign the upstream flow. The slopes are often stabilized with riprap, gabions, cable-tied blocks, or grout-filled bags, while the upstream flow is realigned with guidebanks, dikes, spurs, or in-channel devices such as vanes and bendway weirs. Neither of these approaches has been totally successful—bridge abutments and their approach embankments are the most commonly damaged bridge components during floods.

The objective of this research was to develop and validate selection criteria and guidelines for the design and construction of countermeasures to protect bridge abutments and approach embankments from scour damage. Two common forms of bridge abutments are addressed in this report: wing-wall (vertical face with angled walls into the bank) and spill-through (angled face). Conditions of scour that affect these two types of abutments include abutments threatened by main channel flow (in the cases of single and compound channels), failure of the bank, failure of the floodplain, and failure of the embankment. Countermeasures were tested under both clear-water scour (when the water velocity is slightly below the velocity at which bed sediment is in motion) and live-bed scour (when the bed sediment is in motion), the two most critical conditions for abutment scour. Tests were conducted in compound-channel flow in which the flow has overtopped the main channel and is flowing on the over-bank floodplain area as well. The selection process identifies the countermeasure concepts that may be appropriate for addressing a scour concern, indicates possible construction options, and then provides design relationships associated with the layout and dimensioning of countermeasures developed in the course of this project. Guidelines are provided for the following abutment countermeasures: riprap, cable-tied blocks, geobags (permeable bags filled with gravel), parallel walls (guidebanks with no elliptical end), spur dikes located locally to the abutment, and abutment collars (a horizontal plate attached to the abutment).

The research was performed under NCHRP Project 24-18A by Dr. Brian D. Barkdoll of the Michigan Technological University in cooperation with Dr. Robert Ettema of the University of Iowa, Dr. Bruce W. Melville of the University of Auckland, Arthur Parola of the University of Louisville, Roger Kuhnle and Carlos Alonso of the USDA National Sedimentation Laboratory.

CONTENTS

1	Summary	
4	Chapter 1 Introduction	
4	1.1 Introduction	
4	1.2 Problem Statement	
5	1.3 Objective and Scope	
5	1.4 Relationship to Prior NCHRP Studies	
6	1.5 Abutment Forms	
6	1.6 Countermeasure Concepts	
6	1.7 Research Approach	
6	1.8 Overview of Report	
7	Chapter 2 Abutment Forms and Scour	
7	2.1 Common Forms of Abutments	
7	2.2 Abutment Setting	
9	2.3 Proximity of First Pier	
9	2.4 New Versus Existing Abutments	
10	2.5 Scour Processes and Abutment Failure Mechanisms	
10	2.6 Channel and Bank Scour Processes	
15	2.7 Need for Countermeasures	
19	Chapter 3 Countermeasure Concepts and Criteria	
19	3.1 Introduction	
19	3.2 Approach-Flow Control	
20	3.3 Criteria	
21	3.4 Technical Effectiveness	
21	3.5 Constructability	
21	3.6 Durability and Maintainability	
22	3.7 Aesthetics and Environmental Issues	
22	3.8 Cost	
23	3.9 Bridges over Narrow Versus Wide Channels	
24	Chapter 4 Practitioner Survey	
24	4.1 Introduction	
24	4.2 Summary of State DOT Responses	
36	4.3 Summary of Responses	
38	Chapter 5 Literature Review	
38	5.1 Introduction	
38	5.2 Approach-Channel Alignment	
41	5.3 Vanes	
43	5.4 Guidebanks	
43	5.5 Grade-Control Structures	
46	5.6 Riprap	

63	5.7 Cable-Tied Blocks
66	5.8 Geobags
67	5.9 Other Forms of Armoring
68	Chapter 6 Lab Results I: Preliminary Experiments
68	6.1 Introduction
68	6.2 Program of Experiments
69	6.3 Use of Large Blocks
72	6.4 Use of Large Geobags
73	6.5 Wing-Wall Abutment and Geobags
75	6.6 Influence of Wing-Wall Angle
75	6.7 Influence of Abutment Alignment
78	6.8 Summary of Findings from Preliminary Experiments
79	Chapter 7 Lab Results II: Aprons at Wing-Wall Abutments
79	7.1 Introduction
80	7.2 Experiments on Aprons of Riprap or Cable-Tied Blocks
103	7.3 Experiments on Aprons of Geobags and Riprap
115	7.4 Summary of Results from Riprap, Cable-Tied Blocks, and Geobags
118	Chapter 8 Lab Results III: Aprons at Spill-Through Abutments
118	8.1 Experimental Work
123	8.2 Bridge Abutment Flow Fields
132	8.3 Spill-Through Abutment Clear-Water Study
143	8.4 Two-Dimensional Modelling of Flow Around a Small-Scale Model Abutment
150	8.5 Large-Scale Tests of Riprap Apron Performance
161	Chapter 9 Lab Results IV: Flow Modification
161	9.1 Experimental Apparatus and Procedure
164	9.2 Baseline Experiment
169	9.3 Parallel-Wall Countermeasure
178	9.4 Spur Dike Countermeasure
185	9.5 Abutment Collar Countermeasure
190	9.6 Summary
191	Chapter 10 Design Guidelines
191	10.1 Introduction
191	10.2 Countermeasure Selection and Construction Options
192	10.3 Channel Bed Degradation
195	10.4 Channel Control
198	10.5 Design Guidelines for Localized Abutment Armoring
205	10.6 Design Guidelines for Localized Flow Field Modification
207	10.7 Relation to Existing HEC Guidelines
208	Chapter 11 Conclusions
208	11.1 Wing-Wall Abutments
209	11.2 Spill-Through Abutments
210	11.3 Flow Guidance
212	References
217	Notation

S U M M A R Y

Problem Statement

Most of the techniques and guidelines that are available for protecting bridge abutments against scour have been developed from small-scale, hydraulic modeling conducted in laboratories, and a limited amount of empirical data along with anecdotal observations has been acquired from field sites. Though quite useful advances have been made with scour-protection countermeasures, there is a widely recognized need for a more extensive study, one that links modeling efforts in the laboratory to priorities of countermeasure needs and to observed field performance of countermeasures. In addition, there is a perceived need to explore innovative concepts for scour countermeasures. None of the existing approaches has been totally successful, as bridge abutments and their approach embankments are the most commonly damaged bridge components during floods. It has been recognized, therefore, that along with new countermeasure concepts, better design and construction guidelines need to be developed to protect bridge abutments and approach embankments from scour damage and to reduce the depths to which expensive deep foundations may have to be placed. In addition, there are substantial needs for guidelines and selection criteria that address limitations imposed by environmental regulation, relative cost, availability, serviceability, constructability, and design constraints. Such guidelines will assist practitioners in preventing, reducing, or mitigating the damage incurred with abutment failure owing to scour.

Scour and Abutment Forms

Scour is caused by a complicated flow pattern through the bridge opening consisting of downward flow and vortices around the abutment leading edge and rear. In addition, the riverbank can be eroded and thereby remove soil from behind the abutment. Other processes can also threaten abutments, such as riverbed degradation, headcuts, river meander migration, and embankment-eroding drainage from the roadway.

Two primary types of abutments are commonly used: wing-wall abutments, which have a vertical wall and are typically close to the main channel banks, and spill-through abutments, which are typically located back from the main channel banks on the floodplain. Wing-wall abutments are typically found on smaller streams, while spill-through abutments are on wider rivers. In addition, the orientation of the bridge may vary from being lateral, angled upstream, or downstream in relation to the flow. Each orientation changes the scour behavior in complicated ways. Countermeasure can be located on existing bridges or on new ones, with construction possibly more difficult on existing bridges with limited access to the bridge abutment. The proximity of the first pier to the abutment can be a problem since the scour holes from each can merge and further complicate countermeasure placement.

Countermeasure Concepts and Criteria

Abutment scour can be mitigated by several approaches, including upstream or downstream channel control, armoring, flow modification, bridge modification, and drainage control. Upstream channel control can be accomplished by spur dikes, hard points, or vanes that prevent a channel from migrating laterally and thereby bypassing the bridge opening. Downstream control includes a weir or checkdam to prevent headcuts from migrating upstream and threatening the bridge. Armoring consists of riprap or cable-tied blocks that protect the soil from scour. Bridge modification means adding an additional span to allow increased flow area, and flow modification entails guiding the flow smoothly through the bridge opening, typically with a wall of some kind. Drainage control ensures no adverse impact from drainage water around the bridge. The criteria for selecting a countermeasure usually encompass the following set of considerations: technical effectiveness (including no substantial adverse effects), constructability, durability and maintainability, aesthetics and environmental issues, and cost.

Survey Findings

A survey was conducted of the state offices of the U.S. Departments of Transportation. The results revealed that the most common form of scour countermeasure was riprap. Other methods were employed on a more limited basis, including sheet-piling and grout bags. Monitoring, most often by visual inspection, was employed by all the respondents with varying frequency.

Wing-Wall Experimental Results

Local scour in the general vicinity of a wing-wall abutment next to the main channel cannot be eliminated completely by an apron of riprap or geobags. An apron shifts the scour region away from an abutment. The experiments show that an apron can prevent scour from developing at the abutment itself, but that significant scour can occur readily near the downstream edge of the apron. A possible concern in using an apron is to ensure that shifting of scour does not imperil a nearby pier or portion of riverbank. Moreover, if the scour is likely to extend to an adjacent pier, then the abutment and pier countermeasure apron should be placed so as to protect both elements of a bridge. It is necessary to protect all areas around an abutment. For the use of geobags (sacks of geotextile material filled with gravel), it is necessary to tie them together and extend the mat thus formed at the lowest dune level under the pile cap.

The results obtained show that decreasing wall angle (from 90 degrees) to flow reduces the scour depth under either live-bed or clear-water conditions of scour. Decreasing the wall angle at an abutment was observed to weaken downflow and the horseshoe vortex. Accordingly, an approach-flow guide wall likely can be effective in reducing scour depth at a vertical-wall or wing-wall abutment. The brief ancillary experiments on scour at various alignments of abutment show that scour depth is at maximum when an abutment is perpendicular to the channel crossed.

Spill-Through Abutment Results

The results of the characterization of the flow field through a bridge opening with a spill-through abutment show that the velocity increases at the abutment as the flow accelerates toward and past the end of the abutment, causing a local increase in bed shear stress on the floodplain. There is a small plan-view counterclockwise rotation in the flow field at the upstream corner of the abutment and a larger plan-view counterclockwise rotation in the flow field downstream of the abutment, which extends out past the end of the abutment and increases with abutment length. There is also a smaller clockwise rotation in the flow field at the downstream corner of the abutment next to the larger region of counterclockwise rotation. The apron protection around the abutment inhibited the development of scour at the abutment toe. Scour was initiated at the edge of the apron, increasing in depth with the passage of time. As the scour hole deepened, bed material on the sides of the scour hole would fall into the scour hole, progressively undermining the protection apron. The response of the apron to the undermining process

depended on the protection type. Two-dimensional numerical modelling was also performed on this flow field and was found to be within about 15 percent of the experimental velocity results.

As the riprap aprons were undermined, the stones at the outer edge would roll into the scour hole, protecting the bed of the hole from further scour. This would deflect the erosion zone farther away from the abutment. As the cable-tied block aprons were undermined, the outer edge of the apron would fold down onto the side of the scour hole, because the cables would prevent the blocks from sliding into the scour hole. As the apron folded down onto the side slopes of the scour hole, the horizontal distance between the toe of the abutment and the edge of the apron decreased, allowing the erosion zone to move closer toward the abutment. The scouring process would continue until the equilibrium scour depth was reached.

The velocity flow fields mentioned above, measured at the abutments, showed that the velocity at the contracted bridge section increased with increasing abutment length and floodplain width. Both parameters have the effect of reducing the flow area at the contracted bridge section, thereby increasing the velocity and flow strength. Consequently, the vorticity and bed shear stress also increase with increasing abutment length and floodplain width. Concurrently, similar effects were observed regarding the influence of the abutment length and floodplain width on the equilibrium scour hole depths, showing that the scour hole size is related to the flow field around the abutment.

Flow Modification Experimental Results

Experiments were performed investigating the use of a wall composed of piled rocks. The wall extended parallel to the flow and was higher than the flood level, thereby smoothing flow through the bridge opening and also preventing return floodplain flow from scouring the abutment foundation. These parallel walls were found to work well and reduce scour at the abutment substantially. Solid walls did not work as well and could have foundation problems in a prototype bridge.

Spur dikes located locally to the abutment were also modeled and found to work well. Three dikes were warranted, one upstream of the abutment, one at the upstream abutment corner, and one at the downstream corner. If the abutment were sufficiently long, then other dikes could be located in between the two corner dikes.

Abutment collars were also investigated and found to work well, but could cause problems with debris and could be difficult to construct.

Design Guidelines and Suggestions

A complete set of design guidelines and suggestions have been developed, consisting also of criteria for selection of the most appropriate countermeasure. For bed degradation, some kind of grade-control structure can be used. For meander migration, upstream control needs to be implemented. For local protection of the abutment, either the flow can be modified or the material armored. For flow control, one can align the approach-channel banks, shift the abutment back and add a bridge span, add a relief bridge, or place flow-deflection spur dikes or guidebanks upstream of the bridge. For armoring, one can use riprap, cable-tied blocks at the abutment and/or at the drainage outlets, parallel rock walls, or spur dikes locally at the abutment. Selection should be guided by a life-cycle cost assessment, including environmental impacts.

Study Participants

Work for this project was performed at various locations. The riprap and cable-tied block experiments were carried out at the University of Auckland, New Zealand. Experiments on geobags and a large-scale experiment on riprap on spill-through abutments were carried out at the University of Iowa. Experiments on parallel walls and spur dikes were performed at the U.S. Department of Agriculture Agricultural Research Service (USDA-ARS) National Sedimentation Laboratory. The researchers involved visited the other laboratories involved, and the results are synthesized in this final report.

CHAPTER 1

Introduction

1.1 Introduction

Scour of bridge abutments is a common cause of bridge failure, often resulting in substantial interruption of traffic, and sometimes loss of life, not to mention damage to vehicles. An abutment scour entails hydraulic erosion of the waterway boundary around an abutment and the geotechnical failure of both the soil upon which the abutment is placed and of the soil comprising the embankment at an abutment. Accordingly, it is necessary to protect the abutment structure against hydraulic erosion as well as geotechnical failure. This requirement potentially makes the design of scour countermeasures for abutments a more difficult proposition than countermeasure design for piers. The present project reviews existing countermeasure concepts, explores prospective new concepts, and further develops existing concepts.

It is pertinent to indicate at the outset here that, after extensive investigation, the main advances stemming from this project concern the further development of existing countermeasure concepts. There are, though, several additional relatively new concepts introduced. These concepts are not highly innovative or elegant, but are sensible and practical. This final report documents the extensive amount of investigation and testing completed for the project. The investigation included heuristic, laboratory exploration of countermeasure concepts not documented in the literature on scour, detailed testing aimed at further developing concepts of proven merit, and identification of concepts that have been implemented in a somewhat ad hoc manner at existing abutments.

No panacea was found in the sense that many countermeasure configurations did mitigate scour at the abutment location but shifted the scour somewhere else. Care must be taken to ensure that a pier or other structure is not located in the scour location in order to avoid potential collapse.

Work for this project was performed at various locations. The riprap and cable-tied block experiments were carried out at the University of Auckland, New Zealand. Experiments on

geobags and a large-scale experiment on riprap on spill-through abutments were carried out at the University of Iowa. Experiments on parallel walls and spur dikes were performed at the U.S. Department of Agriculture Agricultural Research Service (USDA-ARS) National Sedimentation Laboratory. The researchers involved visited the other laboratories involved, and the results are synthesized in this final report. The researchers involved and their positions, institutions, and roles in the study are listed in Table 1-1.

1.2 Problem Statement

Most of the techniques and guidelines that are available for protecting bridge abutments against scour have been developed from small-scale, hydraulic modeling conducted in laboratories, and a limited amount of empirical data along with anecdotal observations has been acquired from field sites. Though quite useful advances have been made with scour protection (hereinafter termed scour “countermeasures”), there is a widely recognized need for a further extensive study, one that links modeling efforts in the laboratory to both priorities of countermeasure needs and observed field performance of countermeasures. In addition, there is a perceived need to explore innovative concepts for scour countermeasures.

There are two broad approaches for protecting bridge abutments from scour:

1. Mechanically stabilizing the abutment slopes with armor units, such as riprap, gabions, cable-tied blocks, or grout-filled bags, and
2. Aligning the upstream flow by using guidebanks, dikes, spurs, or in-channel devices such as vanes and bendway weirs.

Neither of these broad approaches has been totally successful, as bridge abutments and their approach embankments are the most commonly damaged bridge components

Table 1-1. Personnel involved in project.

Personnel	Position	Institution	Role in Study
Brian Barkdoll	PI	Michigan Tech University	Project management; experiments on parallel wall, spur dikes, and collars
Carlos Alonso	Co-PI	National Sedimentation Lab	Parallel wall, spur dikes, and collars
Robert Ettema	Co-PI	University of Iowa	Geobags and large-scale riprap
Roger Kuhnle	Co-PI	National Sedimentation Lab	Parallel wall, spur dikes, and collars
Bruce Melville	Co-PI	University of Auckland	Riprap and cable-tied blocks
Art Parola	Co-PI	Riverine Inc.	2D modeling of flow through bridge opening
Recep Korkut	Graduate Student	University of Iowa	Geobag and riprap apron at wing-wall abutments
Hua Li	Graduate Student	Michigan Tech University	Parallel wall, spur dikes, and collars
Emelio Martinez	Graduate Student	University of Iowa	Countermeasure concepts for wing-wall abutments
Reinaldo Morales	Graduate Student	University of Iowa	Large-scale experiment on apron performance at a spill-through abutment
Sjoerd van Ballegooy	Graduate Student	University of Auckland	Riprap and cable-tied blocks

during floods. It has been recognized, therefore, that along with new countermeasure concepts, better design and construction guidelines need to be developed to protect bridge abutments and approach embankments from scour damage and to reduce the depths to which expensive deep foundations may have to be placed.

In addition, there are substantial needs for guidelines and selection criteria that address limitations imposed by environmental regulation, relative cost, availability, serviceability, constructability, and design constraints. Such guidelines will assist practitioners in preventing, reducing, or mitigating the damage incurred with abutment failure owing to scour.

1.3 Objective and Scope

The objective of this project is to develop and validate selection criteria and guidelines for the design and construction of countermeasures to protect bridge abutments and approach embankments from scour. The following countermeasure concepts were considered:

- Armoring countermeasures such as riprap, cable-tied blocks, and geobags at abutments, including the type and extent of filters that could be used under the protective armoring countermeasure layer, the size of the armoring countermeasure, and the extent to which the armoring countermeasure should be placed up an abutment embankment slope, into the channel, and on the approach embankment;

- Methods to increase or maintain the geotechnical stability of the earthfill embankment at an abutment;
- Flow-altering devices such as spur dikes, including the size, type, placement, and feasibility of using these devices; and
- Nontraditional concepts for abutment scour countermeasures, such as collars and parallel walls, and temporary countermeasures, such as geocontainers and extra-large armor units, including the size, type, placement, and feasibility of using these concepts.

1.4 Relationship to Prior NCHRP Studies

Several prior studies have investigated scour countermeasures for bridge abutments or provide suggestions for countermeasures. Notably, the FHWA Hydraulic Engineering Circular No. 23 (HEC 23) addresses various countermeasures for the prevention of river-bend migration and has some relation to the current topic only in that some of the same countermeasures may be applicable. Their design, however, for use at bridge abutments is made clear in the present study. Only single-channel flow conditions are mentioned; therefore, HEC 23 does not address the complicated flow situation of overbank flow interacting with the bridge abutments, as the current study does.

NCHRP Project 24-7 also discusses countermeasures, but in relation to bridge piers. There are similar concepts in the mitigation of scour at piers and abutments, but the issue of compound channel flow is less important for piers due to their farther distance from the bank.

NCHRP Project 24-7(2) further reported on pier selection criteria, guidelines for design and construction, inspection, maintenance, and performance evaluation.

NCHRP Project 24-23 is concurrent with the present study and investigates scour depth prediction only and does not address countermeasures, which the present study does.

Other studies besides NCHRP reports are in the literature and are described further in a later chapter, but none of these studies address abutment scour countermeasures for overbank flow as the current study does. Overbank flow is especially important for abutment scour, since the return flow from the floodplain is one of the more significant causes of scour, as is elaborated later in this report.

1.5 Abutment Forms

Given the wide variety of abutment forms existing and the various conditions of scour, it is understandable that previous studies focused on simplified abutment shapes and geometries. The scour-inducing flow patterns around abutments on compound channels can be quite complicated and counterintuitive. This simplification, however, has led to conclusions that are perhaps not realistic. The current study has chosen abutment shapes that replicate those found on actual waterways, namely wing-wall (vertical face with angled walls into the bank) and spill-through (angled face) shapes. Conditions of scour for spill-through and wing-wall abutments include abutments threatened by main channel flow (in the cases of single and compound channels), failure of bank, failure of floodplain, and failure of embankment.

1.6 Countermeasure Concepts

The primary concepts for abutment scour mitigation are bank hardening, embankment stabilizing, and flow altering. Bank-hardening countermeasures seek to armor or strengthen the surface of a bank so as to withstand the hydrodynamic forces imposed by flow round an abutment. Primary examples of bank-hardening countermeasures are riprap, cable-tied blocks, geobags, partially grouted riprap, and interlocking devices (e.g., Toskanes).

Embankment-stabilizing countermeasures entail increasing the slope stability of the earthfill embankment at an abutment by ensuring that an embankment does not fail geotechnically as scour hole forms at the toe of the embankment.

Flow-altering countermeasures seek to reduce the flow-induced stresses on the bed and banks to a level that will not erode the bed or bank material. Common flow-altering

countermeasures are spur dikes, stone walls, collars, submerged vanes, and guidebanks.

All of the above-listed bank-hardening, embankment-stabilizing, and flow-altering countermeasures (except perhaps collars) can also be used for channel and bank stabilization. A stable channel is paramount in protecting a bridge because if the channel migrates around and bypasses the bridge crossing, then a new bridge must be built.

1.7 Research Approach

The research was broken into seven distinct tasks.

- **Task 1 Literature Review.** All available research was read and summarized to aid in the selection of the research approach and the selection of countermeasures for study.
- **Task 2 Screening Approach.** After consideration of all countermeasures, a select few were chosen for further study.
- **Task 3 Research Alternatives.** Various research options were considered in order to make an informed choice of research approach and the associated work plans.
- **Task 4 Interim Report.** An interim report was prepared for consideration by the NCHRP review panel for the project, and consent was received to proceed.
- **Task 5 Execution of Work Plans.** The approved work plans were carried out between the various parties involved in the form of laboratory work and two-dimensional modeling.
- **Task 6 Selection Criteria and Guidelines.** Upon consideration of the laboratory results and two-dimensional modeling, design guidelines were prepared for each of the countermeasures studied.
- **Task 7 Final Report.** This final report was written to document the findings and recommendations of the project.

1.8 Overview of Report

Following from the introduction given above, Chapter 2 presents abutment forms and failure processes. Chapter 3 outlines countermeasure concepts and criteria. Chapter 4 presents the results of a survey of state departments of transportation. Chapter 5 contains a comprehensive literature review. Chapters 6–9 contain laboratory results of preliminary experiments, wing-wall abutment experiments, spill-through abutment experiments, and flow modification experiments, respectively. Chapter 10 presents the design guidelines stemming from the project, and Chapter 11 presents the project's conclusions and recommendations.

CHAPTER 2

Abutment Forms and Scour

2.1 Common Forms of Abutments

The two principal types of bridge abutment forms are wing-wall abutments and spill-through abutments. These abutment forms may be supported on piled or slab footings. Figures 2-1a and b illustrate the main features of wing-wall and spill-through abutment forms, respectively.

Wing-wall abutments have vertical walls that retain the earthfill material comprising the embankment approach to the abutment. The walls can be angled from about 45 degrees to 90 degrees. The abutment face is vertical as well. The overall form of the abutment is quite bluff, and causes large-scale turbulence structures to develop in the flow around the abutment. Wing-wall abutments are commonly used for small bridges with one to three spans, as the abutment form lends itself to placement on the banks of streams and creeks, or small rivers that do not have a pronounced floodplain.

Spill-through abutments are formed as sloped earthfill placed fully around a pier-like abutment support (often called a standard stub abutment). This abutment form is commonly used for abutments set back on floodplains. The

sloped earthfill material making up the earthfill embankment around the abutment needs protection from scour, as often does the floodplain immediately around the abutment. Accordingly, although some spill-through abutments have a simple grassed surface, it is usual for spill-through abutments to have their front slopes and flanks protected with riprap or sometimes with a concrete slab.

2.2 Abutment Setting

Though there are essentially two basic abutment forms (spill-through and wing-wall), abutments may vary markedly in their setting at bridge waterways. Most abutment settings are unique in abutment placement, soil conditions, channel morphology, and surrounding vegetation. Therefore, the task of providing scour protection through the use of countermeasures inevitably entails tailoring countermeasure techniques to individual bridge sites. This consideration is a major theme in this report.

A second, and related, theme concerns the size of river or stream channel to be bridged. Channel size has a bearing on abutment form and layout and thereby on the nature of the scour countermeasure options to be implemented. There is a correspondence between the size of the channel and the size of the countermeasure concept. For instance, spur dikes are likely not to be an appropriate countermeasure concept for flow and bank control along a small stream; rock hard-points or riprap are better suited scour countermeasures for small channels.

For most state departments of transportation and counties in the United States, a small channel is one whose upstream watershed encompasses about 100 square miles or less. It is usual for such bridges to have one, two, or three spans. Usually, small channels have a negligible floodplain, such that the bridge abutments are practically located at the top of the channel banks, more or less as indicated in Figure 2-2. To be sure, channel width and flow depth can increase as flow

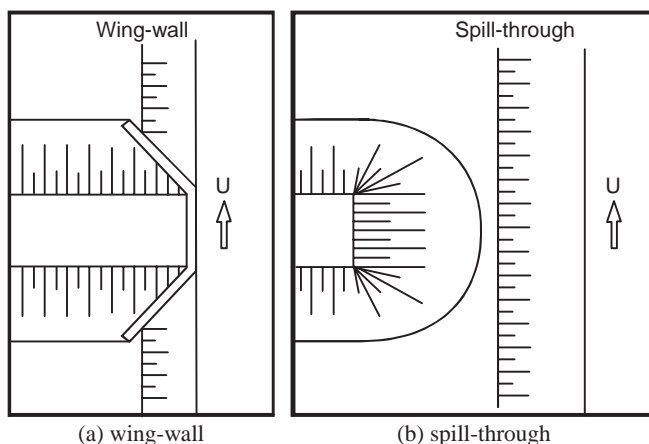


Figure 2-1. Two common forms of abutment.

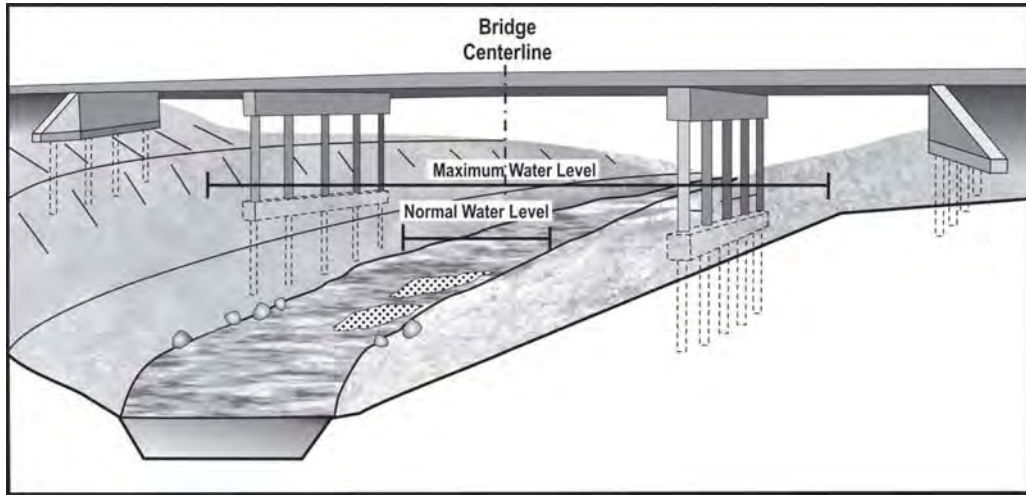


Figure 2-2. Typical features of a bridge set over a small channel, with abutments near the edge of the channel.

increases, yet the abutments cause minimal constriction of flow.

As channel size increases, channels may become more compound in cross section, such that there is a main channel and a floodplain of variable extent, as shown in Figure 2-3. Abutments may still be located at the banks of a main channel, or they may be set back so as to constrict flow to some practical minimal extent and as to reduce the cost of the bridge. Spill-through abutments most commonly are used for bridges over comparatively large channels. Further, for bridges over compound channels, spill-through abutments usually are set back on the floodplain, as illustrated in Figure 2-3. To be sure, a great variety of channel sizes and abutment forms can be found;

wing-wall abutments occasionally are used for bridges spanning portions of floodplains. Also, water elevations and flow patterns can vary enormously with varying discharge in compound channels.

The setting of a bridge across a waterway also may vary in accordance with highway or road orientation relative to the thalweg axis of a channel. These considerations determine abutment skewness to the flow and possibly the extent of set-back from the main channel of the waterway. The skewness angle of the abutment to the waterway can affect scour extent, depth, and location. When aligned upstream into the flow, the flow is retarded upstream of the abutment with scour occurring around the abutment tip. When an abutment is angled

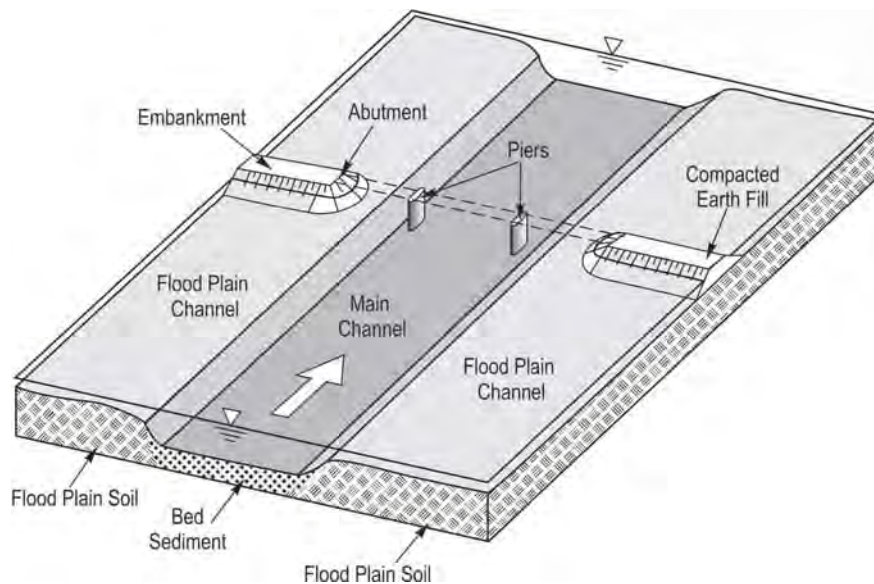


Figure 2-3. Typical features of a bridge over a relatively large and compound channel.



Figure 2-4. Spill-through abutment on a floodplain.

downstream, scour usually occurs around the tip and extends downstream of the abutment. Abutments perpendicular to the flow cause the deepest scour, occurring slightly downstream of the tip.

Figures 2-4 and 2-5 illustrate a spill-through abutment on a floodplain and a wing-wall abutment at a streambank, respectively.

2.3 Proximity of First Pier

Many bridges over rivers are constructed with a comparatively short first deck span such that a pier is located very close to an abutment. There are construction advantages in having the pier close to the abutment and riverbank, and the arrangement often facilitates a clear span over the river. That construction advantage, however, can lead to a potentially severe scour situation whereby local scour at a pier adversely influences scour at a neighboring abutment, or vice versa. Figure 2-6 depicts a fairly common example of a bridge that has a pier located close



Figure 2-5. Wing-wall abutment at a streambank.



Figure 2-6. Pier close to a spill-through abutment.

to an abutment. For such cases, it is important that the protection for the abutment and pier be jointly developed. A risk, otherwise, is that protection of the abutment may aggravate scour at the pier.

2.4 New Versus Existing Abutments

Scour countermeasures may be applied to abutments being constructed for new bridges or be retrofitted to an existing bridge. It is increasingly usual for new abutments to be constructed with some form of scour countermeasure. For such bridges, it is somewhat easier to place the countermeasure, as the abutment site is usually accessible. However, present design practice entails that abutment (and pier) foundations be deep enough that the structural stability of an abutment is not reliant on the performance of a scour countermeasure. The role of the countermeasure is to reduce scour extent so as to minimize erosion of an approach embankment to an abutment or of a channel bank near an abutment.

For existing abutments, scour countermeasures often are required to ensure that a potentially scour-threatened abutment does not fail or to aid in the repair of an abutment. Often a scour countermeasure can be a temporary action to prevent further erosion of an exposed embankment or eroding channel bank. However, a countermeasure may also be intended to extend the remaining design life of a bridge.

One challenge associated with the application of a scour countermeasure for an existing bridge can be access to the abutment region requiring protection. This is a concern especially if a countermeasure has to be placed in water flowing around the abutment. It is important that scour countermeasures be practical to implement, in terms of both construction of the countermeasure components and placement of the countermeasure.

2.5 Scour Processes and Abutment Failure Mechanisms

There are many scour processes and abutment failure mechanisms of concern. The previously described flow patterns cause scour that, if unmitigated, can cause abutment failure. The scour processes are extensively described in the final report for NCHRP Project 24-20, "Prediction of Scour at Abutments"; this study is a companion study to the present study. The ensuing descriptions of abutment scour are largely taken from the findings of NCHRP Project 24-20.

2.6 Channel and Bank Scour Processes

Described here are the flow field and the scour processes leading to abutment scour. Given that several processes contribute to abutment failure, it is useful to first mention the several boundary materials forming the bridge waterway and then indicate the locations where abutment scour can be deepest. Figure 2-7 indicates the usual soil and sediment dispositions in the vicinity of a bridge abutment, in this case for an abutment on a floodplain. The soils and sediments can have different erosion resistance and behavior.

2.6.1 Locations of Abutment Scour

The abutment layout, the flow field, and the erodibility of sediment and soil at bridge sites may cause the deepest scour to occur at any, or all, of three locations near an abutment, as indicated in Figure 2-8:

1. In the main channel near the abutment (Scour Condition 1);
2. A short distance downstream of the abutment (Scour Condition 2); and
3. At the abutment itself (Scour Condition 3).

Scour at these locations occurs at different rates and can differ in the maximum depth attained, in accordance with flow-field and soil conditions. If sufficiently deep, scour at each location can cause the slope-stability failure of the embankment adjoining the abutment.

2.6.2 Flow Field

In its effect on flow in a channel, a bridge abutment may be likened to a short contraction, such as that indicated in Figure 2-9 for flow through a simple orifice. Two flow features are directly evident in the flow field through a contraction:

1. Flow contraction and
2. The generation and shedding of large-scale turbulence structures from the boundaries of the contraction.

As shown schematically in Figure 2-10, the flow field at an abutment typically consists of an acceleration of flow from the upstream approach to the most contracted cross section somewhere at or just downstream of the head of the abutment, followed by a deceleration of flow. A flow-separation region forms immediately downstream of the abutment, and flow expands around the flow-separation region until it fully reestablishes itself across the compound channel. Just upstream of the abutment, a flow-separation point and a small eddy may develop. The size of the upstream eddy depends on the length and alignment of the abutment. The curvature of the flow along the interface between the stagnation region and the flow causes a secondary current that, together with the flow, leads to a spiral motion or vortex motion similar to flow through a channel bend. The vortex in flow around an abutment head is more localized and has a strong scouring action. The

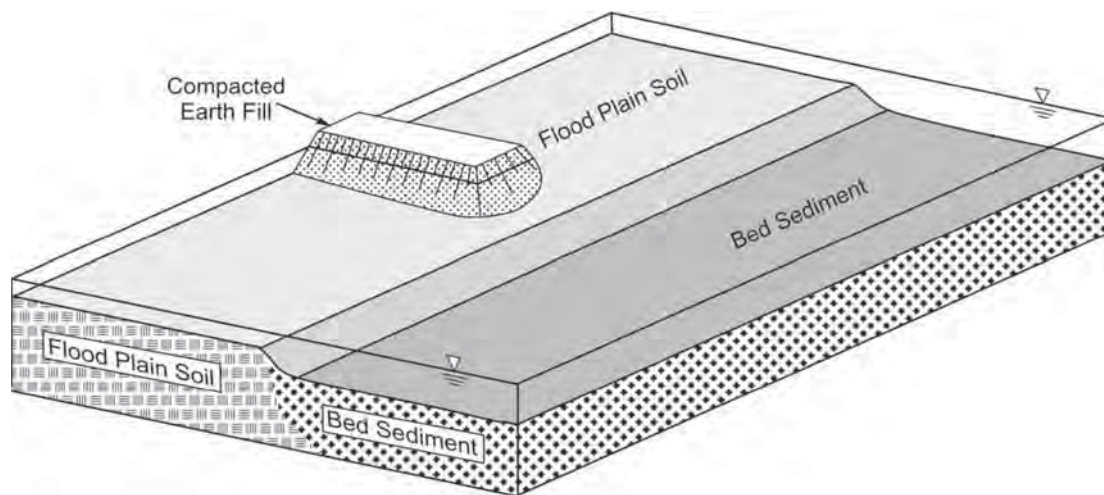


Figure 2-7. Boundary soils and sediments forming the waterway at an abutment.

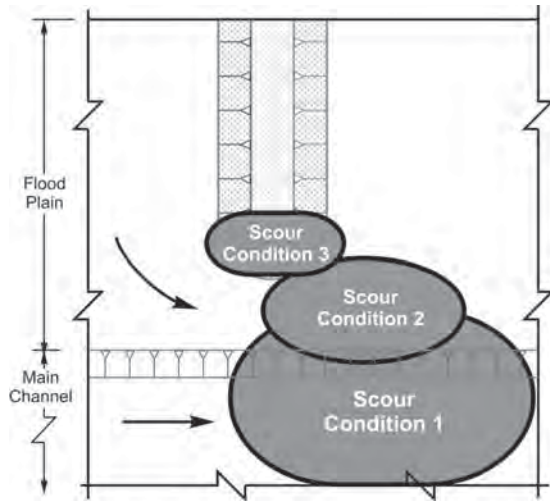


Figure 2-8. Three main regions of abutment scour.

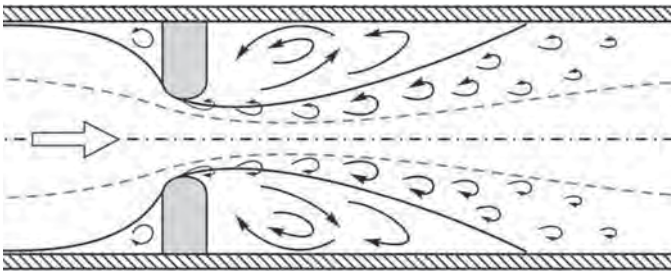


Figure 2-9. Flow through a bridge opening is analogous to flow through an orifice contraction; the flow contracts and turbulence structures develop.

vortex erodes a groove along its path and induces a complex system of secondary vortices.

At abutments with wing-walls (Figure 2-11), the flow impinging on the wall may create a downflow (similar to at a bridge pier), which excavates a locally deepened scour hole at

the wall. The downflow is much weaker for spill-through abutments because of their sloped face.

The two flow features listed above (flow contraction and the generation and shedding of large-scale turbulence structures from the boundaries of the contraction) are related and difficult to separate in the flow field. The region of flow contraction is influenced by the area ratio of the approach flow and the contracted flow, as well as by the form and roughness of the contraction. The large-scale turbulence structures are also influenced by the form and roughness of the contraction. The orifice analogy is somewhat simplistic, but an important point to be made from it is that the flow field through a bridge waterway, like the flow field through an orifice, is not readily delineated as a contraction flow field and local flow field limited to the near zone of the abutment.

The effect of flow contraction on velocity through the contraction can be explained in terms of a contraction coefficient, C , as used in calibrating flow through an orifice. For fully turbulent flow, C is a function of orifice geometry. Likewise, for abutments, the extent of flow contraction and the turbulence generated by the contracting flow depends on abutment shape.

Either of the flow features listed above may become more pronounced, depending on the extent of flow contraction. When an abutment barely constricts flow through the waterway, scour at the abutment may develop largely as a consequence of the local flow field generated by the abutment. At the other extreme situation, flow contraction may dominate the flow field when the flow is severely constricted such that a substantial backwater rise in water level occurs. In this case, the approach flow slows as it approaches the upstream side of the bridge, then it accelerates to high speed as it passes through the bridge waterway. Except for bridges whose spans greatly exceed abutment length, the flow field at a typical bridge waterway will be influenced by the com-

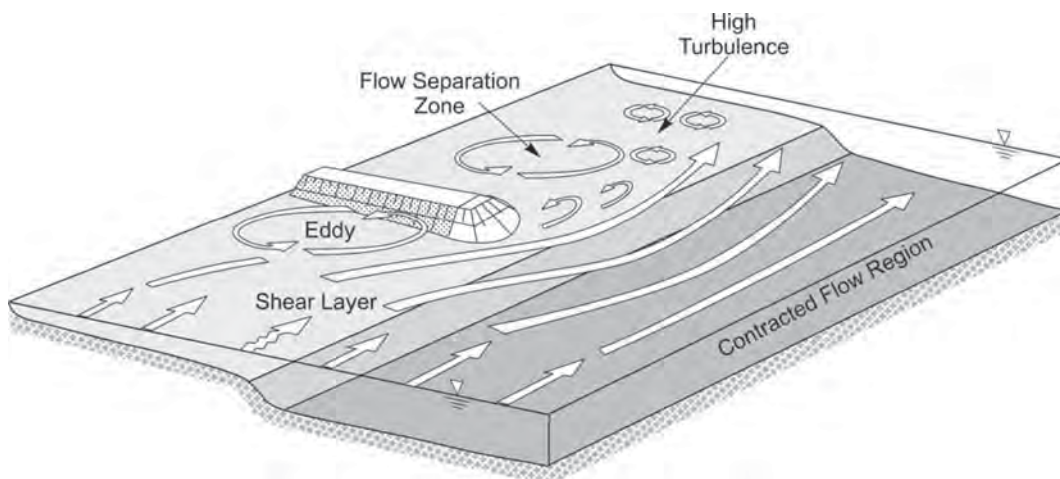


Figure 2-10. Schematic of near-field flow around a spill-through abutment.

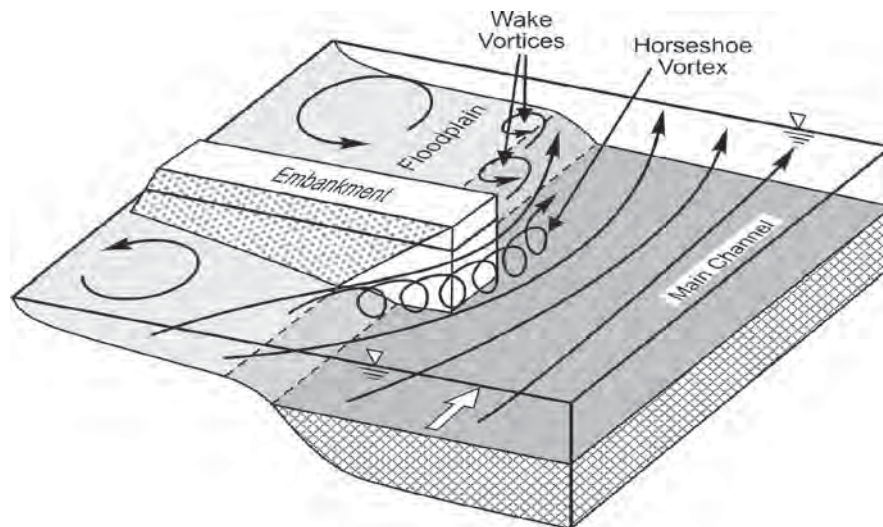


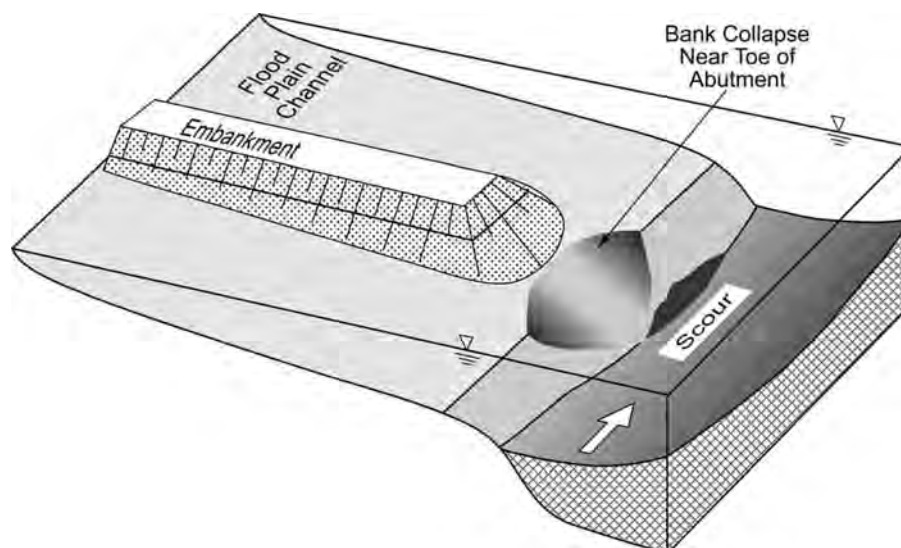
Figure 2-11. Flow field past a wing-wall abutment.

bined effects of flow contraction and flow features generated by the abutment.

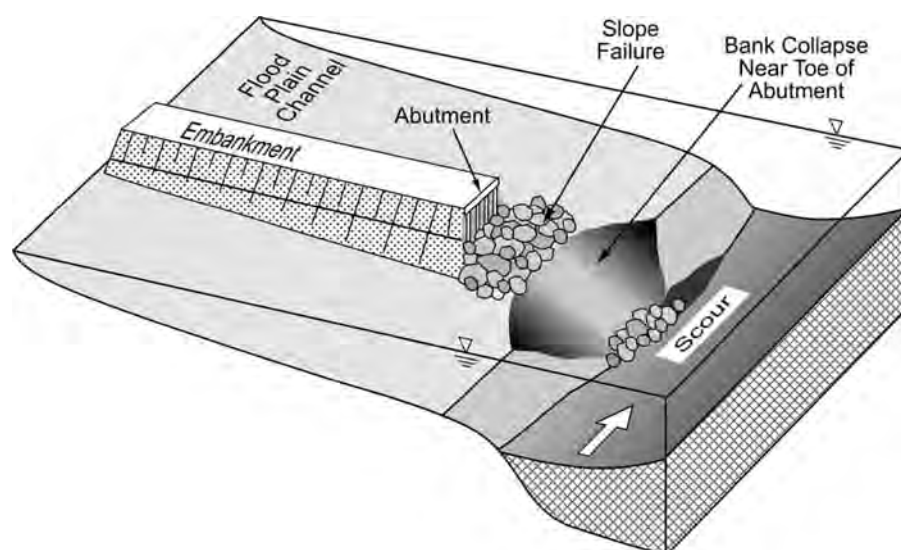
2.6.3 Common Scour Conditions Causing Abutment Failure

The foregoing considerations of scour location, based on flow field and boundary susceptibility to erosion, indicate that scour at the locations indicated in Figures 2-12 through 2-17 can lead to the following conditions of abutment failure (the scour conditions are elaborated in the final report for NCHRP Project 24-20):

- **Condition 1: Scour destabilization of the main-channel bank near the abutment, which is located close to the bank.** The floodplain is relatively resistant to erosion compared with the bed of the main channel. Figure 2-12 illustrates the several-stage failure process, which involves scour leading to geotechnical failure of the main-channel bank and the embankment. Hydraulic scour of the main-channel bed causes the channel bank to become geotechnically unstable and collapse. The collapsing bank undercuts the abutment embankment, which in turn collapses locally. Soil, and possibly riprap, from the collapsed bank and embankment slide into the scour hole.
- For wing-wall abutments, located within the bank of the main channel, several erosion processes in addition to flow contraction can result in failure of the main-channel bank and the approach embankment:
 - The local flow field generated at the corners of the abutment can cause local scour at those locations (see Figure 2-13) and
 - Exposure of the piles beneath the abutment pile cap can cause riverbanks and embankment soil to erode out from beneath the pile cap (see Figure 2-14).
- **Condition 2: Scour of the floodplain around an abutment well set back from the main channel.** The floodplain scours near and slightly downstream of the abutment. The scour hole locally destabilizes the embankment side slope, causing embankment soil, and possibly riprap, to slide into the scour hole (see Figure 2-15).
- **Condition 3: Scour at Locations 1 or 2 just mentioned may eventually cause the approach embankment to be washed out near the abutment, thereby fully exposing the abutment.** In this condition, scour at the exposed stub or wing-wall abutment essentially occurs as if the abutment were a form of pier. Figure 2-16 illustrates this scour condition.
- **Condition 4: Scour may occur at the embankment approach some distance from an abutment.** This is shown in Figure 2-17. The embankment intercepts and deflects flow on the floodplain, but the unprotected floodplain near the embankment may experience eroding velocities that cause a local side slope failure of the embankment. This scour mechanism differs from those shown in Figures 2-15 and 2-16 because that scour does not occur at the bridge opening. In somewhat extreme cases, flow may erode through the embankment or wash out the embankment.
- **Condition 5: Scour can occur when an approach embankment is overtopped by a high flow.** Overtopping can occur because the embankment has a comparatively low crest elevation or because the bridge opening has become clogged with vegetation debris or perhaps (during the early spring season) with ice. In this condition, flow



(a) Hydraulic scour of the main-channel bed causes riverbank instability and failure.



(b) The face of the abutment embankment fails. In this condition, the floodplain is much less erodible than is the bed of the main channel.

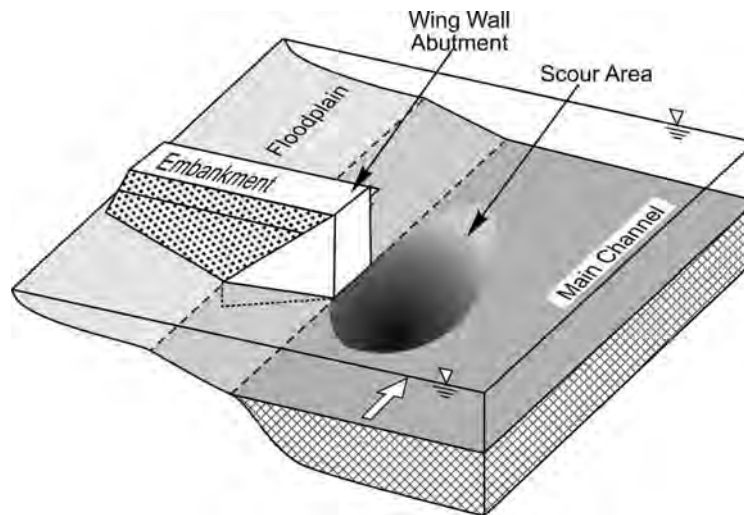
Figure 2-12. The several-stage collapse process associated with one common condition of scour at a spill-through abutment in a compound channel.

spilling over the abutment scours the floodplain along the downstream side of the embankment, and then the embankment side slope may undergo a side slope failure. This scour condition is akin to dam-breaching and possibly to the scour form that develops immediately downstream of an unprotected outlet of a culvert.

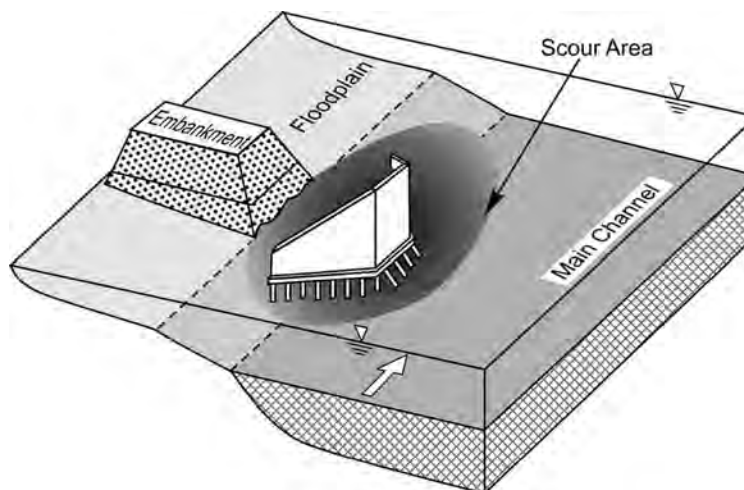
It is important to realize that a scour event (or series of events) at an abutment, however, may involve a sequence of all five scour conditions. When an abutment is close to the main channel, Condition 1 (Figure 2-12) may develop

relatively quickly, with Condition 2 (Figure 2-15) occurring at a slower rate. Either separately or together, Scour Conditions 1 and 2 may eventually cause the approach embankment to undergo a slope-stability failure. If the embankment washes out enough to expose the abutment structure, scour may develop at the abutment structure as if the abutment were a form of pier (Condition 3, Figure 2-16). The combination of scour conditions is suggested earlier in Figure 2-8.

The scour conditions described in this section may occur for pile-supported or spread-footing-supported abutments



(a) Hydraulic scour of the main-channel bed causes riverbank instability and failure.



(b) The channel bank and the face of the abutment embankment fail.

Figure 2-13. The two-stage collapse process associated with one common condition of scour at a wing-wall abutment.

and are of practical importance for the design and monitoring of bridge abutments.

(a) Hydraulic scour of the main-channel bed causes riverbank instability and failure.

(b) The face of the abutment embankment fails. In this condition, the floodplain is much less erodible than is the bed of the main channel.

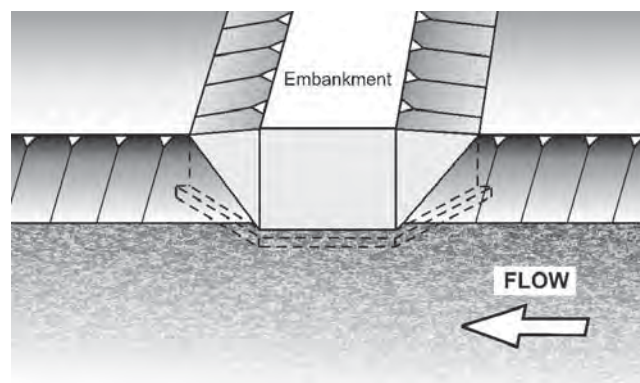
2.6.4 Other Abutment Failure Processes

Other possible scour conditions can be associated with abutments. These processes are attributable to several causes:

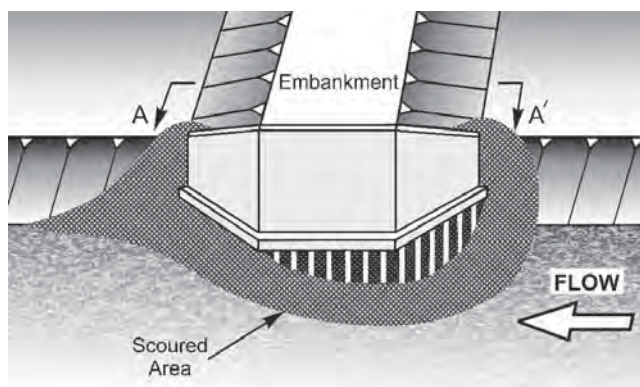
- General scour,
- Head-cut migration along a channel,

- Shifts in channel or channel-thalweg alignment, and
- Erosion associated with poorly maintained drainage channels along the flanks of an abutment.

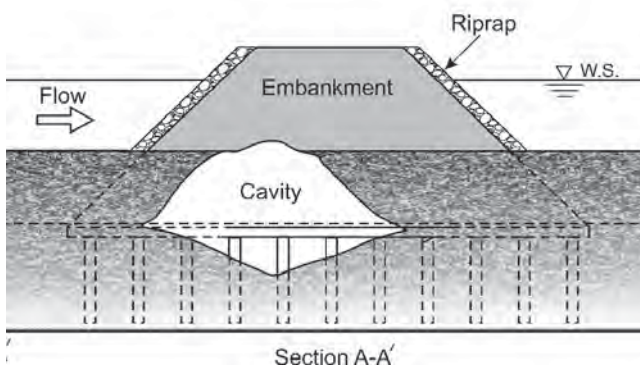
General scour is scour that occurs irrespective of the existence of the bridge. It includes long-term and short-term scour processes. Long-term general scour is scour that occurs over several years or longer and includes progressive degradation and lateral bank erosion due to channel widening or meander migration. Progressive degradation is the almost permanent lowering of the river bed at a bridge site owing to natural changes in the watershed (meander-bend cutoff, head-cut progression, landslides, fire, climate change, etc.) or human activities (channel straightening, dredging, dam construction, agriculture, urbanization, etc.).



(a) Before scour.



(b) Scour develops below the pile cap of a wing-wall abutment.



(c) Embankment soil is sucked from beneath the pile cap and forms a cavity in the embankment.

Figure 2-14. Collapse process.

It is noted here that head-cutting of channel beds and channel migration are two types of channel degradation that are of major concern for bridges and account for numerous abutment failures.

When a main-stem channel experiences bed degradation for some reason, the overall bed slope of a tributary channel

then becomes steeper, with the erosion causing the steepening beginning at the downstream end (or base level) of the tributary channel. The steepening process forms a so-called knickpoint along the bed of the tributary channel; the knickpoint is the location where there is a discontinuity in the channel bed of the tributary. As the downstream extent of the bed of the tributary channel erodes, the knickpoint is moved upstream. For a bed consisting of sandy alluvium, bed erosion and knickpoint movement occur relatively quickly. For a bed consisting of cohesive sediment (clay) or soft sedimentary rock, knickpoint movement can be relatively slow, and the upstream movement of the knickpoint occurs by means of a process called head-cutting.

Head-cut migration along a channel occurs when flow plunges over a head-cut (that is, a vertical or near-vertical drop in the channel bed) and strikes the bed downstream, thereby eroding a scour hole. The scour hole deepens until the face of the head-cut becomes unstable geotechnically, then fails into the scour hole, and the head-cut progresses upstream. The upstream migration of a head-cut induces channel bed and bank instabilities, worsens erosion, and increases the sediment load delivered to downstream reaches. Figure 2-18 illustrates head-cutting occurring within the waterway of a small bridge. The head-cutting destabilized the bridge abutments and exposed the piling support of piers.

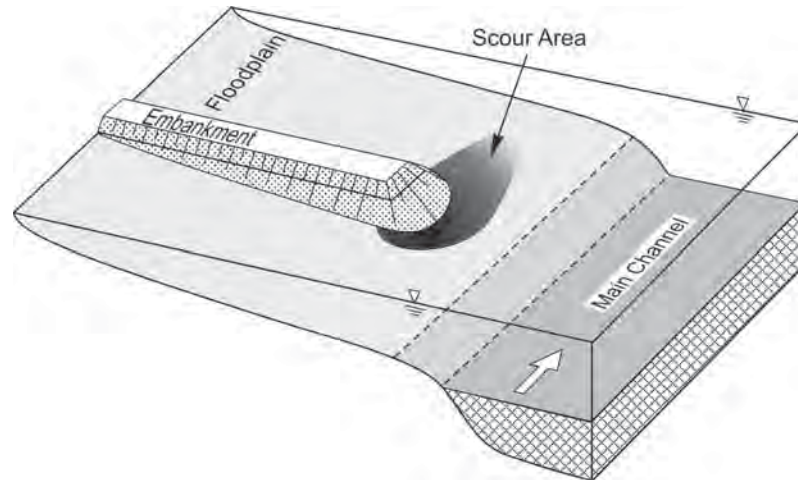
Short-term general scour is scour that develops during a single or several closely spaced floods. It includes scour at a confluence, which includes *shifts in channel thalweg or channel-thalweg alignment*, shifts in bends, and scour arising from bed-form (dune or bar) migration.

A common problem for bridge abutments is erosion attributable to head-cutting at drainage channels along the flanks of an abutment. Figure 2-19 depicts a common situation found for small bridges. The *erosion associated with poorly maintained drainage channel* exposes the abutment to aggravated scour.

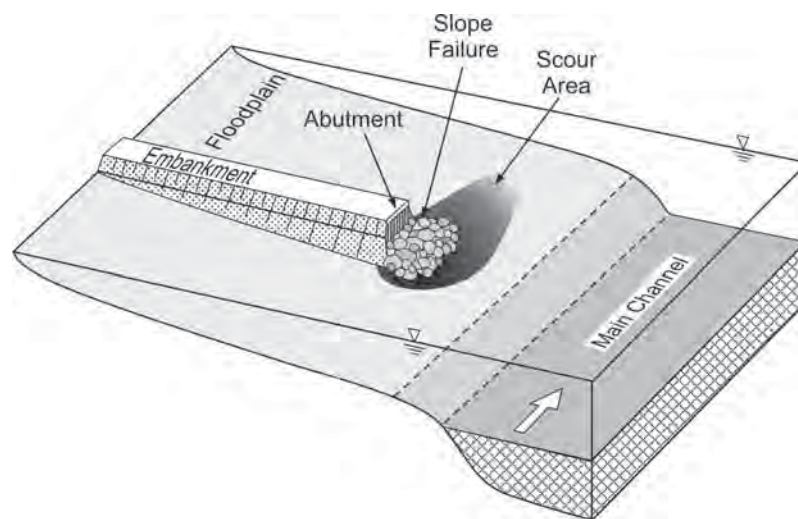
2.7 Need for Countermeasures

To mitigate abutment scour and avoid abutment undermining and failure, countermeasures are needed. These countermeasures can make it more difficult for the flow to cause scour or they can alter the flow pattern so as to lessen its scouring capacity, or a combination of both.

Countermeasures can lessen scour by quite significant amounts and, therefore, provide a fairly inexpensive method of protecting the abutment from failure. Examples are provided in subsequent chapters of scour mitigation by countermeasures.



(a) Hydraulic scour of the floodplain



(b) Failure of the face of the abutment embankment. In this condition, the floodplain is as erodible (more or less) as is the bed of the main channel. The collapse of the embankment soil (and armor protection) into the scour hole modifies the scour area.

Figure 2-15. The collapse process associated with a common condition of scour at a spill-through abutment in a compound channel.

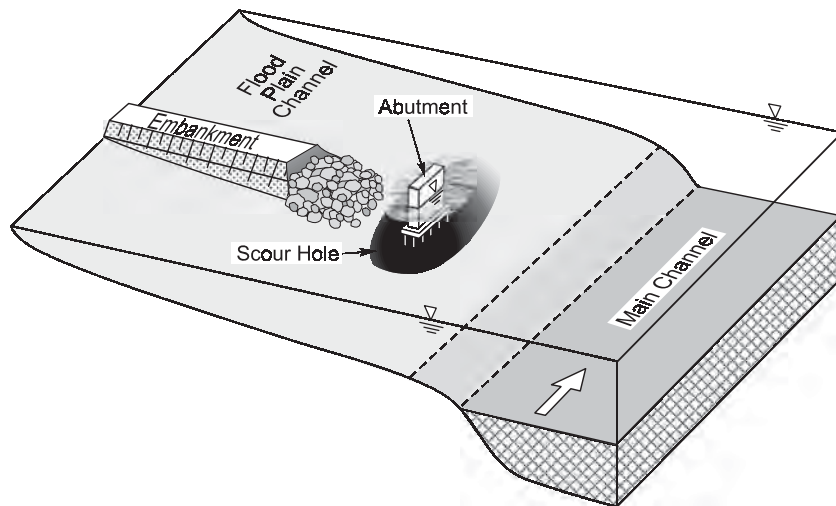


Figure 2-16. Washout of the approach embankment can fully expose the abutment foundation, such that further scour progresses as if the abutment were a form of pier.

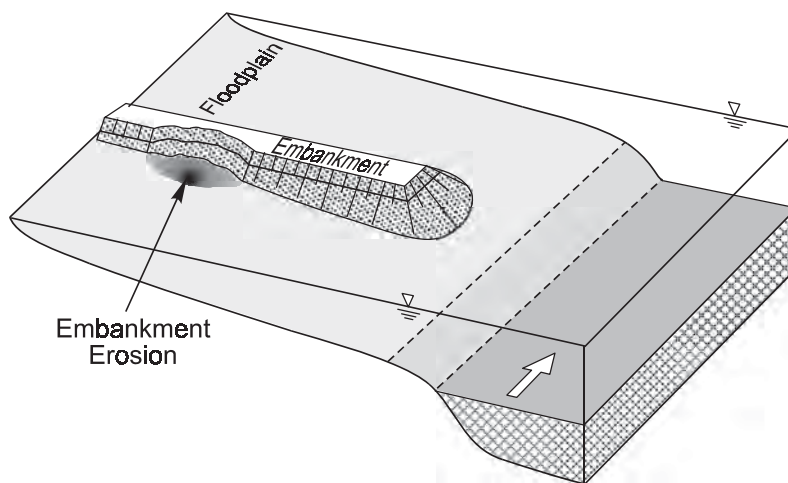


Figure 2-17. Floodplain flow impingement against a long approach embankment can result in erosion of the embankment.



Figure 2-18. Upstream progression of a head-cut through a bridge waterway with exposed pier supports and destabilized adjoining abutments.



Figure 2-19. Erosion of side drainage upstream of right abutment, exposing the abutment to scour.

CHAPTER 3

Countermeasure Concepts and Criteria

3.1 Introduction

This chapter outlines the main concepts employed to mitigate abutment scour and introduces the criteria to be considered when selecting and designing countermeasure concepts. The concepts are evaluated in a preliminary manner here, and the merits of selected concepts are investigated in subsequent chapters that present the results of the laboratory phase of this study.

A point to be emphasized is that effective protection against scour, along with good maintenance and repair of waterways, in concert with regular monitoring, are key considerations for reliable design-life performance of a bridge waterway. Bridge waterways often are fitted with various scour-protection methods that go a long way to mitigate scour concerns. However, it is quite common for bridge waterways to require maintenance and repair because of damage, or possible impending damage, caused by one or more scour processes. For example, adjustments in upstream channel alignment owing to changes in land use, the abrasive impacts of large flows, and head-cut advance along the downstream channel may result in wear and tear of bridge waterways. Figure 3-1 illustrates another situation that may result in the failure of riprap placed on a spill-through abutment.

The present chapter outlines and illustrates concepts for scour protection and repair of bridge waterways.

Waterway maintenance and repair entails undertaking one or more of the following remedial actions:

1. **Approach-channel control.** If the damage is attributable to a troublesome approach flow, such as that caused by channel shifting, the approach flow must be controlled to realign its passage through the bridge waterway.
2. **Downstream-channel control.** If the damage is caused by troublesome changes in the condition of the channel downstream of the bridge, these conditions must be mitigated so that the bridge is no longer affected by them. It is

usual for some channel-control structures to be placed so as to ensure that the adverse condition does not affect the bridge waterway. In western Iowa, for example, a common concern in this regard is the movement upstream of a head-cut or knickpoint in the channel bed. Such knickpoint or head-cut migration may expose the foundations of a bridge and cause embankment failure.

3. **Armoring of bridge opening.** If the foundation of an abutment or a pier is about to be exposed, or an approach embankment or riverbank to be eroded, these locations need to be armored with riprap stone or some other protective surface.
4. **Bridge modification.** Sometimes it is necessary to modify a bridge to enable better passage of flow through a bridge waterway. The bridge modification may be needed because of a change in the approach channel or to improve an inadequate initial design.
5. **Drainage control.** Flow draining along the sides of an approach embankment must be discharged into the waterway without eroding the waterway.

3.2 Approach-Flow Control

Approach-flow control is intended to guide the approach flow directly through the bridge opening, so that the flow does not expose the bridge's piers, abutments, and approach embankments to scour. Flow-control methods seek to streamline the flow through a bridge waterway—in other words, to minimize a bridge's obstruction to flow. It is usual that, for example, approach-flow remediation to reduce the angle between the major horizontal axis of a pier and the approach flow is warranted.

There are several options for approach-flow control. These will be further discussed in the literature review section, but are summarized here. The options vary in accordance with the extent to which the approach flow has to be aligned and guided through the bridge opening. In most cases, the layouts



Figure 3-1. Erosion of channel bank in the outlet of a side drain has made this abutment more prone to scour.

of flow-control structures are determined on a site-by-site basis. The layouts sometimes require investigation by means of a hydraulic laboratory model or a two-dimensional numerical model.

Flow control can be summarized as typically requiring the use of one or more of the following structures for the purpose indicated:

1. **Guidebanks** are fitted to bridge abutments in order to guide flow locally through a bridge opening. Guidebanks are used in situations where a wide flow approaches a bridge opening at an awkward angle or has to be “funneled” through the bridge opening. Guidebanks are often used for guiding floodplain flow through an opening or for guiding flow through bridge openings in broad, braided channels.
2. **Hardpoints** ensure that channel alignment is maintained in situations where the approach channel may otherwise tend to shift laterally.
3. **Spur dikes** are fitted to force the realignment of a channel and/or to increase flow velocities. Channel realignment may be needed when an approach channel is shifting laterally. Increased flow velocities may be needed in situations where a channel has widened, flow velocities decreased, and the approach channel is aggrading. Channel aggradation may reduce the flow area of the bridge opening.
4. **Bendway weirs or barbs** are fitted to stop lateral shifting of a channel and thereby to redirect the channel optimally through a bridge opening.
5. **Vanes** are an alternative to spur dikes, bendway weirs, or barbs for use in improving approach channel alignment.

Note that, in progressing from channel-control structures 1 through 5 outlined above, the repair effort entails dealing

with a widening channel to ensure that the channel passes centrally through the bridge waterway.

Additional channel-control methods include:

6. **Removal of vegetation and sloughed riverbank material**, which is a mundane but very important requirement for ensuring that the bridge opening does not become clogged and that flow within the waterway does not get deflected adversely toward a pier or abutment.
7. **Bridge widening or shifting**, which is an option when channel control is infeasible. For some bridge sites and approach channels, the most technically and fiscally feasible option is to add a span to a bridge. This option becomes attractive if the bridge opening should be increased in area to reduce flow velocities in the opening and if an abutment has experienced damage to the extent that it has been largely washed out.

3.3 Criteria

Bridge waterways often are fitted with various scour-protection methods that may largely mitigate scour concerns. This section outlines and discusses the main issues associated with scour countermeasures and the principal criteria required for acceptable performance of a countermeasure method that substantially reduces scour at or near a bridge abutment.

The main issues that arise with respect to scour countermeasure selection touch on aspects of technical effectiveness, constructability, durability and maintainability, aesthetics, and environmental impact. These issues comprise the essential considerations underlying selection criteria for scour countermeasures.

The literature review chapter discusses the range of options for scour countermeasures to mitigate or lessen scour at bridge abutments. The most common conventional options involve riprap placed in various configurations, and flow guidance by means of guidebanks at the approach to a bridge. In addition, newer countermeasures that show promise are being used, such as alternative materials for armor units (e.g., geobags and cable-tied blocks) and newer forms of structures that work to modify flow behavior (e.g., vanes and purpose-built walls). Whether the countermeasure option being considered is well tried and conventional or is novel, it should be subject to a set of criteria that address the factors associated with implementing the countermeasure.

The criteria for selecting a countermeasure usually encompass the following set of considerations:

- Technical effectiveness (including no substantial adverse effects),
- Constructability,
- Durability and maintainability,

- Aesthetics and environmental issues, and
- Cost.

It is prudent to mention that scour control can be a tricky process. When protecting an abutment against scour or protecting the entire bridge, it is possible that the scour problem is simply shifted elsewhere or that another problem may result. Therefore, when considering possible scour-protection concepts, it is important to evaluate the likely consequences of the protection method. For instance, scour protection of an abutment may concentrate flow locally and aggravate scour at an adjacent pier, and adjustment of the angle at which a channel approaches a bridge opening may result in bank erosion a short distance downstream of the bridge. In the context of bridge waterways, it cannot be assumed that, once set along a prescribed orientation and bed elevation through a bridge waterway, a river or stream channel will hold to its course.

3.4 Technical Effectiveness

The technical effectiveness of a countermeasure method is the first consideration in deciding whether to employ the method. The primary measure of technical effectiveness of a countermeasure is its capacity to substantially reduce scour and thereby prevent abutment failure as well as failure of an adjoining component of a bridge waterway, notably a pier or riverbank. As mentioned above, a further consideration is that the countermeasure does not contribute to a scour problem elsewhere.

Experience, especially as obtained from the extensive testing conducted for the present project, shows that no countermeasure totally eliminates scour at a bridge waterway. It is common for a countermeasure to reduce scour depth, but also to shift the location of deepest scour. A scour countermeasure may be considered effective if it accomplishes the following goals:

- For spill-through abutments, scour is limited such that the embankment side slopes around the abutment structure (e.g., standard stub abutment) do not erode hydraulically or collapse owing to a geotechnical instability.
- For wing-wall abutments, the scour depth is limited to be above the top of the pile cap (if the abutment is on a pile foundation) or the top of the footing slab (if the abutment is on a slab footing).
- The countermeasure does not inadvertently cause or worsen scour at another location in the bridge waterway.

As mentioned at the outset of this report, channel width spanned by a bridge has a significant bearing on the selection of scour countermeasures. Accordingly, it is useful to reiterate briefly here that the scour-protection methods applied to

short bridges usually are limited to armoring of the bridge waterway and the approach channel. The comparative narrowness of a bridged channel makes the use of certain channel-control methods infeasible, as is mentioned subsequently. For narrow channels (as defined in Chapter 2), channel control normally is limited to the use of riprap armoring, possibly along with stubby structures like rock hardpoints. The debris-blockage risk for bridges over narrow channels is exacerbated by scour countermeasures involving the use of relatively elaborate or long structures, such as spur dikes or flow-guidance vanes.

3.5 Constructability

To be practicable, a countermeasure method must be constructible. Though some countermeasures may seem to have technical merit in laboratory tests or when sketched out on paper, they may not be constructible. Accordingly, they cannot be implemented. This criterion is especially significant when considering retrofitting a countermeasure to an existing abutment for which site access is very difficult, or when the countermeasure requires a high degree of precision in its placement, but site conditions (e.g., swift flowing water) hamper precise placement. Many rivers flow perennially, and their beds are never dry to allow for easier construction.

The construction and placement of a countermeasure in flowing water is a common difficulty that limits the use of some countermeasure methods. Not only is it not always possible to plan the construction schedule for periods of low flow in the river, but physical access to regions beneath the bridge deck can be limited. Locating large equipment under an existing bridge with small clearance is not always feasible.

3.6 Durability and Maintainability

The use of durable construction materials is important for the success of a countermeasure, at least with respect to the intended working life of the countermeasure. Any material used as part of a countermeasure method must be able to withstand the potentially severe natural conditions of the river. Depending on bridge location, these conditions may include loads and abrasions owing to contact with water flow, ice, and woody debris. Moreover, scour-induced changes in local bathymetry of the channel may alter structural loads on the countermeasure (e.g., as the countermeasure becomes more exposed to flow or readjusts its disposition). Corrosion and decay may weaken some countermeasure methods (for example, rust and rotting are also common modes of failures of steel cable and wood, respectively).

Materials such as stone, steel cable, concrete, geotextiles, and wood are sometimes used for countermeasures.

Suitably durable stone should be used. Not all stone is suitable for use as riprap, and some stone has a shorter working life than does other stone; for example, dolomite is not as durable as granite. Steel cable, such as is used in cable-tied blocks, is subject to rust unless coated with epoxy or another protective material. Concrete is durable, but is subject to cracking, spalling, and the corrosion of the internal rebar. Geotextile fabrics can be obtained in various thicknesses and, therefore, can be quite durable, but lose strength with time. Wood has been used to support or shore up piers and abutments, but is subject to rotting when repeatedly wetted and dried, as occurs in rivers with fluctuating water levels.

Care must be taken, therefore, to select durable materials for countermeasure construction that are commensurate with the intended life of the countermeasure.

The ongoing costs of maintaining a countermeasure can be substantial and, therefore, should be taken into consideration from the onset of the design process. When considered over the entire design life of the bridge, maintenance costs can be more than the initial construction costs. To be kept in mind is the concern that certain scour countermeasures may be difficult to maintain, especially for durations beyond the intended nominal design life of the countermeasure. Some commonly expected maintenance activities include the replacement of dislodged riprap stone and care of grassed side slopes of guidebanks. Ensuring adequate drainage can also pose a maintenance problem for earthfill embankments forming the approach to an abutment or used to form guidebanks. Cable-tied blocks that form large mats for scour protection can be displaced by the uplifting of the upstream row of blocks, and the entire mat might then be moved as a result. Steel cables can corrode, and concrete blocks can be cracked or chipped. Geobags can be torn or lose strength with age. Consideration of maintenance is a real concern in countermeasure selection and design. It is important that the state of a countermeasure method be checked regularly, especially immediately following a major flood flow. One further conclusion from the present study is that many countermeasures themselves suffer damage while mitigating a serious scour condition at an abutment.

3.7 Aesthetics and Environmental Issues

While normally somewhat of a secondary consideration, but of high value regarding public acceptance, the aesthetics of the appearance of a countermeasure method can be an important criterion in countermeasure selection. The degree of importance may depend on the urgency of protecting an abutment or on local attitudes. It is a criterion to be evaluated during countermeasure selection and design; countermea-

asures that impair the appearance of the bridge waterway may not be suitable for long-term use.

Pertinent environmental issues in abutment countermeasures include the disruption of the ecology by blocking fish passage along the river, and increased water levels (and thereby flood levels) upstream of a bridge because of flow blockage by a countermeasure. Some countermeasures, such as a low weir or grade-control wall, have the potential to block the migration of fish and amphibians along a stream or river. For example, a check dam extending across the entire width of the river can halt bed degradation attributable to head-cutting, thereby averting the threat of abutment. Other than to point out environmental concerns as a criterion for countermeasure selection, the present report does not address environmental aspects of bridge waterways.

3.8 Cost

The cost of the countermeasure, or rather the cost-benefit analysis associated with the countermeasure, is a significant criterion in the selection of countermeasures. For an existing bridge, it may be the deciding consideration as to whether the existing bridge should be replaced as opposed to protected. Cost-benefit estimates should include costs and benefits estimated for the design life of the countermeasure. The present project did not address the criterion of countermeasure cost. That criterion must necessarily be evaluated in accordance with the constraints prevailing in the geographic region containing the bridge being considered for countermeasure protection. The ensuing discussion, by way of example, outlines some of the considerations entailed in selecting the extent of armor blankets or the construction of spur dikes.

The extent of coverage by blankets of riprap, cable-tied blocks, or geobags is an important consideration in their performance as a scour countermeasure. Measuring this coverage entails consideration of cost; in general, a larger extent of coverage results in better performance, but incurs a higher cost. Better performance occurs as increased protection is provided against such failure mechanisms as edge erosion, uplifting of filter layers, or the washing away of armor units. Edge erosion effects, for instance, can pose a major problem when flow creates scour around the leading block in the case of a protective blanket. Once the flow has created scour around the upstream blocks or rocks, then uplifting can occur that will compromise the integrity of the countermeasure. It is a simple truism that consideration of the failure of a countermeasure method is an important aspect of assessing the technical feasibility of a countermeasure.

The filter requirements for riprap blankets or cable-tied blocks are important to their effective performance and cost. The finer the pore spaces in a filter cloth, the better the

protection against bed material winnowing upward through the filter and riprap and thereby causing undesirable settling. It is necessary, to be sure, that the filter cloth must remain porous, but filter cloths with finer pores typically cost more. The largest size of filter that prevents winnowing is sought. In addition, the durability of the filter cloth is important for its long-term performance.

As described subsequently in the chapters on the literature review and laboratory experiments on flow control, spur dikes are walls that extend into the waterway and direct flow away from a bank. The choice of construction material for the spur dikes can affect their performance, constructability, cost, and aesthetics. The main materials used for spur dikes are concrete, rock, and timber. Concrete and rock have the advantages of durability, but can be more costly and difficult to construct and maintain. Timber spur dikes are easier to place (for example, by means of pile driving), but may not be as durable.

Additionally, to be sure, the dimensions of the spur dike (length, width, and height) are important to performance and cost. The dike with the smallest dimension that effectively reduces scour to an acceptable amount is desirable. The length of a spur dike can excessively push the flow out into the waterway and thereby cause scour on the far bank. If constructed of rock, then the wall width and height are linked through the angle of repose of the rock. The spacing between spur dikes is important to cost and performance. A close spacing may increase the costs, and an excessive spacing between dikes may allow the flow to reattach to the near-abutment bank and not reduce scour.

3.9 Bridges over Narrow Versus Wide Channels

For narrow channels, scour countermeasures are limited largely to channel-bank and bed-armoring concepts, rather than concepts aimed at modifying flow distribution within a channel. There is insufficient channel width to accommodate structures intended for redistributing flow within a narrow bridge waterway. A further concern with flow-guidance structures located in narrow channels is that such structures may aggravate the debris blockage of a bridge waterway. In some situations, though, guidebanks are still used to direct floodplain flow into the bridge waterway.

Scour countermeasure concepts for small bridges typically entail the use of riprap, other armoring such as cable-tied blocks, and possibly hardpoints, which essentially act to locally deflect flow away from a vulnerable bank. The ensuing sections of this chapter discuss the main considerations associated with armor design for abutments.

In many situations, narrow channels are not connected to floodplains. Instead, they flow as channels eroded through comparatively steep, undulating, or hilly terrain. Armoring of abutments in these situations poses a problem that heretofore has been inadequately resolved. It is a problem similarly faced when protecting so-called bottomless culverts against scour damage (Kerenyi et al., 2005). The problem concerns adequate placement of some form of armor cover at the upstream and downstream corners of the abutment (or bottomless culvert) without substantially blocking flow through the bridge waterway.

CHAPTER 4

Practitioner Survey

4.1 Introduction

To assess existing practices with regard to the use of abutment scour countermeasures, a survey form was sent to the department of transportation office of each state in the United States. Additionally, general information and experience were obtained from certain other entities, such as county engineer offices, and overall experience in New Zealand, the home country of one of the co-investigators. The information obtained from the survey responses was used in determining the program of experiments to be carried out for this project.

The survey sought the following information regarding abutment scour countermeasures:

- The extent to which bridges are fitted with abutment scour countermeasures
- Countermeasures that have been successful in terms of the ensuing considerations:
 - Technical effectiveness (including no substantial adverse effects)
 - Constructability
 - Durability and maintainability
 - Aesthetics and environmental issues
 - Cost

- Method of countermeasure selection
- Design method for selected countermeasures
- Procedure for evaluation of countermeasure effectiveness
- Countermeasure construction
- Pertinent conditions at abutment failure sites:
 - Bed material
 - Abutment design
 - Flow
- Additional information (e.g., on aesthetics of countermeasure design)

Of the 50 states contacted, responses were received from 36 states. An overall summary of countermeasure practice in New Zealand was developed by Dr. B. Melville, New Zealand's leading authority on scour. The responses varied from a simple statement that scour was not a problem to complete sets of design guidelines used for certain scour countermeasures.

4.2 Summary of State DOT Responses

The responses provided by the state DOTs to survey Questions 1 through 8 are summarized in Tables 4-1 through 4-9.

Table 4-1. Question 1. "Is bridge abutment scour a problem for your agency?"

Response	# of States Responding	Name of States Responding
Definitely	4	AZ, DE, FL, VT
Occasionally	16	AK, AR, CO, CT, GA, ID, IL, KS, KY, MD, MA, MI, MO, OH, OK, VA
No, due to successful countermeasures	13	AL, HI, IA, MN, MT, NV, NM, NY, NC, OR, PA, TN, TX
No, due to favorable site conditions	3	LA, MS, RI

Table 4-2. Question 2. "Please give information on the number of abutments where countermeasures (i.e., riprap, cable-tied blocks, guidebanks, spur dikes, vanes, or any method to reduce abutment scour) have been used (add additional pages as necessary)."

Countermeasure (none is also an option)	Bridge Name	Year Bridge Constructed	Year Countermeasure Constructed	# successful	# unsuccessful
MD - grout bags				48	5
MD - riprap				10	0
MD - sheeting				2	0
MI - riprap				Most (65)	
MI - guidebanks				2	0
MI - articulating blocks				0	3
MT - riprap				All but 1	1

Table 4-3. Question 3. "Please give information on the extent of benefit achieved by providing each countermeasure on the below listed six parameters (see rating scale for each effect)."

Counter-Measure, Bridge Name, Year Constructed	Consideration					
	Environmental Effects (0=high negative effects; 10=high positive effects)	Debris Problems (0=many problems; 10=no problems)	Ice Problems (0=many problems; 10=no problems)	Scour Problems (0=deep scour; 10=no scour)	Construction Cost (0=high cost; 10=low cost)	Maintenance Cost (0=high cost; 10=low cost)
AL, riprap	10	10	na		9	9
AK, riprap	5	9	8	8	5	7
AR, riprap	5	9	na	9	8	8.5
CT, riprap	5	9	9	8	5	8
FL, riprap	5		10	10	4	4
GA, riprap	10	10	na	8	4	8
GA, spur dike	10	10	na	8	6	8
IL, riprap	10	10	10	8	10	7
IL, Reno mat	10	9	9	9	9	9
IL, gabions	10	9	9	9	9	9
IL, Fabri-form	10	10	10	7	8	8
KS, riprap	9	10	10	9	9	7
KS, guidebanks	9	10	10	9	4	10
KS, gabion	9	10	10	10	5	10
KS, sheet-pile	9	8	10	8	4	10
MA, pavement	0	10	10	10	0	10
MA, sheeting	10	10	10	2	8	9
MA, new construction	10	6	10	9	8	9
MD, riprap	5	10	10	5	8	10
MD, grout bags	10	10	10	5	10	10
MN, riprap	5	10	9	4	5	8
MT, riprap	6	10	9	8	na	10
NM, guidebank	9	9	10	8	6	9
NM, spur dike	8	7	10	7	7	9
NM, riprap	5	10	10	3	10	8

Table 4-4. Question 4. “What method do you use to select if a countermeasure is needed?”

State	Response
AL	Used to use pavement on slopes. Had failure. Now use riprap with good results.
AK	Mostly use riprap. Recently trying cable-tied blocks. Too early to comment on results.
AZ	Case by case consensus of DOT divisions.
AR	Structural needs or maintenance requirement.
AR, CT	Own classification system.
DE	FHWA “Recording and Coding Guide for the Structure Inventory and Appraisal of the Nation’s Bridges.” Fix worst 6 bridges.
FL	Historical scour evidence, existing conditions, hydraulic and geotechnical software, experience and judgment.
GA	FHWA recommendation for riprap, HEC 20 for spur dike.
IL, IA	Use adequate waterway openings, spur dikes and guidebanks when significant overbank flow. 2.5:1 slope. Only riprap if unstable.
KS	Scour analysis, determine depths, rock riprap with toe. Guidebanks if high return flow.
LA	Use spill-through shape with flexible revetment and riprap.
MD	Hydraulic, geotechnical analysis to determine vulnerability. Get flow velocities. Determine construction method. Consider grout bags as an alternative to riprap. Get cost.
MA	Use existing foundation to maintain waterway opening and minimize environmental impact. Build new abutments behind existing ones.
MI	HEC 18.
MN	Screening and evaluation: field review, historical info, cal velocity.
MS	Experience.
MT	Use HEC RAS and determine abutment scour for Q-design, Q-100, and Q-overtopping.
NV	Past history, determine erodibility of existing abutment protection, estimate scour of abutment using pier scour equations assuming river migrates through the foundation and the abutment acts as a pier.
NM	HEC 18, 20, 23. Inspection reports, field inspection.
NY	HEC 18, 20, 23.
OR	Always use riprap.
TN	Place riprap on all abutment fill slopes at stream crossings. We take revetment up to 1 foot above the design flood. Sometimes use gabions on steep slopes. Use filter fabric under gabions and riprap. Use H47 and H49 for hydraulic analysis.
VT	Evaluation by team consisting of Structure Design/Inspection, Hydraulics, and Materials.
VA	HEC 18.

Table 4-5. Question 5. “What design method do you use for each countermeasure?”

State	Response
AK	Velocity-based analysis.
AZ	HEC 23 and team consensus.
AR	HEC 18 and 20, site history.
CO	HEC 18 and 23.
CT	HEC 23.
DE	USGS Report # 95-4153, HEC 18, WSPRO.
FL	Incipient motion analysis.
GA	FHWA recommendation for riprap, HEC 20 for spur dike.
IL	HEC 23.
KS	HEC 23 for riprap, guidebanks, and gabions. Classic methods for sheet pile.
LA	HEC 18.
MA	HEC 18.
MD	Has own standard guidelines.
MI	HEC 18 for riprap.
MN	Use Class III Random Riprap or greater. Check velocity. Use spur dike if necessary. Use spill through abutment. Set abutment back from main channel. Use HEC 18 and 23.
MS	Experience.
MT	Typical section with 2:1 slopes, a riprap key, and the thickness will depend on the size rock used. Construction fabric added underneath the riprap to minimize loss of fine material.
NC	Spill-through slope. Old bridges on unstable rock have been replaced.
NM	HEC 18, 20, 23.
NV	HEC 23, riprap HEC 11. Abutments coincide with banks. Lots of river migration. Solved by river training with riprap or spur dikes. Design abutment as if it were a pier using HEC 18. Banks protected with riprap (HEC 11).
NY	HEC 23, standard policy or state policy.
OH	Size riprap according to velocity using HEC publications.
OK	HEC 11, 14, and 23.
OR	HEC 18 and 11.
PA	State DOT design manual.
TN	HEC 18.
VT	Place riprap until area stabilizes.
VA	HEC 23.

Table 4-6. Question 6. “What evaluation procedure do you use for each countermeasure?”

State	Response
AK	Biennial inspection.
AR	Regular bridge inspection and maintenance district.
AZ	Regular bridge inspection and maintenance district.
CO	HEC 18 and 23.
CT	Biennial inspection.
DE	Always use riprap.
FL	Choose two most appropriate alternatives, give to DOT reviewing engineering departments.
GA	Riprap: two times the depth of the 100-year storm adjacent to the abutment. Spur dike: length is based on natural overbank flow adjacent to abutment. Length must be greater than 150 ft.
IL	Visual observation.
KS	2-year inspections.
MD	Biennial inspections.
MI	Biennial inspections.
MS	Experience.
MT	HEC 18.
NM	Biennial inspection.
NV	Biennial inspection.
NY	Field inspection.
PA	Procedures for Scour Assessments at Bridges in Pennsylvania.
VT	Inspection team.

Table 4-7. Question 7. "What are the construction methods used for each countermeasure?"

State	Response
AR	Spurs use earth-moving equipment, riprap from barge, temporary work platforms, or from shore.
CT	Dump riprap from barges (large rivers), pump area dry (small rivers).
DE	Excavate, cofferdam, geotextile, place stone, key riprap into channel.
FL	Floating platform barges, filter fabric.
GA	Riprap: filter fabric first, then dump riprap. Spur dike: earth-moving equipment. Hand place filter fabric, then dump stone.
KS	Kansas Standard Specs for State Road and Bridge Construction.
MD	Riprap: earth-moving equipment. Grout bag: fill bags on site.
MT	Backhoe or crane to place rock. Placed during low flow.
NV	River diversion, dewatering.
OH	Place rock by land or barge.
TN	Dozer or track excavator. Rock is countersunk.
VA	Riprap dumped directly on fill slope and excavate as necessary around toe to preclude riprap reducing the flow across the sectional area.

Table 4-8. Question 8. "Please summarize the conditions at the 5 worst abutment scour sites (please send drawings, if possible)."

Abutment Characteristics		5 Worst Scour Sites				
		1	2	3	4	5
ARKANSAS						
Name (Bridge Number)		AB5109	01432	02549	02819	
Location (Nearest Town)		Mulberry	Malvern	Texarkana	Marble	
Bed Material	Scour depth (ft)	10	7	6	18	
	% gravel	40 (w/ boulders)	0		Below road fill is 100% gravel & boulders	
	% sand		80			
	% silt					
	% clay	60	20	100		
	d ₉₀					
	d ₅₀	Est. 0.25"	Est. 0.02"	0.00004" Est.	Est. 6"	
	d ₃₀					
Abutment Properties	Bedload (high, med., low)	Med.	Low	Low	Low	
	Setback from riverbed (ft)	200	30	0	0	
	On floodplain?	Yes	Yes	No	No	
	Abutment slope (V:H)	1:2	Vertical	1:1.5	1:1.5	
	Abutment height (ft)	25	16	13	17.5	
	Abutment length (ft)	1,000	1,300	500	36	
	Span between abutment and nearest pier or opposite abutment (ft)	33 from toe of slope	35	6 from toe of slope	18	
	Abutment plan shape	See drawing	See drawing	See drawing	See drawing	
	Straight approach?	No	Yes	No	Yes	
	On a river bend?	Yes	No	Yes	No	
	Near tributary?	No	No	No	No	
Flow Parameters	Velocity range (ft/s)	Unknown	4.1	13.4	12 avg.	
	Discharge range (ft ³ /s)	Unknown	7,000	7,480	3,600 approx.	
	Flow depth range (ft)	15	13.1	14	17	
	Max. scour depth (ft)	12	7	6	18	
	Upstream channel width (ft)	70	20	30	45	
	Channel width under bridge (ft)	410	68	72	20	
	Downstream channel width (ft)	70	20	30	45	
	Ice problems?	NA	NA	NA	NA	
	Debris problems?	Yes	No	No	Yes, major	
	Environmental problems?	No	No	No	No	

Table 4-8. (Continued)

Abutment Characteristics CONNECTICUT		5 Worst Scour Sites				
		1	2	3	4	5
Name		BN02781	BN 01048	BN01383	BN05419	BN08014R
Location		Stinington	Oxford	Haddam	Sherman	Stamford
Bed Material	Scour depth (ft)	6	4	0-3	2	4-5
	% gravel	50		10	10	
	% sand	50		75		
	% silt			15		
	% clay					
	d ₉₀		58 mm	10 mm		
	d ₅₀	38 mm	3 mm	1.6 mm		
	d ₃₀		0.7 mm	0.75 mm		
Bedload (high, med., low)		Med.	Med.	High	Med.	Med.
Abutment Properties	Setback from riverbed (ft)	1	0	0	0	0
	On floodplain?	No	Yes	No	No	No
	Abutment slope	Vertical	Vertical	Vertical	Vertical	Vertical
	Abutment height (ft)	8.5	5-6	21	10	9.5
	Abutment length (ft)	43	32	87	50	98
	Span between abutment and nearest pier or opposite abutment (ft)	22	21	71.5	20	26
	Abutment plan shape	Skewed flared wings	Flared wings	Flared wings	Wings ext. of abut.	Flared wings
	Straight approach?	No	No	No	No	No
	On a river bend?	Yes	Yes	Yes	Yes	Yes
	Near tributary?	No	No	Yes	Yes	No
Flow Parameters	Velocity range (ft/s)		4.9-7.7	4.5-5.1	9.8-15.9	10.3-15.0
	Discharge range (ft ³ /s)	1,086 (10 yr) 3,631 (500 yr)	950 (10 yr) 3,800 (500 yr)	6,924 (10 yr) 2,587 (500 yr)	390 (10 yr) 1,720 (500 yr)	1,180 (10 yr) 3,200 (500 yr)
	Flow depth range (ft)	6.7-14.4	4.9	9.4-19.8	2.4-8.0	10-22
	Max. scour depth (ft)	19.8	17	34.7	10	
	Upstream channel width (ft)	20	10-20	80-90	18-20	28-30
	Channel width under bridge (ft)	22	40	150	13.7	26
	Downstream channel width (ft)	20	30	130	22	28-30
	Ice problems?	No	No	Yes	No	No
	Debris problems?	No	No	No	No	No
	Environmental problems?	Yes	Yes	Yes	Yes	Yes

(continued on next page)

Table 4-8. (Continued)

Abutment Characteristics FLORIDA		5 Worst Scour Sites				
		1	2	3	4	5
Name		070026				
Location						
Bed Material	Scour depth (ft)	Abutment scour was not calculated due to low projected velocities, nor were geotechnical data obtained.				
	% gravel					
	% sand					
	% silt					
	% clay					
	d ₉₀					
	d ₅₀					
	d ₃₀					
Bedload (high, med., low)						
Abutment Properties	Setback from riverbed (ft)	10				
	On floodplain?	Yes				
	Abutment slope (V:H)	2:1				
	Abutment height (ft)	20				
	Abutment length (ft)	50				
	Span between abutment and nearest pier or opposite abutment (ft)	15				
	Abutment plan shape	Spill-through				
	Straight approach?	No				
	On a river bend?	Yes				
Near tributary?	Yes					
Flow Parameters	Velocity range (ft/s)	3-5				
	Discharge range (ft ³ /s)	1,000				
	Flow depth range (ft)	5-7				
	Max. scour depth (ft)	7-8				
	Upstream channel width (ft)	60				
	Channel width under bridge (ft)	50				
	Downstream channel width (ft)	60				
	Ice problems?	No				
	Debris problems?	Yes				
Environmental problems?	No					

Table 4-8. (Continued)

Abutment Characteristics GEORGIA		5 Worst Scour Sites				
		1	2	3	4	5
Name		SR 38	SR 38			
Location		Long. Co	Lowndes Co.			
Bed Material	Scour depth (ft)	30	25			
	% gravel	0	0			
	% sand	80	80			
	% silt	10	10			
	% clay	10	10			
	d ₉₀					
	d ₅₀					
	d ₃₀					
Bedload (high, med., low)		Low	Low			
Abutment Properties	Setback from riverbed (ft)	Yes	Yes			
	On floodplain?	Yes	Yes			
	Abutment slope (V:H)	2:1	2:1			
	Abutment height (ft)	20	15			
	Abutment length (ft)	40	30			
	Span between abutment and nearest pier or opposite abutment (ft)	33	38			
	Abutment plan shape	Spill-through	Spill-through			
	Straight approach?	Yes	Yes			
	On a river bend?	No	Yes			
	Near tributary?	No	No			
Flow Parameters	Velocity range (ft/s)		3.5-3.75			
	Discharge range (ft ³ /s)		40,000-50,000			
	Flow depth range (ft)	40	30			
	Max. scour depth (ft)	25	20			
	Upstream channel width (ft)					
	Channel width under bridge (ft)	1,089	920			
	Downstream channel width (ft)					
	Ice problems?	No	No			
	Debris problems?	No	No			
	Environmental problems?	No	No			

(continued on next page)

Table 4-8. (Continued)

Abutment Characteristics		5 Worst Scour Sites				
		1	2	3	4	5
MICHIGAN						
Name		B01	B03/04			
Location		81,032	61,075			
Bed Material	Scour depth (ft)	4				
	% gravel					
	% sand	90	100			
	% silt					
	% clay					
	d ₉₀					
	d ₅₀	0.0005				
	d ₃₀					
Bedload (high, med., low)		Med.	Low			
Abutment Properties	Setback from riverbed (ft)	0				
	On floodplain?		Yes			
	Abutment slope (V:H)	Arch	Vertical			
	Abutment height (ft)		2.5			
	Abutment length (ft)	85	70			
	Span between abutment and nearest pier or opposite abutment (ft)	117	72			
	Abutment plan shape		Rectangular			
	Straight approach?	No	No			
	On a river bend?	Yes	Yes			
	Near tributary?	No	Yes			
Flow Parameters	Velocity range (ft/s)	6.9-9.2	3.5-5.8			
	Discharge range (ft ³ /s)	7,100-11,000	14,525-29,208			
	Flow depth range (ft)	17.5-20	22.6-25.5			
	Max. scour depth (ft)	26	26			
	Upstream channel width (ft)	130	300			
	Channel width under bridge (ft)	117	324			
	Downstream channel width (ft)	110	300			
	Ice problems?	No	No			
	Debris problems?	No	No			
	Environmental problems?	No	No			

Table 4-8. (Continued)

Abutment Characteristics MINNESOTA		5 Worst Scour Sites				
		1	2	3	4	5
Name		5236	87007	87015		
Location		TH 212 - Lac Qui Parle R.	TH 23 - Minnesota R. Overflow	TH 212 - Minnesota R. Overflow		
Bed Material	Scour depth (ft)	4 observed	7 observed	7 observed		
	% gravel	10	NA	NA		
	% sand	70	NA	NA		
	% silt	20	NA	NA		
	% clay	-	NA	NA		
	d ₉₀	2 mm	NA	NA		
	d ₅₀	300 um	NA	NA		
	d ₃₀	150 um	NA	NA		
Bedload (high, med., low)		NA	NA	NA		
Abutment Properties	Setback from riverbed (ft)	0	0/8	0		
	On floodplain?	No	No	No		
	Abutment slope (V:H)	1:2	1:2	1:2		
	Abutment height (ft)	21	9	13		
	Abutment length (ft)	54	107	52		
	Span between abutment and nearest pier or opposite abutment (ft)	31	40	117		
	Abutment plan shape	Spill-through	Spill-through	Spill-through		
	Straight approach?	No	Yes	No		
	On a river bend?	Yes	No	Yes		
Near tributary?	No	No	No			
Flow Parameters	Velocity range (ft/s)	6	9	16		
	Discharge range (ft ³ /s)	5,500 ²	15,000 ³	15,000 ³		
2 design or approximate 100 yr event	Flow depth range (ft)	13.3	16	10		
	Max. scour depth (ft)	17 pier	25 abut	NA		
3 500 yr	Upstream channel width (ft)	80	65	70		
	Channel width under bridge (ft)	90	55	100		
	Downstream channel width (ft)	95	80	180		
	Ice problems?	No	No	No		
	Debris problems?	No	No	No		
	Environmental problems?	No	No	No		

(continued on next page)

Table 4-8. (Continued)

Abutment Characteristics NEW MEXICO		5 Worst Scour Sites				
		1	2	3	4	5
Name		6479	8996	8979	5714	
Location		Cuba	Clayton	US 285	Pecos River	
Bed Material	Scour depth (ft)	None so far	None so far	Aggregation, 1'	None so far	
	% gravel					
	% sand					
	% silt					
	% clay					
	d ₉₀					
	d ₅₀					
	d ₃₀					
Abutment Properties	Bedload (high, med., low)	Low	Low	Low	Low	
	Setback from riverbed (ft)	No	No	No	100	
	On floodplain?	No	Yes	Yes	Yes	
	Abutment slope (V:H)	1:1.5	1:1.5	1.5:1	1.5:1	
	Abutment height (ft)	9	9.75	20	20	
	Abutment length (ft)	45	43	200	100	
	Span between abutment and nearest pier or opposite abutment (ft)	35	99	80	40	
	Abutment plan shape					
	Straight approach?	No	No	Yes	Yes	
	On a river bend?	Yes	Yes	Yes	No	
	Near tributary?	No	No	Yes	No	
	Flow Parameters	Velocity range (ft/s)	12	10	8.7	5-10
Discharge range (ft ³ /s)		5,000	13,500	77,200	54,000	
Flow depth range (ft)		8	16	16.1	24	
Max. scour depth (ft)		9 calc.	9.1 calc.	Aggregation	30' calc.	
Upstream channel width (ft)		150	82	400	80	
Channel width under bridge (ft)		120	150	400	80	
Downstream channel width (ft)		150	78	200	80	
Ice problems?		No	No	No	No	
Debris problems?		Silt	Silt	Silt and Debris	No	
Environmental problems?		No	No	No	No	

Table 4-8. (Continued)

Abutment Characteristics OKLAHOMA		5 Worst Scour Sites				
		1	2	3	4	5
Name		East Clay Creek/US 64				
Location		Alfalfa Co.				
Bed Material	Scour depth (ft)	82				
	% gravel					
	% sand					
	% silt					
	% clay					
	d ₉₀					
	d ₅₀	0.002				
	d ₃₀					
	Bedload (high, med., low)					
Abutment Properties	Setback from riverbed (ft)	10				
	On floodplain?					
	Abutment slope (V:H)	Vertical				
	Abutment height (ft)	3				
	Abutment length (ft)	24				
	Span between abutment and nearest pier or opposite abutment (ft)	25				
	Abutment plan shape	7 concrete piles 25' long				
	Straight approach?	Yes				
	On a river bend?	Close				
Near tributary?	No					
Flow Parameters	Velocity range (ft/s)	10-24				
	Discharge range (ft ³ /s)	1,060- 17,370				
	Flow depth range (ft)	2-25				
	Max. scour depth (ft)	82				
	Upstream channel width (ft)	100				
	Channel width under bridge (ft)	26				
	Downstream channel width (ft)	80				
	Ice problems?	No				
	Debris problems?	No				
Environmental problems?	No					

Table 4-9. Question 9. "Please give any additional information that you feel the NCHRP 24-18 research team should know when deciding which countermeasures to further study and develop design guidelines for."

State	Response
AK	Failure consists of embankment loss due to toe loss.
AZ	Abutment failure can occur in nonwaterway bridges due to deck drainage, nuisance water, or roadway drainage. 246/850 waterway bridges have protection: 128 concrete slope, 23 soil cement, 190 rail bank protection, 9 grouted rock, 68 riprap, 30 gabions, 124 combination of countermeasures, 51 other types.
DE	There already exist sufficient design guidelines for riprap.
FL	Abutment scour only a problem when no abutment protection.
HI	Abutment scour not a problem; use riprap if it is.
IL	Abutment scour not a problem; use riprap if it is.
KS	Meandering of streams is the biggest problem. Need lab testing on cohesive soil and develop more reliable scour equations.
MA	Channel relocation a problem. Bends cause problems.
MD	Grout bags good for gradual slopes, silt, or small stones. They save money and are better for environment. Less construction time and equipment. Can install in low-access areas. Need study to determine how to reduce grout leaching out of bags and optimal design patterns and sizes of grout bags for various conditions.
MN	Spur dikes and riprap work well. We do not have significant flooding. Need guidance on riprap on bends, contraction scour. Difficult to distinguish between various types of scour in the field.
MO	Most damage to roadways with inadequate overflow capacity. Riprap used primarily. Less paperwork involved in getting permission from the COE [U.S. Army Corps of Engineers] and DNR [Department of Natural Resources]. Some use of gabions and dumping old concrete slabs as toe protection. Grouting or concreting the rock blanket has NOT been successful.
MT	Only scour problems occurred during the 64 floods (500 yr). Need better method for determining abutment scour using HEC RAS.
OH	Riprap protection is environmentally unfriendly initially until vegetation is established. Extent can be large. Use riprap for river training. Need study on riprap armoring.
OR	Have no confidence in scour-predicting equations in HEC 18.
PA	Use riprap mostly.
TX	No fixed strategy due to wide variation of site conditions. Hydraulics branch has been encouraging use of flexible riprap. Use TxDOT Hydraulics Manual.

4.3 Summary of Responses

The responses obtained from the survey of the state department of transportation offices can be summarized as follows:

- Most states either have a moderate scour problem or would have one if they did not use scour countermeasures.
- There are relatively few states that have severe scour problems and an approximately equal number of states that have site conditions that are not conducive to scour.
- Riprap seemed to be used often and only failed in one reported case.
- Grout bags were used extensively by one state and worked most of the time, but there were some noted failures.
- Sheeting and pavement were reported to cause scour and environmental problems, but were not used very often.
- Riprap seemed to perform well in general, but was reported to have environmental problems.
- A wide variety of countermeasure selection methods were reported, but HEC 18 and 20 were the most cited.
- Countermeasure design was performed using the HEC reports primarily.
- Visual inspection was the method most often used for evaluation of existing countermeasures.

- Construction methods include heavy equipment, including barges sometimes.

In addition, the main points arising from county engineers consulted can be summarized as follows:

- County bridges are inspected usually once every 2 years. The inspection teams vary greatly in their hydraulic engineering expertise.
- The county engineers are concerned primarily with protecting comparatively small bridges against scour. Such bridges typically have one to three spans and are sited at channels draining watersheds smaller than about 100 square miles.
- Wing-wall abutments are usual for small bridges over channels that do not have flood plains.
- Spill-through abutments are used for larger bridges over channels that have substantial floodplains.
- The countermeasure concepts of greatest relevance for small bridges are simple armoring countermeasures. In this respect, riprap or comparable armor elements are of interest. In some locations, suitable rock for armor unit use is not available, and so there is interest in alternative armor concepts.

- Countermeasure structures placed in the waterway or that rely on approach-flow alignment are generally not desired.

The main points arising from bridge scour experience in New Zealand are as follows:

- Bridge waterways are inspected regularly.
 - The monograph “Bridge Scour” by Melville and Coleman (2000) is a good example of standard practice in New Zealand.
 - Several bridge authorities in New Zealand use a national code of practice for estimating abutment scour and scour countermeasure needs: “Code of Practice for the Design of Bridge Waterways,” M.W.D. Civil Division Publication 705/C, 1979. More recently, several agencies have updated their design methods in line with the work of Dr. S.T. Maynard et al. (1989).
 - Riprap is used extensively because it is generally readily available and very effective. A majority of new bridges feature riprap protection to foundations and approaches. Riprap is also used to protect “problem” bridges. Other types of armor protection (e.g., gabions) have been used successfully, but are much less common than riprap.
 - Riprap rock usually is placed by machine. End dumping is not normally permitted. Handwork, where necessary, is required to obtain a satisfactory nesting, with each rock having a three-point bearing. Filters are used under riprap, where the natural ground contains a high proportion of fine sediments.
-

CHAPTER 5

Literature Review

5.1 Introduction

The literature on scour at bridge abutments and similar structures, such as spur dikes, is extensive. Useful overviews of the literature are given by Melville and Coleman (2000) and FHWA (1995) and (1997). This chapter is a concise review of the literature pertaining to scour countermeasures for abutment protection. The review encompasses the following scour countermeasure concepts:

- Structures for controlling channel alignment,
- Guidebanks for approach-flow entry into a bridge waterway,
- Structures for controlling channel grade,
- Armoring of flow boundaries, and
- Local modification of flow around abutments.

Channel-bank control serves to ensure that flow remains in a predetermined channel, thereby minimizing flow capacity to erode the boundaries (bed and bank) of the predetermined channel. Channel-grade control structures are used to limit bed erosion so as to impede the upstream progress of channel degradation. For bridges in compound channels (a main channel with flanking floodplains), flow must be guided into a bridge waterway. Guidebanks direct flow into a bridge waterway in a manner that enhances flow alignment, minimizes flow turbulence, and thereby reduces scour of the waterway.

By far the most common form of scour countermeasure is the armoring of flow boundaries prone to erosion. Armoring substantially increases the capacity of a boundary to resist erosion. Riprap is the customary form of armoring. Other forms of armoring that have been attempted for abutment scour mitigation are tied mats, ensembles of Toskanes, tetrapods, and soil reinforcement.

The basic intent of locally modifying the flow field at an abutment is to reduce the scour capacity of the local flow field

around an abutment by modifying the flow. The modification hypothetically could be achieved by attaching a form of vane, plate, collar, delta wing, or something similar to the abutment. No published studies appear to exist on the use of appurtenances for reducing scour at bridge abutments.

The present review also includes the considerations associated with the performance of countermeasure methods subject to the effects of woody debris, ice, scour of cohesive soil, and modeling issues.

5.2 Approach-Channel Alignment

5.2.1 Introduction

The most common method for controlling approach-channel alignment to a bridge waterway entails the use of spur dikes or structures similar in function to spur dikes. Spur dikes have been used extensively in all parts of the world as river training structures to enhance navigation, improve flood control, and protect erodible banks (Copeland, 1983). Spur dikes are structures that project from the bank into the channel (Figure 5-1). There are a variety of terms that refer to these transverse structures, including spur dikes, transverse dikes, cross dikes, spurs, wing dams, jetties, groins, and deflectors. While there are some differences in the use of these terms, they may be taken to be generally synonymous. Following usage of the U.S. Army Corps of Engineers (Franco, 1982; Copeland, 1983), the term spur dikes will be used here. Spur dikes may be permeable, allowing limited passage of water at a reduced velocity, or they may function to completely block the current (impermeable). They may be constructed out of a variety of materials, including masonry, concrete, earth and stone, steel, timber sheet-piling, gabions, timber fencing, or weighted brushwood fascines. They may be designed to be submerged regularly by the flow or to be submerged only by the largest flow events.

The main function of spur dikes is to reduce the current adjacent to the streambank, often at the outside (concave



Figure 5-1. A hardpoint on Goodwin Creek Experimental Watershed, Mississippi. Flow direction is from right to left.

bank) eroding bank of meander bends, the placement of which reduces the erosive ability of the flow and may cause deposition near the bank. Because of the deposition induced by spur dikes, spur dikes may protect a streambank more effectively and at less cost than revetments (Lagasse et al., 2001). Spur dikes are usually built in a group of two or more and may be at right angles to the bank, angled upstream, or angled downstream. The crest of the individual dikes might be level or sloping from the bank toward the channel. The crest of each succeeding dike in a system might be at the same elevation as, higher than, or lower than the one upstream, based on the low-water plane (Franco, 1982).

There have been many studies on spur dikes for river training, notably Kuhnle et al. (1997, 1998, 1999), Farsirotou et al. (1998), Molinas et al. (1998b), Zhang and Du (1997), Soliman et al. (1997), Tominaga et al. (1997), Wu and Lim (1993), Khan and Chaudhry (1992), Shields et al. (1995a, 1995c), Molls et al. (1995), Mayerle et al. (1995), and Muneta and Shimizu (1994). Richardson and Simons (1984) give design recommendations based on the literature. Lagasse et al. (1995) and Richardson et al. (1991) give design guidelines for impermeable and permeable spur dikes, guidebanks, and riprap stability factor design.

Even with the widespread use of spur dikes, there has been no definitive hydraulic design criteria developed. Design guidance is based largely on experience and practice within specific geographical areas, usually on an ad hoc basis. Several hydraulic model studies have investigated the use of spur dikes upstream of abutments at specific sites (e.g., Herbich [1967]). The wide range of variables affecting the performance of the spur dikes complicates the development of general guidelines for spur dike use. The main site-specific parameters affecting the performance of the spur dikes include channel width, depth, flow velocity, shape of flow hydrographs, sinuosity of the channel, bed material size,

distribution and transport rate, and material characteristics of the bank (Copeland, 1983). Parameters that affect the performance of spur dikes include: length, width, height, shape, orientation angle, permeability, construction materials, and longitudinal extent of the spur dike field (Melville and Coleman, 2000).

Spur dikes may be classified based on their permeability: high permeability (retarder spur dikes), impermeable (deflector spur dykes), and intermediate permeability (retarder/deflector). Permeability of a spur dike may be defined as the percentage of the spur dike surface facing the flow that is open. A qualitative guide as to the type of spur dike to use for a specific situation is given in Table 5-1. This table provides preliminary advice on the type of spur dike that may be most suitable for a given circumstance.

5.2.2 Local Scour at Spur Dikes

The flow adjacent to a spur dike is characterized by a system of vortices that is formed as the flow is diverted around the structure (Figure 5-2). Flow velocity is greatest at the edge of the structure, where the protrusion into the channel is greatest. This flow velocity peak and high turbulence causes bed material to be suspended intermittently and transported by the flow. For simple-shaped spur dikes (i.e., flat plates without overtopping flow), the maximum depth of scour occurs at the tip of the structure (Figure 5-3). For more complicated spur dike shapes and overtopping flows, the shape of the scour hole may become more complex (Figure 5-4). Predicting the vertical and lateral extent of the local scour is critical for determining the length of bank that the spur dike will protect and determining the depth of spur dike required to protect its base. Stable scour holes associated with spur dikes have been shown to benefit aquatic ecology in degraded streams (Shields et al., 1995a).

Currently, there is no established procedure for predicting the maximum scour depths associated with spur dikes. The many complicating parameters of the stream and the spur dike design (see above) are undoubtedly a factor in the lack of established procedure for prediction of scour in the vicinity of spur dikes. Equations to predict the maximum depth of scour have been developed by several researchers. These equations were derived from experiments in laboratory flumes, in which the maximum depth of scour associated with spur dikes was measured. Even with modern equipment, the maximum scour depth associated with spur dikes in the field is very difficult to determine. Unsteady flows, nonuniform and sometimes varying sediment sizes, and the difficulty of determining the actual location of the stream bottom make collection of field data challenging and rare. Table 5-2 shows the variety of equations used to predict the maximum depth of scour at a spur dike. As is shown in the table, there has been a

Table 5-1. Spur dike performance chart (from Lagasse et al., 2001).

Table 1. Spur Type Performance																						
Spur Type	Function			Erosion Mechanism				Sediment Environment			Flow Environment						Bend Radius			Ice/Debris Environment		
	Project Ext. Bank	Re-est. Prev. Align.	Flow Construction	Transport	Shear Stress - Toe	Shear Stress - Upper Bank	Abrasion	Regime/Low Threshold	Medium Threshold	High	Velocity			Stage			Large	Medium	Small	Minimal	Light Debris	Large Debris/Ice
											Low	Medium	High	Low	Medium	High						
Retarder																						
Fence Type	3	2	2	3	3*	1	1	4	3	2	3	3	2	3	2	1	3	2	1	3	3	2
Jack/Tetrahedron	3	3	1	3	3	1	1	4	3	1	3	2	1	3	2	1	3	2	1	2	4	1
Retarder/Deflector																						
Light Fence	3	3	3	3	3	2	2	3	3	2	3	3	2	3	3	2	3	3	2	3	4	2
Heavy Divorter	3	4	4	3	3	4	3	2	3	3	3	3	2	3	4	4	3	3	2	3	4	3
Deflector																						
Hardpoint	3	4	4	3	3	3	4	2	3	4	3	3	4	3	3	2	3	4	4	3	3	5
Transverse Dike	3	4	4	3	3	3	4	2	3	4	3	3	4	3	3	2	3	4	3	3	3	5
*Henson spur jetties are rated a 4 for this condition.																						
1. Definite disadvantage to the use of this type structure. 2. Some disadvantage to the use of this type structure. 3. Adequate for condition. 4. Some advantage to the use of this type structure. 5. Significant advantage to the use of this type structure.																						

general lack of agreement on the important variables needed to predict maximum scour depth. This disagreement has been possibly settled by Melville (1992, 1997), in whose equations the ratio of the length of the structure to the flow depth determines the form of the equation. Melville's (1992) equations were technically derived for bridge abutments; however, in many cases, particularly in experimental studies, model bridge abutments are similar to spur dikes.

5.2.3 Design Considerations for Spur Dikes

There are three main design considerations for spur dikes:

- **Length and spacing of spur dikes.** The spacing and length dimensions of spur dikes have been related to the length of bank that is protected by each structure. The relationships vary with local variables, such as bank curvature, flow velocity, and whether the structures are designed for navigation of bank protection. Recommendations from several sources are given in Table 5-3.
- **Orientation of spur dikes.** There is a lack of agreement as to the most advantageous orientation to construct spur dikes (Figure 5-5). Permeable spur dikes are usually

designed to decrease the flow near the bank. They are generally not strongly affected by the angle and are usually built at 90 degrees from the bank to have the maximum effect on near-bank velocity and to use the least material (Lagasse et al., 2001). From studies of single spur dikes (orientation angles of 45, 90, and 135 degrees) in a straight channel, Kuhnle et al. (1998) concluded that the volume of the scour hole was greatest for upstream-facing spur dikes (135 degrees), while the potential for bank erosion was greatest for the downstream-facing spur dikes (45 degrees). There are proponents of both upstream-facing and downstream-facing spur dikes (Copeland, 1983). As in other design factors of spur dikes, the best orientation is most likely a function of the local conditions and the purpose of the structures.

- **Permeability.** Spur dikes with permeability up to about 35 percent do not affect the length of the channel bank protected. For permeability values above 35 percent, the length of bank protected decreases with increased permeability. High-permeability spur dikes generally are most suitable for mild bends where small reductions in flow are sought. Permeable spur dikes may be susceptible to damage from debris and ice (Lagasse et al., 2001).

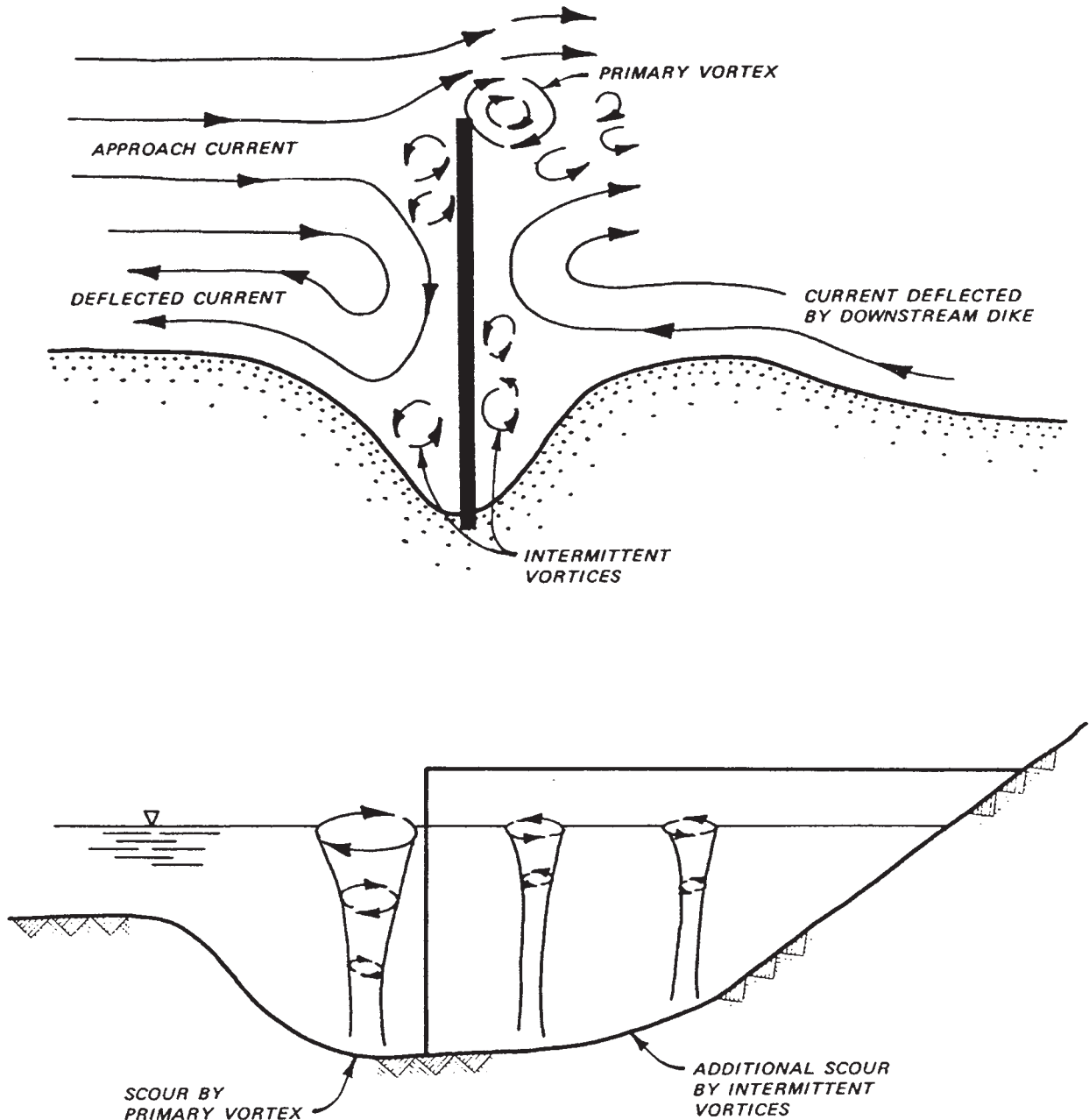


Figure 5-2. Flow patterns at a spur dike: (top) plan view and (bottom) cross-sectional view (from Copeland, 1983).

Spur dikes situated at the bridge crossing oriented 90 degrees to the main channel are studied for the first time in this study, and the results are presented in Chapter 6.

5.2.4 Application to Abutment Scour Countermeasure

Spur dikes are commonly used to maintain predetermined alignment of the upstream-channel approach to a bridge abutment. A bridge abutment may be in danger of being severely eroded when it is subjected to high-velocity flow

from a channel that has changed course due to meandering of the channel (Figure 5-6). Spur dikes may also be used to establish and maintain the alignment of a channel. They have been used to decrease the length of the bridge required and reduce the cost and maintenance of the bridge in actively migrating braided channels (Lagasse et al., 2001)

5.3 Vanes

Vanes comprise a set of panels placed within a channel and oriented slightly obliquely to the flow through the channel.

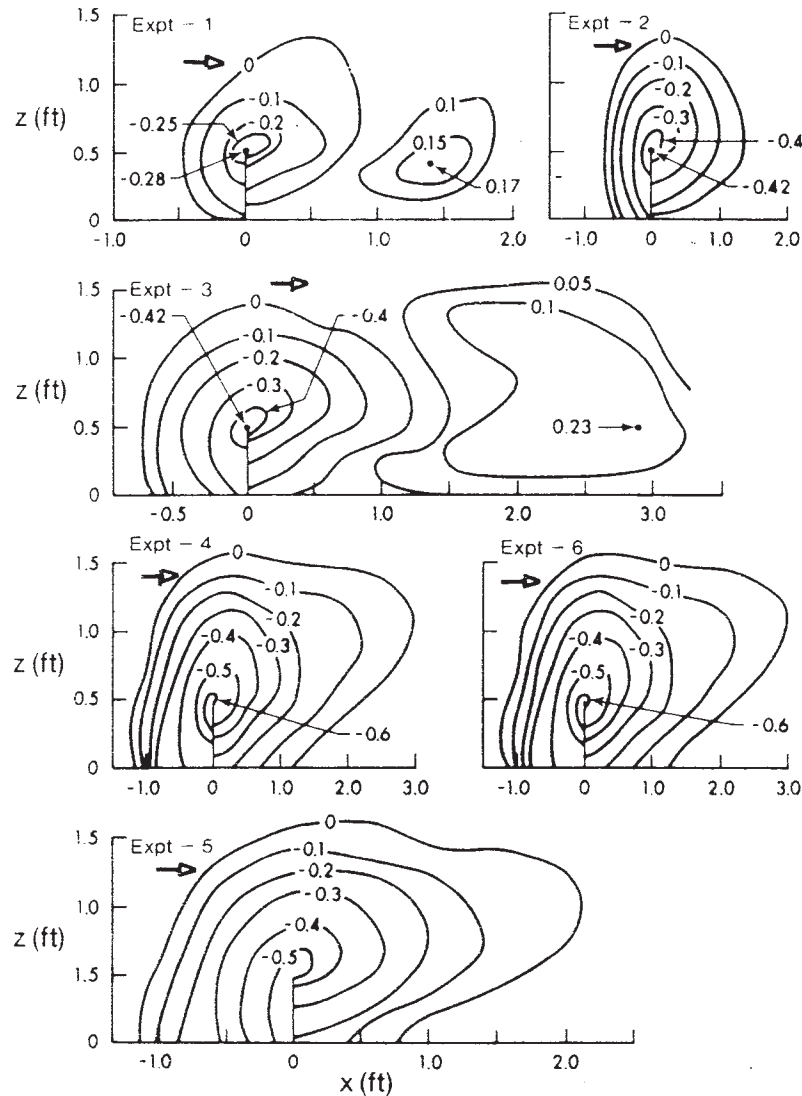


Figure 5-3. Scour hole contours at the end of spur dike experiments (from Rajaratnam and Nwachukwu, 1983a). Arrow indicates flow direction.

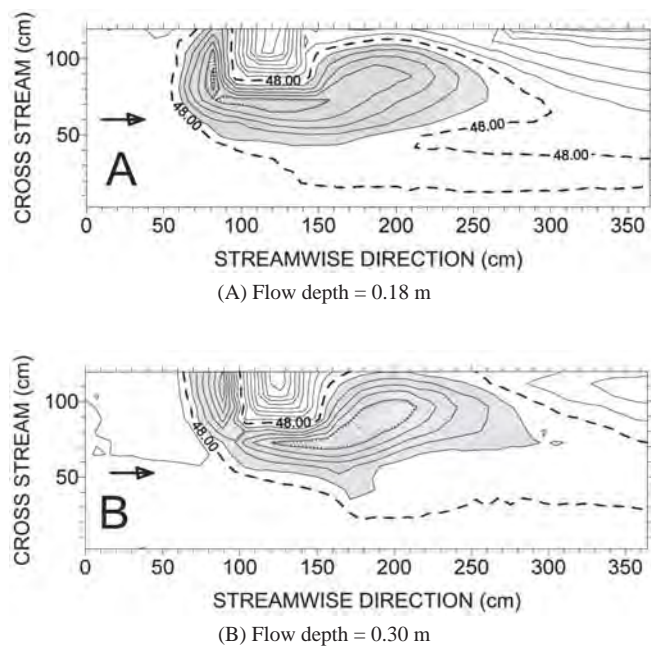
The set of vanes acts to direct bed sediment toward a river bank, or the set (if vane orientation is suitably altered) may scour sediment from a region within a channel. The modest amount of work to date suggests that vane use likely is effective primarily for guiding flow to a bridge opening. Vane use, though, is limited to reasonably well-defined, and comparatively wide, channel conditions whereby the flow indeed will hold its alignment in its approach to a series of vanes, and to channels in which the vanes will not be damaged by material conveyed by channel flow (ice, logs, large bed material, etc.).

Vanes have been used for erosion reduction on river bends (Ettema, 1990, 1992; Odgaard and Kennedy, 1982; Odgaard

and Kennedy, 1983; Odgaard and Lee, 1984; Odgaard and Mosconi, 1987; Odgaard and Spoljaric, 1986; Odgaard et al., 1988; Odgaard and Wang, 1987, 1990a, 1990b, 1991) and for reducing sediment ingestion in intakes (Barkdoll et al., 1999). The installation of vanes and their effects on bank stabilization after 2 years are shown in Figure 5-7.

The main utility of vanes is to ensure channel alignment toward a bridge opening. Prominent concerns incurred with channel shifting are

- Outflanking of an abutment or bridge approach and
- Adverse flow orientation to the abutment.



Reprinted with permission from ASCE.

Figure 5-4. Topographic map of scour hole experiments conducted at National Sedimentation Laboratory, USDA-ARS (Kuhnle et al., 1999). Contour interval = 2 cm. Flow direction indicated by arrows.

A factor associated with these concerns is the common propensity of scour at an abutment to attract a thalweg, especially during conditions of diminished or constricted flow (ice, debris, etc.). Scour at an abutment may be minimized if the channel thalweg is kept at a distance from an abutment or pier. In concept, a series of vanes could be used to direct flow optimally through a bridge opening. This use might be explored further. A possible scenario entails vanes placed immediately upstream of a bridge opening in such a manner as to keep flow from impinging directly against an abutment, or to direct flow away from an abutment, and to promote sediment accumulation at an abutment or pier.

There are only a few cases of vane use to mitigate channel shifting at a bridge site. Odgaard (unpublished report) describes the use of vanes to align the West Fork of the Cedar River at a bridge site in northeast Iowa (Figure 5-8). In both cases, the vanes, set in an array (two wide and about ten long), act to stop a river bend from migrating and severing an approach to a bridge.

One study purports to use vanes for mitigating local scour at abutments (Johnson et al., 2001). However, that study actually looked at submerged, angled dikes. The dikes, built from piled rock, are intended to direct flow away from an abutment and possibly to induce some sedimentation at an abutment. In effect, the submerged, angled dikes shift the channel thalweg away from an abutment. That study did not examine the

effects of submerged, angled dikes on flow blockage (with or without debris or ice). The application of such dikes may be fraught with inadvertent effects, such as directing flow adversely toward a pier.

5.4 Guidebanks

When embankments span wide floodplains, the flows from high waters must be aligned to go smoothly through the bridge opening. Overbank flows on the floodplain can severely erode the approach embankment and can increase the depth of the scour at the bridge abutment. Guidebanks can be used to redirect the flow from the embankment and to transfer the scour away from the abutment. Guidebanks serve to reduce the separation of flow at the upstream abutment face and maximize the total bridge waterway area, and reduce the abutment scour by lessening the turbulence at the abutment face (Lagasse et al., 2001).

Guidebanks are earth or rock embankments placed at abutments to improve the flow alignment and move the local scour away from the embankment and bridge abutment. The guidebank provides a smooth transition for flow on the floodplain to the main channel. Design guidelines for guidebanks are given by Bradley (1978), Neill (1973), Ministry of Works and Development (1979), Lagasse et al. (1995), and Central Board of Irrigation and Power (1989).

Typically, the length of the guidebank will be longer than the width of the bridge opening. The plan shape is usually elliptical and is designed to provide acceptable flow alignment without flow separation. This requires long radius curves. The important factors for guidebank design are orientation relative to the bridge opening, plan shape, length (upstream and downstream of the abutment), cross-sectional shape, crest elevation, and protection of the structure from scour (Figures 5-9 and 5-10). Protection from scour on the flow-facing side of guidebanks, usually by using riprap stone protection, is critical.

5.5 Grade-Control Structures

Channel bed degradation poses a common erosion problem for bridge abutments, as it does for piers. The problem is especially a concern for short bridges over smaller streams farther up within watersheds, because the degradation typically is proportionately more severe with distance up a watershed. A fairly usual form of bed degradation is head-cutting, which especially occurs in streams with beds having significant clay content.

To stop head-cut migration upstream, various hydraulic structures have been developed, including sheet-pile weirs, concrete spillways, and rock drop-structures. The methods used to

Table 5-2. Equations to predict the maximum depth of scour at spur dike.

Equation	Reference	Equation #
$y_s = k \left(\frac{Q}{f} \right)^{0.33}$ <i>k</i> varies between 0.8 and 1.8	Inglis (1949)	(5-1)
$y_s = k \left(\frac{q^2}{F_{bo}} \right)^{0.33}$ <i>k</i> varies between 2.0 and 2.75	Blench (1969)	(5-2)
$y_s = kq^{0.67}$	Ahmad (1953)	(5-3)
$y_s = yK \left(\frac{B_1}{B_2} \right) F_n^n$	Garde et al. (1961)	(5-4)
$y_s = y + 1.1y \left(\frac{L_{sd}}{y} \right)^{0.4} F_n^{0.33}$	Liu et al. (1961)	(5-5)
$y_s = 8.375y \left(\frac{d_{50}}{y} \right)^{0.25} \left(\frac{B_1}{B_2} \right)^{0.83}$	Gill (1972)	(5-6)
$\frac{L_{sd}}{y} = 2.75 \frac{y_s - y}{y} \left[\left(\frac{1}{r_s} \frac{(y_s - y)}{y} + 1 \right)^{1.70} - 1 \right]$	Laursen (1962a)	(5-7)
Here, B_1 = original channel width, B_2 = constricted channel width, C_D = drag coefficient, d_{50} = median grain size, F_{bo} = Blench's zero bed factor (which is a function of grain size), F_n = Froude number, f = Lacey silt factor, k = function of approach conditions, K = function of C_D (which varies between 2.5 and 5.0), L_{sd} = effective length of spur dike, n = Manning coefficient, Q = total stream discharge, q = discharge per unit width at constricted section, r_s = assumed multiple of scour at dike taken as 11.5 by Laursen, y = average depth in unconstricted section, y_s = equilibrium scour depth measured from water surface.		

halt the upstream advance of a knickpoint have been required to change in recent years because of concerns that fish and other aquatic species can be able to move along a stream or river.

Though there has been extensive work done on the use of grade-control structures to impede the upstream progression of bed degradation, there has not been much work

done regarding the effect of bed degradation on the stability of bridge abutments. There exists, though, several ad hoc grade-control structures placed in channels so as to protect bridges.

Early work to stop knickpoint migration on small streams requiring single-span bridges sometimes entailed the con-

Table 5-3. Spur dike spacing recommendations.

Reference	Spacing to length ratio	Comments
Acheson (1968)	3-4	depends on curvature and slope
Ahmad (1951)	4.3 5	straight channels curved channels
Copeland (1983)	2-3	concave banks
Grant (1948)	3	concave banks
Neil (1973)	1.5 2.0 2.5	concave banks straight banks convex banks
Maza Alvarez (1989)	5.1-6.3 2.5-4	straight channels curved channels
Neill (1973)	2 4	if fewer than 2 dikes if 2 or more dikes
Richardson et al. (1990)	2-6	depends on flow and dike characteristics
Strom (1962)	3-5	
Suzuki et al. (1987)	< 4	straight channels
United Nations (1953)	1 2-2.5	concave banks convex banks

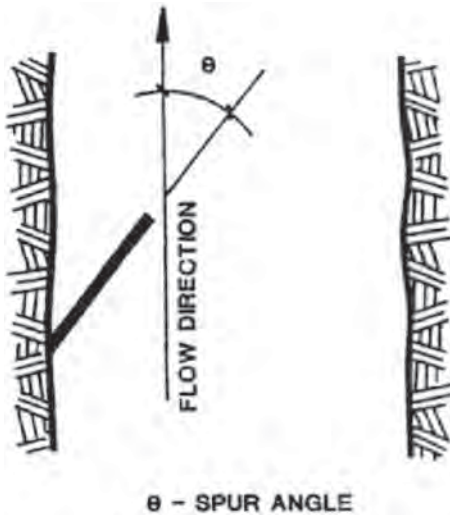


Figure 5-5. Definition sketch for spur dike angle (from Lagasse et al., 2001).

struction of a bridge waterway as a weir. The resulting bridge was called a Greenwood bridge, named for the county engineer who developed the concept for this form of bridge waterway. An example is shown in Figure 5-11. Sometimes a simple sheetpile wall was placed across the channel. Such weirs now are not well received by environmental biologists because fish migrations upstream are prohibited.

Vertical drop structures typically include weirs, check dams, grade-control dams, and stilling basins constructed of materials able to maintain sharp, well-defined crests over

which river or stream flow spills. Drop structures constructed of logs and tightly constructed rock can also be used as vertical drop structures. Structures constructed of loose rock usually form a sloping sill. Figure 5-12 shows the typical configuration of flow and scour at such structures. A grade-control weir is depicted in Figure 5-13. Such weirs are (or at least were) commonly used to stop the upstream progression of general degradation of a channel bed. One concern with them these days is that they may inhibit fish passage along a stream.

The literature on scour at weirs and drop structures is quite extensive. Novak (1955, 1961) conducted early experiments on weir scour. Useful and accessible summaries are given by Laursen and Flick (1983), Peterka (1984), Breusers and Raudkivi (1991), Hoffmans and Verheij (1997), and Raudkivi (1998).

The two leading equations for estimating scour depths caused by flow pouring over a vertical drop structure were developed to estimate scour immediately downstream of vertical drop structures and sloping sills. Equation 5-8 was developed by Peterka (1984) and is recommended for predicting scour depth immediately downstream of a vertical drop structure and for determining a conservative estimate of scour depth for sloping sills. Equation 5-9 was proposed by Laursen and Flick (1983) and is specifically developed for scour downstream of sloping sills constructed of rock. When designing check dams, weirs, grade controls, and similar structures, it is recommended that the designer use these equations as needed (using professional judgment) to estimate expected scour depth immediately downstream of the structure.

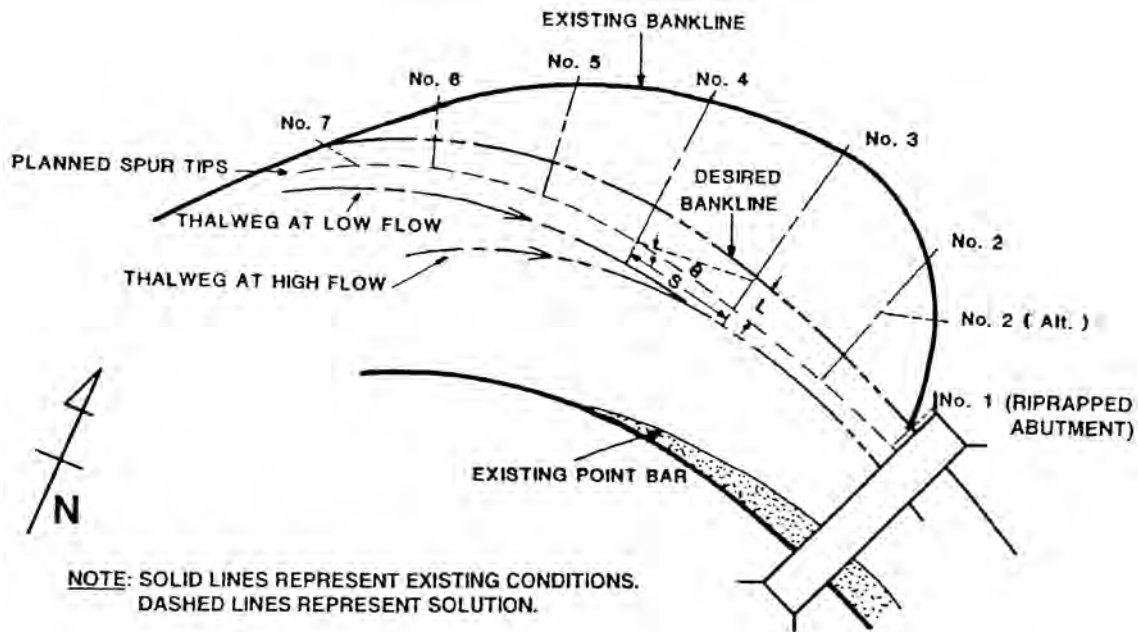


Figure 5-6. Example of spur dike design for realignment of a channel at a bridge crossing (from Lagasse et al., 2001).

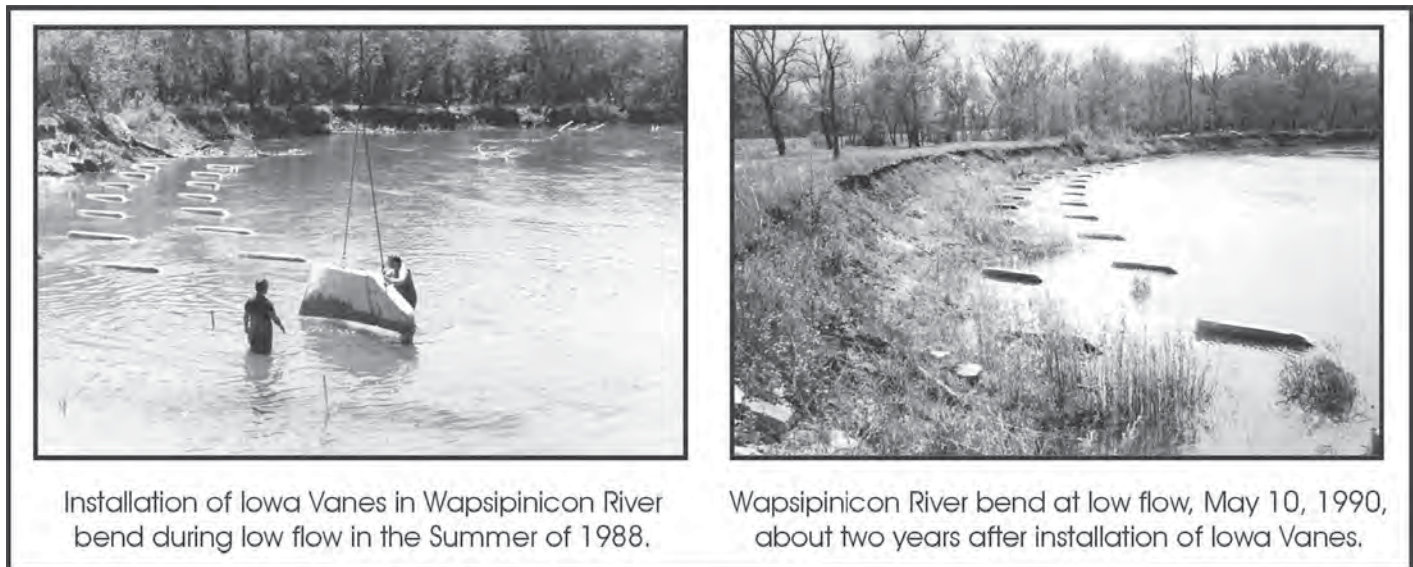


Figure 5-7. Vanes installed along the concave bank just upstream from the bridge crossing and their effectiveness in stabilizing eroded bank, Wapsipinicon River in Iowa.

$$d_s = KH_t^{0.26} q^{0.54} - d_M \quad (5-8)$$

Where:

d_s = local scour depth (below the unscoured bed level) immediately downstream of the vertical drop (m);

q = discharge per unit width ($m^3/s/m$);

H_t = total drop in head, measured from the upstream to downstream energy grade line (m),

d_M = tail water depth immediately downstream of scour hole (m),

$K = 1.9$, a dimensionless coefficient.

The depth of scour calculated in Equation 5-8 is independent of bed particle diameter. If the bed contains large or resistant materials, it may take years or decades for scour to reach the depth calculated in Equation 5-9.

$$d_s = \left\{ \left[4(y_c / d_{50})^{0.2} - 3(R_{50} / y_c)^{0.1} \right] y_c \right\} - d_M \quad (5-9)$$

Where:

d_s = local scour depth (below unscoured bed level) immediately downstream of vertical drop (m or ft);

y_c = critical depth of flow (m or ft);

d_{50} = median grain size of material being scoured (m or ft);

R_{50} = median grain size of stone that makes up the grade control, weir, or check dam (m or ft); and

d_M = tail water depth immediately downstream of scour hole (m or ft).

In recent years, considerable effort has been devoted to developing channel-control structures that do not block fish

and aquatic creatures from moving along streams, as illustrated in Figures 5-14 through 5-16. The structures typically have replicated the form and flow features of rock riffles, like small-scale rapids (Figures 5-14 and 5-15), or a weir fitted with a fish ladder (Figure 5-16). The rock riffle drop structure is favored by biologists because it resembles a natural rock riffle and enables fish and aquatic creature migration upstream or downstream. In some instances, grout is applied over the riprap rocks to prevent them from moving during extreme flow events.

5.6 Riprap

This section discusses procedures already used for sizing and placing riprap at bridge abutments, and it includes an outline of the recommended practice.

Riprap, one of the most commonly used materials for erosion protection, consists of loose, coarse elements of natural stone. The use of stone to help prevent erosion is certainly not new; for example, a 1914 researcher (Forchheimer, 1914) refers to an equation for choosing stone size, which is based on flow velocity.

The increased weight of the riprap stones enables them to resist the increased flow velocities and turbulence associated with flow around an abutment and thereby provides an armor layer protection to the underlying sediments. Interlocking forces between adjacent stones also act to stabilize the riprap layer. Typically, the riprap is placed on the embankment slopes to protect the sediment from scour. In many applications, riprap bank protection has traditionally been placed from the toe of the slope to the top of the bank and has been kept free of vegetation. On large rivers like the Mississippi, however, riprap on the upper part of the bank is often combined with

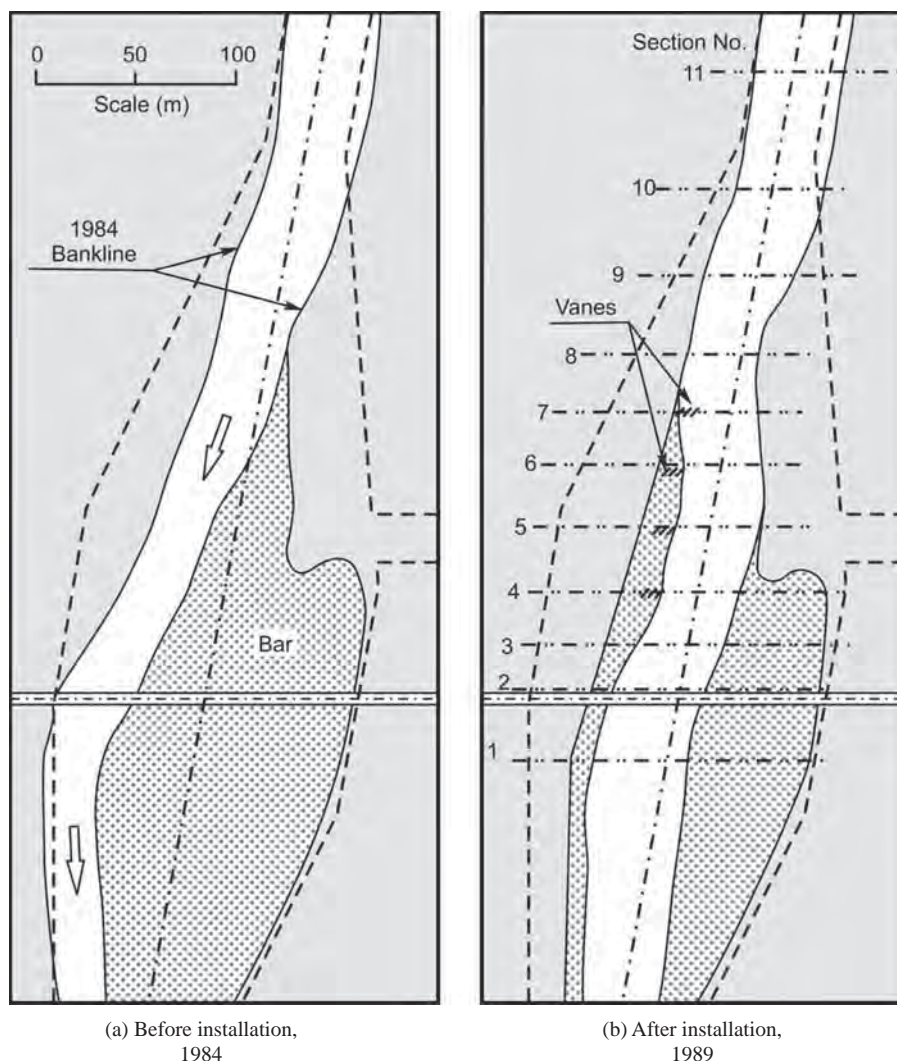


Figure 5-8. Plan view of changes in channel alignment before and after installation of vanes, West Fork Cedar River, Butler County, Iowa.

articulated concrete mattress on the lower portion because of the difficulty and uncertainty of placing riprap underwater in large depths and high velocities. Conversely, riprap can be used on the lower portion of the bank, with vegetation on the upper portion, a technique used on some smaller streams.

An alternative to extending the riprap down to the expected scour depth is to lay an equivalent blanket of riprap, known as a launching apron, onto the sides of a developing scour hole. This riprap acts to reduce the scour depth and protect the abutment foundation from undermining. The launchable apron method was apparently first used for large alluvial rivers in India and is described by the Central Board of Irrigation and Power (1989) in India.

Advantages of using riprap include

- Relative ease of construction,
- Flexibility,
- Tendency to be self-healing,

- Extensive experience and design guidance to support its use,
- Ease of repair of local failures, and
- Natural appearance that can be enhanced by vegetation.

Potential disadvantages of using riprap include

- Limited availability and relatively high cost in some areas,
- Environmental restrictions on use,
- Variations in quality, and
- Difficulties of transport and placement in some locations.

Fairly numerous guides exist for sizing and placing riprap. Thorne et al. (1995) usefully summarize five general requirements for riprap sizing and placement:

- Riprap must be capable of withstanding the combined impact of all the forces of water flow (and wave attack) responsible for erosion and destabilization. This determination is based on

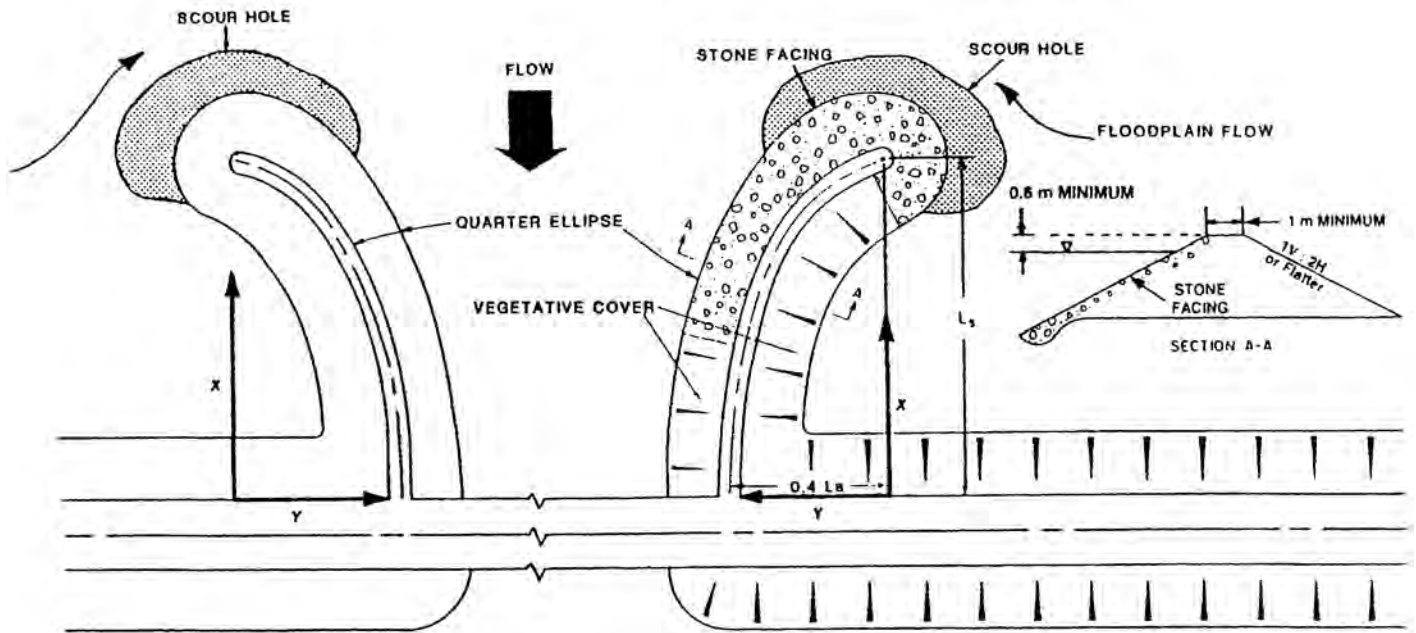


Figure 5-9. Design details for guidebanks at bridge crossing (from Lagasse et al., 2001).

such factors as stable stone size, lateral and vertical extent of protection, and alignment.

- Riprap layout must be safe with regard to geotechnical stability, foundation settlement, and groundwater seepage.
- Riprap must be composed of sufficiently durable materials to retain the required erosion resistance and mass stability over the design life of the project.
- Ecological impacts and aesthetics of the riprap have to be acceptable.

- Riprap layout must be economical to build using available materials, equipment, and labor.

5.6.1 Riprap Failure Mechanisms

Riprap is subject to certain failure mechanisms, depending on where it is placed with respect to a bridge abutment. Riprap placed in the apron is subject to failure mechanisms similar to those of riprap placed about a bridge pier, whereas riprap placed on the embankment slopes are subject to not only dislodgement by the flow, but also slump and slide failures where the riprap moves down the embankment slope.

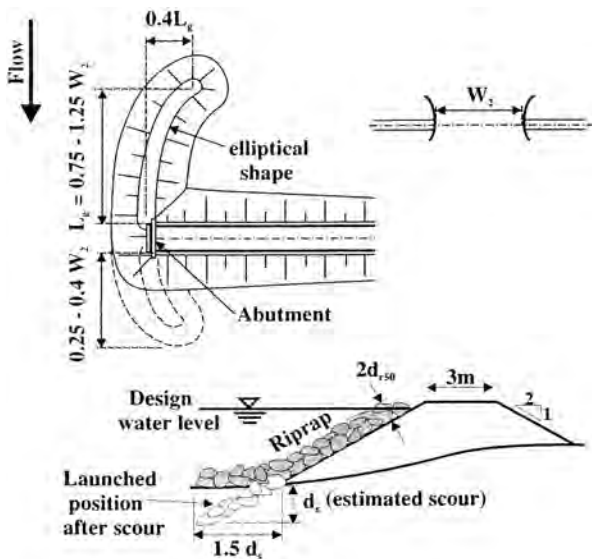


Figure 5-10. Design details for guidebanks at bridge crossing (from Melville and Coleman, 2000).



Figure 5-11. A concrete weir helps protect bridge abutments against general scour produced by head-cutting.

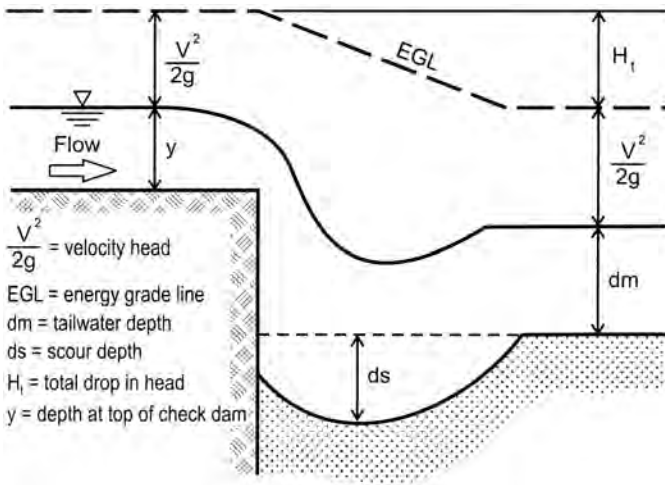


Figure 5-12. Flow and scour over a simple drop structure.

Riprap placed in an apron at the base of wing-wall abutments may be subjected to shear failure, edge failure, winnowing failure, and bed-form undermining (Parola, 1993; Chiew, 1995; Parker et al., 1998; Lauchlan, 1999). Shear failure occurs where the individual riprap stones are not large enough to resist entrainment by the flow. Scour of the riprap stones at the edges of the riprap layer is termed edge failure, while winnowing describes the erosion of the finer bed material between voids in the riprap layer. Filter layers are often placed to prevent winnowing failure. Shear failure may be triggered at the edges of the riprap layer (i.e., shear and edge failure are often linked and are both a consequence of undersized riprap). Bed-form undermining occurs under mobile-bed conditions due to the migration of the troughs of large bed forms through the bridge section. The riprap stones settle into the troughs of the passing bed forms, which may



Figure 5-13. A grade-control weir helps protect a bridge against general degradation of a stream bed. Riprap is placed along the downstream side to protect against scour.

destabilize the riprap layer. In general, riprap size selection can be based on stability against shear and edge failure, as long as the other possible modes of failure are also addressed appropriately.

The following four failure mechanisms of riprap layers at the embankments of spill-through abutments were observed during laboratory studies and in the field (e.g., Blodgett and McConaughy, 1985):

- Particle erosion failure.** The hydrodynamic forces of the flowing water are able to dislodge individual riprap stones. Possible causes of particle erosion failure include the stone size being too small, the riprap gradation being too uniform, the side slopes being too steep, and the removal of

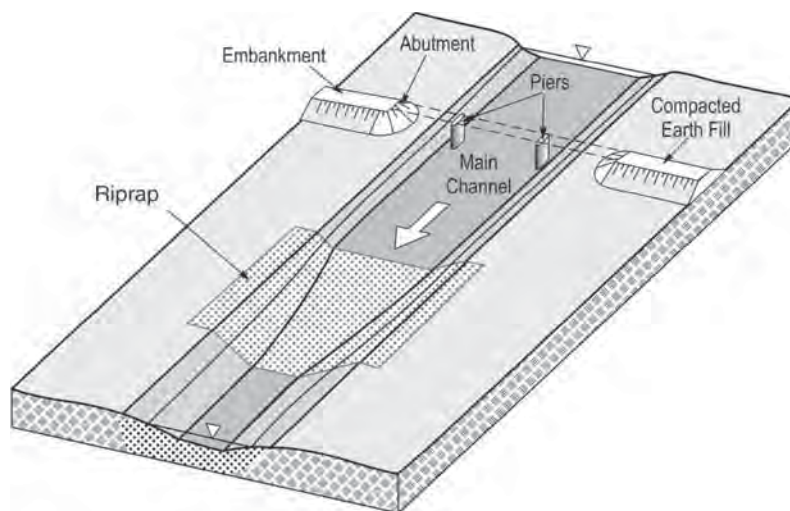


Figure 5-14. A riprap stone riffle placed to arrest head-cut progression upstream toward a bridge waterway. The riffle halts erosion, but enables the passage of aquatic creatures.



Figure 5-15. A rock riffle grade-control structure placed downstream of a bridge.

individual stones by impact and abrasion. This mode of failure is similar to shear failure, with an additional factor being the effect of the slope.

- **Translational slide failure.** This type of failure occurs when a mass of riprap stones moves down the embankment slope, with a horizontal fault line. Failure is usually initiated by undermining of the riprap blanket by a scour hole in the channel. Possible causes include excess pore pressures in the embankment slope, undermining of the riprap toe, and the side slopes being too steep.
- **Modified slump failure.** Modified slump failure is a mass movement of riprap material occurring along an internal slip surface within the riprap layer. Possible causes include disturbance of critical material in the lower levels of the riprap layer and side slopes being too steep.
- **Slump failure.** A movement of material occurs along a ruptured surface that has a concave upward curve, when a shear failure of the underlying base material occurs. Possible causes of slump failure include the presence of nonhomogeneous base material with layers of impermeable material that can act as fault lines when subjected to excess pore pressure and side slopes being too steep.

Abutment side slope is a significant factor in riprap stability. Accordingly, it is desirable to decrease side slope steepness, thus increasing the stability of the riprap on the slopes. Recommendations by various authors for the minimum value for side slopes vary from 1:2 to 1:1.5 (H:V).

Parker et al. (1998) undertook an extensive survey of scour countermeasures installed at bridges throughout the United States. They noted two primary methods of failure for riprap, beside direct entrainment by the flow. These



Figure 5-16. A sheetpile grade-control structure placed downstream of a bridge. The structure includes a fish ladder.

are failures caused by instability of the riverbed and failures caused by an inadequate filter. Instability of the riverbed affects countermeasure stability by altering the flow conditions that the countermeasure experiences.

5.6.2 Riprap Stability

Many early equations for riprap stability were based on flatbed conditions, several having origins in the research of Isbash (1935, 1936), who was concerned with the stability of rock dumped in flowing water. He proposed the following stability criterion:

$$N_{sc} = 2E^2 \quad (5-10)$$

Where N_{sc} is a dimensionless stability factor for the stone given as

$$N_{sc} = \frac{V_{cr}^2}{g(S_r - 1)d_{50}} \quad (5-11)$$

Where:

- V_{cr} = critical threshold velocity for the stone,
- S_r = specific gravity of the riprap stones, and
- d_{50} = effective diameter of the stone.

The parameter E has a value of 0.86 for loosely placed stones in flowing water and 1.2 for those that have become embedded.

Neill (1976) studied incipient motion of uniform gravel on a flatbed. From dimensional analysis and empirical results, the following stability equation was developed:

$$N_{sc} = 2.5 \left(\frac{d_{50}}{y} \right)^{-0.20} \quad (5-12)$$

Where y is flow depth.

Neill (1973) provides a graph of correctly sized riprap material, as shown in Figure 5-17, based on the recommendations of four U.S. agencies for embankment protection. The local velocity is to be taken as approximately 1.5 times the mean velocity through the waterway opening.

The results of Neill (1967) were generalized by Maynard (1987) for graded riprap to produce

$$N_{sc} = 2.63 \left(\frac{d_{30}}{y} \right)^{-0.20} \quad (5-13)$$

Where d_{30} denotes the riprap size for which 30 percent by weight are finer.

The following equation was proposed by Maynard (1993) for determining riprap stone sizes for use in channels with low turbulence:

$$d_{30} = S_f C_s C_v C_T y \left[\left(\frac{\gamma_w}{\gamma_s - \gamma_w} \right)^{1/2} \frac{V}{\sqrt{K_1 g y}} \right]^{2.5} \quad (5-14)$$

Where:

- S_f = safety factor (>1);
- C_s = stability coefficient for incipient failure: 0.3 (angular rock), 0.375 (rounded rock);
- C_v = vertical velocity distribution coefficient,
 - = 1.0 for straight channels on the inside of bends,
 - = $1.283 - 0.2 \log(R_b/W)$ for outside of bends,
 - = 1.25 for downstream of concrete channels, and
 - = 1.25 at end of dykes;
- R_b = centerline radius of curvature of bend,
- W = water surface width at upstream end of bend,
- C_T = blanket thickness coefficient, given by Figure 1 in Maynard (1993),
- y = local depth of water,
- γ_w = unit weight of water,
- γ_s = unit weight of stone,
- V = local depth-averaged velocity,
- K_1 = side slope correction factor, and
- g = gravitational constant.

Maynard et al. (1989) provide a riprap design procedure for application when riprap is placed in channels, whether natural or human-made, that are not adjacent to structures that induce high turbulence levels. The procedure is based on local depth-averaged velocity in a low-turbulence environment. It is applicable to a wide range of gradations for riprap blanket thickness equal to the maximum stone size.

The following riprap sizing equation was proposed by Faraday and Charlton (1983) for the general water environment, with an additional coefficient to account for flow changes in certain situations:

$$\frac{d_{50}}{y} = C^* Fr^3 \quad (5-15)$$

Where:

C^* = coefficient determined from laboratory and field testing and

Fr = flow Froude number = $V/(gy)^{0.5}$.

The mean channel flow velocity (V) should be multiplied by the following factors: 2.0 at noses of groins and guidebanks, 1.5 at bends, and 1.25 in straight reaches.

For determining the recommended rock sizes to protect a streambed conveying uniform flow, Brown and Clyde (1989) give

$$d_{50} = 0.387 \frac{V^3}{y^{1/2} g^{3/2} (S_r - 1)^{3/2}} \quad (5-16)$$

Where V is the average stream velocity.

Pilarczyk (1990) suggested Equation 5-17 in the form of stability criteria for revetments under either wave or current attack. Instead of using the traditional threshold values such as the Shields (1936) criterion, Pilarczyk combined many empirical formulas into the criteria:

$$\Delta_m t_p \geq \delta_c K_T \frac{0.035}{\phi_{cr}} K_h K_d^{-1} \frac{V^2}{2g} \quad (5-17)$$

Where:

- t_p = thickness of the protection unit,
- Δ_m = relative density of protection system,
- δ_c = stability factor for current,
- K_T = turbulence and/or shear stress adjustment factor,
- K_h = depth (or velocity profile factor),
- K_d = slope factor,
- ϕ_{cr} = critical shear stress parameter, and
- V = depth-averaged velocity.

It is suggested that Equation 5-17 can also be used for other armoring devices, such as blocks, block mats, and gabions. Values for the various factors are given in Pilarczyk (1990).

An alternative approach to the methods outlined above is to consider the stability of individual riprap stones. This approach is outlined by Stevens and Simons (1971), Stevens et al. (1976), and Simons and Senturk (1977). The method is based on the ratio of the moments of forces resisting overturning of the stone and the moments of forces promoting overturning. A disadvantage of using moment analysis to size riprap stones is that the interaction between the stones in the layer, which can enhance the stability of the stones, cannot be incorporated.

5.6.3 Current Guidelines for Riprap Use at Abutments

HEC 23 is the FHWA document that specifies bridge scour and stream instability countermeasures, including rock riprap design, for piers and abutments. In addition, the guidelines in Table 5-4 customarily are used for sizing and placing

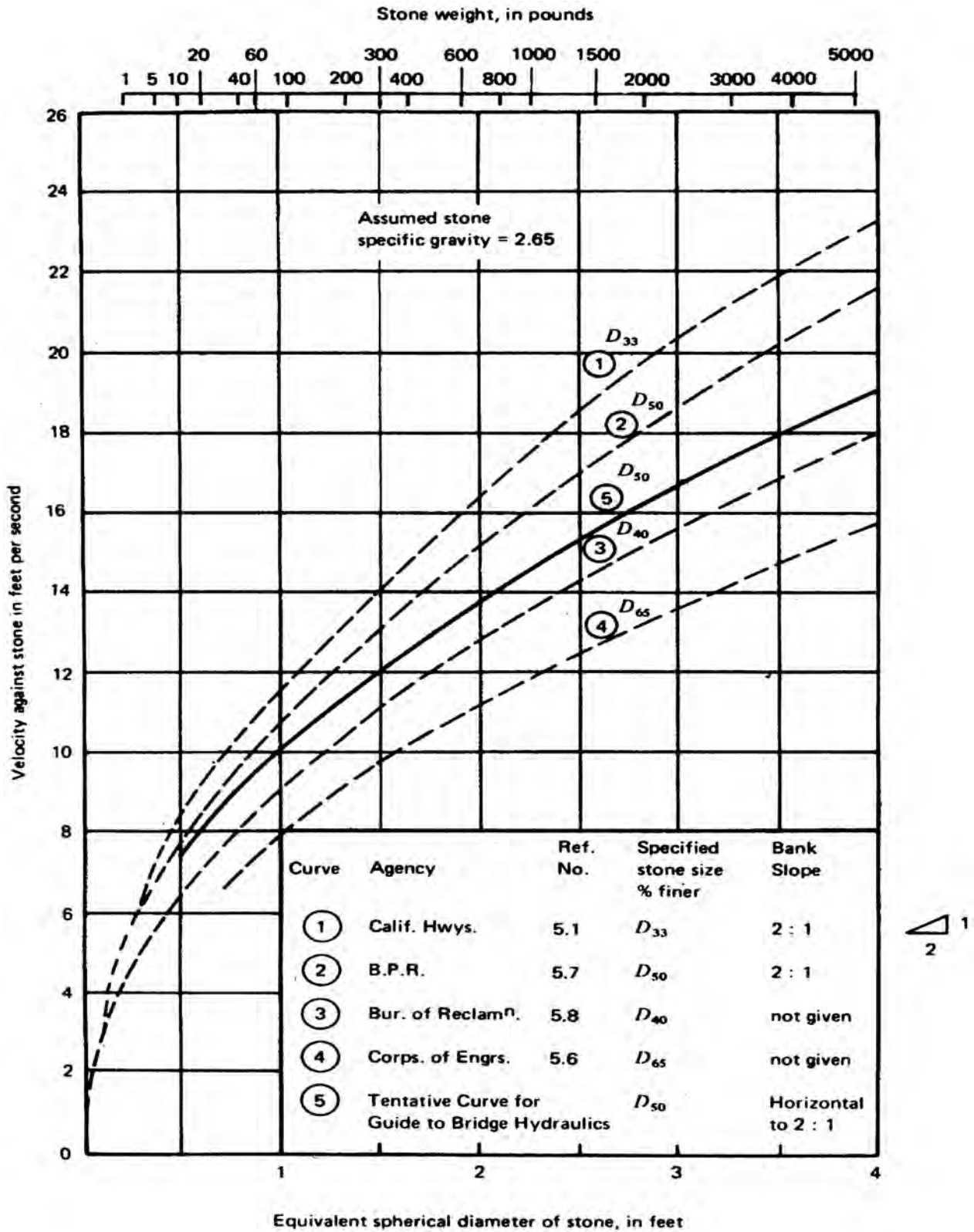


Figure 5-17. Riprap size selection (Neill, 1973).

Table 5-4. Guidelines for sizing and placing riprap.

Country	Guidelines
United States	Richardson et al. (1998) Brown and Clyde (1989) Richardson and Davis (1995)
Canada	Harris (1988)
India	Central Board of Irrigation and Power (1989)
Australia	Austrroads (1994)
New Zealand	Ministry of Works and Development (1979) Gregorius (1985) Melville and Coleman (2000)

riprap at bridge abutments. The recommendations cover some or all of the following riprap parameters: size, extent of protection, layer thickness, gradation, and filter design. The following sections discuss each of these parameters.

Size

A list of the riprap sizing equations for abutment protection is provided in Table 5-5. The equations by Simons and Lewis (1971), Croad (1989), Pagan-Ortiz (1991) for spill-through abutments, Austrroads (1994), and Atayee et al. (1993) for $Fr < 0.8$ can be arranged into the form

$$\frac{d_{50}}{y} = \frac{C}{(S_r - 1)} Fr^2 \quad (5-18)$$

Where C is a coefficient. For $Fr < 0.8$ and flatbed conditions, the Simons and Lewis (1971) relation at the critical location of failure can be considered identical to that of Atayee et al. (1993) if the local velocity one-rock diameter over the bed is considered as 1.15 times the average contracted flow velocity on the floodplain. For the same flow range and conditions, the Croad (1989) equation can be considered identical to that of Atayee et al. (1993) if the depth-averaged velocity at the critical point of failure is considered to be 1.48 times the average contracted-flow velocity on the floodplain.

A graphical comparison of the various equations for $S_r = 2.65$ is shown in Figure 5-18. The equations of Pagan-Ortiz (1991) and Richardson and Davis (1995), which are expressed in terms of flow velocity and depth in the contracted (bridge) section, are plotted for different values of the contraction ratio, β , where β is the ratio of the channel width to the bridge opening width. It can be seen that the various equations give a wide range of recommended riprap sizes. The equations given by Croad (1989) and Richardson and Davis (1995) give larger riprap sizes in comparison with the other equations, whereas the equations given by Brown and Clyde (1989) and Pagan-Ortiz (1991) give relatively small riprap sizes.

Three of these equations are applicable to wing-wall abutments, namely Brown and Clyde (1989), Pagan-Ortiz (1991), and Lagasse et al. (2001). The three equations give a wide range

of suggested riprap size, with the equation by Brown and Clyde giving significantly smaller riprap than the other two equations.

The basis of each of the three equations is limited, as discussed below. The equation given by Brown and Clyde (1989) was derived from a simple tractive force consideration for uniform flow. The analysis uses the Manning equation for flow resistance and the Shields entrainment function for stone stability. The equation was calibrated using field observations from a number of sites on U.S. rivers, but the data set did not include bridge sites. The recommended stability factors for riprap placed at bridge abutments were taken as equivalent to those for “high-turbulence” and “sharp-bend” sites. The Pagan-Ortiz (1991) equation is based on a simplified laboratory investigation of wing-wall abutments sited on the floodplain. The experiments were undertaken using an idealized fixed-bed channel on which the test riprap stones were placed. The study consistently indicated failure of the riprap occurring at the apron toe upstream of the abutment centerline. The equation is of the same form as the classic Isbash (1936) equation. The equation recommended by Lagasse et al. (2001) is also based on the experiments of Pagan-Ortiz (1991) and can be expressed in the same form.

Extent of Protection

The recommended practice (e.g., Richardson and Davis, 1995; Austrroads, 1994) is to extend the riprap right around the abutment and down to the expected scour depth.

As mentioned previously, an alternative to extending the riprap down to the expected scour depth is to lay an equivalent blanket of riprap, known as a launching apron, on the existing bed. The launching apron protects the side of the scour hole as erosion occurs. Macky (1986) notes that this is seldom practiced in New Zealand and that the riprap rarely extends below the existing riverbed.

Specific guidelines for riprap layout for a launching apron are as follows:

- The apron at the toe of the abutment slope should extend along the entire length of the abutment toe, around the curved portions of the abutment to the point of tangency

Table 5-5. Equations for size of riprap.

Reference	Applicability	Equation	Symbols
Simons and Lewis (1971)	Spill-through abutments	$\eta = \frac{0.4V_r^2}{(S_r - 1)gd_{50}} \quad (5-A)$	d_{50} = riprap stone size V_r = velocity at a level of one-rock diameter above the bed S_r = specific gravity of rock η = stability factor = 0.595, for flow over a horizontal bed
Croad (1989)	Spill-through abutments	$d_{50} = 0.025V_b^2 K_{sl}^{-1}$ $K_{sl} = \sqrt{1 - \frac{\sin^2 \phi_{sl}}{\sin^2 \theta_r}} \quad (5-B)$	V_b = velocity at abutment end = 1.5V K_{sl} = embankment slope factor ϕ_{sl} = slope angle θ_r = angle of repose
Brown and Clyde (1989)		$d_{50} = \frac{0.0127V^3}{y^{0.5} K_{sl}^{1.5} (S_r - 1)^{1.5}} \left(\frac{S_{fa}}{1.2}\right)^{1.5} \quad (5-C)$	S_f = stability factor varying from 1.6 to 2.0 for abutment protection y = flow depth
Pagan-Ortiz (1991)	Wing-wall abutment	$d_{50} = \left(\frac{1.064V_2^2 y_2^{0.23}}{(S_r - 1)g}\right)^{0.81} \quad (5-D)$	V_2 = mean velocity in contracted (bridge) section y_2 = flow depth in contracted section
Pagan-Ortiz (1991)	Spill-through abutment	$d_{50} = \frac{0.535V_2^2}{(S_r - 1)g} \quad (5-E)$	
Austrroads (1994)		$\frac{d_{50}}{y} = \frac{1.026}{(S_r - 1)} Fr^2 \quad (5-F)$	Fr = flow Froude number = $V/(gy)^{0.5}$
Atayee et al. (1993) and Lagasse et al. (2001)	$Fr_2 \leq 0.8$	$\frac{d_{50}}{y_2} = \frac{K_s}{(S_r - 1)} Fr_2^2 \quad (5-G)$	Fr_2 = Froude number in the contracted section K_s = shape factor = 0.89 for spill-through abutments = 1.02 for wing-wall abutments
	$Fr_2 > 0.8$	$\frac{d_{50}}{y_2} = \frac{K_s}{(S_r - 1)} Fr_2^{0.14} \quad (5-H)$	K_s = 0.61 for spill-through abutments = 0.69 for wing-wall abutments

with the plane of the embankment slopes (Richardson and Richardson, 1993a).

- The apron should extend from the toe of the abutment into the bridge waterway a distance equal to twice the flow depth in the overbank area near the embankment, but need not exceed 7.6 m (Lagasse et al., 1997).

The recommendations shown in Figure 5-19 are based on the studies carried out by Pagan-Ortiz (1991) and Atayee (1993). Atayee (1993) recommended that the width of the apron not exceed 7.5 m.

Gregorius (1985) states that “the apron should have a thickness of 1.25 times the largest stone size and a horizontal length such that, in the launched position, the apron extends

to below the estimated scour depth.” No allowance is made for the fact that the presence of the riprap will reduce the scour depth and also affect the position of the scour hole.

Eve (1999) conducted riprap tests with approach-flow conditions at 90 percent of the threshold condition for the approach sandbed. Based on observations of progressive failure of the abutment embankments, Eve developed the following relation for determining the extent of protection:

$$\frac{W_a}{y} \left(\frac{0.5W_a + r_t}{y + r_t} \right) = \left(0.5 - 1.82 \frac{d_{50}}{y} \right) \left(\frac{B}{B - L_a} \right) \left(\frac{180}{180 - (\theta + \phi_{ai})} \right) \quad (5-19)$$

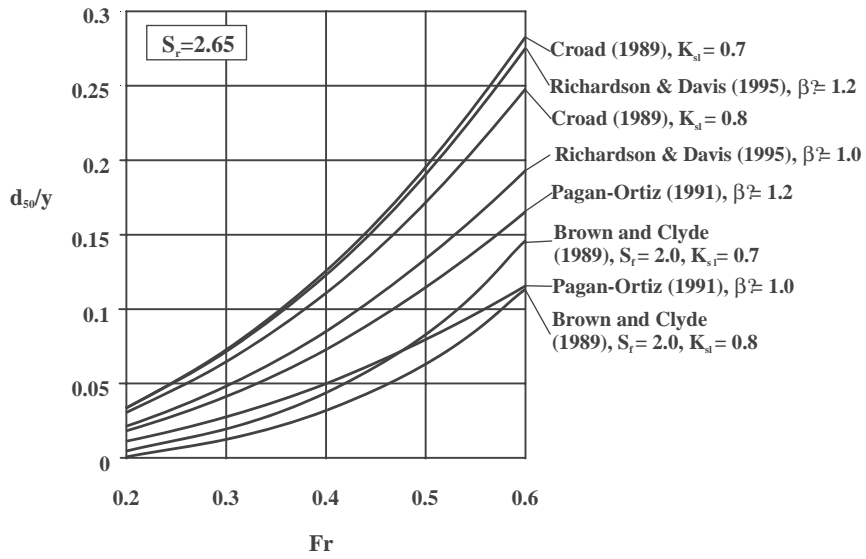


Figure 5-18. Comparison of equations for riprap sizing at bridge abutments.

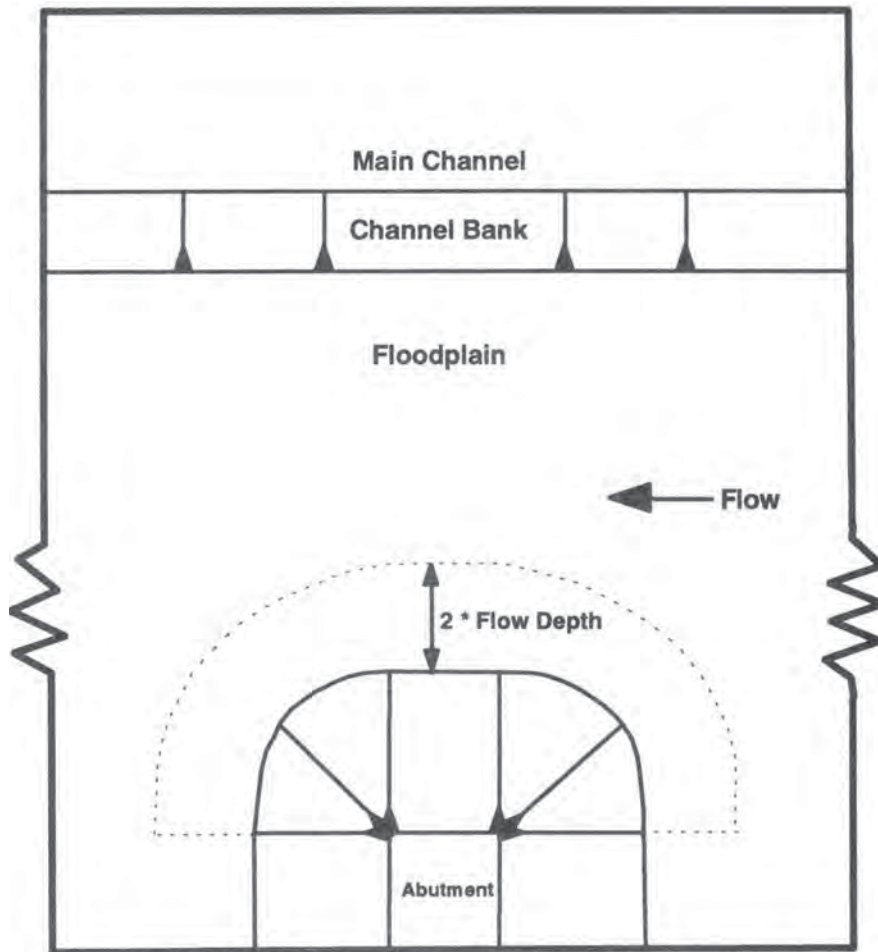


Figure 5-19. Plan view of the recommended extent of rock riprap apron (Lagasse et al., 1997).

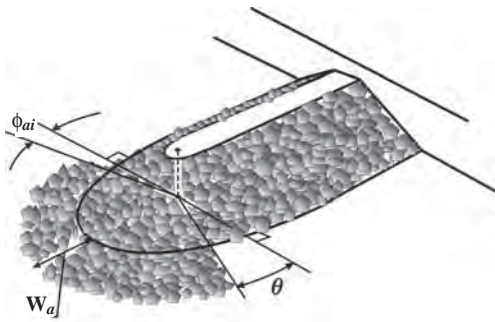


Figure 5-20. Definition diagram for placement of a riprap launching apron at a spill-through abutment (after Eve, 1999).

Where:

y = approach-flow depth,

B = upstream width of the flume,

L_a = abutment length, and

r_t = radius of the spill-through abutment toe

W_a , θ , and ϕ_{ai} are defined in Figure 5-20.

Layer Thickness

To a certain extent, riprap layer thickness affects the stability and durability of riprap protection. Thickness is generally specified as a multiple of maximum size d_{100} or of median size d_{50} . For relatively low-turbulence applications such as bank protection, the U.S. Army Corps of Engineers (1994) specifies a minimum thickness of d_{100} or $1.5d_{50}$, whichever is greater. For high-turbulence applications, the same reference specifies $1.5d_{100}$.

Maynard (1988) showed that additional thickness above these minimums generally results in increased stability. It is common practice to use 50 percent more thickness underwater because of uncertainties in placement.

For New Zealand conditions, the Ministry of Works and Development (1979) recommends a layer thickness of $2d_{50}$,

as well as a suitably graded filter layer or filter cloth. Lagasse et al. (2001) recommend that the rock riprap thickness be at least the larger of 1.5 times d_{50} or d_{100} . To allow for the uncertainties associated with placing riprap underwater, it is also recommended that the rock riprap thickness be increased by 50 percent when it is placed underwater.

Austrroads (1994) gives specific recommendations of riprap size and thickness for specific water velocity values. Table 5-6 shows the riprap diameter D as computed by Austrroads from a recommended rock weight, assuming a roughly spherical shape and a specific gravity of 2.65. The table also shows the value of t_r/D for the Austrroad recommendations and shows an average value of 1.77. The small variances from this value are negligible when considering that riprap placement is inexact in practice.

Gradation

Riprap gradation is often specified in the form of upper and lower limit curves, with any intermediate gradations being regarded as acceptable. Generally, the narrower the specified limits, the higher the production costs.

If the riprap is not correctly graded, the Ministry of Works and Development (1979) recommends the use of a filter for New Zealand conditions. Figure 5-21 shows the grading curve recommended by the Ministry of Works and Development.

A criterion for correctly grading riprap for bridge abutment protection, given by Brown and Clyde (1989), is shown in Table 5-7. If gradation is sufficient, a filter fabric is not required. It is acknowledged that this gradation may be restrictive, and the 85-percent specification may be ignored if the riprap cannot be sourced to this specification.

Austrroads (1994) recommends that a filter be required when “the face stones are nearly uniform in size and embankment material is vulnerable to scour.” No criterion is given to ascertain when riprap is nearly uniform in size, although it is assumed that this is true when riprap gradation is more uniform than that stated in the Austrroads guidelines.

Table 5-6. Design of rock slope protection (Austrroads, 1994).

Velocity (m/s)	Riprap Diameter, D (m)	t_r/D	Riprap Thickness, t_r (m)
<2.0	None	---	---
2.0-2.6	0.30	1.67	0.50
2.6-2.9	0.40	1.87	0.75
2.9-3.9	0.55	1.82	1.00
3.9-4.5	0.70	1.79	1.25
4.5-5.1	0.90	1.77	1.60
5.1-5.7	1.15	1.74	2.00
5.7-6.4	1.45	1.72	2.50
>6.4	Special	---	---

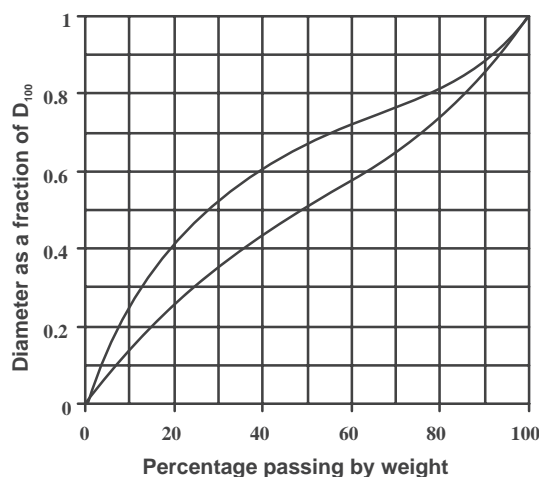


Figure 5-21. Optimum riprap grading curve (Ministry of Works and Development, 1979).

Filter Design

Filters include granular filters, which make use of the filtering effect of graded sediments, and synthetic filters, commonly called geotextiles. Filters are placed beneath riprap layers to meet one or both of the following objectives:

- To prevent groundwater behind the riprap from transporting bank material through the riprap (i.e., piping). The filter should be fine enough to prevent the base material from passing through, but more permeable than the sediment being protected.
- To prevent large-scale turbulence in front of the riprap layer from sucking bank material through the riprap (i.e., winnowing).

Granular filters. According to conventional theory, granular filter material is placed in layers of decreasing size, where the filter material follows the Terzaghi and Peck (1958) filter criterion. Terzaghi and Peck recommended that the 15-percent size be at least four times as large as the coarsest particles of the material being protected, but not more than four times as large as the 85-percent size of the finest soil to be protected by the filter.

Advantages of granular filters include

- Self-healing ability,
- Durability,
- Ability to deform without serious damage, and
- Relative ease of repair.

Potential disadvantages include

- The careful control required to achieve specified gradation and thickness,

Table 5-7. Rock riprap gradation (Brown and Clyde, 1989).

Stone Size Range	Percent of gradation smaller than the stone range
$1.5d_{50}$ to $1.7d_{50}$	100
$1.2d_{50}$ to $1.4d_{50}$	85
$1.0d_{50}$ to $1.15d_{50}$	50
$0.4d_{50}$ to $0.6d_{50}$	15

- Difficulty of compaction on steep slopes, and
- Difficulties in control of underwater placement.

In practice, it is difficult to place a multilayered filter. A single layer is simple to construct and less likely to contain defects. Riprap produced to exact specifications is usually expensive to source locally. An alternative to granular filters is the use of synthetic filters.

De Sousa Pinto (1959) tested the Terzaghi and Peck criterion for applicability to the riprap protection of piers. Favorable results were determined, with no winnowing of the finer material.

Synthetic filters. Brown and Clyde (1989) identified the following advantages for the use of synthetic filters (compared to granular filters) in riprap revetments:

- Lower costs;
- Consistent, more reliable material quality;
- Faster, more labor-efficient installation; and
- Lack of limits on design based on local availability of suitable granular filter material.

Disadvantages of synthetic filters include the following:

- Problems with placement underwater;
- Unproven durability;
- Propensity for clogging;
- Bacterial activity, which can affect performance;
- Relative movement between fabric and bank material;
- Failure on steep slopes, due to sliding (the technique is typically limited to slopes 2H:1V or flatter);
- Requirements for edge protection, especially in turbulent flow conditions (sudden failure can result if the scour exposes the filter fabric edge [Escameia and May, 1992], a phenomenon that is not observed with granular filters).
- Susceptibility to damage;
- Difficulty of repair; and
- The careful design and installation needed to accommodate settlement.

Filter recommendations. The important parameters in selecting a filter fabric are pore size, permeability, and long-term soil/fabric permeability and shear strength, according to Hudson and East (1991). Gregorius (1985)

summarized various suggested guidelines for the use of synthetic filters beneath riprap for channel protection as follows:

- **Piping.** To prevent fines from passing through the filter fabric, the average filter fabric pore size, O_{50} , must be less than the d_{85} size of the bed sediment.
- **Permeability.** The permeability of the filter should be greater than that of the unprotected sediment to prevent hydrostatic pressure buildup in the protected bed.

5.6.4 Ecological Impacts

Riprap has been shown to support dense, diverse populations of macroinvertebrates (Shields et al., 1995b). Also, Farabee (1986) found that uniform riprap supports higher fish populations than does graded riprap, presumably because the larger interstitial openings provide better habitat.

5.6.5 Riprap Placement

Riprap performance as a scour countermeasure at bridge abutments depends on the accuracy of the placement of the riprap at the site. Riprap is often placed inaccurately because of the inherent difficulties of handling the large riprap stones, especially when they are being placed underwater. There are two main methods of placement—end dumping, where the riprap is tipped off the back of a truck, and individual placement by grab, where each riprap stone is positioned individually. Individual placement is more costly, but results in a more effective riprap blanket. These placement methods are illustrated in Figures 5-22 and 5-23.

5.6.6 Prior Laboratory Experiments on Riprap Protection of Abutments

Relatively few laboratory studies of abutment scour protection have been conducted. Notable studies are those conducted



Figure 5-22. End dumping of riprap (Smart, 1990).



Figure 5-23. Riprap placement by grab (Smart, 1990).

by Pagan-Ortiz (1991), Macky (1986), Atayee (1993), Croad (1989), and Eve (1999).

Pagan-Ortiz (1991)

Pagan-Ortiz made laboratory-flume measurements of flow velocities near model abutments and observed the stability of riprap protection placed on the bed surrounding the abutment—that is, in the region where a launching apron would be sited. A vertical wall abutment and a spill-through abutment were modeled. The riprap was placed directly on the floor of the flume, rendering the study essentially a fixed-bed investigation—that is, scour did not occur at the abutment. Therefore, the study is useful in determining the likely position in which riprap, placed in an apron around an abutment, will first fail while the riverbed remains level. This information is useful only until a scour hole begins to develop, at which time the flow regime changes, and riprap in other positions of the apron may become unstable.

The tests were carried out under clear-water conditions, with V/V_{cs} values of approximately 0.9, where V is the mean approach-flow velocity and V_{cs} is the threshold value of V . The spill-through abutment was 116.9 cm (46 inches) wide and 25.4 cm (10 inches) high, as shown in Figure 5-24. The length of the model abutment varied from 63.52 cm to 101.63 cm in increments of 12.70 cm.

The experiments were conducted in a 21.34-m long by 1.78-m wide rectangular flume with glass walls. The abutment model was placed against the side wall of the flume and surrounded by an observation area consisting of a gravel bed

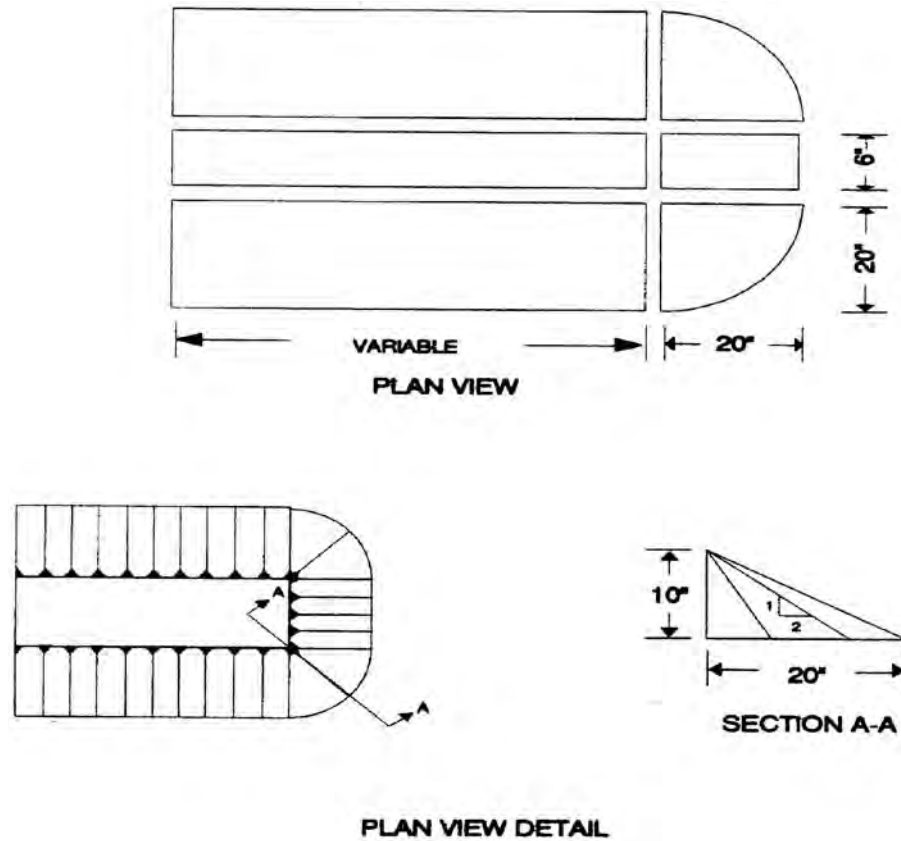


Figure 5-24. Diagram of spill-through abutment model (Pagan-Ortiz, 1991).

placed on the floor of the flume. The gravel-covered observation area spanned the width of the flume and extended for 1.78 m of the length of the flume, with equal areas upstream and downstream from the abutment model. Gravel sizes of 7.6 mm and 10.2 mm were used. Experiments were performed to determine the location of the vulnerable zone for initial failure and critical condition for displacement of gravel. Flow conditions were those to simulate 100- and 500-year return period floods, the latter based on FHWA recommendations.

The significant findings from this study are as follows:

- For a spill-through abutment, the initial failure zone begins at the armored floodplain downstream of the contraction near the toe.
- For a wing-wall abutment, the initial failure zone occurs at the upstream corner of the abutment.
- The rock riprap apron should be extended along the entire length of the abutment, both upstream and downstream, and to the parallel face of the abutment to the flow.
- It is reasonable to limit the rock riprap apron to a relatively small portion of the contraction at a bridge crossing

because the velocity amplification decays rapidly with distance from the toe of the abutment.

- Equations 5-D and 5-E in Table 5-5 were recommended for sizing riprap at vertical-wall and spill-through abutments, respectively.

Macky (1986)

Macky undertook laboratory experiments under clear-water conditions ($V/V_{cs} = 0.9$) to compare the effectiveness of different methods of protecting bridge abutments, using an idealized scale model of an actual bridge (Waiharakeke River Bridge). Bridge piers with 20-m spans were included in the model. Alternatives to riprap protection were examined because of the high cost of riprap in some parts of New Zealand.

Rock riprap, concrete akmon units (commonly used at coastal sites), flexible concrete mattresses, gabions laid on the abutment slope, stacked gabions staggered up the abutment slope, and boulder-filled wire mattresses laid on the bed sediment with stacked gabions above were tested in the study.

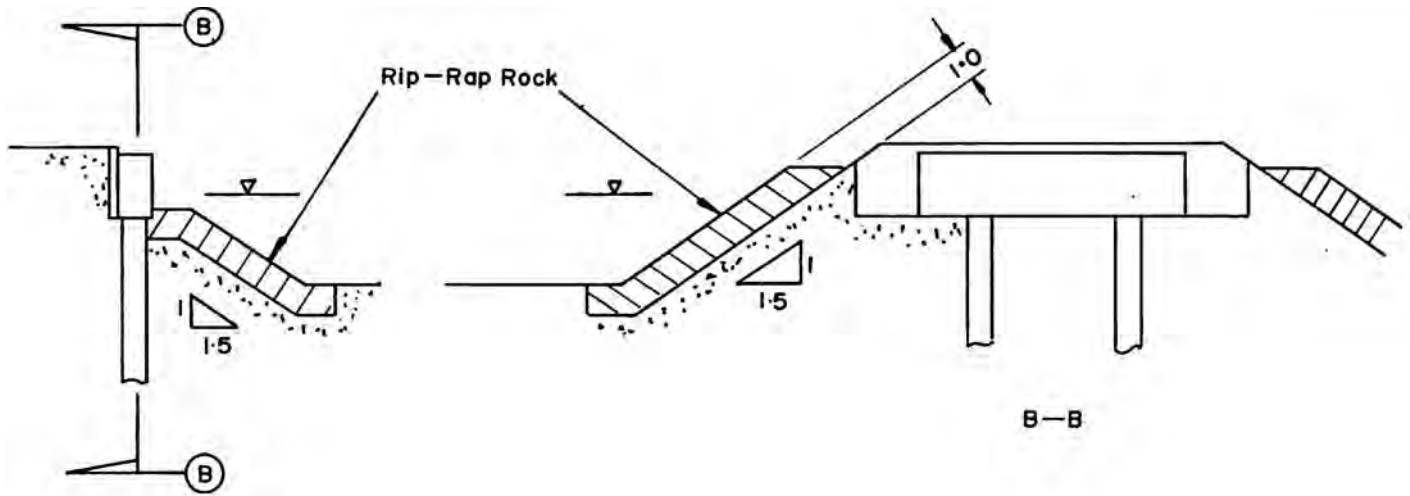


Figure 5-25. Riprap placement used by Macky (1986).

The tests were conducted to simulate typical construction practice rather than recommended construction practice. Thus, the protection measure was terminated at a level slightly below the existing bed levels. This differs from recommended practice, according to which the protection material should be placed to cover the entire face of the scour hole that is expected to develop.

The riprap was placed upon an abutment constructed of the bed sediment material. The configuration used to test typical riprap practice is illustrated in Figure 5-25. It is noted that the riprap terminates at the abutment toe without an apron.

Macky observed that the flow conditions at the start of the testing period were characterized by very high velocities near the front face of the abutment, especially the upstream corner. Sediment was rapidly eroded from this region, and several rocks were lost from the riprap layer. Over time, the abutment face slumped to a gentler slope that became stable.

Despite being undermined, the riprap continued to protect the abutment structure. The protected slope slumped considerably, which enabled a stable, flatter abutment slope to be formed, which was armored by the riprap. A stable scour hole was attained with the abutment substantially undamaged.

The principal findings from this study are as follows:

- While the downstream side of the abutment requires nominal protection only, the upstream corner of the abutment in particular is subject to strong attack and requires protection not only above the existing bed but also down the slope of the developing scour hole.
- The high initial velocities in some of the experiments caused damage, which could possibly have been avoided by pre-excavating the scour hole.
- The bridge pier adjacent to any abutment needs special protection because it can be sited in the abutment scour hole.

Atayee (1993)

Atayee studied the stability of a riprap apron using a model spill-through abutment situated on the floodplain of a compound channel (see Figure 5-26). The study was intended to build on that of Pagan-Ortiz (1991) by measuring the threshold of movement of the gravel material used to protect the floodplain and channel in the vicinity of the abutment. The hydraulic conditions that initiate gravel movement were measured.

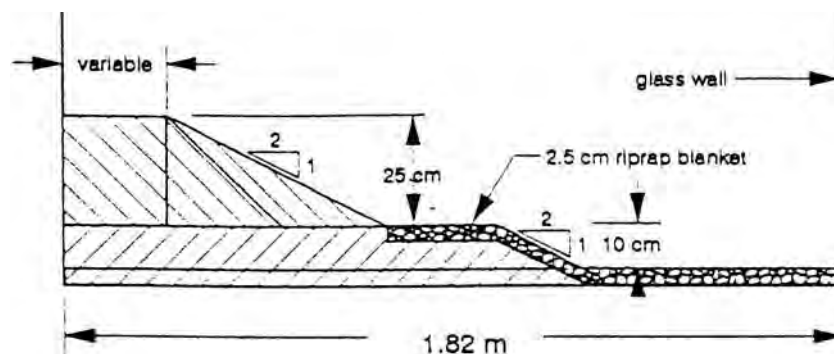


Figure 5-26. Atayee experimental setup (Atayee, 1993).

The abutment was 150 mm wide on an embankment 1.17 m wide, 0.25 m high, varying in length from 130 to 510 mm, with side slopes of 2:1 (H:V). Two sizes of uniformly graded gravels, with $d_{50} = 7.94$ mm and 11.11 mm, were used as model riprap. The riprap apron thickness was equal to two layers of gravel.

Atayee (1993) defined failure as occurring at the instant when the unprotected surface (in this case, the bed of the flume) was clearly exposed. Degradation of the gravel layer to expose the flume bed could happen very rapidly (in seconds). In all experiments, failure occurred at the toe of the embankment just downstream of the abutment centerline, as shown in Figure 5-27.

Croad (1989)

As a follow-up study to Macky (1986), Croad investigated the performance of riprap protection in pre-excavated scour holes under clear-water conditions ($V/V_{cs} = 0.95$). Results were compared with two cases not involving a pre-excavated scour hole: (1) riprap placed down to just below the initial bed level and (2) riprap placed down to the initial bed level with a launching apron.

A spill-through abutment, formed from the bed sediment, was used (Figure 5-28). A model bridge foundation was placed in the model and protected using riprap.

The flume used for the experiments was 10.6 m long and 2.0 m wide. The tests were run for 24 hours with a flow depth of 75 mm. The experiments used a uniform bed sediment with a mean sediment size of 2.2 mm and riprap material with a mean stone size of 18 mm.

Croad does not define his criterion for "Degree of Damage." Photographs included in the report suggest that the degree of damage is related to the amount of sediment removed from the abutment around the model foundation.

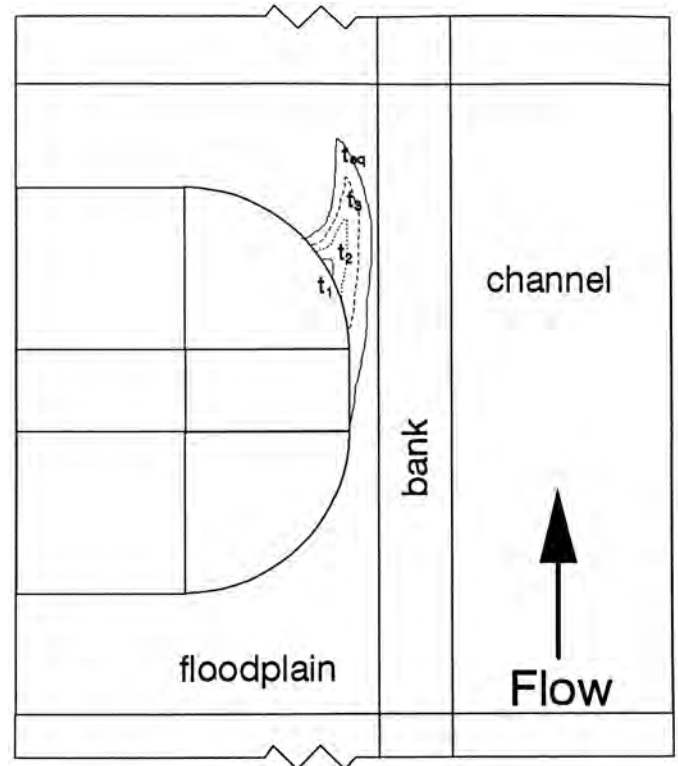


Figure 5-27. Typical riprap failure zone (Atayee, 1993).

Examples of slight, moderate, and severe failure for Croad's tests are shown in Figure 5-29.

Croad concluded that pre-excavation of the scour hole that is expected to develop at an abutment is effective in reducing the amount of damage to the abutment and riprap protection at the abutment. The pre-excavated scour hole needs to be aligned around the upstream corner of the abutment, and the riprap protection needs to extend to the bottom of the pre-excavated hole.

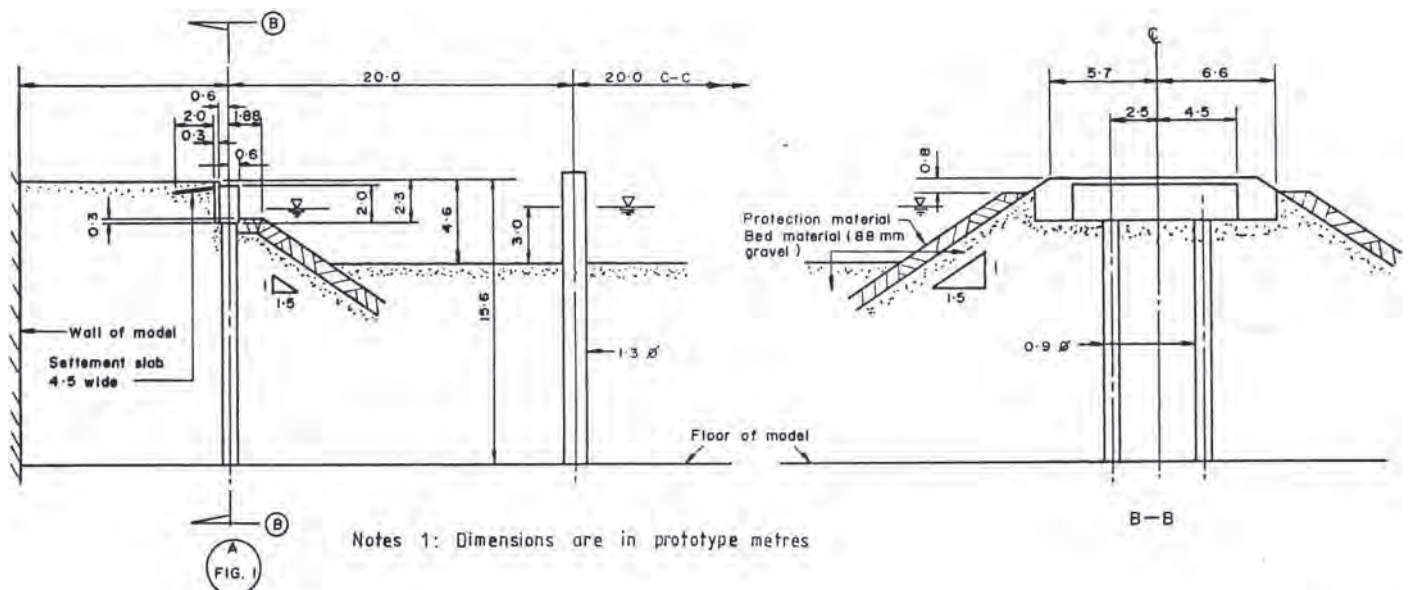
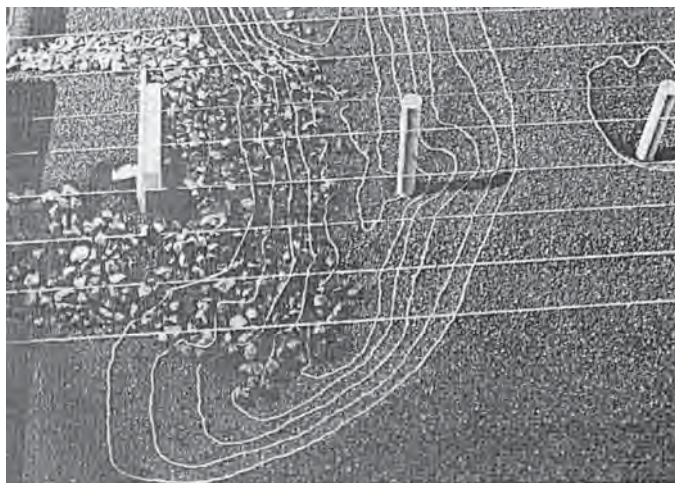
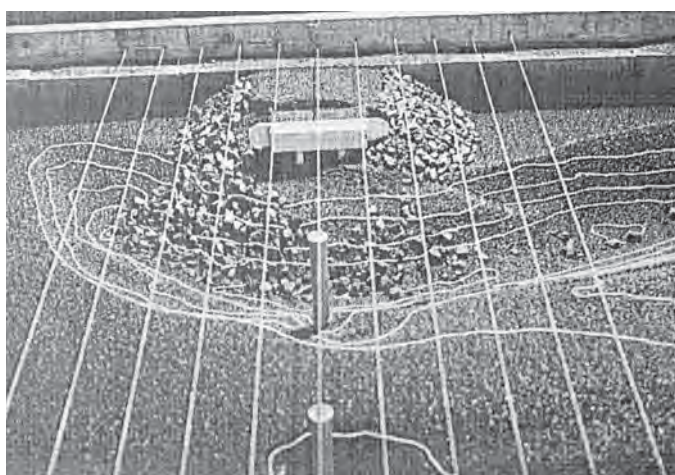


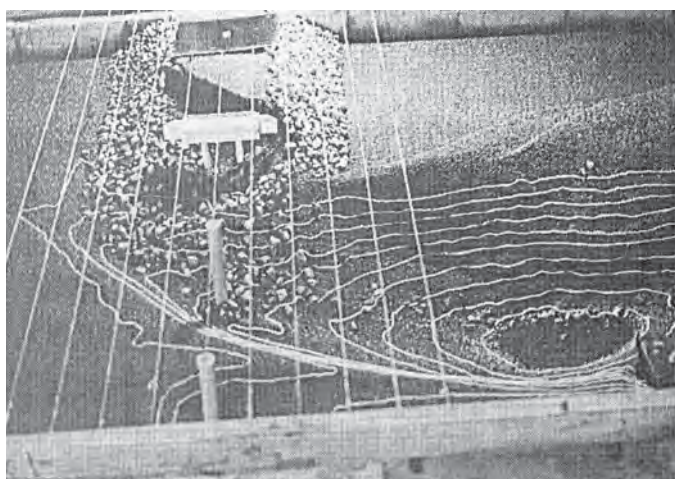
Figure 5-28. Bridge abutment and pier model, scale 1:40 (Croad, 1989).



(a) Slight failure



(b) Moderate failure



(c) Severe failure

Figure 5-29. Examples of slight, moderate, and severe failure (Croad, 1989).

Eve (1999)

Eve studied criteria for selection of riprap protection at spill-through bridge abutments with launching apron protection under clear-water and live-bed conditions. The size of the riprap and the extent of the launching apron were varied systematically in the tests. Experiments were run for 24 hours, at the end of which the abutment was assessed for failure. The abutment embankments were constructed using the bed sediment material.

Three failure conditions were defined:

- **Total failure**, where large-scale movement of sediment and riprap occurred on the abutment slopes. The abutment fill material slumped and large areas of sediment were exposed.
- **Partial failure**, where the movement of riprap and sediment was initiated in one part of the embankment, but did not result in a change of the embankment slope as a whole. Partial failure was typically observed at the water level, where a few riprap stones would be displaced and would move down the slope, and at the base of the slope if undermining of the toe occurred.
- **No failure**, where no change was observed in the embankment slope and the riprap stones did not move.

Examples of each failure type are shown in Figure 5-30.

For the clear-water tests, two abutment lengths and three riprap sizes were used. Eve measured the position at which the maximum scour depth occurred in all experiments. Generally, the point of maximum scour moved away from the toe of the abutment as the size of the launching apron and riprap stone size increased, as expected.

The lateral extent of the riprap launching apron was initially set at twice the flow depth, based on the HEC 18 recommendations (Richardson and Davis, 1995). This criterion was found to be conservative in all cases. For subsequent experiments, the lateral extent (as defined by θ , ϕ , and W in Figure 5-20) was reduced in increments until failure occurred. Eve (1999) proposed Equation 5-19 on the basis of these tests.

The live-bed experiments were conducted at 125 and 150 percent of the threshold velocity for the bed sediment. These tests were preliminary in nature, and Eve recommended further study under live-bed conditions. In all cases, the riprap failed rapidly, apparently because of winnowing of bed sediment through voids between the riprap stones. Some of the tests were repeated with the addition of a filter fabric, which was found to improve the stability of the protection, especially at the lower flow velocity. At the higher flow velocity, the abutments failed, in spite of the presence of the geotextile, because of undermining of the



(a) Total failure



(b) Partial failure



(c) No failure

Figure 5-30. Examples of clear-water failure criteria defined by Eve (1999).

abutment toe, which led to slumping of the sediment beneath the filter fabric.

Three types of failure were observed in the live-bed tests:

- **Catastrophic rapid failure**, which occurred without a geotextile where the embankment fill material was rapidly winnowed from between the riprap stones, leading to disintegration of the structure.
- **Slumping failure**, where the abutment failed due to exposure of the underlying geotextile at the abutment toe, allowing the embankment fill material to slump beneath the geotextile. Exposure of the geotextile at the toe of the embankment slope exacerbated the failure process.
- **Riprap failure**, where the riprap layer failed, but the embankment remained intact at the end of the test.

5.7 Cable-Tied Blocks

Cable-tied blocks consist of concrete blocks or slabs interconnected with metal or nonmetal cables. The cables used can be fabricated from steel, copper, or synthetic materials, such as polypropylene (Pzedwojski et al., 1995). An example of cable-tied blocks is given in Figure 5-31.

A key feature of cable-tied blocks is the interconnecting of small units, which may be unstable as individual blocks, into a framework capable of withstanding much higher flow velocities. The term is used typically to describe relatively small units. Articulated concrete mattresses, which rely on the same principles, are larger units commonly used for bank protection.

Previous studies and experiments on the use of cable-tied blocks for scour protection of bridge foundations are limited and are focused on bridge piers (McCorquodale et al., 1993; Bertoldi and Jones, 1994; Jones et al., 1995; Parker et al., 1998). McCorquodale et al. (1993) conducted an experimental investigation of the use of cable-tied blocks for protection of bridge piers (see Figure 5-32). They studied concrete blocks in the shape of truncated pyramids, interconnected by stainless steel cables. Their clear-water tests indicated that, in

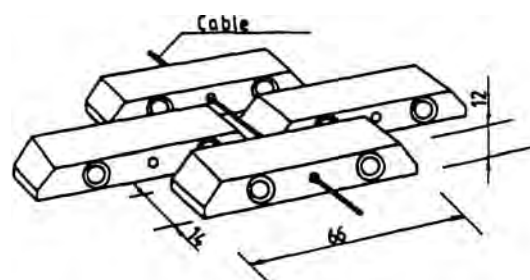
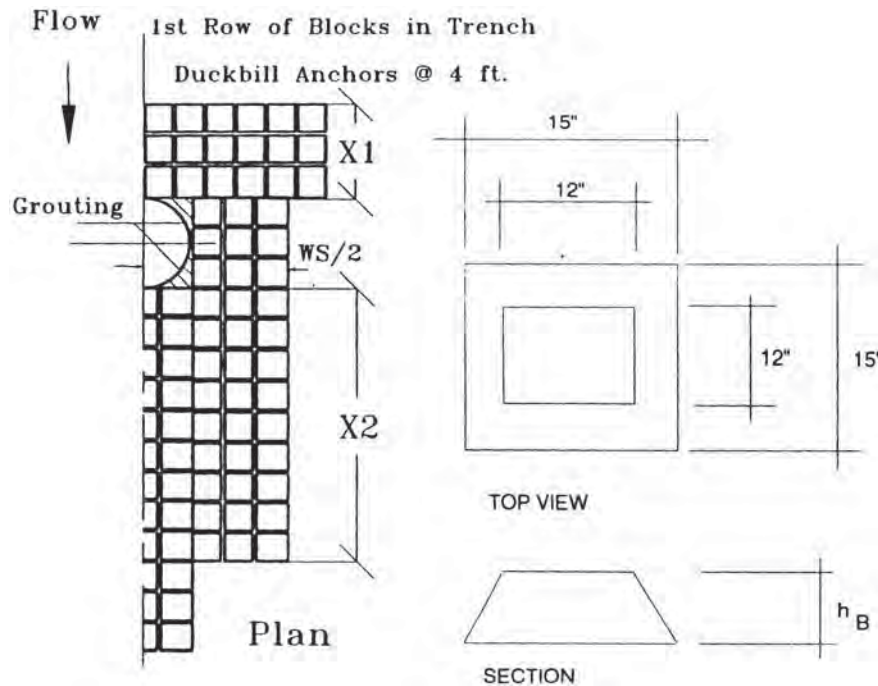


Figure 5-31. Cable-tied blocks used as bank protection (Pzedwojski et al., 1995).



Reprinted with permission from ASCE.

Figure 5-32. Scour protection using cable-tied blocks (McCorquodale et al., 1993).

the absence of a filter layer, the underlying sediment could be entrained by the winnowing process. Subsequent tests by Jones et al. (1995) and Parker et al. (1998) confirmed the need for filter layer protection.

Escarameia (1995) conducted a series of experiments with cable-tied concrete blocks in a highly turbulent environment. A block mat containing rectangular concrete blocks with vertical holes was used for the tests. The blocks were joined using horizontal cables running through two cable ducts in each block. An interlocking effect was achieved as the blocks were joined in a staggered fashion. Results of testing indicated that collapse was more easily reached under rapid flow conditions than under highly turbulent flows and that the amount of tension applied to the block mat did not appear to have a strong effect on the stability of the mattress. Higher stability was achieved when the cable direction was transverse, rather than parallel, to the main flow direction.

Escarameia (1995) recommended the following equation for selecting block size for cable-tied blocks with similar geometric characteristics to those tested:

$$D_n = C \frac{1}{(S_s - 1)} \frac{V_b^2}{2g} \quad (5-20)$$

Where:

V_b = velocity defined at 10 percent of the water depth above the bed;

S_s = specific gravity of sediment;

D_n = design diameter of the cable-tied blocks; and

$C = 0.05$ for $TI \leq 0.43$ and

$= 1.79 TI - 0.72$ for $0.43 < TI \leq 0.90$; and

TI = turbulent intensity defined at 10 percent of the water depth above the bed.

Choi et al. (2000) investigated the potential to use “G-blocks,” a type of cable-tied block available in Korea, as scour protection at bridge piers. Two types of G-block were tested, as shown in Figure 5-33. The G2 blocks are designed to be tied by U-bolts in one direction and to be self-interlocked in the other direction, whereas the G3 blocks are tied using U-bolts in both directions. Generally, the G-blocks were found to be more stable than the equivalent weight of riprap stone. Plots of critical block weight, W_{CR} , for stability in terms of mean flow velocity, U , are shown in Figure 5-34.

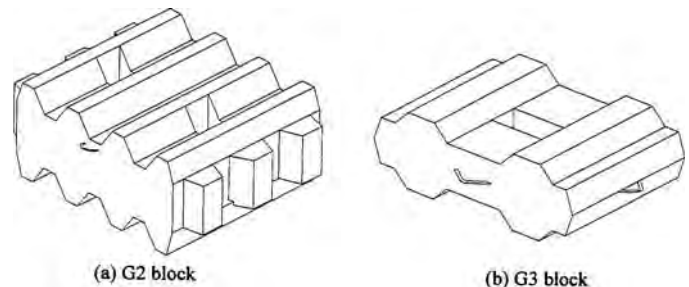


Figure 5-33. G-blocks tested by Choi et al. (2000).

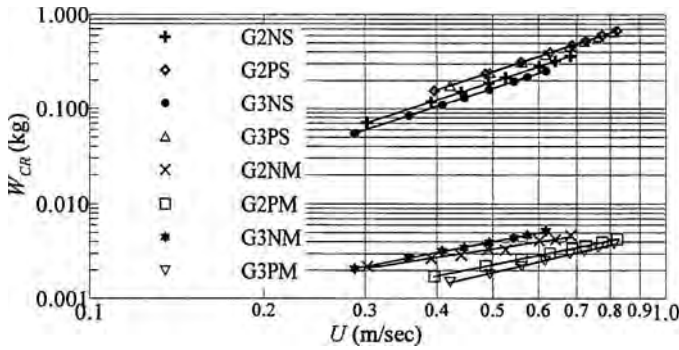


Figure 5-34. Stability of G-blocks tested by Choi et al. (2000).

Parker et al. (1998) identified three possible failure mechanisms:

- Overturning and rolling up of the leading edge, which is exacerbated if the edge is not anchored;
- Uplift of the center of the mat, which typically occurs in cases where the edge is not adequately anchored; and
- Winnowing of sediment between the mat and the bridge pier, which typically occurs if the mat is not sealed tightly to the pier.

Also, Parker et al. (1998) identified six instances of the use of cable-tied blocks as bridge pier protection in the United States. They also noted the significant use of an articulated concrete mattress—using very large, flat concrete slabs—as bank protection by the U.S. Army Corps of Engineers. More recently, various cable-tied block mattress configurations have been developed by a number of manufacturers for erosion protection, including flood-control protection works, bank stabilization, and erosion protection at outfalls.

The extensive laboratory investigation by Parker et al. (1998), as part of NCHRP Project 24-7, demonstrated that cable-tied blocks can be designed to be a highly effective countermeasure against scour at piers. Parker et al. proposed the following relation for design of cable-tied block mattresses at bridge piers, which indicates that the concrete block units can be smaller than riprap:

$$\zeta = 0.20 \frac{\rho_{cb}}{\rho_{cb} - \rho} \rho V^2 \quad (5-21)$$

Where:

- ζ = weight per unit area of the mattress,
- ρ = fluid density,
- ρ_{cb} = density of the concrete blocks, and
- V = approach-flow velocity.

The height of concrete blocks, H_{cb} , and the volume fraction pore space in the mattress, p , are related to ζ as follows:

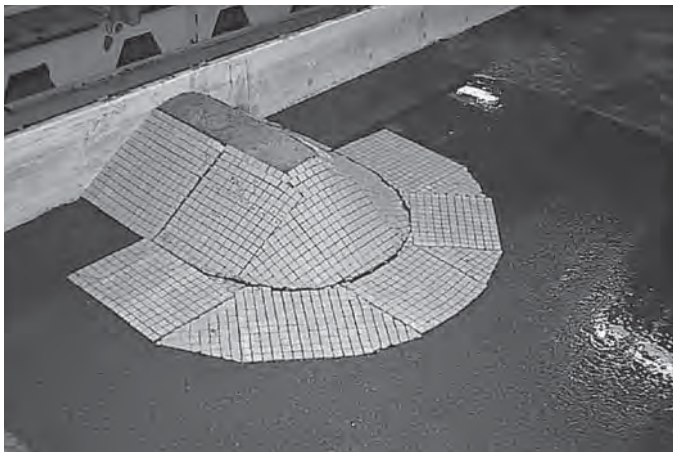
$$\zeta = \rho_{cb} g H_{cb} (1 - p) \quad (5-22)$$

Parker et al. (1998) assessed the use of cable-tied blocks for pier protection to be feasible in sand and gravel-bed streams, but not for rivers with large cobbles or rock, and made the following recommendations for their use:

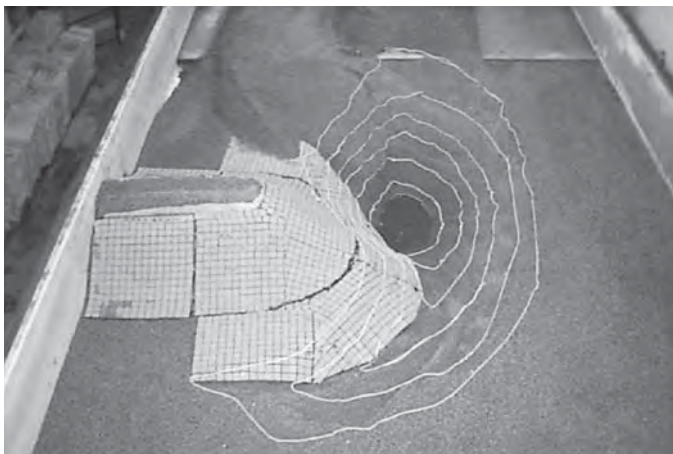
- **Spacing between cable-tied block units:** make spacing adequate to allow the mattress a sufficient degree of flexibility.
- **Cable material:** use stainless steel cable for harsh environments, given the critical nature of cable durability. Where galvanized cable is used, it should be single-strand galvanized.
- **Mattress size:** Make mattress length = $L_p + 3B/\cos\beta$, mattress width = $4B/\cos\beta$, in which L_p is pier length, B is pier width, and β is pier skewness to the flow.
- **Geotextile filter:** use it in sand-bed streams, but not in gravel-bed streams.
- **Geotextile size:** make length = $L_p + 2B/\cos\beta$, width = $3B/\cos\beta$.

Additionally, Parker et al. (1998) undertook an extensive field survey of countermeasures at bridge sites throughout the United States. They reported two instances of concern related to U.S. Army Corps of Engineers' designed cable-tied block installations. Galvanized cables at the I-880 crossing of the Guadalupe River in San Jose, California, had rusted between the inner strands in spite of detailed design specifications. At another site, where cable-tied blocks were installed to prevent erosion downstream from a grade-control structure, geotextile matting beneath the cable-tied blocks had pulled away from the edge of the grade-control structure, allowing the blocks to be undermined.

Hoe (2001) undertook preliminary tests of the use of cable-tied blocks to protect bridge abutments. The model spill-through abutment was constructed from the bed sediment (0.85-mm uniform sand) using the same mold as that used by Eve (1999). Ceramic tiles—measuring 25 mm square and about 5 mm thick and with specific gravity about 2.1—were used to model the blocks. The tiles were joined together by gluing them onto a flexible, loose-weave net fabric. Tests were conducted under clear-water conditions with and without the use of a geotextile filter. Figure 5-35 shows before and after photographs of a typical test, which incorporated a filter and was conducted at $V/V_{cs} = 0.66$ (where V_{cs} is the critical velocity for bed sediment movement), with flow depth = 150 mm. In spite of significant scour development, the spill-through slope remained stable at the end of the experiment (a 24-hour duration).



(a) Prior to testing, looking from upstream



(b) After testing, looking from upstream

Figure 5-35. Laboratory test of spill-through abutment protection using cable-tied blocks, Hoe (2001).

5.8 Geobags

Geobags can be used in lieu of riprap stone or other armor cover, such as cable-tied blocks, that in certain regions can be difficult and expensive to obtain. The potential advantages of the geobags are that they are readily transported (when empty), they can be filled with local sediments and soils (sometimes concrete), and they can be formed to a range of sizes—geobags can be tailored to fit specific application situations (e.g., Pilarczyk, 2000; and Heibaum, 2002, 2004). Geobags, however, rarely have been used as a scour countermeasure to prevent erosion or scour of the abutments of bridges spanning rivers and streams.

Geobags, also called geosynthetic containers, are quite commonly used as an erosion countermeasure in various applications, but have seen limited application for bridge abutments. Small geobags are extensively used during land-development activities to protect exposed soil against erosion.

Geobag use is quite common for coastal engineering applications (e.g., Ray, 1977; Pilarczyk, 2000; and Heibaum, 2002, 2004) and as temporary protection against scour at exposed banks and embankments in river channels. Geobags are especially useful for containing and protecting exposed soil during earthwork construction projects. They are also especially useful for use during repair or renovation work. Figure 5-36 shows geobags used to form and protect a bridge abutment that had experienced scour damage.

Geobags are sized in accordance with a design method proposed by Pilarczyk (2000). The method estimates a geobag's thickness, D_B . The aerial extent of a geobag should exceed D_B and otherwise can be sized for handling ease or to fit a site. The general form of Pilarczyk's relationship for geobag thickness is as follows:

$$D_B = \frac{0.035 \phi_{st} K_T K_h V^2}{(S_{SB} - 1) \theta_C K_{sl} 2g} \quad (5-23)$$

Where:

- S_{SB} = specific gravity of the geobag,
- V = depth-averaged mean velocity,
- g = gravity acceleration,
- ϕ_{st} = stability parameter,
- θ_C = critical value of the Shields parameter for particle (geobag) entrainment,
- K_T = turbulence factor,
- K_h = depth parameter, and
- K_{sl} = slope parameter in which

$$k_{sl} = \sqrt{1 - \left[\frac{\sin^2 \alpha_b}{\sin^2 \theta_C} \right]} \quad (5-24)$$



Figure 5-36. Geobags form and protect a bridge abutment that had recently experienced damage owing to abutment scour.

Where:

α_b = angle of the boundary on which the geobag is placed and

θ_c = angle of repose of the sediment forming the boundary.

For the experiments, α and θ were 26.7 and 30 degrees, respectively. Pilarczyk (2000), who gives the background to Equation 5-24, recommends for geobags that ϕ , θ_c , and K_T be 0.75, 0.05, and 2.0, respectively. The depth parameter K_h is defined as a function of water depth, y , and equivalent roughness k_s . Pilarczyk (2000) suggests using $k_s = D_n$. However, since D_n is unknown initially, the measured thickness of the geobag sample was used as a trial value. The required thickness of the geobags, D_n , was calculated as 22 mm, using a bulk-specific gravity of the model geobags measured to be 1.46.

Several investigators studied the stability of geobags as a slope-protection unit in coastal applications (Ray, 1977; Jacobs and Kobayashi, 1983; Gadd, 1988; Pilarczyk, 1998). Pilarczyk (1990) provided an empirical equation for stability of revetment material under flow attack. His formula can be used for different materials—such as riprap, geobags, geomattresses, gabions, and block or block mats—using different coefficients provided for each material.

Placing geobags, geosynthetic bags filled with sand, as an abutment countermeasure has an important advantage compared with riprap. A geobag is less prone to winnowing of the fine underlying bed sediment particles. To overcome winnowing failure of riprap, geosynthetic or granular filters are used in combination with riprap, commonly when riprap is used as a scour countermeasure. However, laying filters is difficult to control in practice, especially in flowing water. Geobags do not require filters and, therefore, are relatively easy to place. Moreover, the size and weight of individual bags are solely the discretion of the designer, and one can always design large enough geobags so that they can resist shear erosion. Figure 5-37 shows several arrangements of geobags.

As is discussed above, there are distinct advantages of using geobags as an abutment countermeasure over its riprap counterpart. However, before one can use geobags, a confirmation of their performance and suitable deployment is needed.

5.9 Other Forms of Armoring

Besides riprap and cable-tied blocks, various other forms of armoring have been used to protect bridge abutments against scour. Frequently, the other forms of armoring have entailed the use of large elements, notably Toskanes, dolos, and large blocks of concrete or rock. Figure 5-38 depicts the use of large concrete blocks (locally termed hedgehogs), linked together by cables to armor the channel bank immediately upstream of an abutment. The channel bed in front of the abutment is armored with large, hinged concrete slabs.



Figure 5-37. Geosynthetic containers: bag (top), and mesh with plant openings (bottom) (Heibaum, 2002).

diately upstream of an abutment. The channel bed in front of the abutment is armored with large, hinged concrete slabs.

Burns et al. (1996) developed Toskanes as an alternative scour countermeasure where riprap is not feasible. Results of model studies and design guidelines are presented. Ruff et al. (1995) used Toskanes to protect bridge piers.

Adams et al. (1999) used reinforced soil by bridge abutments, but they concluded that reinforced soil is not suitable for permanent bridges in scour zones.



Figure 5-38. Heavy hinged slabs and cable-tied blocks (termed hedgehogs) used to protect a bridge abutment on an ephemeral river.

CHAPTER 6

Lab Results I: Preliminary Experiments

6.1 Introduction

This chapter presents observations and data from sets of brief, preliminary laboratory experiments conducted to evaluate scour countermeasures for protecting abutments. The experiments were carried out using small-scale replicas of a simple abutment form: a wing-wall abutment extending at a depth into a cohesionless bed of a rectangular channel. As mentioned at the outset of this report, wing-wall abutments are commonly used for short bridges, such as those that span relatively narrow channels. Given the large number of small bridges, especially in the U.S. Midwest, the great majority of abutment failures have occurred for small single- or double-span bridges that commonly have wing-wall abutments. Accordingly, it was thought useful to expend laboratory effort exploring the responses of such abutments to various scour countermeasure concepts.

In most cases of subsequent bridge repair, and increasingly for the design of new bridges, it is usual to consider use of a protective armor layer placed to prevent erosion of the channel bed and bank around abutments. Also, to a lesser extent, consideration is given to wing-wall angle and abutment alignment (relative to the channel crossed) to minimize scour. Adjustment of angle and alignment would seek to minimize local flow velocities and turbulence in the vicinity of the abutment, thereby reducing scour. The experiments focused chiefly on the use of armoring countermeasures and to a lesser extent on flow-altering countermeasures. The experiments investigated the performance of armor elements, aprons of riprap and geobags placed around pile-supported wing-wall abutments retaining erodible embankments, and subject to clear-water flow conditions. Also investigated were the influences of wall angle and abutment alignment on scour depth.

In particular, the exploratory experiments investigated the following questions:

- Are there simple configurations of large armor units that could be an effective scour countermeasure method for wing-wall abutments?

- Can aprons of smaller armor units or riprap be used as a scour countermeasure for wing-wall abutments, and, if so, to what extent should a riprap apron extend around a wing-wall abutment?
- How do large geobags perform as an alternative to riprap or cable-tied blocks for preventing abutment scour?
- How does the wing-wall angle of an abutment affect scour depth?
- How does the abutment alignment to a channel affect scour depth?

The findings to these questions consist of general observations and small-scale laboratory data about armor unit, riprap, and geobag performance at small bridges.

6.2 Program of Experiments

In accordance with the set of questions enumerated above, the program of exploratory experiments consisted of the following four series of experiments:

- Experiments on the scour countermeasure effectiveness of large blocks,
- Experiments on the use of large geobags,
- Experiments on the scour influence of wing-wall angle, and,
- Experiments on the influence of abutment alignment on scour depth.

The experiments were heuristic (i.e., trial-and-error discovery) and exploratory in nature. They were carried out using a simple wing-wall abutment to explore the efficacy of using large armor units as a scour countermeasure. The units consisted of two sizes of concrete block, one or more large geobags, and a combination of large geobag and riprap stone.

The use of large armor units held particular practical initial appeal because such large blocks would not be moved by the flow and because their roughness and bulk would redirect

flow partially. Also, placing and positioning blocks around an abutment would seem relatively practicable, even in flowing water.

The test armor units were tried in various combinations and layout extents to gage the sensitivity of scour development and depth with respect to the placement and location of individual large armor units. The experiments were heuristic, involving considerable adjustment and exploration of armor unit placement. Only a representative overview of the experiment results need be mentioned herein. The experiments are fully documented by Martinez (2003).

6.3 Use of Large Blocks

6.3.1 Experiment Layout

A simplified configuration of wing-wall abutment was used for the experiments, which were all conducted using a laboratory flume at the University of Iowa. The overall layout and dimensions of the flume are given in Figure 6-1, which also indicates the location of the test region in the flume. A sand-roughened false-floor approach conveyed flow to the sediment recess making up the test section. The test abutments were placed in the sediment recess region. An overall view of the flume is shown in Figure 6-2, which also depicts the sediment recess.

The preliminary experiments were done under conditions of clear-water scour, with $u_*/u_{*c} = 0.8$, where u_* is the shear

velocity and u_{*c} is the critical value of the shear velocity associated with bed-particle movement. The main hydraulic parameters for the flume flow were the following: mean velocity, $V_0 = 0.55$ m/s; and flow depth, $Y_0 = 0.10$ m. The sediment parameters were the following: median particle size, $d_{50} = 0.45$ mm; standard deviation of sediment size, $\sigma_g = 1.4$; specific gravity of particles = 2.4; and the angle of sediment repose, $\alpha_r = 30$ degrees.

Similitude between laboratory experiments and field scale was satisfied by the use of the aforementioned u_*/u_{*c} ratio, of which a value of just below 1.0 represents a condition called “clear-water scour.” This condition is extreme for scouring because the velocity is as high as possible without the movement of the channel bed, which causes infilling of the sediment hole.

The layout and dimensions of the wing-wall abutment used are given in Figure 6-3. The abutment was made of a simple approximate form, in keeping with the exploratory nature of the preliminary experiments. The figures indicate the layout extents of the armor units placed around the test abutments.

Also indicated in Figure 6-3 are the two locations where scour depth was greatest. Point A is at the face of the abutment, and Point B is somewhat downstream of the abutment. A consequence of extensive armoring of the bed around the abutment was that the location of deepest scour was forced downstream.

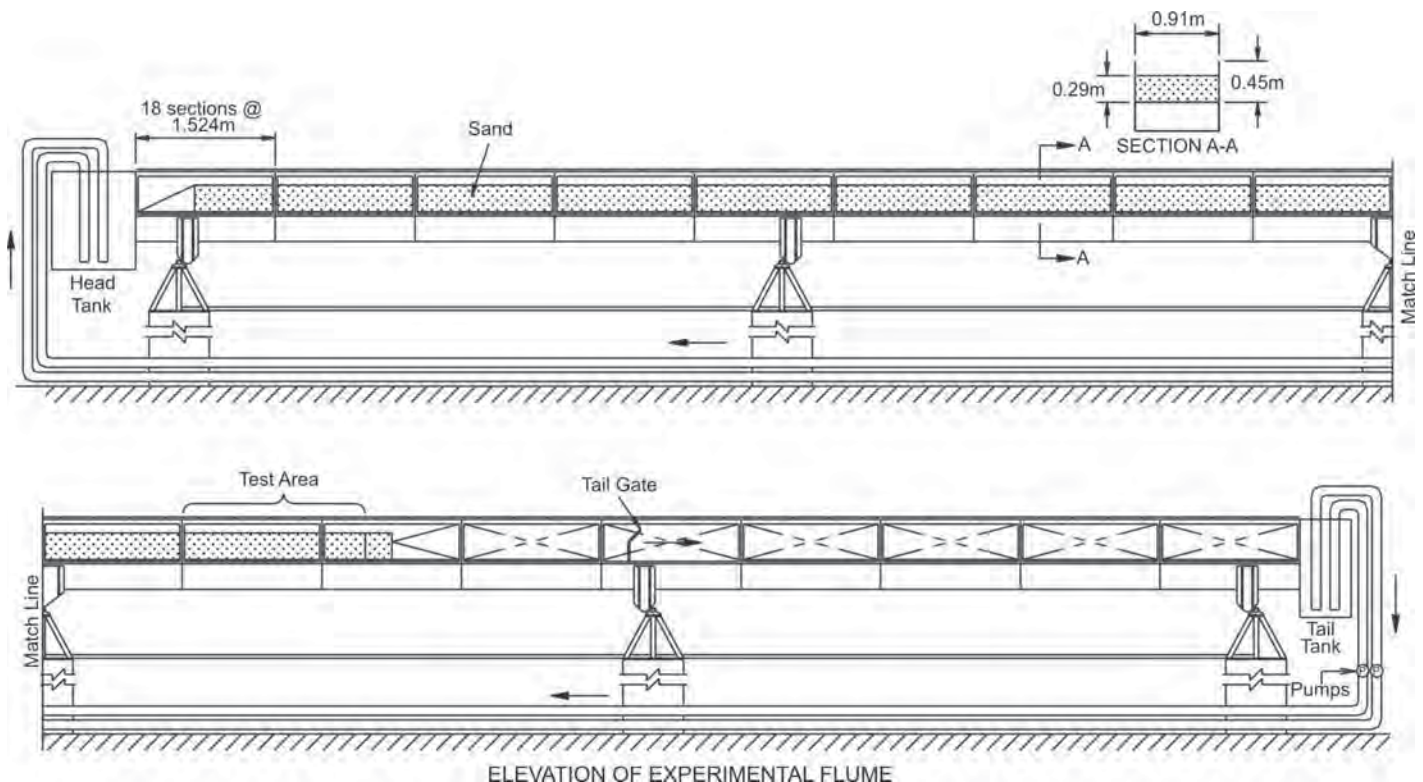


Figure 6-1. Layout and dimensions of the flume, including the false floor and sediment recess.



Figure 6-2. View of the sediment flume.

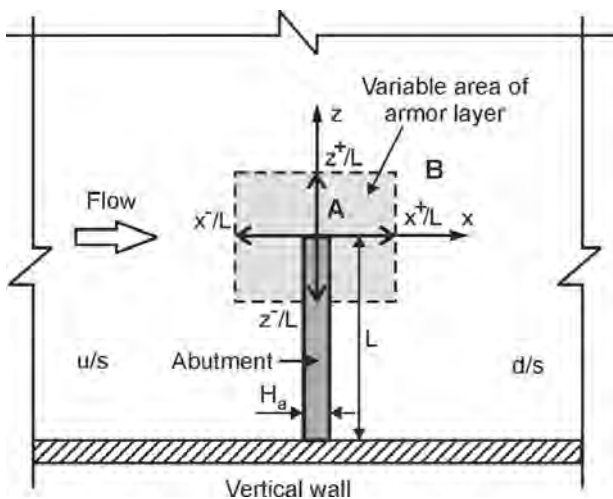


Figure 6-3. Layout and dimensions of simple wing-wall abutment used in preliminary experiments, $L = 160 \text{ mm}$, $H_a = 32 \text{ mm}$.

Two sizes of blocks made of cement and sand were tested in the flume: blocks with 22-mm side lengths and blocks with 11-mm side lengths. The specific gravity of the blocks was estimated as 2.30. The blocks were placed in different arrangements to investigate as a scour countermeasure.

6.3.2 Observations

The experiments showed that single large individual armor units, or ensembles of blocks (or such units as dolos and tetrapods), alone, are of limited effectiveness as a scour countermeasure. Scour of the bed sediment around the armor units diminished armor unit effectiveness as a scour countermeasure. Figure 6-4 shows the scour that formed around the wing wall without a countermeasure. Figures 6-5 and 6-6 show before-and-after photos of the 22-mm blocks and 11-mm blocks, respectively. Table 6-1 lists the scour depths from three of the experiments. Without the presence of the blocks, a scour depth (ds_{A0}) of 140 mm developed at the face of the abutment (Point A).

Flume observations showed that edge erosion of bed sediment occurred around the blocks, caused the formation of a local scour hole around each exposed block, and that the block subsequently slid into the scour hole. As water flowed past the blocks, vortices were shed, which entrained bed sediment from around the blocks. Bed sediment particles were winnowed through the gaps of the overlying concrete blocks, causing the local scour hole to expand in area and eventually envelop the blocks.

The placement of concrete blocks reduced scour depth at the abutment. Ten large concrete blocks (of side length 22 mm) that were placed around the abutment as shown in Figure 6-5 reduced the scour depth by 32.2 percent compared with the baseline scour depth at the unprotected

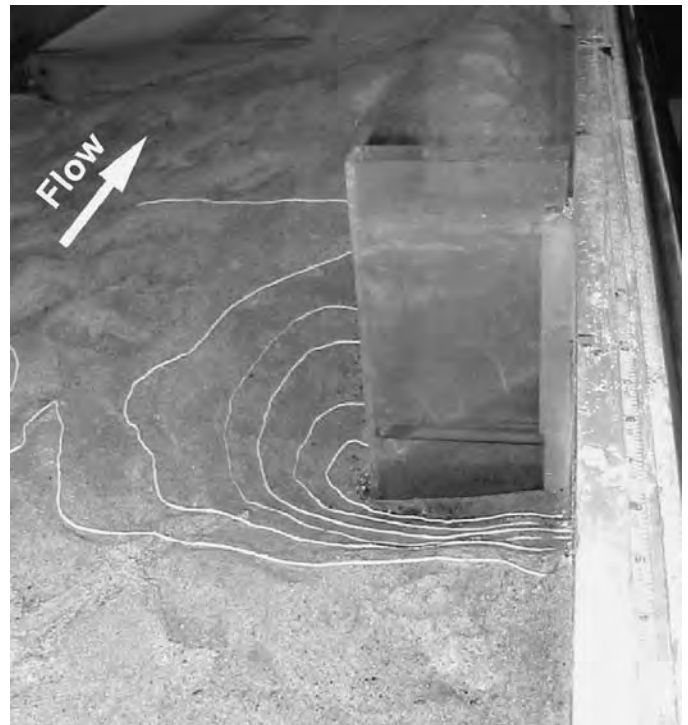
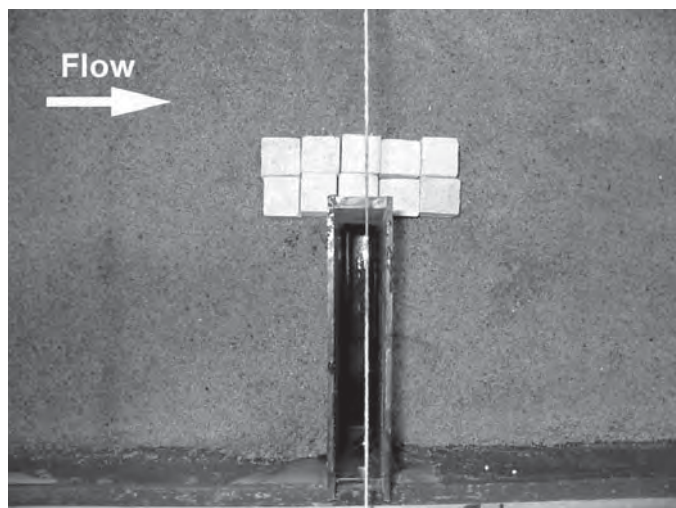
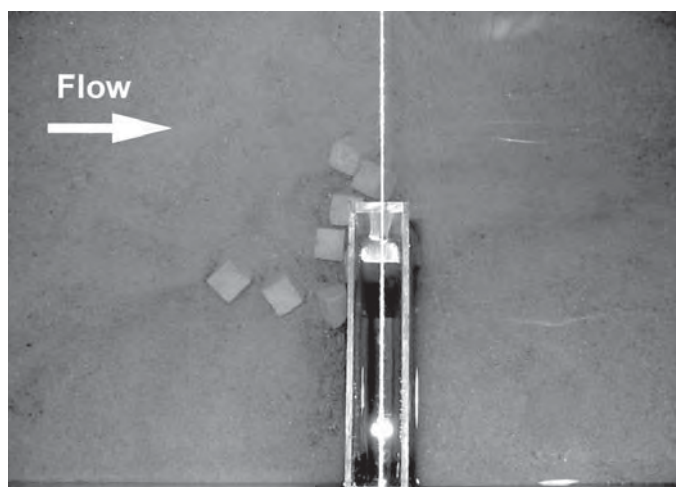


Figure 6-4. View of scour hole formed at wing-wall abutment.



(a) At start of experiment

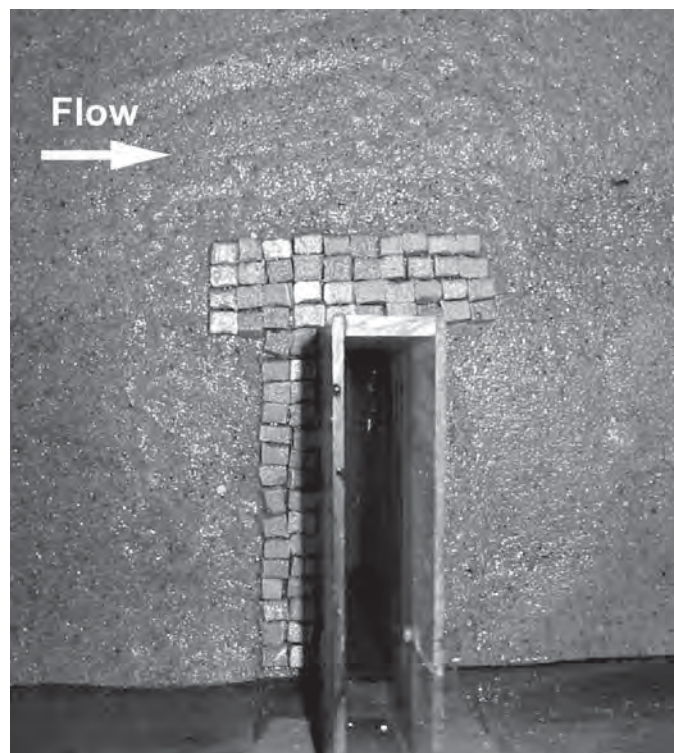


(b) At end of experiment

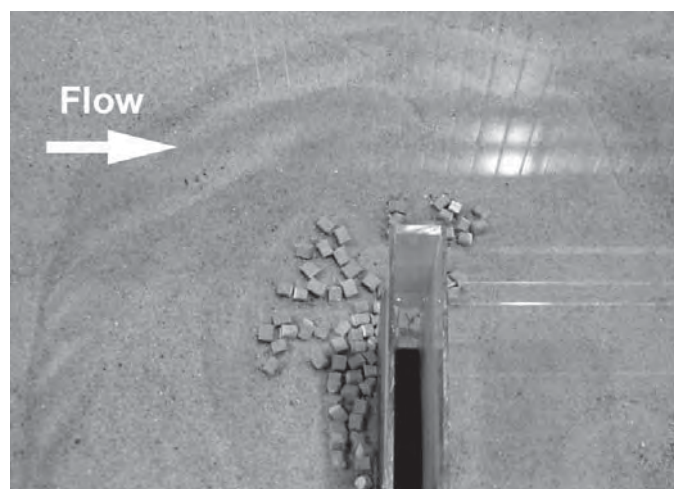
Figure 6-5. Experiment with large (22-mm) blocks placed at front of wing-wall abutment.

abutment. The large blocks, acting as exposed large elements, produced locally increased flow velocities and turbulence, such that bed sediment readily scoured from around the blocks. In due course, the scour hole developed around the abutment, and the blocks gradually slid toward the base of the scour hole.

An important finding is that the smaller concrete blocks (of side length 11 mm) covering the same area as the large blocks performed essentially the same in reducing scour depth. The equilibrium depth of scour was identical to that conducted with large concrete blocks. In other words, provided that the blocks were not entrained by the flow, block size is less important than the extent of bed covered and the presence of a filter-cloth underlay to reduce the winnowing of bed sediment. A critical consideration that emerges from the experiments is that the size of the block



(a) At start of experiment



(b) At end of experiment

Figure 6-6. Experiment with small (11-mm) blocks placed at front of wing-wall abutment.

chosen must be large enough to resist shear erosion, yet small enough to substantially reduce any winnowing of bed-form sediment.

To demonstrate the influence of aerial coverage on scour depth, two additional rows of the smaller (11-mm) blocks were placed upstream of the abutment and perpendicular to the flow direction, thereby increasing the coverage. The arrangement is shown in Figure 6-6. This experiment showed that ds_A was reduced by 60 percent. The reduction

Table 6-1. Local scour depths at wing-wall abutment with concrete blocks.

Layout	X^+/L	X^-/L	Z^+/L	Z^-/L	ds_A (mm)	ds_A/ds_{A0} (%)
No blocks	0	0	0	0	140	100.00
10 blocks $a_1/L = 0.13$	0.33	0.33	0.27	0	94	67
40 blocks $a_1/L = 0.13$	0.33	0.33	0.27	0	94	67
70 blocks $a_2/L = 0.07$	0.33	0.33	0.27	1	56	40

ds_A = scour reduction at the abutment with scour countermeasure.

ds_{A0} = scour depth at the abutment without scour countermeasure.

in scour depth is attributable to the increased area of bed protection around the abutment. The placement of two rows upstream of the abutment helped to minimize erosion of bed sediment from around the leading edge of the abutment, thereby resulting in an enlarged extent of scour hole, but a shallower depth of scour. Furthermore, when the scour hole eventually developed fully around the abutment, the larger number of blocks provided greater coverage of the base of the scour hole, thereby reducing scour depth.

The two mechanisms of scour reduction explained above produce a much shallower scour hole. These experimental results agree with prior observations on riprap stones as a pier-scour countermeasure (e.g., Chiew 1995), where sufficient riprap stones could significantly reduce winnowing failure.

6.4 Use of Large Geobags

The main problems concerning the use of large armor units, such as concrete blocks, for scour reduction are the winnowing of bed sediment around blocks and edge erosion around the blocks. To reduce these problems, experiments were carried out to examine the use of a large geobag formed from geotextile fabric and filled with sand. A large geobag has

a flat profile and rounded edges, thereby reducing local acceleration of flow velocities around the geobag. Also, a large geobag essentially provides its own filter cloth base as well as acts as an armoring layer. A further possible advantage of a geobag is the prospect of making a geobag that conforms to a desired shape and size for particular abutment sites. Experiment-scale geobags of approximately equivalent weight were used as the large blocks and were sized as 90 mm × 70 mm × 18 mm. The geobags were densely filled with sand.

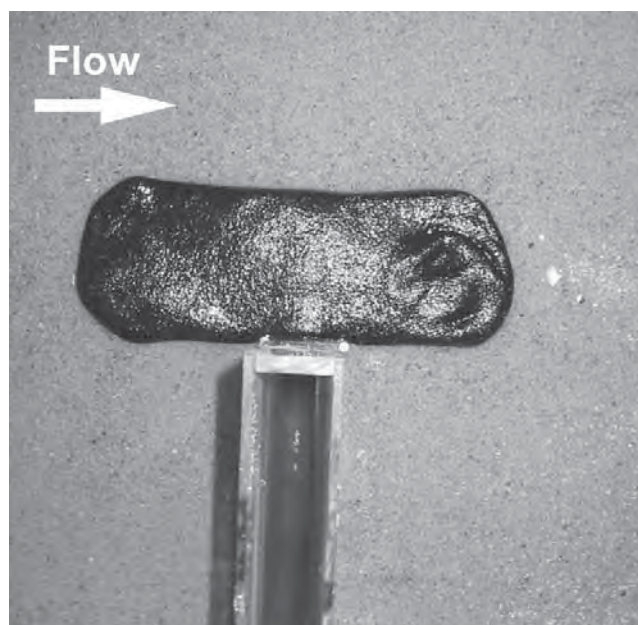
6.4.1 Observations

Table 6-2 summarizes the results of the test with a single large geobag. While winnowing erosion did not occur between the geobag and the abutment, edge failure remained an unresolved concern. Figure 6-7 shows the formation of a large scour hole adjacent to the geobag, into which the geobag slid. Note that the geobag setup in this experiment is hinged to the abutment; otherwise, it would have slid completely into the scour hole.

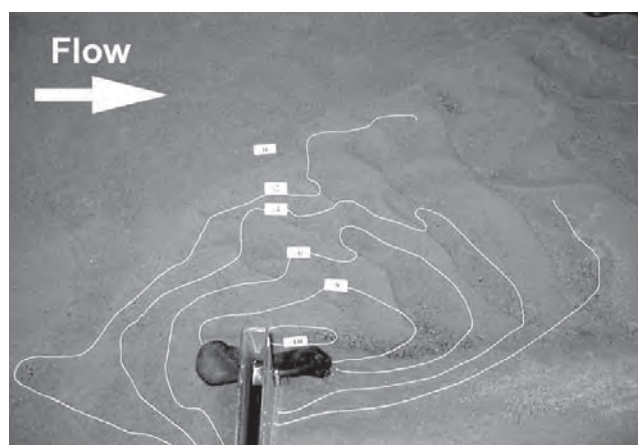
The experiment showed that, though the geobag protected the abutment, scour continued at a location shifted away from the abutment to a location downstream of the abutment. Accordingly, two values of scour reduction need to be considered: one at the abutment, ds_A , and the other at the

Table 6-2. Local scour depths at wing-wall abutment with geobag.

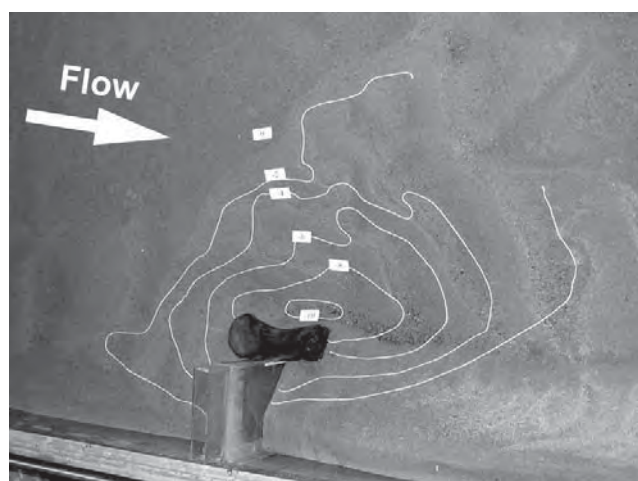
Layout	X^+/L	X^-/L	Z^+/L	Z^-/L	ds_A (mm)	ds_A/ds_{A0} (%)	ds_B (mm)	ds_B/ds_{A0} (%)
No bag	0.00	0.00	0.00	0.00	140	100	140	100
bag	0.69	0.69	0.50	0.00	84	60	102	73
bag+rock	0.69	0.69	0.50	0.00	60	43	102	73
bag	0.69	0.69	0.50	1.00	52	37	100	71
bag+rock	0.69	0.69	0.50	1.00	58	49	104	74
bag	0.69	0.69	1.00	1.00	0	0	112	80



(a) At start of experiment



(b) At end of experiment, view from above



(c) At end of experiment, side view

Figure 6-7. Experiment with a single large geobag placed at front of wing-wall abutment.

maximum deepest point of scour, ds_B . The values for these two locations were $0.40ds_{A0}$ and $0.27ds_{A0}$, respectively.

6.4.2 Geobag and Riprap Stone

In an effort to control edge erosion, simulated riprap stones (median diameter $d_{50} = 8$ mm) were placed around the geobag. Minor improvements resulted such that ds_{AR} at the abutment was increased from the original 40 percent to 60 percent, though the ds_B at the deepest point of the scour hole remained almost the same. Therefore, placing loose riprap stones around the geobag in order to prevent edge failure had marginal success. Figure 6-8 shows how the geobag was at risk of sliding into the scour hole.

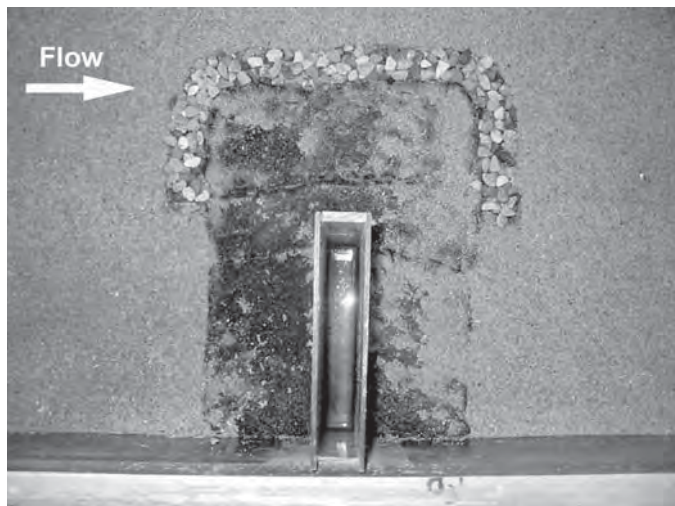
When the area of geobag protection was enlarged around the abutment so that the geobag covered the bed beneath the large-scale turbulence structures generated by flow around the abutment, the geobag completely prevented scour development at the nose of the abutment, but the scour hole downstream of the abutment persisted. A further experiment investigated whether the placement of riprap stones on the geobags would reduce the depth of the scour hole downstream of the abutment. The idea explored in this experiment was whether the riprap on the geobag would roll into the developing scour hole and consequently retard its deepening. The results from both tests show that the deepest point of the scour hole is about $0.48ds_{A0}$. No scour occurred at the nose of the abutment. While the formation of the scour hole downstream of the abutment seems to be unavoidable, the present test shows that armoring the bed would be able to control its development and protect the scour countermeasure.

6.5 Wing-Wall Abutment and Geobags

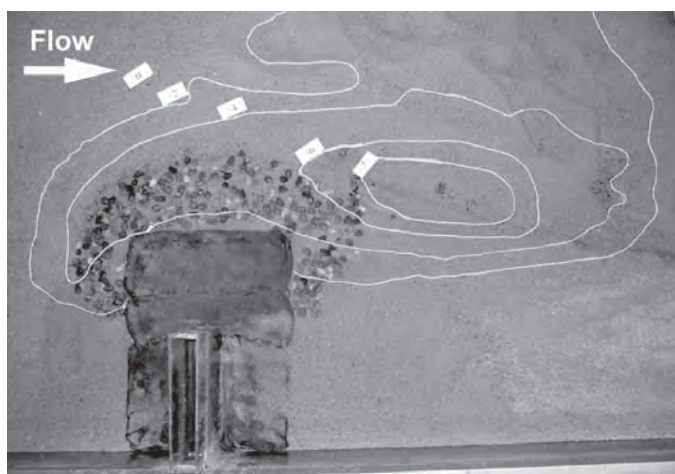
Experiments with a wing-wall abutment and geobags entailed the same flume conditions as those used for the experiments described in Section 6.3. However, now the abutment was of wing-wall shape. The wing-wall abutment form used for the experiment replicated, at a scale corresponding to approximately 1:40, the width of abutments typical of two-lane roads in the United States when the road width is about 12 m (40 ft). The abutment's wing-walls were set at an angle of 45 degrees. Figure 6-9 shows the dimensions of the model abutment used.

Table 6-3 shows the ratio among geometric variables as well as scour depths for four of the experiments conducted. The scour at the unprotected abutment is shown in Figure 6-10. Scour was deepest at the abutment face.

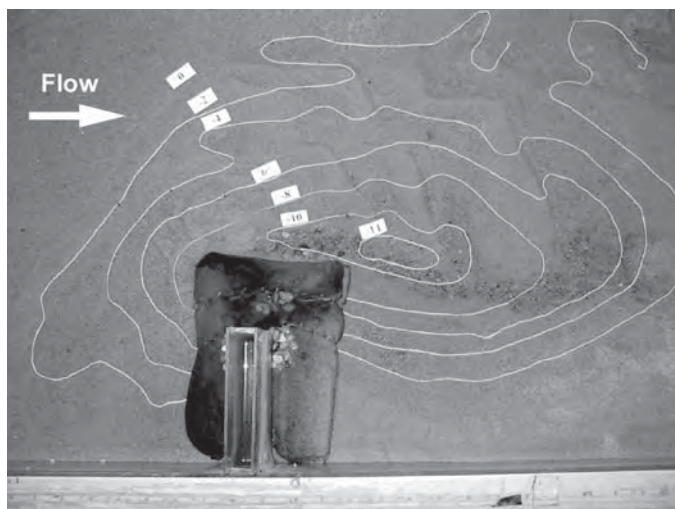
When a large geobag was placed around the wing-wall abutment, scour did not occur at the abutment face; that is,



(a) At start of experiment



(b) At end of experiment, view from above



(c) At end of experiment, side view

Figure 6-8. Experiment with a large geobag placed around the wing-wall abutment and with stone placed along geobag edges.

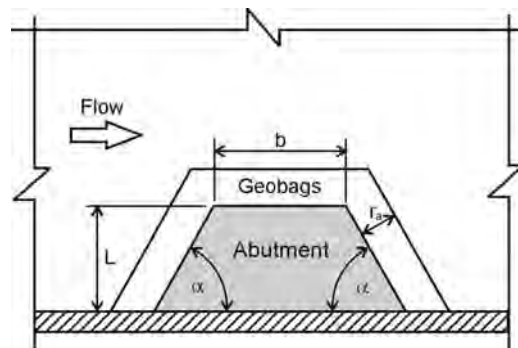


Figure 6-9. Dimensions of simple wing-wall abutment used in preliminary experiments; $L = 160$ mm, $b = 160$ mm, $\alpha = 45$ degrees, $r_a = 160$ mm, thickness of geobag layer = 20 mm.

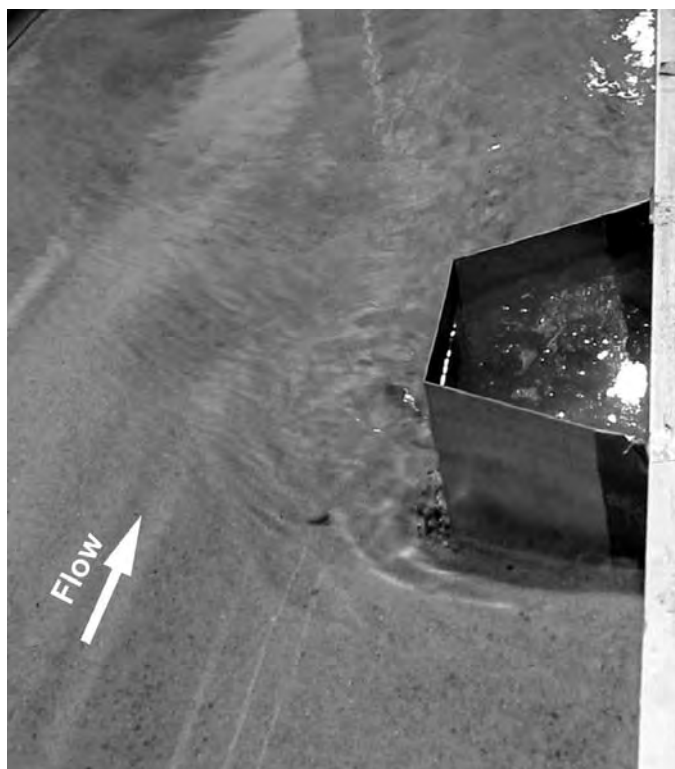
scour reduction was 100 percent ($ds_A = 0$). However, turbulence generated by flow around the abutment and over the geobag eroded the sand bed immediately downstream of the geobag, thereby shifting the scour and creating a deeper scour hole. Figure 6-11 depicts the initial state and the eventual scoured state of the bed. The erosion of the bed at the downstream edge of the geobag gradually propagated upstream around the edge of the geobag. It is noteworthy to point out that this process of edge erosion was observed to occur for all the experiments with geobags. The deepest scour hole for this experiments was $ds_B = 143$ percent of ds_{A0} . Its location is shown in Figure 6-11(b) and (c). As the scour hole reached the downstream edge of the geobag, an additional row of geobags was used to further reduce the scour. Figure 6-12 shows the initial condition and the eventual scour condition. Although scour was eliminated at the abutment, the scour hole immediately downstream of the abutment and geobags remained, though it was somewhat shallower. Figure 6-12 shows that the extra row of geobags diminished the erosion attributable to wake vortices. The maximum deepest scour was 119 percent of the scour depth at the unprotected abutment (ds_A).

In addition, when a fringe of riprap stone was placed around the geobags in an effort to limit edge erosion, the maximum scour depth was reduced further to 97 percent of ds_A . The stones provided partial armoring of the scour hole.

Dune-bed conditions pose the severest test for the stability of an armor cover, such as riprap or geobags, because the passage of dunes may dislodge portions of a cover. This certainly was found in the present study, and it is amply shown for efforts at armoring beds around piers (e.g., Chiew, 2000). It is of interest to note that existing guidelines for riprap design are based on laboratory experiments performed exclusively in clear-water scour and do not account for the dislodging effects of bed forms passing the riprap.

Table 6-3. Local scour depths at wing-wall abutment with geobag.

Test	Layout	ds_A (mm)	ds_A/ds_{A45} (%)	ds_B (mm)	ds_B/ds_A (%)
W1	no geobag	65	100	0	0
W2	1 geobag row	0	0	93	143
W4	2 geobag rows	0	0	77	119
W5	2 geobag rows plus stone at edge	0	0	63	97

**Figure 6-10. Scour development at the unprotected wing-wall abutment.**

6.6 Influence of Wing-Wall Angle

A series of experiments was conducted in which the wing-wall angle was varied. No additional scour countermeasure was used in these experiments. The angle α (Figure 6-13) was set at 15, 30, 45, 65, and 90 degrees to the flow.

Figure 6-13 and Table 6-4 show the resulting trends for the variation with α of equilibrium scour depth at the abutment, ds_A . The values of ds_A are normalized with ds_A obtained for the 90-degree wing wall (i.e., the vertical wall). Scour depths reduced as α decreased. As is to be expected, a smaller angle of wing-wall produces less velocity component normal to the wall. Consequently, the strength of the horseshoe vortex in the scour hole was reduced. Also, the intensity of wake turbulence was reduced. Figure 6-13 shows that the reductions in scour depth are substantial, at least for the length of abutment used in the experiments; for instance, the scour

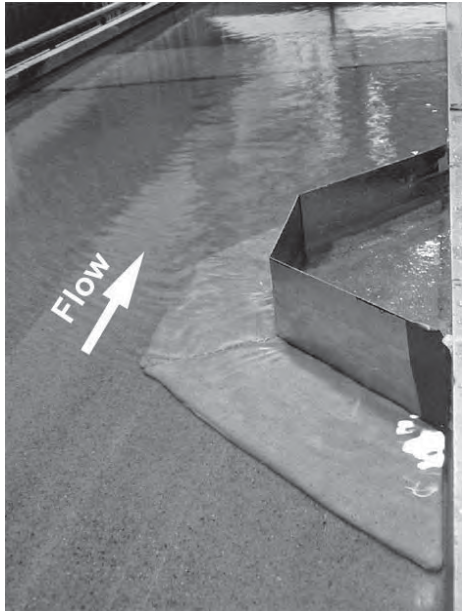
depth using a 15-degree wall angle was only 23 percent of the scour depth that developed for a 90-degree (vertical-wall) wing-wall abutment.

The findings on wall angle presented here indicate the scour-reducing merit of (a) decreasing the bluffness of an abutment's upstream profile and (b) streamlining the downstream profile to greatly weaken wake vortices. The findings do not necessarily imply that angling the approach of a wing-wall abutment produces the same extent of scour depth reduction, because the downstream side of an angled abutment may still produce strong wake vortices. Also, as pointed out by Dongol (1994), reducing the scour at one abutment by reducing its angle to the flow may aggravate scour at the opposite abutment on the river bank; the opposite abutment has an adverse angle to the approach flow. This concern, however, applies to long abutments that substantially contract the flow at a bridge crossing. It is not a concern that affects short abutments, such as wing-wall abutments.

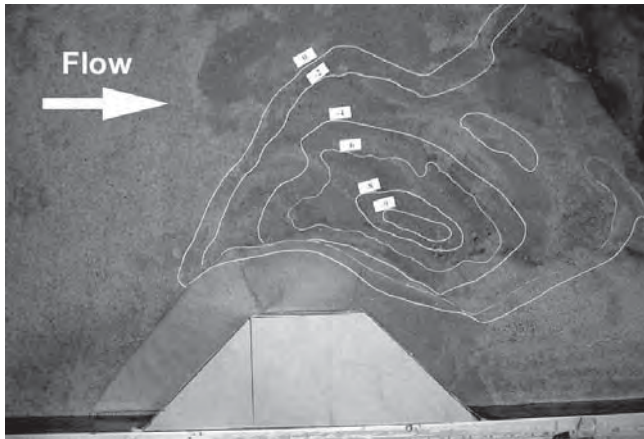
6.7 Influence of Abutment Alignment

A brief further set of exploratory experiments examined the influence of abutment alignment on scour depth. These experiments, conducted for the present study but using a different flume than that shown in Figure 6-1, are reported by Martinez (2003). The corollary question addressed by these experiments is whether scour depth is minimized or aggravated by aligning a bridge at some angle other than 90 degrees to a channel. The experiments were conducted with a thin wall replicating a simplified abutment.

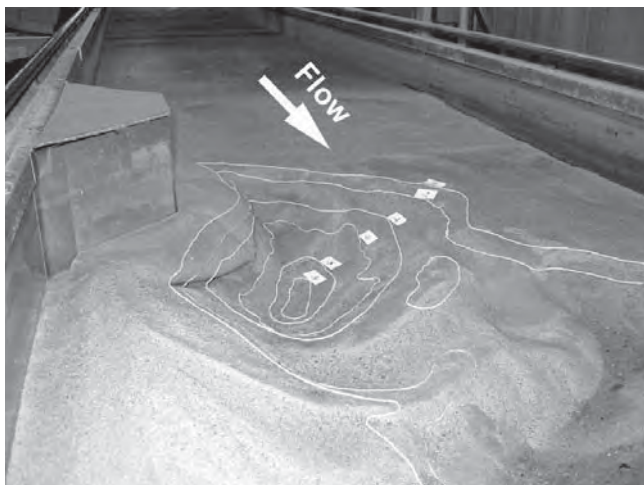
Figure 6-14 shows that the scour depth, ds_A , increased as alignment angle increased from 15 to 90 degrees, and then the scour depth decreased as the angle further increased from 90 to 150 degrees. The variation of ds_A with angle appears to be almost symmetrical for alignments upstream or downstream. For all angles, the deepest scour occurred at the end of the abutment. Dye observations from the present experiment indicate that the downflow and horseshoe vortices around the end of the abutment weakened as the abutment pointed upstream, as they also did when the abutment pointed downstream. These flow features play major roles in scour, and weakening them is one way to minimize scour.



(a) At start of experiment

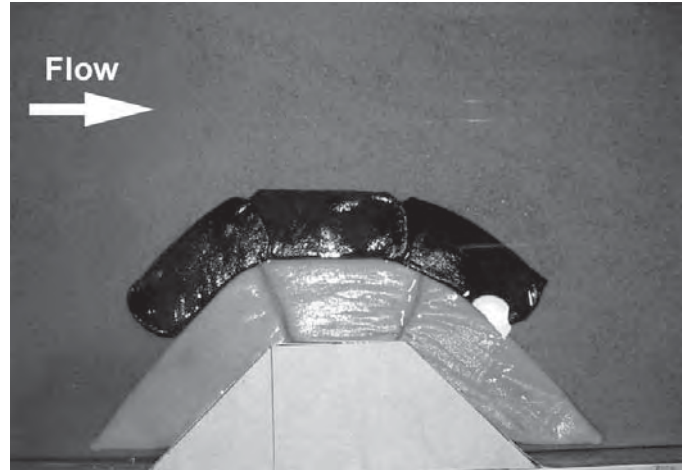


(b) At end of experiment, view from above

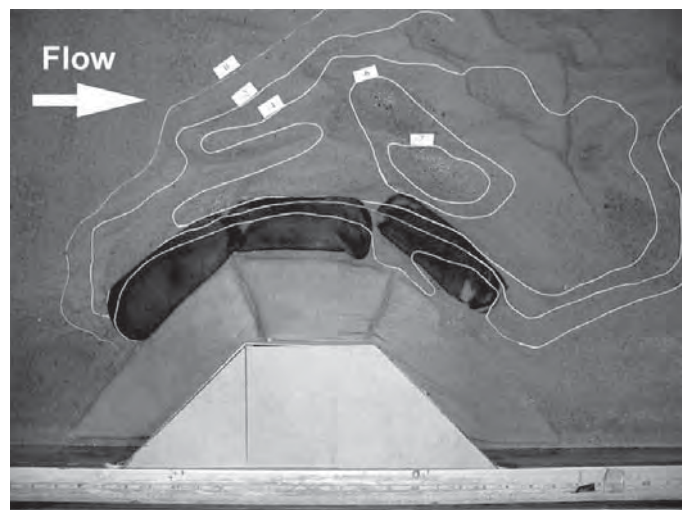


(c) At end of experiment, view from the side

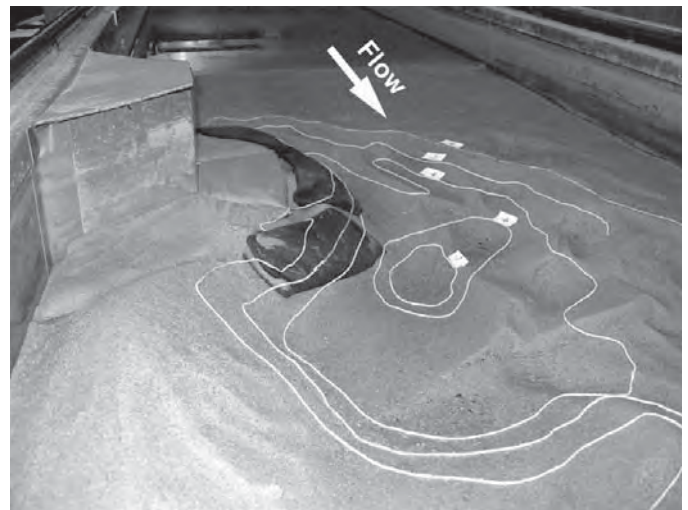
Figure 6-11. Experiment with a large geobag placed around the wing-wall abutment.



(a) At start of experiment



(b) At end of experiment, view from above



(c) At end of experiment, view from the side

Figure 6-12. Experiment with two rows of large geobags placed around the wing-wall abutment.

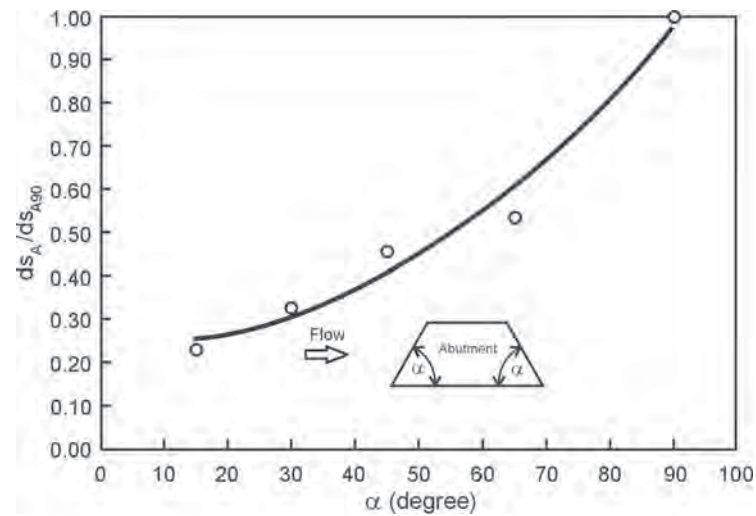


Figure 6-13. Influence of wall angle α on scour depth at a wing-wall abutment.

Table 6-4. Influence of wing-wall alignment on scour depth.

α (degrees)	ds_A (mm)	ds_A/ds_{A0} (%)
90	140	100.00
65	75	53.57
45	65	46.43
30	46	32.86
15	32	22.86

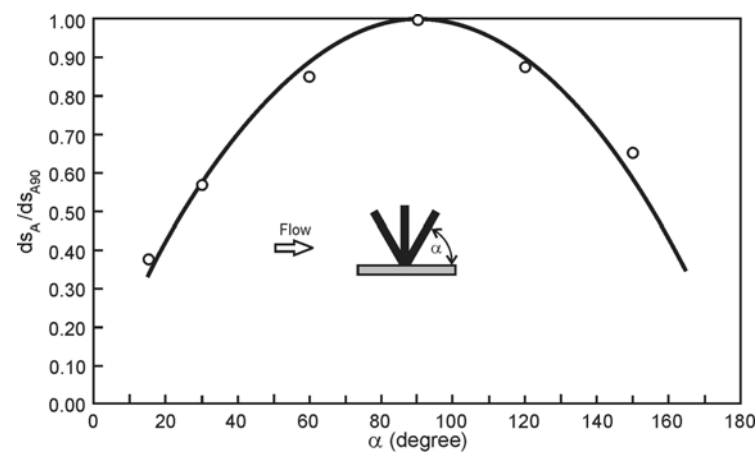


Figure 6-14. Influence of abutment alignment on scour depth at a wing-wall abutment.

6.8 Summary of Findings from Preliminary Experiments

The results from the preliminary experiments led to the following findings in answer to the questions posed at the outset of this chapter. The findings are of significance for the more detailed sets of experiments that were conducted subsequently for the project:

- Large concrete blocks placed around an abutment are insufficiently effective as a scour countermeasure for reducing scour depth at an abutment. The winnowing of the bed material from around the blocks enables scour to progress, though possibly not as deep as may occur if the blocks were not present. Sediment winnowing, edge erosion, and local scour around the blocks are processes that need to be addressed in order for armoring to function as an effective scour countermeasure.
 - Once a critical block size is attained (with respect to resistance to entrainment by flow), increasing block size does not result in reduced scour depth. Of greater importance than block size is aerial coverage of blocks. Smaller concrete blocks closely arranged were more effective than the larger blocks because they caused less winnowing of sediment.
 - A large geobag or a continuous mat of relatively small geobags holds promise of functioning as an effective scour countermeasure for wing-wall abutments when the mat extends over an area defined approximately as $r_a/L_a \geq 1$, where r_a is radial distance out from the end of the abutment and L_a is abutment length. Edge erosion remains a concern because the geobag is thick. However, edge erosion likely can be reduced by use of riprap stone, or smaller geobags, placed around the geobags.
 - The results obtained show that decreasing wall angle (from 90 degrees) to flow reduces the scour depth under either live-bed or clear-water scour conditions. Decreasing the wall angle at an abutment was observed to weaken down-flow and the horseshoe vortex. Accordingly, an approach-flow guide wall likely can be effective in reducing scour depth at a wing-wall abutment.
 - The brief ancillary experiments on scour at various alignments of abutment show that scour depth is a maximum when an abutment is perpendicular to the channel crossed.
-

CHAPTER 7

Lab Results II: Aprons at Wing-Wall Abutments

7.1 Introduction

The findings of the DOT survey presented in Chapter 4, the literature review presented in Chapter 5, and the preliminary experiments presented in Chapter 6 indicate that suitably positioned aprons of riprap, cable-tied blocks, or geobags hold promise as an effective scour countermeasure for wing-wall abutments. The present chapter investigates such aprons in further detail. Observations and data were obtained from a series of laboratory experiments. In particular, the experiments focused on the performance of riprap, cable-tied blocks, and geobags placed as an apron around pile-supported wing-wall abutments retaining erodible embankments.

Furthermore, the aprons were subject to live-bed flow conditions in which the channel bed was in a dune regime. It is of interest to note that existing guidelines for abutment apron design are based on laboratory experiments performed exclusively in clear-water scour and do not account for the dislodging effects of bed forms passing around or over an apron. In this respect, the findings from the experiments reported here are novel. The capacity of dunes to destabilize riprap, cable-tied blocks, or geobags around the edges of an apron poses a severe test of the stability of an armor apron formed from riprap, cable-tied blocks, or geobags. The present experiments showed that the passage of dunes may readily dislodge portions of a protective apron if the edges are not protected. This finding concurs with similar findings from efforts at armoring beds around piers (e.g., Chiew, 2000).

A further novel aspect of the experiments is the finding regarding the importance of protecting the embankment region beneath and immediately behind the pile cap of wing-wall abutments supported by piles. Heretofore, little diagnostic attention has been given to the manner whereby the earthfill embankment immediately behind a wing-wall abutment may erode when a scour hole develops.

Besides observations on the performance of cable-tied blocks and small geobags as riprap alternatives, the findings from the experiments include an evaluation of geobags used as a substitute for filter-cloth underlay to riprap. The findings also include a summary of the maximum scour depths associated with the baseline scour conditions, the use of a riprap or cable-tied blocks apron, and selections from the geobag arrangements tested. Design guidelines are given and include using current riprap configurations for sizing and placing geobags.

Two sets of experiments were conducted:

- **Use of riprap and cable-tied blocks for protection of an abutment sited near the bank of a narrow channel.** The aim of the experiment was to investigate the use of riprap and cable-tied blocks as wing-wall abutment scour countermeasures. Both riprap and cable-tied block aprons were placed around abutments to protect them from scour, which could potentially undermine the abutments if no protection were provided. A series of experiments were conducted with live-bed conditions. Flow depth, flow velocity, and apron extent were systematically varied for both protection types to determine the minimum required apron extent to sufficiently protect the abutment from scour. Different riprap sizes and apron burial depths were also investigated.
- **The use of geobags and riprap for protection of an abutment sited near the bank of a narrow channel.** The aim of this study was to determine whether an apron of geobags in addition to riprap, or without riprap, could be an effective countermeasure for wing-wall abutments. As geobags are relatively easy to transport and place, they hold promise as a potentially useful temporary armor material for use when riprap is not immediately available. Therefore, there is interest to determine if and how geobags may function in minimizing scour.

7.2 Experiments on Aprons of Riprap or Cable-Tied Blocks

This section describes the experiments conducted to determine the performance behavior of an apron of riprap or cable-tied blocks placed around a wing-wall abutment under live-bed conditions. The experiments were completed at the University of Auckland, New Zealand.

7.2.1 Experiment Layout

A 1.5-m wide, 1.2-m deep, and 45-m long recirculating flume was used to conduct the experiments. The flume is supported on two universal beams that are centrally pivoted so that the slope of the flume can be adjusted by electrically driven screw-jack supports at either end of the flume. The flume's channel consists of an inlet section, a 35-m long channel, and an outlet section. A false floor 0.4 m high was placed along the length of the channel section, with a 3-m long recess located 26 m downstream of the inlet section. Figure 7-1 shows the flume looking in the downstream direction, and Figure 7-2 shows a longitudinal cross section of the flume.

Water enters the flume at the base of the inlet section, and the sediment slurry enters the flume at the top of the inlet section. As the flow enters the inlet section, it passes through a wave skimmer that suppresses surface wave formation.

The floor of the channel section slopes up to the false floor height 0.4 m above the channel floor. The water and entrained sediment flow from the inlet section down the channel section of the flume and into the outlet section. The sediment entrained in the flow collects in the sand trap and is pumped back to the inlet section of the flume as a sand slurry using a 30-kW pump and a 100-mm diameter pipeline. The sediment-free water passes over the sediment trap and is pumped



Figure 7-1. The 1.5-m wide flume used for experiments on riprap and cable-tied blocks.

back to the inlet section of the flume through 250-mm and 300-mm diameter pipelines using 22-kW and 45-kW pumps, respectively. The pumps are controlled by variable-speed controllers that regulate the flow rate in the flume.

The flume is filled from the laboratory reservoir via an inflow pipe located at the back of the outlet section of the flume and is drained by an outlet valve in the bottom of the outlet section. During experiments, the water levels in the flume are controlled by an overflow pipe in the outlet section of the flume.

Model Channel and Abutment

A fixed floodplain 0.4 m wide was constructed along the length of the rectangular channel section of the flume, as shown in Figure 7-3. The floodplain was constructed from concrete blocks 240 mm high. The main channel bank was constructed from sheet metal glued to the concrete blocks on the floodplain and riveted to the false floor of the flume, with a side slope of 1:1 (H:V). The sheet metal lining the main channel bank was painted and sprinkled with sand to simulate the roughness of the sediment bed. Figure 7-4 shows the construction of the floodplain in the flume. The main channel and the recess were filled with bed sediment to a depth of 140 mm above the false floor level. This sediment allowed sufficient depth for the equilibrium bed forms to fully develop in the main channel along the length of the flume.

In order to generate appropriate flow velocities on the floodplain, it was necessary to increase the roughness. Rows of five evenly spaced $35 \times 35 \times 30$ mm roughness blocks were glued onto the floodplain with a row spacing of 400 mm along the entire floodplain (Figure 7-3).

A 600-mm wide Perspex wing-wall abutment model with a 45-degree flare angle was used for this study. Detailed dimensions of the wing-wall abutment are given in Figure 7-5. The abutment model protruded 150 mm into the main channel from the edge of the floodplain. The top of the abutment was placed 75 mm above the top of the floodplain. The abutment extended to the bottom of the recess in the flume and was fixed to the floor of the flume. The fixed main channel bank was extended down under the same angle (1:1) to the bottom of the recess and fitted around the abutment model. The edge of the sheet metal forming the main channel bank around the abutment was sealed onto the abutment.

A concrete embankment 75 mm high, 400 mm long, and 600 mm wide at the crest, with side slopes of 2:1 (H:V) was cast on top of the floodplain behind the abutment model. Figure 7-6 shows a photo of the embankment and the wing-wall abutment, with the sediment in the main channel leveled 100 mm below the top of the floodplain.

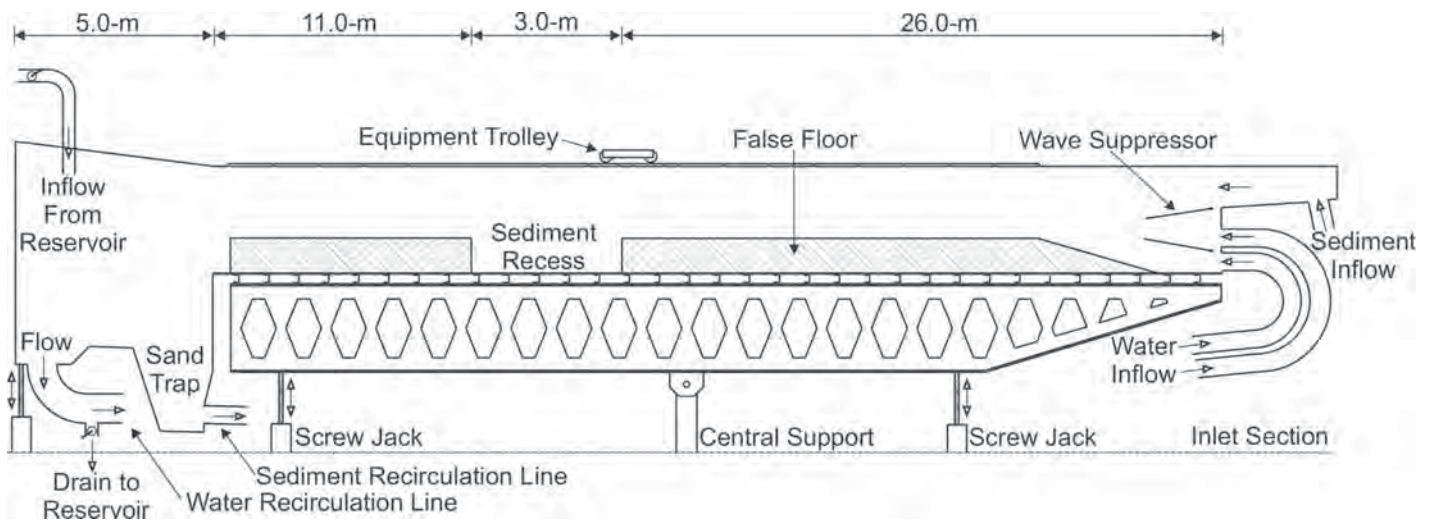


Figure 7-2. Dimensions of the 1.5-m wide flume.

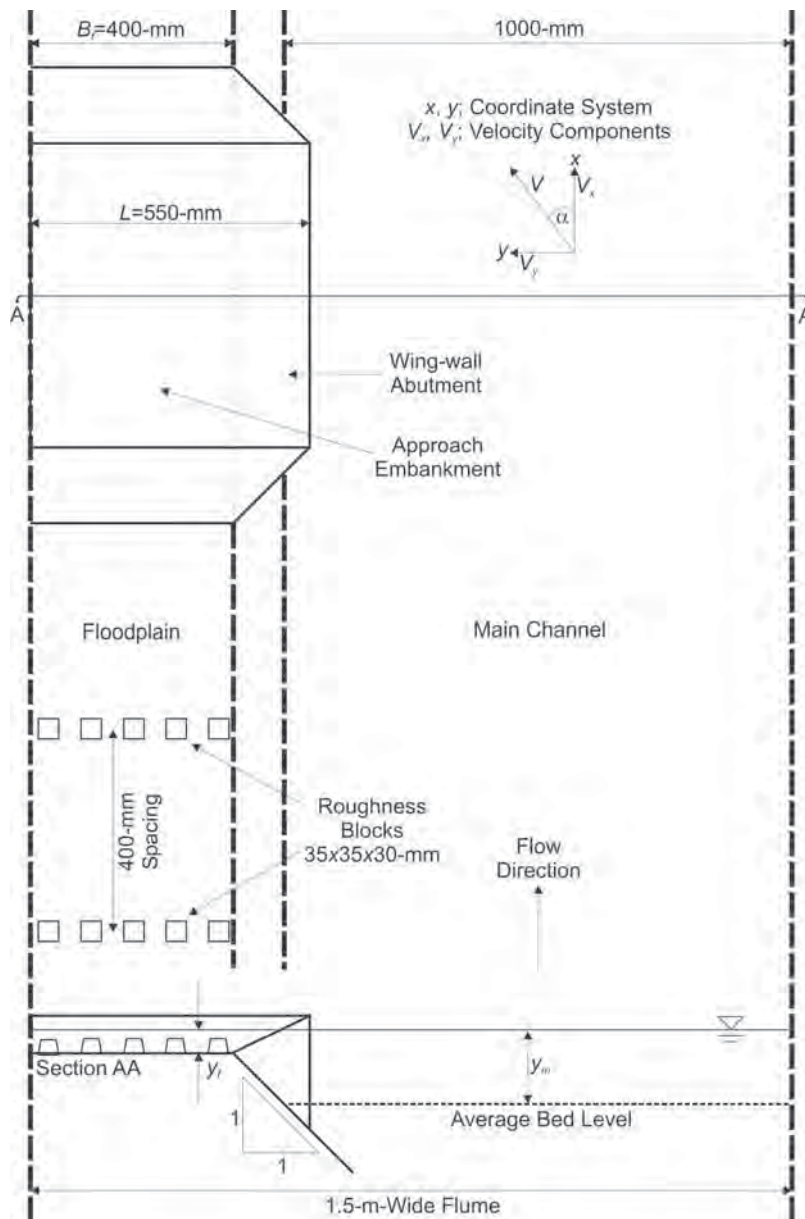


Figure 7-3. Layout of the channel and the wing-wall abutment.



Figure 7-4. Floodplain construction in the 1.5-m wide flume.

Bed Sediment

Uniform coarse sand was used as the bed material for all the experiments. A sieve analysis was carried out for the sand (Van Ballegooy, 2005). The sediment properties are summarized in Table 7-1.

The geometric standard deviation σ_g was calculated from $\sigma_g = (d_{84}/d_{16})^{0.5}$. The bed material was considered to be uniform because $\sigma_g < 1.5$. Using the Shields entrainment function, the critical shear velocity for the sediment was determined.

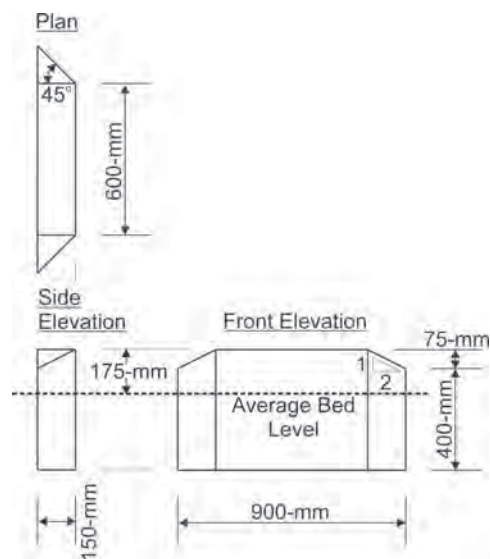


Figure 7-5. Wing-wall abutment dimensions.

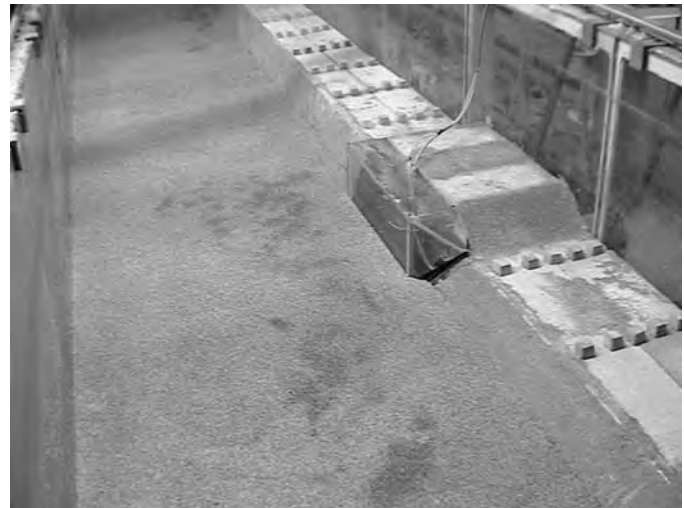


Figure 7-6. Wing-wall abutment and approach embankment setup in the 1.5-m wide flume, with the sand in the main channel leveled.

Model Riprap Stone

Four different riprap sizes were used for the scour countermeasure experiments. The riprap properties are summarized in Table 7-2 and illustrated in Figure 7-7.

Riprap type R2 was painted yellow, R3 was painted orange, and R4 was painted green. The reason for painting the riprap was to allow for better visibility in the flow and for clearer photographs of each experiment. The paint also facilitated retrieving the riprap stones at the conclusion of each test. The critical shear velocity for each riprap size was determined in the same way as for the bed sediment.

Model Cable-Tied Blocks

Conventionally, cable-tied blocks are constructed from precast concrete and are joined together using stainless steel

Table 7-1. Bed sediment data.

Description	d_{16} (mm)	d_{84} (mm)	d_{50} (mm)	σ_g	S_s	u_{*c} (ms^{-1})
Filter sand	0.62	1.04	0.82	1.30	2.65	0.020

Table 7-2. Riprap properties.

Description	d_{16} (mm)	d_{84} (mm)	d_{50} (mm)	σ_g	S_s	u_{*c} (ms^{-1})
R1	20	21	18	1.08	2.65	0.137
R2	28	32	25	1.13	2.65	0.162
R3	40	43	38	1.06	2.65	0.193
R4	61	66	56	1.09	2.65	0.239



Figure 7-7. The four riprap sizes used.

or synthetic cables to form a mattress. By adopting the McCorquodale et al. (1993) and Parker et al. (1998) recommendations for cable-tied block design, the required block height to satisfy the stability criteria was determined using

$$\zeta = a_{cb} \frac{\rho_{cb}}{\rho_{cb} - \rho} \rho V^2 \quad (7-1)$$

Where:

- ζ = weight per unit area of the block mattress as a whole,
- $a_{cb} = 0.1$,
- ρ_{cb} = block density,
- ρ = fluid density, and
- V = approach velocity.

The minimum required block height, H_b , can be calculated from

$$H_b = \frac{\zeta}{\rho_{cb} g (1 - p_m)} \quad (7-2)$$

Where p_m is the volume fraction pore space within the mattress.

Assuming a block density of $\rho_{cb} = 2,400 \text{ kg/m}^3$ and a volume fraction pore space of $p_m = 0.15$, the minimum required height of the block was determined to be 2 to 13 mm (depending on the flow velocity). A block height of 10 mm was used. This ensured that the cable-tied block mats would remain stable for all test conditions.

The blocks had the shape of a truncated square pyramid similar to the shape of cable-tied blocks used in practice. The dimensions for the three different blocks are given in Figure 7-8. The blocks used (see Figure 7-9) were dimensionally identical to those used in the Cheung (2002) experiment. The blocks were made from concrete using molds. A 1:5:1 water to sand to cement ratio was used to

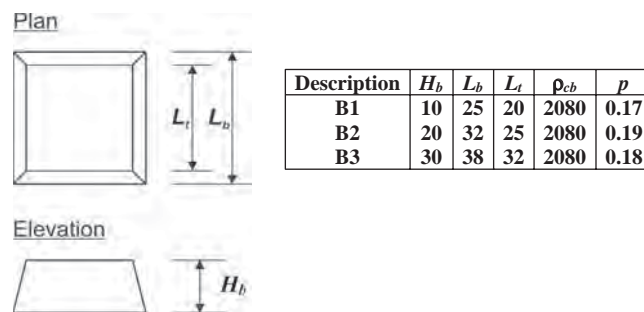


Figure 7-8. Dimensions (mm) of the blocks used for the cable-tied block mats.

yield a saturated block density of $\rho_{cb} = 2,080 \text{ kg/m}^3$. The mixture was left to set in the mold for at least 24 hours before the concrete blocks were carefully removed. The edges were smoothed using a fine grit sand paper.

The blocks were glued with a two-part epoxy glue to a porous shade cloth with a grid size of 5 mm to form a mattress. Attaching the blocks to the shade cloth simulated the linking together of actual blocks with cables. A 1-mm gap was left between each concrete block. For each of the experiments, sections of block matting were tied together to form the required apron extent at the abutments.

Model Geotextile

Most of the experiments were carried out with a geotextile placed underneath the countermeasure apron to eliminate the winnowing of sand from between the riprap stones or cable-tied blocks. The geotextile used for testing was flexible enough to ensure that the riprap or cable-tied blocks would be in contact with the bed at all times.

The geotextile used was a commercial nonwoven geotextile identical to the geotextile used in the Cheung (2002) experiment. The properties of the geotextile are given in Table 7-3.

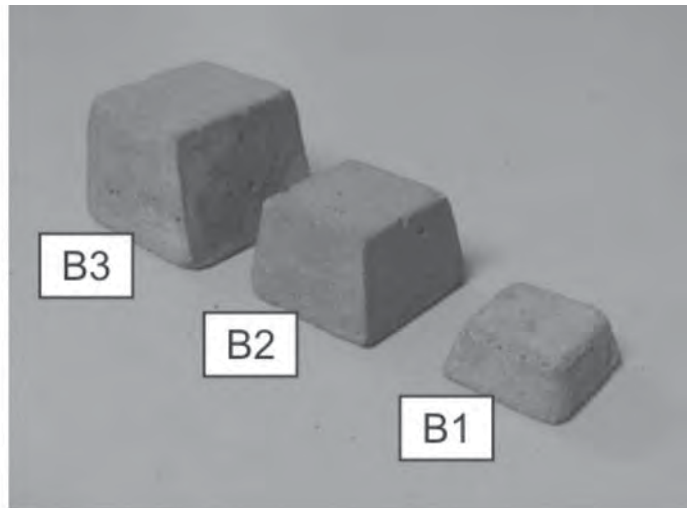
Approach-Flow Distribution

Uniform flow was established along the flume for four different flow velocities (approximately $V/V_c = 1.1, 1.4, 1.8$, and 2.1) and two different flow depths ($y_m = 100$ and 170 mm). With live-bed conditions, bed forms develop in the flume. As the bed forms developed, the slope of the flume was increased to maintain a uniform flow. When the bed forms were fully developed, the flow velocity upstream of the abutment was measured using the particle-tracking velocimetry (PTV) technique, and the bed profiles were measured using the acoustic depth sounder.

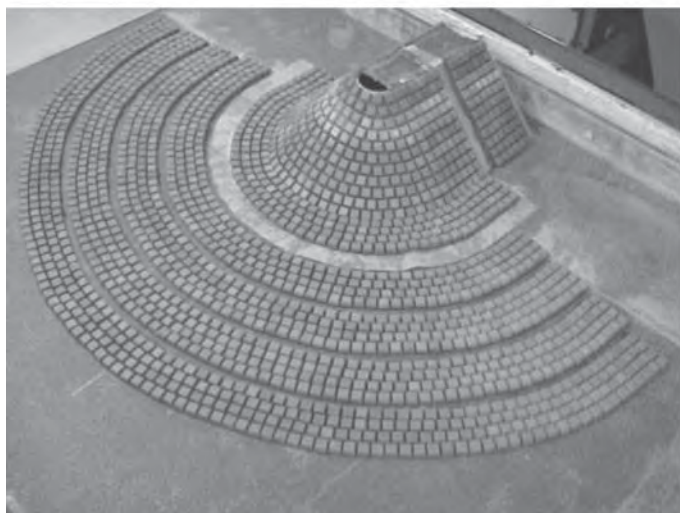
Similitude between laboratory experiments and field scale was satisfied by the use of the aforementioned u^*/u^* .



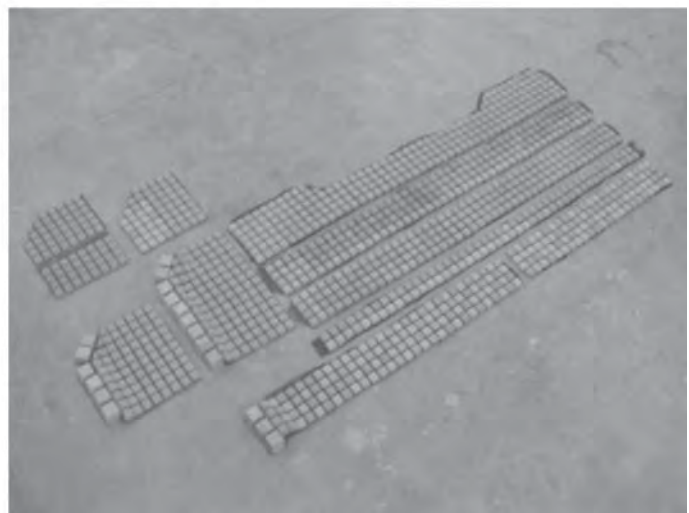
(a) mold for making the concrete blocks



(b) block types used in the experiment



(c) radial sections of the cable-tied block mat for the experiments reported in Chapter 8



(d) rectangular sections of cable-tied block mat for the experiments discussed herein

Figure 7-9. Cable-tied block mats.

ratio, of which values above 1.0 represent a condition called “live-bed scour.” This condition is extreme for scouring of armouring units such as riprap, cable-tied blocks, and geobags because the bed forms travelling past the armouring units can dislodge individual units and therefore cause failure.

Table 7-3. Characteristic properties of the geotextile material used.

Properties	Geotextile Information
Name	T500S
Puncture Strength (kN)	500
Elongation Strength (%)	60
Trapezoid Tear (kN)	100
Apparent Opening Size (mm)	0.35
Permeability (lm^2s^{-1})	130

Figure 7-10 shows the surface velocity distributions across the flume for the four flow velocities at two different flow depths. The major grid lines on the vertical axis of the graphs are multiples of the critical velocity for sediment entrainment. The lower graph shows the velocity distributions for the flow depth $y_m = 100$ mm. These velocity distributions finish at the edge of the main channel bank because there is no overbank flow at this flow depth. The upper graph shows the velocity distributions for the flow depth $y_m = 170$ mm. These velocities are highest in the main channel and are lowest in the floodplain ($y_f = 70$ mm).

The minor anomaly that the surface velocity using the PTV technique for $1.8V_c$ is lower in the floodplain than for $1.5V_c$ is not considered significant because the flows on the floodplain were relatively low and the prime interest was in the live-bed conditions in the main channel.

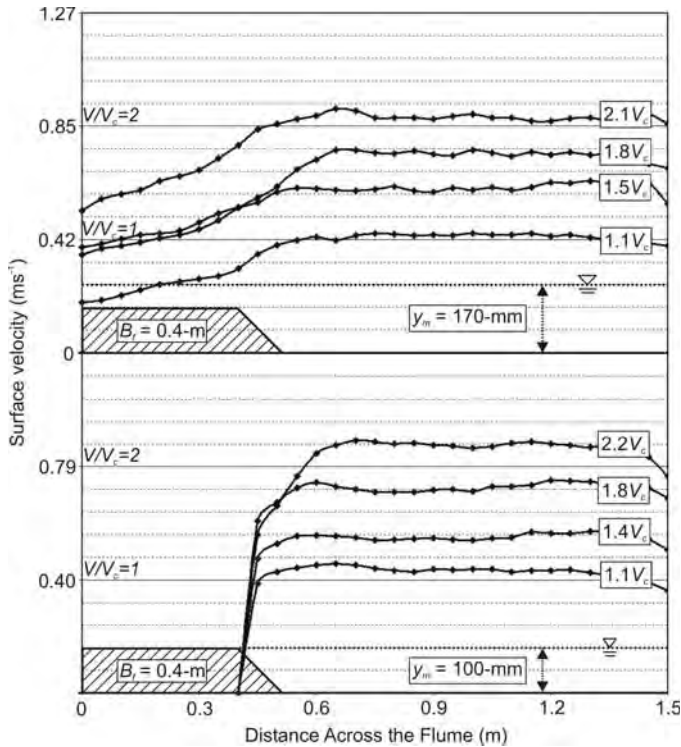


Figure 7-10. Velocity distributions across the 1.5-m wide flume for the four different flow velocities and two different flow depths.

Bed Forms

Bed forms can be seen in Figure 7-11. After the velocity distributions were measured, the flow was stopped and 10-m long bed profiles were measured longitudinally in the flume at 100-mm spacings. Average and maximum bed-form heights λ_H , lengths λ_L , and trough depths λ_D were determined for each flow condition from the bed profiles and are summarized in Table 7-4.

Layout of Riprap and Cable-Tied Block Aprons

The aprons of riprap stones were carefully placed to a thickness of $2d_{50}$ (equivalent to two riprap layers) at different

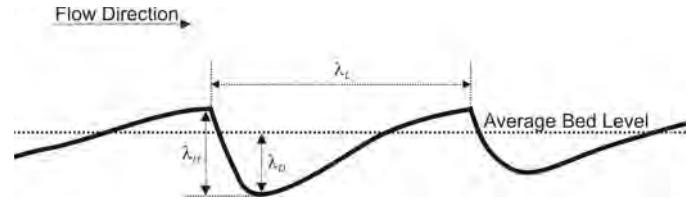


Figure 7-11. Bed-form parameter definition diagram.

elevations relative to the initial bed level, termed the average bed level. The placement level of the apron, d_b , is defined as the distance between the average bed level and the bottom of the apron (Figure 7-12). For the riprap type R3, three placement levels were used with the riprap aprons: $d_b = 2d_{50}$ (80 mm) with the top of the apron flush with the average bed level, $d_b = 1d_{50}$ (40 mm) with one riprap layer placed above the average bed level, and $d_b = 0$ with both layers placed on top of the average bed level. For the other riprap types (R1, R2, and R4), the placement levels were $d_b = 1d_{50}$ (20, 27, and 60 mm, respectively) with the top of the first riprap layer buried flush with the average bed level and the other riprap layer placed on top of the average bed level.

The cable-tied block mat was placed on the surface of the average bed level and was attached to the abutment face. For the experiments at higher velocities, larger blocks were glued to the leading edge of the cable-tied block mat to prevent failure of the mat from uplift, which could result in overturning of the mat.

The riprap and cable-tied block aprons were 1.35 m long in all cases. The 0.5-m upstream extension was selected as a result of preliminary experiments, which demonstrated that the 0.5-m extension was adequate to ensure that undermining of the leading edge of the aprons did not extend as far as the upstream corner of the abutment (i.e., the extent of undermining was always less than 0.5 m).

At the downstream end, the longitudinal extent of undermining of the apron was negligible. Therefore, a 0.25-m downstream extension was selected to give a reasonable margin of protection downstream of the abutment. A filter was placed beneath the aprons to prevent winnowing of the bed

Table 7-4. Bed-form characteristics (m).

Flow Parameters		λ_H		λ_L		λ_D	
y_m	V/V_c	Mean	Max.	Mean	Max.	Mean	Max.
0.100	1.1	0.048	0.073	1.221	2.140	0.031	0.060
	1.4	0.054	0.086	1.022	1.904	0.032	0.081
	1.8	0.051	0.080	0.984	1.736	0.033	0.066
	2.2	0.056	0.088	1.005	1.957	0.033	0.074
0.170	1.1	0.064	0.110	1.142	2.151	0.043	0.088
	1.5	0.080	0.138	1.295	2.172	0.059	0.106
	1.8	0.085	0.132	1.184	2.191	0.041	0.085
	2.1	0.078	0.135	1.389	2.521	0.048	0.099

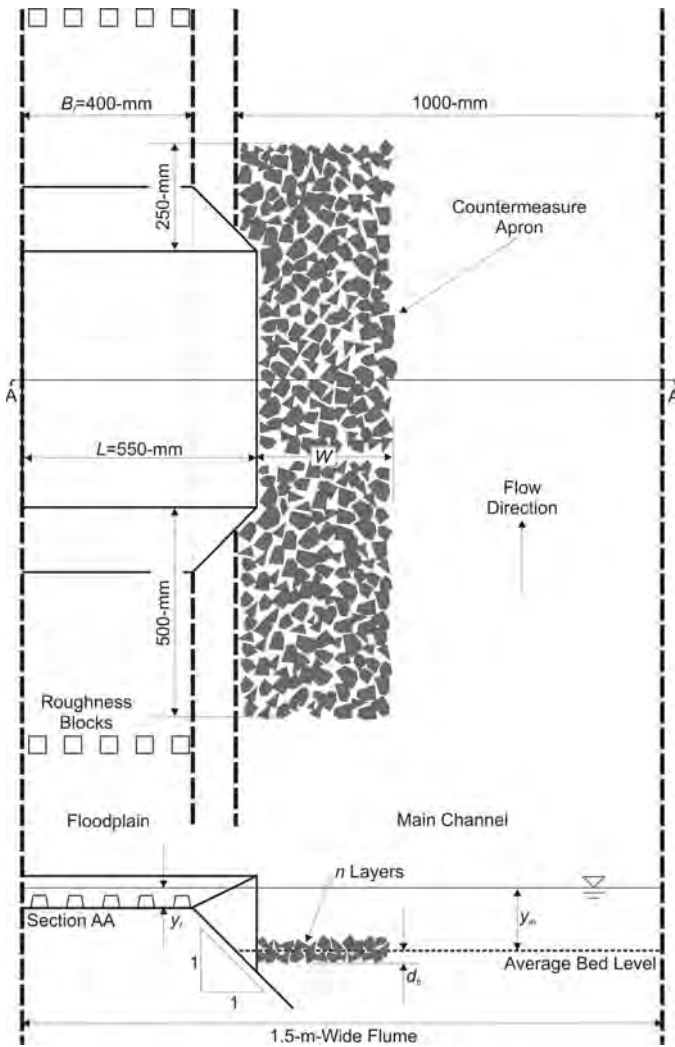


Figure 7-12. General layout of riprap apron.

sediment from between the riprap stones and the cable-tied blocks.

The experiments were conducted with two flow depths, $y_m = 100$ mm (bank-full) and $y_m = 170$ mm (maximum flood level without overtopping the embankment). At each flow depth, four different flow velocities were used. For the bank-full condition, the experiments were conducted with average main channel velocity ratios of $V/V_c = 1.1, 1.4, 1.8,$ and 2.2 . Likewise, for the maximum flood-level condition, the velocities tested were $V/V_c = 1.1, 1.5, 1.8,$ and 2.1 . Each run commenced from a flatbed, as shown in Figure 7-6. Experimental durations ranged from 8 hours to 72 hours, based on a requirement that at least 50 bed forms would propagate past the abutment during the run.

At the end of each experiment, any sand covering the apron was carefully removed and the settlement of the apron was measured. The depth to which the outer edge of the apron had settled was taken as the maximum scour depth at that point, where settlement depth is defined as the distance from

the average bed level to the top of the apron after settlement. Two cases of settlement were observed depending on the extent of undermining of the apron. These are identified in Figure 7-13 and discussed below.

The settlement of the apron at the abutment face d_{s1} , the settlement of the outer edge of the apron d_{s2} , the horizontal distance from the abutment face to the outer edge of the apron α_2 , and the horizontal distance to the point where the apron was undermined W_{min} were measured at both the upstream and downstream corners of the abutment. Accuracy of measurements was ± 5 mm.

7.2.2 Experimental Results

Summary of Results

The measurements from the experiments are summarized in Table 7-5.

Two cases of settlement were observed depending on the extent of undermining of the apron. These are identified in Figure 7-13. For Case I, no settlement occurred at the abutment face, while for Case II the entire apron was subject to settlement. For Case I, d_{s1} was taken to be negative when the top of the apron was above the average bed level ($nd_{50} > d_b$) and vice versa. For Case II, $W_{min} = 0$ because the entire apron was subject to settlement.

General Trends

Figures 7-14 and 7-15 show the results for two series of riprap experiments ($y_m = 100$ mm and $y_m = 170$ mm, respectively), and Figures 7-16 and 7-17 show the results for the equivalent series of cable-tied block experiments ($y_m = 100$ mm and $y_m = 170$ mm, respectively). For the two riprap experimental sets, R3 riprap was used for the aprons and was placed at a burial depth $d_b = 80$ mm (nd_{50}). For the two cable-tied block experiments, R1 riprap was used for the aprons and placed at a burial depth $d_b = 0$. In Figures 7-14 through 7-17, apron width increases across the page from $W = 100$ mm to $W = 400$ mm, while the flow velocity increases down the page from $V/V_c = 1.1$ to $V/V_c = 2.1$ (or 2.2 for the experiments with $y_m = 100$ mm).

The results for four riprap experimental series with different apron widths ($W = 100$ mm to $W = 400$ mm) and varying apron burial depths are shown in Figures 7-18 and 7-19. For these experimental sets, R3 riprap was used for the aprons, which were tested at a flow depth of $y_m = 170$ mm. Apron burial depth increases down the page from $d_b = 0$ to $d_b = 80$ mm (nd_{50}), while flow velocity increases across the page from $V/V_c = 1.1$ to $V/V_c = 2.1$.

Riprap size was varied in a final experimental series, as shown in Figure 7-20. R1 riprap was used for $d_{50} = 20$,

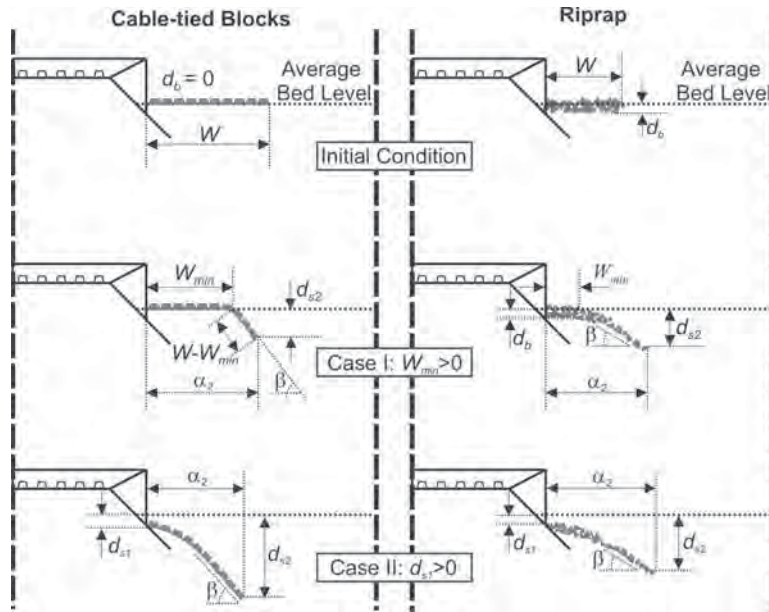


Figure 7-13. Definition diagram of the apron settlement measurements.

R2 riprap was used for $d_{50} = 27$, R3 riprap was used for $d_{50} = 40$, and R4 riprap was used for $d_{50} = 60$. For these experiments, a 200-mm wide apron was used, placed at a burial depth $d_b = 1d_{50}$, such that one riprap layer was buried flush with the average bed level and the other riprap layer was placed on top. The aprons were tested with a flow depth of $y_m = 170$ mm. Riprap size increases across the page from $d_{50} = 20$ mm to $d_{50} = 60$ mm, while flow velocity increases down the page from $V/V_c = 1.1$ to $V/V_c = 2.6$. Riprap type R4 was tested at a high flow velocity ($V/V_c = 2.6$) to determine the flow velocity at which shear failure of the riprap would occur.

Figures 7-14 to 7-20 depict the systematic variations in scour formation at the wing-wall abutment as a consequence of variations in y_m , V/V_c , W , d_b , and d_{50} . The data from Table 7-5 are scattered due to the variability in bed-form height and consequent apron settlement, but a trend of increased settlement of the outer edge of the apron with both increasing flow depth and increasing flow intensity is apparent. Also, the corresponding scour depth at the upstream end of the apron was typically larger than that at the downstream end because the bed forms were larger at the upstream end. The data also show that lowering the placement level of the apron did not affect the settlement depth at the outer edge of the apron, although the apron remained more intact (i.e., W_{min} was larger for lower apron placement levels), because less material was undermined from the apron. Apron type (riprap or cable-tied blocks) and increasing apron width both had little effect on the settlement depth.

7.2.3 Experimental Observations

Riprap and Cable-Tied Block Apron Behavior

The movement of bed forms through the bridge section undermined the outer edges of the protective apron, as illustrated in Figure 7-21. Whenever bed-form troughs propagated past the apron, the bed was lowered locally and the apron would be undermined and settle if the bed lowering was more than had occurred previously during the experiment. The edge of the apron was more susceptible to undermining, thereby causing deeper settlement of the apron at its outer edge. This settling process continued as subsequent bed forms with deeper troughs propagated past the apron, thereby further undermining the toe of the apron. Subsequent bed forms with shallower troughs propagated over the apron without causing further settlement. The outer edge of the apron typically settled to the level of the deepest bed form that propagated past the abutment during the particular run. After a sufficient number of bed forms had passed, the edge of the apron was assumed to have settled to its equilibrium position.

The cable-tied block aprons, consisting of interconnected blocks and being attached to the abutment face, were constrained to settle downward when undermined. The more loose nature of riprap aprons resulted in apron stones rolling down into the bed-form troughs and the apron spreading as erosion took place.

Comparison of Riprap Observations with Lauchlan (1999)

The three clear-water failure mechanisms for riprap aprons identified by Chiew (1995) were confirmed in the

Table 7-5. Apron settlement measurements.

y_m (m)	V/V_c	W (m)	d_{50} (m)	d_b (m)	Upstream				Downstream			
					d_{s1} (m)	d_{s2} (m)	W_{min} (m)	α_2 (m)	d_{s1} (m)	d_{s2} (m)	W_{min} (m)	α_2 (m)
Riprap Protection												
0.100	1.1	0.100	0.040	0.080	0.000	0.080	0.050	0.200	0.000	0.060	0.070	0.165
0.100	1.4	0.100	0.040	0.080	0.005	0.085	0.000	0.200	0.000	0.065	0.070	0.165
0.100	1.8	0.100	0.040	0.080	0.010	0.095	-	0.230	0.000	0.075	0.050	0.200
0.100	2.2	0.100	0.040	0.080	0.040	0.110	-	0.240	0.000	0.105	0.000	0.240
0.170	1.1	0.100	0.040	0.080	0.000	0.105	0.040	0.300	0.000	0.085	0.060	0.250
0.170	1.5	0.100	0.040	0.080	0.000	0.105	0.000	0.230	0.000	0.085	0.060	0.230
0.170	1.8	0.100	0.040	0.080	0.000	0.135	0.000	0.260	0.000	0.105	0.040	0.250
0.170	2.1	0.100	0.040	0.080	0.105	0.175	-	0.325	0.000	0.145	0.040	0.305
0.100	1.1	0.200	0.040	0.080	0.000	0.075	0.100	0.300	0.000	0.055	0.150	0.270
0.100	1.4	0.200	0.040	0.080	0.000	0.085	0.080	0.310	0.000	0.055	0.150	0.280
0.100	1.8	0.200	0.040	0.080	0.000	0.120	0.060	0.320	0.000	0.065	0.150	0.300
0.100	2.2	0.200	0.040	0.080	0.000	0.125	0.040	0.340	0.000	0.085	0.150	0.300
0.170	1.1	0.200	0.040	0.080	0.000	0.103	0.100	0.300	0.000	0.100	0.130	0.320
0.170	1.5	0.200	0.040	0.080	0.000	0.130	0.080	0.350	0.000	0.100	0.130	0.320
0.170	1.8	0.200	0.040	0.080	0.000	0.140	0.060	0.360	0.000	0.095	0.130	0.345
0.170	2.1	0.200	0.040	0.080	0.025	0.145	-	0.360	0.000	0.115	0.100	0.360
0.100	1.1	0.300	0.040	0.080	0.000	0.200	0.200	0.380	0.000	0.045	0.250	0.360
0.100	1.4	0.300	0.040	0.080	0.000	0.200	0.200	0.390	0.000	0.065	0.250	0.370
0.100	1.8	0.300	0.040	0.080	0.000	0.180	0.180	0.415	0.000	0.065	0.230	0.380
0.100	2.2	0.300	0.040	0.080	0.030	0.150	0.150	0.470	0.000	0.075	0.220	0.410
0.170	1.1	0.300	0.040	0.080	0.000	0.200	0.200	0.400	0.000	0.075	0.230	0.390
0.170	1.5	0.300	0.040	0.080	0.000	0.180	0.180	0.405	0.000	0.075	0.230	0.380
0.170	1.8	0.300	0.040	0.080	0.000	0.150	0.150	0.410	0.000	0.105	0.200	0.390
0.170	2.1	0.300	0.040	0.080	0.000	0.100	0.100	0.470	0.000	0.115	0.150	0.390
0.170	1.1	0.400	0.040	0.080	0.000	0.085	0.330	0.480	0.000	0.350	0.500	0.075
0.170	1.5	0.400	0.040	0.080	0.000	0.105	0.320	0.500	0.000	0.330	0.520	0.075
0.170	1.8	0.400	0.040	0.080	0.000	0.130	0.280	0.550	0.000	0.300	0.540	0.095
0.170	2.1	0.400	0.040	0.080	0.000	0.150	0.210	0.580	0.000	0.280	0.610	0.135
0.170	1.1	0.100	0.040	0.040	0.005	0.130	-	0.300	-0.035	0.115	0.040	0.280
0.170	1.5	0.100	0.040	0.040	0.020	0.135	-	0.305	-0.035	0.115	0.040	0.285
0.170	1.8	0.100	0.040	0.040	0.070	0.160	-	0.305	0.005	0.115	-	0.285
0.170	2.1	0.100	0.040	0.040	-	0.190	-	0.350	0.025	0.165	-	0.360
0.170	1.1	0.200	0.040	0.040	-0.035	0.120	0.090	0.385	-0.035	0.090	0.100	0.355
0.170	1.5	0.200	0.040	0.040	-0.035	0.125	0.050	0.385	-0.035	0.090	0.100	0.355
0.170	1.8	0.200	0.040	0.040	-0.035	0.130	0.050	0.360	-0.035	0.110	0.090	0.370
0.170	2.1	0.200	0.040	0.040	0.075	0.165	-	0.450	-0.035	0.165	0.050	0.430
0.170	1.1	0.300	0.040	0.040	-0.035	0.105	0.150	0.400	-0.035	0.075	0.200	0.400
0.170	1.5	0.300	0.040	0.040	-0.035	0.130	0.150	0.470	-0.035	0.120	0.200	0.460
0.170	1.8	0.300	0.040	0.040	-0.035	0.135	0.150	0.470	-0.035	0.130	0.200	0.460
0.170	2.1	0.300	0.040	0.040	0.045	0.165	-	0.530	-0.035	0.145	0.150	0.515
0.170	1.1	0.400	0.040	0.040	-0.035	0.120	0.270	0.560	-0.035	0.090	0.320	0.560
0.170	1.5	0.400	0.040	0.040	-0.035	0.130	0.240	0.560	-0.035	0.105	0.310	0.580
0.170	1.8	0.400	0.040	0.040	-0.035	0.155	0.220	0.590	-0.035	0.115	0.280	0.580
0.170	2.1	0.400	0.040	0.040	-0.035	0.175	0.120	0.650	-0.035	0.155	0.200	0.640
0.170	1.1	0.100	0.040	0.000	0.005	0.115	-	0.360	-0.075	0.095	0.040	0.350
0.170	1.5	0.100	0.040	0.000	0.045	0.145	-	0.360	-0.075	0.105	0.040	0.350
0.170	1.8	0.100	0.040	0.000	0.075	0.165	-	0.360	-0.005	0.145	-	0.430
0.170	2.1	0.100	0.040	0.000	-	0.000	-	-	-	0.000	-	-
0.170	1.1	0.200	0.040	0.000	-0.075	0.130	0.060	0.430	-0.075	0.120	0.090	0.420
0.170	1.5	0.200	0.040	0.000	-0.075	0.140	0.040	0.430	-0.075	0.125	0.090	0.430
0.170	1.8	0.200	0.040	0.000	-0.025	0.140	-	0.440	-0.075	0.125	0.060	0.440
0.170	2.1	0.200	0.040	0.000	0.035	0.155	-	0.450	-0.075	0.145	0.000	0.460

Table 7-5. (Continued).

y_m (m)	V/V_c	W (m)	d_{50} (m)	d_b (m)	Upstream				Downstream			
					d_{s1} (m)	d_{s2} (m)	W_{min} (m)	α_2 (m)	d_{s1} (m)	d_{s2} (m)	W_{min} (m)	α_2 (m)
0.170	1.1	0.300	0.040	0.000	-0.075	0.115	0.150	0.490	-0.075	0.095	0.200	0.470
0.170	1.5	0.300	0.040	0.000	-0.075	0.125	0.150	0.490	-0.075	0.100	0.200	0.480
0.170	1.8	0.300	0.040	0.000	-0.075	0.135	0.090	0.510	-0.075	0.115	0.150	0.490
0.170	2.1	0.300	0.040	0.000	0.045	0.145	-	0.510	-0.075	0.135	0.150	0.530
0.170	1.1	0.200	0.020	0.020	-0.020	0.130	0.110	0.410	-0.020	0.105	0.150	0.360
0.170	1.5	0.200	0.020	0.020	0.065	0.180	-	0.420	-0.020	0.165	0.120	0.460
0.170	1.8	0.200	0.020	0.020	-	-	-	-	-	-	-	-
0.170	2.1	0.200	0.020	0.020	-	-	-	-	-	-	-	-
0.170	1.1	0.200	0.027	0.027	-0.025	0.105	0.110	0.340	-0.025	0.100	0.145	0.340
0.170	1.5	0.200	0.027	0.027	-0.025	0.140	0.100	0.400	-0.025	0.105	0.120	0.340
0.170	1.8	0.200	0.027	0.027	-0.025	0.140	0.060	0.400	-0.025	0.120	0.100	0.380
0.170	2.1	0.200	0.027	0.027	0.085	0.170	-	0.470	-0.025	0.155	0.070	0.480
0.170	1.1	0.200	0.061	0.061	-0.060	0.105	0.110	0.390	-0.060	0.075	0.120	0.300
0.170	1.5	0.200	0.061	0.061	-0.060	0.115	0.070	0.400	-0.060	0.085	0.120	0.310
0.170	1.8	0.200	0.061	0.061	-0.060	0.130	0.060	0.410	-0.060	0.085	0.060	0.320
0.170	2.1	0.200	0.061	0.061	-0.015	0.155	-	0.440	-0.060	0.115	0.050	0.340
Cable-Tied Block Protection												
0.100	1.1	0.100	-	0.000	-0.005	0.065	-	0.071	-0.005	0.060	-	0.076
0.100	1.4	0.100	-	0.000	0.020	0.090	-	0.071	0.015	0.080	-	0.076
0.100	1.8	0.100	-	0.000	-	-	-	-	-	-	-	-
0.100	2.2	0.100	-	0.000	-	-	-	-	-	-	-	-
0.170	1.1	0.100	-	0.000	0.075	0.145	-	0.071	0.065	0.135	-	0.071
0.170	1.5	0.100	-	0.000	-	-	-	-	-	-	-	-
0.170	1.8	0.100	-	0.000	-	-	-	-	-	-	-	-
0.170	2.1	0.100	-	0.000	-	-	-	-	-	-	-	-
0.100	1.1	0.150	-	0.000	-0.005	0.065	-	0.133	-0.005	0.060	0.000	0.137
0.100	1.4	0.150	-	0.000	0.000	0.085	-	0.124	-0.005	0.075	0.000	0.130
0.100	1.8	0.150	-	0.000	0.000	0.085	-	0.124	-0.005	0.075	-	0.127
0.100	2.2	0.150	-	0.000	-	-	-	-	-	-	-	-
0.170	1.1	0.150	-	0.000	0.005	0.110	-	0.107	0.000	0.085	0.000	0.124
0.170	1.5	0.150	-	0.000	0.035	0.120	-	0.124	0.000	0.105	0.000	0.107
0.170	1.8	0.150	-	0.000	-	-	-	-	-	-	-	-
0.170	2.1	0.150	-	0.000	-	-	-	-	-	-	-	-
0.100	1.1	0.200	-	0.000	-0.005	0.070	0.100	0.171	0.100	0.176	0.100	0.176
0.100	1.4	0.200	-	0.000	-0.005	0.080	0.100	0.160	0.075	0.179	0.075	0.179
0.100	1.8	0.200	-	0.000	0.010	0.085	0.100	0.153	0.100	0.166	0.100	0.166
0.100	2.2	0.200	-	0.000	0.015	0.085	-	-	0.075	0.167	0.075	0.167
0.170	1.1	0.200	-	0.000	-0.005	0.105	0.050	0.157	0.075	0.175	0.075	0.175
0.170	1.5	0.200	-	0.000	0.005	0.135	0.025	0.136	0.025	0.147	0.025	0.147
0.170	1.8	0.200	-	0.000	0.000	0.135	0.025	0.136	0.075	0.175	0.075	0.175
0.170	2.1	0.200	-	0.000	Over-turned				0.000	0.120	0.000	0.120
0.100	1.1	0.300	-	0.000	-0.005	0.070	0.200	0.271	0.200	0.276	0.200	0.276
0.100	1.4	0.300	-	0.000	-0.005	0.070	0.200	0.271	0.175	0.279	0.175	0.279
0.100	1.8	0.300	-	0.000	0.005	0.150	0.125	0.215	0.175	0.267	0.175	0.267
0.100	2.2	0.300	-	0.000	0.010	0.155	0.100	0.226	0.150	0.262	0.150	0.262
0.170	1.1	0.300	-	0.000	-0.005	0.070	0.175	0.279	0.225	0.276	0.225	0.276
0.170	1.5	0.300	-	0.000	-0.005	0.125	0.100	0.256	0.150	0.280	0.150	0.280
0.170	1.8	0.300	-	0.000	0.005	0.130	0.125	0.242	0.175	0.262	0.175	0.262
0.170	2.1	0.300	-	0.000	0.035	0.185	-	-	0.100	0.243	0.100	0.243
0.100	1.1	0.400	-	0.000	-0.005	0.070	0.300	0.371	0.300	0.376	0.300	0.376
0.100	1.4	0.400	-	0.000	-0.005	0.075	0.300	0.366	0.300	0.371	0.300	0.371
0.100	1.8	0.400	-	0.000	-0.005	0.095	0.275	0.356	0.275	0.367	0.275	0.367
0.100	2.2	0.400	-	0.000	0.005	0.150	0.200	0.332	0.200	0.352	0.200	0.352
0.170	1.1	0.400	-	0.000	-0.005	0.065	0.300	0.376	0.300	0.384	0.300	0.384
0.170	1.5	0.400	-	0.000	-0.005	0.090	0.250	0.370	0.300	0.376	0.300	0.376
0.170	1.8	0.400	-	0.000	-0.005	0.135	0.200	0.348	0.275	0.367	0.275	0.367
0.170	2.1	0.400	-	0.000	-0.005	0.195	-	-	0.250	0.325	0.250	0.325

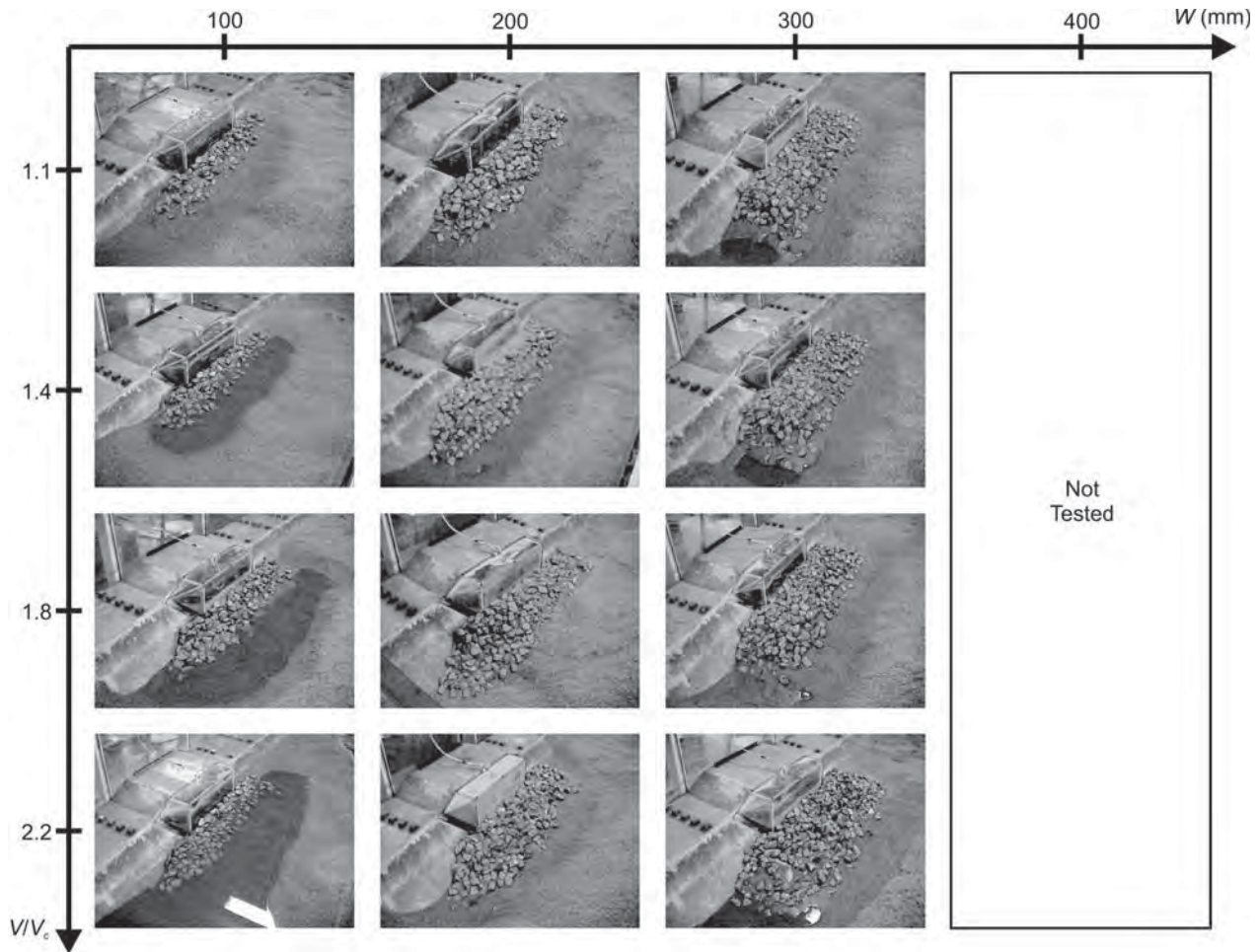


Figure 7-14. Performance of riprap apron protection at wing-wall abutments under live-bed conditions ($d_b = 2d_{50} = 80$ mm, and $y_m = 100$ mm).

present study. Shear, winnowing, and edge failure were all found to occur in both the clear-water experiments with spill-through abutments and the live-bed experiments with wing-wall abutments. Additionally, under mobile bed conditions, Lauchlan (1999) identified destabilization of the riprap through the propagation of bed forms as another failure mechanism for riprap aprons. Both in the present wing-wall abutment scour countermeasure study and in the pier scour countermeasure study by Lauchlan (1999), destabilization of the riprap through the propagation of bed forms was observed to be the dominant failure mode of riprap aprons. Shear failure of the riprap occurred when the flow velocity exceeded the critical velocity of the riprap stones (Figure 7-20).

Winnowing failure was the dominant failure mode at the upstream corner of the abutment for the preliminary experiment that was run without filter fabric placed underneath the apron. Lauchlan (1999) observed that sediment beneath the riprap apron cannot be winnowed through the riprap layers when a filter is used, also preventing the riprap from subsiding into the bed. However, under high flow velocities,

the filter layer could become exposed if riprap shear failure or excessive apron settlement occurred—that is, for the experiment, $d_{50} = 27$ mm and $V/V_c = 2.1$ shown in Figure 7-20 and the experiment $d_b = 0$ and $V/V_c = 1.8$ shown in Figure 7-18.

Lauchlan (1999) concluded that increasing the riprap apron layer thickness increases the scour protection by reducing the winnowing of bed sediment from underneath the riprap blanket. This conclusion could not be made in the current wing-wall abutment scour countermeasure study because all of the experiments were run with a filter placed underneath the riprap apron, thereby preventing winnowing from occurring. However, the preliminary experiments showed that increasing the riprap layer thickness increased the scour protection by reducing the extent of the apron destabilized by the propagation of bed forms.

Lauchlan (1999) identified the apron placement level relative to the average bed level as the most important parameter affecting the performance of the riprap apron. Because bed-form destabilization is the prominent failure mechanism under mobile-bed conditions, and because less mate-

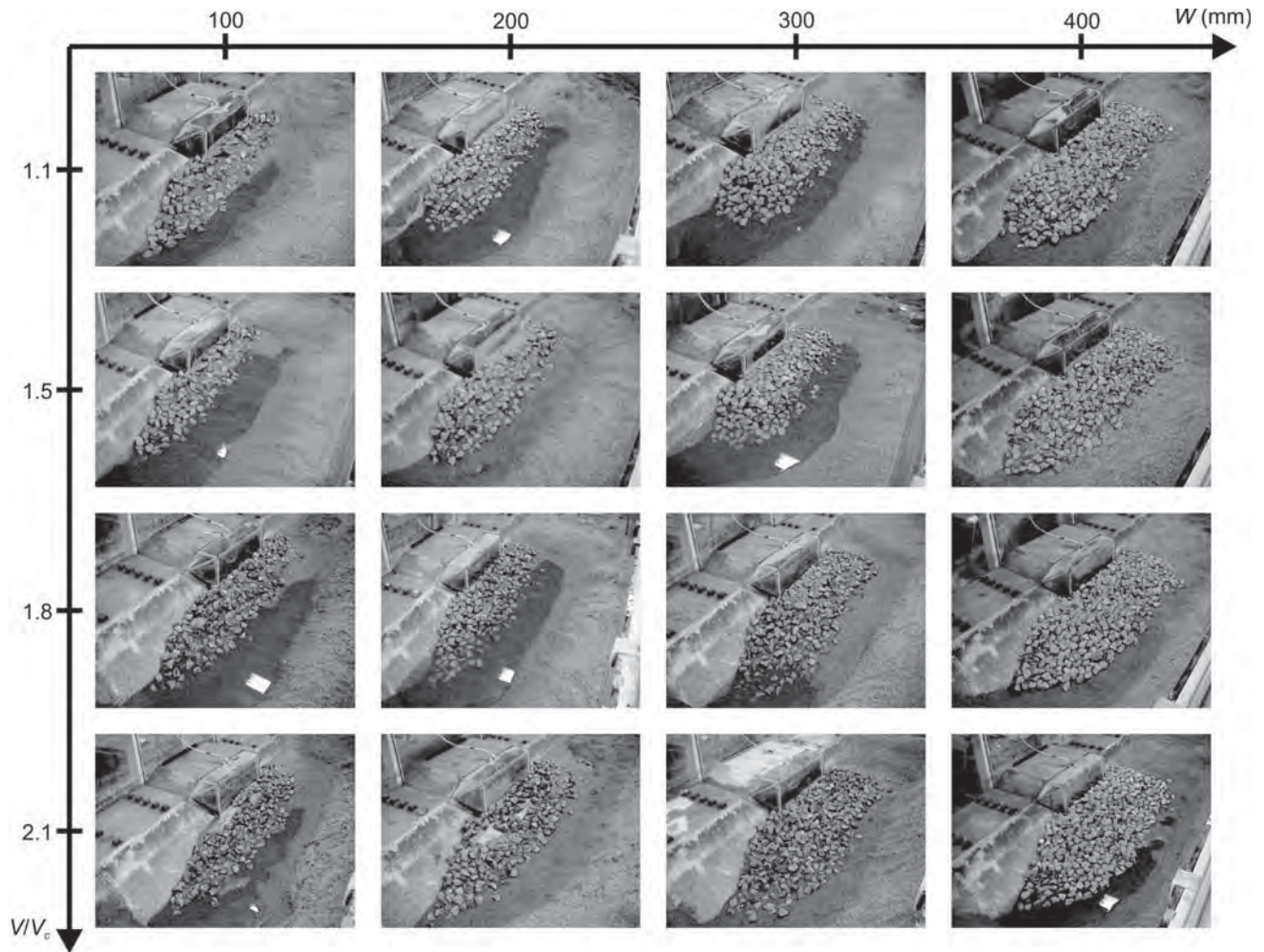


Figure 7-15. Performance of riprap apron protection at wing-wall abutments under live-bed conditions ($d_b = 2d_{50} = 80$ mm, and $y_m = 170$ mm).

rial is undermined from the apron by the troughs of the propagating bed forms, increasing the burial depth increases the stability of the apron. The current experiments show that as the burial depth is increased, apron width can be reduced to afford similar levels of scour protection at the abutment.

Lauchlan (1999) also observed that, with increased burial depths, the riprap stones are less susceptible to shear failure, but this effect was not investigated in this experiment.

7.2.4 Discussion

Comparison of the Experimental Results with the Clear-Water Spill-Through Abutment Study

For the spill-through abutment clear-water scour countermeasure experiments, settlement (or scour) depth reduced with increased apron width (for the case where $\alpha_e < B_f$), because the local scour hole was deflected farther from the abutment. Similar trends would also be expected for live-bed conditions, but were not observed in the present study.

Similitude between laboratory experiments and field scale was satisfied by the use of the aforementioned u_* / u_{*c} ratio, of which a value of just below 1.0 represents a condition called “clear-water scour.” This condition is extreme for scouring because the velocity is as high as possible without the movement of the channel bed, which causes infilling of the sediment hole.

The maximum equilibrium scour depth as a function of the mean flow velocity occurs at threshold conditions and decreases slightly thereafter with increasing velocity (Melville and Coleman, 2000). The two preliminary experiments that were run just below threshold conditions with no protection gave the maximum equilibrium local scour depth at the abutment for the two flow depths used. For both experiments, the deepest point of scour occurred at the upstream corner of the abutment face, with maximum scour depths of 80 mm for the 100-mm flow depth and 100 mm for the 170-mm flow depth. The preliminary experiments were repeated with a 200-mm wide apron in place, for which the maximum scour depth was significantly reduced, consistent with the results in the clear-water spill-through abutment study.

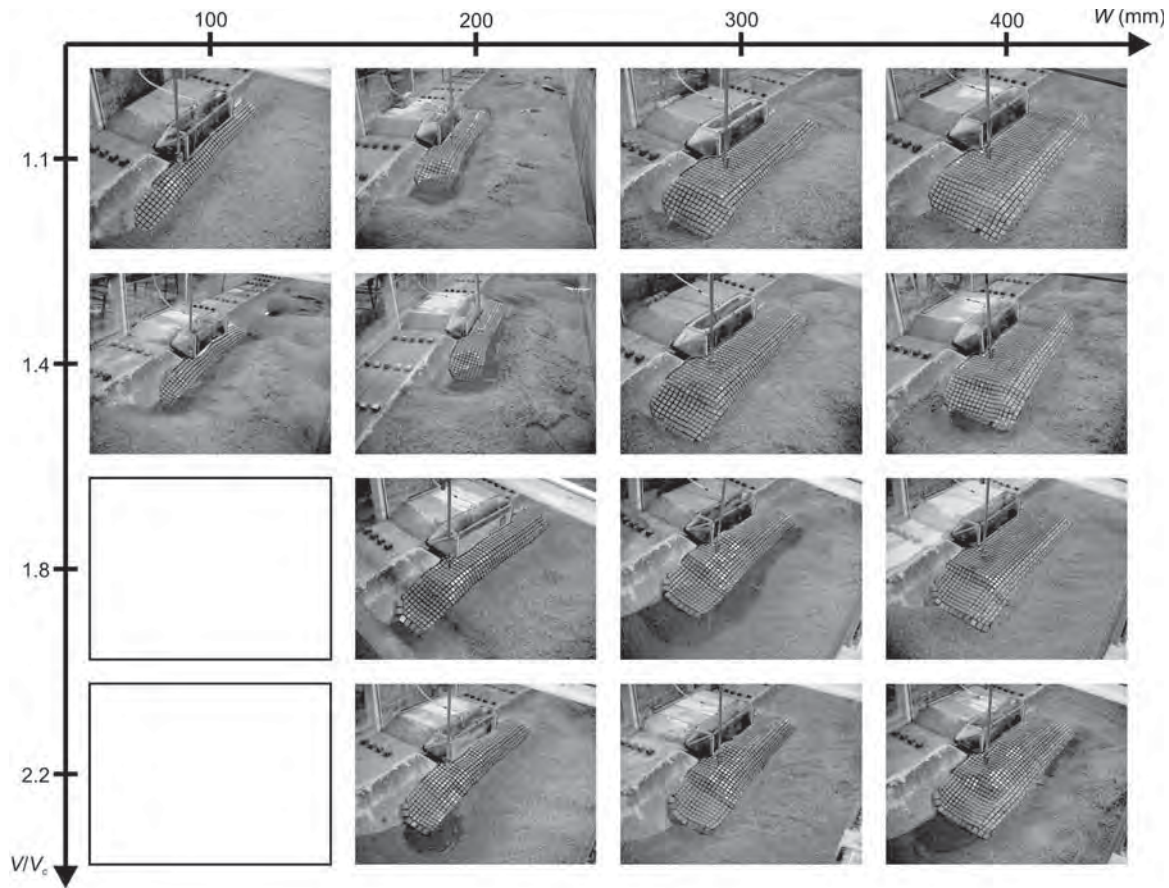


Figure 7-16. Performance of cable-tied block apron protection at wing-wall abutments under live-bed conditions ($d_b = 0$, and $y_m = 100$ mm).

Contrary to expectations, the measured scour depths for clear-water conditions are considerably smaller than the measured scour depths at the outer edge of the apron for live-bed conditions. It is apparent that the troughs of the bed forms in the live-bed experimental work were very much deeper than the local scour at the abutment; the former, therefore, dominated the maximum scour depth d_{s2} .

Bed Forms

Section 7.2.3 outlines how the bed forms affect the countermeasure aprons, and the previous paragraph shows that the scour at the abutment is governed by the largest bed forms that propagate past the abutment (for the wing-wall abutment configuration tested). Van Rijn (1984) and Yalin (1992) both presented methods to predict the average equilibrium bed form heights and lengths, but it is the maximum equilibrium bed form height that dominates the scour at the abutment. Ashley (1990) compared bed form height-to-length ratios for 1,500 subaqueous bed forms and developed an expression for the maximum bed form height λ_{H-max} :

$$\lambda_{H-max} = 0.16\lambda_{L-ave}^{0.84} \quad (7-3)$$

Where λ_{L-ave} is the average bed form length. Figure 7-22 compares the measured λ_{H-max} values from Table 7-4 with the predicted λ_{H-max} values from Equation 7-3 for the eight different flow conditions run in the flume. There is a good correlation between the measured and predicted λ_{H-max} values, confirming that Equation 7-3 developed is a good estimate for predicting λ_{H-max} where λ_{L-ave} is estimated from the expression developed by Yalin (1992).

Riprap Stability

For the experimental series shown in Figure 7-20, the flow velocity was systematically increased for the different riprap sizes until shear failure of the riprap occurred. Shear failure occurs where the flow dislodges the riprap stones from the apron and carries them downstream. The experiments for which shear failure occurred can be seen in Figure 7-20 at the bottom of each of the columns. The dislodged riprap stones that were carried downstream by the flow are circled for each of these experiments. Table 7-6 summarizes the upstream and bridge section surface flow velocities V_{2-surf} and the bridge section depth-averaged flow velocities V_{2-ave} for each of the experiments shown in Figure 7-20. The bridge section velocities were obtained from

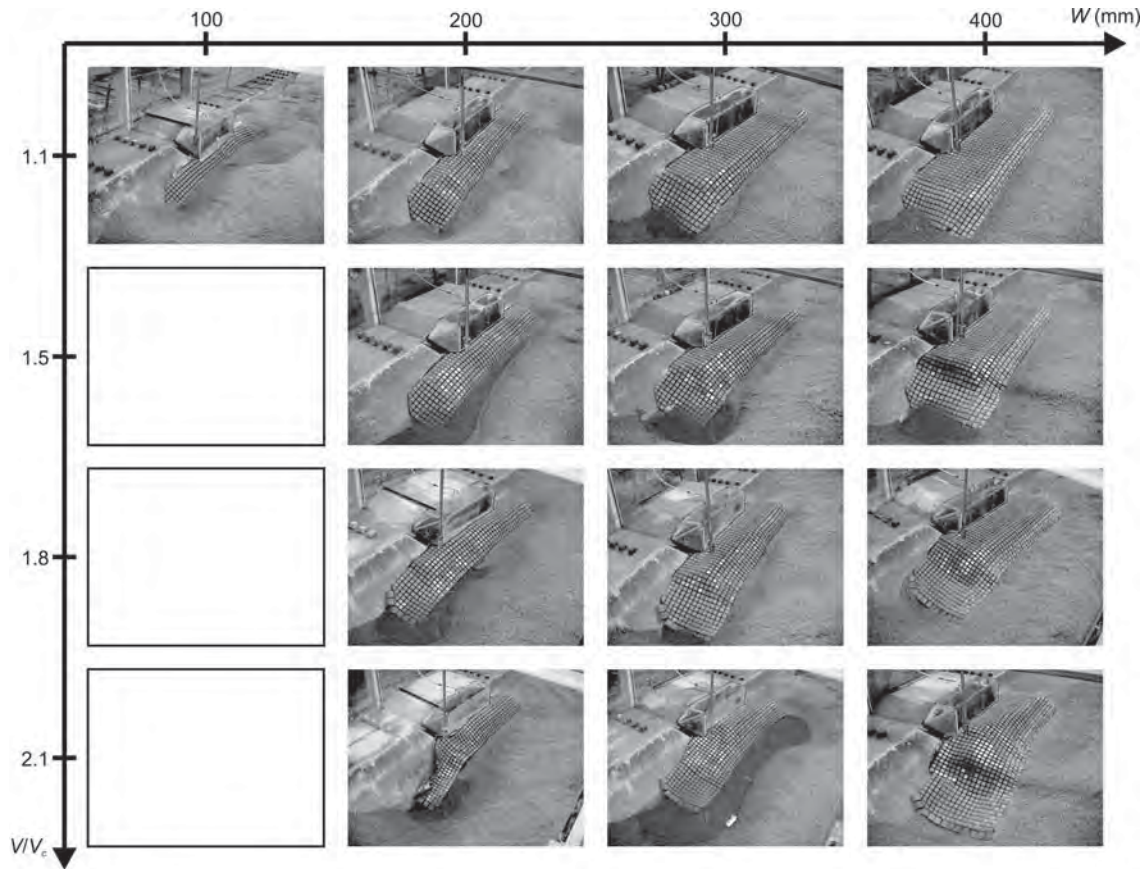


Figure 7-17. Performance of cable-tied block apron protection at wing-wall abutments under live-bed conditions ($d_b = 0$, and $y_m = 170$ mm).

the PTV flow field measurements and acoustic Doppler velocimeter measurements of the vertical velocity distribution.

Figure 7-23 shows the riprap size normalized with the flow depth as a function of the Froude number at the bridge section Fr_2 , as well as the riprap sizing equation from Lagasse et al. (2001) for vertical-wall abutments. The experimental data for the stable riprap are depicted by solid black symbols and lie above the curve. Likewise, the experimental data for the unstable riprap (experiments where shear failure occurred) are depicted by hollow symbols and lie below the curve.

The comparison in Figure 7-23 confirms that either the Lagasse et al. (2001) equation or the Pagan-Ortiz (1991) equation, with appropriate factors of safety, is suitable for predicting riprap stone sizes that are resistant to shear failure at wing-wall abutments. As noted above, riprap size selection is appropriately based on stability against shear and edge failure, although consideration of the possibility of winnowing or bed form undermining is also important in design.

Cable-Tied Block Stability

Cable-tied block aprons are subject to two observed flow-induced failure modes, as described by Parker et al. (1998). The failure modes are overturning and roll-up of the leading

edge of a cable-tied block mat, which can occur in the absence of sufficient anchoring or toeing in of the leading edge, and uplift of the inner mat, which occurs at higher flow velocities when the leading edge is sufficiently anchored. The cable-tied block aprons used in the countermeasure experiments were sized so that the blocks were large enough for the mat to resist uplift failure at the highest flow velocity condition. In the preliminary cable-tied block experiments, overturning of the leading edge of the mat was observed to occur for the two highest flow velocity conditions. To prevent the leading edge of the cable-tied block mat from overturning at the higher flow velocities, type B3 blocks were fixed onto the front of the mat to anchor the leading edge.

Van Ballegooy (2005) investigated the stability against overturning of the leading edge of cable-tied block mats, recommending the following expression:

$$\theta_c = 0.002 + 0.06 \exp\left(-12 \frac{P_b}{L}\right) \quad (7-4)$$

Where:

- θ_c = critical dimensionless shear stress,
- P_b = protrusion of the blocks above bed level, and
- L = horizontal dimension of the blocks.

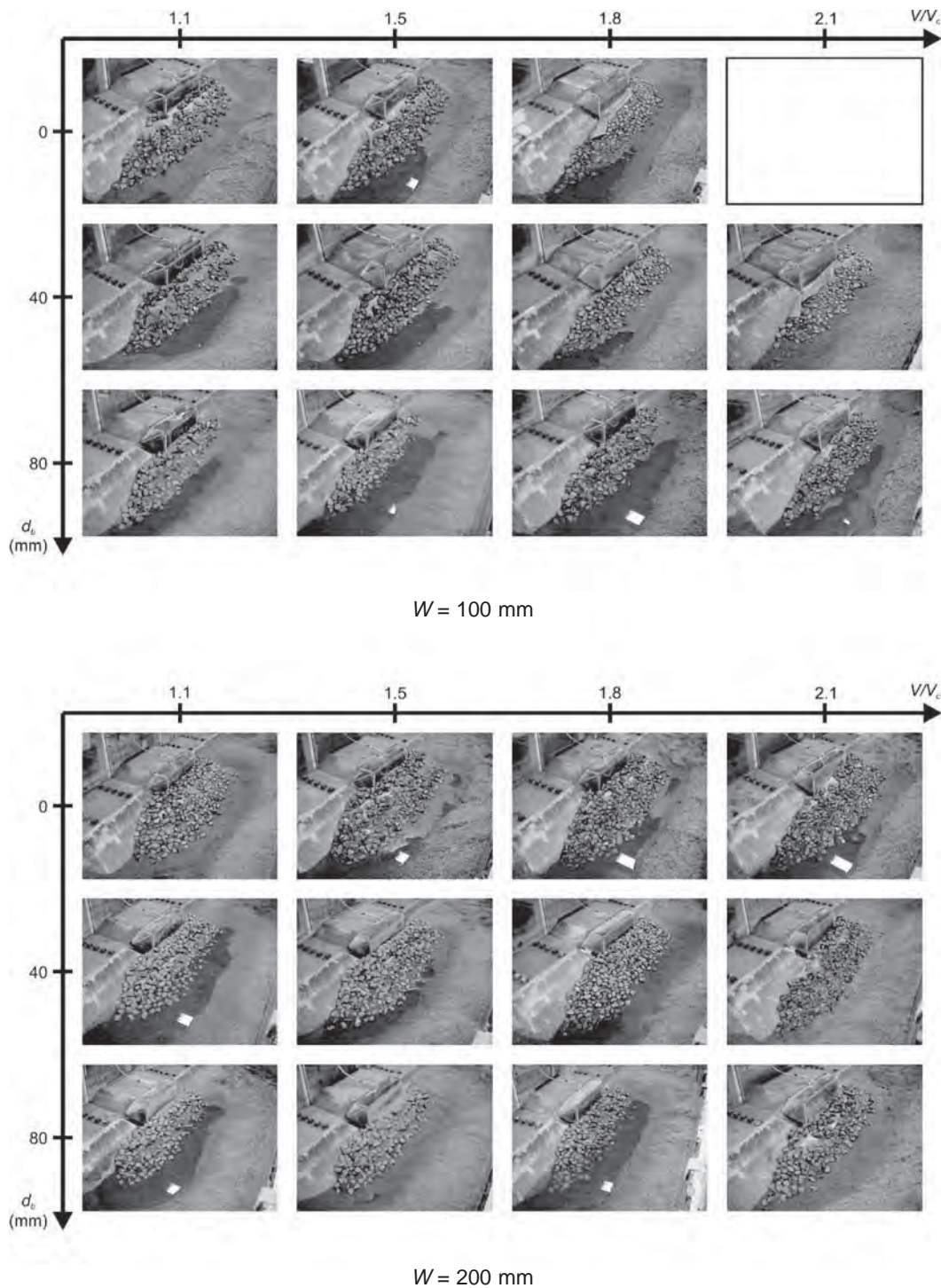


Figure 7-18. Performance of riprap apron protection at wing-wall abutments under live-bed conditions ($d_{50} = 40$ mm, and $y_m = 170$ mm).

Van Ballegooy showed that this equation was conservative when applied to a cable-tied block mat buried with its surface flush with the surrounding sediment bed—that is, for zero protrusion ($P_b = 0$). For this condition, $\theta_c = 0.062$ and Equation 7-4 can be expressed in the following form using the Manning equation for flow resistance:

$$\frac{H_b}{Y} = \frac{158}{(S_{cb} - 1)} Fr^2 \frac{n^2}{Y^{0.33}} \quad (7-5)$$

Where:

S_{cb} = specific gravity of the blocks and
 n = Manning coefficient.

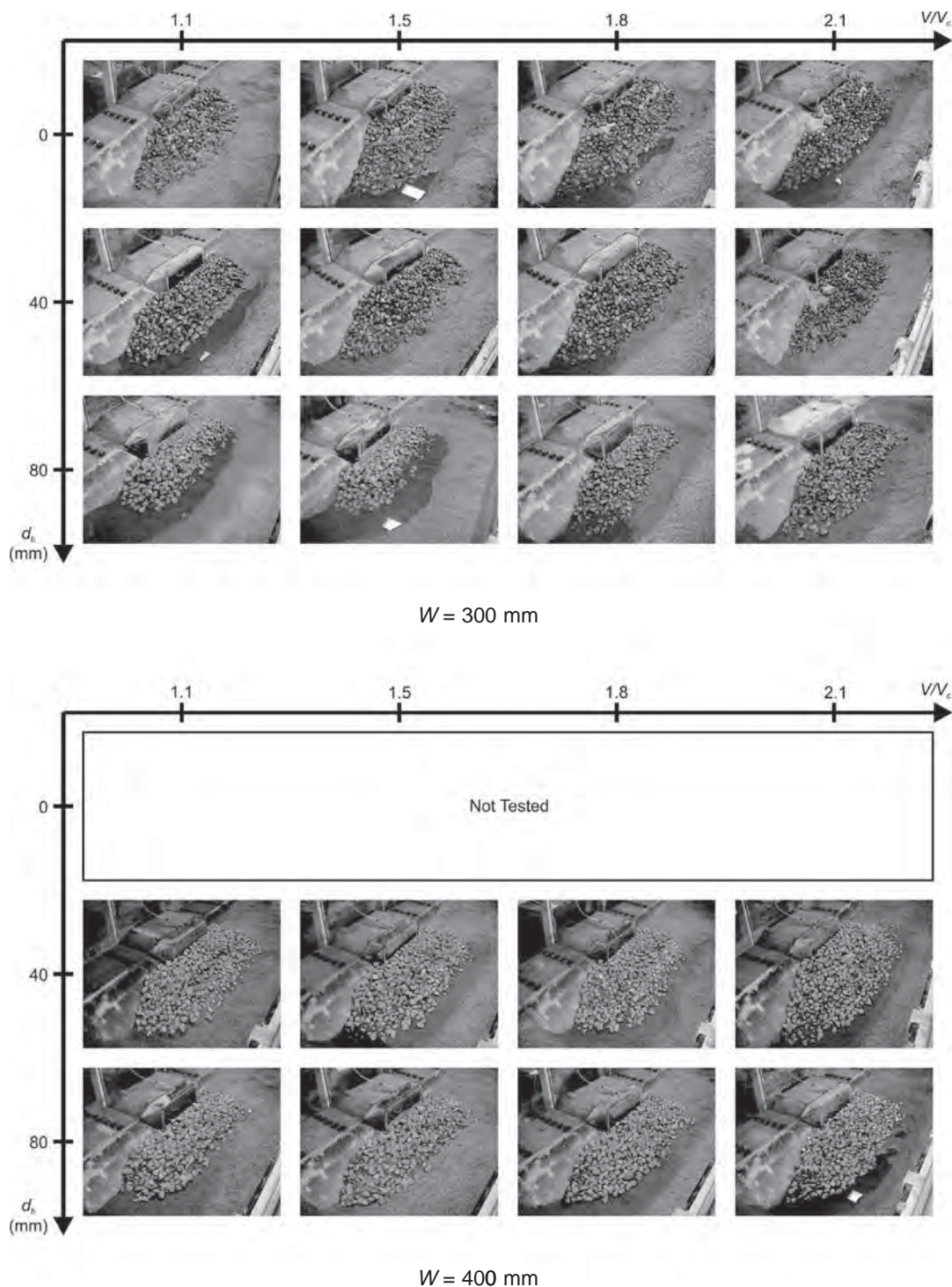


Figure 7-19. Performance of riprap apron protection at wing-wall abutments under live-bed conditions ($d_{50} = 40 \text{ mm}$, and $y_m = 170 \text{ mm}$).

Equation 7-5 provides a simple means of estimating block size to resist failure due to overturning and roll-up of the leading edge. In use of Equation 7-5, care needs to be taken to ensure that the leading edge of the mat remains buried.

Data Analysis

As is apparent from the data in Table 7-5, apron settlement and corresponding scour depths at the upstream end of the apron were typically larger than equivalent values at the

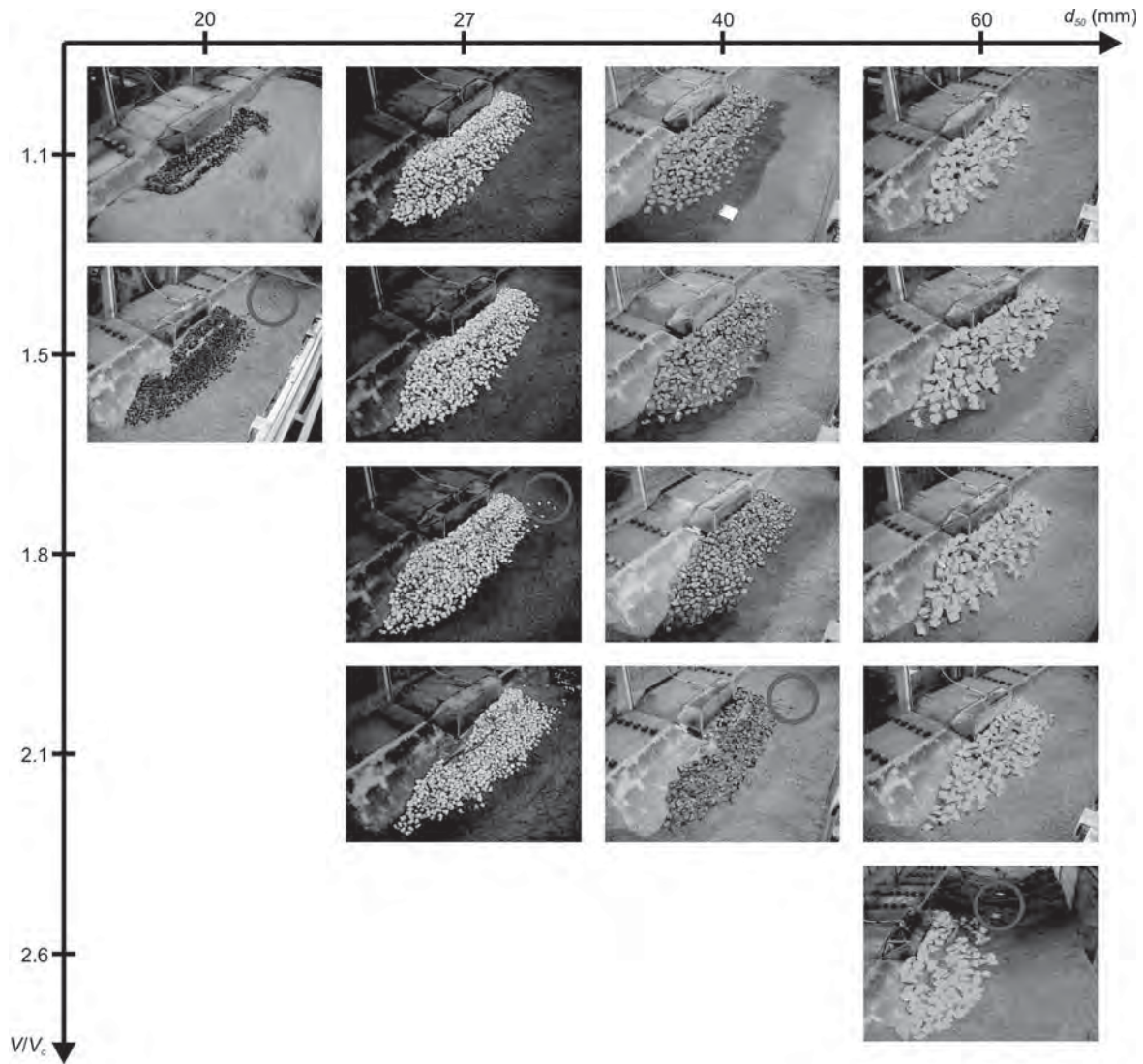


Figure 7-20. Performance of riprap apron protection at wing-wall abutments under live-bed conditions ($d_b = 1d_{50}$, $W = 200$ mm, and $y_m = 170$ mm).

downstream end because the bed forms were larger at the upstream end. At the downstream end of the abutment, the flow was fully contracted in the main channel. Consequently, the velocity increased, which caused the crests of the bed forms to wash out and the troughs to fill in because of a

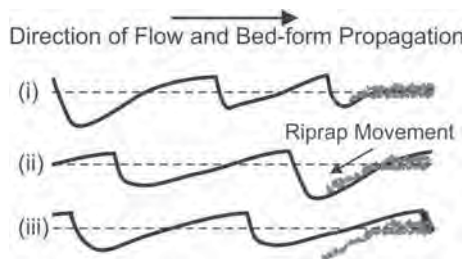


Figure 7-21. Riprap movement in response to bed-form propagation.

limitation of sediment supply. The measured scour depths are shown in Figure 7-24 as a functions of approach-flow intensity V/V_c .

The data are scattered due to the variability in bed form height and consequent apron settlement, but a trend of increased settlement with both increasing flow depth and increasing flow intensity is apparent. Since bed form height increases with both flow depth and flow velocity, the measured scour depths were plotted as a function of the maximum bed form height λ_{H-max} . Again, the data are scattered, but a trend of increased settlement with increasing λ_{H-max} is apparent. Most of the settlement depths for the upstream corner of the abutment are less than $1.2\lambda_{H-max}$, and for the downstream corner of the abutment they are equal to about $1.0\lambda_{H-max}$. Figure 7-25 shows the scour depth as a function of the maximum bed-form height.

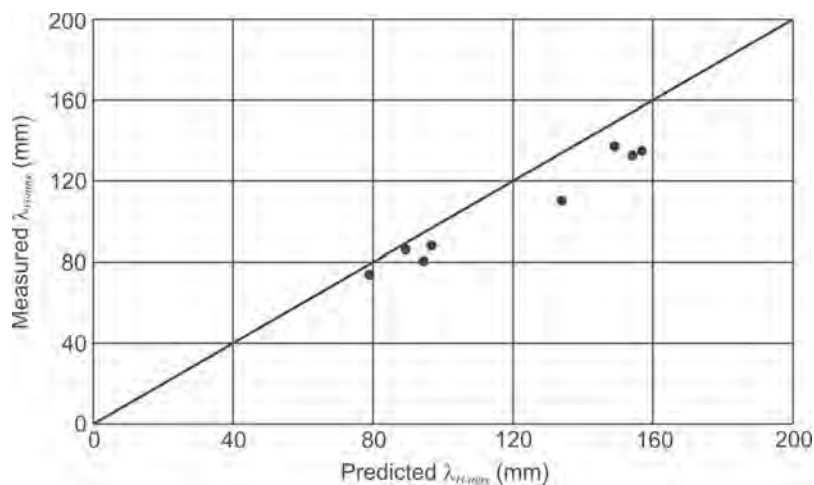


Figure 7-22. Comparison of measured maximum bed-form heights with predicted maximum bed-form heights using Equation 7-3.

Because the apron settlement d_{s2} is a function of the maximum bed form height λ_{H-max} , an approximate envelope approximation for the settlement depth is given by the following equation:

$$d_{s2} \approx C_4 \lambda_{H-max} = 0.16 C_4 \lambda_{L-ave}^{0.84} \quad (7-6)$$

Where $C_4 = 1.2$ and 1.0 for the upstream and downstream abutment corner positions, respectively, and λ_{L-ave} can be approximated from Yalin (1992). Figure 7-26 shows the measured apron settlements plotted against the predicted apron settlements using Equation 7-6. From the figure, it can be seen that Equation 7-6 envelops the bed form induced settlements reasonably well.

The angle β (see Figure 7-13) was calculated for each experiment from the measured values of d_{s1} , d_{s2} , W_{min} , and α_2 using the following expression:

$$\beta = \tan^{-1} \left(\frac{d_{s2} - d_{s1}}{\alpha_2 - W_{min}} \right) \quad (7-7)$$

The values of β for the wing-wall abutment scour experiments are shown in Figure 7-27, with average values of 25 degrees for the riprap aprons and 40 degrees for the cable-tied block aprons at both the upstream and downstream corners of the abutment. The different values of β for the riprap and cable-tied block protection can be directly related to the

Table 7-6. Flow parameters at the wing-wall bridge section.

y_m (m)	V/V_c	V_{2-surf} (ms^{-1})	V_{2-ave} (ms^{-1})	Fr_2	d_{50} (m)	d_{50}/y_m	Riprap Stability
0.170	1.1	0.50	0.43	0.33	0.020	0.12	Stable
0.170	1.5	0.71	0.62	0.48	0.020	0.12	Shear Failure
0.170	1.1	0.50	0.43	0.33	0.027	0.16	Stable
0.170	1.5	0.71	0.62	0.48	0.027	0.16	Stable
0.170	1.8	0.79	0.69	0.53	0.027	0.16	Shear Failure
0.170	2.1	0.96	0.84	0.65	0.027	0.16	Shear Failure
0.100	1.1	0.49	0.43	0.43	0.040	0.40	Stable
0.100	1.4	0.59	0.51	0.51	0.040	0.40	Stable
0.100	1.8	0.78	0.64	0.64	0.040	0.40	Stable
0.100	2.2	1.01	0.87	0.88	0.040	0.40	Shear Failure
0.170	1.1	0.50	0.43	0.33	0.040	0.24	Stable
0.170	1.5	0.71	0.62	0.48	0.040	0.24	Stable
0.170	1.8	0.79	0.69	0.53	0.040	0.24	Stable
0.170	2.1	0.96	0.84	0.65	0.040	0.24	Shear Failure
0.170	1.1	0.50	0.43	0.33	0.060	0.35	Stable
0.170	1.5	0.71	0.62	0.48	0.060	0.35	Stable
0.170	1.8	0.79	0.69	0.53	0.060	0.35	Stable
0.170	2.1	0.96	0.84	0.65	0.060	0.35	Stable
0.170	2.6	1.10	0.96	0.74	0.060	0.35	Shear Failure

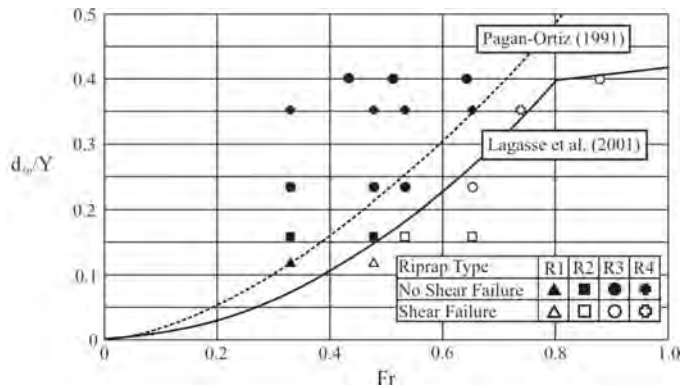


Figure 7-23. Normalized riprap size for apron protection at the bridge abutments as a function of the Froude number of the flow in the contracted bridge section.

manner in which the aprons settled. Because the cables prevented the cable-tied block aprons from increasing in width, sand was eroded from beneath the apron, and the outer edge of the apron folded down, retaining the sand at an angle larger than the repose angle of the sand. When a riprap apron was undermined, the apron increased in width as the riprap stones

rolled forward and down into the bottom of the troughs. The slope of the undermined section of the riprap apron was typically slightly less than the repose angle of the sand.

Figure 7-28 is a schematic diagram showing the settlement of an idealized riprap apron. The thickness of the apron is nd_{50} , where n is the number of layers of riprap. For cable-tied block mats, $n = 1$ and nd_{50} is taken equal to the block height H . For the case when $W_{min} > 0$, d_{s1} and d_b are related as follows:

$$d_{s1} = d_b - nd_{50} \tag{7-8}$$

Where d_{s1} is taken to be negative when the top of the apron is above the average bed level ($nd_{50} > d_b$) and vice versa.

Figure 7-28 shows the settlement and spreading of five riprap stones. From the experimental work, the portion of apron that settled ($W - W_{min}$) was observed to increase with increasing d_{s2} and decrease with increasing d_b , as shown in Figure 7-29. The spread length (slope length) L_s of the apron after settlement can be given by the following equation:

$$L_s = \frac{C_3 [d_{s2} - d_b + (n-1)d_{50}]}{n \sin \beta} \tag{7-9}$$

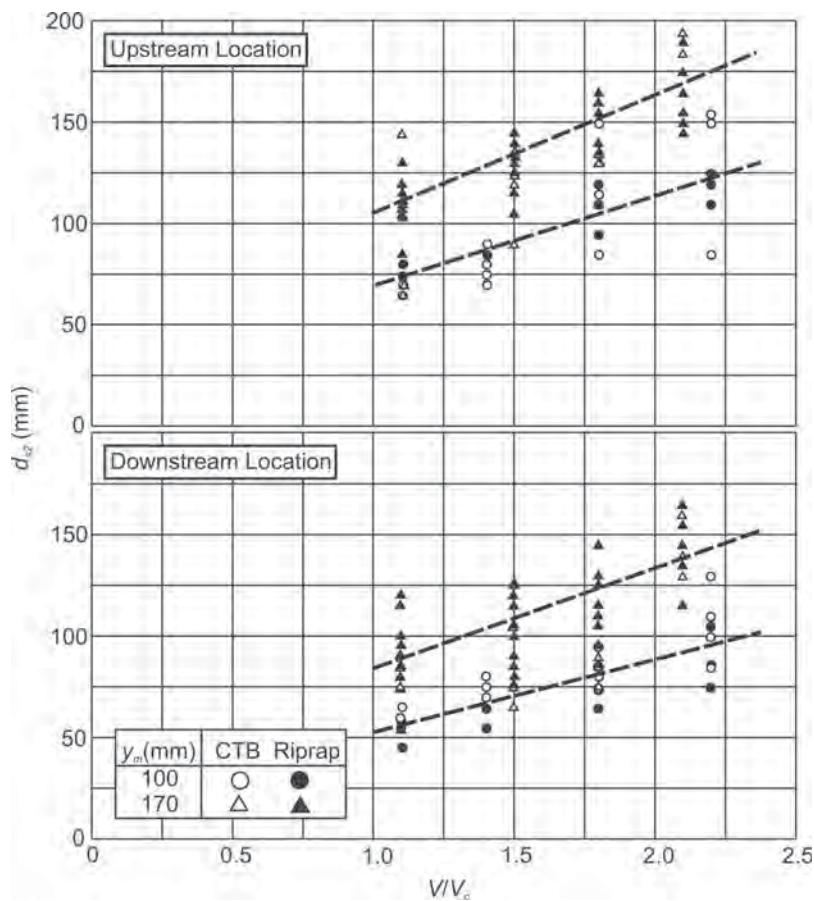


Figure 7-24. Scour depth as a function of flow intensity for both the upstream and downstream corners of the abutment.

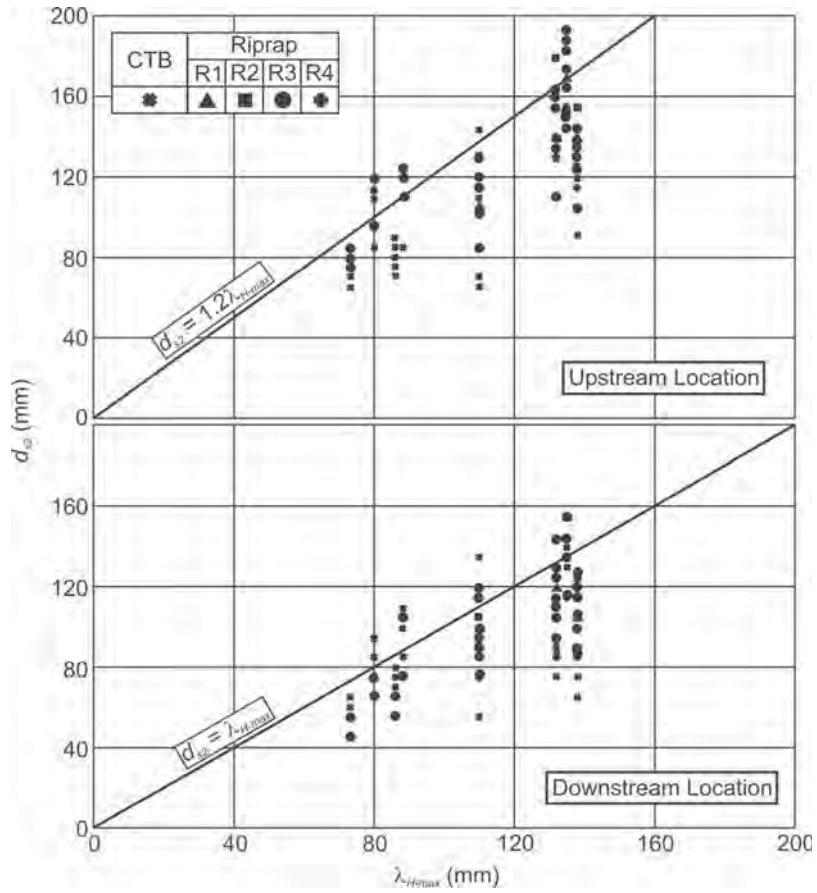


Figure 7-25. Scour depth at the abutment as a function of the maximum bed-form height for both the upstream and downstream corners of the abutment.

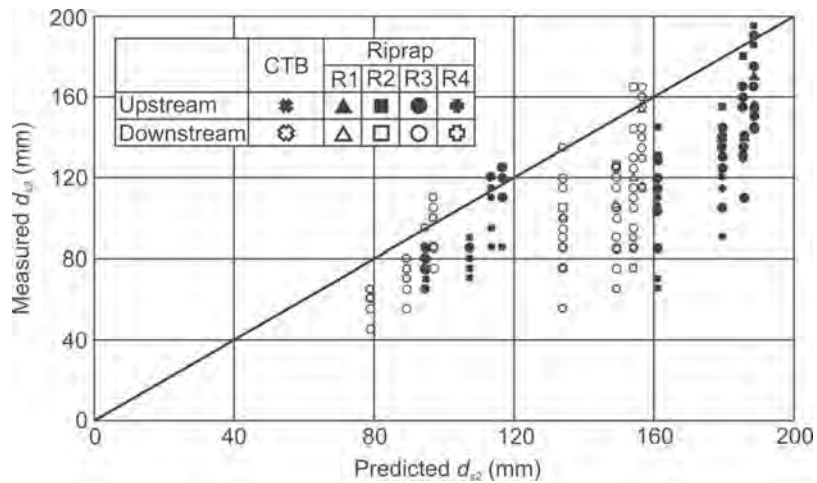


Figure 7-26. Comparison of the predicted scour depths using Equation 7-6 with the measured scour depth for both the upstream and downstream corners of the abutment.

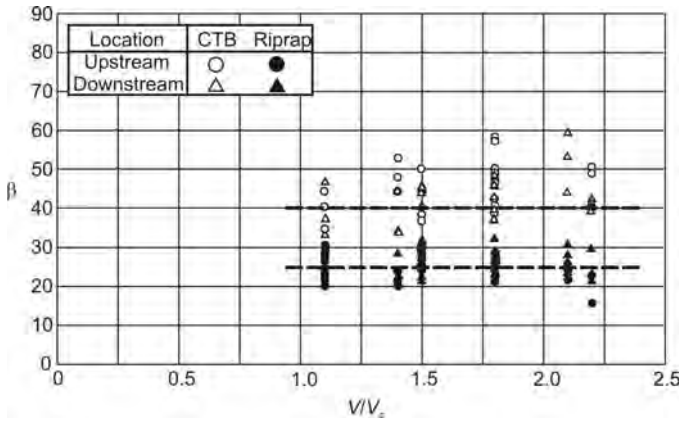


Figure 7-27. Angle of apron settlement as a function of flow intensity for both the upstream and downstream corners of the abutment.

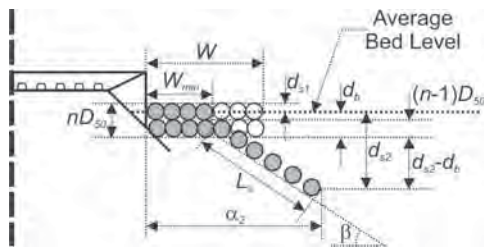


Figure 7-28. Apron settlement due to undermining of an idealized riprap apron.

Where the coefficient C_5 varies for the upstream and downstream locations depending on the direction of movement of the undermined riprap stones. At the upstream corner of the wing-wall abutment, the riprap stones moved both laterally away from the abutment and upstream when rolling into the scour regions. The distance L_s for the upstream corner was aligned 45 degrees to the abutment face, and $C_5 = \sqrt{2}$. At the downstream corner of the wing-wall abutment, the riprap stones rolled laterally away from the abutment into the scour region. The distance L_s for the downstream corner was aligned perpendicular to the abutment face, and $C_5 = 1$. A value of $C_5 = 1$ applied to cable-tied block aprons, irrespective of the location.

An expression for W_{min} can be derived as follows:

$$W_{min} = W - C_6 L_s = W - \frac{C_5 C_6 [d_{s2} - d_b + (n-1)d_{50}]}{n \sin \beta} \quad (7-10)$$

Where the coefficient C_6 represents the proportion of L_s that was covered by riprap stones. Figure 7-30 shows a plot of the experimental data for riprap aprons in a rearranged form of Equation 7-10. The figure shows that a value of $C_6 = 0.8$ is appropriate.

For riprap, $C_5 = 1$ at the downstream corner of the riprap layer, $C_5 = \sqrt{2}$ at the upstream corner, $C_6 = 0.8$, and $\beta = 25$

degrees. The limiting condition for design is when $W_{min} = 0$, when Equation 7-10 reduces to the following:

$$W = C_1 (d_{s2} - d_b + d_{50}) \quad (7-11)$$

Where the coefficient $C_1 = 1.68$ and 1.19 at the upstream and downstream corners of the riprap layer, respectively.

For cable-tied block aprons, $C_6 = 1$ because the cables in the mat prevented spreading. Hence, Equation 7-11 reduces to

$$W_{min} = W - \frac{[d_{s2} - d_b]}{\sin \beta} \quad (7-12)$$

The limiting condition for design is when $W_{min} = 0$. With $\beta = 40$ degrees for cable-tied blocks, Equation 7-12 reduces to:

$$W = 1.55(d_s - d_b) \quad (7-13)$$

Equations 7-12 and 7-13 both imply that W_{min} increases linearly with W , which is in agreement with the experimental data from Table 7-5. The equations also imply that W_{min} decreases with increasing d_{s2} and increases with increasing d_b . The reduced minimum apron width for increased scour depth is a consequence of larger bed forms propagating through the bridge section as a result of deeper flows and higher flow velocities. Regarding placement level, the deeper the apron is buried below the average bed level, the smaller the volume of the material undermined from the apron during bed form propagation (consistent with the experimental study of Korkut, 2004). When the apron is buried below the expected scour depth ($d_b > d_s$), the apron cannot be undermined, so there is no apron loss ($W = W_{min}$). When the predicted values of W_{min} (from Equations 7-12 and 7-13) are less than zero, settlement occurs at the abutment face. Figure 7-31 compares the measured W_{min} data with the predicted W_{min} values using Equations 7-12 and 7-13.

Figure 7-31 demonstrates a reasonable agreement between the measured and predicted W_{min} values, even though there is a lot of scatter in the measured values of W_{min} . The protective aprons settled in response to the propagation of bed forms through the bridge section. The bed forms are inherently variable in size and shape, and, as a result, the associated apron settlement is also inherently variable. This is the reason for the scatter in measured values of W_{min} shown in Figure 7-31.

Equations 7-12 and 7-13 have a similar structure with the exception of the factor $C_5 C_6 / n \sin \beta$, which takes values of 1.34 and 0.95 for riprap protection ($n = 2$) at the upstream and downstream corners, respectively, and 1.56 for cable-tied block protection. At the upstream corner of the abutment, W_{min} is slightly less for cable-tied block aprons than for riprap aprons, while W_{min} values are considerably larger for riprap aprons at the downstream corner. The implication is

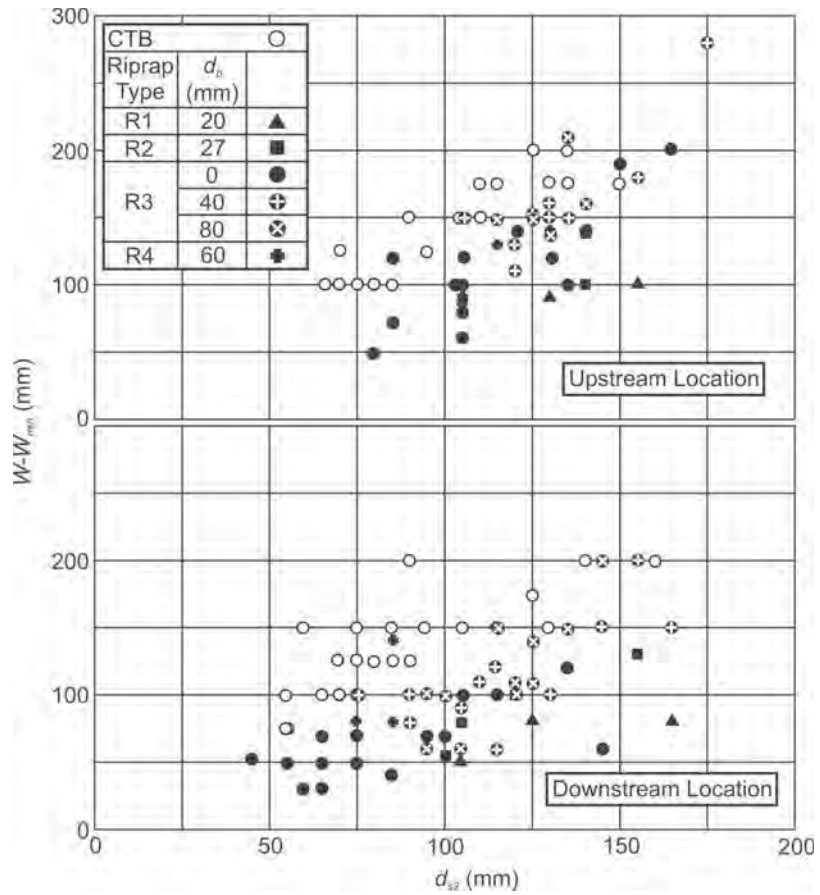


Figure 7-29. Portion of apron that was undermined ($W-W_{min}$) as a function of the scour depth for both the upstream and downstream corners of the abutment.

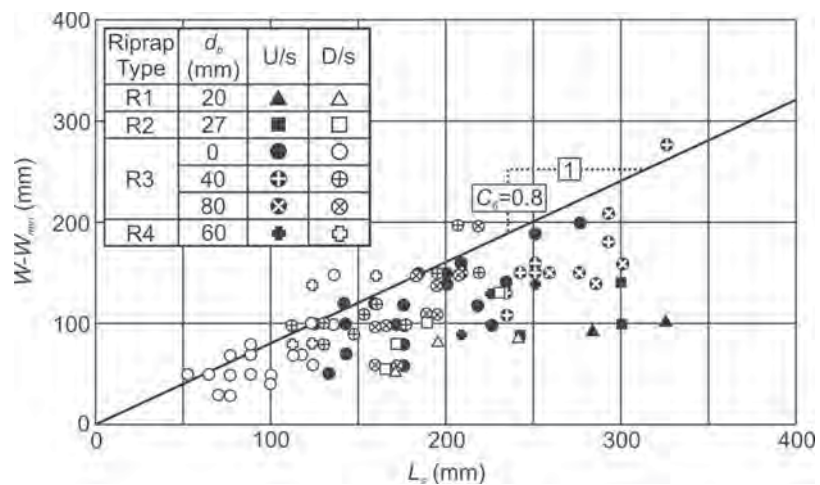


Figure 7-30. Portion of apron that was undermined ($W-W_{min}$) as a function of the riprap spread distance for both the upstream and downstream corners of the abutment.

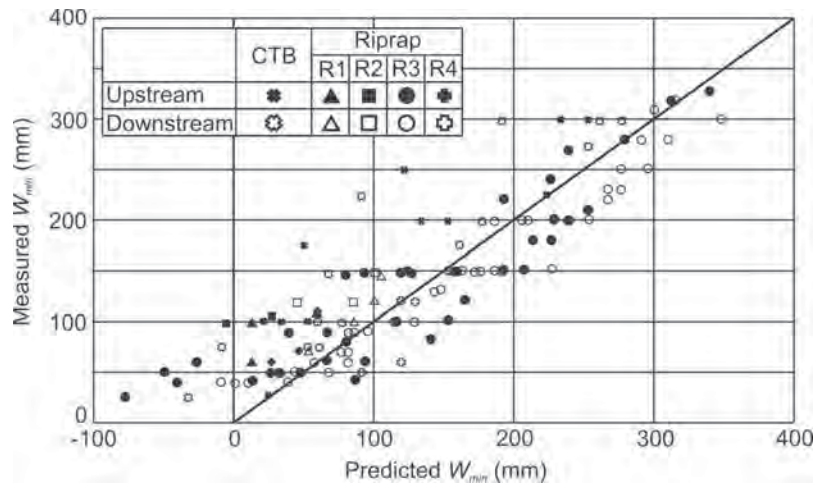


Figure 7-31. Comparison of the predicted values of W_{min} using Equations 7-12 and 7-13 with the measured values of W_{min} for both riprap and cable-tied block protection.

that cable-tied block aprons need to be wider than riprap aprons (with two riprap layers) to afford the same level of protection at wing-wall abutments. Conversely, for the case where only one layer of riprap is used in an apron, such an apron will need to be considerably wider than a cable-tied block apron to afford the same level of protection at the abutment.

For Case I in Figure 7-13, where $W_{min} > 0$, an expression for α_2 can be developed (as shown in Figure 7-30) as follows:

$$\alpha_2 = W_{min} + \frac{[d_{s2} - d_b + (n-1)d_{50}]}{\tan\beta} \tag{7-14}$$

By substituting Equation 7-12 into 7-14, a simplified expression can be developed for α_2 as follows:

$$\alpha_2 = W + \left(\frac{n \cos\beta - C_5 C_6}{n \sin\beta} \right) [d_{s2} - d_b + (n-1)d_{50}] \tag{7-15}$$

For cable-tied block protection, C_5 , C_6 , and n all equal 1, so Equation 7-15 reduces to the following:

$$\alpha_2 = W + \left(\frac{\cos\beta - 1}{\sin\beta} \right) [d_{s2} - d_b] \tag{7-16}$$

Figure 7-32 compares the measured α_2 data with the predicted α_2 values using Equations 7-15 and 7-16. Equations 7-15

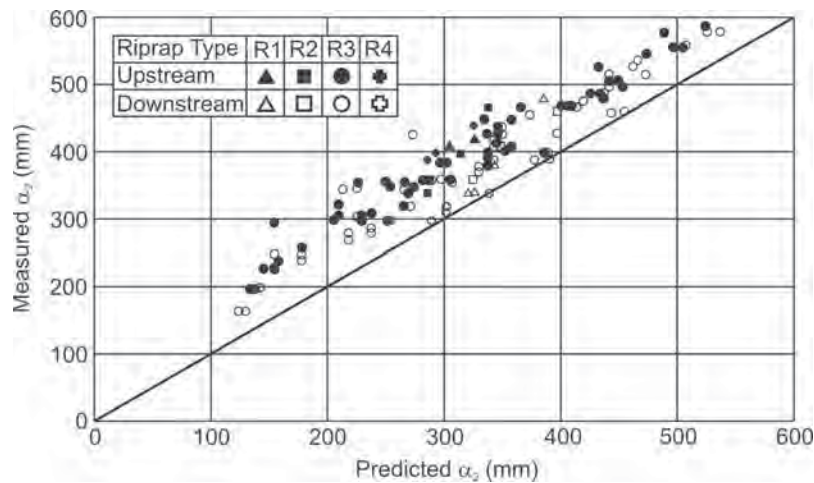


Figure 7-32. Comparison of the predicted values of α_2 using Equations 7-15 and 7-16 with the measured values of α_2 , for both riprap and cable-tied block protection.

and 7-16 tend to underpredict the α_2 values slightly, but overall there is a good agreement between the measured and predicted α_2 values. Underprediction of the α_2 values is conservative, however, because the troughs of the bed forms are predicted to pass closer to the abutment face.

Equations 7-15 and 7-16 have a similar structure with the exception of the factor $(n\cos\beta - C_5C_6)/n\sin\beta$, which takes values of 0.81 and 1.19 for riprap protection ($n = 2$) at the upstream and downstream corners, respectively, and -0.36 for cable-tied block protection. This shows that α_2 exceeds W for riprap aprons after settlement. The stones from the riprap apron tend to settle and move away from the abutment face, deflecting the troughs of the bed forms farther away from the abutment. Conversely, α_2 is slightly less than W for cable-tied block aprons after settlement, allowing the troughs of the bed forms to pass closer to the abutment face.

For the case where $d_{s1} > 0$ (Case II in Figure 7-13), insufficient protection has been placed around the abutment ($W_{min} < 0$). In this situation, a riprap apron, which settles at the abutment face due to insufficient extent, will still afford some protection because the scour depth at the abutment face is typically less than what it would be if no protection had been provided. Conversely, a cable-tied block apron with insufficient apron width offers minimal protection and typically induces deeper scour at the abutment face because the apron, being attached to the abutment face, creates a larger obstruction to the flow.

7.3 Experiments on Aprons of Geobags and Riprap

The program of experiments consisted of the following sets of investigations:

1. Diagnostic experiments on geobag stability at solid abutment;
2. Baseline scour condition at the single, pile-supported abutment (without an apron);
3. Scour performance of riprap aprons at a single, pile-supported abutment;
4. Scour performance of geobag aprons at a single, pile-supported abutment; and
5. Scour performance of an armor apron across the entire bed of a short bridge.

By virtue of the inherent trial-and-error nature of the study—to determine how well an apron worked—considerably more experiments were conducted than are presented herein. Many of the experiments were ended without the scour having reached an equilibrium state; if a test apron

failed, there was little point in continuing the experiment. Korkut (2004) and Morales (2006) provide full documentation of the experiments.

7.3.1 Experiment Layout

Flume experiments were conducted using the same flume as that used for the preliminary experiments described in Chapter 6. The flume was 27.4 m long, 0.91 m wide, and 0.45 m deep. The flume recirculated sediment. The flume was fitted with a 200-mm deep bed of sand. Figure 7-33 shows the sand bed along the flume.

Approach-Flow Conditions

The experiments were conducted under live-bed flow conditions, with $u^*/u_{*c} = 1.5$ (here u^* is the shear velocity, and u_{*c} is the critical value of the shear velocity associated with bed particle movement). The main hydraulic parameters for the flume flow were the following: mean velocity, $V_0 = 0.55$ m/s; and flow depth, $y_0 = 100$ mm. The sediment parameters were the following: median particle size, $d_{50} = 0.45$ mm; standard deviation of sediment size, $\sigma_g = 1.4$; specific gravity of particles = 2.4; and, the angle of sediment repose, $\alpha = 30$ degrees. The average height of the dunes moving along the flume bed was 34 mm.

Similitude between laboratory experiments and field scale was satisfied by the use of the aforementioned u^*/u_{*c} ratio, of which a value above 1.0 represents a condition called “live-bed scour.” This condition is extreme for scouring of armouring units such as geobags because the high velocity can dislodge a geobag and therefore constitute failure.



Figure 7-33. Flume with sand bed in dune regime.

Wing-Wall Configurations

The bulk of the experiments were conducted using a single wing-wall abutment that replicated, at a scale corresponding to about 1:40, the width of abutments typical of two-lane roads in the United States; the road width is about 12 m (40 ft). Three variations on this abutment form were used:

1. **A solid wing-wall abutment whose walls extended the full bed depth.** Such an abutment in practice would be founded on sheet piles. The abutment was made from Plexiglas to facilitate observation of geobag behavior and scour development. Figure 7-34 shows this test abutment. These experiments were useful for obtaining bed-level observations concerning the manner whereby the flow field around a wing-wall abutment could entrain geobags and at times erode sand from around geobags.
2. **A wing-wall abutment on a pile cap supported on two rows of circular piles.** Figure 7-35 shows the dimensions of this model abutment, which was used for the final performance testing of riprap and geobag aprons.
3. **A pair of opposing wing-wall abutments, representing the layout of a small short-span bridge.** Figure 7-36 illustrates this layout, which was used for determining

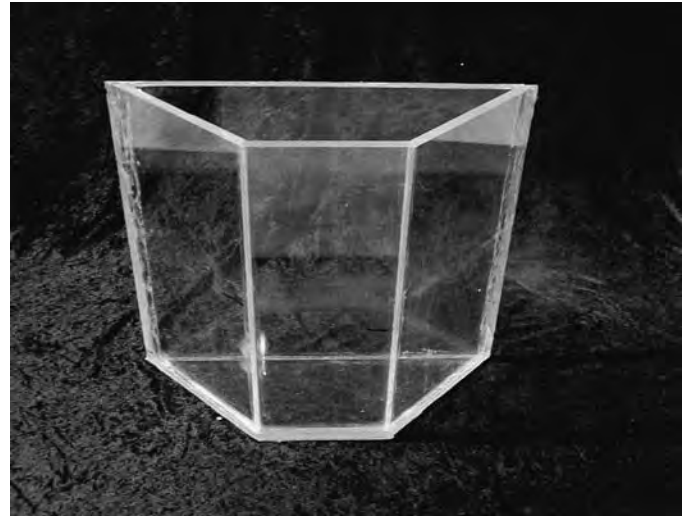


Figure 7-34. Plexiglas abutment used for viewing geobag stability.

the performance of an apron extending between two opposing abutments.

Depending on the presence and the arrangement of an apron at an abutment, the maximum depth of scour could occur at any of three locations, as indicated in Figure 7-37: in

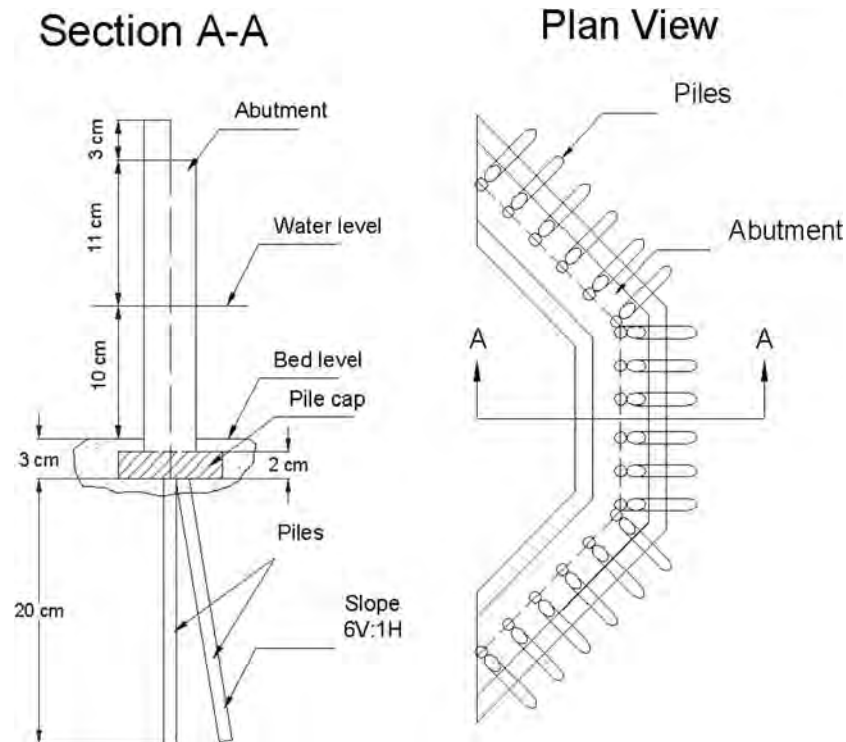


Figure 7-35. Model dimensions of a 45-degree wing-wall abutment of the pile-supported form commonly used in the United States.

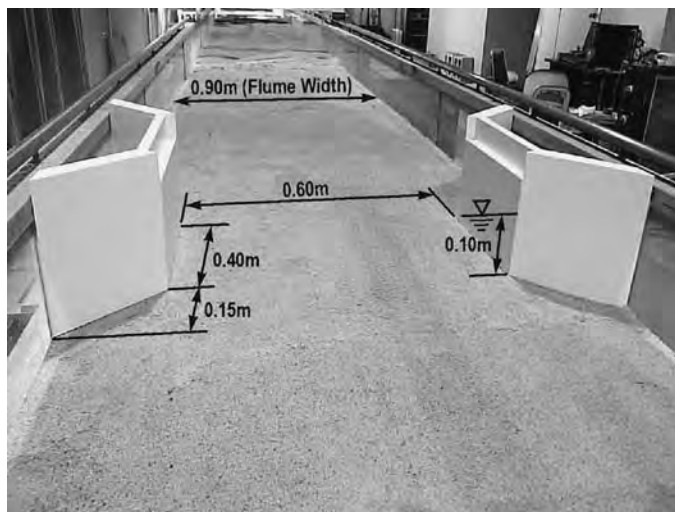


Figure 7-36. Layout of two opposing wing-wall abutments.

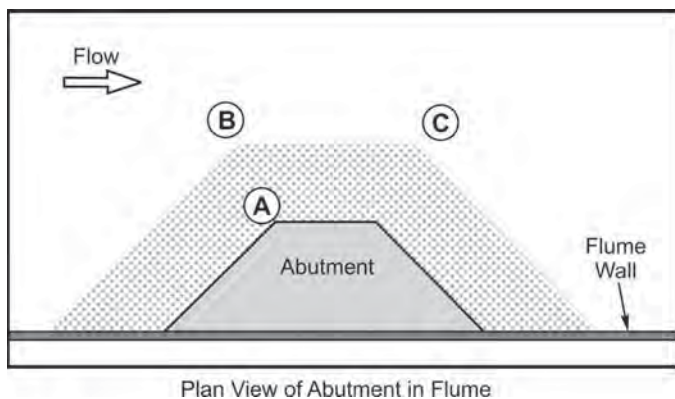


Figure 7-37. Locations of deepest scour: A, no protective apron; B, loose protective apron that partially fails; C, protective apron tied to abutment.

front of the abutment itself (A), in front of loose apron protection (B), and downstream of an apron formed of armor elements linked like a mattress (C). Table 7-5 lists the selection of scour experiments reported herein.

Riprap Sizing

The diameter of riprap stone used was estimated using the relationship proposed by Richardson and Davis (1995):

$$\frac{D_R}{Y} = \frac{K_s}{(S_s - 1)} Fr^n \quad (7-17)$$

Where:

- D_R = equivalent riprap diameter,
- Y = flow depth in the bridge section,
- K_s = shape factor associated with abutment shape (wing-wall or spill-through),

Table 7-7. Values of K_s and n for Equation 7-17 (Richardson and Davis, 1995).

Fr	K_s	n
≤ 0.8	1.02	2.0
> 0.8	0.69	0.1

$$Fr = U/(gY)^{0.5}$$

= Froude number for the mean flow in the bridge (contracted) section, and

S_s = specific gravity of riprap stone.

For wing-wall abutments, values of K_s and n are given in Table 7-7 (Richardson and Davis, 1995).

For the flow conditions used in the experiments using $S_s = 1.4$ and determined for the available stone, Equation 7-17 gives $D_R = 22$ mm, which is about the same as the required thickness of geobag estimated using Equation 7-15. The riprap stone that was selected for the flume tests was sieved so that $D_R \approx 22$ mm, with a shape factor (major axis/minor axis) of about 2.1.

Geobag Sizing

The simulated, large geobags were sized in accordance with a design method proposed by Pilarczyk (2000). The method estimates a geobag thickness, D_B . The aerial extent of a geobag should exceed D_B and otherwise can be sized for handling ease or to fit a site. The general form of Pilarczyk's relationship for geobag thickness is as follows:

$$D_n = \frac{0.035}{(S_{SB} - 1)} \frac{\phi}{\theta_c} \frac{K_T K_h}{K_{st}} \frac{V^2}{2g} \quad (7-18)$$

Where:

- S_{SB} = specific gravity of the geobag;
- V = depth-averaged mean velocity;
- g = gravity acceleration;
- ϕ = stability parameter;
- θ_c = critical value of the Shields parameter for particle (geobag) entrainment;
- K_T = turbulence factor;
- K_h = depth parameter; and
- K_{st} = slope parameter, expressed as:

$$K_{st} = \sqrt{1 - \left[\frac{\sin^2 \alpha}{\sin^2 \theta} \right]} \quad (7-19)$$

Where α is the angle of the boundary on which the geobag is placed, and θ_c is the angle of repose of the sediment forming the boundary. For the experiments, α and θ were 26.7 degrees and 30 degrees, respectively. Pilarczyk (2000), who gives the background to Equation 7-19, recommends for geobags that ϕ , θ_c , and K_T be 0.75, 0.05, and 2.0, respectively.

The depth parameter K_h is defined as a function of water depth y and equivalent roughness k_s . Pilarczyk suggests using $k_s = D_n$. However, since D_n is unknown initially, the measured thickness of the geobag sample was used as a trial value. The required thickness of the geobags, D_n , was calculated as 22 mm using a bulk-specific gravity of the model geobags measured to be 1.46. Accordingly, the model geobags used in the experiments were selected to be 22 mm thick and 95×55 mm in plan area.

7.3.2 Procedure

In general terms, the experimental procedure was similar to that used for the experiments at the University of Auckland. The bed sediment was placed as a 0.2-m thick layer along the whole length of the flume. A trial-and-error procedure was used to adjust the flow through the flume so as to obtain uniform flow 0.1 m deep and an average velocity (discharge/flow area) that was 1.5 times greater than the critical velocity for incipient motion of the bed sediment. Achieving this flow condition required adjustment of flume slope once the appropriate discharge had been set. Water depth in the flume was controlled by means of a tailgate. The tailgate was adjusted to set the water depth, yet still enable sediment to pass into the tail box.

Once the flow condition had been set, the flow was left running through the flume for about 2 days so that the bed forms (i.e., dunes) over the bed would attain nominally steady dimensions. The average height and length of the dunes was fairly constant along the flume, though some scatter in magnitudes occurred. Once the bed forms were fully developed, the flume slope was adjusted so as to ensure that the requisite flow depth occurred for the discharge over the dune bed. To check for overall uniformity of flow depth, water surface elevations were measured at 10 positions along the flume. Additionally, an acoustic Doppler velocimeter (ADV) was used to measure the velocity profiles to check with the estimated velocity based on flow depth and discharge.

With the flow condition determined and the flume slope set, the flume was drained and the test abutment placed in the flume. The bed at the abutment location was levelled when the abutment was placed, but the bed elsewhere in the flume remained in the dune regime condition, thereby enabling the flow to quickly establish itself when the experiment began. The flume was filled to the prescribed depth, the flume's pump started, and the experiment then begun. Slight adjustment of water level occurred early in the experiment to ensure that the prescribed average water depth prevailed along the flume.

The experiments varied in their duration. Tests in which the apron arrangement failed were stopped soon after the failure occurred. Typically, the scour reached an equilibrium condition

shortly after apron failure, owing mainly to the live-bed condition of the experiment. Tests in which the apron remained intact were run for 2 days, over which time the bed conditions were monitored periodically. At the end of each experiment, the location and depth of maximum scour were recorded.

7.3.3 Results: Solid-Wall Abutments

Described in this section are experiments conducted to measure the performance of the geobags as a scour countermeasure. The experiments progressed from a baseline condition that was used as a reference for the subsequent experiments toward the solution. The effectiveness of each countermeasure was assessed in terms of the reduction of the scour depth that occurred when the abutment was not protected by a countermeasure. The geometry of the wing-wall abutment used throughout the experiments is given in Figure 7-38.

Baseline Scour

This experiment produced a reference, baseline scour depth for use in evaluating the effect of the countermeasure applied to reduce the scour depth. The baseline experiment was conducted without a countermeasure. The maximum scour depth occurred at the upstream corner of the abutment and was 162 mm. As mentioned above, the dunes moving along the flume had a height of 34 mm.

Geobags on Bed Surface

In this experiment, an apron of loose geobags was placed on the bed surface around the abutment. The geobags were 55 mm wide, 95 mm long, and 14 mm thick. Figure 7-39 shows the apron.

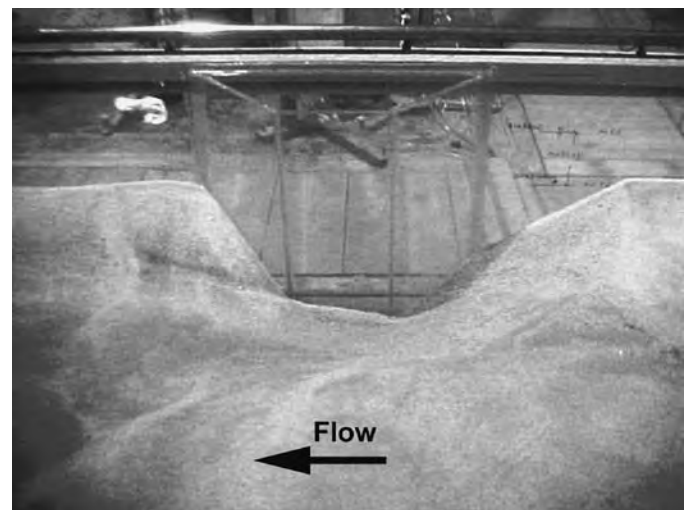


Figure 7-38. Maximum scour depth for baseline scour.

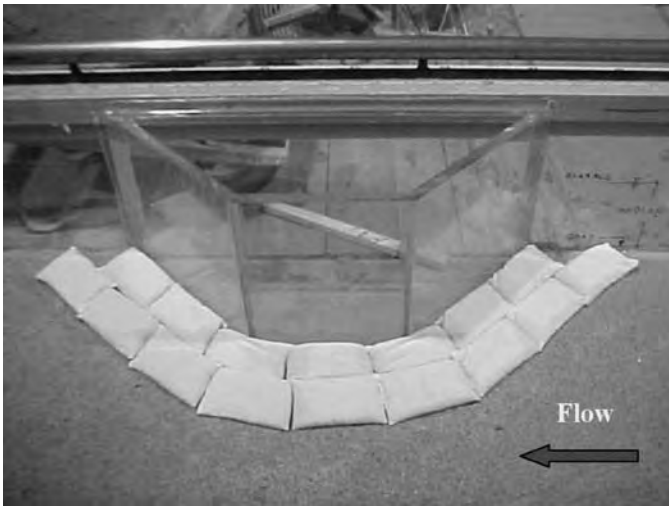


Figure 7-39. Layout of loose geobags placed as an apron.

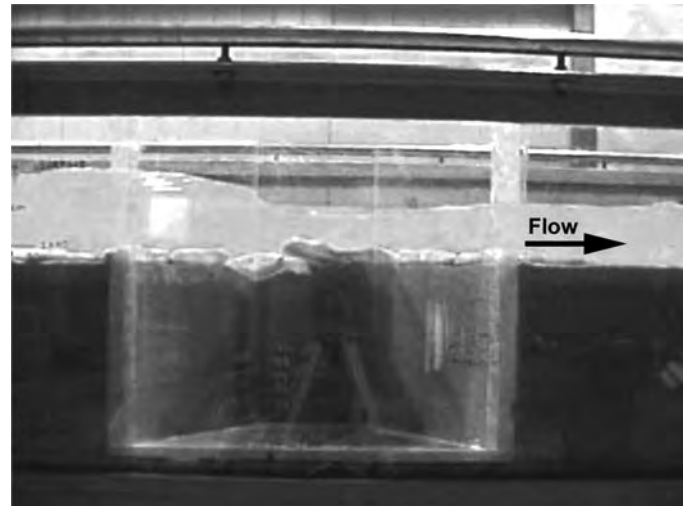


Figure 7-41. Flow entrains a geobag at abutment face.

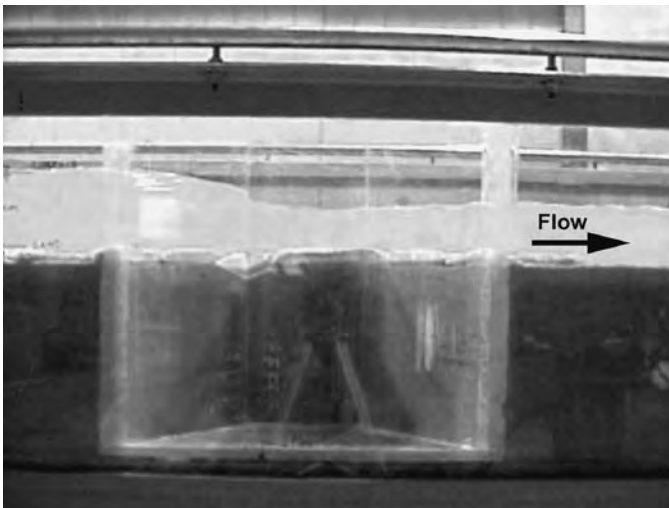


Figure 7-40. Scour begins at the interface of the geobag apron and the abutment.

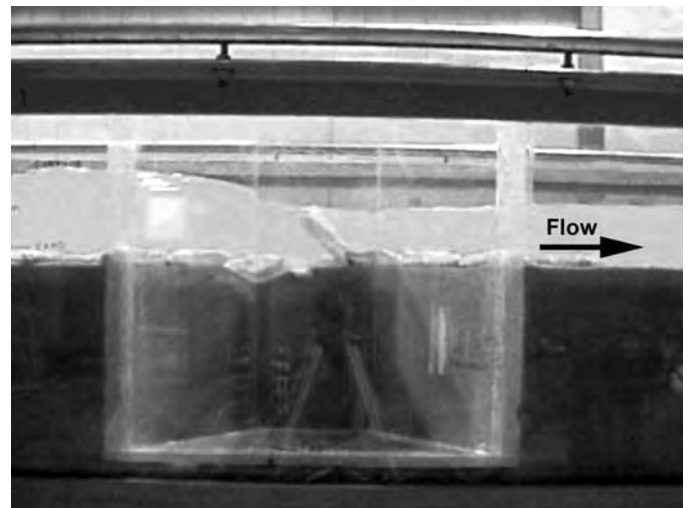


Figure 7-42. Flow lifts a geobag from the apron.

The geobag apron failed to withstand the flow. Some geobags became embedded in the sediment, and some were rolled away from the abutment. The apron began failing along the abutment's streamwise face. Bed sediment was winnowed from around the edges of the geobags and the face of the abutment. Consequently, scour still began around the abutment's sides and beneath the geobags. As scour progressed, some geobags became exposed to higher flow velocity and subsequently became unstable. Eventually, the flow forces caused some of these geobags to turn over and move away from the abutment. Gradually, the apron disintegrated. Figures 7-40 through 7-44 depict this failure process. The maximum scour depth, measured at the upstream corner of the abutment, was 156 mm, only a 4-percent reduction of the baseline scour depth (Figure 7-44).

Geobags on Filter Cloth

For this experiment, a geotextile underlay fabric, acting as a geofilter cloth, was used in combination with geobags. Figure 7-45 shows the layout of the geobags and filter cloth. The gap between the filter cloth and abutment was sealed in order to minimize the sediment winnowing. Figure 7-45 shows the apron at the start of the experiment.

During this experiment, however, sediment was eroded from around the perimeter of the apron. This erosion undermined the apron's upstream row of geobags and gradually led to the apron's complete failure. Geobags slid into the scour hole that formed around the apron. The collapse of the front row of geobags exposed the latter rows and filter cloth. Water flow lifted the filter cloth and caused most of the remaining geobags to slide into the scour hole. Subsequently, a highly

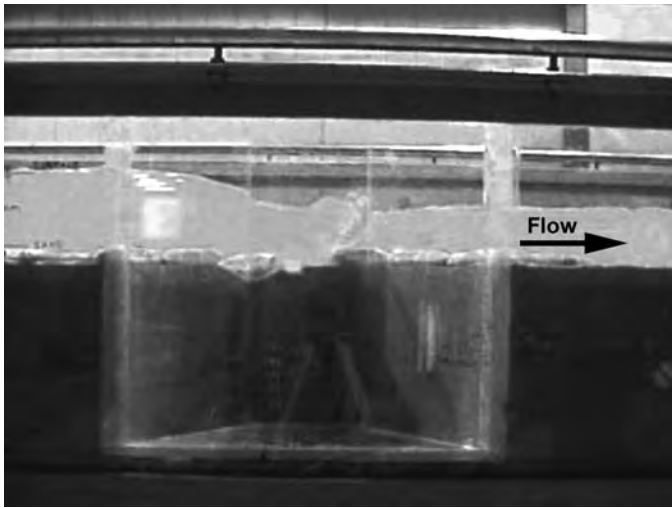


Figure 7-43. The geobag is swept from the apron, which then begins to break up.

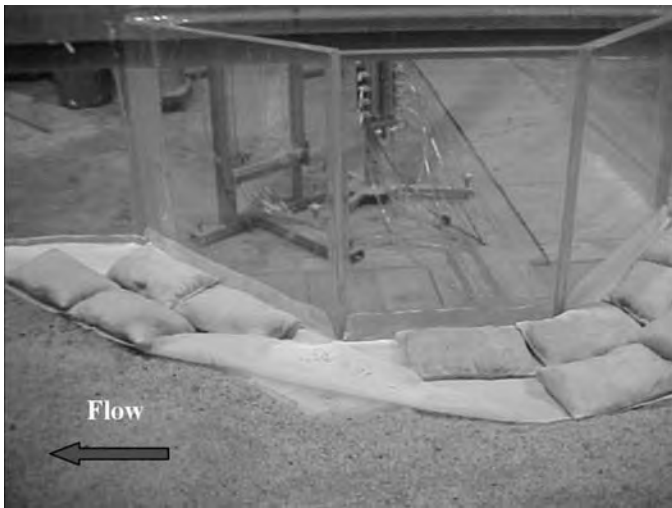


Figure 7-44. An apron of geobags is placed on a geofilter cloth, which was fixed to the abutment.

turbulent flow formed around the abutment and jumble of the filter cloth and geobags and resulted in a scour hole that was deeper than the baseline scour hole. The failure process is shown in Figures 7-46 through 7-49.

Apron of Tied Geobags on Filter Cloth

In this experiment, the geobags were tied to each other along their longitudinal axis, which extended around the perimeter of the abutment. The geobags were tied to prevent them from being entrained by flow or sliding into the scour hole and to enable them to form overall a more flexible apron around the abutment.

This apron arrangement remained stable during much of the experiment, but eventually it too failed, owing to the same

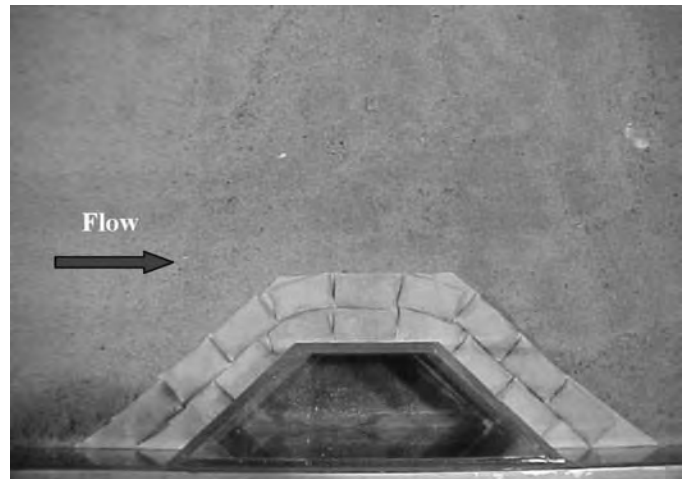


Figure 7-45. Apron of geobags on a geofilter cloth.

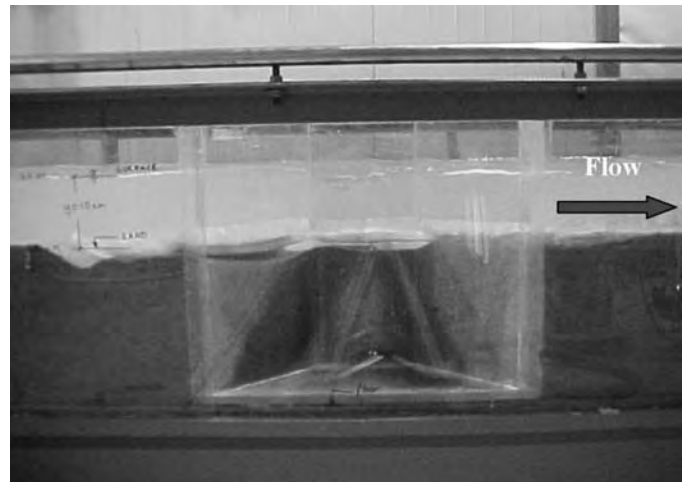


Figure 7-46. Sediment erosion from around and beneath the apron; geobags on geofilter.

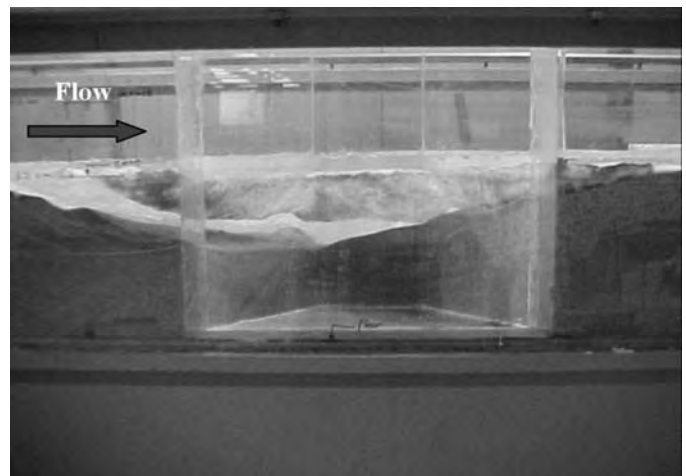


Figure 7-47. Side view of the final scour hole; geobags on geofilter.

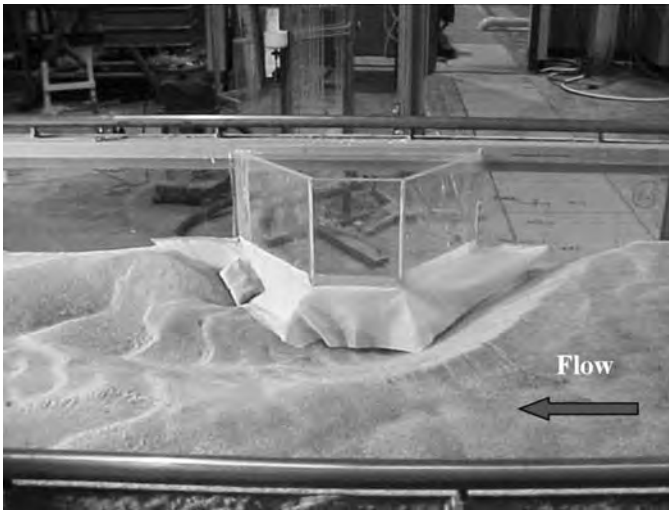


Figure 7-48. Front view of the scour hole; geobags on geofilter.

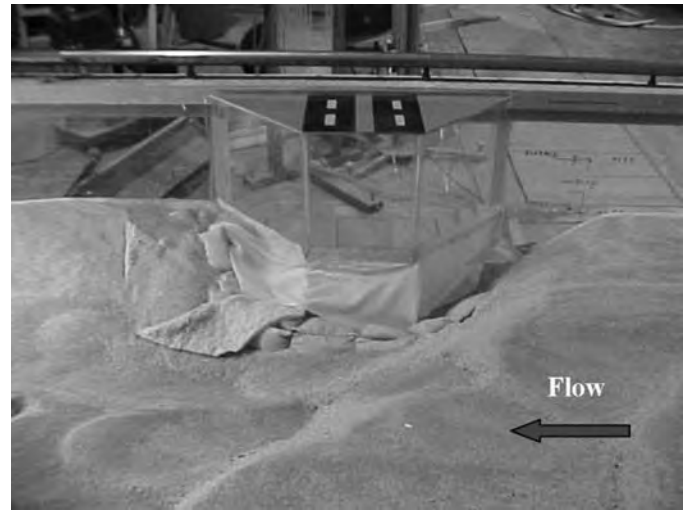


Figure 7-50. Scour hole formed after the experiment; fully tied geobags were on a geofilter.

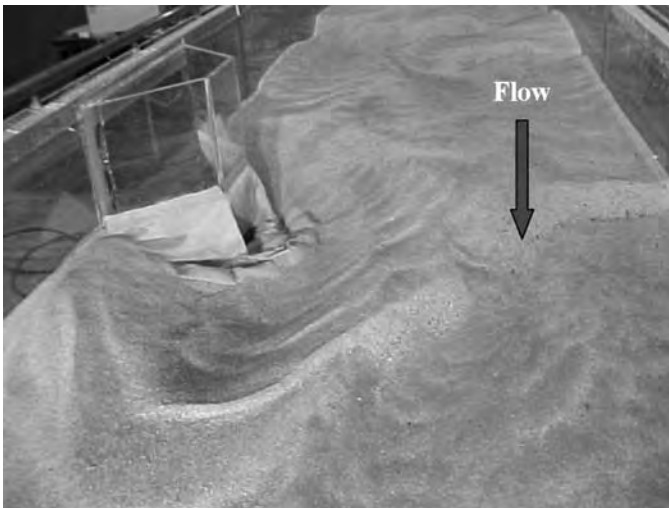


Figure 7-49. The apron failed once the geobags were rolled into the scour hole that formed around the edge of the apron; circumferentially tied geobags were on a geofilter.

scour process described above. The resulting scour hole is shown in Figure 7-50. It is evident that the upstream corner of the front row of the tied geobags slid into the scour hole. Since the geobags were tied to each other, the movement at the corner led the rear bags to slide toward the direction of the scour hole. Once the rear bags were displaced, the filter cloth along the upstream face of the abutment began to lift and expose the underlying sediment. Subsequently, the two other rows of the geobags forming the apron slid apart.

This same experiment was repeated with the geobags tied in all side directions (i.e., geobags were tied to geobags all around). The intent was to prevent the front row of geobags

from sliding into the scour hole developing around the geobag system. However, again the apron eventually failed, though taking longer to do so. Apron undermining started at its upstream corner, then progressed in the manner described previously. Figure 7-50 shows a view after the experiment.

Apron of Layered Geobags

An apron was formed of geobags placed in three vertical and two horizontal rows; it was toed into the bed around the abutment. No geofilter cloth was laid below the geobags. Instead, the lower layer of geobags, together with a shingled, overlapping placement of geobags, served as a geofilter as well as increased apron bulk. The toe of geobags was used in an effort to prevent undermining of the apron's upstream edge. Although the toe protected the apron from being undermined along its upstream side, the apron still failed because of the scour hole formed around the apron's lower perimeter. Once the scour hole formed, the geobags slid into the hole simultaneously. The system failed after an hour.

Geobag Apron Sloped into the Bed

The aim of this experiment was to test the performance of an apron of geobags placed on a slope into the bed around the abutment. Geobags were placed at a slope of 1:2 (V:H) with a toe that consisted of three rows of geobags stacked vertically around the two rows of geobags, as can be seen in Figure 7-51. The bottom elevation was just below the average trough elevation of dunes moving along the flume. The geobags were placed in an overlapping manner like roofing shingles such that the overlap of bags prevented sediment from being winnowed through gaps between adjoining geobags.

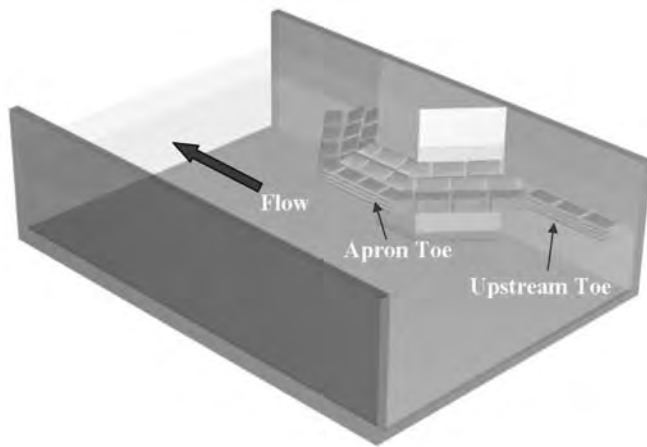


Figure 7-51. Sloped apron formed of overlapping geobags, with the base of apron toe at the average trough level of dunes.

This apron proved to be very effective. It completely prevented the scour from occurring at the abutment. However, scour still developed around the geobag system, especially immediately downstream of the apron. The maximum depth of that scour was 85 mm—that is, 48 percent of the maximum depth when the scour hole occurred at the abutment. Considering the average dune height as 34 mm, it can be said that the scour depth was decreased considerably. Figures 7-52 and 7-53 show the final state of the bed around the abutment.

7.3.4 Results: Pile-Supported Abutments

Next, experiments were performed to evaluate scour at pile-supported abutments, these being common in many rivers. Initially, a baseline case was tested without any countermeasure,

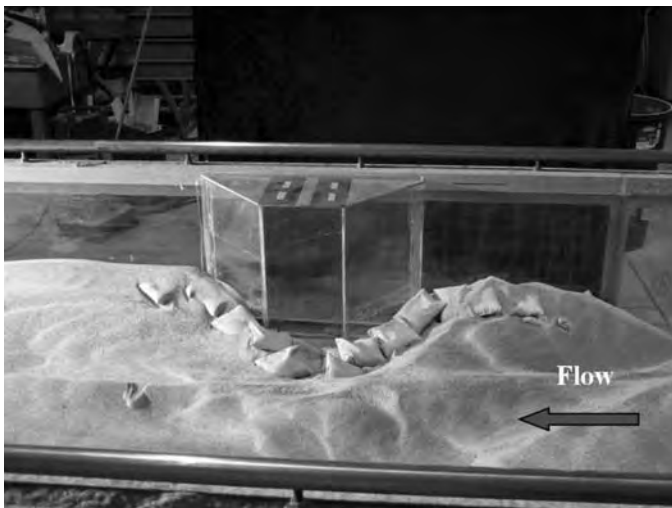


Figure 7-52. A view after the experiment, including a double layer of tied geobags with no geofilter.

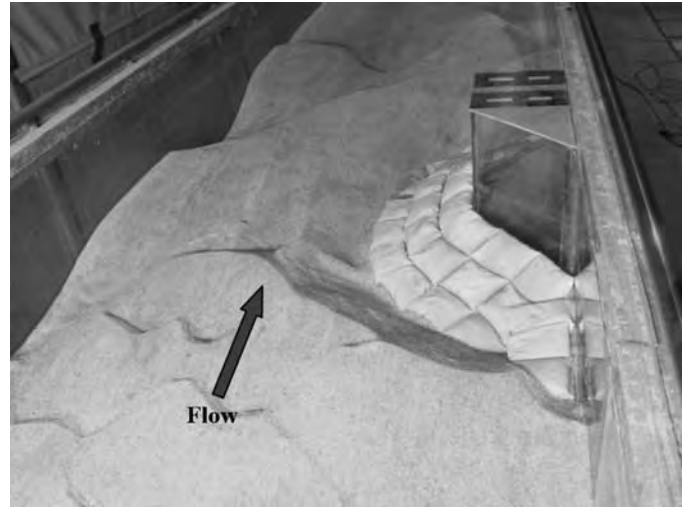


Figure 7-53. The sloped apron of tied geobags worked well. Scour did not occur at the abutment, but was shifted out from it.

followed by riprap and then by geobags. The experiments are described herewith and summarized in Table 7-8.

Baseline Scour Condition

The initial experiments were conducted to observe scour development and to measure scour depth at the pile-supported abutment when the abutment was not protected with an apron of any form, and to determine a baseline depth against which geobag performance could be compared. As no prior study has tested wing-wall abutments, it is useful to include here a brief description of the scour process.

Figure 7-54 shows the consequent scour form that developed at the abutment with the pile cap at the level of the main-channel bed. The maximum scour depth, d_{Smax} occurred at the leading corner of the abutment (point A in Figure 7-37), where the flow contraction was greatest and wake eddies were generated. The maximum scour depth extended 146 mm below the average bed level of the flume (about 5.2 m at full scale).

The baseline experiments revealed two important mechanisms whereby the wing-wall abutment could eventually fail. One mechanism was the mass failure of the embankment that occurred once the scour hole had deepened to the extent that the embankment's earthfill lost its geotechnical stability.

The second mechanism had not been reported heretofore, largely because it is difficult to observe. It occurred as follows. As the scour deepened to below the pile cap and exposed the piles, the embankment's earthfill was eroded out from beneath the pile cap. Gradually, a cavity developed within the embankment, undermining the embankment immediately behind the abutment. This development is depicted in Figure 7-55.

Table 7-8. List of representative principal experiments (Korkut 2004 and Morales 2006 document full list of exploratory experiments).

Experiment	Description
1: Baseline Scour	This experiment was conducted to produce reference baseline scour depth that can be used to determine the scour-reducing influence of a geobag apron.
2: Embankment Protected with Geobags	The side slopes of erodible embankment behind pile-supported abutment were protected with geobags. No geobag apron.
3: Geobag Protection Under the Pile Cap	Geobags were placed under the pile cap in addition to the side slopes to prevent winnowing.
4: Testing Performance of Riprap I	This experiment tested performance of riprap to protect pile-supported wing-wall abutment with erodible embankment.
5: Testing Performance of Riprap II	This experiment repeated Experiment 4, but with rigid embankment.
6: Protection of Apron and Embankment	This experiment placed geobags in a manner replicating the riprap configuration found to be commonly used for Iowa DOT bridges.
7: Apron with Geobags also under the Pile Cap	This experiment repeated Experiment 6, but with geobags placed under the pile cap as a filter.
8: Partially Tied Geobag Apron	Only the geobags at the upper and the lower layers of the apron were tied together.
9: Geobag Mattress	In addition to the two rows of the apron, the geobags at the half downstream part of the upper layer of the apron toe were tied together.
10: Fully Tied Apron of Geobags	The entire apron of geobags was tied together.
11: Steep Embankment Slope	Performance of the geobag system used in the previous experiment was tested for a steeper embankment side slope.
12: Pile Cap Lowered, No Geobags	The pile cap was placed deeper in the bed.

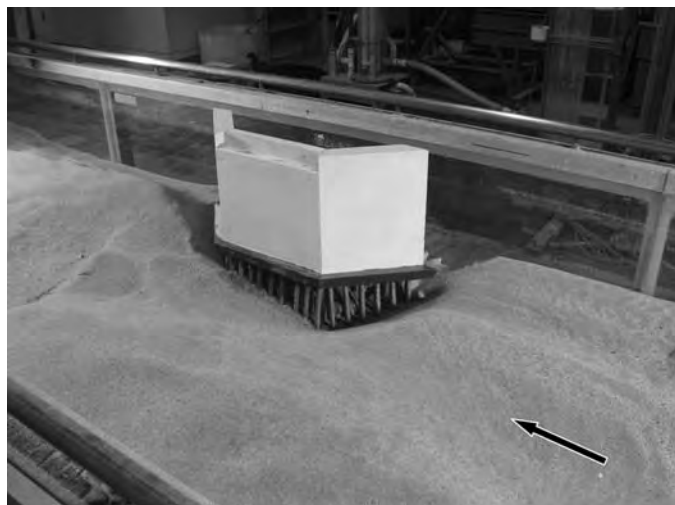
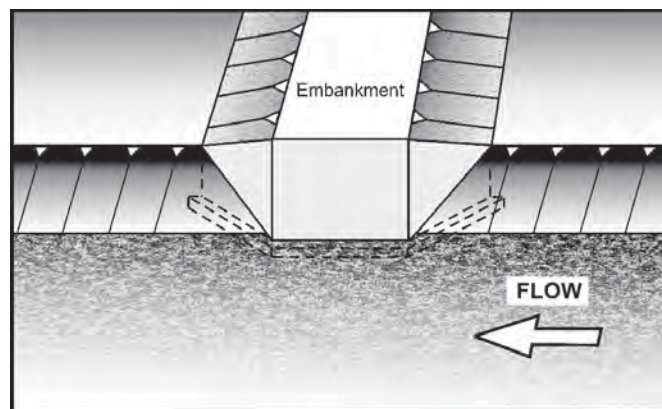
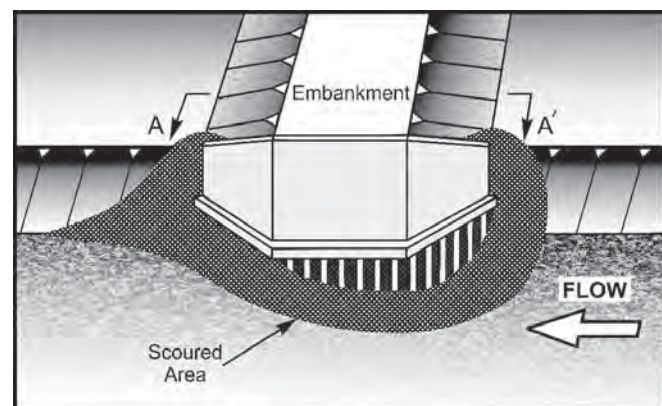


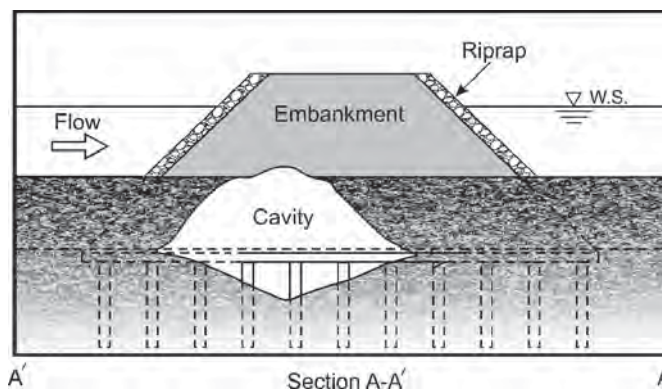
Figure 7-54. Scour development at the abutment and embankment when unprotected.



(a) Before scour



(b) Scour exposes piles



(c) Cavity forms behind the pile cap

Figure 7-55. As scour exposes piles (shown in a and b above), embankment soil may be sucked under the pile cap, forming a cavity behind the pile cap (shown in c).

Eventually, scour deepening caused the embankment side slopes to become unstable and to slide into the scour hole, where sediment had been removed by the flow. As the embankment collapsed, the flow passed around the exposed abutment.

A countermeasure-related observation from these experiments is that the embankment's earthfill beneath and behind the pile cap must be protected. Two options for doing this are to place armor material immediately behind the pile cap and to place the pile cap at a lower elevation. These options were tested in the experiments. The experiment with riprap placed immediately behind the pile cap produced a deeper scour (165 mm at the leading corner), but the embankment did not fail. The experiment with the pile cap lowered showed that a lower pile cap resulted in a still larger maximum scour depth of 182 mm, at the abutment's upstream corner. Although this scour depth exceeded the baseline scour depth (Experiment 3 in Table 7-8), scour could not progress substantially lower than about the pile-cap base. Use of scour protection immediately behind the pile cap, or use of a lowered pile cap, therefore enables a wing-wall abutment and its approach embankment to better withstand scour.

Abutment with Riprap Apron

A series of experiments were conducted to determine how scour develops when an apron of riprap stone is placed around the abutment, an example of which is shown in Figure 7-56. The riprap apron consisted of a layer of riprap about two stones thick, with a toe three to four stones thick. The riprap stones simulated were scaled down to uniform-sized riprap of $d_{50} = 22$ mm.

Figure 7-57a illustrates the initial arrangement of the riprap apron used in the flume experiments, and Figure 7-57b shows the resultant scour hole, whose maximum depth occurred at the upstream corner of the abutment and was 85 mm. The experiments showed that edge failure of the riprap apron led to apron failure and to scour progression beneath and around the abutment, including the abutment pile cap. The failure started at the apron's upstream edge, where accelerated flow and the passage of dunes destabilized the apron's riprap toe, and resulted in large parts of the entire

riprap apron sliding into the scour hole forming around the apron. As the riprap apron slid, it exposed the pile cap so that embankment sediment was winnowed from beneath the pile cap. The embankment then failed due to winnowing of sediment from beneath the pile cap. Additionally, the deepening scour hole caused the embankment side slope to become unstable.

The manner of riprap apron failure essentially was the same as that reported by Chiew (2000) and Parker et al. (1989) for riprap aprons placed around model bridge piers. It is evident from the experiment that riprap aprons placed locally around an abutment may not work in dune-bed channels unless the apron toe extends deep enough to be below the trough elevation of dunes moving through the bridge opening.

Abutment with Geobag Apron

A series of trial-and-error experiments was conducted to determine whether and how scour would be prevented by one or more large geobags fitted as an apron around the perimeter of the test wing-wall abutment. All of these experiments essentially showed that, for large geobags to be effective at preventing scour depth at an abutment, the geobags must be tied together so as to form a more or less continuous apron, and the apron itself should be tied to the abutment. Otherwise, the geobags would slide away from the abutment, expose the abutment footing, and cause scour of sediment from beneath the footing. However, even though an apron of tied geobags eliminated scour at the abutment, it caused the location of deepest scour to shift downstream of the abutment. The maximum scour depth d_{Smax} was 110 mm, which was about equal to the flow depth. Figure 7-58 illustrates a typical result from the experiments. The location of maximum scour depth moved from location A to C in Figure 7-37.

It was found that, as additional geobags were placed around the abutment, the scour shifted farther downstream of the abutment. Therefore, to be effective, the geobags have

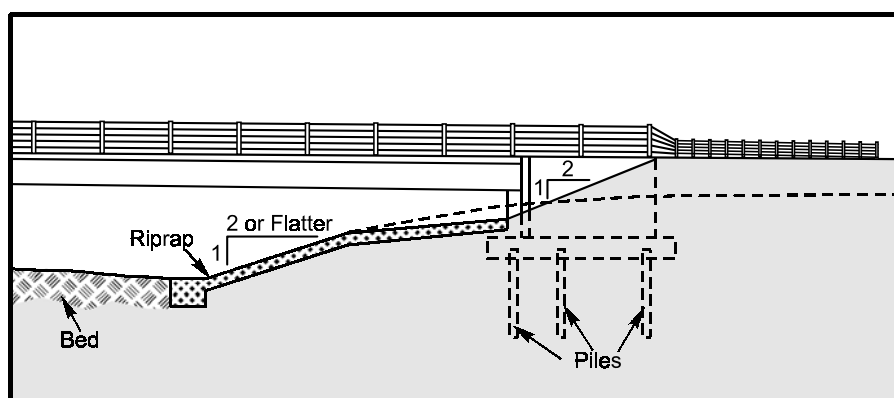
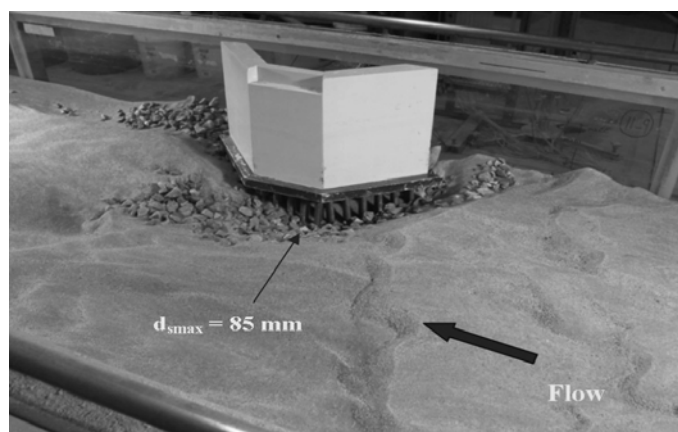


Figure 7-56. Example of an actual apron at a wing-wall abutment.



(a) Before scour



(b) After scour

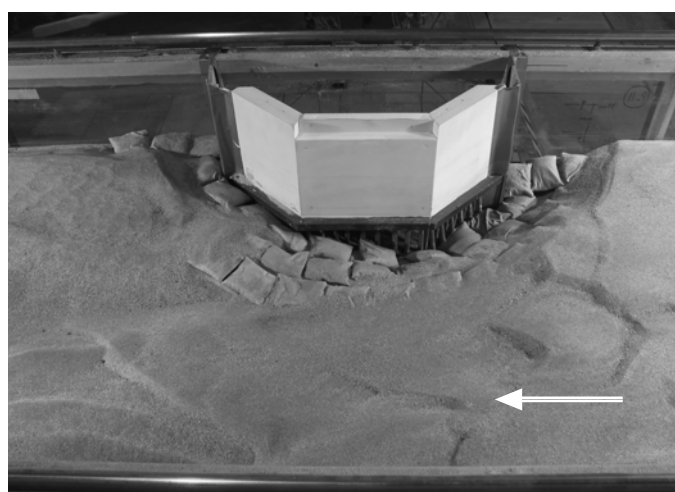
Figure 7-57. The failure of a riprap apron due to scour (Experiment 4, Table 7-8). The location of deepest scour is indicated.

to extend out a substantial distance from the abutment. The present experiments and the preliminary experiments indicate that apron width should exceed road width. This finding indicates that, for single- or double-span bridges, the apron formed of geobags (or riprap) should extend across the full width of the bridge waterway. Also, if the additional geobags were not secured to the abutment, they would slide into the scour hole. In sizing the bag thickness using Equations 7-17 through 7-19, it should be kept in mind that the slope angle may increase substantially as scour develops and that bag thickness should be based on the anticipated slope associated with scour hole formation.

Because an advantage of geobags is that they can be formed and placed by hand, especially in circumstances where an immediate temporary countermeasure is needed, series of experiments were conducted to determine how an apron of relatively small geobags would perform as an alternative to a riprap apron. The experiments involved an apron of geobags placed in a design layout essentially the same as for the riprap apron described above. The apron consisted of a layer of



(a) Before scour



(b) After scour

Figure 7-58. Scour failure of an apron formed of loosely placed small geobags. The deepest scour is indicated with the arrow.

geobags, two bags thick, with a toe three to four bags thick. The apron generally conformed with the layout of the riprap apron shown in Figure 7-56. Early experiments revealed that, though the geobags that were loosely placed reduced scour depth, they might not fully protect the abutment pile cap.

The experiments showed that an apron of suitably positioned and connected geobags (acting like cable-tied blocks), such as one generally conforming to the apron in Figure 7-56, can reduce the scour depth at an abutment. However, as with a riprap apron, scour may occur at position B on the perimeter of the geobag apron if the geobags are loosely placed or at position C downstream from the apron if the geobags are tied together as a mattress. Once edge scour occurs, at either position B or position C, the edge geobags (as with riprap) are dislodged into the scour hole.

The experiments showed that the edge failure is the principal factor that results in the failure of the geobag apron, just as it is for the riprap apron. It was found that such failure can be eliminated or substantially reduced by fully linking the geobags to form a flexible apron, by then sloping the apron into the bed, and by forming a suitably deep toe of geobags (as for riprap) around the apron's perimeter. Also, it was found that geobag size did not affect the performance of a tied apron of geobags for the experiment conditions tested. Of greater importance was that the geobag elements be linked to form a flexible apron of sufficient coverage around the abutment.

Scour at the abutment itself was eliminated when geobags or riprap were placed under the pile cap to prevent the winnowing erosion of riverbank and embankment soil through the exposed region beneath the pile cap (Experiment 7 in Table 7-8). Though the abutment itself was protected, the bed scoured downstream of the geobag apron, with scour depths exceeding the maximum scour depth at the abutment for the baseline case.

Summary of Scour Data

The scour depth results associated with the experiments are plotted in Figure 7-59, which shows how appropriate geobag use may reduce scour depth at the abutment (d_{sA}), but with the consequence of shifting scour to positions B (d_{sB}) and C (d_{sC}) (positions are indicated in Figure 7-37). In shifting the scour location, geobag use may not eliminate scour at a bridge. As is shown in the ensuing discussion, it quickly becomes evident

that the protection (geobag or riprap) must extend as a mat across essentially the full opening of a bridge waterway.

7.3.5 Mat Across Bridge Waterway

The foregoing findings with aprons show that the bridge waterway should be fully lined with a large protective apron, or mat, that essentially links the aprons extending from each abutment. Further experiments investigating the extent and layout that are required for an effective mat led to the mat layout design guide presented in Figure 7-60, which reflects the following recommendations:

- The mat should extend upstream and downstream of the abutment by a distance of minimally one bridge width to ensure that the waterway bed is protected from the accelerating flow through the waterway. Mats providing this extent of waterway coverage were able to prevent scour in the waterway.
- The mat should be sloped. The bottom of the slope should coincide approximately with the trough elevation of bed sediment dunes passing through the bridge waterway. At this bottom elevation, dunes do not cause the upstream or downstream edges of the mat to be undermined and fall apart. An additional advantage of the sloped mat is that it enables low flows to concentrate at the center of the waterway; this is an advantage for fish passage. Additionally, the center slope minimizes flow blockage through the waterway.
- The mat should have a toe and a heel, each of which are three geobag- or riprap-stone-thicknesses deep below the mat.

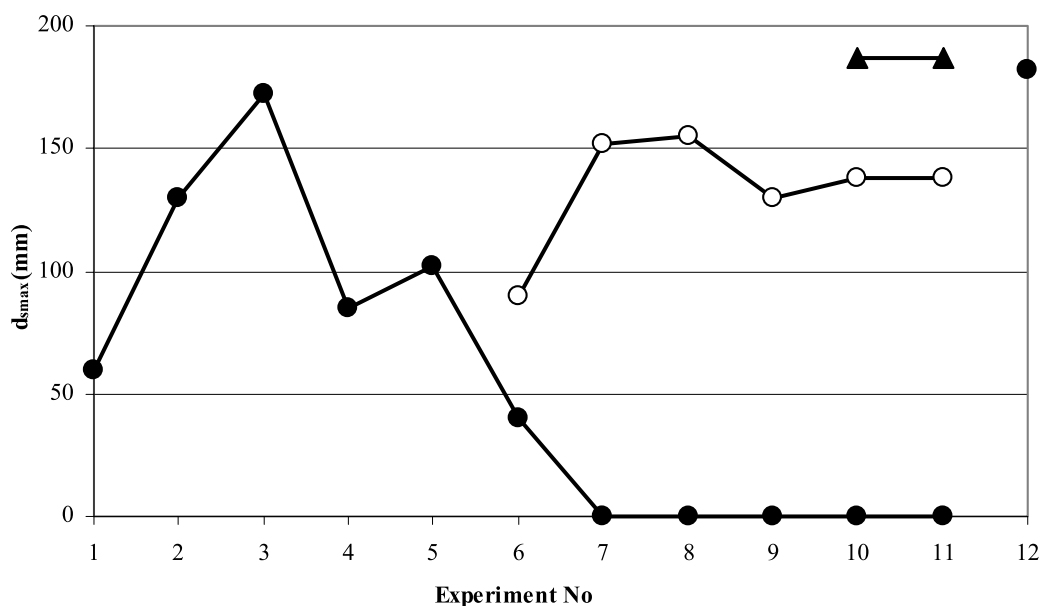


Figure 7-59. Maximum scour depths for experiments described in Table 7-8; depths of scour at locations A (●), B (○), and C (▲) in Figure 7-37. When a full mat (double layer) was placed across the channel, scour depth was zero.

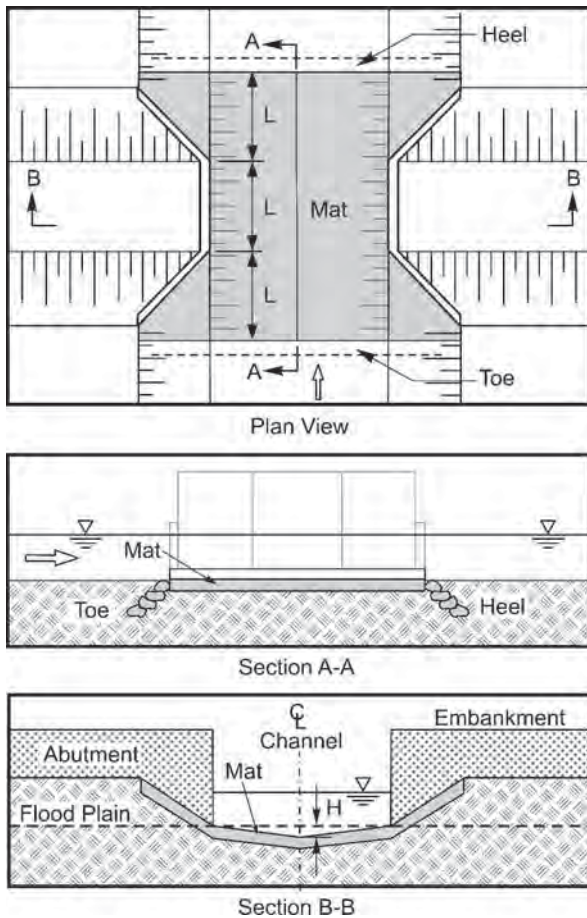


Figure 7-60. Recommended minimum extent of mat formed from geobags or riprap for single-span bridges.

An early series of tests with a single layer of geobags not tied to each other resulted in local failure of the mat near the abutments, owing to the winnowing of sand from between the geobags. The same result occurred with a single layer of riprap. An illustrative geobag mat failure is given in Figure 7-61. If repeated with a double layer of geobags, or a double layer of riprap, minimal winnowing of sand occurred, and no scour developed at the bridge opening. For example, the performance of a mat formed from a double layer of riprap is shown in Figures 7-62. The mat remained in tact and inhibited scour at the either abutment.

Geobags as Filter Under Riprap Mat

The flume tests showed that, for geobags to serve as an effective form of filter cloth beneath a single layer of riprap, and for the riprap to be stable, it was necessary for the geobags to be placed slightly below the local level of the channel bed. For this arrangement, the riprap remained stable. Otherwise, when the geobags were placed on top of the channel bed or the riprap was placed on the geobags,



(a) Setup



(b) After test, showing failure of mat owing to winnowing of sand from between bags

Figure 7-61. Performance of a geobag mat (single-bag thick) with riprap toe and heel.

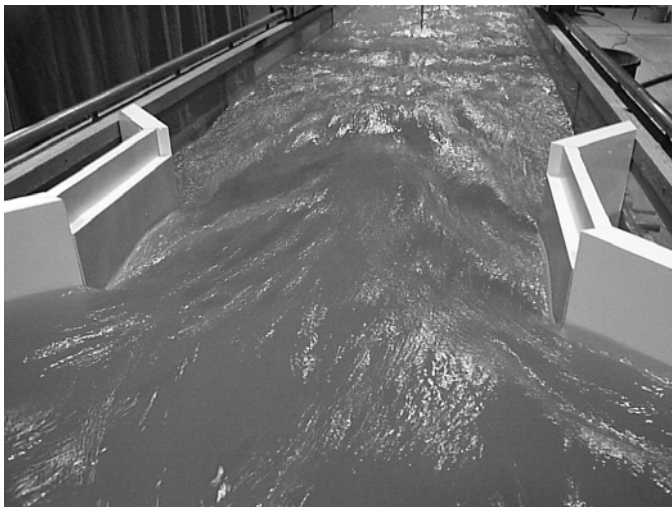
the riprap was exposed such that the riprap stone was less stable than when the geobags were placed below level. A larger size of riprap stone would be needed in this situation.

7.4 Summary of Results from Riprap, Cable-Tied Blocks, and Geobags

Local scour in the general vicinity of an abutment cannot be eliminated completely by an apron of riprap or geobags. An apron shifts the scour region away from an abutment. The experiments show that an apron can prevent scour from developing at the abutment itself, but that



(a) Before flow



(b) During flow



(c) After flow

Figure 7-62. Performance of riprap mat (double-stone layer) for a single-span bridge. Mat layout is as given in Figure 7-60.

significant scour can occur readily near the downstream edge of the apron. A possible concern in using an apron is to ensure that shifting of scour does not imperil a nearby pier or portion riverbank. Moreover, if the scour is likely to extend to an adjacent pier, then the abutment and pier countermeasure apron should be placed so as to protect both elements of a bridge.

The experiments show that it is necessary to protect the following regions of the river bed and banks near an abutment:

- The river bed at the abutment pile cap,
- The riverbank immediately upstream of the abutment and a short distance downstream of the abutment,
- The side slopes of embankment immediately behind the abutment (standard stub for a wing-wall abutment or spill-through abutment), and
- The area beneath and immediately behind the pile cap.

For use of riprap or cable-tied block alone, the following conclusions emerged from this study:

- For the range of experimental investigation in this study, the scour at wing-wall abutments in live-bed conditions is directly related to the level of the deepest bed form trough that propagates past the abutment, which is predictable using existing expressions, together with any localized scour that may occur.
- Stones on the outer edge of riprap aprons tend to settle and move away from the abutment, pushing the troughs of the bed forms farther away from the abutment. Conversely, cable-tied block mats remain intact during settlement. The outer edge of the apron settles vertically, allowing the troughs of the bed forms to pass closer to the abutment face than for an equivalent riprap apron.
- Equations 7-10 and 7-11 allow prediction of the minimum apron width remaining horizontal after erosion. Equation 7-12 allows prediction of the horizontal distance between the abutment face and the point of deepest scour. These predictions, along with prediction of apron settlement, facilitate assessment of the stability of an abutment structure.

With regard to the specific use of geobags for wing-wall abutments, the following conclusions can be drawn:

- Geobags are a promising alternative to riprap for use as a bridge abutment scour countermeasure.
- It is necessary to connect the geobags placed as an apron around an abutment. The initiation of the failure of geobag apron shown in Figure 7-58 was due to the failure of an individual geobag placed in front of the abutment.
- The apron should have a perimeter toe whose lower level approximately coincides with the average elevation of

dunes moving through the channel in the vicinity of the bridge.

- The geobags should be placed in a shingled manner, whereby adjoining geobags overlies joints between underlying geobags.
 - It is necessary to place geobags (or riprap) immediately under the pile cap in order to prevent the winnowing of embankment sediment from beneath the pile cap.
- Geobags may serve as a useful alternative to a geotextile filter cloth placed beneath a riprap apron because geobags are more readily placed than is an underlay cloth for blocking the winnowing of sediment from between bed-armor elements like riprap stone. The geobags, though, should be placed somewhat below bed level so as not to increase riprap exposure to flow.
-

CHAPTER 8

Lab Results III: Aprons at Spill-Through Abutments

8.1 Experimental Work

8.1.1 Introduction

The aim of the experiments reported in this chapter was to investigate the use of riprap and cable-tied blocks as bridge abutment scour countermeasures. Both riprap and cable-tied block aprons were placed around spill-through bridge abutments to protect them from scour, which could otherwise potentially undermine the abutments.

A series of experiments was conducted in the Fluid Mechanics Laboratory of the School of Engineering, University of Auckland, in New Zealand, with clear-water conditions at flow velocities just below the threshold velocity of the sediment. A spill-through abutment model, molded from the bed material, was sited on the floodplain of the compound channel. For these experiments, abutment length, floodplain width, and apron extent were systematically varied for both riprap and cable-tied blocks to determine the minimum required apron extent to sufficiently protect the abutment. The results from these experiments are presented in Section 8.3.

Flow fields around the bridge abutments were measured for all abutment and compound channel configurations to provide insight into the development of scour and the interaction between the developing scour formations and the apron countermeasures protecting the abutment. The flow field measurements are presented in Section 8.2.

The measured flow fields described above were compared with flow distributions obtained from a two-dimensional shallow-water numerical model. The two-dimensional shallow-water model developed for analysis of bridges for Federal Highway Administration, FESWMS (Finite Element Surface Water Modeling System), is used by highway agencies throughout the United States; therefore, it was used in this study. The results are given in Section 8.4.

A further set of experiments was undertaken in a relatively large-scale flume at the University of Iowa to validate the main recommendations from the extensive parametric flume

experiments described above. These experiments are presented in Section 8.5.

8.1.2 University of Auckland Experimental Equipment and Set-Up

A 2.4-m wide, 0.3-m deep, and 16.5-m long nonrecirculating flume was used to conduct the clear-water, spill-through abutment scour countermeasure study. The flume is supported by two universal beams that pivot about a central support. Screw jacks support the beams at either end so that the flume slope is adjustable. The flume consists of an inlet tank, a flow straightener, a 13-m long channel, a sediment collection tank, and an outlet tank. A 2.8-m long, 0.45-m deep sediment recess is located 7 m downstream of the inlet tank. Figure 8-1 shows the flume in the upstream direction, and Figure 8-2 shows a longitudinal cross section of the flume.

Water is supplied to the flume inlet from the laboratory constant-head tank via two 150-mm and one 200-mm diame-

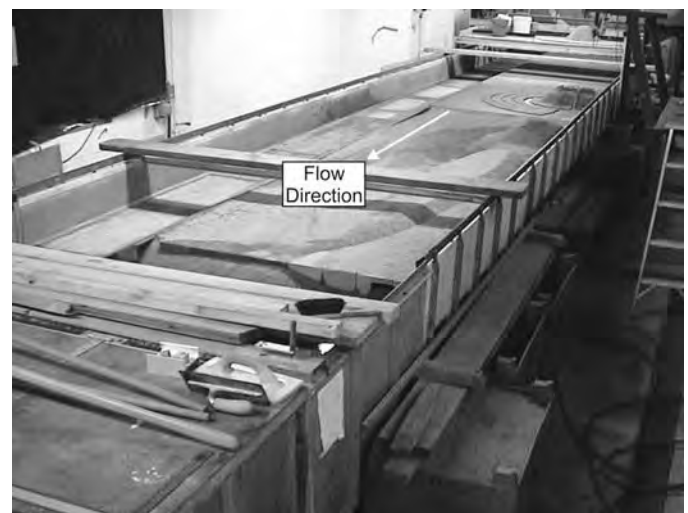


Figure 8-1. The 2.4-m wide flume in the upstream direction.

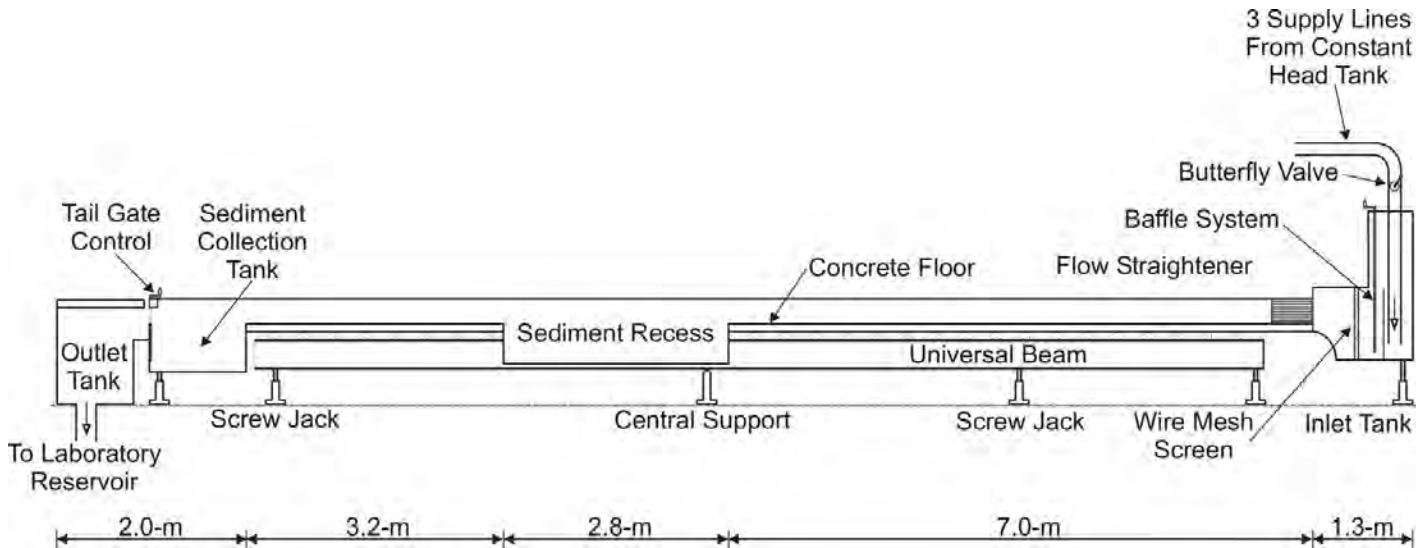


Figure 8-2. Longitudinal cross section of the 2.4-m wide flume.

ter pipes. The discharge from each pipe is regulated by butterfly valves, and the flow rate is measured by measuring the pressure difference across an orifice plate in each pipeline.

The inlet tank consists of a 1.8-m high header tank with a baffle system to regulate and distribute the flow evenly across the flume. The flow passes through a baffle system at the bottom of the header tank, through a wire mesh screen to smooth the flow, and then through a flow straightener into the channel section of the flume. The flume channel consists of fiberglass sides and a concrete floor. The recess was filled with bed sediment such that the surface of the sand was level with the flume floor prior to any scouring. From the flume channel, the flow passes into the sediment collection tank. The tailgate controls the water depth in the flume.

A sediment feed system is located 1.2 m downstream of the flow straightener, as seen in Figure 8-3. Dry sediment stored in the hopper falls onto a conveyor belt, which carries the sediment away. The sediment discharge is controlled by a variable-sized triangular orifice. A rotating brush sweeps the sediment from the conveyor belt into the flume.

Sediment can be prevented from being fed into the floodplain section by removing sections of the rotating brush, so that some of the sand on the conveyor belt is carried across the flume, where it falls off the belt and is deposited over the side of the flume.

A moveable floodplain was constructed along the length of the rectangular channel section of the flume, as shown in Figure 8-4. The main channel bank was constructed in sections of sheet metal folded into wedge profiles 150 mm high with a side slope of 2:1 (H:V). The wedge sections were placed lengthwise in the flume, with the top edge of the main channel bank running parallel to the side of the flume at the desired floodplain width, B_f . The sheet metal lining the main

channel bank and the top of the floodplain was painted and sprinkled with sand to simulate the roughness of a sediment bed. The four different floodplain widths, B_f , used in this study are 0.8, 1.2, 1.6, and 2.0 m. Figure 8-4 shows a floodplain in the flume. In the figure, B_f equals 1.6 m.

Four different spill-through abutments were used in this study. All the abutments had the same frontal shape and dimensions, but varied in length, L . The lengths of the abutments used in this study are 0.4, 0.6, 0.8, and 1.0 m. The dimensions of the frontal section of the abutment are given in Figure 8-5. The abutments were placed on the floodplain in the sediment recess section of the flume and were molded from the same sediment as that used for the floodplain and in the recess of the flume. Sheet metal molds were used to construct the abutments. The

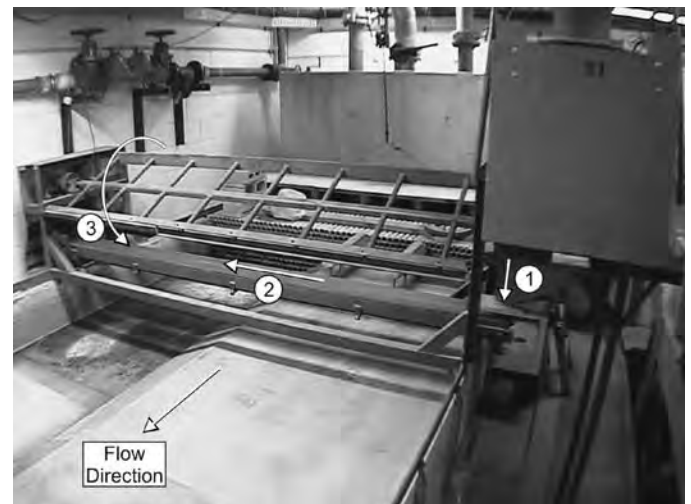


Figure 8-3. Sediment feed system in the upstream section of the 2.4-m wide flume.

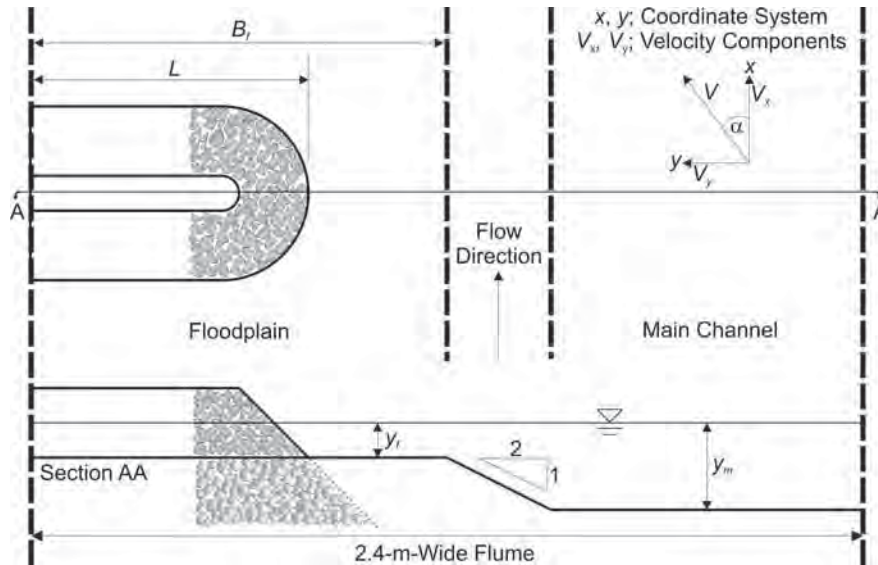


Figure 8-4. Experimental set-up for the spill-through abutment study.

mold was split into a 0.4-m frontal section and several extension sections with varying lengths, as shown in Figure 8-6.

8.1.3 Bridge Abutment Flow Field Measurements

A particle-tracking velocimetry (PTV) technique was developed to measure the two-dimensional surface flow fields around the spill-through abutment models. PTV is based on the principle of capturing sequences of images of specially illuminated, particle-seeded fluid flow, from which quantitative information about the flow field can be extracted. A particle-seeding density of approximately 15-blocks/m² was used.

Uniform flow was established along the length of the flume, with a flow depth of 100 mm on the floodplain and 250 mm in the main channel. For each compound channel configuration ($B_f = 0.8, 1.2, 1.6,$ and 2.0 m), the flow field was measured in the test section of the compound channel using the PTV technique. The flow distribution across the flume was adjusted at the flume inlet by blocking off sections in the flow straightener until there was no net transfer of flow over the main channel bank boundary. The average flow velocity in the main channel was set to the threshold velocity for sediment movement, while the average velocities on the floodplain were typically 80 to 90 percent of the threshold velocity. Figure 8-7 shows the surface velocity distributions across the flume for the four different compound channel configurations. A small

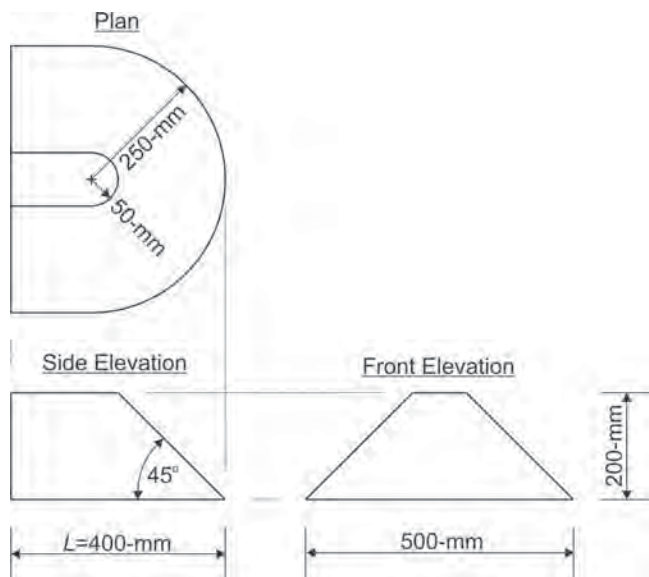


Figure 8-5. Spill-through abutment dimensions.

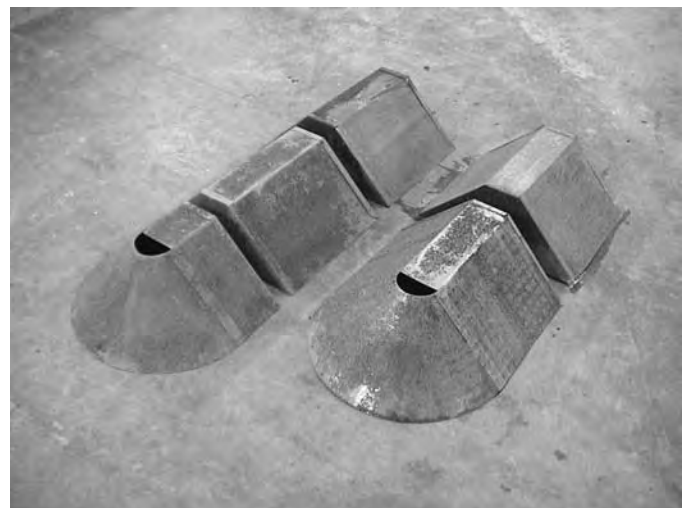


Figure 8-6. Spill-through abutment molds.

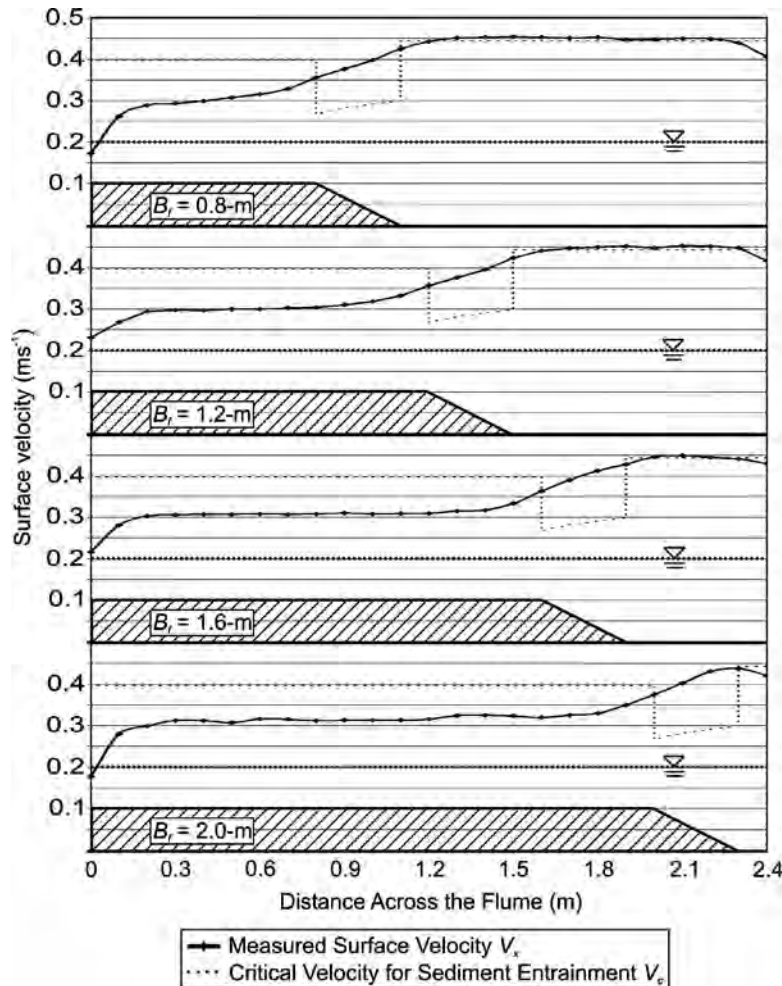


Figure 8-7. Velocity distributions across the 2.4-m wide flume for the four different compound channel geometries.

diagram of the cross section of the corresponding compound channel is shown under each velocity distribution. The critical velocity for sediment entrainment V_c , determined using Shields criterion adjusted for lateral slope, is shown on each velocity distribution. The adjustment for lateral slope was made using the method given in Vanoni (1977).

For the spill-through abutments, the flow measurements were undertaken using the experimental set-up in Figure 8-8 at the initial (i.e., unscoured) stage of the experiments. The flow fields were measured for the abutment lengths 0.4, 0.6, 0.8, 1.0, 1.2, 1.4, and 1.6 m, situated on the various floodplain widths, B_f , of 0.8, 1.2, 1.6, and 2.0 m.

8.1.4 University of Auckland Experimental Procedure

The purpose of the study was to determine the amount of scour countermeasure protection required to protect spill-through bridge abutments from failure. The test models used in this experimental study were designed to be representative

of spill-through abutments situated on the floodplain of wider compound river channels. At such river crossings, the natural vegetation typically protects the flood channels from general erosion, and approach-flow conditions can be taken as clear-water during floods. An idealized compound channel geometry was used, as shown in Figure 8-8.

Similitude between laboratory experiments and field scale was satisfied by the use of the aforementioned u_* / u_{*c} ratio, of which a value of just below 1.0 represents a condition called “clear-water scour.” This condition is extreme for scouring because the velocity is as high as possible without the movement of the channel bed, which causes infilling of the sediment hole.

The primary objective was to determine (a) the scour hole geometry under clear-water conditions due to variations in the compound channel and abutment geometries and (b) the extent and type of scour protection provided. The extent of apron protection W , the length of the abutment and bridge approach embankment L , and the width of the floodplain B_f were systematically varied for both riprap and cable-tied block protection

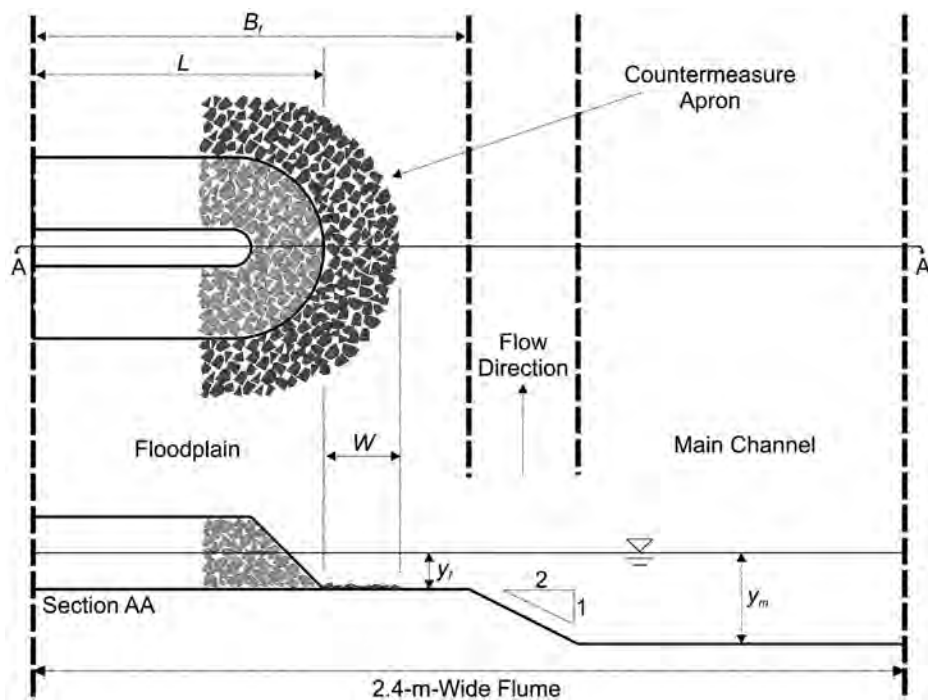


Figure 8-8. Experimental configuration of the countermeasure placement for the spill-through abutment study.

(Figure 8-8). The aspect ratio of the floodplain width B_f/y_f ranged from 8 to 20, and the aspect ratio of the abutment length L/y_f ranged from 4 to 10, where y_f is flow depth on the floodplain.

The compound channel consisted of an erodible sand bed for the floodplain and erodible sand boundaries for the main channel bed and bank in the test section. Uniform coarse sand was used as the bed material for all the experiments. The sediment properties are identical to those of the sediment used in the wing-wall experiments described in Chapter 7 and are summarized in Table 8-1.

Riprap protection was placed on the erodible bank and bed of the main channel. This was necessary to prevent erosion of the main channel bank, which would have occurred in the absence of any abutment structure due to the influence of the bank slope. Filter fabric was placed over the abutment and covered with riprap or cable-tied block protection. The filter layer was also placed beneath the horizontal apron for cable-tied block protection (i.e., to prevent winnowing of the bed sediment), but was not used for riprap protection because this could induce edge failure of the riprap (Eve, 1999).

Experiments were run under uniform flow conditions (with flow depths of 100 mm on the floodplain and 250 mm in the

main channel). Initially, experiments were run with no apron protection ($W = 0$, as per the experimental set-up in Figure 8-8). Instead, the spill-slope protection was extended below the surface of the floodplain to a depth greater than the expected scour hole depth to protect the toe of the abutment, based on existing recommendations. Next, experiments were run with a 0.5-m wide apron, and thereafter the aprons were successively reduced in size by 0.1 m until the edge of the equilibrium scour hole occurred adjacent to the abutment slope. Figure 8-9 shows such experimental set-ups in the flume. All data apply to the case of “no failure” of the abutment and approach embankment.

For experiments where the scour hole would encroach on the main channel bank, the riprap stones lining the main channel bank were removed just before they were about to fall into the scour hole. In this way, the scour hole formation was not affected by the riprap protection covering the main channel bank.

Using the Richardson and Davis (1995) method for calculating the required riprap size to prevent dislodgement of the stones by the flow, the required riprap size, d_{50} , for the most critical flow conditions was calculated to be 15 mm. The riprap size (Type R1 in Table 7-2 and Figure 7-7) used for the experimental study was larger than the required riprap size, ensuring the stability of the riprap for all the abutment-compound channel configurations tested. In the same way, the cable-tied blocks used in the experiments (Type R1 in Table 7-2 and Figure 7-7) were sized so that they would remain stable for all test conditions.

Table 8-1. Sediment properties.

Description	d_{16} (mm)	d_{84} (mm)	d_{50} (mm)	σ_g	S_s	u_{*c} (ms^{-1})
Filter sand	0.62	1.04	0.82	1.30	2.65	0.020



(a) Riprap extended below the surface of the floodplain



(c) Riprap apron protection



(b) Levelled floodplain with riprap protection extended below the bed



(d) Cable-tied block apron protection

Figure 8-9. Initial set-up of experiments.

The experiments were carried out with a geotextile placed underneath the countermeasure apron to eliminate the winnowing of sand from between the riprap stones or cable-tied blocks. The geotextile used for testing (shown in Table 7-3) was flexible enough to ensure that the riprap or cable-tied blocks would be in contact with the bed at all times.

All experiments were run for 72 hours to ensure that the local scour hole had reached the equilibrium depth. At the conclusion of each experiment, the resulting scour hole formation was contoured in 50-mm increments for photographic purposes. Figures 8-10 and 8-11 show examples of the contour lines.

The position of the deepest point of the scour hole defined by α_x and α_y , the depth of the scour hole relative to the floodplain d_{sf} , the horizontal distance from the floodplain wall to the opposite edge of the scour hole α_e , and the minimum distance between the edge of the scour hole and the abutment W_{min} were measured. Figure 8-12 shows these measurements. The accu-

racy of the measurements of d_{sf} was ± 5 mm, whereas the accuracy of the measurements of α_x , α_y , α_e , and W_{min} was ± 10 mm.

8.2 Bridge Abutment Flow Fields

8.2.1 Introduction

The flow fields around the model bridge abutments were measured for all abutment and compound channel configurations with a flat fixed bed to provide insight into the development of scour and the interaction between the developing scour formations and the apron countermeasures protecting the abutment.

8.2.2 Data Analysis

The measured flow field data sets were used to plot time-averaged, two-dimensional velocity-vector fields. An example

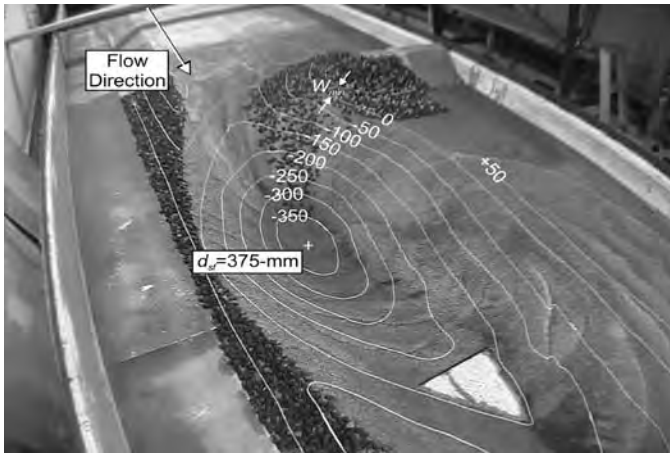


Figure 8-10. Contour lines placed in the equilibrium scour hole for a spill-through abutment protected by a riprap apron ($B_f = 1.6$ m, $L = 0.8$ m, and $W = 0.3$ m).

of the velocity vector field around a 0.8-m long spill-through abutment situated on a 1.6-m wide floodplain is shown in Figure 8-13.

The associated vorticity, ω , for each flow field was calculated by using the time-averaged velocity measurements and adopting a central-difference approximation for the following vorticity expression:

$$\omega = \frac{\partial V_y}{\partial x} - \frac{\partial V_x}{\partial y} \approx \frac{V_y^{[x+\Delta x]} - 2V_y^{[x]} + V_y^{[x-\Delta x]}}{\Delta x^2} - \frac{V_x^{[y+\Delta y]} - 2V_x^{[y]} + V_x^{[y-\Delta y]}}{\Delta y^2} \quad (8-1)$$

Where V_x and V_y are velocity components in the x and y directions, respectively, as defined in Figure 8-4 and Δx and $\Delta y =$

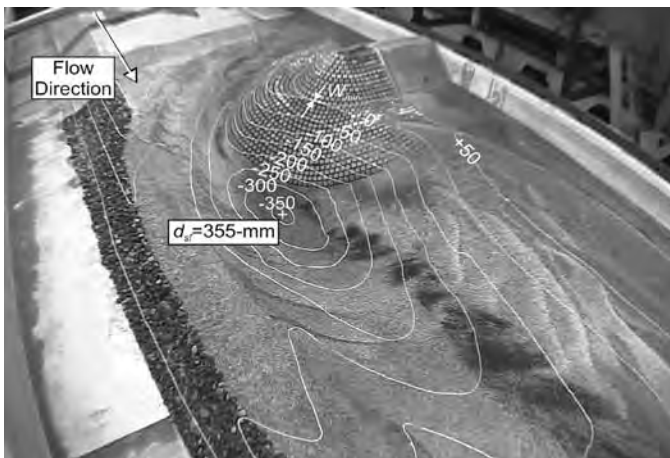


Figure 8-11. Contour lines placed in the equilibrium scour hole for a spill-through abutment protected by a cable-tied block apron ($B_f = 1.6$ m, $L = 0.8$ m, and $W = 0.4$ m).

0.1 m. An example of the calculated vorticity fields at the spill-through abutment is shown in Figure 8-14.

The bed shear stress, τ , was calculated by using the time-averaged surface velocity measurements. Assuming a logarithmic velocity profile, the shear velocity u_* was estimated by an iterative process:

$$\frac{V}{u_*} = 5.75 \log \frac{z}{k_s} + a_r \quad (8-2)$$

Where V is the velocity, measured using an acoustic Doppler velocimeter at an elevation z above the bed level and $k_s = 2d_{50}$. The parameter a_r is given by the following:

$$a_r = 5.75 \log \left(\frac{u_* k_s}{\nu} \right) + 5.5 \quad \text{if } \frac{u_* k_s}{\nu} < 3.5 \quad (8-3)$$

$$a_r = 5.75 \log \left(\frac{u_* k_s}{\nu} \right) + 8.5 \quad \text{if } 3.5 < \frac{u_* k_s}{\nu} < 70 \quad (8-4)$$

$$a_r = 0.85 \quad \text{if } \frac{u_* k_s}{\nu} > 70 \quad (8-5)$$

Where ν is the kinematic viscosity of the water in the flume. The shear stress exerted on the bed by the flow ν was calculated as follows:

$$\tau = \rho u_*^2 \quad (8-6)$$

where ρ is the density of the water in the flume. The bed shear stress values were normalized using idealized values of τ_c , the critical stress for sediment entrainment, estimated from

$$\tau_c = \theta_c (S_s - 1) \rho g d \quad (8-7)$$

Where θ_c is the nondimensional critical shear stress parameter obtained from the Shields diagram, the specific gravity of the bed sediment S_s is 2.65, g is 9.81 ms^{-2} , and d is the sediment diameter. For the spill-through abutment flow fields, the τ_c values were adjusted for localized bed slope τ_{wc} using the following equation given by Vanoni (1977):

$$\frac{\tau_{wc}}{\tau_c} = \sqrt{\left(\frac{\sin \beta \sin \alpha}{\tan \phi'} \right)^2 + \cos^2 \beta} \left[1 - \left(\frac{\tan \beta}{\tan \phi'} \right)^2 \right] - \frac{\sin \beta \sin \alpha}{\tan \phi'} \quad (8-8)$$

Where the main channel bank slope angle α_s is 26.6 degrees, or 2:1 (H:V), the repose angle of the bed material ϕ' is 30 degrees and β is the direction of the flow defined in Figure 8-14. An example of the normalized bed shear

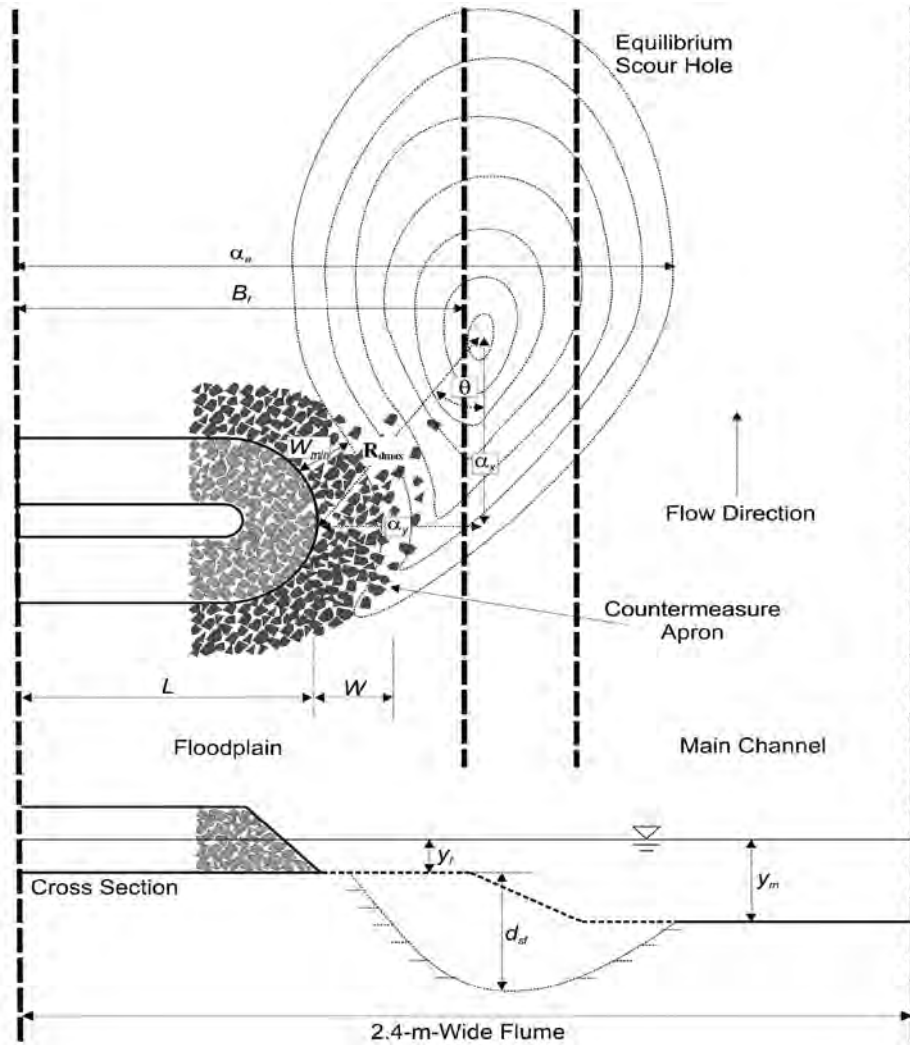


Figure 8-12. Scour hole parameters measured for each experiment in the 2.4-m wide flume.

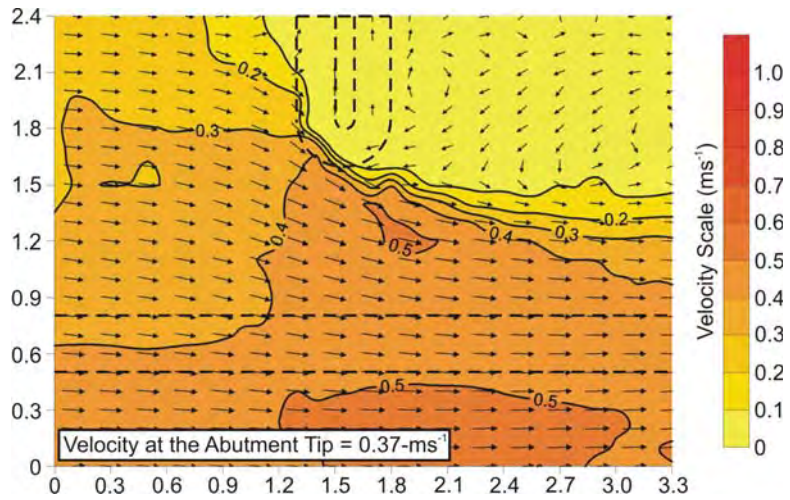


Figure 8-13. Velocity vector field around a spill-through abutment ($B_r = 1.6 \text{ m}$; $L = 0.8 \text{ m}$).

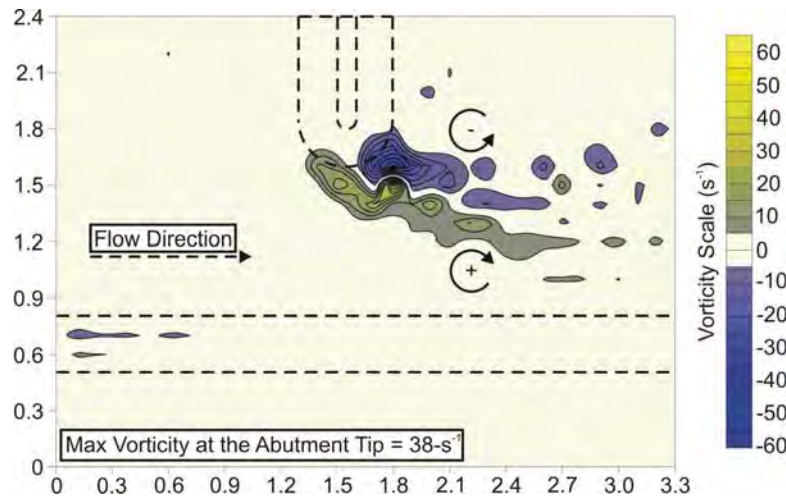


Figure 8-14. Vorticity field around a spill-through abutment ($B_f = 1.6$ m; $L = 0.8$ m).

stress fields at the spill-through abutment is shown in Figure 8-15.

8.2.3 Results

Figures 8-16 and 8-17 give lateral distributions of flow velocity.

The series of velocity, vorticity, and normalized bed shear stress plots are shown in Figures 8-18, 8-19, and 8-20, respectively, for the spill-through abutment flow fields. In these three figures, the abutment length L increases down the page from $4y_f$ to $16y_f$, the floodplain width B_f increases across the page from $8y_f$ to $20y_f$, and the flow velocity V/V_c increases down the page from 1.1 to 2.2.

The increase in velocity at the abutment, shown in Figure 8-16, causes a local increase in bed shear stress on the floodplain, shown in Figure 8-18. This observation is most obvious for the case where L/y_f is 8 and B_f/y_f is 16. Upstream of the abutment, the backwater on the floodplain caused by the abutment diverts flow from the floodplain into the main channel. The velocity in the main channel increases as the flow accelerates through the contracted section, causing an increase in bed shear stress in the main channel, as seen in Figures 8-16 and 8-18. These two observations were also observed by Biglari and Sturm (1998) and Lim and Nugroho (2004) in both their experimental and numerical work on flow around abutments in compound channels.

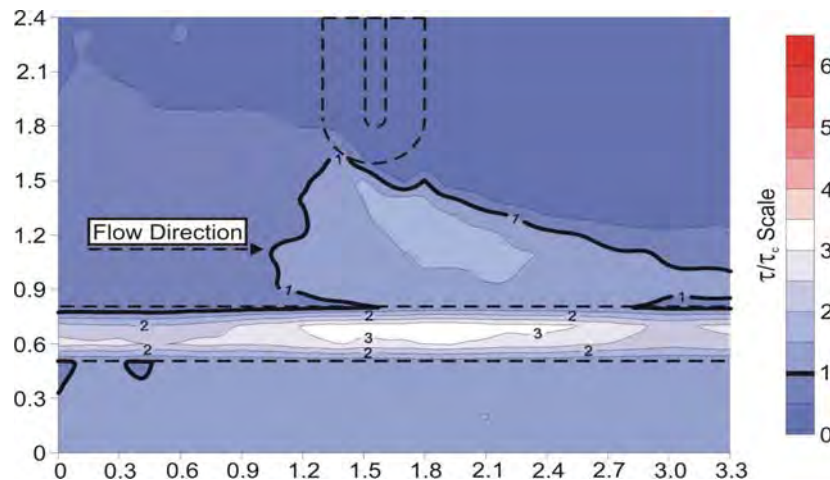


Figure 8-15. Normalized bed shear stress field at a spill-through abutment ($B_f = 1.6$ m; $L = 0.8$ m).

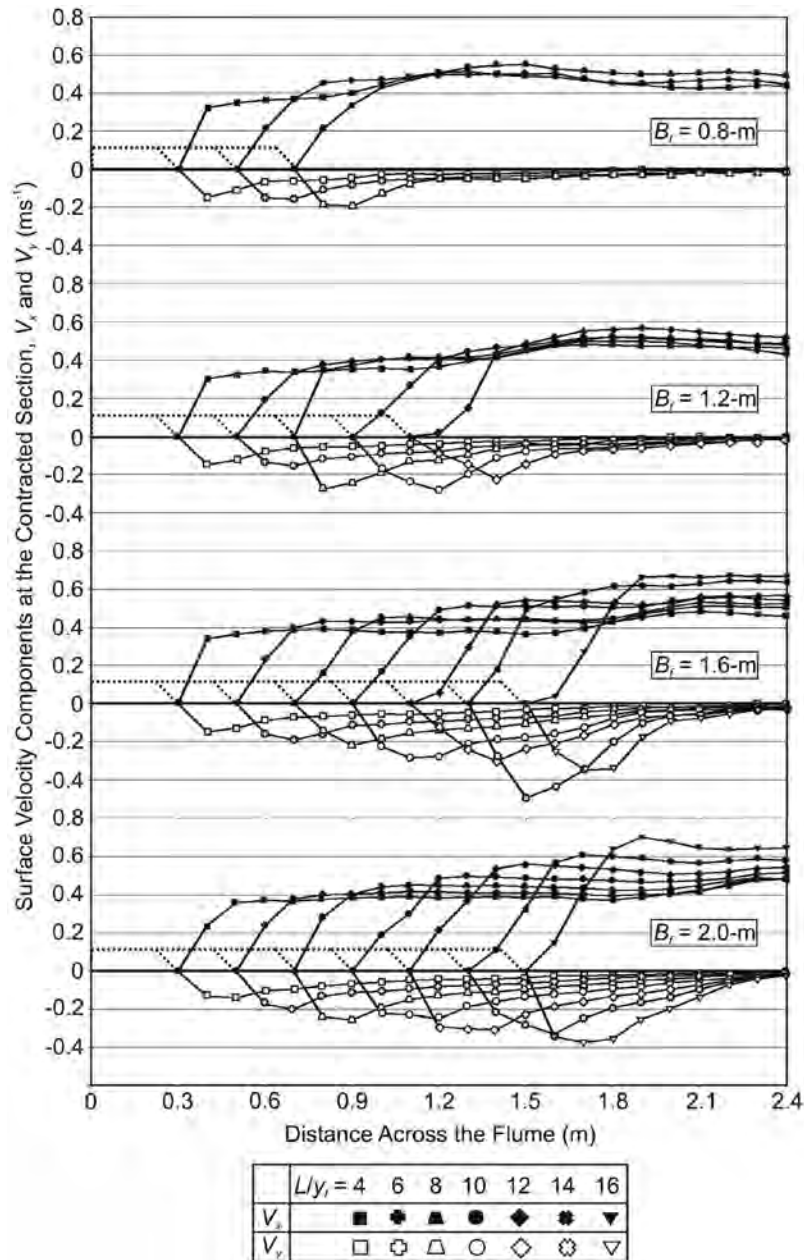


Figure 8-16. Velocity distributions across the bridge section (in terms of V_x and V_y , defined in Figure 8-7) for all the experimental configurations given in Figure 8-32.

There is a small counterclockwise rotation in the flow field at the upstream corner of the abutment (also observed by Kwan, 1984) and a larger counterclockwise rotation in the flow field downstream of the abutment, which extends out past the end of the abutment (see Figure 8-16), the latter increasing with abutment length. There is also a smaller clockwise rotation in the flow field at the downstream corner of the abutment next to the larger region of counterclockwise rotation. This clockwise rotation is more obvious with increasing abutment length

and is most obvious for the spill-through abutment case where L/y_f is 10 and B_f/y_f is 16.

Atayee (1993) studied the stability of riprap in aprons around spill-through abutments situated on the floodplain of a compound channel. Atayee observed that failure occurred consistently at the toe of the embankment just downstream of the end of the abutment, regardless of abutment length and proximity to the main channel. From Figure 8-17, it can be seen that the vorticity strength of the flow field around the abutment is strongest at the toe of the embankment just down-

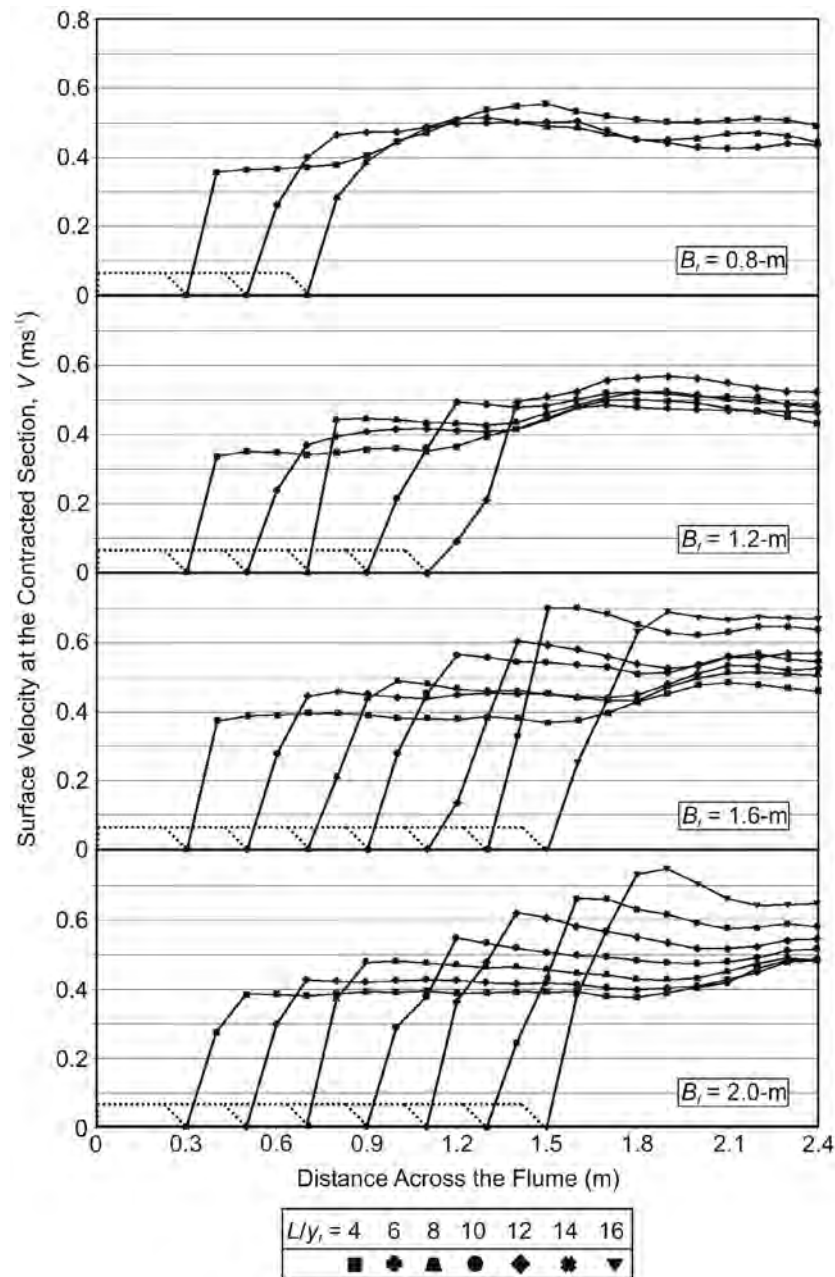


Figure 8-17. Velocity distributions across the bridge section (in terms of the velocity magnitude) for all the experimental configurations given in Figure 8-32.

stream of the abutment end, irrespective of abutment length and proximity to the main channel. The zone of strongest vorticity at the abutment corresponds to the zone where riprap shear failure occurred in the study by Atayee, suggesting that the vorticity strength may be the dominant parameter initiating riprap shear failure in an apron around an abutment.

The bed shear stress fields were calculated based on the assumption that the vertical velocity distribution could be represented by a logarithmic velocity profile. The validity of this

assumption has not been verified by measuring the bed shear stress at different points in the flume, so the results should be interpreted with caution. Lim and Nugroho (2004) measured vertical velocity profiles around a vertical-wall abutment situated on the floodplain of a compound channel both before and after scour occurred. Their work showed that in the unscoured state (when the flow is mainly two-dimensional), the velocity distributions are represented reasonably well by the log-law relationship. This suggests that it is reasonable to

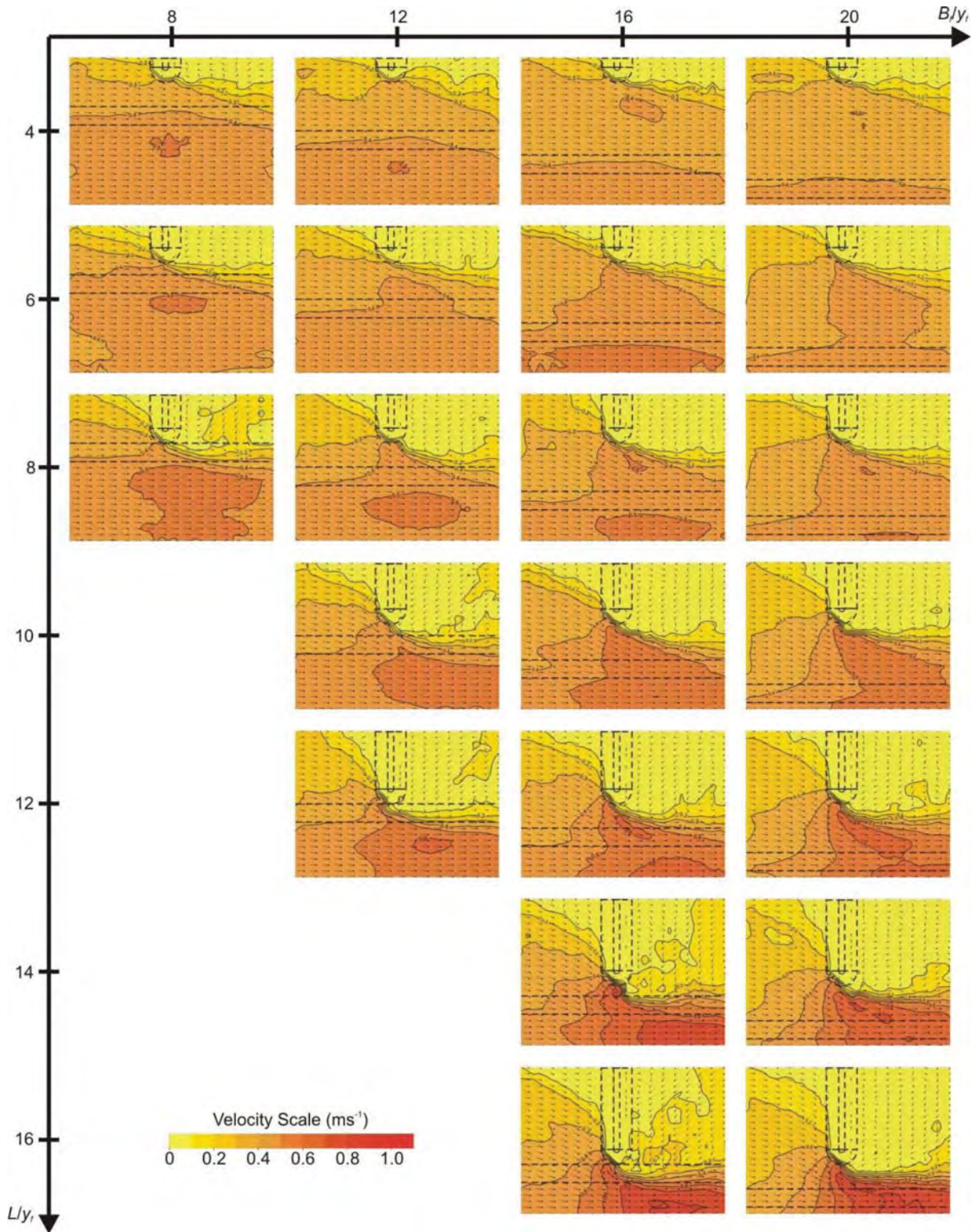


Figure 8-18. Velocity contour plots for various flow scenarios.

assume a logarithmic velocity distribution to calculate the bed shear stress.

Although the normalized shear stress plots must be interpreted with caution, they can effectively indicate zones where the shear stress increases relative to other areas in the flow field.

Figures 8-16 through 8-20 all show that the velocity, vorticity strength, and shear stress at the end of the abutment increase with increasing abutment length as a result of more flow being diverted around longer abutments. It can also be seen that the velocity in the main channel increases with increasing abutment

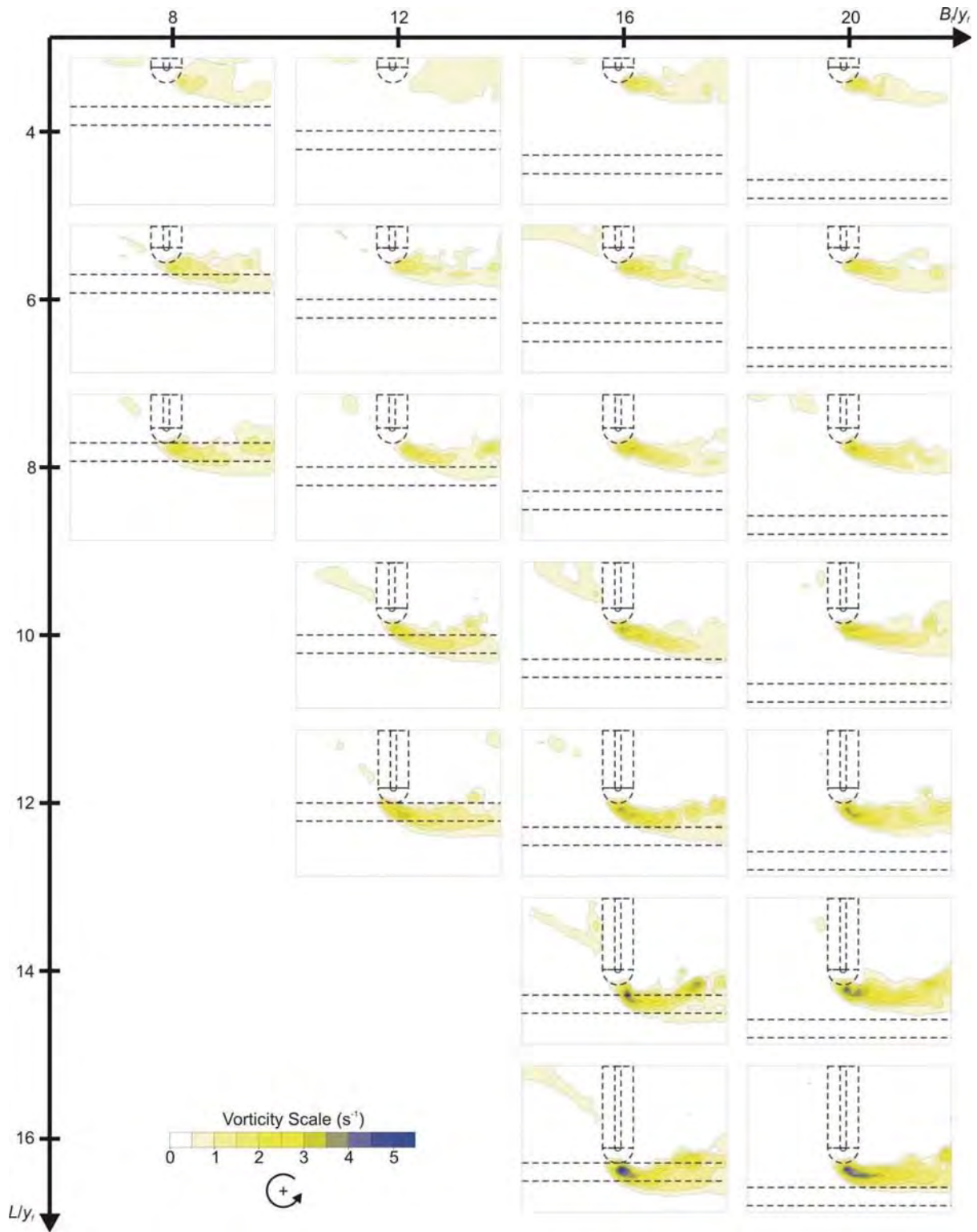


Figure 8-19. Vorticity contour plots for various flow scenarios.

length because of a greater contraction at the bridge section. Figure 8-16 shows that the velocity component across the flume in the y -direction increases with increasing abutment length as the flow is diverted around the abutment. Equation 8-8 allows for flow direction in the calculation of the critical shear stress on

the main channel bank. Consequently it can be seen from the normalized shear stress plots that the normalized shear stress on the main channel bank increases considerably with increasing abutment length because of the increasing component of the flow in the y -direction.

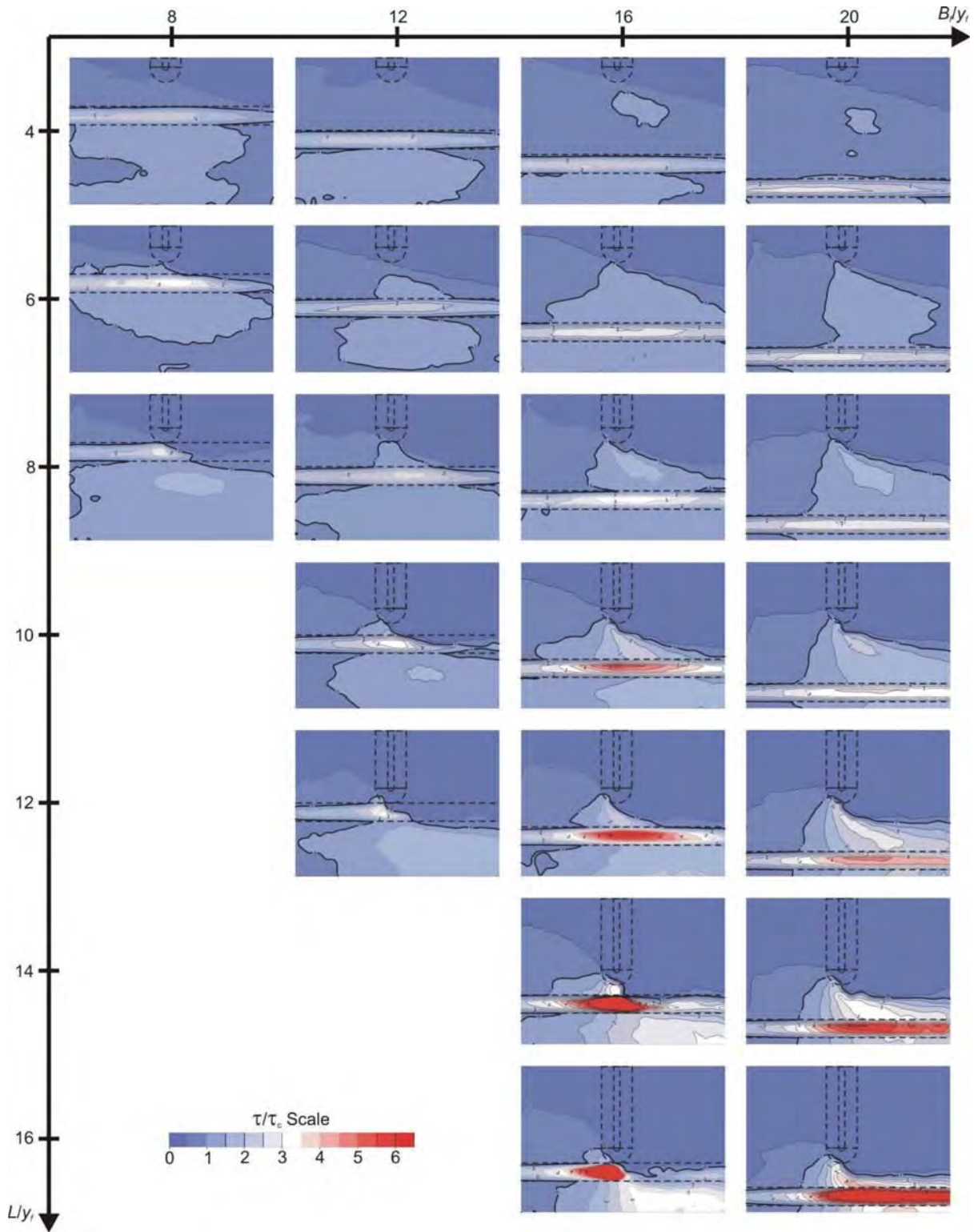


Figure 8-20. Bed shear stress contour plots for various flow scenarios.

Figures 8-16 and 8-17 show that, for most cases, the velocity, vorticity strength, and shear stress at the abutment end increase slightly with increasing floodplain width. These trends are explained as follows. As the floodplain width increases, the flow area at the bridge section decreases,

increasing the flow velocity at the bridge section. As a result of the increasing flow velocity at the bridge section, stronger vortices are shed from the end of the abutment.

Sections 8.3.3 and 8.3.4 describe the relationship between the measured flow fields around the spill-through abutments

and the development of scour at the abutments. These sections also describe how the flow fields can be used to determine the zones around the abutment that need to be protected from scour.

8.3 Spill-Through Abutment Clear-Water Study

8.3.1 Introduction

The aim of the study was to investigate the use of riprap and cable-tied blocks as spill-through abutment scour countermeasures. Both riprap and cable-tied block aprons were placed around abutments to protect them from scour, which could potentially undermine them if no protection were provided. A series of experiments were conducted with clear-water conditions just below the threshold velocity of the sediment. Abutment length, floodplain width, and apron extent were systematically varied for both riprap and cable-tied blocks to determine the minimum required apron extent to sufficiently protect the abutment.

Similitude between laboratory experiments and field scale was satisfied by the use of the aforementioned u_* / u_{*c} ratio, of which a value of just below 1.0 represents a condition called “clear-water scour.” This condition is extreme for scouring because the velocity is as high as possible without the movement of the channel bed, which causes infilling of the sediment hole.

8.3.2 Experimental Results

The measurements from the experiments are summarized in Table 8-2. For the experiments marked with an asterisk in Table 8-2, d_{sf} and W_{min} were also measured during the experiments. These measurements are given in Table 8-3. The distance to the deepest point of the scour hole from the abutment end R_{dmax} (as shown in Figure 8-12), is also given in Table 8-2 and can be determined as follows:

$$R_{dmax}^2 = \alpha_x^2 + \alpha_y^2 \quad (8-9)$$

The F values given in Table 8-2 were developed as part of the data analysis and are discussed in Section 8.3.4.

The position of the deepest point of the scour hole for all of the experiments is shown in Figure 8-21. As the abutment length increases, the distance to the deepest point of the scour hole from the end of the abutment increases. The scour hole position is independent of the floodplain width. For the case where the scour hole forms entirely on the floodplain ($\alpha_e < B_f$), the size of the scour hole tends to decrease slightly with increasing apron width and increase slightly with increasing floodplain width. Conversely, for the case where part of the scour hole forms beyond the floodplain ($\alpha_e > B_f$), the size of

the scour hole increases with increasing apron width and decreases with increasing floodplain width. As the apron width increases, the scour hole is deflected farther away from the end of the abutment.

The systematic trends of the scour hole geometry inherent in each of the experimental series is discussed in Section 8.3.4, including the equations derived from the data, which allow prediction of the position, extent, and depth of the scour hole and provide a method for estimating the minimum extent of apron protection to ensure adequate toe protection for the abutment.

8.3.3 Experimental Observations

The apron protection around the abutment inhibited the development of scour at the abutment toe. Scour was initiated at the edge of the apron and increased in depth with the passage of time. As the scour hole deepened, bed material on the sides of the scour hole fell into the scour hole, progressively undermining the protection apron. The response of the apron to the undermining process depended on the protection type.

As the riprap aprons were undermined, the stones at the outer edge would roll into the scour hole, protecting the bed of the hole from further scour. This would deflect the erosion zone farther away from the abutment.

As the cable-tied block aprons were undermined, the outer edge of the cable-tied block apron folded down onto the side of the scour hole because the cables prevented the blocks from sliding into the scour hole. As the apron folded down onto the side slopes of the scour hole, the horizontal distance between the toe of the abutment and the edge of the apron decreased, allowing the erosion zone to move closer toward the abutment. The scouring process would continue until the equilibrium scour depth was reached.

The velocity flow fields measured at the abutments showed that the velocity at the contracted bridge section increased with increasing abutment length and floodplain width. Both parameters have the effect of reducing the flow area at the contracted bridge section, thereby increasing the velocity and flow strength. Consequently, the vorticity and bed shear stress also increase with increasing abutment length and floodplain width. Similar effects were observed regarding the influence of the abutment length and floodplain width on the equilibrium scour hole depths, showing that the scour hole size is related to the flow field around the abutment.

The flow fields were overlaid on the associated equilibrium abutment scour formation photographs to compare some of the flow field features with the resultant scour hole formations. This comparison was undertaken only for the experiments where the spill-slope protection was extended below the surface of the floodplain ($W = 0$)—that is, for experiments with no apron. For the experiments with the protection aprons ($W > 0$), comparison of the flow field features

Table 8-2. Equilibrium scour hole measurements.

B_f (m)	L (m)	W (m)	d_{sf} (m)	α_x (m)	α_y (m)	α_e (m)	W_{min} (m)	R_{dmax} (m)	F
Riprap Protection									
0.800	0.400	0.000	0.200	0.620	0.250	0.980	-	0.669	0.27
0.800	0.400	0.100	0.190	0.660	0.290	0.990	0.000	0.721	0.28
0.800	0.400	0.200	0.185	0.790	0.350	1.000	0.070	0.864	0.29
0.800	0.400	0.300	0.210	0.880	0.430	1.080	0.170	0.979	0.38
0.800	0.400	0.400	0.285	0.960	0.530	1.230	0.250	1.097	0.53
0.800	0.400	0.500	0.280	1.050	0.560	1.350	0.310	1.190	0.61
0.800	0.600	0.000	0.355	0.780	0.320	1.430	-	0.843	0.89
0.800	0.600	0.300	0.330	1.000	0.500	1.500	0.005	1.118	0.91
0.800	0.600	0.400	0.380	1.040	0.550	1.730	0.060	1.176	0.96
0.800	0.600	0.500	0.370	1.080	0.625	1.810	0.135	1.248	0.97
0.800	0.800	0.000	0.435	0.850	0.435	2.020	-	0.955	1.00
0.800	0.800	0.500	0.400	0.900	0.700	2.200	0.000	1.140	1.00
1.200	0.400	0.000	0.180	0.380	0.155	0.860	-	0.410	0.00
1.200	0.400	0.100	0.160	0.450	0.260	1.010	0.040	0.520	0.00
1.200	0.400	0.200	0.155	0.650	0.290	1.065	0.120	0.712	0.00
1.200	0.400	0.300	0.100	0.780	0.360	1.120	0.250	0.859	0.00
1.200	0.400	0.400	0.080	0.860	0.410	1.180	0.380	0.953	0.00
1.200	0.400	0.500	0.070	1.050	0.410	1.300	0.465	1.127	0.07
1.200	0.600	0.000	0.250	0.500	0.220	1.260	-	0.546	0.07
1.200	0.600	0.200	0.280	0.650	0.410	1.360	0.010	0.769	0.17
1.200	0.600	0.300	0.300	0.810	0.560	1.480	0.180	0.985	0.28
1.200	0.600	0.400	0.315	0.920	0.600	1.540	0.280	1.098	0.32
1.200	0.600	0.500	0.325	1.030	0.650	1.610	0.350	1.218	0.38
1.200	0.800	0.000	0.315	0.795	0.440	1.630	-	0.909	0.54
1.200	0.800	0.300	0.365	0.990	0.550	1.840	0.010	1.133	0.69
1.200	0.800	0.400	0.385	1.100	0.690	2.000	0.125	1.298	0.77
1.200	0.800	0.500	0.400	1.120	0.725	2.100	0.210	1.334	0.81
1.600	0.400	0.000	0.205	0.450	0.230	1.060	-	0.505	0.00
1.600	0.400	0.100	0.205	0.600	0.290	1.090	0.010	0.666	0.00
1.600	0.400	0.200	0.210	0.750	0.440	1.260	0.065	0.870	0.00
1.600	0.400	0.300	0.215	0.790	0.440	1.280	0.165	0.904	0.00
1.600	0.400	0.400	0.200	0.870	0.475	1.350	0.275	0.991	0.00
1.600	0.400	0.500	0.210	1.010	0.530	1.390	0.385	1.141	0.00
1.600	0.600	0.000	0.290	0.500	0.270	1.470	-	0.568	0.00
1.600*	0.600*	0.200*	0.305*	0.790	0.490	1.600	0.020*	0.930	0.00
1.600	0.600	0.300	0.300	0.830	0.530	1.680	0.150	0.985	0.05
1.600	0.600	0.400	0.270	0.950	0.580	1.710	0.230	1.113	0.06
1.600	0.600	0.500	0.260	1.010	0.720	1.770	0.350	1.240	0.10
1.600	0.800	0.000	0.315	0.610	0.330	1.690	-	0.694	0.08
1.600	0.800	0.200	0.330	0.820	0.510	1.780	0.000	0.966	0.14
1.600	0.800	0.300	0.375	0.880	0.650	1.950	0.090	1.094	0.26
1.600	0.800	0.400	0.400	1.060	0.750	2.060	0.210	1.298	0.33
1.600	0.800	0.500	0.390	1.120	0.780	2.120	0.320	1.365	0.36
2.000	0.400	0.000	0.200	0.470	0.190	0.960	-	0.507	0.00
2.000	0.400	0.100	0.190	0.530	0.260	1.000	0.000	0.590	0.00
2.000	0.400	0.200	0.180	0.640	0.310	1.080	0.110	0.711	0.00
2.000	0.400	0.300	0.160	0.770	0.370	1.130	0.250	0.854	0.00
2.000	0.400	0.400	0.120	0.955	0.380	1.190	0.380	1.028	0.00
2.000	0.400	0.500	0.105	1.040	0.400	1.210	0.480	1.114	0.00
2.000	0.600	0.000	0.260	0.540	0.240	1.420	-	0.591	0.00
2.000	0.600	0.200	0.260	0.630	0.425	1.505	0.025	0.760	0.00
2.000	0.600	0.300	0.270	0.720	0.500	1.610	0.180	0.877	0.00
2.000	0.600	0.400	0.255	0.810	0.530	1.700	0.290	0.968	0.00
2.000	0.600	0.500	0.250	0.880	0.615	1.750	0.410	1.074	0.00
2.000	0.800	0.000	0.290	0.580	0.180	1.715	-	0.607	0.00
2.000	0.800	0.200	0.295	0.650	0.510	1.820	0.000	0.826	0.00
2.000	0.800	0.300	0.310	0.750	0.610	1.950	0.120	0.967	0.00
2.000	0.800	0.400	0.300	0.800	0.600	1.990	0.220	1.000	0.00
2.000	0.800	0.500	0.305	0.990	0.715	2.090	0.320	1.221	0.04
2.000	1.000	0.000	0.325	0.660	0.370	2.080	-	0.757	0.05

(continued on next page)

Table 8-2. (Continued).

B_f (m)	L (m)	W (m)	d_{sf} (m)	α_x (m)	α_y (m)	α_e (m)	W_{min} (m)	R_{dmax} (m)	F
Cable-Tied Block Protection									
0.800	0.400	0.200	0.210	0.480	0.190	0.950	0.000	0.516	0.23
0.800	0.400	0.300	0.235	0.580	0.260	0.990	0.050	0.636	0.28
0.800	0.400	0.400	0.275	0.620	0.380	1.100	0.100	0.727	0.41
0.800	0.400	0.500	0.260	0.690	0.410	1.150	0.160	0.803	0.45
0.800	0.600	0.400	0.370	0.640	0.360	1.530	0.000	0.734	0.92
0.800	0.600	0.500	0.385	0.735	0.405	1.620	0.100	0.839	0.94
0.800	0.800	0.500	0.415	0.755	0.260	2.040	0.000	0.799	1.00
1.200	0.400	0.200	0.185	0.300	0.185	0.950	0.015	0.352	0.00
1.200	0.400	0.300	0.180	0.420	0.280	1.010	0.060	0.505	0.00
1.200	0.400	0.400	0.170	0.530	0.320	1.100	0.200	0.619	0.00
1.200	0.400	0.500	0.130	0.700	0.360	1.230	0.375	0.787	0.02
1.200	0.600	0.300	0.300	0.380	0.250	1.310	0.000	0.455	0.12
1.200	0.600	0.400	0.315	0.480	0.370	1.400	0.070	0.606	0.21
1.200	0.600	0.500	0.295	0.540	0.480	1.480	0.130	0.722	0.28
1.200	0.800	0.400	0.380	0.615	0.440	1.715	0.010	0.756	0.61
1.200	0.800	0.500	0.405	0.760	0.510	1.900	0.085	0.915	0.72
1.600	0.400	0.300	0.215	0.425	0.260	1.110	0.025	0.498	0.00
1.600	0.400	0.400	0.200	0.520	0.350	1.240	0.150	0.627	0.00
1.600	0.400	0.500	0.215	0.635	0.440	1.310	0.250	0.773	0.00
1.600*	0.600*	0.300*	0.305*	0.360	0.280	1.390	0.000*	0.456	0.00
1.600	0.600	0.400	0.300	0.530	0.330	1.500	0.050	0.624	0.00
1.600	0.600	0.500	0.280	0.615	0.380	1.630	0.145	0.723	0.02
1.600	0.800	0.400	0.355	0.400	0.360	1.800	0.000	0.538	0.16
1.600	0.800	0.500	0.350	0.630	0.400	1.850	0.070	0.746	0.19
2.000	0.400	0.200	0.190	0.310	0.180	0.940	0.000	0.358	0.00
2.000	0.400	0.300	0.190	0.430	0.250	1.035	0.100	0.497	0.00
2.000	0.400	0.400	0.190	0.470	0.365	1.160	0.130	0.595	0.00
2.000	0.400	0.500	0.200	0.630	0.390	1.250	0.330	0.741	0.00
2.000	0.600	0.300	0.250	0.340	0.250	1.320	0.000	0.422	0.00
2.000	0.600	0.400	0.250	0.460	0.360	1.420	0.080	0.584	0.00
2.000	0.600	0.500	0.250	0.550	0.440	1.540	0.180	0.704	0.00
2.000	0.800	0.400	0.305	0.410	0.350	1.790	0.005	0.539	0.00
2.000	0.800	0.500	0.300	0.460	0.460	1.860	0.100	0.651	0.00
2.000	1.000	0.500	0.330	0.530	0.420	2.150	0.005	0.676	0.10

with the scour formation was difficult, because the scour hole development occurred away from the abutment because of the presence of the apron. Figure 8-22 shows an example of the equilibrium scour hole at a 0.8-m long abutment situated on a 1.6-m wide floodplain, with spill slope protection extended below the surface of the floodplain. Figures 8-23, 8-24, and 8-25 show the corresponding velocity, vorticity, and relative bed shear stress, respectively, overlaid on top of the equilibrium scour formation at the abutment.

It is apparent that the region of high vorticity in the wake of the abutment corresponds to areas where scour is initiated, as shown in Figure 8-24. During the development of the scour hole, erosion develops down the face of the riprap protection surface and downstream along the line of high vorticity.

The effect of placing a riprap apron or similar protection layer around an abutment is to prevent the initiation of scour at the point where the vorticity is strongest. The scour hole is deflected downstream and generally reduces in size. Figure 8-24 shows that the vorticity strength decreases farther away from the abutment, which is consistent with the reduced scour depth observed when wider aprons are placed around the abutments.

The deepest point of scour occurs on a line extending from the end of the abutment at an approximate angle of 30 degrees to the downstream direction, irrespective of the apron size (discussed in Section 8.3.4). Figure 8-24 shows that the dividing line of positive and negative vorticity at the end of the abutment also occurs at an approximate angle of 30 degrees to the downstream direction. This shows a strong correlation between the scour hole position and zone of strongest vorticity at the abutment. Therefore, using a two-dimensional numerical model to determine strong vorticity regions at a bridge abutment could enable better prediction of the expected scour hole location.

Coupled with regions of strong vorticity at the abutment end are regions of increased flow velocity and associated bed shear stress, where the bed shear stress exceeds the critical bed shear stress. Such regions typically occur upstream of, and in front of, the abutment. The excess shear stresses are responsible for the erosion that occurs farther toward the main channel where the vorticity is weaker. Because the bed of the main channel was fixed for these experiments, the increase in the bed shear stress in the main channel as a result of the contracted flow did not result in contraction scour.

Table 8-3. Non-equilibrium scour measurements for the experiments marked with an asterisk in Table 8-2 ($B_f = 1.6$ m and $L = 0.6$ m).

Time (hrs)	Riprap Protection $W = 0.2$ m		Cable-Tied Block Protection $W = 0.2$ m		Cable-Tied Block Protection $W = 0.3$ m	
	d_{sf} (m)	W_{min} (m)	d_{sf} (m)	W_{min} (m)	d_{sf} (m)	W_{min} (m)
0.0	0.000	0.200	0.000	0.200	0.000	0.300
0.5	0.050	0.190			0.040	0.275
1.0	0.080	0.190	0.080	0.140	0.060	0.265
1.5	0.090	0.190	0.105	0.100	0.090	0.250
2.0	0.100	0.160	0.125	0.100	0.115	0.225
2.5	0.105	0.130	0.135	0.075	0.125	0.220
3.0	0.110	0.130	0.145	0.030	0.135	0.200
3.5	0.115	0.130	0.150	0.010	0.140	0.170
4.0	0.125	0.130	0.155	0.000		
5.0	0.135	0.110	0.160	0.000	0.160	0.150
6.0	0.155	0.100			0.170	0.125
7.0	0.170	0.100			0.175	0.115
8.0	0.170	0.100				
9.0	0.180	0.090			0.190	0.080
10.0	0.195	0.080				
11.0	0.200	0.070				
12.0						
13.0	0.220	0.070			0.210	0.050
14.0	0.225	0.070				
15.0					0.225	0.030
30.0	0.255	0.025				
72.0	0.305	0.020			0.305	0.000

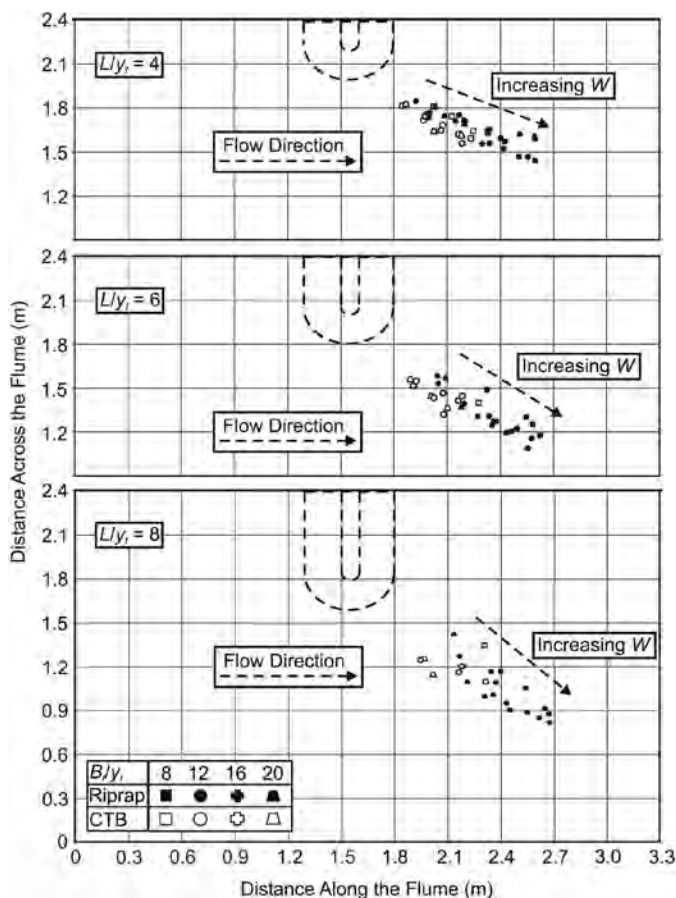


Figure 8-21. Position of the deepest point of scour relative to the spill-through abutment for the experimental data recorded in Table 8-3.

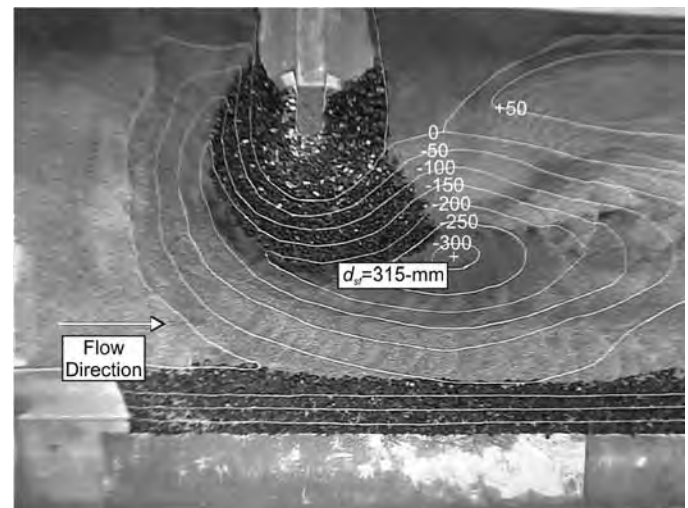


Figure 8-22. Equilibrium scour hole at a spill-through abutment with the spill-slope riprap protection extended below the floodplain ($B_f = 1.6$ m; $L = 0.8$ m).

If the flow fields at the abutment had been remeasured after the development of a scour hole at the abutment, the velocity around the abutment would have decreased because the flow depth would have been deeper as a result of the scour at the abutment. Consequently, the bed shear stresses around the abutment would also have decreased. It is postulated that the bed shear stresses around the abutment would progressively decrease with the development of scour at the abutment. This process would continue until the stage where the bed shear

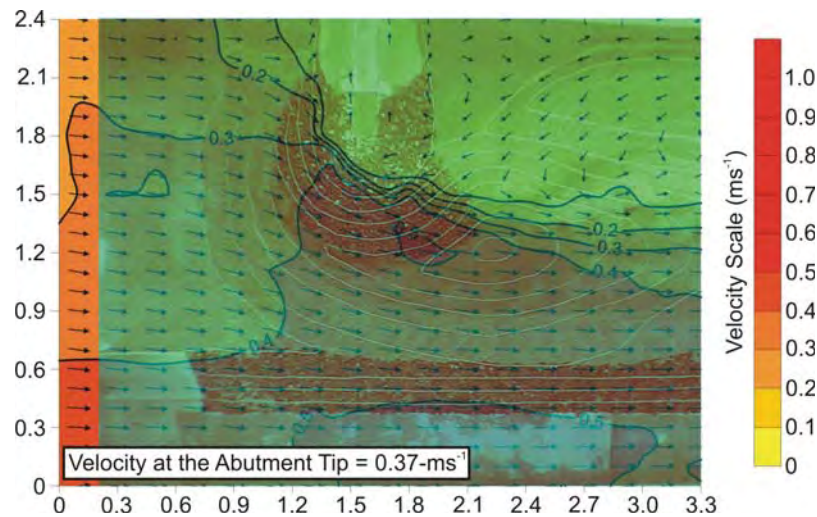


Figure 8-23. Velocity vector field overlaid on the corresponding equilibrium scour formation.

stresses would decrease to the critical bed shear stress level, at which point equilibrium scour conditions would be attained.

The problem with remeasuring the flow fields around the abutment after the development of a scour hole at the abutment is that the measured flow fields would not be representative of the actual flow fields at the abutment. The reason is that the measuring technique used is a surface particle-tracking technique. At the initial stages of the experiment, the flow can be represented reasonably well by a two-dimensional flow field, but at equilibrium scour conditions the flow field becomes significantly three-dimensional. Consequently, the surface velocity field is not representative of the flow structure around the abutment, as shown by the experimental work of Lim and Nugroho (2004).

8.3.4 Discussion

A comparison between the experimental scour depth data with the data presented in Sturm and Chrisochoides (1998a) for the scour depths at abutments situated in compound channels is shown in Figure 8-26. The data from Sturm and Chrisochoides apply to unprotected solid abutment structures. Therefore, only the experiments where the spill-slope protection was extended below the surface of the floodplain ($W = 0$) are included for the purpose of comparison. The flow directly upstream of the bridge opening Q_o , as a fraction of the total flow in the compound channel upstream of the bridge crossing Q_T , was determined from the velocity flow fields. The data from the present study agree reasonably well

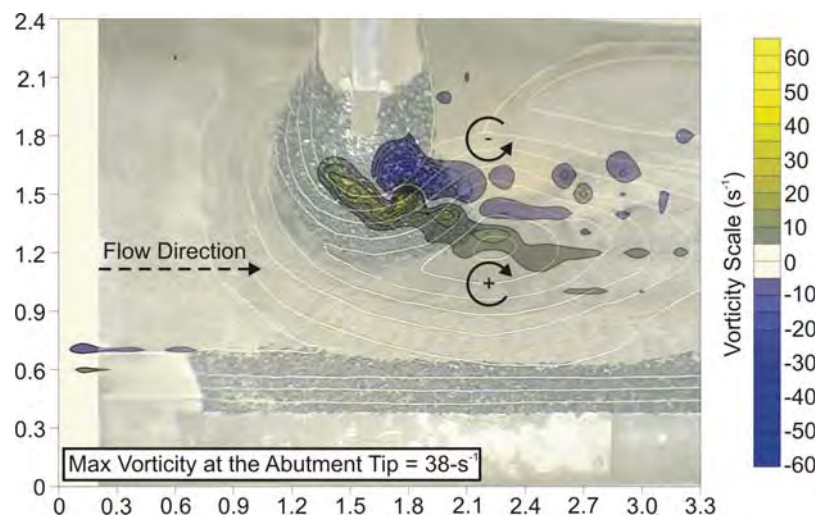


Figure 8-24. Vorticity field overlaid on the corresponding equilibrium scour formation.

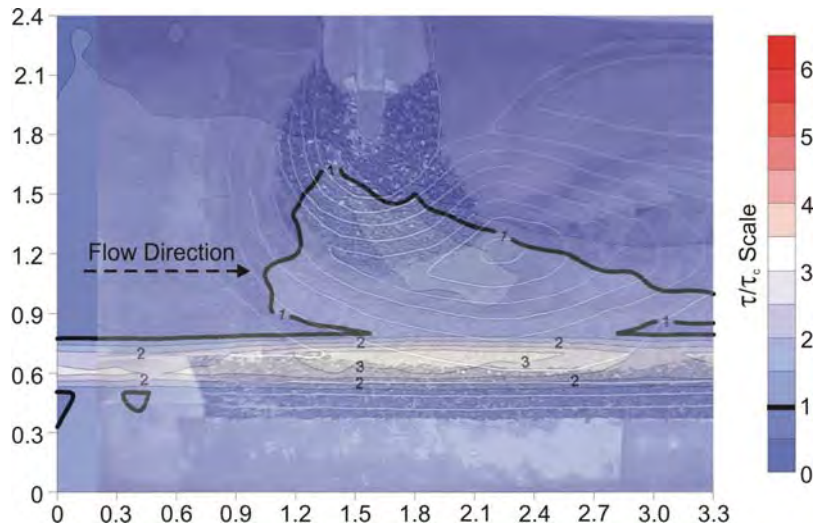


Figure 8-25. Normalized bed shear stress field overlaid on the corresponding equilibrium scour formation.

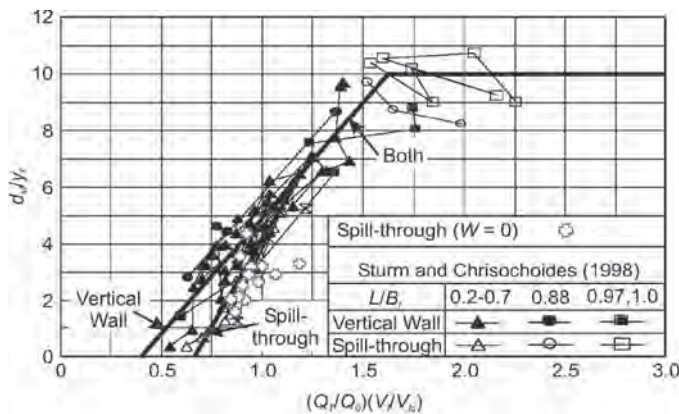
with the trend for spill-through abutments given by Sturm and Chrisochoides (1998a).

Figure 8-27 compares the scour depths from the present study with the results of experimental studies by Gill (1972), Wong (1982), Tey (1984), Kwan (1984, 1988), Kandasamy (1989), and Dongal (1994), as presented by Melville and Coleman (2000). The envelope suggested by Melville and Coleman (2000) gives a reasonable upper estimate of the scour depth for the experiments where the scour development at the abutment occurred on the floodplain only ($\alpha_e < B_f$). However, for experiments where part of the scour hole

forms beyond the floodplain ($\alpha_e > B_f$), the data points lie above the envelope suggested by Melville and Coleman (2000). For the latter experiments, scour depths are affected by the compound channel geometry, which increases the scour depths compared with those for abutments situated in equivalent rectangular channels. This effect is discussed further in the following section.

Scour Hole Position

The position of the center of the scour hole was recorded for each experiment in terms of α_x and α_y . The position of the center of the scour hole can also be defined by R and θ (see Figure 8-12) using trigonometric expressions. The values of R were calculated for each experiment using



Reprinted with permission from ASCE.

Figure 8-26. Normalized scour depth as a function of the upstream flow parameters (reproduced from Sturm and Chrisochoides, 1998a). Also included are data from the current experiments where the riprap protection was extended below the surface of the floodplain.

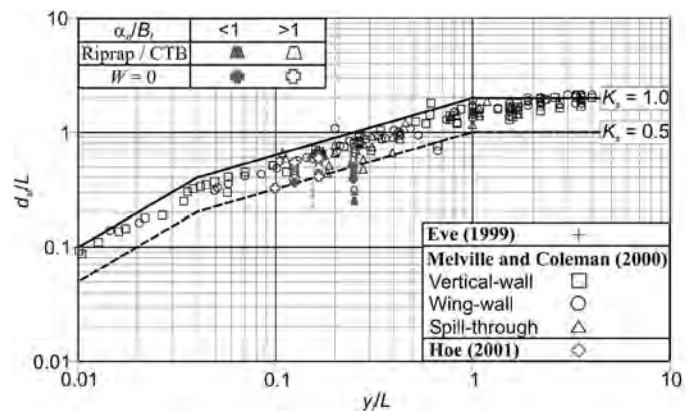


Figure 8-27. Normalized scour depth as a function of the normalized flow depth (reproduced from Melville and Coleman, 2000). Also included are scour data from the current spill-through abutment experiments.

Equation 8-9, while the angle θ was calculated from the following:

$$\tan\theta = \frac{\alpha_y}{\alpha_x} \tag{8-10}$$

Figure 8-28 is a plot of α_y against α_x for all of the experiments. The gradient of the line of best fit in Figure 8-28 is $\tan\theta$, where a value of $\theta = 30$ degrees was determined.

Expressions for R and α_e were derived from the data of Table 8-2 using regression analysis. Figures 8-29 and 8-30 show the results of the regression analysis for R and α_e , respectively, which were found to be dependent on L and W and independent of B_f . The expressions for R and α_e are as follows:

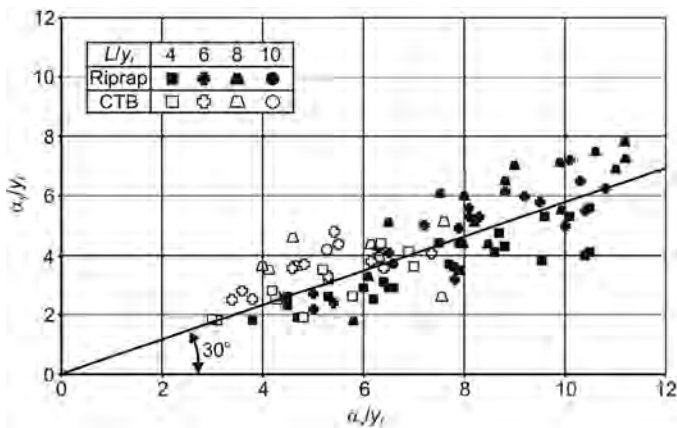


Figure 8-28. Normalized longitudinal position of the deepest point of the scour hole as a function of the normalized lateral position of the deepest point of the scour hole.

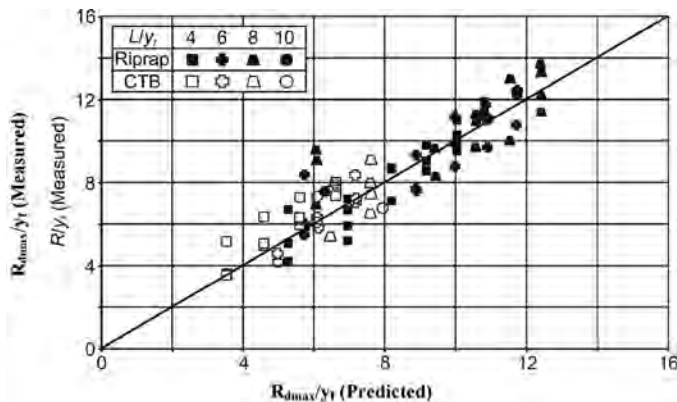


Figure 8-29. Comparison of the predicted distance from the end of the abutment to the deepest point of the scour hole using Equation 8-9 with the measured data.

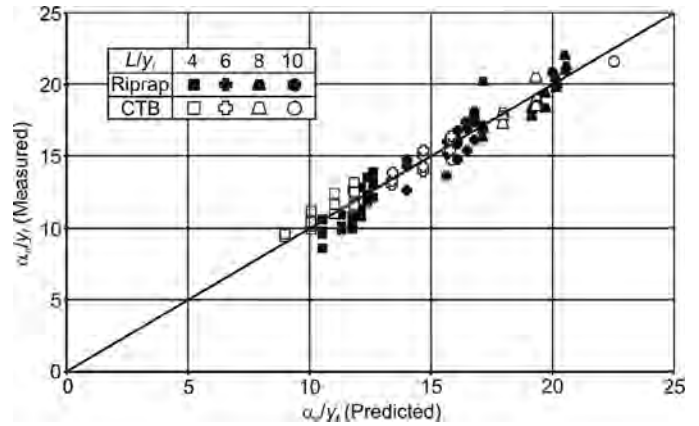


Figure 8-30. Comparison of the predicted distance from the side of the flume to the outer edge of the scour hole using Equation 8-10 with the measured data.

$$\frac{R}{y_f} = C_1 \left(\frac{L}{y_f} \right)^{0.2} \left(1 + \frac{W}{y_f} \right)^\phi \tag{8-11}$$

$$\frac{\alpha_e}{y_f} = C_2 \left(\frac{L}{y_f} \right)^{0.7} \left(1 + \frac{W}{y_f} \right)^\varphi \tag{8-12}$$

Where C_1 , C_2 , ϕ , and φ depend on the type of protection. For riprap, $C_1 = C_2 = 4$, $\phi = 0.4$, and $\varphi = 0.1$, while for cable-tied blocks, $C_1 = 1.0$, $C_2 = 2.2$, $\phi = 0.9$, and $\varphi = 0.4$.

Longer abutments (larger L) induced deeper scour holes and correspondingly increased R_{dmax} and α_e . Increasing W deflects the scour hole farther away from the end of the abutment, thereby increasing R_{dmax} and α_e , consistent with the results from the experimental studies of Croad (1989), Eve (1999), Hoe (2001), Cheung (2002), and Martinez (2003). Scour holes at abutments protected by cable-tied blocks form closer to the abutment than scour holes at abutments protected by equivalent riprap aprons—that is, R and α_e are larger for riprap protection than for cable-tied block protection, as discussed in Section 8.3.

Scour Depth

Three different cases of scour development were identified in this study, depending on the position of the scour hole in relation to the boundary between the main channel and the floodplain (shown schematically in Figure 8-31):

- The scour hole formed entirely on the floodplain ($\alpha_e < B_f$).
- The scour hole extended beyond the floodplain onto the main channel bank and, in some cases, into the main channel ($\alpha_e > B_f$).

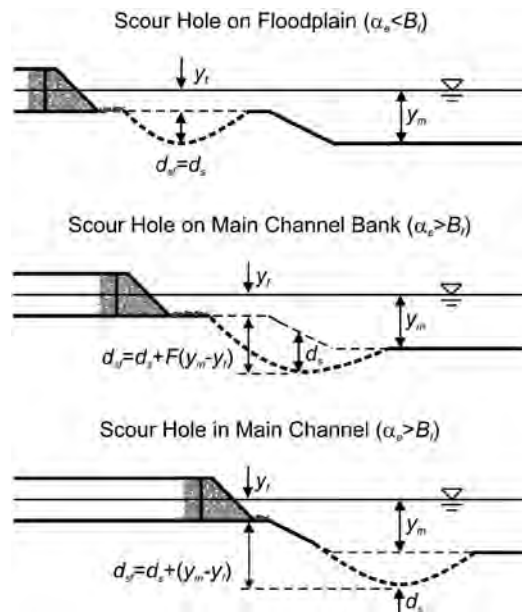


Figure 8-31. Three different cases of scour development at the spill-through abutment.

- The scour hole formed in the main channel ($\alpha_e > B_f$).

For all the cases, the scour depth is measured relative to the bed level of the floodplain d_{sf} and can be related to the scour depth relative to the local bed level d_s by the following equation:

$$d_{sf} = d_s + F(y_m - y_f) \quad (8-13)$$

Where F is a function that accounts for the effects of α_e/B_f and L/B_f on the scour development, and α_e/B_f and L/B_f represent the relative position of the scour hole and abutment in the compound channel, as illustrated in Figure 8-12. F , which takes values between zero and unity, is given as follows:

$$F = 1 - \left(1 - \frac{L}{B_f}\right)^2 \left(\frac{\alpha_e - 1}{B_f}\right) \quad \text{when } \frac{\alpha_e}{B_f} > 1 \quad (8-14)$$

$$F = 0 \quad \text{when } \frac{\alpha_e}{B_f} < 1 \quad (8-15)$$

The exponent in Equation 8-14 was determined from a regression analysis of the data, as discussed below. Equation 8-14 is plotted in Figure 8-32 for different values of α_e/B_f and L/B_f . Equations 8-13 and 8-14 apply only to the channel geometry cases C and D, which means that $L \leq B_f$. For this rea-

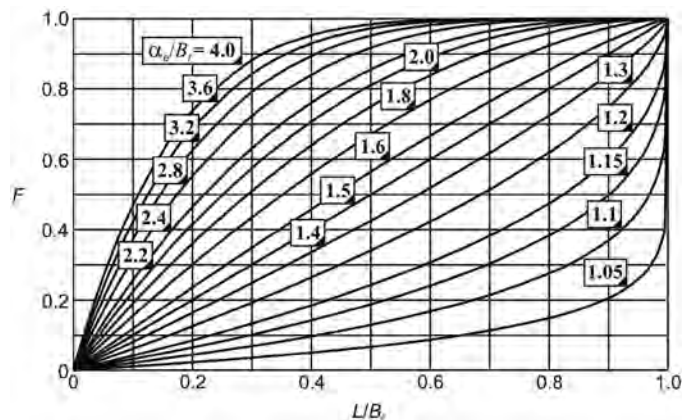


Figure 8-32. Plot of Equation 8-14 for the F function.

son, L/B_f takes values between zero and unity only, as shown on the horizontal axis of Figure 8-32.

When the scour hole forms entirely on the floodplain—that is, when $\alpha_e < B_f$ and $F = 0$ —then Equation 8-13 reduces to $d_{sf} = d_s$. When $L = B_f$, then the scour depth forms mostly in the main channel, $F = 1$, and $d_{sf} = d_s + (y_m - y_f)$. Values of F for each of the experiments are given in Table 8-4.

For the riprap experiments, the normalized (i.e., equilibrium) scour depth data of Table 8-2 are plotted in Figure 8-33 in terms of L/y_f , W/y_f , and B_f/y_f . The solid and hollow symbols signify scour data where $\alpha_e < B_f$ and $\alpha_e > B_f$, respectively. Figure 8-33 shows that the influences of W/y_f and B_f/y_f on the scour depth depend on α_e/B_f , as discussed in the following paragraphs.

Table 8-4. Flow field characteristics and scour depths ($W = 0$).

B_f (m)	L (m)	V_{rip} (ms^{-1})	ω_{max} (s^{-1})	d_{sf} (m)	F	d_s (m)
0.800	0.400	0.36	1.9	0.200	0.27	0.146
0.800	0.600	0.40	2.3	0.355	0.89	0.224
0.800	0.800	0.39	2.9	0.435	1.00	0.285
1.200	0.400	0.34	0.8	0.155	0.00	0.155
1.200	0.600	0.37	2.0	0.250	0.07	0.219
1.200	0.800	0.45	2.6	0.315	0.54	0.223
1.200	1.000	0.49	3.2	-	-	-
1.200	1.200	0.50	3.5	-	-	-
1.600	0.400	0.37	2.4	0.205	0.00	0.205
1.600	0.600	0.40	2.6	0.290	0.00	0.290
1.600	0.800	0.44	3.2	0.315	0.08	0.301
1.600	1.000	0.51	3.7	-	-	-
1.600	1.200	0.61	3.9	-	-	-
1.600	1.400	0.70	4.7	-	-	-
1.600	1.600	0.63	5.5	-	-	-
2.000	0.400	0.36	2.4	0.200	0.00	0.200
2.000	0.600	0.43	2.6	0.260	0.00	0.260
2.000	0.800	0.48	3.5	0.290	0.00	0.290
2.000	1.000	0.55	3.5	0.325	0.00	0.325
2.000	1.200	0.62	3.8	-	-	-
2.000	1.400	0.66	4.6	-	-	-
2.000	1.600	0.73	4.9	-	-	-

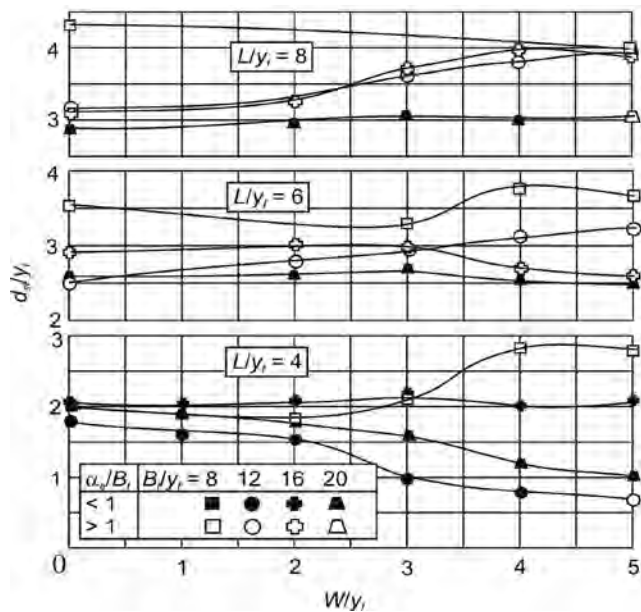


Figure 8-33. Variation of the scour depth with abutment length, floodplain width, and apron extent.

The lines in Figure 8-34 represent Equation 8-13 for the four different B_f/y_f values used in the experimental study. As in Figure 8-33, the solid and hollow symbols in Figure 8-34 signify scour data where $\alpha_e < B_f$ and $\alpha_e > B_f$, respectively. The lower line applies to the case where $\alpha_e < B_f$ (i.e., $F = 0$), while the upper lines incorporate the adjustment corresponding to F . When $\alpha_e < B_f$, the data follow the power-law relation of Equation 8-13. However, when $\alpha_e > B_f$, the data diverge from this line. This divergence can also be seen in Figure 8-33, particularly for the $L/y_f = 4$ data with increasing W/y_f .

When $\alpha_e < B_f$ the scour depth tends to decrease with larger W/y_f (Figure 8-33), and increase slightly with increasing B_f/y_f (Figure 8-34), although this trend is less marked. As B_f

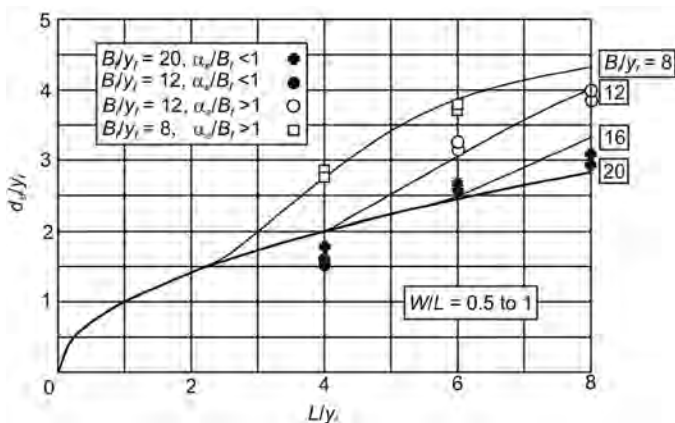


Figure 8-34. Variation of the scour depth with abutment length.

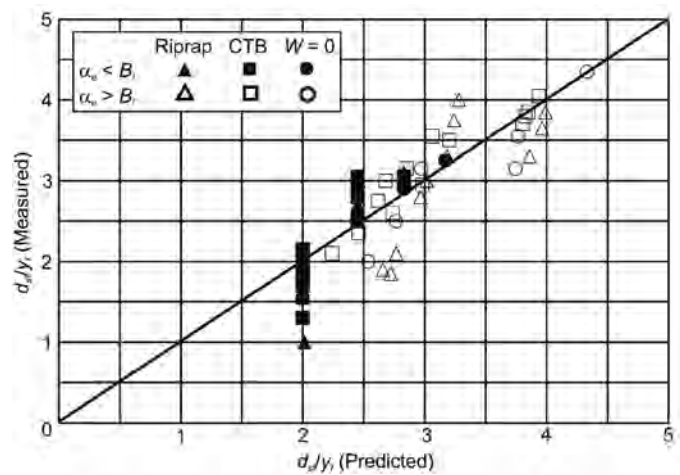


Figure 8-35. Comparison of the predicted scour depth using Equation 8-13 with the measured scour depth data.

increases, the flow area at the bridge section decreases and the mean flow velocity is correspondingly higher, resulting in deeper scour. This trend is consistent with that noted by Sturm and Janjua (1993) and was observed also in flow field measurements undertaken in the present study (discussed in Section 8.1). For smaller apron widths ($W/L < 0.75$), scour depth is approximately independent of W , while for wider aprons, scour depth decreases with increasing W/y_f . The reduced scour for wider aprons is a consequence of the lateral flow distribution in the flood channel. The strongest flow occurs at the end of the abutment, and the flow strength decreases away from the abutment.

When $\alpha_e > B_f$, scour depth increases with increasing W/y_f (Figure 8-33) and decreases as B_f/y_f increases (Figure 8-34). The latter trend is a consequence of the abutment set-back distance being larger with larger B_f/y_f , for which more of the scour hole is situated on the floodplain. With wider protective aprons, the scour hole develops farther away from the abutment. When $\alpha_e > B_f$, the scour hole development occurs farther into the main channel, where deeper scour occurs relative to the floodplain bed level.

Figure 8-35 compares the measured scour depth data with the predicted scour depths using Equation 8-13. Most of the scour data from Table 8-3 are included in Figure 8-35, although a few data points for very wide aprons at short abutments ($W > 0.75L$) are excluded because such aprons are impractically wide.

Figure 8-35 demonstrates a good agreement between the measured and predicted scour depths, supporting the incorporation of the new F function (to account for compound channel effects for Cases C and D, as shown later in Figure 8-46) in the scour depth prediction equation of Melville and Coleman (2000).

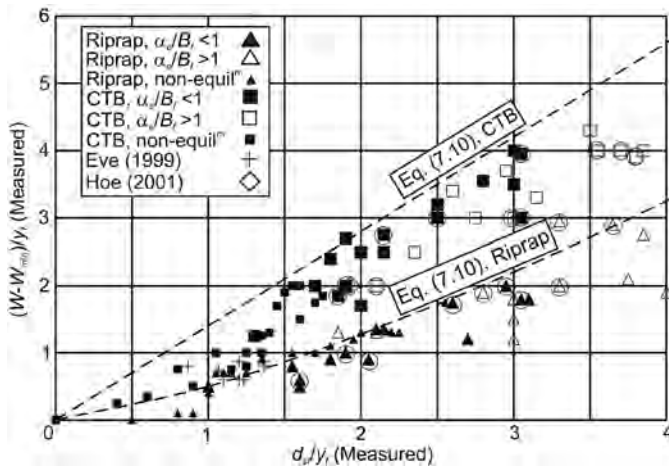


Figure 8-36. Minimum apron extent W_o as a function of scour depth.

Minimum Apron Extent

The apron extent W_o , for which $W_{min} = 0$, was measured for each experimental configuration—that is, for every combination of L/y_f and B_f/y_f . The data are plotted in Figure 8-36, where the encircled data represent values for which W_o was measured directly. In the plot, W_o is approximated by $W - W_{min}$ for data in the range $W/L < 0.75$. This assumption is discussed below. The plot also includes data by Hoe (2001) and Eve (1999).

The following expression for W_o is an envelope to the equilibrium scour data (shown in Figure 8-36) and additional nonequilibrium scour depth data for a few experiments:

$$\frac{W_o}{y_f} = C_3 \left(\frac{d_{sf}}{y_f} \right)^\lambda \quad (8-16)$$

Where $C_3 = 0.5$ and 1.4 and $\lambda = 1.35$ and 1.0 for riprap and cable-tied blocks, respectively. In applying Equation 8-16 to nonequilibrium scour depths, it is assumed that the equation is applicable during scour development as well as at the equilibrium condition. The assumption is reasonable, given the similarity of the scour hole shape throughout its development and the inclusion of some nonequilibrium scour depth data from Table 8-3 in Figure 8-36, as noted above.

As a consequence of the dependencies of scour depth on L and B_f , Equation 8-16 implies that W_o/y_f increases with increasing L/y_f and tends to decrease as B_f/y_f increases when $\alpha_e > B_f$. Larger scour holes are developed at longer abutments, requiring wider aprons for protection. Narrower aprons are required for abutments situated on wider floodplains because a greater portion of the scour hole develops on the floodplain as the floodplain width increases, resulting in smaller scour depths relative to the floodplain.

The dependency of the minimum required apron width with scour depth is consistent with the experimental studies of Hoe (2001) and Cheung (2002). Both of the experimental studies showed that with increasing approach-flow velocity (resulting in deeper scour holes), wider aprons were required to prevent abutment failure.

It is apparent from Figure 8-36 that W_o is larger for cable-tied block aprons, compared with equivalent riprap aprons, because scour holes at abutments protected by cable-tied blocks form closer to the abutment than for equivalent riprap aprons (as discussed in Section 8.3.3). Therefore, a narrower riprap apron will afford a greater level of protection to the base of the abutment spill slope compared with an equivalent cable-tied block apron. This implies that cable-tied block aprons need to be larger than riprap aprons to afford the same level of protection at abutments, consistent with the experimental studies of Croad (1989), Eve (1999), Hoe (2001), and Cheung (2002). The cable-tied block experimental studies of Hoe (2001) and Cheung (2002) showed that cable-tied block apron widths equal to twice the flow depth did not provide sufficient protection for the abutment, whereas the riprap experimental studies of Croad (1989) and Eve (1999) showed that riprap apron widths equal to twice the flow depth provided adequate protection for the abutment. This implies that the use of riprap aprons is preferable to the use of cable-tied block aprons to protect spill-through abutments from clear-water scour.

By definition, $W = W_o$ when $W_{min} = 0$. Thus, W_o defines the minimum apron width to prevent erosion of the toe of the abutment. If the toe is not sufficiently protected (i.e., $W < W_o$), the scour hole undermines the spill-slope fill material, causing the fill material to slump into the scour hole. For the case when $W > W_o$ (i.e., $W_{min} > 0$), the edge of the scour hole is deflected away from the toe of the abutment, and W_{min} is given as follows:

$$W_{min} = W - W_o \quad (8-17)$$

If the apron width increases to a width greater than $W/L = 0.75$, the scour hole reduces in size until eventually the apron is wide enough to eliminate all local scour at the abutment.

8.3.5 Comparison of the Scour Depth Prediction Method with Other Experimental Data

Other experimental data for scour depth at abutments situated on floodplains of compound channels are reported in Sturm and Janjua (1993) and Cardoso and Bettess (1999). Figure 8-37 compares these experimental data with the

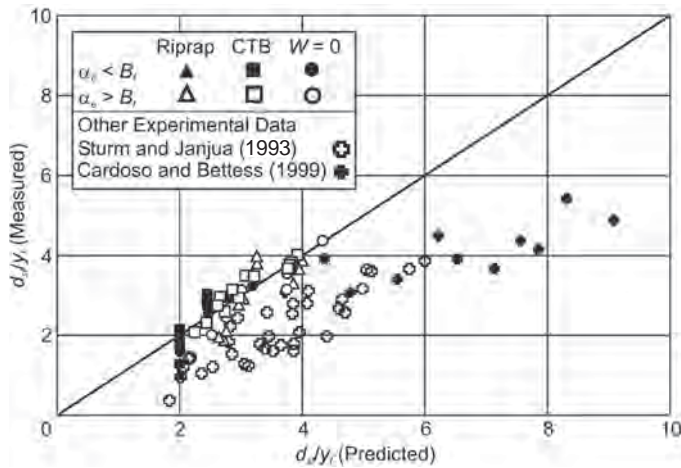


Figure 8-37. Comparison of the predicted scour depth using Equation 8-13 with the measured scour depth data shown in Figure 8-35 and the measured data from Sturm and Janjua (1993) and Cardoso and Bettess (1999).

predicted scour depths of Equation 8-13. Figure 8-37 also includes the data given in Figure 8-35.

Figure 8-37 shows that the data of Sturm and Janjua (1993) and Cardoso and Bettess (1999) are overpredicted by Equation 8-13. The measured data from Sturm and Janjua are smaller than predicted because the scour experiments were run for only 12 hours—that is, the scour depths recorded were less than the equilibrium scour depths. The measured data from Cardoso and Bettess are smaller than predicted because the velocities in the main channel were above the threshold conditions for sediment motion. For the cases when the scour hole formed partly in the main channel, the live-bed conditions in the main channel reduced the maximum clear-water scour depth.

Flow Field Correlations with Scour Hole Depths

The velocity just outside the separation zone at the end of the abutment V_{tip} and the vorticity strength ω_{max} for each abutment and compound channel configuration were determined from the flow field measurements. These are summarized in Table 8-4. The corresponding equilibrium scour depths d_{sf} and adjusted scour depth d_s are also given in Table 8-4 for the $W = 0$ experiments.

Figure 8-38 shows a positive correlation between d_s and V_{tip} , consistent with the results of Sturm and Janjua (1993). Figure 8-38 also shows a positive correlation between d_s and ω_{max} , consistent with the experimental work of Kirkil et al. (2004), which showed that the normalized scour depth increases with increasing vorticity strength at bridge piers.

The scour hole depth increases with increasing velocity at the abutment end and vorticity strength because the increas-

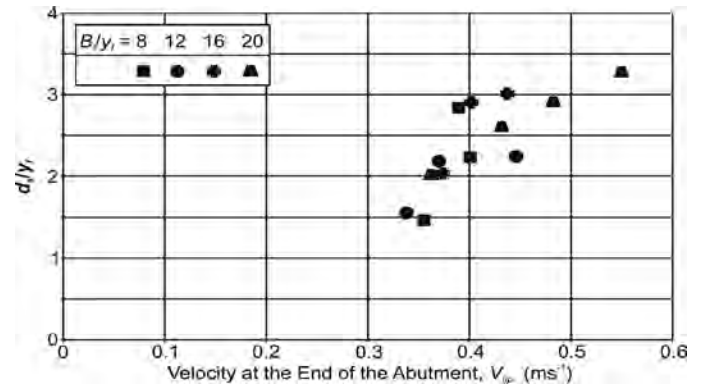


Figure 8-38. Normalized scour depth plotted against the measured velocity at the end of the abutment just outside the separation zone.

ing flow strength is capable of eroding more bed material from the scour hole.

The V_{tip} and ω_{max} parameters were used in a regression analysis to develop an empirical expression to predict the scour depth using the values obtained from the measured abutment flow field data. The results from the regression analysis of the normalized scour depth data (d_s/y_f) with V_{tip} and ω_{max} are shown in Figure 8-39.

Figure 8-40 shows the effect of a dimensionless expression containing ω_{max} on normalized d_s . It can be seen that the dimensionless expression $2.4(\omega_{max} V_{tip}/g)^{0.35}$ collapses the data well and could be used as an alternative scour depth prediction method when the flow fields around bridge abutments are modeled numerically. Thus, the alternative scour depth prediction method can be expressed as follows:

$$\frac{d_s}{y_f} = 2.4 \left(\frac{\omega_{max} V_{tip}}{g} \right)^{0.35} \quad (8-18)$$

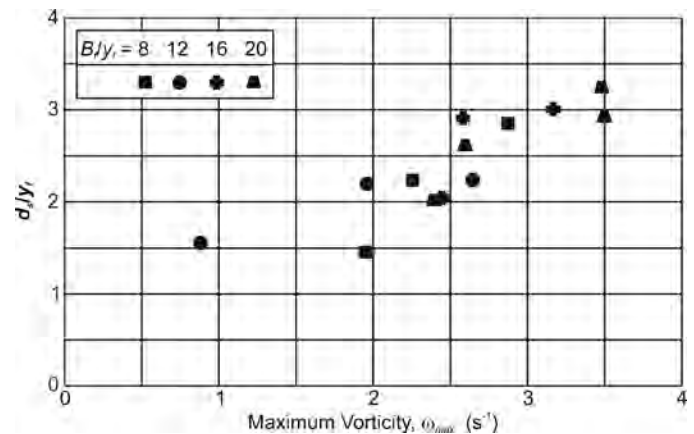


Figure 8-39. Normalized scour depth plotted against the maximum vorticity in the flow field at the abutment.

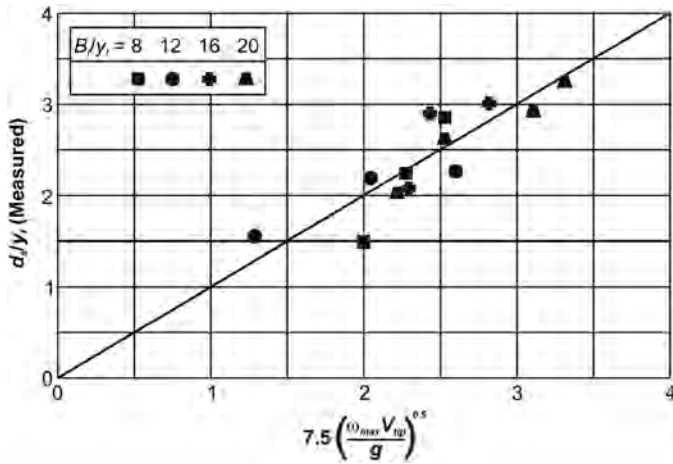


Figure 8-40. Comparison of the predicted scour depth using the flow field parameters from Table 8-4 in Equation 8-16 with the measured scour depth data for $W = 0$.

Figure 8-41 compares scour depth predictions using Equation 8-13 with those using Equation 8-18 in terms of the flow field parameters listed in Table 8-4. Figure 8-41 shows that there is a good agreement between Equations 8-13 and 8-18.

By substituting Equation 8-18 into Equation 8-13, the geometric parameters of the abutment can be related to the flow field parameters at the abutment as follows:

$$d_s = \sqrt{Ly_f} = 2.4y_f \left(\frac{\omega_{max} V_{tip}}{g} \right)^{0.35} \quad (8-19)$$

Equation 8-19 shows that scour depth increases with increasing L , V_{tip} , and ω_{max} consistent with the observations noted above. The direct implication is that V_{tip} and ω_{max}

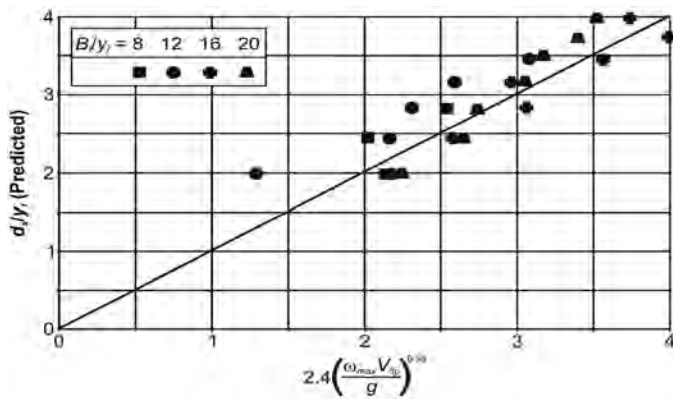


Figure 8-41. Comparison of the predicted scour depths of Equation 8-13 with the predicted scour depth of Equation 8-18 for $W = 0$.

increase with L , consistent with the observations noted in Section 8.3. It is important to note that Equations 8-18 and 8-19 are limited to when the abutment is aligned perpendicular to the flow—that is, when $V/V_c \leq 1$, $y_f/y_m = 0.4$, and $4 < L/y_f < 10$. Further investigation into the effects of V_{tip} and ω_{max} on the scour depth at the abutment is needed before Equations 8-18 and 8-19 can be applied beyond the data range tested.

8.4 Two-Dimensional Modelling of Flow Around a Small-Scale Model Abutment

8.4.1 Introduction

Selection of countermeasures to protect bridges from scour requires estimates of velocity distributions in the bridge opening. Estimates of the peak velocity in what is typically a highly nonuniform flow distribution near the tip of the abutment is necessary to determine whether countermeasures are necessary and, if so, to determine the type, size, and extent of countermeasures to protect bridge abutments from scour. Laboratory physical models have been developed to determine the size, type, and location of protection for a relatively small range of flow conditions at bridges; however, the laboratory models represent very simplistic geometric conditions. Effective transfer of laboratory model results to the complex hydrodynamic conditions of real bridge sites requires that flow velocity be predicted in the vicinity of bridge abutments using numerical models; however, the degree to which numerical models, typically used by highway engineers, can represent the highly nonuniform flow around abutments has not been examined.

The main purpose of this component of the study was to compare flow distributions obtained from a two-dimensional shallow water numerical model to flow distributions measured in small-scale laboratory model studies of flow around abutments. The two-dimensional shallow water model FESWMS (Finite Element Surface Water Modeling System), developed for analysis of bridges for the Federal Highway Administration, is used by highway agencies throughout the United States; therefore, it was used in this study. Also, the mesh-generating and postprocessing program SMS 8.1 was used in developing the computational mesh and in postprocessing the numerical results. This study illustrates the comparison of numerical and physical model results and an evaluation of the effectiveness of the two-dimensional model to simulate flow around abutments under small-scale laboratory conditions.

As noted previously, a particle-tracking velocimetry (PTV) was used to estimate the surface velocity of flow for two model abutments and four different channel and floodplain

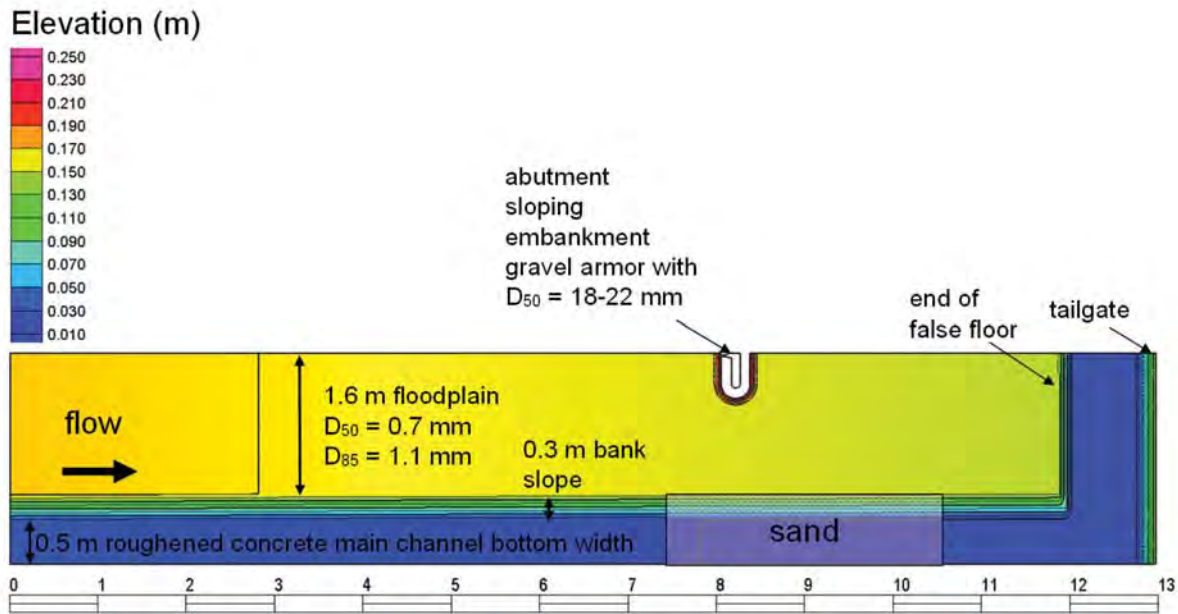


Figure 8-42. Plan view of the physical model as represented in the numerical model for the 600-mm spill-through abutment.

configurations. The physical model's configuration of abutment, channel, and floodplain, diagrammed in Figure 8-42, was chosen to evaluate the numerical model.

The physical model configuration included a spill-through abutment 600mm long with 1:1 side slopes, a floodplain 1.6m wide, and a main channel 0.8m wide. The flow rate was constant at 127.4l/s; the flow depth was 100mm in the floodplain and 250mm in the main channel. The flume slope was set at 0.002m/m. The floodplain surface was sand with a d_{50} of 0.7mm, and the channel surface was roughened concrete except for the test section, which was composed of sand of the same gradation as the floodplain. The abutment face was covered with uniformly graded riprap with intermediate axis between 18 and 22mm.

8.4.2 Finite Element Mesh and Hydraulic Coefficients of the Two-Dimensional Model

A finite element mesh was created using SMS Version 8.1. Figure 8-43 shows the developed mesh at two different scales. The mesh was composed of a combination of 11,966 nine-noded quadrilateral elements and 679 six-noded triangular elements, requiring 49,786 nodes. Element dimensions varied from 5mm in the region of suspected flow separation around the abutment to 352mm at the model upstream and downstream boundaries. Variation of mesh size was controlled by restricting the change in element area

by adjacent elements to less than 40 percent. Nine-noded quadrilateral elements were used wherever possible. Triangular elements were used to change element density or where ambiguous bed slope developed in quadrilateral elements, thereby requiring that one quadrilateral be divided into two triangular elements.

Slopes along the main channel, on the face of the abutment, at the downstream end of the flume false floor, and at the tailgate all exceed 10 percent. At the locations where substantial components of the flow are in the direction of the slope, significant error in flow acceleration is possible (Froehlich, 2002).

The two-dimensional model roughness coefficient for the channel and floodplain was calibrated such that the numerical model depth matched the measured depth (100mm) in the physical model floodplain and, to the extent possible, the velocity distribution observed for the floodplain at the upstream and downstream extents of the flume and for the cross-flume velocity distribution prior to placement of the abutment in the model. This two-dimensional model calibration resulted in a Manning n of 0.019 for the channel and 0.016 for the floodplain. The eddy viscosity for the main channel was also calibrated as 0.001m²/s. The two-dimensional model eddy viscosities for the floodplain varied from 0.00002 to 0.002m²/s. The largest values of eddy viscosity were applied in the entrance and exit of the two-dimensional model and in straight reaches with large elements, whereas the smallest values of eddy viscosity were applied in

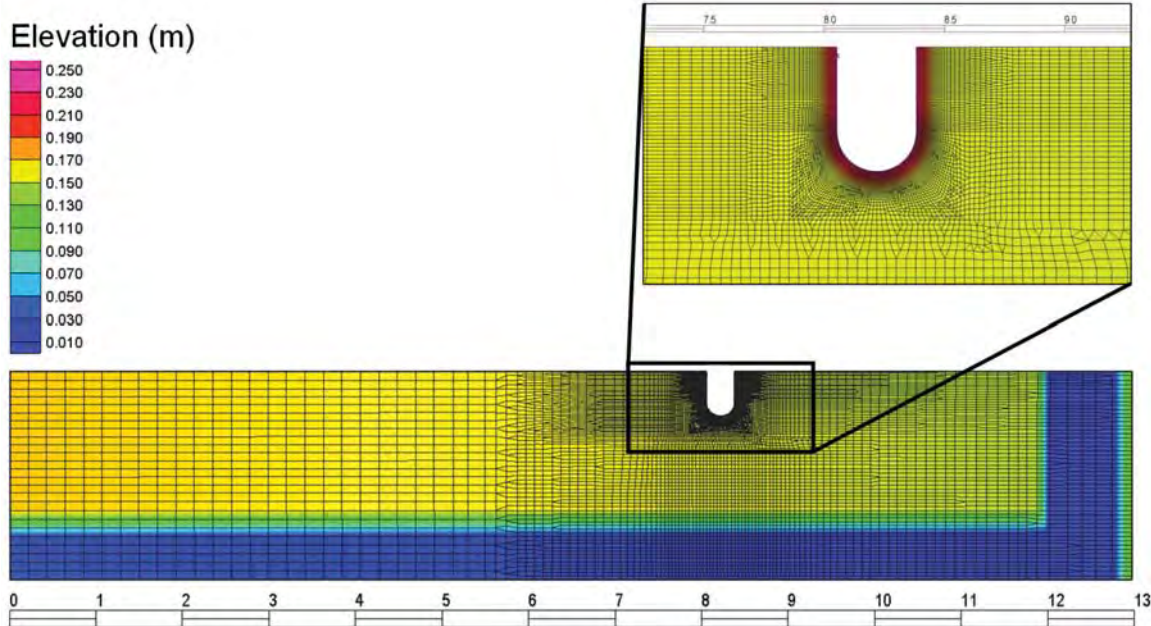


Figure 8-43. Finite element mesh composed primarily of nine-node quadrilateral and six-node triangular elements.

the low-velocity regions of the wake. No further calibration was performed.

The Peclet number is defined as:

$$Pe = \frac{LV}{E_v}$$

Where:

- L = characteristic length of an element (m),
- V = representative velocity magnitude (m/s), and
- E_v = kinematic eddy viscosity (m^2/s).

The Peclet number varied from 4.5 in the low-velocity region of the wake downstream of the abutment to 150 near the high-velocity regions of the flow boundary. In the floodplain and in the complex flow region near the abutment, the element size and the eddy viscosity were reduced until flow separation was simulated upstream of the abutment centerline. A combination of an element length of 5mm and an eddy viscosity of 0.0001 was required to model separation upstream of the abutment centerline.

8.4.3 Boundary Conditions and Roughness Characteristics of the Two-Dimensional Model

Boundary conditions for the numerical simulation included upstream flow input (127.4 l/s), downstream water

surface elevation based on the flow depth (100 mm), and semi-slip conditions along the walls and abutment (Manning n for flume walls). A flume slope of 0.002 m/m, as determined from a survey, was used in the model. Manning n values were determined from the roughness characteristics of the channel, bank, and floodplain of the model. The downstream extent was complicated by the end of the false floor used to model the floodplain and trap sediment and the tailgate. Earlier simulations indicated that a large recirculation zone downstream of the abutment extended beyond the end of the false floor. Consequently, flow was entering the computational model from a large part of the downstream boundary. To numerically model the entire recirculation zone, the mesh was extended to the flume tailgate.

8.4.4 Two-Dimensional Model Results

The two-dimensional simulation showed an increase in velocity both on the floodplain and in the main channel, as indicated in Figures 8-44 through 8-46. The location of simulated maximum increase in velocity associated with flow contraction was predicted to be on the abutment's sloping face upstream of its centerline; however, the flow in the remaining floodplain and channel continues to contract and accelerate to a point well downstream of the abutment. The point of highest simulated velocity on the embankment face is in an area of the flow field with high curvature; therefore,

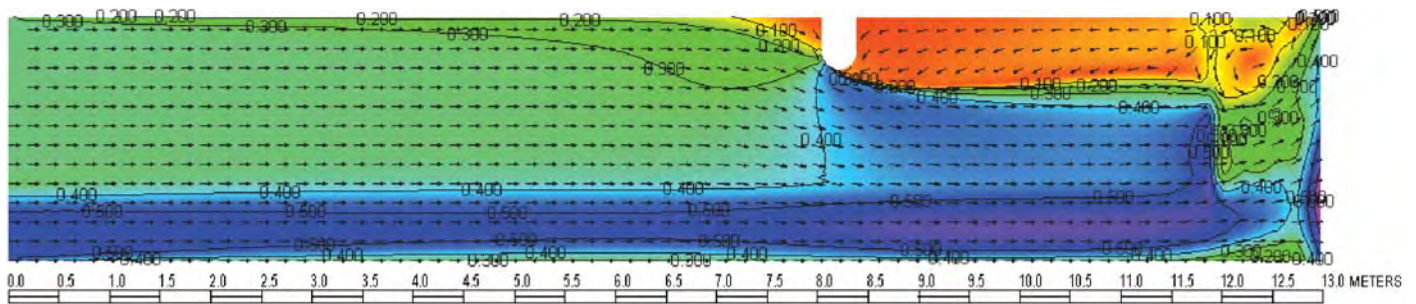


Figure 8-44. Numerically simulated velocity field over the entire model reach of the flume for 600-mm spill-through abutment (velocity contours in m/s).

the depth-averaged velocity at this location is likely to be inaccurate.

Depth-averaged velocity and computed boundary shear stress were plotted for four cross-flume transects, as shown in Figures 8-47 and 8-48. The first transect was obtained at the flume station of 5 m and represents the approach flow, although backwater effects have developed at this location. The second transect, at station 8.18m, was across the abutment, approximately 40mm upstream of the transect representing the abutment centerline. This transect at 8.18m passes through the region of highest local velocity (0.48m/s) and highest boundary stress (5.0N/m^2) computed by the two-dimensional model. The high boundary stress can, in part, be attributed to a combination of high local flow velocity and high local roughness caused by the layer of gravel on the face of the abutment slope. The rapid decrease in boundary shear stress in the 8.1-m transect is caused by the rapid change in

roughness from the abutment slope to the adjacent model floodplain (sand grain roughness). Flow separation, as indicated in Figure 8-47, was computed to occur along a transect approximately 50mm upstream of the abutment centerline transect and approximately the same distance downstream of the maximum velocity and stress transect.

Although flow separation from the abutment tip was simulated in the approximate location anticipated (upstream of the abutment centerline), the increase in flow velocity in the vicinity of the abutment tip was not as high as expected.

8.4.5 Comparison of Flume PTV-Measured and Two-Dimensional Modelled Velocity Magnitude

Figures 8-49 and 8-50 show plots of both PTV and two-dimensional model velocity magnitude data. Again, keep in

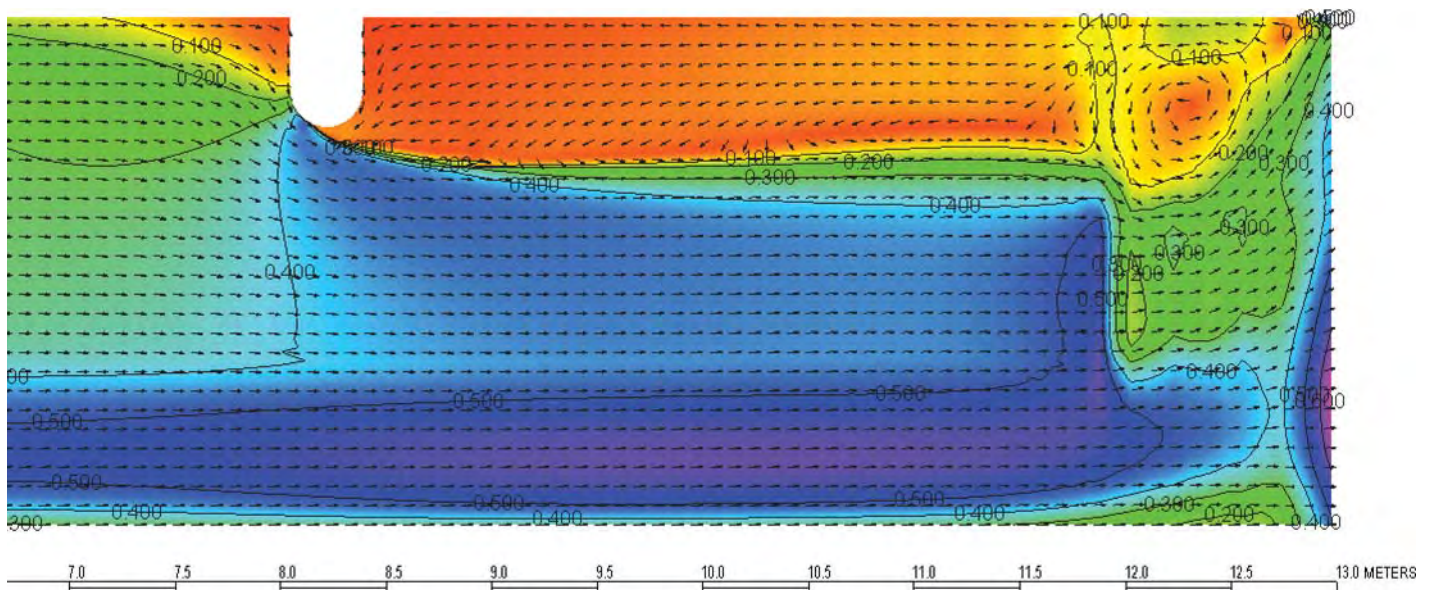


Figure 8-45. Numerically simulated velocity field in the region of the significant channel and floodplain contraction and expansion for 600-mm spill-through abutment (velocity contours in m/s).

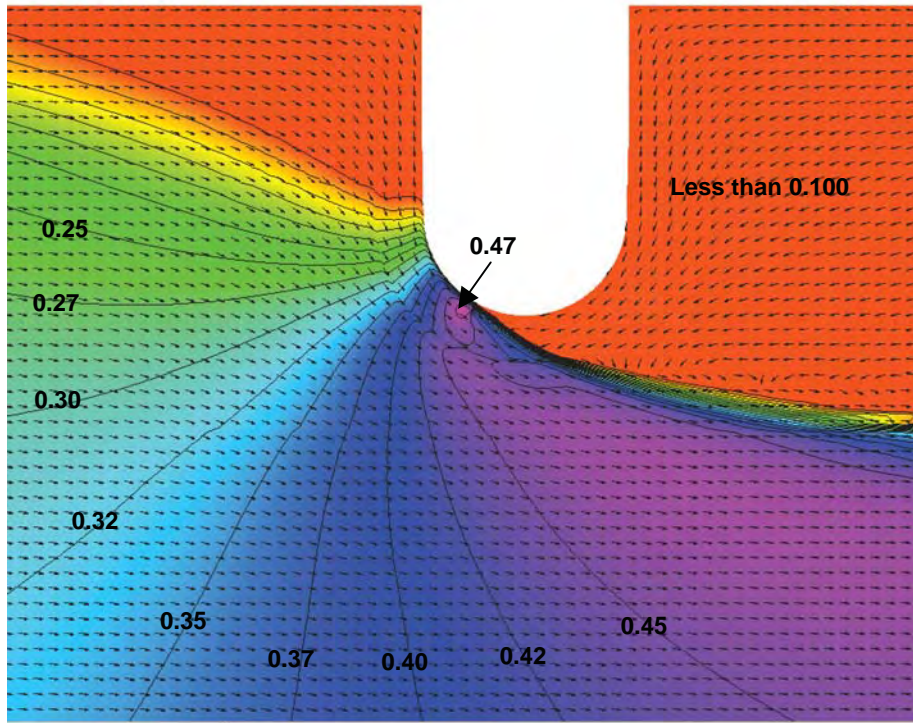


Figure 8-46. Numerically simulated velocity field near the abutment tip for 600-mm spill-through abutment (velocity contours in m/s).

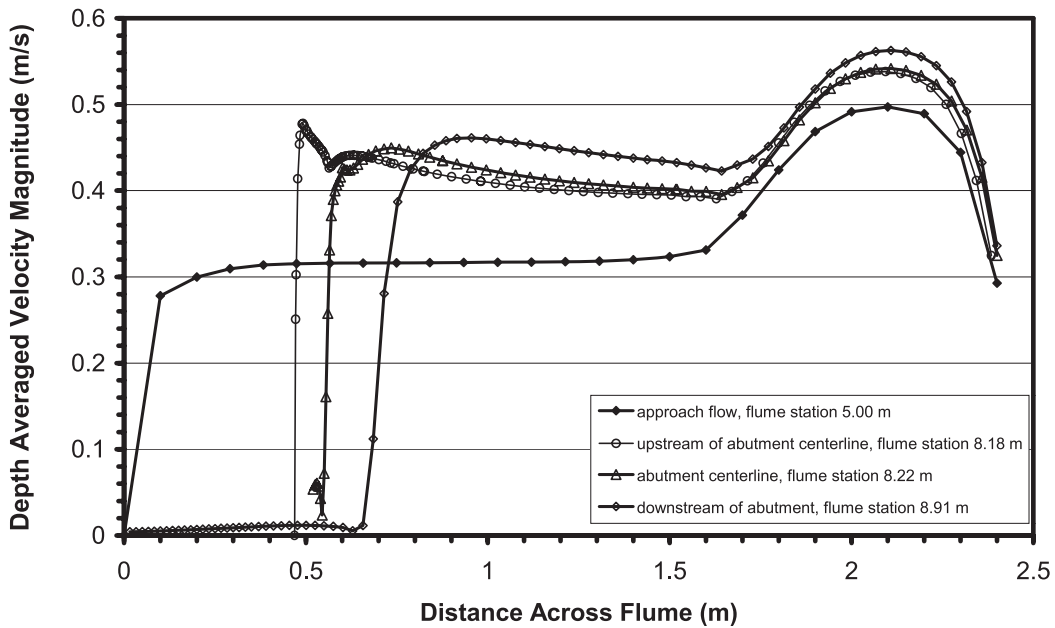


Figure 8-47. Depth-averaged velocity along transects across flume. The transects are located at flume stations 5.00 m, 8.18 m, 8.22 m, and 8.91 m, as indicated in Figure 8-42.

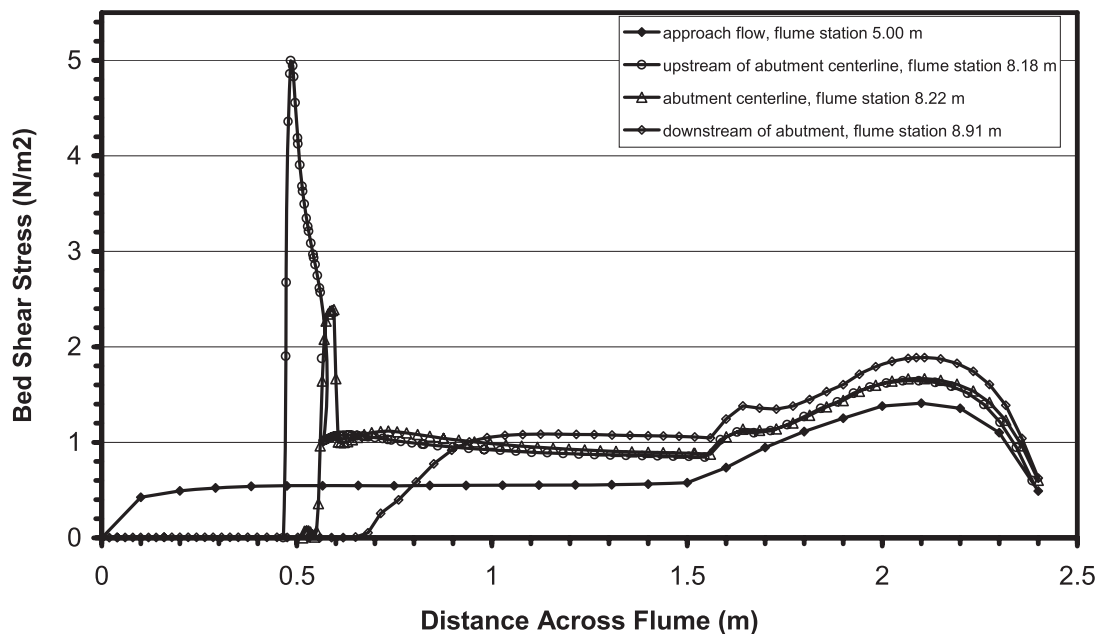
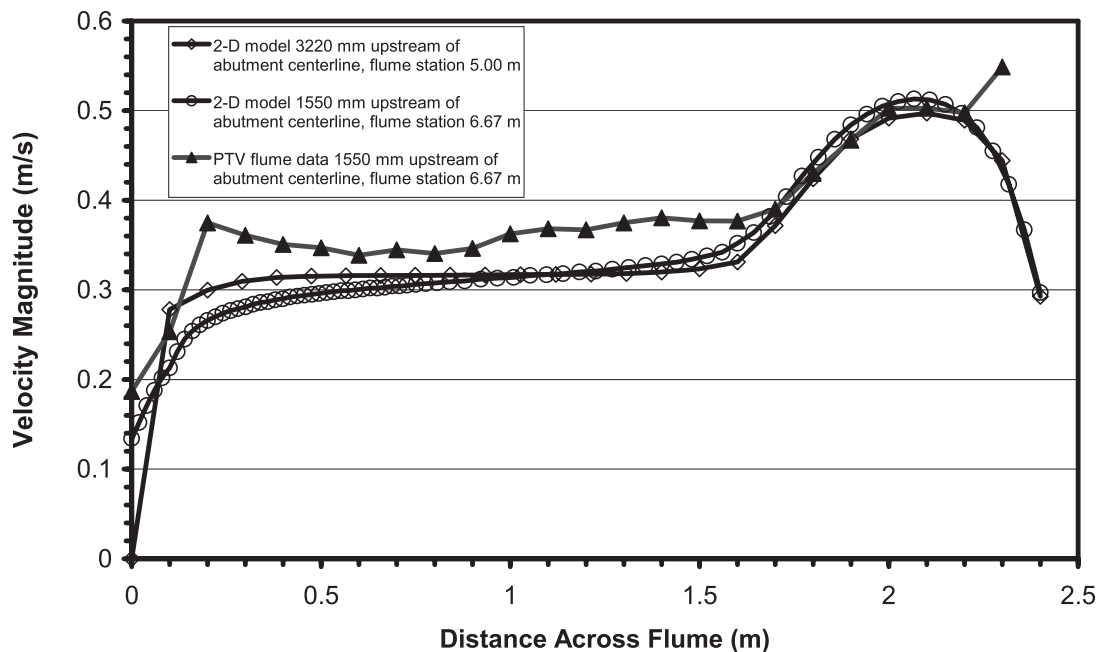
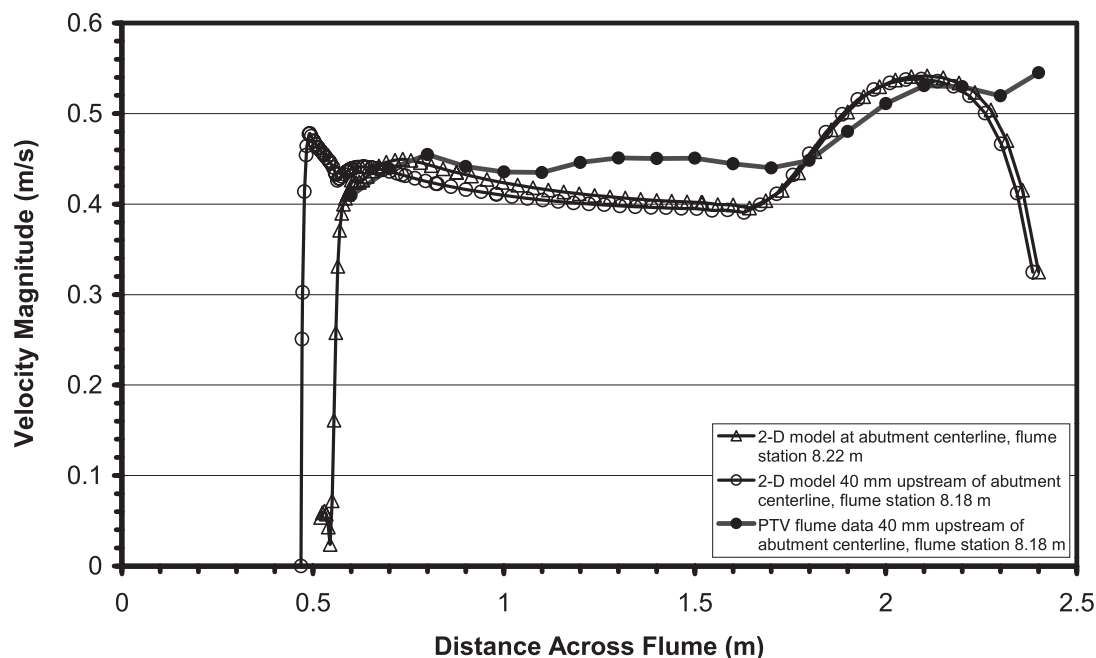


Figure 8-48. Bed shear stress along transects across flume. The transects are located at flume stations 5.00 m, 8.18 m, 8.22 m, and 8.19 m, as indicated in Figure 8-42.



Note: two-dimensional model velocities are depth-averaged, and PTV velocities are from the water surface only.

Figure 8-49. Comparison of PTV-measured velocity magnitude along transects upstream of the model abutment with that computed from the two-dimensional model simulation.



Note: two-dimensional model velocities are depth-averaged, and PTV velocities are from the water surface only.

Figure 8-50. Comparison of PTV-measured flow velocity magnitude along a transect 40 mm upstream of the model abutment centerline, with flow velocity magnitude obtained from the two-dimensional model simulation.

mind that the PTV data represent flow velocity at the water surface in the physical model, while two-dimensional model data represent computed depth-averaged flow velocity. Comparisons of local peak velocity and average velocity over the floodplain and main channel are provided below.

Local Peak Velocity

Because of the tendency for flow to accelerate around abutments, the local peak in flow velocity is used in some scour prediction methods or in the design of scour protection. Table 8-5

Table 8-5. Direct comparison of maximum velocity magnitude at abutment transects.

Source of Data	Transect Station (m)	Over Riprap Slope of Abutment (m/s)	Over Floodplain (m/s)	In Main Channel (m/s)
Two-Dimensional Model	8.22	0.43	0.45	0.54
Two-Dimensional Model	8.18	0.48	0.44	0.54
Flume PTV	8.18	0.41	0.45	0.53*
Two-Dimensional Model/PTV Difference	8.18	17%	2%	2%

*Velocity taken from center of channel rather than along flume wall, where a slightly higher velocity was reported.

shows that local peak velocity on the floodplain and in the main channel was predicted well by the two-dimensional model, although the location of the local maximum was not. In addition, the two-dimensional model computes the highest velocity along the transect over the riprap; PTV data, however, were not available at precisely the same location.

Table 8-6 compares the average velocities of the two models for the floodplain of the flat part of the channel. Regions

Table 8-6. Comparison of average velocity magnitude.

Source of Data	Transect Station (m)	Over Floodplain (m/s)	In Main Channel (m/s)
Two-Dimensional Model	5.00	0.31	0.46
Two-Dimensional Model	6.67	0.29	0.46
Flume PTV	6.67	0.36	0.46
Two-Dimensional Model	8.18	0.39	0.50
Flume PTV	8.18	0.44	0.52
Two-Dimensional Model	8.22	0.34	0.50
Two-Dimensional Model/PTV Difference	6.67	20%	0%
Two-Dimensional Model/PTV Difference	8.18	11%	4%

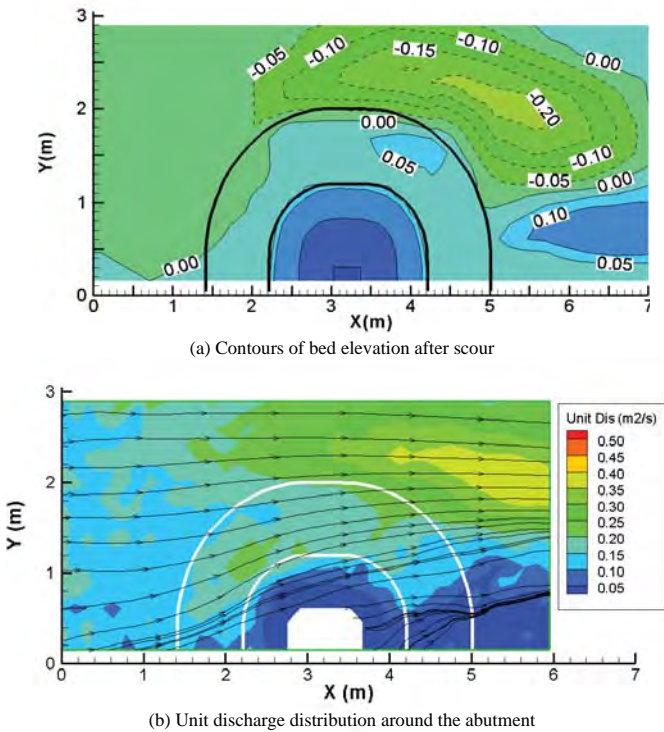


Figure 8-51. Velocity observations obtained from the flume PTV measurements (apron length = 0.80 m).

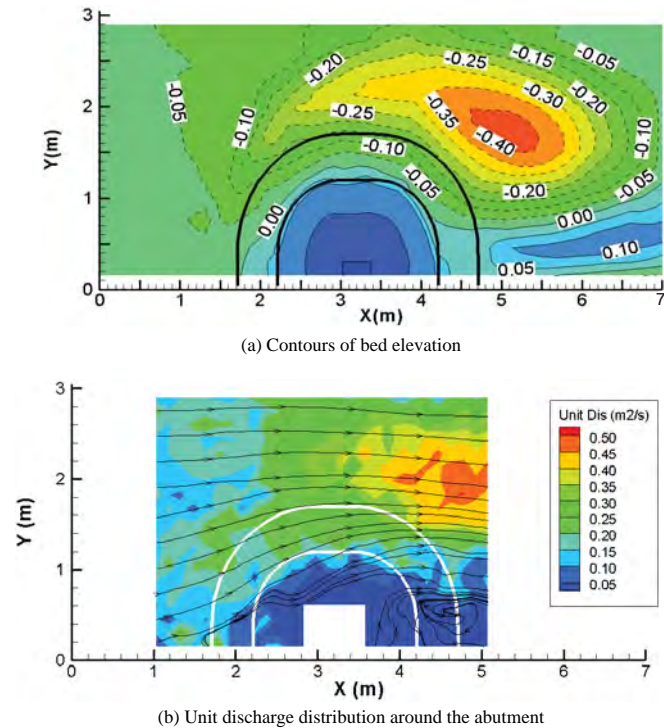


Figure 8-52. Velocity observations computed from FESWMS (apron length = 0.50 m).

of flow over the abutment slope and over the sloping channel bank were not included in the averages for the floodplain and channel, respectively. The average velocity in the channel is well predicted by the two-dimensional model.

Flow velocity observations obtained from the flume PTV measurements and those computed by FESWMS are plotted in Figures 8-51 and 8-52, respectively. As shown in Figure 8-51, one unusual velocity observation in the PTV measurements causes the PTV point data to deviate from the two-dimensional model results. The average velocity for the PTV floodplain data is significantly higher than that of the two-dimensional model for transects 8.18 and 8.67. The velocity magnitudes were plotted along transects perpendicular to the flume walls in the flow upstream of the modeled abutment and near the abutment centerline. The transect representing the upstream extent of PTV measurements (approximately 1,550mm upstream of the abutment centerline transect) is compared with two-dimensional, depth-averaged velocity magnitudes at the same location and at a second location 3,220mm upstream of the abutment centerline. The PTV-measured velocity in the floodplain (from 0m to 1.6m along the transect) is higher than that computed by FESWMS.

Overall, good agreement is demonstrated between the two-dimensional model results and the PTV measurements.

8.5 Large-Scale Tests of Riprap Apron Performance

8.5.1 Introduction

Described here are the findings from relatively large-scale flume experiments conducted to validate the main recommendations from the extensive parametric flume experiments, which are described in Section 8.3. In particular, these tests had two objectives:

- To ascertain the minimum width (W_0) of riprap apron placed around a spill-through abutment that has a much larger size than, though nominally similar flow geometry to, the abutments described in Section 8.1.
- To obtain additional detailed information on apron performance.

The large-scale tests were run for clear-water scour conditions that replicated a spill-through abutment located on a floodplain and at some distance back from the main channel of a river. However, the large-scale tests were done at a geometric size approximately four times larger than the abutment size used in Section 8.1; here, the standard size is taken to be the top (i.e., road) and base widths of abutment, as well as abutment height. Flow depth was slightly more than five times the flow depth; a larger depth factor was dictated by constraints in flume operation. The extent of the riprap apron

and the stone size conform in scale to the values mentioned in Section 8.1. Also, the clear-water approach-flow condition matched those for the experiments described in Section 8.1. Flume tests on abutment scour at this scale have not been undertaken heretofore. Morales (2006) fully documents the flume tests.

Similitude between laboratory experiments and field scale experiments was satisfied by the use of the aforementioned u_w/u_{*c} ratio, of which a value of just below 1.0 represents a condition called “clear-water scour.” This condition is extreme for scouring because the velocity is as high as possible without the movement of the channel bed, which causes infilling of the sediment hole.

8.5.2 Tests

The test layout consists of a subcase of the test program described in Section 8.1. The layout is not an exact up-scaling of an abutment and floodplain layout in Section 8.1. The layout was designed with the intent of having maximum length and height of abutment for the given constraints of flume width and pump capacity.

Test Layout

The experiments were performed using a large flume at a facility in IIHR, a unit of the University of Iowa’s College of



Figure 8-53. Environmental flow facility.

Engineering (Figure 8-53). The flume, shown in Figure 8-54, was fitted with a simulated portion of floodplain. The flume consisted of a rectangular open channel 3.05 m (10 ft) wide, 19.81 m (65 ft) long, and 2.29 m (7.5 ft) deep. The test abutment was placed on a sediment recess in the simulated floodplain. The recess was 0.9 m (3 ft) deep and 7.00 m (23 ft) long. The approach to the test section was roughened with blocks so as to trip the flow boundary layer and thereby create a fully turbulent velocity profile for the flow approach to the

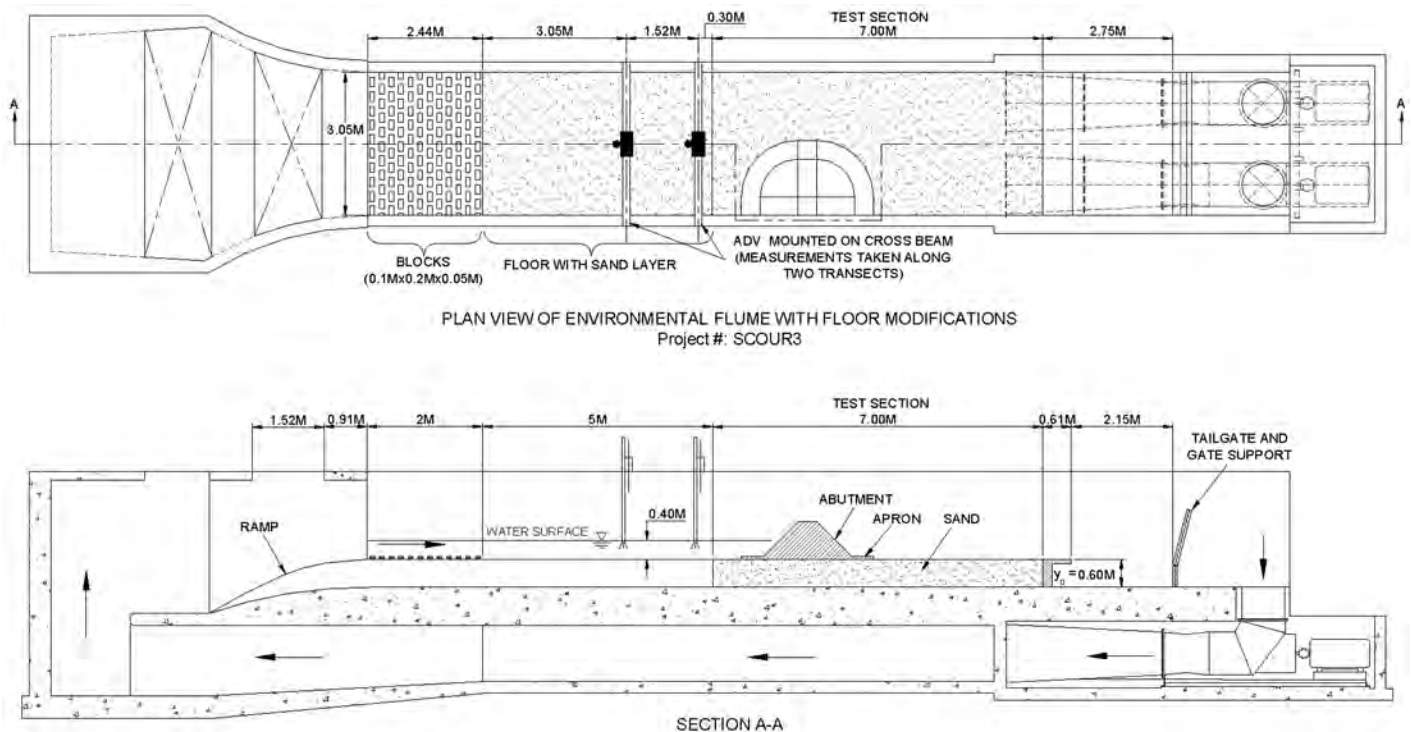


Figure 8-54. Layout of the large-scale experiment in the flume.

abutment. Downstream of the roughened entry was a 4.87-m (16-ft) long planar surface that was of sand-grain roughness; the grain diameter was 1.05 mm. At the downstream end of the simulated floodplain, an adjustable tailgate was used to control water surface elevations preceded by a sediment trap to prevent the sand from going into the pump.

The flow was provided by two 36-in. diameter propeller pumps driven by variable-speed motors operated to produce a regular velocity distribution of the flow upon entering the test area with the desired average velocity. The discharge range attainable with these pumps is 0.60 to 3.54 m³/s (22 to 125 ft³/s). A flow depth of 0.53 m (1.76 ft) was selected because it gave the prescribed clear-water condition of approach flow, yet suitably exceeded the minimum discharge limit for the flume's pumps; a flow depth of 0.40 m would have required too low a discharge for the pumps to deliver. Flow depth through the test section was controlled by means of a tail gate at the end of the test section.

A bed of uniform quartz sand was formed in the recess. The sand had a median diameter of 1.05 mm and a geomet-

ric standard deviation of 1.3. The estimated value of the critical shear velocity for the sand is $u_{*c} = 0.024$ m/s.

The abutment model was four times the top and base widths, as well as height, of the spill-through abutment used in Section 8.1. It was constructed of wood and sheet metal, painted with a layer of epoxy paint, and placed on the sand recess; it was held in position by internal weighting and vertical struts. The abutment's location in the flume is shown in Figure 8-55, and its form and main dimensions are shown in Figure 8-56; the main dimensions are a top width of 0.40 m, a bottom width of 2.00 m, a height of 0.80 m, and a length of 1.20 m. The abutment's length was chosen so that the abutment would not contract flow entirely between the abutment and the opposite wall of the flume. The base of the model abutment was surrounded by a band of sheet metal, which in effect simulated a sheet pile skirt. Figure 8-57 shows the skirt. This configuration differed from the abutment form used for the experiments conducted at Auckland University insofar that the latter used an abutment form whose slope continued into the bed.

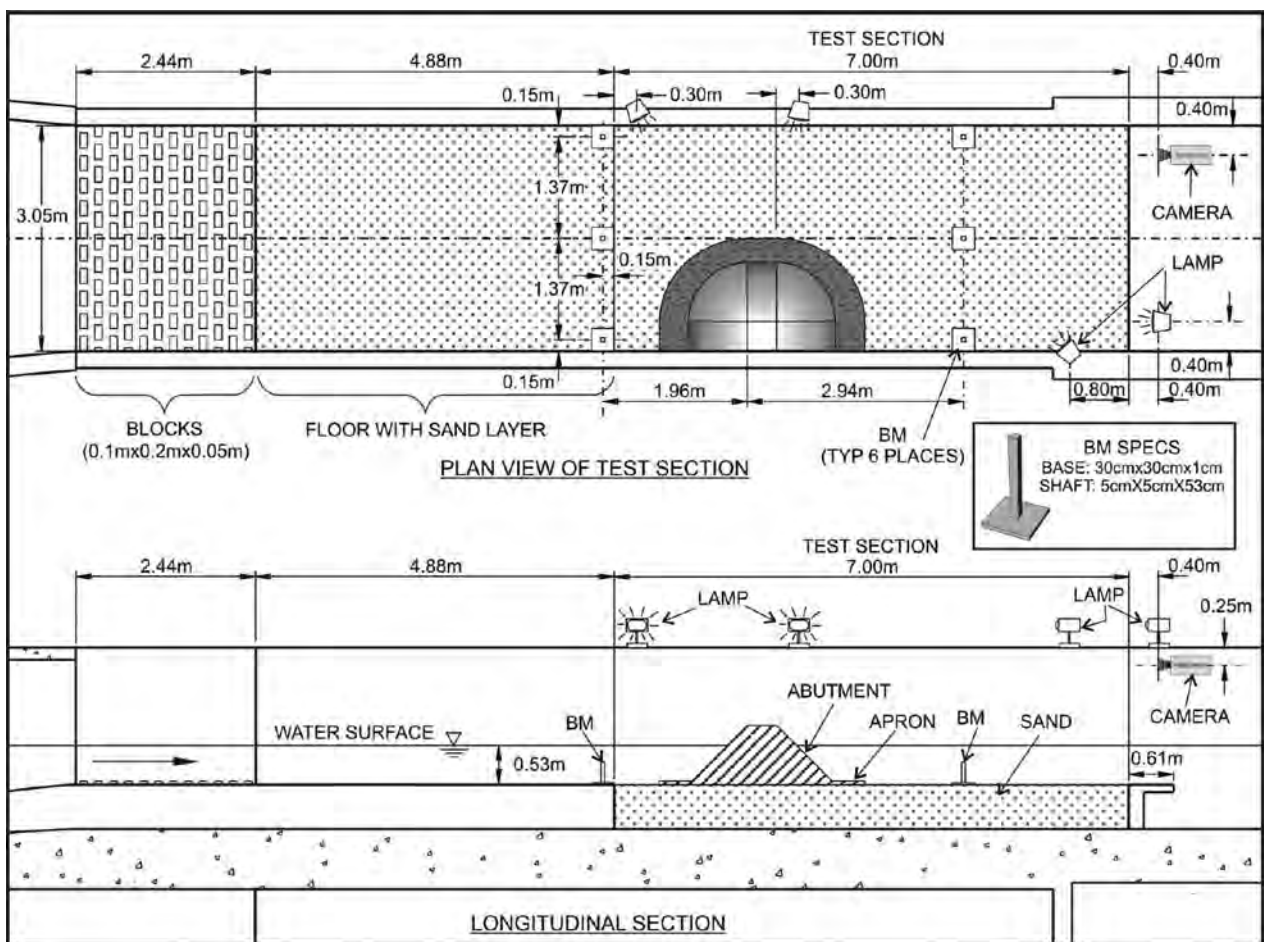


Figure 8-55. Layout of the model abutment in the flume, including the lighting and benchmark system used for the LSPIV measurements of water-surface velocities.

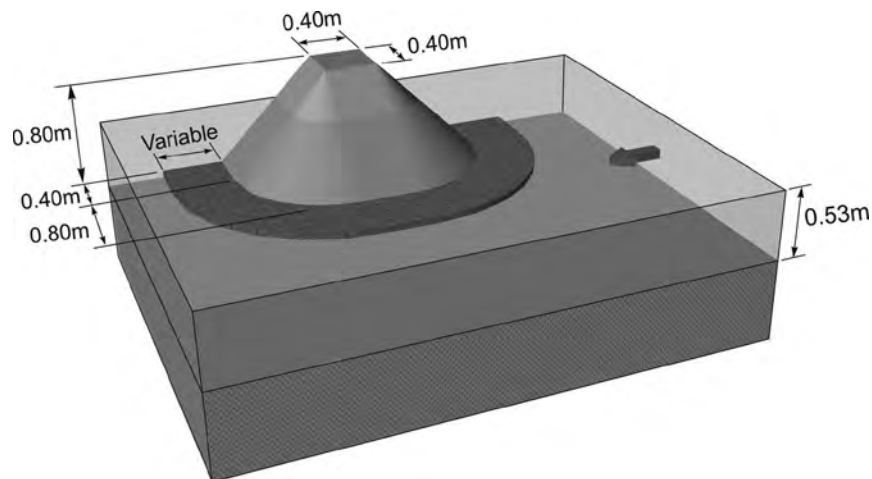


Figure 8-56. Dimensions of the model abutment and apron.

An initial experiment was conducted with an abutment formed of loose sand embankment placed around a standard stub abutment structure, as shown in Figure 8-58. This experiment sought to illustrate scour development around an unprotected abutment formed of an erodible earthfill embankment. This abutment form was wider than the fixed abutment because of the sand's angle of repose used for the embankment.

The apron of riprap was placed as a circumferential band around the abutment. The apron was formed of two stone layers, giving an average thickness of about 1.5 times the median diameter of stone, and was placed on the simulated floodplain surface. The riprap stone consisted of uniform, crushed rock of median diameter estimated by sieve analysis to be 75 mm and a geometric standard deviation of about 1.4.



(a) Before scour



Figure 8-57. Model abutment with skirt.



(b) After scour

Figure 8-58. Scour at abutment without apron.

The estimated critical shear velocity for this stone u_{*c} was calculated to be 0.26 m/s. Apron width was the principal variable in the experiments, and it was adjusted from 0 to 1.0 m; in terms of flow depth, Y , apron width W varied from 0 to about $2Y$; this upper limit is the design width recommended by Lagasse et al. (1997). The width restriction of the flume limited the upper value of W . Figure 8-58a shows the prerun set-up of riprap around a semi-circular spill-through abutment fitted with a 0.50-m wide riprap apron with a leveled sediment bed (simulating a floodplain). Figure 8-58b shows the abutment after the experiment.

In terms of the parameters used in Section 8.1, the present abutment's details are $V/u_{*c} = 0.90$, $D_{\text{riprap}}/d_{50} \approx 75$, $B_f/y_f = 5.75$, $L/y_f = 2.23$, $B_f/L = 2.5$, and $W/L = 0.33$ to 0.83. The values of B_f/y_f , L/y_f , and B_f/L are less than those discussed in Section 8.1.

Flow Conditions

For the flow depth set at 0.53 m, and with $u^*/u_{*c} = 0.90$, the average velocity of flow V was 0.48 m/s. The values of flow velocity in the approach to the abutment were determined by means of acoustic Doppler velocimetry (ADV), and velocity profiles over the flow depth were confirmed to conform to the general form associated with flow in a fully developed turbulent boundary layer.

Measurements

Large-scale particle image velocimetry (LSPIV) was used to visualize and document the free surface of the flow field around the abutment. Figure 8-55 indicates the system of lighting and benchmarks used in obtaining the LSPIV data.

The flow field was documented at the start and end of each test. The flow field measurements were analyzed to obtain estimated distributions of depth-averaged velocity, unit discharge, and bed-shear stress around the abutment and its apron. Depth-averaged values of velocity are estimated using the velocity profiles associated with fully turbulent flow in the channel. The LSPIV technique and the associated analyses are documented by Morales (2006).

The velocity measurements obtained by way of LSPIV and ADV were also augmented by numerical simulations of the flow field around the abutment. These simulations, which were carried out using the depth-averaged, two-dimensional simulation code FESWMS-2DH, are also documented by Morales (2006). Only selected findings from the simulations are presented herein.

The bed elevations at the end of the experiment were taken using a Total Station TOPCON® GTS 226 with resolution up to ± 0.0003 m. Readings were taken at regular intervals. Downstream of the scour hole, measurements were taken at 0.25-m intervals. Around the abutment and in the scour hole, measurements were taken at 0.10-m intervals. Because there was no erosion of the bed near the abutment, the bed elevations there were measured at 0.45-m intervals.

Test Program

Table 8-7 provides the test program, as well as the maximum depths of scour measured for each test. Note that, because the abutment was placed on top of the sand bed and did not extend into the sand bed, as scour developed the abutment was undermined. Had the abutment been built of an earthfill embankment around an abutment structure, the embankment would have failed by way of slope instability.

Table 8-7. Test program and maximum scour depth measured in the experiments.

Test Number	Abutment Length L (m)	Channel Half-Width B_f (m)	Flow Depth y_f (m)	Apron Width W (m)	Maximum Scour Depth d_{smax} (m)	Scour Depth at Axis d_c (m)
1	1.20	3.05	0.53	0.00	0.315	0.300
2	1.20	3.05	0.53	0.15	0.355	0.330
3	1.20	3.05	0.53	0.20	0.347	0.312
4	1.20	3.05	0.53	0.25	0.200	0.170
5	1.20	3.05	0.53	0.25	0.385	0.307
6	1.20	3.05	0.53	0.30	0.397	0.305
7	1.20	3.05	0.53	0.40	0.457	0.352
8	1.20	3.05	0.53	0.50	0.443	0.306
9	1.20	3.05	0.53	0.60	0.451	0.257
10	1.20	3.05	0.53	0.70	0.337	0.254
11	1.20	3.05	0.53	0.70	0.335	0.193
12	1.20	3.05	0.53	0.80	0.228	0.155
13	1.20	3.05	0.53	1.00	0.281	0.183

W = average width of apron. Actual width varied $\pm d_{50}/2$, where d_{50} = median diameter of riprap stone.

8.5.3 Results

The results presented herein include data on the maximum depth and location of the consequent region of scour, along with information illustrating the variations in flow field corresponding to the scour region. As clear-water scour asymptotically approached an equilibrium condition over time, each experiment was run for about 72 to 80 hours until negligible change was observed in the scour hole dimensions.

Scour Depth and Location

The location and depth of scour at the model abutment depend on the resistance of the abutment form to erosion and on the placement of the abutment within (or on) the floodplain base. The scour tests with the abutment surrounded by a skirt, and with an abutment of erodible embankment, produced markedly different scour forms than those that appeared when the abutment was surrounded by an apron.

Without the protection of an apron of riprap stone, the scour region developed immediately around the edge of the fixed abutment and exposed the simulated sheet pile skirt underneath the abutment toe. Figure 8-58 shows this effect as observed in the flume experiments. Two experiments were carried out on the abutment without an apron. In both experiments, the deepest scour was located approximately below the midpoint of the upstream round corner. The subsequent discussion of the flow field around the abutment shows that this particular region in the channel is subject to the highest level of turbulence and shear stress. Figure 8-58a shows the initial abutment condition, and Figure 8-58b shows the exact location of the deepest scour. The measured



Figure 8-59. *View of the model abutment and apron before test ($W = 0.50$ m).*

maximum scour depth was $0.315 \text{ m} \pm 5 \text{ mm}$ in both cases. This scour depth was proportionately less than that predicted using FESWMS.

Also observed in these experiments was the presence of small dunes inside the scour region, especially on the exit slope of the scour hole. These dunes, having a maximum height of about 15 mm, increase the resistance to flow through the scour region. In effect, the flat dunes add form resistance to flow. By so doing, the dunes in the scour area dissipate flow energy and act to reduce scour depth.

The abutment formed of the unprotected embankment eroded completely, leaving the stub abutment structure fully exposed. Scour then developed around the stub abutment. Though the abutment was completely washed out, the actual scour depth was comparatively modest.

By way of illustration of one test with an apron, Figure 8-59 shows the abutment and a 0.50-m apron before a test, and Figures 8-60 and 8-61 show the apron after the test. The apron stayed intact around the upstream perimeter of the abutment, but the apron frayed around the end of the abutment. As expected from the findings described earlier in this



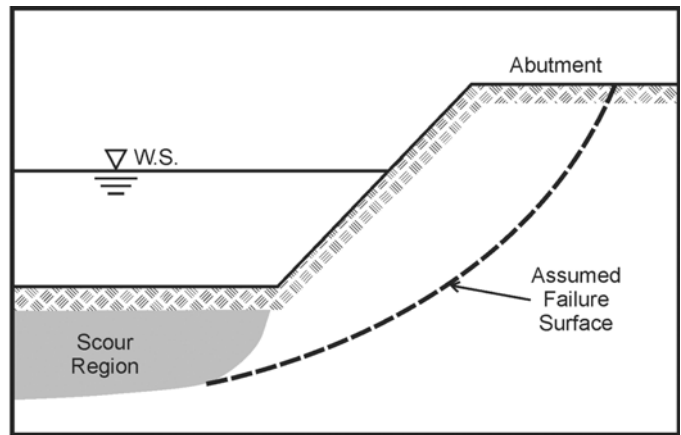
Figure 8-60. *View of apron launched into scour region downstream of abutment after the test ($W = 0.50$ m).*



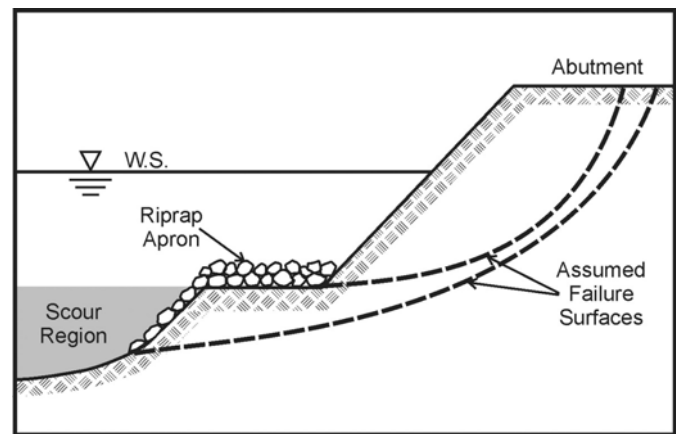
Figure 8-61. View of upstream condition of apron around abutment after the test ($W = 0.50$ m).

chapter (and earlier chapters), the apron did not prevent scour development, but shifted its position away from the abutment. The apron, though, did inhibit scour immediately at the abutment. Riprap stone forming the apron slid (or launched) into the scour region. Subsequently, in this section, Figure 8-61 presents the bed bathymetry of the scour region.

It is important to mention the geotechnical stabilizing influence of an apron. In viewing Figures 8-58 through 8-61, along with Figure 8-62, it is evident that, by forcing the scour region to shift away from the abutment, the apron not only impedes scour at the toe of the abutment but also reduces the effective slope of the embankment face. This effect, indicated in Figure 8-62, increases the geotechnical slope stability of the embankment face. Seen in terms of a slope-stability failure surface, the apron serves to lengthen the arc of the failure surface (thereby adding stability to the embankment slope). Additionally, the counterweight effect of the apron at the toe of the embankment slope has a stabilizing effect.



(a) No apron



(b) Apron adds stability by lengthening slip circle or counter-ballasting slip circle in embankment earthfill

Figure 8-62. Influence of apron on slope stability of abutment embankment.

Figure 8-63 summarizes the overall scour trends obtained from the tests by presenting a matrix of views and bathymetry measurements of the scour regions that occurred as the apron width was widened. The views and bathymetry data assembled in Figure 8-63 show that increasing apron width from $0.76y$ to about $1.00y$ barely alters scour depth or location. As apron width increases from about $1.00y$ to $2.00y$, scour depth drops significantly, although the location of maximum depth changes only slightly, as evident in Table 8-7. When $W \approx 2.00y$, the maximum depth of scour corresponds approximately to the thickness of the apron, which is about 0.15 m. In effect, for the widest apron tested, scour occurs mainly because of turbulence shed by flow passing over the edge of the apron and impinging on the bed downstream. The eventual scour form produced by a relatively wide apron is akin to scour immediately downstream of a submerged apron in the absence of the abutment.

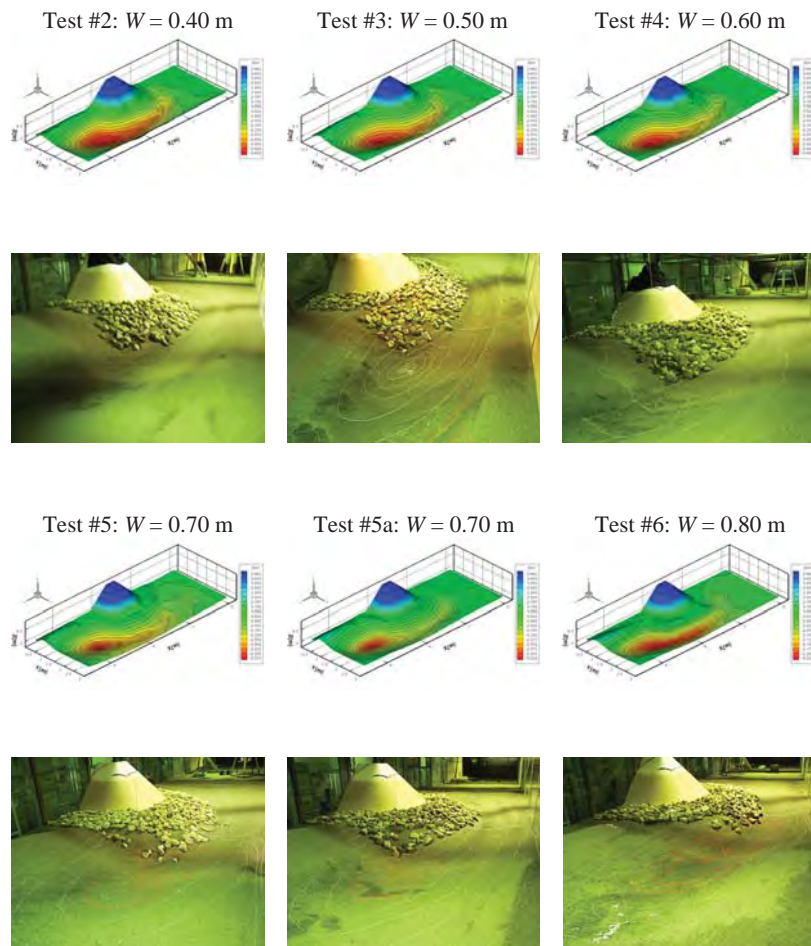


Figure 8-63. Assembled views of the scoured region for the variable apron widths.

Figure 8-64 plots maximum scour depth, d_{smax} , versus apron width, W . This figure indicates three regions of scour depth trends:

- Scour attributable to abutment form and erodibility,
- Scour development attributable to the combined structural form of abutment and apron, and
- Scour attributable to flow over apron.

The first region is likely to be highly variable in depth value, because scour depth and location depend on the abutment foundation condition and erodibility of the abutment embankment. The second region shows a reduction in scour depth as apron width increases, until apron width is sufficiently large that scour around the apron's trailing edge is not substantially influenced by abutment presence. The third region shows that flow over the end of the apron causes some scour of the bed.

For the abutment with apron, the location of d_{smax} was slightly downstream of the abutment, as evident in Figure 8-64.

Also indicated in Figure 8-64 is the scour depth immediately in front of the abutment, d_{SO} , along the abutment's centerline axis. The figure also indicates the average thickness of the apron, about 0.12 m. The initial placement of an apron (of width $0.76y$) around the abutment substantially reduced d_{smax} , but then slight increases of apron width only slightly reduced d_{smax} further. As W increases so that W/y approaches and exceeds about 2, however, d_{smax} decreased to a minimum approximately equivalent to the nominal thickness of the apron. Values of d_{SO} decreased monotonically for the range of widths considered as apron width increased.

Values of the resulting minimum extent of apron, W_{min} , at the end of each test versus initial apron width, W_0 , are plotted in Figure 8-65. The trend here indicates convergence of W_0 and W_{min} as W_0 increases. The tests suggest that riprap stone at the edge of the apron may usually fray from the apron, such that $W_{min} \approx W_0$ only when W_0 becomes very large. Figure 8-66 shows views of the minimum extent of riprap after each test for values of $W = 0.4, 0.5, 0.6, 0.7, 0.8,$ and 1.0 m.

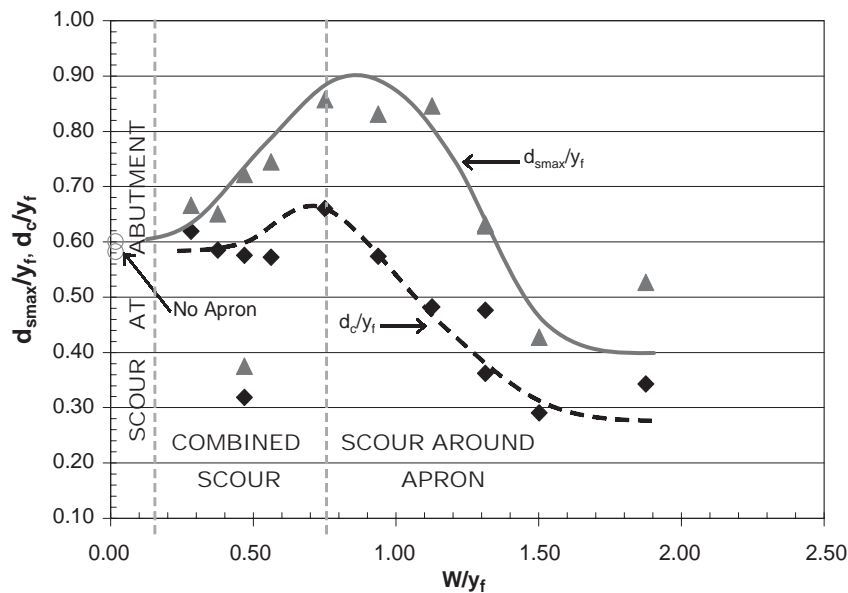


Figure 8-64. Maximum scour depth, d_{smax} versus apron width, W .

Flow Field Over Apron

The trends for scour depth and location are explainable in terms of the flow field around the abutment and over the apron, as well as in terms of apron extent. In this regard, the flow field insights provided by the LSPIV measurements, along with the findings from the two-dimensional numerical simulation, usefully show the following trends in flow field as apron width increases:

- The median mean value of depth-averaged velocity of the approach flow to the abutment, with the 0.40-m wide apron,

is 0.45 m/s. As the flow passes around the abutment, the flow contracts, producing an overall depth-averaged velocity of 0.55 m/s at the plane extending through the center of the abutment. For all the tests, the maximum value of depth-averaged velocity around the abutment was 0.60 m/s before scour had developed. This velocity occurred a short distance downstream of the abutment and was slightly beyond the downstream edge of the apron, thereby more or less coinciding with the area of maximum scour depth.

- Slight reductions in maximum velocity and unit discharge over the scour region were observed for increasing apron

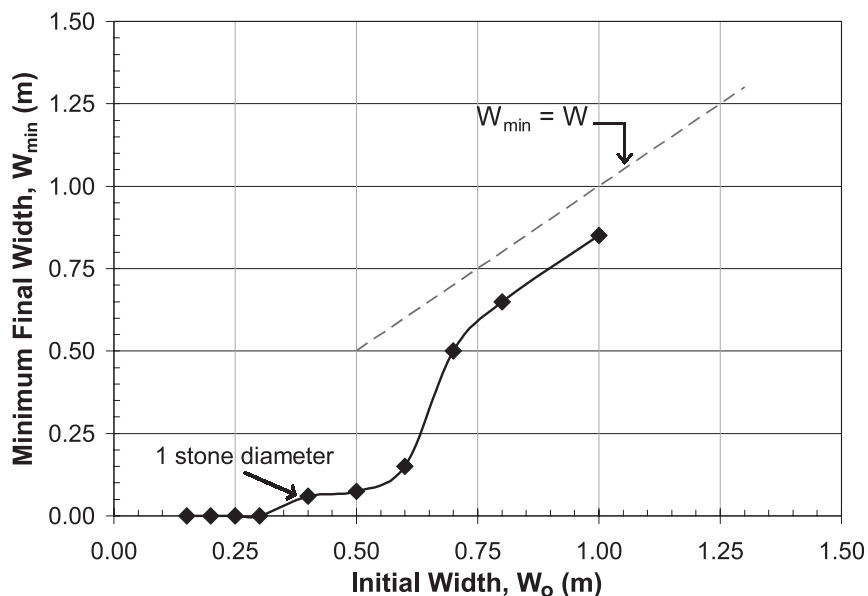


Figure 8-65. Minimum final width of apron, W_{min} , versus initial width, W_0 , for test conditions.



(a) $W = 0.4$ m



(b) $W = 0.5$ m



(c) $W = 0.6$ m



(d) $W = 0.7$ m



(e) $W = 0.8$ m



(f) $W = 1.0$ m

Figure 8-66. Views of the minimum extent of riprap after each test.

lengths. The scour deepening of the bed drew more flow to the scour region, thereby locally increasing unit discharge of water in the region of scour. The lesser scour depths for the wider aprons drew less flow to the scour region. Figures 8-51 and 8-52 show the bathymetry contours and distributions of unit discharge for apron widths of 0.50 to 0.80 m.

- Because bed shear stress and flow velocity are related ($\tau = \rho u^2$), it is possible to estimate the maximum bed shear stress near the location of the maximum scour depth. For the approach flow, the bed shear stress is on average 0.34 N/m^2 ; the shear rises at the section through the center of the abutment to attain a value of 0.43 N/m^2 . The maximum bed shear downstream of the abutment is 0.62 N/m^2 .
- The numerical simulations show that increased apron width mildly decreases the bed shear stress near the abutment, though increasing it away from the abutment. This influence of an apron is attributable to the influence of apron roughness in reducing flow velocities near the abutment.

8.5.4. Comparison with University of Auckland Results

The overall scour forms observed in the large-scale tests concurred with those found in the flume tests described in Section 8.1, especially those described in Figures 8-7, 8-10, and 8-11. Relative to abutment position, the locations of deepest scour coincide reasonably well. Scour depths, though, were proportionately less for the large-scale tests.

The difference in location of maximum scour for the present test with the large abutment without apron protection is due to the different form of the abutment below the bed level; the model abutment at Auckland continued its side slope below the bed level. The depth of scour was smaller, relative to flow depth, at the unprotected abutment in the present tests than at the test abutments at Auckland. The lesser scour depth was due to the larger scale of the model. Ettema et al. (2006) explain how scale effects that are incurred with simulating the vorticity of eddies generated by flow around a cylinder may produce an amplified scour depth in a smaller model. The vorticity of eddies is smaller in the larger model. Additionally, as mentioned above, the presence of dunes inside the scour region formed on the exit slope of the present large-scale abutment increased the resistance to flow through the scour region and thereby reduced scour depth.

The scour depth trend obtained for the large-scale abutment, which replicates a short abutment on a comparatively wide floodplain, is similar to the trend obtained in the small-scale tests when $L/B_f = 0.2$. Scour depth decreases in two stages as apron width is increased. For small values of L/B_f , the

presence of the main channel does not affect the abutment flow field and scour development. The lesser depths for the large abutment can be attributed to two factors:

- The value of L/y_f for the large abutment is 2.23, which is less than the values used for the small-scale abutments ($L/y_f = 4$ to 8). The values of L/B_f , however, are in the same range; $L/B_f = 0.39$ for the large-scale abutment and $L/B_f = 0.20$ to 0.50 for the small-scale abutment. A smaller value of L/y_f , for an equivalent value of L/B_f , means that less floodplain flow must pass around the abutment. Accordingly, flow velocities at the abutment are proportionately less; therefore, less scour depths will result.
- Magnitudes of flow vorticity generated by flow around the abutment and over the apron are proportionately larger in the small-scale tests than in the large-scale tests. As both series of tests were conducted with the parameter V/V_c as the principal criterion for dynamic similitude, and both test series involved beds of coarse sand, tests at the smaller scale have the greater exaggeration of flow vorticity and therefore experience greater entrainment and movement of bed sediment.

The design recommendation can be used to estimate the minimum initial width of apron, W_0 , such that scour would not fully launch the apron and thereby begin to undermine the embankment of the abutment used in the present, large-scale tests. From Equation 8-16, the scour depth estimated for the present test is 0.74 m; from $y_f = 0.53 \text{ m}$, $L = 1.20 \text{ m}$, and $V/V_c = 0.90$. Equation 8-16 is repeated here as

$$\frac{W_0}{y_f} = C_3 \left(\frac{d_{sf}}{y_f} \right)^\lambda \quad (8-20)$$

Where:

$$C_3 = 0.9 \text{ and} \\ \lambda = 1.35.$$

In accordance with this equation, the predicted value of W_0 is 0.42 m. This value compares favorably with the test result, in which W_0 is 0.4 m, as indicated in Figures 8-64 and 8-65. In this test, the minimum width of apron W_{min} was about one riprap stone width. The large-scale test results also agree with the design recommendation that, for relatively short abutments at least, an apron width of $2y_f$ practically eliminates substantial scour in the vicinity of an abutment. However, the tests show that some modest extent of scour will occur around the edge of even a wide apron.

Given the differences in geometric scale and layout of abutment for the large-scale test, this agreement is a substantial validation of the design relation developed from the small-scale tests presented in Section 8.1.

CHAPTER 9

Lab Results IV: Flow Modification

This chapter reports laboratory results of three flow modification countermeasures: parallel walls, spur dikes, and abutment collars. Section 9.1 describes the laboratory equipment and procedure, including a description of the flume, the abutment model, the velocity ration, the sediment characteristics, instrumentation, and the experimental procedure employed. Section 9.2 describes the baseline experiment results—that is, the scour depth at the bridge abutment without any countermeasures. Sections 9.3, 9.4, and 9.5 discuss the results of the tests using parallel walls, spur dikes, and abutment collars, respectively. Section 9.6 summarizes the findings.

9.1 Experimental Apparatus and Procedure

9.1.1 Flume

All of the experiments were conducted in a flume located in the hydraulic laboratory at the USDA-ARS National Sedimentation Laboratory in, Oxford, Mississippi. The flume channel was 30 m long, 1.2 m wide, and 0.6 m deep. It was supported in the center at two points and on the ends by four screw jacks that allowed the channel slope to be adjusted. The wing-wall abutment model was located over a 3-m long, 1.2-m wide, and 1.2-m deep recessed section of the flume 22 m downstream of the inlet tank. The test section was 22 m downstream from the inlet, and the channel was 1.2 m wide, thereby making the test section a distance downstream from the inlet of 18 times the channel width. This distance was enough to ensure fully developed flow at the test section. Uniform flow was established for each experimental run by the adjustment of the flume slopes and pump speed until the water surface line, the bed surface, and the flume slope were parallel to one another along a 12-m transect in the approach channel. The channel plan and section views of the experiments are illustrated in Figure 9-1. Figure 9-2 shows all of the elements in the flume, such as the abutment model, flood-

plain, main channel, instrument carriage, and flume inlet and outlet. It also shows scour by the abutment. All experiments used a compound channel, consisting of a 320-mm wide, asymmetric floodplain next to a main channel with a bank slope of 1:1. The elevation difference between the top of the floodplain and the main channel bed was 80 mm. The rigid floodplain was made of a galvanized steel plate and glued down onto the flume bottom. A layer of sand was glued onto the floodplain to add roughness. In addition, since most floodplains are heavily vegetated and therefore have high roughness, gravel with a mean diameter of 4.5 cm was placed in a staggered arrangement on the floodplain in later runs of baseline cases. Figure 9-3 shows this arrangement. By measuring the velocity profiles both in the main channel and on the floodplain, and by using Manning's equation, the roughness of the floodplain and the main channel bed under clear-water conditions (a velocity ratio of 0.9) were found to be 0.030 and 0.014, respectively.

9.1.2 Abutment Model

The wing-wall abutment model was made of sheet steel. The dimensions of the model are shown in Figure 9-4. The abutment terminated on the bank slope of the main channel, as illustrated in Figure 9-1, which corresponds to the Type III abutment of Melville (1992). The distance between the top of the floodplain and the top of the abutment was 60 mm. The abutment length was about one-third of the channel width and was observed not to alter the flow enough to interact with the far flume wall.

9.1.3 Sediment Characteristics

The bed material sediment used in the main channel had a diameter of 0.8 mm. The standard deviation of the sediment diameter, $[\sigma_g = (D_{84}/D_{16})^{1/2}]$, was equal to 1.37. According to a modified version of the Shields diagram (Miller et al., 1977),

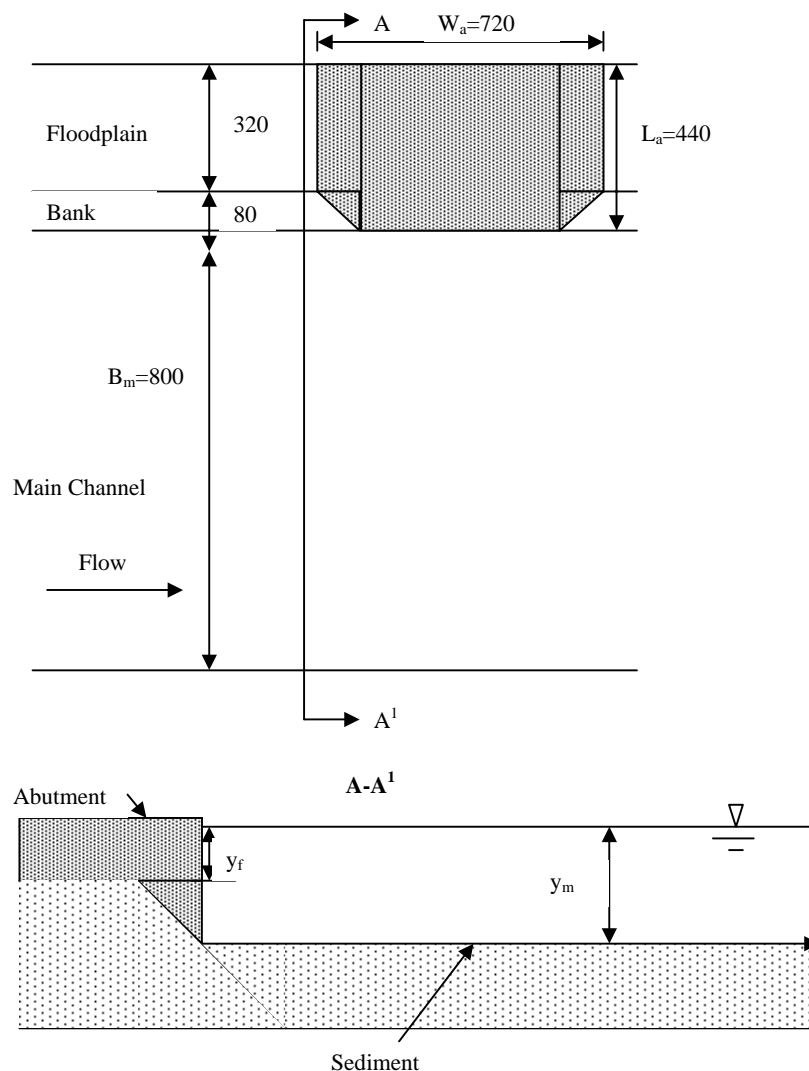


Figure 9-1. Dimensions of experimental compound channel (mm).

the critical shear velocity of the bed sediment is 1.995 cm/s. In experiments under live-bed conditions, the sediment was recirculated with the water. At the upstream inlet of the flume, a gradual-transition contraction was built to guide the sediment into the main channel.

9.1.4 V/V_c Ratio

For all clear-water scour experimental conditions herein, a V/V_c ratio of 0.9 was used, with V being the overall average velocity in the whole cross section of the compound channel and V_c being the critical velocity of the sediment.

Similitude between laboratory experiments and field scale was satisfied by the use of the aforementioned u_*/u_{*c} ratio, of which a value of just below 1.0 represents a condition called “clear-water scour.” This condition is extreme for scouring because the velocity is as high as possible without the movement of the channel bed, which causes infilling of the sediment hole.

The mean velocity of the flow is given by the following equation:

$$\frac{V}{u_*} = 5.75 \log \left(\frac{Y_o}{k_s} \right) + 6.0 \quad (9-1)$$

Where:

k_s = roughness height of the bed and

Y_o = distance above the bed.

At the threshold condition,

$$\frac{V_c}{u_{*c}} = 5.75 \log \left(\frac{Y_o}{k_s} \right) + 6.0 \quad (9-2)$$

So for clear-water conditions, where the bed is stable and k_s is constant,

$$\frac{V}{V_c} = \frac{u_*}{u_{*c}} \quad (9-3)$$



Figure 9-2. View of the flume looking upstream.

For the experiments of this research project, $u_{*c} = 0.01995$ m/s.

Thus, given that clear-water scour is

$$\frac{V}{V_c} = \frac{u_*}{u_{*c}} = 0.9, \text{ then}$$

$$u_* = 0.017955 \text{ m/s}$$

If the flow depth is set, then

$$u_* = \sqrt{gRS} \quad (9-4)$$

Thus, the slope of the flow should be able to be determined. V and V_c can also be determined by selecting $k_s = 2d_{50} = 1.6$ mm.

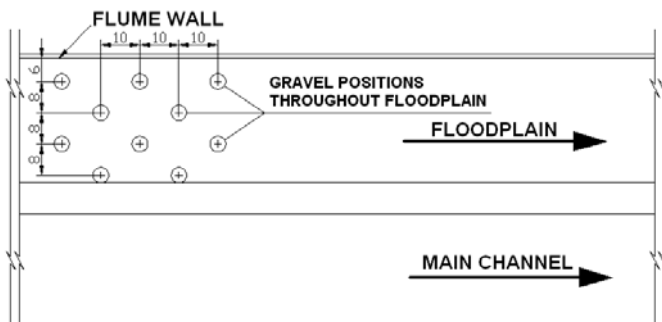


Figure 9-3. Staggered placement of gravel on floodplain to provide roughness (cm).

Three flows were used with velocity ratios, V/V_c , of 0.9, 1.5, and 2.3. The critical velocity of the bed material was calculated using the velocity distribution relation for a rectangular cross section, rough wall, and free surface, as shown in Equation 9-2 above.

For clear-water conditions ($V/V_c = 0.9$), the experiments were run for 80 hours so that the local scour had reached a near equilibrium value. For live-bed conditions ($V/V_c = 1.5$ and 2.3), all experiments were run for 50 hours to ensure that at least 125 bed forms migrated past the abutment.

9.1.5 Instrumentation

Velocity profiles were collected 15 m downstream of the inlet tank, with a 2-mm outside diameter total head tube mounted on a point gage at the channel centerline. Flow rate in the flume was measured using a pressure transducer connected to a Venturi meter in the return pipe. Flow depth was controlled by the volume of water in the flume and measured by taking the difference in elevation between the bed and water surface over a 12-m long transect in the approach section. Water surface and bed surface profiles were collected using two acoustic distance measurement devices, the remote measurement unit (RMU) that operates in air and the bed form and sediment information system (BASIS) that operates underwater. These instruments were mounted on an instrument carriage that traveled on rails over the channel. The instrument carriage was equipped with a computer-controlled, three-axis precision positioning system that allowed transects of the scour hole to be automatically collected using the BASIS. The bed elevation of the area in the vicinity of the abutment was measured at the completion of the clear-water experiments using the BASIS. For the live-bed experiments, the bed elevation of a 2.5-m long flow-parallel transect from 13 to 50 mm from the abutment (depending on the size of the bed forms) was measured continuously for 125 minutes after the scour reached equilibrium state. The probe of the BASIS detects the bed elevation once every minute at a certain point along this transect. The distance between two successive points detected along the transect by the probe is about 1.5 cm. The time-averaged and instantaneous scour depth values adjacent to the abutment were determined from this record. Flow depth was also measured and checked using the point gage.

9.1.6 Experimental Procedure

For this experiment, the researchers took the following steps:

1. Placed the abutment model (with or without counter-measure models) in the flume;
2. Leveled the sediment bed surface;

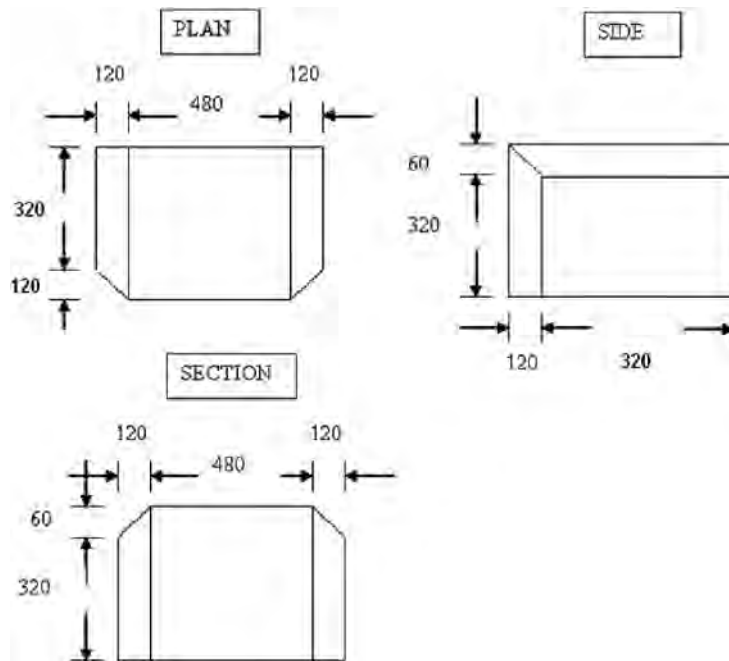


Figure 9-4. Dimensions of abutment model (mm).

3. Wet and drained the flume completely;
4. Collected the profile of the bed surface using the RMU;
5. Filled the flume with water and obtained the desired depth;
6. Collected an initial set of transects of the scour region around the abutment using the BASIS program;
7. Set the predetermined flume slope and started the pump;
8. Adjusted the pump speed to obtain uniform flow at the selected flow depth by measuring the water surface elevation at both ends of the 12-m transect in the center of the channel;
9. Checked the water surface slope along the 12-m transect using the RMU device to ensure the uniformity of the flow;
10. Maintained the same rate of flow and approach depth for the entire experimental run;
11. Collected transects of the scour region at 30-minute intervals;
12. Increased the time intervals to 60 to 90 minutes or more as the experiment progressed and as changes in the scour region became slower;
13. Continued the experiment until the changes in the scour hole became very slow (approximately 80 hours);
14. Stopped the pump, dewatered the flume carefully, and contoured the scour hole; and
15. Took a photo of the scour hole.

9.2 Baseline Experiment

In order to study the efficiency of a certain type of countermeasure in preventing scour at the bridge abutment, the baseline scour—that is, the scour depth at the bridge abutment without any countermeasures—was determined as a reference.

9.2.1 Clear-Water Scour Baseline Experiments

Experimental Results

Several runs of experiments were carried out under clear-water scour conditions with a velocity ratio of 0.9 to determine the worst scour scenario at the bridge abutment. These experiments were done with varying flow depths both in the floodplain and in the main channel. The floodplain was first roughened only with sand of the same size as the bed material and later was further roughened with staggered gravel, as mentioned previously. The gravel was used to simulate a rough floodplain and had a mean diameter of 4.5 cm. The placement of the gravel is shown in Figure 9-3. Table 9-1 gives the experimental results of these baseline tests.

Scour Pattern

Two scour patterns were discovered, depending upon the difference of the roughness on the floodplain. Without gravel on the floodplain, the scour pattern of Figure 9-5 occurred, in which there were five scour locations. Tests B1 through B4 (not roughened with gravel) had similar scour patterns. The first scour hole, Zone A, was at the upstream corner of the abutment and posed the greatest threat to the stability of the abutment. Scour in Zone B was located some distance away from the abutment face in the bridge crossing and was where the maximum scour hole was located. Since it was away from the abutment, it was considered not to be a threat to the abutment. Scour in Zone C was a short distance downstream

Table 9-1. Baseline clear-water experimental results with $V/V_c = 0.9$.

Experimental Result	Test B1	Test B2	Test B3	Test B4	Test B5
Run time, t_e (min)	4,800	2,920	4,800	4,800	4,800
Total discharge, Q (m^3/s)	0.0366	0.0335	0.0387	0.0353	0.0387
Flow depth on floodplain, y_f (cm)	4.5	1.2	5.2	3.0	5.2
Flow depth in main channel, y_m (cm)	13.2	9.9	13.2	11.0	13.2
Main channel bank height, h_1 (cm)	8.7	8.7	8.0	8.0	8.0
Scour depth at upstream corner of abutment, $d_{max,up,abut}$ (cm)	3.60	5.00	5.30	4.70	7.77
Scour depth at a short distance downstream of the downstream corner of the abutment, $d_{max,dn,abut}$ (cm)	3.83	--	3.91	3.44	2.90
Scour depth in the channel away from the abutment, $d_{max,ch}$ (cm)	4.00	--	7.00	4.00	1.50
Floodplain roughness	Sand (0.8 mm)	Sand (0.8 mm)	Sand (0.8 mm)	Sand (0.8 mm)	Sand (0.8 mm) plus staggered gravel (Figure 9-3)

of the abutment. This scour zone may pose a threat to the main channel bank immediately downstream of the abutment. Scour in Zone D was far out into the main channel and, therefore, posed no threat to the abutment. Scour in Zone E was located at a short distance upstream of the abutment corner and seemed to be the upstream extent of Scour Zone B. For Test B5, which did have gravel on the floodplain to provide roughness, there was a slightly different scour pattern, as shown in Figure 9-6, where scour Zones A, B, and E merged to be the maximum scour location, which was located at the upstream corner of the abutment.

Scour Mechanism

In the baseline experiments, it was found that each of the scour zones identified in Tests B1 through B5 was formed by different mechanisms. Figure 9-7 shows the flow patterns responsible for the various scour patterns observed. In Zone A, scour was caused by a combination of a downward roller from the water striking the upstream abutment corner, return

flow from the floodplain flowing down toward the main channel bed, and vortex shedding from the upstream abutment corner. In Zone B, scour was caused by a secondary vortex oriented horizontally and parallel to the streamwise flow direction. Scour in Zone C was caused by the wake vortex induced by flow separation. Scour in Zone D was caused by an increase in main channel velocity above the critical value for sediment movement caused by abutment-induced contraction scour. Scour in Zone E was simply the initial part of scour in Zone B and was caused by the flow coming down from the floodplain into the main channel.

Effect of Floodplain Roughness on Scour Depth at Upstream Corner of the Abutment

The mechanisms of the formation of the four scour holes in Tests B1 through B4 were explained above. In addition to these flow patterns, it was seen that the maximum scour depth was found in the bridge crossing a distance away from the abutment instead of being at the upstream corner

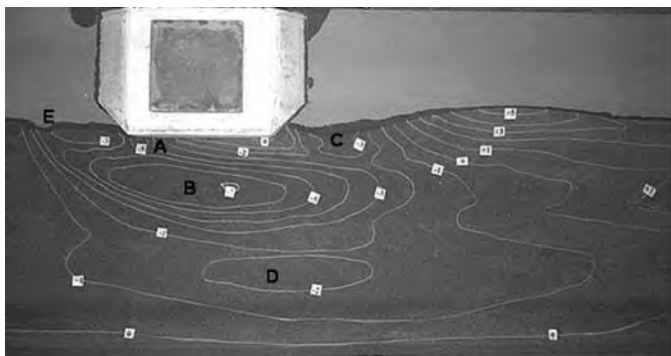


Figure 9-5. String contour of baseline Test B3 (flow is from left to right).

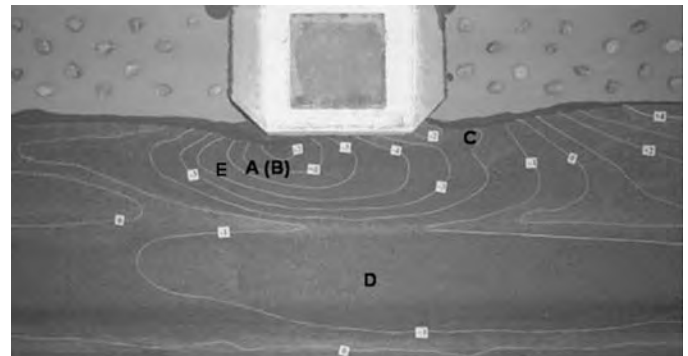


Figure 9-6. String contour of B5 with gravel on the floodplain (flow is from left to right).

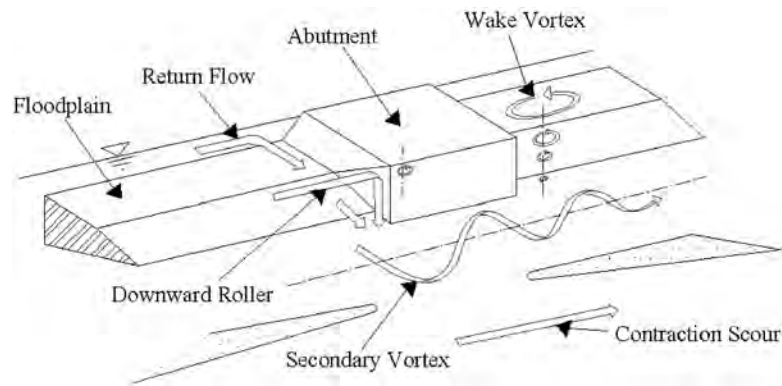


Figure 9-7. Flow patterns around a wing-wall abutment (flow is from left to right).

of the abutment. The reason why the maximum scour depth was not located right at the upstream corner of the abutment was that the velocity ratio between the floodplain flow and the main channel flow was so high that the floodplain flow was able to jet into the main channel a distance away from the bank. To solve this problem with the hope of the maximum scour depth taking place right at the upstream corner of the abutment, the floodplain was further roughened with gravel of an average diameter of 45 mm, as shown in Figure 9-3. As was expected, and as is shown in Figure 9-6, the scour in Zones A, B, and E merged and the maximum scour hole was found right at the upstream corner of the abutment.

Effect of Main Channel Height on Scour

In addition to the velocity ratio of floodplain and main channel, another factor in the location of scour away from the bank is the bank height. When the bank height approaches zero, the scour pattern turns into Type I scour (Melville 1995), which is abutment scour in a rectangular channel. In this case, the maximum scour will happen around the upstream corner of the abutment because the approach flow obstructed by the protrusion of the abutment always makes contact with the bed around the abutment corner upon entering the bridge crossing. Therefore, the downflow and secondary vortex will exert significant shear stress on the bed and cause scour. When the bank height increases, the flow coming from the floodplain must travel a distance before it hits the bed in the main channel after it enters the bridge crossing. In this process, the flow may avoid contacting the corner of the abutment. Figure 9-5 showed that when the velocity ratio between the floodplain and the main channel flow was relatively high, the floodplain flow came off the floodplain edge at a distance upstream of the upstream corner of the abutment (Point E) and made full contact with the main channel bed at Point B, where the maximum scour hole

was found. However, Figure 9-6 (slower floodplain velocity) showed that the flow contacted the main channel bed at the upstream corner of the abutment.

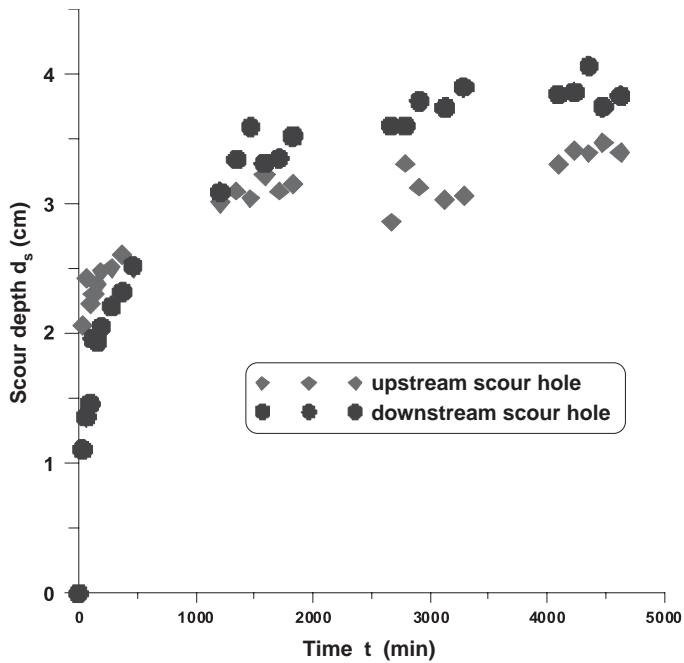
Formation of Scour Holes

Clear-water data of all runs indicated that the upstream scour holes (A and B in Figure 9-5 or EA(B) in Figure 9-6) developed faster at the beginning of the experiment than the downstream scour holes (C in Figures 9-5 and 9-6) because the vortex systems at the upstream corner of the abutment were generally stronger than those at the downstream end of the abutment. Therefore, the upstream scour hole reaches equilibrium more quickly than the downstream scour hole. Figure 9-8 shows the time evolution of the scour depths of both the upstream and downstream scour holes with time for the case with a smooth floodplain (Test B1) and a rough floodplain (Test B5).

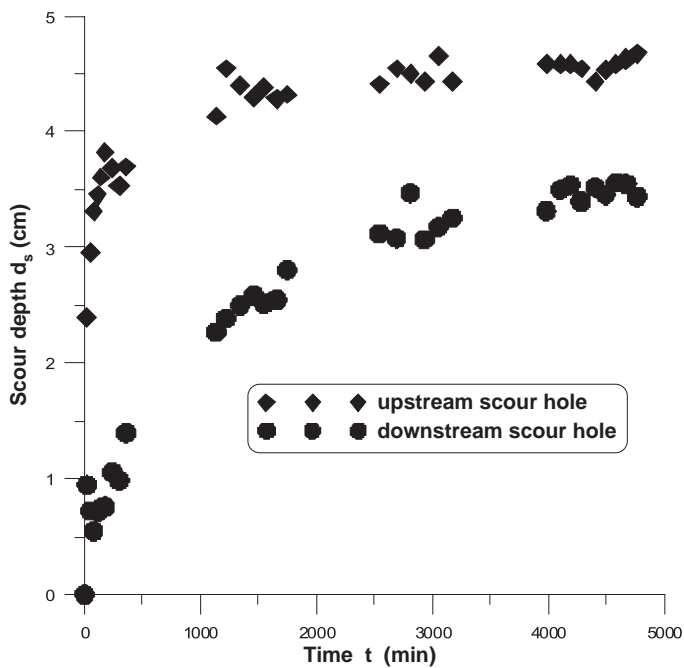
9.2.2 Live-Bed Scour Baseline Experiments

When the velocity of the flow gets higher and the velocity ratio or the shear stress ratio of the flow exceeds one, then the bed materials of the river begin to move and bed forms are initiated. Under live-bed conditions, it is believed that the fluctuating bed forms and the higher shear stress may pose more threat to the stability and practicability of the countermeasures, even though bed-load sediment may fill in the scour holes. Therefore, live-bed experiments were conducted to test successful countermeasures for clear-water conditions to confirm their efficiency in all scour conditions. The live-bed baseline—that is, the scour depth at the bridge abutment without any countermeasures—was determined first as a reference. The live-bed baseline scour results were obtained under the flow conditions shown in Table 9-2.

In the live-bed condition, because of the wavy water surface and the fast-moving and fluctuating bed forms, velocity



(a) Test B1



(b) Test B5

Figure 9-8. Plot of the time evolution of the scour depth of both the upstream (A) and downstream (C) scour holes at the abutment.

profile measurements turned out to be difficult. Therefore, the flow was mainly controlled by the discharge and the average water surface profile and the average bed profile along a 12-m transect in the middle of the approach channel, where

Table 9-2. Experimental results for baseline scour depth for three velocity ratios, V/V_c .

Experimental Result	$V/V_c = 0.9$	$V/V_c = 1.5$	$V/V_c = 2.3$
Instantaneous maximum scour at abutment, $d_{max.abut.inst}$ (mm)	77.7	150.0	172.8
Time-averaged baseline scour depth, $d_{abut.avg}$ (m)	77.7	72.3	75.2
Run time, t (hr)	80	50	50
Total discharge, Q (m^3/s)	0.0387	0.0622	0.0966

Flow depth in flood plain, y_f , is 52 mm. Flow depth in main channel, y_m , is 132 mm.

each bed profile was monitored. First, the discharge was set to be 1.5 times the discharge at the critical condition, and then the slope was adjusted until the average water surface slope and average bed surface slope were equal to the flume slope (i.e., the uniform live-bed flow condition was set through trial and error). The flow depth was also adjusted to be 132 mm deep because it was in the clear-water case.

Similitude between laboratory experiments and field scale was satisfied by the use of the aforementioned V/V_c ratio, of which a value of above 1.0 represents a condition called “live-bed scour.” This condition is extreme for scouring of objects in the flow, such as rock, that make up the flow-altering countermeasures described in this chapter because the high velocity can cause dislodging of individual rocks and therefore constitute failure.

Also, because of the fast change of the bed profiles at the bridge crossing, it was impractical to measure the bed profile in the same manner as was done in the clear-water scour condition, which took 14 transects and more than 13 minutes to cover the whole scour region. Therefore, in the live-bed case, only one 2.5-m long transect at the main channel side of the abutment was chosen to monitor the time evolution of the scour at the edge of the abutment. This transect started from a point 1.5 m upstream of the upstream abutment tip and traveled parallel to the flow just to the right of the abutment. Each pass of the transect took 54.90 seconds, and a total of 133 loops were taken to capture the local scour, as well as the bed forms along this transect, in a period of 2 hours. The data obtained from this transect enabled the determination of the maximum local scour location at the abutment and how it evolved with time.

The bed form shape across the channel was not uniform. Close to the opposite wall, where there was no floodplain, the bed form amplitude was relatively small; close to the floodplain, the bed form amplitude was relatively high.

Figure 9-9 shows the time-averaged local scour depth along the 2.5-m transect at the abutment versus the distance starting from a point 1.5 m upstream of the upstream abutment corner for the 1.5 velocity ratio case. Figure 9-10 shows the time evolution of baseline scour at the upstream abutment corner versus the time after the scour reached equilibrium.

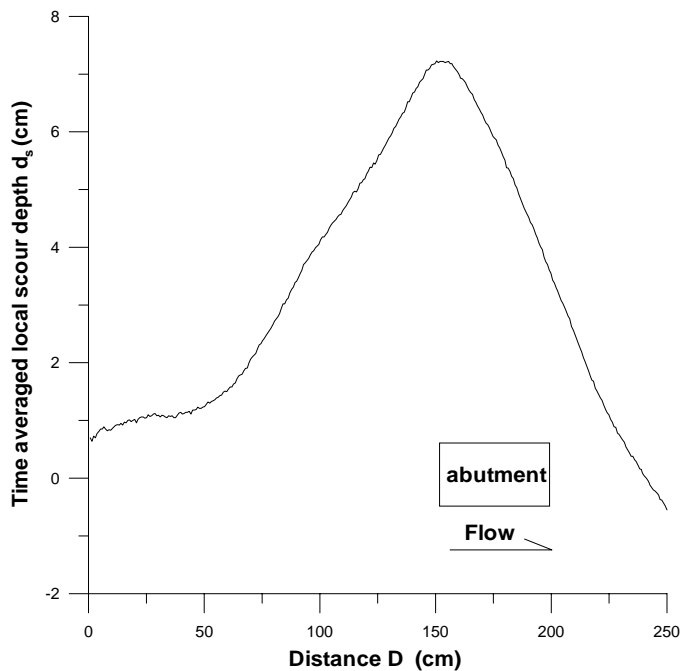


Figure 9-9. Time-averaged local scour depth along the 2.5-m transect at the abutment versus distance starting from a point 1.5 m upstream of the upstream abutment corner.

From Figure 9-9, it can be seen that the maximum time-averaged local scour still took place at the upstream corner of the abutment, with a scour depth of 7.23 cm. This finding agreed with the baseline scour pattern in the clear-water scour condition. The scour depth dropped to 4.01 cm as it approached the downstream end of the abutment. Deposition began to occur at a point 45 cm downstream of the downstream abutment end.

From Figure 9-10, it can be seen that the scour depth at the upstream abutment corner varied from near 0 to 14 cm with time. However, the mean value was 7.23 cm, and the amplitude of variation was about 7 cm. The fluctuation was mainly due to the bed forms. When the crest of the bed forms passed, the scour depth reached its minimum value, which is a few millimeters above zero; when the trough of the bed forms came, the scour depth reached its maximum value.

9.2.3 Conclusions

The following findings were made from the baseline experiments in a compound channel with various flow depths on the floodplain and main channel, various floodplain roughness values, and various bank heights.

Under clear-water conditions:

- Five zones of scour were found for equal floodplain and main channel roughness values and relatively high velocity

ratio between the floodplain and the main channel velocities. The floodplain flow tended to shoot into the main channel at a distance away from the upstream corner of the abutment instead of being fully located at the abutment corner. Under this condition, the maximum scour in the whole region was normally found in Zone B (see Figure 9-5).

- The closer the floodplain flow was to the abutment, the deeper the scour hole was. By increasing the roughness on the floodplain, and thereby decreasing the velocity ratio between the floodplain and the main channel, the floodplain flow was located closer to the upstream abutment corner. As a consequence, the scour Zones A, B, and E were combined and the maximum scour depth was found at the upstream corner of the abutment.
- The principal and secondary vortex systems at the upstream corner of the abutment were stronger than the wake vortex systems at the downstream corner of the abutment. Consequently, the upstream scour hole reached equilibrium more quickly than the downstream scour hole.
- Test B5 was used as the clear-water baseline condition for subsequent countermeasure experiments with a scour depth of 77.7 cm.

Under live-bed conditions:

- Maximum scour took place at the upstream corner of the abutment. Time-averaged scour depth at the upstream corner was less than the scour depth under critical clear-water conditions, whereas instantaneous scour depths were

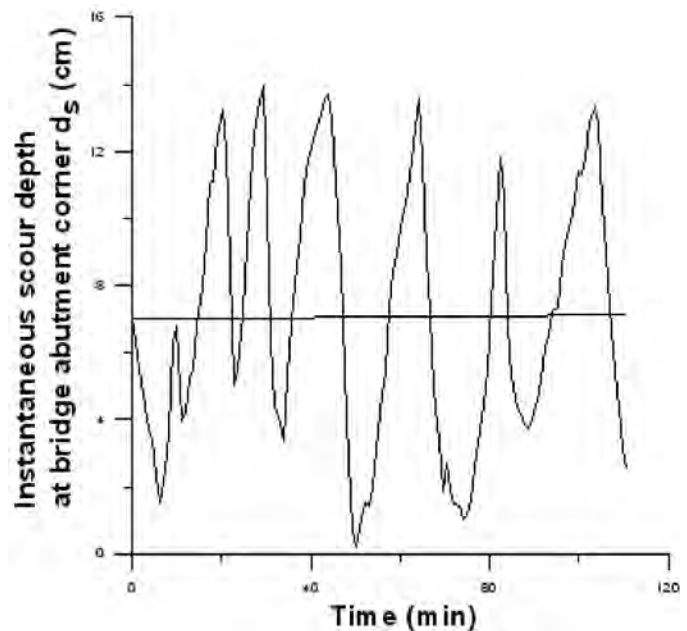


Figure 9-10. Time evolution of baseline scour at the upstream abutment corner after equilibrium was reached.

between values near zero and values nearly twice the maximum scour under clear-water flows because of the superposition of the trough of bed forms (see Figure 9-10).

- Live-bed scour reaches equilibrium more quickly than clear-water scour.

Results in Table 9-2 will be used as the references to evaluate the efficiency of countermeasures that will be tested later.

9.3 Parallel-Wall Countermeasure

The first countermeasure reported herein is the parallel wall. It consists of a wall parallel to the flow attached to the upstream corner of the abutment. After a brief introduction, this section describes the flow patterns and then details solid flat wall countermeasures and rock wall countermeasures.

9.3.1 Introduction

Scour at an abutment can cause damage or failure of bridges and result in excessive repairs, loss of accessibility, or even death. Scour mitigation at bridges has received much attention in the past few decades. Hydraulic countermeasures against bridge abutment scour can be classified as either river training structures or armoring countermeasures. Other than design constraints, considerations in choosing the appropriate method of mitigation include maintenance and inspection requirements, enhancement of the physical environment, and constructability. Design specifications for many of these scour mitigation techniques can be found in *Hydraulic Engineering Circular 23* (Lagasse et al., 2001).

Guidebanks are earth or rock embankments placed at abutments to improve the flow alignment and move the local scour away from the embankment and bridge abutment. The guidebank provides a smooth transition for flow on the floodplain to the main channel. The major use of guidebanks in the United States has been to prevent erosion by eddy action at bridge abutments or piers where concentrated flood flow traveling along the upstream side of an approach embankment enters the main flow at the bridge (Lagasse et al., 2001). There also have been various studies on guidebanks. Among those studies are Spring (1903), Karaki (1959, 1961) Neill (1973), Bradley (1978), Chitale (1980), Smith (1984), Richardson and Simons (1984), and Lagasse et al. (2001). Guidebank orientation, length, crest height, shape, size, downstream extent, and other aspects were investigated. Design guidelines for guidebanks are given by Neill (1973), Bradley (1978), Ministry of Works and Development (1979), Central Board of Irrigation and Power (1989), and Lagasse et al. (1996, 1999, 2001).

However, despite the design guidelines and studies in the literature, issues remain to be dealt with for certain types of

bridges in certain environments. For instance, for small bridges where wing-wall abutments prevail and terminate on the riverbanks, specific design guidelines have not been developed. Guidebanks have been specifically designed for spill-through abutments on rivers with wide floodplains; in such designs, the slope of the guidebank can be made tangent to the slope of the abutment so that there is no protrusion of the abutment into the flow beyond the slope of the guidebank. However, in a wing-wall abutment, this design may not be achieved readily because of the vertical front faces of the abutment. In this situation, either the slope of the guidebank protrudes out beyond the abutment face or the abutment face protrudes out beyond the guidebank slope. The impacts of these configurations on local scour at abutments need to be studied.

Another issue is that a careful review of the guidelines for determining the length of guidebanks shows that the guidelines designed for spill-through abutments in wide floodplain rivers may not apply to smaller bridges (Bradley, 1978). Many factors were not addressed that may be important for small bridges. For instance, first, it is recommended that if the length read from the design chart is less than 9.1 m (30 ft), a guidebank is not needed. This might not be true for a small two-lane bridge whose width is about 9 m; for such a bridge, a 9-m long guidebank may make a great difference in protecting the bridge abutments. Second, it is recommended in the guidelines that for charts 9 to 30 m long, a guidebank no less than 30 m long be constructed. However, according to Herbich (1967), the length of the guidebank appears to be unimportant in reducing velocities provided that the length is greater than a certain minimum length. Therefore, an unnecessarily long guidebank may increase the cost of the structure and not improve its effectiveness. Yet another issue is that the parameters defined and used in determining the length of guidebanks may not be easily available—for instance, the total stream discharge, Q ; the lateral or floodplain flow discharge, Q_f ; and the discharge in the 100 feet of stream adjacent to the abutment, Q_{100} (Bradley, 1978).

In addition, although an elliptical-shaped end seems to be favorable by all design recommendations because the curved head can direct the flow smoothly into the main channel and reduce scour at the guidebank end, the floodplain flow velocity may be relatively low and a curved head may not be justified for small rivers and streams whose floodplains are relatively narrow and are mostly farmlands under cultivation. Most importantly, for abutments terminating on the riverbanks, a curved end stretching out from the bank into the farmland may be aesthetically and practically unacceptable.

This section deals with design issues for parallel-wall countermeasures on small rivers with wing-wall abutments. These parallel walls are essentially scaled-down, simplified versions

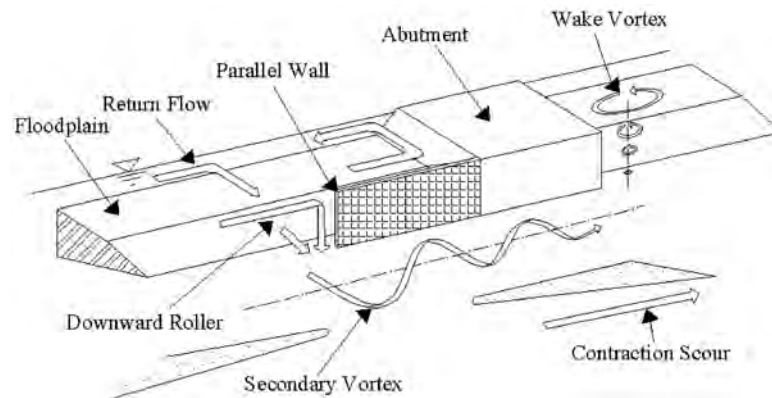


Figure 9-11. Conceptual model of the parallel-wall countermeasure against abutment scour in a compound channel.

of guidebanks. The work fills a need for low-cost countermeasures for small bridges with wing-wall abutments.

9.3.2 Conceptual Model

Figure 9-11 shows the conceptual model of a parallel-wall countermeasure against abutment scour in a compound channel. A wall is attached at the upstream end of the abutment and is parallel to the flow direction.

There are multiple ways in which the parallel-wall countermeasure alters the flow field favorably. First, it can push the scour-inducing downflow and secondary vortex upstream away from the abutment so that scour will not occur at the upstream corner of the abutment provided that the length of the wall is long enough. Second, the wall can create a slow-moving or dead-water zone behind itself on the floodplain. In the case where there is no dead-water zone, the return flow from the floodplain would flow along the roadway and bridge abutment embankment toward the main channel, causing embankment scour. The presence of this wall, and thus the dead-water zone, helps slow down the scour and erosion of

the embankment. Third, the wall helps straighten and improve the flow through the bridge crossing.

9.3.3 Solid Parallel-Wall Countermeasure Results

A series of rectangular solid walls made from 13-mm thick plywood of different lengths, L_s , attached to the upstream end of the abutment and parallel to the flow direction were tested first as preliminary, proof-of-concept experiments. Solid walls are tested because, in certain geographical areas, rocks may not be readily available and cost efficient. All the solid parallel walls were seated at the bottom of the bank slope and aligned with the abutment face parallel to the flume wall. The top of each wall was the same height as the top of the abutment except in one clear-water case, in which the wall height was 52 mm lower than the water surface. The flow depth on the floodplain, y_f , was equal to 52 mm, and the flow depth in the main channel, y_m , was 132 mm. The velocity ratio, V/V_c , was about 0.9, 1.5, and 2.3 in the center of the entire channel for each of the three flow conditions tested. Table 9-3 gives

Table 9-3. Solid-wall experimental results for clear-water scour (run time = 80 hours, $Q = 0.0379 \pm 0.003 \text{ m}^3/\text{s}$, $V/V_c = 0.9$).

Solid-Wall Length, L_s	Maximum Scour Depth at Abutment, d_s (mm)	Scour Reduction Rate (%)	Maximum Scour at the Countermeasure, d_c (mm)
0.3 L , rectangular	62.5	19.6	86.5
0.5 L , rectangular	40.1	48.4	81.0
0.6 L , rectangular	29.5	62.0	77.1
0.7 L , rectangular	21.5	72.3	78.3
0.8 L , rectangular	14.3	81.6	76.2
1.0 L , rectangular	3.3	95.8	77.1
1.2 L , rectangular (Figure 9-14)	-4.0*	105.1	83.0
1.0 L , submerged, top even with floodplain	40.0	48.5	55.0

* Negative scour depth indicates deposition.

Table 9-4. Solid-wall experimental results for live-bed scour for six wall lengths, L_{spw} (run time = 50 hours, $Q = 0.0619 \pm 0.0015 \text{ m}^3/\text{s}$ for $V/V_c = 1.5$, and $Q = 0.0619 \pm 0.0015 \text{ m}^3/\text{s}$ for $V/V_c = 2.3$; all walls were rectangular-shaped and emergent).

Experimental Results	$L_{spw} = 0.6L$	$L_{spw} = 0.9L$	$L_{spw} = 1.2L$	$L_{spw} = 1.5L$	$L_{spw} = 1.6L$	$L_{spw} = 1.9L$
Velocity ratio, V/V_c	1.5	1.5	1.5	1.5	2.3	2.3
Time-averaged scour depth at abutment, $d_{abut,avg}$ (cm)	5.05	4.04	2.57	0.22	2.23	3.57
Percent reduction in time-averaged scour depth at abutment, % $_{max,abut,avg}$	30	44	63	92	70	53
Maximum instantaneous scour depth at abutment, $d_{max,abut,inst}$ (cm)	12.98	9.56	10.12	5.49	8.84	8.94
Percent reduction in maximum instantaneous scour depth at abutment, % $_{max,abut,inst}$	13	36	33	63	49	48
Time-averaged scour depth at the countermeasure, $d_{cm,avg}$ (cm)	7.57	7.90	7.74	7.86	9.21	9.82
Maximum instantaneous scour depth at the countermeasure, $d_{max,cm,inst}$ (cm)	14.36	15.86	13.81	14.20	16.43	16.73

results of the solid-wall experiments under clear-water conditions, and Table 9-4 gives results under live-bed conditions. Figure 9-12 is a string contour of the $1.2L$ solid wall run in clear-water scour conditions, where y_m is 132 mm, y_f is 52 mm, Q is $0.0379 \text{ m}^3/\text{s}$, and t_c is 80 hours. Flow was from left to right.

Discussion of Solid-Wall Length

Figure 9-13 shows the maximum scour depths at the abutment and the maximum scour depth in the vicinity of the upstream end of the wall versus the length of the wall in terms of the abutment length, L_a , for both clear-water ($V/V_c = 0.9$) and live-bed ($V/V_c = 1.5$) experiments. It is seen that, as the length of the wall increases from $0.3L_a$ to $1.2L_a$, the scour at the abutment decreases rapidly. There was no scour at the abutment corner in 80 hours of running when the wall reached a length of $1.1L_a$.

It is also seen from Figure 9-13 that as the length of the wall increases from $0.6L_a$ to $1.5L_a$, the scour at the abutment

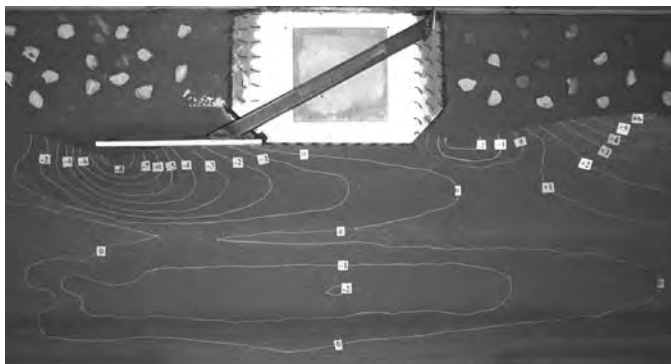
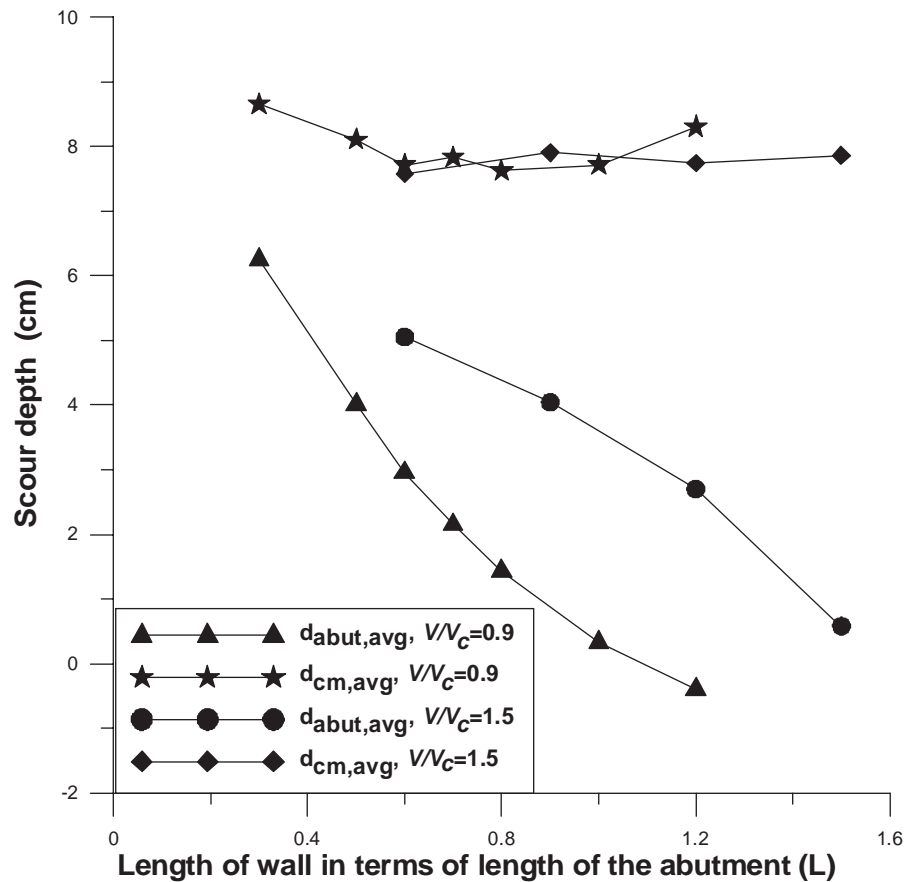


Figure 9-12. A string contour of the $1.2L$ solid wall run in clear-water scour (contour interval = 1 cm).

decreases rapidly for the live-bed case. The average scour depth at the abutment corner tends to zero if the wall length reaches a length of $1.6L_a$. The amplitudes of the bed forms were significant, however. For instance, the maximum trough depths of the bed forms in the approaching channel ranged from 9.32 to 11.50 cm. The presence of the solid wall did not affect the dune amplitudes because the bed forms migrated past the wall and abutment, thereby causing the scour depth at the abutment to fluctuate about its average value, as mentioned above. From the live-bed experimental data, it is seen that as the time-averaged scour depth at the bridge abutment changes from 5.05 cm ($0.6L_a$ case) to 0.22 cm ($1.5L_a$ case), the maximum contribution from the bed forms to the scour depth varies from 7.93 to 4.91 cm. It can be seen that although increases in solid-wall length decreased the amplitude of the bed forms, the decreases are not significant. Therefore, if the height of bed forms constitutes a large part of the local instantaneous scour depth, scour can only be completely eliminated when the presence of the solid wall can change the flow condition in the bridge crossing into a transition regime under which the dunes completely disappear and a flat bed with bed material transport is formed. This transition regime may or may not be readily achieved depending on the approach-flow conditions and the constriction ratio of the channel.

It was also found from the live-bed experimental data that, with a velocity ratio of 2.3, when the length of the wall was increased from $1.6L_a$ to $1.9L_a$ the scour reduction rate at the abutment decreased from 70 percent to 53 percent instead of increasing. This decrease may be due to imperfect construction of the floodplain or wall, or it may be that these two scour values are within the range of scatter of the scour data for this high-sediment-transport flow.

In summary, it was found that, in general, a solid parallel-wall countermeasure attached to the upstream end of the



Subscript “abut” denotes scour at the abutment that could threaten the abutment, and subscript “cm” denotes scour at the upstream end of the parallel-wall countermeasure tested (not threatening to the abutment).

Figure 9-13. Scour depth at both abutment and upstream end of solid walls versus wall length in terms of abutment length, L_w , for $V/V_c = 0.9$ (clear-water scour conditions) and 1.5 (live-bed scour conditions).

abutment was able to move the scour hole upstream from the abutment corner and, therefore, was effective as a scour countermeasure. It was also found that, for clear-water scour conditions, as the length of the wall increased, the scour at the abutment declined. In live-bed experiments, however, when the length of the wall becomes longer than $1.6L_w$, then the scour at the abutment begins to increase.

9.3.4 Rock Parallel-Wall Countermeasure Results

While the preliminary experiments mentioned above using a solid plate for a parallel-wall countermeasure were successful, there may be some bridge sites where rock is available. In these cases, it may be more economical and easier to construct if the parallel-wall countermeasure is a pile of rocks instead of a solid plate. Therefore, a series of rock walls of different

lengths, L_w , and different protrusion lengths, L_p , were tested under both clear-water and live-bed conditions, as shown in Figure 9-14. In these experiments, the flow depth on the floodplain, y_f , was 52 mm, and the flow depth in the main channel, y_m , was 132 mm. The velocity ratio was 0.9 along the centerline of the entire channel for clear-water experiments and 1.5 and 2.3 for live-bed experiments. The top of each wall was the same height as the top of the abutment so that they were not submerged by the flow. The experimental results are tabulated in Table 9-5 for clear-water scour conditions and Table 9-6 for live-bed scour conditions.

From Tests 1, 2, and 3 in Table 9-5, it was found that with a protrusion length of the wall base of $0.5W$ beyond the abutment face into the main channel, there tended to be a separation zone behind the downstream end of the wall, causing a significant local scour hole. When the length of the wall was $1.5L_w$, the scour hole was relatively small (8.81 cm) and did

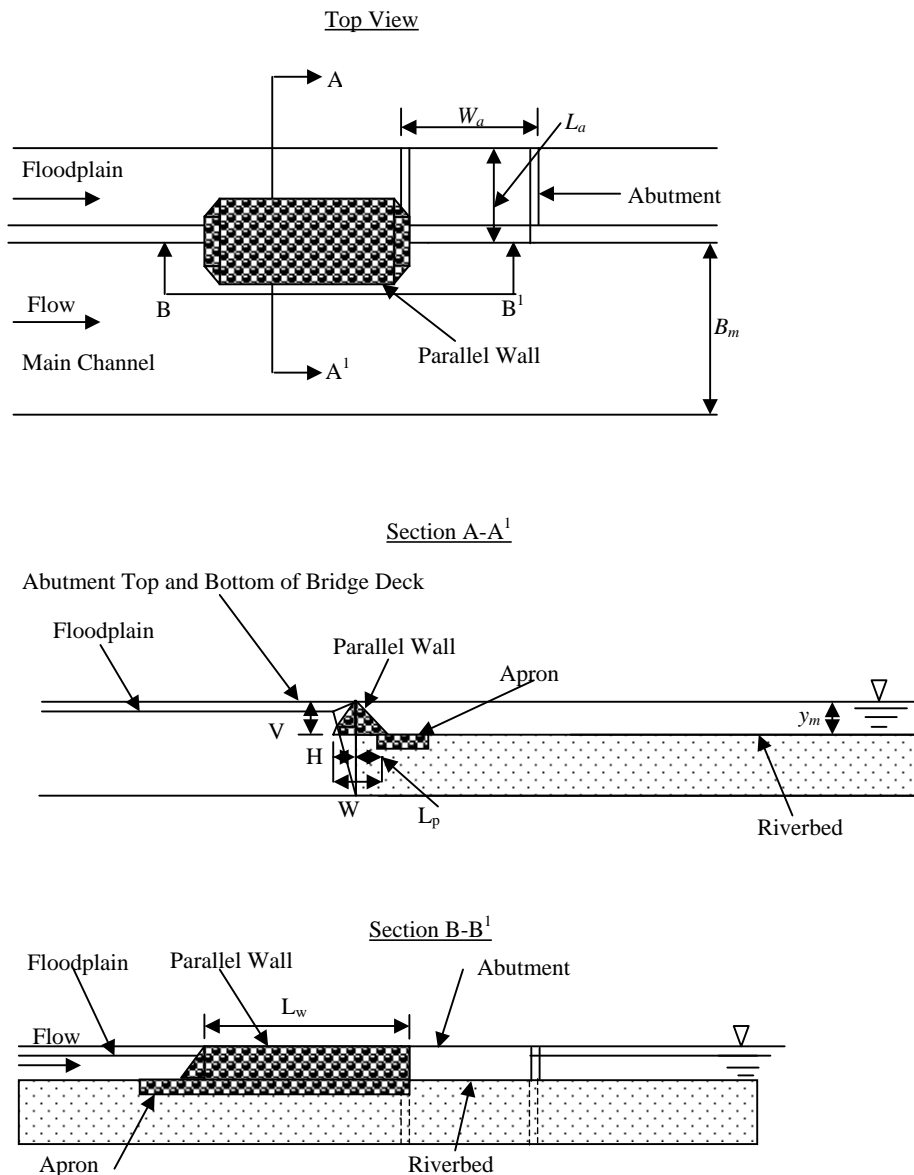


Figure 9-14. Parallel wall (aprons were present only in live-bed experiments) with $L_w = 1.2L$.

Table 9-5. Experimental data of parallel rock walls in clear-water scour ($Q = 0.0385 \pm 0.003 \text{ m}^3/\text{s}$; $t_e = 80$ hours; $V/V_c = 0.9$; side slope, $S_b = 18/13.2$; end slope, $S_n = 30/13.2$).

Experimental Result	Test 1	Test 2	Test 3	Test 4	Test 5	Test 6	Test 7	Test 8	Test 9	Test 10	Test 11	Test 12
Gravel diameter, D (mm)	6.7~9.5	6.7~9.5	6.7~9.5	6.7~9.5	6.7~9.5	6.7~9.5	6.7~9.5	6.7~9.5	6.7~9.5	6.7~9.5	6.7~9.5	19.0~50.0
Wall length, $L_w \times L_a$	1.5	0.5	1.0	1.5	0.5	1.0	1.5	1.0	0.5	0.25	2.0	1.5
Wall protrusion, $L_p \times W$	0.5	0.5	0.5	0.3	0.3	0.3	0.0	0.0	0.0	0.0	0.0	0.0
Maximum scour at abutment, d_s (mm)	2.0	52.1	50.6	4.5	53.0	23.5	19.0	19.5	20.0	28.0	20.0	3.0
Scour reduction (%)	97	29	35	94	32	70	76	75	74	64	74	96

Table 9-6. Rock wall experimental results in live-bed scour for three different wall lengths, L_w .

Experimental Result	$L_w = 0.5L_a$	$L_w = 1.0L_a$	$L_w = 1.5L_a$	$L_w = 0.5L_a$
Velocity ratio, V/V_c	1.5	1.5	1.5	2.3
Time-averaged scour depth at abutment, $d_{abut,avg}$ (mm)	31.9	25.9	18.7	22.3
Maximum instantaneous scour depth at abutment, $d_{max,abut,inst}$ (mm)	51.3	51.4	47.3	40.7
Percent reduction in time-averaged scour depth at abutment, % $_{max,abut,avg}$	56	64	74	70
Percent reduction in maximum instantaneous scour depth at abutment, % $_{max,abut,inst}$	66	66	68	76

$t_e = 50$ hours. All walls were rectangular shaped and emergent.

$Q = 0.0619 \pm 0.0015$ m³/s for $V/V_c = 1.5$.

$Q = 0.0966 \pm 0.003$ m³/s for $V/V_c = 2.3$.

not pose a direct threat to the abutment. However, when the length of the wall was $0.5L_a$, the scour hole was 12.96 cm and the abutment was highly threatened. These scour holes could pose significant threat to a pier if a pier is located near the abutment.

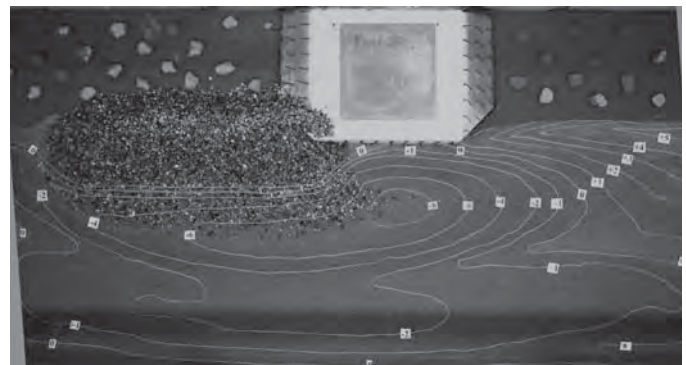
From Tests 4, 5, and 6 in Table 9-5, it was found that with a protrusion of the wall base of $0.25W$ beyond the abutment face into the main channel, there was still a separation zone right behind the downstream end of each wall. However, the scour holes caused by the separation in the $0.25W$ protrusion cases were smaller than they were in the corresponding $0.5W$ cases. For instance, the scour hole depths were 43.0 mm, 56.7 mm, and 80.4 mm for wall lengths of $1.5L_a$, $1L_a$, and $0.5L_a$, respectively. However, these holes were closer to the abutment because of the reduced protrusion of the wall into the main channel.

From Tests 7, 8, 9, 10, and 11 in Table 9-5, it was found that when the wall base did not protrude beyond the abutment, separation that appeared in the $0.25W$ and $0.5W$ protrusion cases disappeared. However, the abutment now was partly protruding out beyond the wall slopes, causing constriction of the flow coming from the wall slope. Fortunately, because of the high roughness of the wall, the near-wall velocity of the flow was retarded; as a result, the constriction of the flow did not cause significant scour at the abutment. It was found that the scour depth at the abutment ranged from 19 to 20 mm when the length of the wall varied from $0.5L_a$ to $2L_a$. The scour depth was about 28 mm when the wall was $0.25L_a$ long, which indicated that for zero wall base protrusion, the scour depth at the upstream corner was not significantly affected by the length of the wall.

Figures 9-15, 9-16, and 9-17 show the scour contours of Tests 3, 6, and 9, respectively, in Table 9-5.

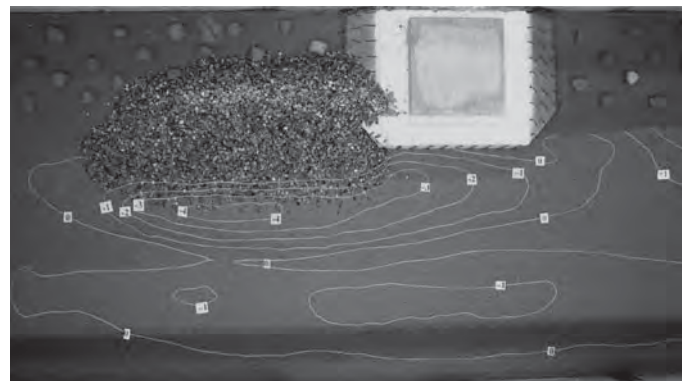
For live-bed scour conditions, it can be seen in Table 9-6 that a length of $0.5L$ requires the least amount of rock to build the wall and results in the same level of scour protection as longer walls. Even with a velocity ratio of 2.3, there is a

76-percent reduction in the maximum instantaneous scour depth at the abutment. The instantaneous scour depth is considered to be more critical than the average scour depth because the abutment could collapse even in the short time in which the instantaneous scour depth was at its deepest level.



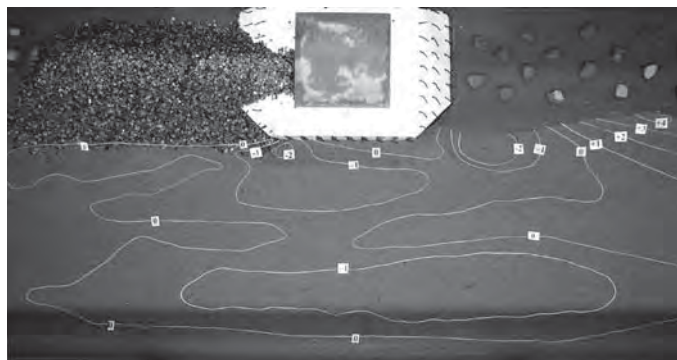
There is a small apron at the end. The wall base protruded out into the main channel from the abutment half-wall width. Flow is from left to right.

Figure 9-15. Scour contours of Test 3 in Table 9-5.



There is a small apron at the end. The wall base protruded out into the main channel from the abutment a quarter-wall width. Flow is from left to right.

Figure 9-16. Scour contours of Test 6 in Table 9-5.



There is a small apron at the end. The wall base was even with the abutment. Flow is from left to right.

Figure 9-17. Scour contours of Test 9 in Table 9-5.

Discussion

Figure 9-18 shows the scour depth at the bridge abutment versus rock wall length for different wall protrusion amounts for clear-water scour conditions. It can be seen that, for protrusion lengths, L_p , of $0.25W$ and $0.5W$, increases in wall lengths can reduce scour at the abutment significantly. However, for the case of no protrusion, increases in wall lengths do not show obvious effects in reducing scour at the abutment except when the wall is less than $0.5W$.

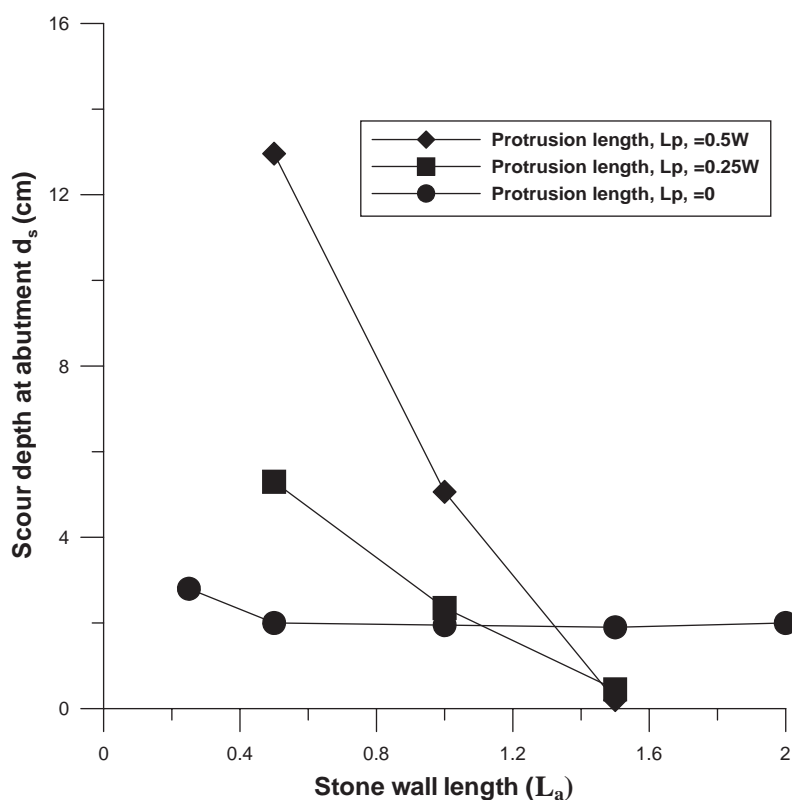


Figure 9-18. Scour depth at bridge abutment versus rock wall length for different wall protrusion lengths under clear-water conditions ($V/V_c = 0.9$).

Figure 9-19 shows the maximum scour depth caused by the wall in the channel versus rock wall length for different wall protrusion lengths for the clear-water experiments. The figure shows that for the $0.25W$ and $0.5W$ protrusion lengths, increases in wall lengths can significantly reduce the maximum scour depth that is induced by the presence of the walls. For walls with protrusion length of zero, increases in wall length result in essentially no reduction in scour depth (i.e., scour at abutment) when wall lengths are greater than $0.5L$.

Figure 9-20 shows both time-averaged and maximum instantaneous scour depth at the bridge abutment versus rock wall length for zero protrusion length under live-bed conditions. The time-averaged scour depth was calculated by measuring the scour depth at regular time intervals and then averaging the depths over time, thereby giving a sense of the average depth of scour. The maximum instantaneous scour depth is the maximum scour measured at any time in the scour time series data collected. Even though this maximum scour value would not persist at the abutment, it could cause some brief undermining of the abutment structure and, therefore, is reported here as a parameter of interest. It is found that increases in wall lengths from $0.5L$ to $1.5L$ were able to reduce the time-averaged scour depth at the bridge abutment from 31.9 to 18.7 mm (a 41-percent reduction).

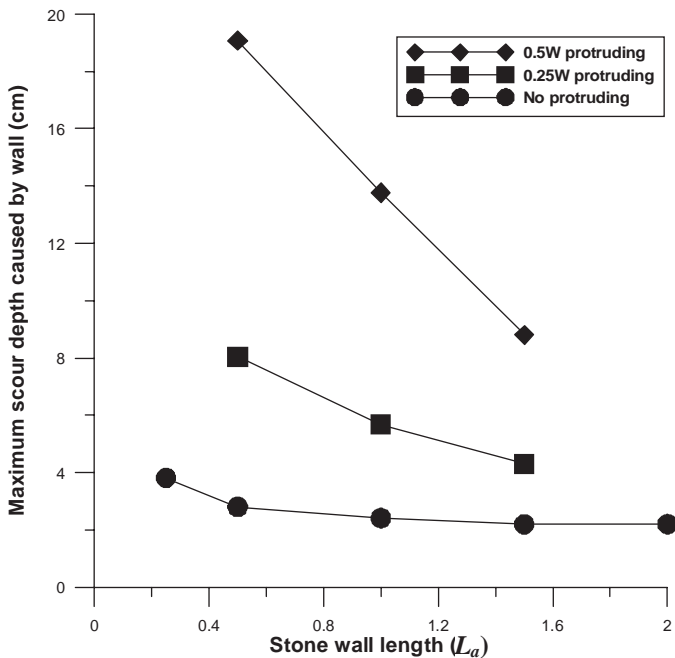


Figure 9-19. Maximum scour depth caused by the wall in the entire channel versus rock wall length for different wall protrusion lengths under clear-water conditions ($V/V_c = 0.9$).

However, the increases in wall lengths only reduced the maximum instantaneous scour from 51.3 to 47.3 mm (an 8-percent reduction).

The following general findings were made:

- Walls that were set back onto the floodplain such that the base of the walls were even with the abutment (protrusion length, $L_p = 0$) were most effective in protecting the abutment.
- For zero protrusion length ($L_p = 0$), the scour protection of the walls was not sensitive to the length of the wall unless the length was less than $0.5L$.
- Walls whose base protruded into the main channel beyond the abutment ($L_p = 0.25W$ or $0.5W$) tended to produce significant scour in the bridge crossing and potentially threaten the middle and downstream abutment end when the length of these walls became shorter than a certain length.

Regarding the amount of mass transfer or water flow through the rock wall itself during the experiments, dye was injected in the floodplain side of the parallel walls. For all of the flow conditions investigated, no significant amount of dye

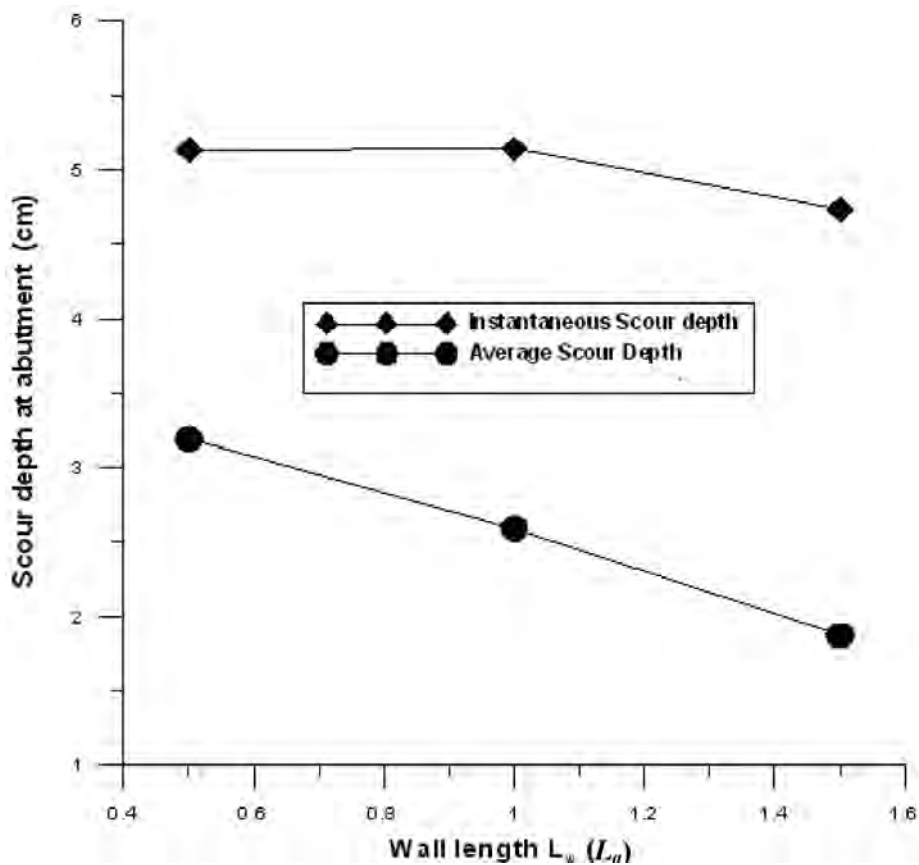


Figure 9-20. Time-averaged and maximum instantaneous scour depth at bridge abutment versus rock wall length for zero protrusion under live-bed conditions ($V/V_c = 1.5$).

was observed to flow through the rocks. This indicated that there is no significant flow transfer through the wall. In addition, a parallel solid wall with length $0.8L_a$, with 85 circular 8-mm diameter holes uniformly distributed on the wall, was tested and compared with the $0.8L_a$ impermeable wall. The results were similar. This showed that when the permeability of the wall is smaller than a certain value, the solid wall acts like an impermeable one.

Cases of clear-water and live-bed scour were investigated. It could be that during flow conditions in which there was less downstream velocity, there is more flow through the wall. This would most likely not be critical for scour, however, since clear-water and live-bed scour are the two worst scour cases.

In all of the experiments described in this report, there was no physical gap between the countermeasure and the abutment. Care should be taken to ensure this, as a high-velocity jet may form if such a gap exists, which could exacerbate the scour depth in unknown ways.

9.3.5 Design of Parallel-Wall Countermeasure for Scour Prevention at Wing-Wall Abutments

General preliminary design guidelines can be established for the use of parallel solid walls and parallel rock walls to reduce scour at typical bridges with wing-wall abutments terminating on or protruding beyond the main channel banks.

Protrusion of Wall

The best position for solid walls would be such that the solid wall's face is aligned with the abutment's face so that there is no protrusion by either structure.

For parallel rock walls with lateral protrusions of $0.25W$ and $0.5W$, a separation zone is formed behind the walls, causing scour holes and threatening the abutment foundation. Also, the protrusion of the wall into the main channel further constricts the bridge crossing and reduces its conveyance capacity. Therefore, parallel rock walls of zero protrusion are recommended.

Length of Wall

For a solid parallel-wall countermeasure, the clear-water experimental results showed that a solid wall with a length of $1.1L_a$ will completely eliminate the local scour at the bridge abutment, while a solid wall of length $1.6L_a$ with a velocity ratio of 1.5 will be able to reduce the time-averaged scour to zero. For a velocity ratio of 2.3, a solid wall of length $1.6L$ will reduce the time-averaged scour up to 70 percent. Further increases in the length of the wall will result in a decrease in

scour reduction rate. Therefore, it is recommended that the length of the parallel solid wall be $1.6L_a$.

For a parallel-wall countermeasure made of piled rock of zero protrusion, a rock wall length of $0.5L_a$ is recommended.

Height and Width of Wall Crest

Heights for both solid and rock parallel-wall countermeasures should be high enough to prevent the flow from entering the bridge crossing at the abutment, even in the worst case scenario.

Slope of Wall and Apron

The side slope of the rock wall must be less than the rock's angle of repose to ensure stability. However, the side slope should be as high as possible so that the protrusion of the abutment beyond the wall slope is a minimum. It is recommended that the side slope of the wall be about 5 degrees less than the angle of repose of the rocks.

Aprons are always needed at both the bottom of the side slope and the upstream end slope. When scour occurs in the riverbed adjacent to those locations, the rocks from the apron will launch (that is, fall) into the scour hole. This allows the rocks that make up the side slope and upstream end slope to remain intact. Apron thickness, area limit, and relative position with the parallel rock wall should be determined according to the scour depth and position of the scour hole along the wall. Even though Figure 9-11 shows the water hitting the abutment and coming back, the water's velocity is so slow that erosion will be negligible.

Comparison of Solid and Rock Parallel Walls

If the best designs for both solid and rock parallel-wall countermeasures are compared, it can be seen that the rock walls have advantages over the solid walls. Table 9-7 shows scour depths for both solid and rock walls for both clear-water and live-bed scour conditions. The table shows that the rock wall allows less scour at the abutment than the solid wall does. The solid wall, therefore, seems to be feasible only when the cost of rocks is prohibitively high.

9.3.6 Conclusions Regarding Parallel-Wall Countermeasures

The following conclusions were made about parallel-wall countermeasures:

- A parallel solid wall attached at the upstream corner of the abutment parallel with the flow can be used as a countermeasure against abutment scour. The length of the solid

Table 9-7. Comparison of rock and solid wall countermeasure performance (scour depth, mm).

Countermeasure Type	Clear-Water Scour	Live-Bed Scour
Solid Parallel Wall	-4.0 at abutment* 83.0 at solid wall	54.9 at abutment 78.6 at solid wall
Rock Parallel Wall	3.0 max. at abutment 43.3 max. at rock wall	47.3 max. at abutment 85.8 max. at rock wall

* Negative scour depth indicates deposition.

wall should be $1.6L_a$ to obtain acceptable scour reduction rate at the abutment for the conditions tried in this study.

- A parallel solid wall attached at the upstream corner of the abutment parallel with the flow may or may not be able to reduce the amplitude of the bed forms that pass through the bridge opening, depending on the changes of the flow parameters from the approaching channel after entering the bridge crossing.
- There may be significant scour at the upstream solid wall end, so no other structures should be located in this region.
- Parallel rock walls attached at the upstream of the abutment can also be used as countermeasures against scour at the abutment. The foot of the wall should not protrude into the main channel beyond the abutment, and a top wall length of $0.5L$ will provide sufficient protection. The side slope of the rock wall should be on the order of 30 degrees, but in no case should it be steeper than about 70 percent of the rocks' angle of repose.
- Rock walls have more advantages than solid walls in terms of efficiency, stability, and cost.

9.4 Spur Dike Countermeasure

The next flow-altering countermeasure described is a combination of spur dikes located locally to the abutment. The problem is described, and then the results of the lab tests are given.

9.4.1 Introduction

Spur dikes—structures that project from the bank into the channel—have been used extensively in all parts of the world as river training structures to enhance navigation, improve flood control, and protect erodible banks (Copeland, 1983). They may be classified according to their permeability: high-permeability spur dikes are “retarder” spur dikes, impermeable spur dikes are “deflector” spur dikes, and intermediate-permeability spur dikes are “retarder/deflector” spur dikes (Brown, 1985b). They may be constructed out of a variety of materials, including masonry, concrete, earth and rock, steel, timber sheet-piling, gabions, timber fencing, or weighted brushwood fascines. They may be designed to be submerged regularly by the flow or to be submerged only by the largest flow events.

A spur dike serves one or more of the following functions:

- It trains the stream flow. For instance, spur dikes are commonly used to realign streams as they approach a bridge abutment. A bridge abutment may be in danger of being severely eroded when it is subjected to high-velocity flow from a channel that has changed course because of meandering.
- It protects the stream bank (which may or may not contain bridge abutments) from erosion.
- It increases the flow depth for navigation (Garde et al., 1961) or improves aquatic habitat.

In recent years, porous and overflow-type spur dikes have been shown to provide improved pool habitats for fish and other aquatic life in severely degraded streams (Shields et al., 1995c). Volumes of the scour hole in the vicinity of model spur dikes were measured in a laboratory flume under clear-water overtopping flows with varying angles and contraction ratios to maintain bank protection and enhance aquatic habitats (Kuhnle et al., 1997, 1998, 1999). In addition, because of the deposition that spur dikes induce, spur dikes may protect a stream bank more effectively and at less cost than revetments (Lagasse et al., 2001).

Spur dikes constructed on or adjacent to an abutment to counter local scour have not been previously tested. This technique would constitute a combination of bank hardening and flow altering to counter local scour. When spur dikes are properly placed around the abutment, the flow can be redirected and scour near the abutment can be reduced. Local scour can threaten the spur dike itself, however, as shown in Figure 9-21.

9.4.2 Conceptual Model

Figure 9-22 shows the flow patterns around a spur dike as a countermeasure against abutment scour in a compound channel. A spur dike is placed a certain distance upstream of the abutment and is perpendicular to the flow direction. Flow on the floodplain can only go around the main channel end of the spur dike. A spur dike thus installed is expected to be able to block the floodplain flow from hitting the abutment face and

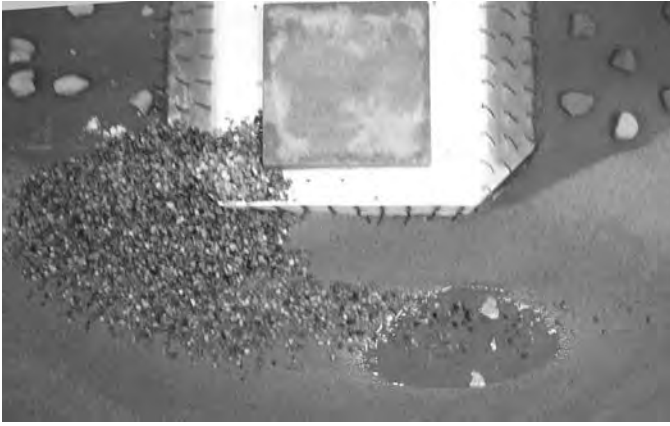


Figure 9-21. Excessive scour around a poorly positioned spur dike (flow is from left to right).

direct the flow into the main channel. It may create wake vortices behind itself. The effects of these wake vortices at the spur dike structure on the abutment scour were evaluated experimentally to determine the best configuration of spur dikes as countermeasures. In the experimental studies described next, the number of spur dikes, the distance between spur dikes and between spur dikes and abutment, the protrusion length, and the construction material of spur dikes will be tested as parameters. Figure 9-23 shows the variables involved.

9.4.3 Results

Results are given next for both solid and rock spur dikes.

Solid Spur Dikes

A preliminary proof-of-concept series of solid spur dike experiments were performed first. The spur dike was made from 13-mm thick plywood and was tested under the same flow condition as in the clear-water baseline test ($V/V_c = 0.9$).

The flow depth in the main channel, y_m , was 132 mm, and the flow depth in the floodplain, y_f , was 52 mm. Only one spur dike located upstream of the abutment was tested in each experiment. The variables experimented with for the solid spur dikes were length, L_{sp} ; distance upstream of the abutment, D_s ; and orientation angle with respect to the flow, θ . In all cases, the top of the spur dikes was higher than the water surface. The experimental results are listed in Table 9-8.

The flow perpendicular length of the spur dike was found to be an important variable in protecting the abutment. Flow perpendicular lengths were restricted to the length of the abutment or less in this experimental series to prevent excessive contraction of the flow in the main channel or backwater effects. The six test cases showed that spur dikes of the same flow perpendicular length as the abutment do not protect the abutment from scour regardless of spacing or orientation angle, as shown in Figures 9-24, 9-25, and 9-26. When the spacing (D_s) of the spur dikes was less than the flow perpendicular length of the abutment (L_a), the scour hole induced by the spur dike will encompass the upstream corner of the abutment (Figure 9-26). When the spur dikes were far away ($D_s \geq 1.5L_a$) from the abutment, a narrow channel formed between the deposited sand and the abutment corner (Figure 9-25). This caused scour at the upstream corner of the abutment. In addition, the spur dikes caused the formation of huge scour holes that would undoubtedly threaten the stability of the stream bank and the stability of the spur dike itself. In summary, the effective reduction of local scour at bridge abutments using spur dikes requires that their flow perpendicular length be greater than the flow perpendicular length of the abutment.

Rock Spur Dikes

Four cases of rock spur dikes, each with the same length perpendicular to the flow, were tested under clear-water flows. These rock spur dikes were constructed from the flume wall

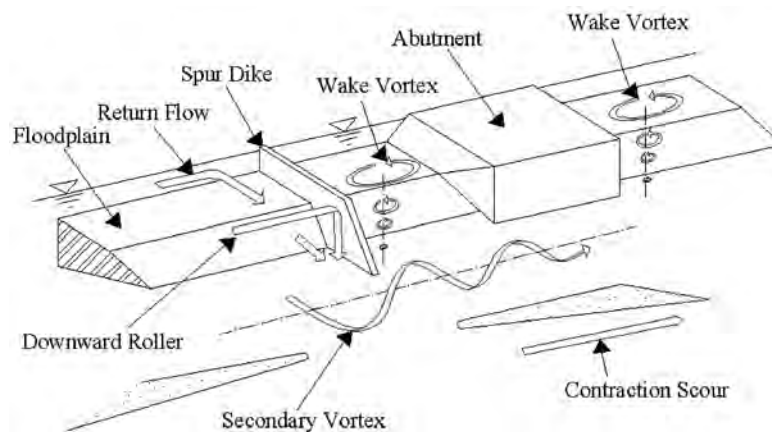


Figure 9-22. Flow patterns around a spur dike as a countermeasure against abutment scour in a compound channel.

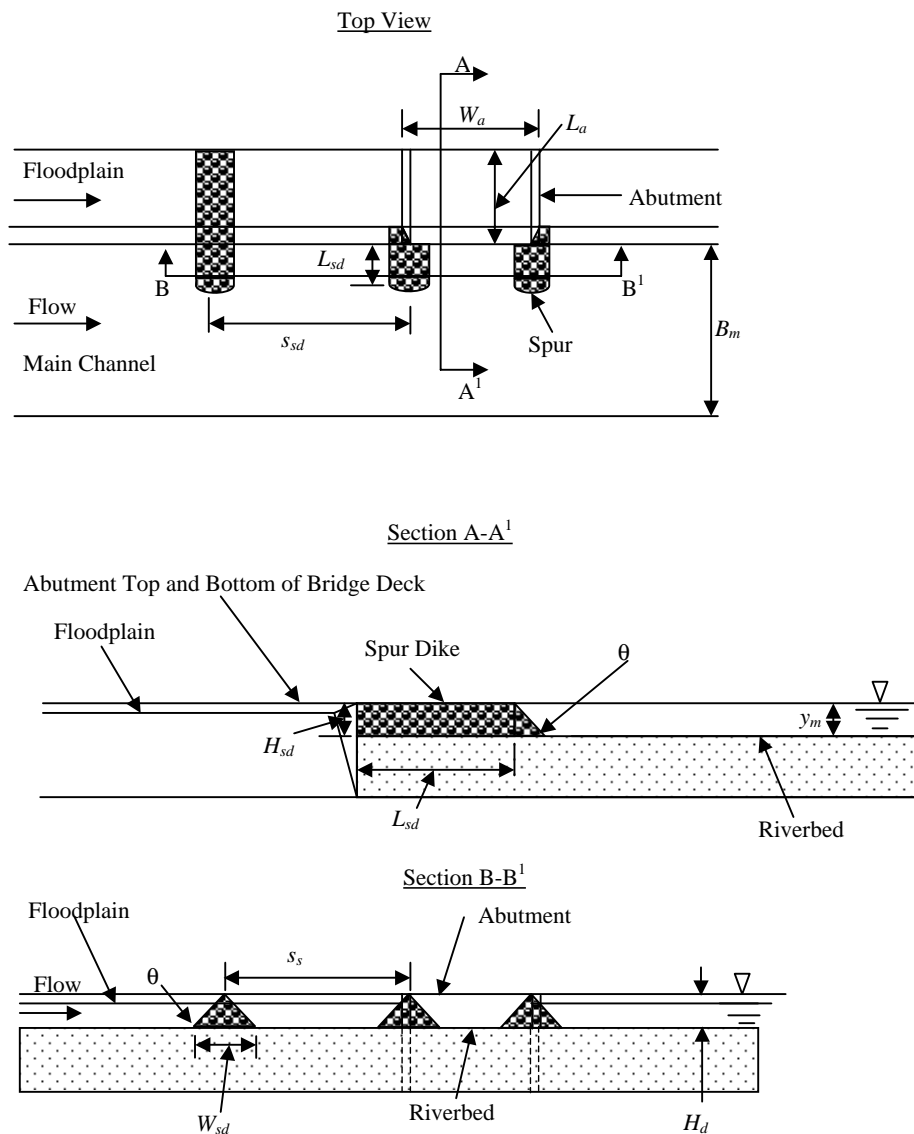


Figure 9-23. Definition sketch for spur dike scour countermeasure.

Table 9-8. Preliminary solid spur dike experimental results ($Q = 0.0387 \pm 0.003 \text{ m}^3/\text{s}$, $V/V_c = 0.9$, $y_m = 132 \text{ mm}$, $y_f = 52 \text{ mm}$).

Experimental result	Test Sp-1	Test Sp-2	Test Sp-3	Test Sp-4	Test Sp-5	Test Sp-6
Spur dike description notes	Rectangular, protrusion length equal to the width of floodplain		Figure 9-24		Figure 9-25	Figure 9-26
Spur dike protrusion length, $L_{sdp} (L_a)$	0.7	1.0	0.7	0.7	0.7	1.0
Distance between the farthest spur dike tip at the main channel end and abutment tip, $D_s (L_a)$	2.0	2.0	1.0	1.5	1.5	0.6
Spur dike orientation angle with respect to the flow, θ (deg)	90	90	45	45	45	90
Run time, t_e (hours)	20.9	25.7	80.0	28.0	24.0	43.0
Time-averaged scour depth at abutment, $d_{abut,avg}$ (mm)	45.2	46.0	46.9	45.0	43.3	58.0
Percent of scour reduction, $\%_{max,abut,avg}$ (%)	32.2	34.8	39.6	35.2	36.5	20.6
Maximum scour depth at spur dike, $d_{max,sp,avg}$ (mm)	--	105.2	144.0	139.0	135.3	--

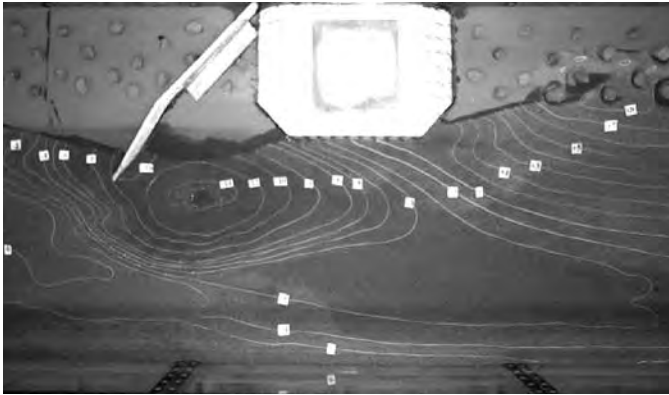


Figure 9-24. Photograph of Sp-3 (flow is from left to right).

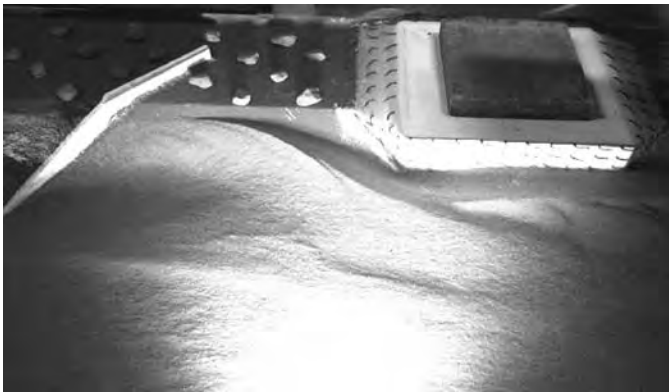


Figure 9-25. Photograph of Sp-5 (flow is from left to right).

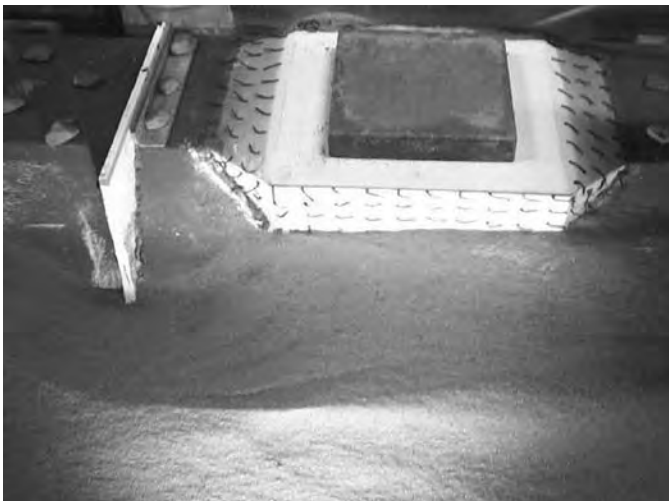


Figure 9-26. Photograph of Sp-6 (flow is from left to right).

extending out into the main channel perpendicular to the flow direction. At the stream end of each spur dike was a transverse slope of 22/13.2. Therefore, the top protrusion length of the spur dike was L_a (44 cm) and the bottom protrusion length

was $1.5L_a$ (66 cm). Each spur dike had a top width of 100 mm and a bottom width of 400 mm. The rocks were 6.7 to 9.5 mm in diameter. In these cases, the flow depth on the floodplain, y_f , was 52 mm and the flow depth in the main channel, y_m , was 132 mm. The mean velocity ratio, V/V_c , was 0.9 in the middle of the main channel. The top of each spur dike was the same height as the top of the abutment. The experimental data for rock wall spur dikes in clear-water scour conditions are summarized in Table 9-9.

The clear-water rock spur dike data, illustrated in Figures 9-27 through 9-30, show that spur dikes with a top length of $1.0L_a$ and bottom length of $1.5L_a$ provided protection to the bridge abutment from scour. These lengths are the minimum lengths required to be sufficient to protect the abutment.

It was found from Tests Sp-8 (Figure 9-28) and Sp-9 (Figure 9-29) that as the distance between two successive spur dikes increased from $1.0L_a$ to $2.0L_a$, the scour depth between the first two spur dikes increased from 76.2 mm to 131.4 mm, more than a 70-percent increase. Although this increase in scour depth did not pose a direct threat to the abutment, it did threaten the two spur dikes and could have caused these spur dikes to partially fail. Therefore, the increase in scour depth ultimately may pose an indirect threat to the abutment. From the scour condition between the second and the third spur dikes in these two tests, it was found that in Test Sp-8, the scour depth was 66.1 mm and greater than the scour depth in Test Sp-9. However, the scour hole in Test Sp-8 was deflected out into the main channel by the spur dikes and had no effect on the abutment, while in Test Sp-9, the abutment was threatened. Therefore, the best spacing between spur dikes is concluded to be $1.0L_a$.

Generally, the larger the number of spur dikes, the better the abutment will be protected, but at a higher cost. To minimize the cost, the number of spur dikes should be minimized. With this in mind, Sp-10 (Figure 9-30) was performed with only two end-slope spur dikes attached at the upstream and downstream corners of the abutment. It was found that the two spur dikes located in this configuration directed the flow away from the abutment, thereby protecting the abutment and upstream and downstream banks.

The advantages of these two end-slope spur dikes are that (1) they can direct the flow away from the abutment and protect the abutment; (2) they can provide extra stabilization to the abutment, especially when some rocks fill in the existing scour holes at both corners of the abutment; (3) as the scour in the bridge crossing develops, the two spur dikes sink and collapse to the original bed level and the rock material is distributed by the flow such that they are still able to function as riprap to protect the abutment; and (4) the two spur dikes attached at the abutment face use less rock than spur dikes attached at the floodplain bank. The disadvantage of the two end-slope spur dikes is that they may cause

Table 9-9. Clear-water experimental data of rock spur dikes ($Q = 0.0368 \pm 0.0016 \text{ m}^3/\text{s}$, $t_e = 80$ hours).

Experimental Result	Test Sp-7 (Figure 9-27)	Test Sp-8 (Figure 9-28)	Test Sp-9 (Figure 9-29)	Test Sp-10 (Figure 9-30)
Number of spur dikes, N_{sd}	2	3	3	2
Spacing between spur dikes or spur dike and abutment $D_s (L_a)$	1	1	2	1
Time-averaged scour depth at abutment, $d_{abut,avg}$ (mm)	0	0	20.0	0
Percent of scour reduction, $\%_{max,abut}$ (%)	100	100	74.3	100
Maximum scour depth behind the first spur dike, $d_{max,sp1,avg}$ (mm)	87.5	76.2	131.4	75.6
Maximum scour depth behind the second spur dike, $d_{max,sp2,avg}$ (mm)	110.0	66.1	35.0	103.0
Maximum scour depth behind the third spur dike, $d_{max,sp3,avg}$ (mm)	--	77.1	68.9	--

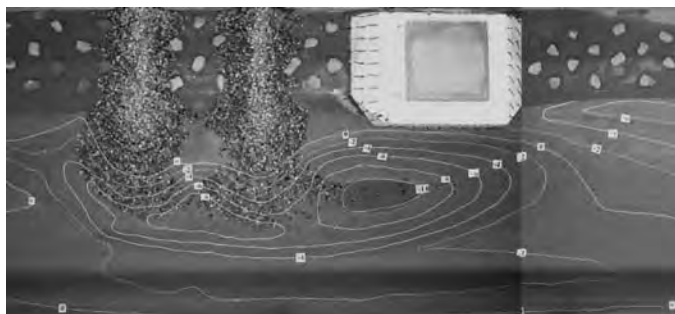


Figure 9-27. Scour contour of Test Sp-7 with two spur dikes upstream of the abutment (flow is from left to right).

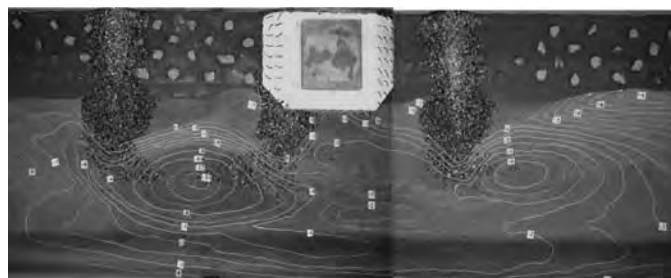


Figure 9-29. Scour contour of Test Sp-9 with three spur dikes, including the one formed by the abutment (flow is from left to right).

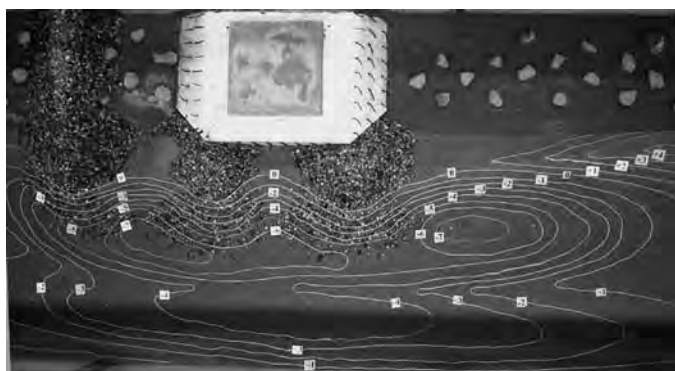


Figure 9-28. Scour contour of Test Sp-8 with three spur dikes, including the two formed by the abutment (flow is from left to right).

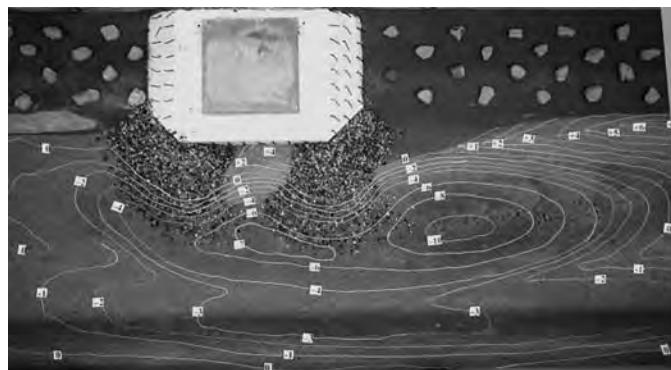


Figure 9-30. Scour contour of Test Sp-10 with two spur dikes, both located at the abutment (flow is from left to right).

contraction scour. In relatively wide bridge crossings, this may not cause a significant problem, but it may be a problem for narrower ones. No significant backwater increase due to the addition of the rock spur dikes was observed in any of the experiments, so increased backwater is not seen as a disadvantage.

Positioning of the spur dikes is important to the protection of the abutment. As shown in the baseline case, the upstream

corner of the abutment was the point that was most likely to scour. Another scour-prone location would be the downstream end of the abutment where the flow leaves the bridge crossing and separates. Therefore, spur dikes located at both ends of the abutment yielded the best results, as shown in Test Sp-10. The advantage of this configuration is that by being attached to the face of the abutment instead of the bank of the flood channel, the amount of rock material is minimized and the cost of the construction of the spur dikes is reduced.

Table 9-10. Live-bed experimental data of rock spur dikes ($Q = 0.0627 \pm 0.003$ m³/s for a velocity ratio of 1.5 and 0.0985 m³/s for a velocity ratio of 2.3, $y_m = 132$ mm, $y_f = 52$ mm, running time, $t_e = 50$ hours).

Experimental Result	Test Sp-11 (Figure 9-31)	Test Sp-12	Sp-13 (Figure 9-32)	Sp-14 (Figure 9-33)
Number of spur dikes, N_{sd}	2	3	3	2
Velocity ratio, V/V_c	1.5	1.5	1.5	2.3
Time-averaged scour depth at abutment, $d_{abut,avg}$ (mm)	-10.3*	-14.2*	-26.6*	-3.0*
Percent reduction in time-averaged scour depth at abutment, % $_{max,abut,avg}$ (%)	114	120	136	100
Time-averaged scour depth in front of the first spur dike, $d_{max,sp1,avg}$ (mm)	51.1	44.5	53.9	69.7
Maximum instantaneous scour depth in front of the first spur dike, $d_{max,sp1,inst}$ (mm)	103.5	95.1	89.0	109.4
Time-averaged scour depth at the second spur dike, $d_{max,sp2,avg}$ (mm)	49.2	50.3	46.8	--
Instantaneous scour depth at the second spur dike, $d_{max,sp2,inst}$ (mm)	99.3	74.9	77.4	--

* Negative scour depths indicate deposition.

From the clear-water experimental data, the configurations of Test Sp-8 and Sp-10 were considered to have the most potential for protecting the abutment and were tested further under live-bed flows. No further experiments were conducted with the configurations used in Sp-7 or Sp-9.

The same spur dike configurations used in Tests Sp-8 and Sp-10 were tested under live-bed conditions as countermeasures against scour at the abutment. Test Sp-11 had basically the same spur dike configuration as Case Sp-10. Test Sp-12 had a similar spur dike configuration as Test Sp-11 except that there was initially a semicircular ring-shaped apron around each of the spur dike ends. Each apron had a width of about 200 mm and was about three rock diameters thick. Tests Sp-13 and Sp-14 had similar spur dike configurations as Test Sp-10 except the aprons and rock size varied. There were similar aprons around the first two spur dikes in the later cases. In these cases, the flow depths were the same as for the clear-water experiments. The velocity ratios used were 1.5 and 2.3. The rock diameters used were 19 to 50 mm for the 1.5 velocity ratio and 500 to 700 mm for the 2.3 velocity ratio. These rock sizes were chosen to avoid rock entrainment and transport by the flow. The top of each spur dike was approximately the same height as the top of the abutment. The live-bed experimental data are listed in Table 9-10.

Data of Test Sp-11, illustrated in Figure 9-31, showed that with a velocity ratio of 1.5, two dikes attached at both ends of the abutment were able to reduce scour over 100 percent (i.e., cause deposition). Deposition of 10 to 40 mm occurred between the two slopes at the abutment during 50 hours of running time. The maximum scour at these spur dikes happened at Point A, where the foot of the upstream bank and the upstream side of the first spur dike meet. This was different from the scour pattern in clear-water scour conditions. Sediment moved along a scour zone starting from Point A and

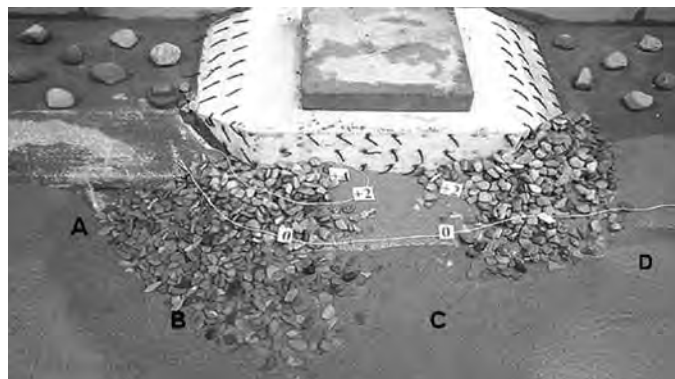


Figure 9-31. Test Sp-11 with two spur dikes, one at each end of the abutment (flow is from left to right).

proceeded along the edge of the launched apron of the spur dikes toward Points B, C, and D, covering part of these aprons and extending past the bridge crossing while keeping a distance from the abutment face. Therefore, after equilibrium was reached, the deposition between the two slopes at the abutment was not affected any more. Local scour holes were found at Points C and D, where flow separated between the two spur dikes. The top of the two spur dikes was initially as high as the flow surface in Test Sp-11. As the scour developed, the rocks on the slope of the spur dikes kept sliding into the scour hole, causing the top of the two spur dikes to subside until the equilibrium state of the scour process was reached. At the end of the test, the top of the first spur dike sank 75.0 mm and the top of the second spur dike sank 20.0 mm. To reduce this sinking, Test Sp-12 was performed with two semicircular aprons of 200-mm width and three-rock-diameter thicknesses placed around the edge of each spur dike. After 50 hours of running time, the presence of the aprons helped improve the deposition between the two spur

dikes at the abutment and reduced the scour depth at the upstream side of the first spur dike, as shown in Table 9-10. However, the top of the first spur dike still sank 50.0 mm.

Although the configuration in Tests Sp-11 and Sp-12 can protect the bed around the abutment, there is a concern about the portion of the floodplain at the upstream corner of the abutment. For erodible floodplains, the spur dikes thus placed are not able to protect the floodplain. Compared with Tests Sp-11 and Sp-12, data in both Table 9-10 and Figure 9-32 showed that the configuration of Test Sp-13 can protect not only the channel bed around the abutment but also the floodplain and the abutment fill. The minimum deposition of sediment around the abutment was found to be 26.6 mm. Also, because of the protection of the first spur dike, the spur dikes at both corners of the abutment experienced very little subsidence.

The same spur dike configuration as in Test Sp-13 was tried further in Test Sp-14 with a velocity ratio of 2.3. The spur dikes were made of rocks with diameter sizes 500 to 700 mm in order to resist transport by the flow. The spur dikes still protected the abutment from scour successfully, as shown in Table 9-10 and Figure 9-33.

Rock spur dikes have more advantages than solid spur dikes. First, unlike solid spur dikes, rock spur dikes do not need a traditional foundation. Instead, they can use aprons around the structure edges as the scour holes develop and

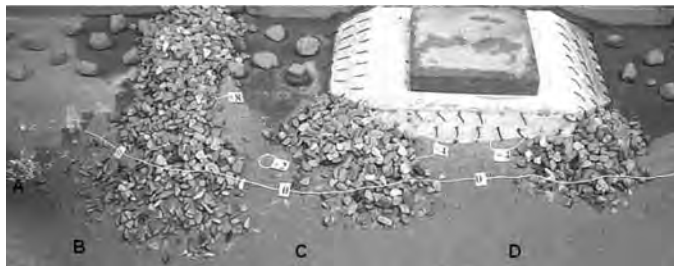


Figure 9-32. Test Sp-13 with three spur dikes (flow is from left to right).



Figure 9-33. Test Sp-14 with three spur dikes (flow is from left to right).

prevent them from failing. Second, a sloped end at the main channel end of a spur dike whose top protrusion length is L_a will provide extra protrusion length and more deflection. Third, rock spur dikes may make deposition at the upstream end of the abutment possible. The reason that the sediment did not deposit at the upstream corner of the abutment is that the abutment structure had a very smooth surface, and the flow velocity near the abutment surface was relatively high. This unimpeded velocity prevents settling of sediment. To conquer this problem, a pile of gravel placed at the upstream abutment end increases the roughness of the abutment and decreases the flow velocity so that sediment can deposit at the upstream corner of the piled rocks. Fourth, upward-sloping rock spur dikes with relatively high friction roughness slow and guide the flow to climb up the slope instead of producing scour-inducing downflow.

9.4.4 Design of Spur Dikes for Scour Prevention at Wing-Wall Abutments

From the experimental results, it was concluded that spur dikes with a top protrusion length of $1.0L_a$ and a bottom length of $1.5L_a$ were sufficiently long to protect the bridge abutment. The amount of material in the spur dikes can be greatly reduced if the spur dikes are attached at the face of the abutment. The top length $1.0L_a$ is believed to be the minimum length required to protect the abutment, while the bottom length is designed as a function of the rock's angle of repose. It was concluded that, for straight channels, the best spacing between successive spur dikes was $1.0L_a$. A spacing of $1.0L_a$ or less was able to restrict the flow from full separation behind each spur dike. As a consequence, the scour depth behind each spur dike was reduced, and the scour hole was pushed farther away from the spur dike end into the main channel.

It was concluded that three spur dikes, with the first one located $1.0L_a$ distance upstream of the upstream abutment corner, and the remaining two attached at the upstream and downstream corners of the abutment, would be the best configuration for preventing scour of the bed near the abutment for this experimental setup (streamwise width of abutment is around $1.0L_a$). For a bridge abutment whose streamwise width is longer than $1L_a$, a spur dike attached at the downstream end is still recommended, but with additional spur dikes located upstream at distances of $1.0L_a$ until the upstream corner of the abutment is met. One more spur dike is preferred upstream of the one at the upstream corner of the abutment. For a bridge abutment whose streamwise width is less than the flow-perpendicular length of the abutment (L_a), three spur dikes are recommended: one at the upstream corner of the abutment, one at a distance of $1.0L_a$ upstream of the abutment, and the other at the downstream corner of the abutment.

In addition to the variables directly tested in the laboratory experiments described above, the following design guidelines are offered. The top height of each spur dike should be high enough so that it is not overtopped by the flow during flooding, since all of the experiments described here are for emergent spur dikes and the flow patterns will be greatly altered if the spur dikes were overtopped. The rock size of the spur dikes should be great enough to resist the flow stress in the worst flood situation. It was observed in the laboratory that end slopes of spur dikes can be constructed as steep as possible since they are able to adjust themselves to a stable state as scour holes develop around them. Semicircular aprons launch rocks into the scour hole during its development.

9.4.5 Conclusions Regarding Spur Dike Countermeasure

For the clear-water and live-bed scour at a Type III abutment configuration in a straight channel, it can be concluded that:

- A single spur dike made of a solid plate, having a protrusion length the same as or shorter than the abutment, and placed upstream of the abutment was not able to protect the abutment. The downflow and the principal vortex are very strong at the stream end of the structure. As a consequence, a significant scour hole was always found at the end of the structure, and this hole threatened both the structure and the channel bank.
- Rock spur dikes show several advantages over rigid spur dikes and are preferred.
- Three rock spur dikes, as configured in Tests Sp-9 and Sp-13, were considered the best configuration for protecting the abutment. This configuration can provide 100-percent protection to the abutment under the velocity ratios of 0.9, 1.5, and 2.3. Two spur dikes at the upstream and downstream

corners of the abutment were also successful at preventing scour in both clear-water and live-bed experiments.

9.5 Abutment Collar Countermeasure

A flow-altering countermeasure that has not previously been tested for abutments in a compound channel is a horizontal collar. After describing the flow patterns around a collar, results are given for various collar configurations.

9.5.1 Introduction

Collars attached to piers have been studied as either an armor layer of the bed or a downflow-halting device by Kapoor and Keana (1994), Kumar et al. (1999), and Borghei et al. (2004). Collars block the downflow found at the leading edge of piers and abutments and eliminate scour-inducing secondary vortices.

This chapter describes laboratory experiments with collars at a vertical-face wing-wall abutment placed at the main channel edge, an abutment configuration typical of older bridges on smaller streams.

9.5.2 Flow Pattern at Collar Attached to Abutment

Figure 9-34 shows the flow patterns of a collar as a countermeasure against abutment scour in a compound channel. A collar is attached around the bridge abutment and has a certain aerial coverage. A collar thus installed is expected to be able to prevent the bed materials from being entrained by the return flow from the floodplain, the downflow, and the secondary vortex systems. In the experimental studies described in this section, the aerial extent in all directions and the vertical elevation of the collar were studied under clear-water

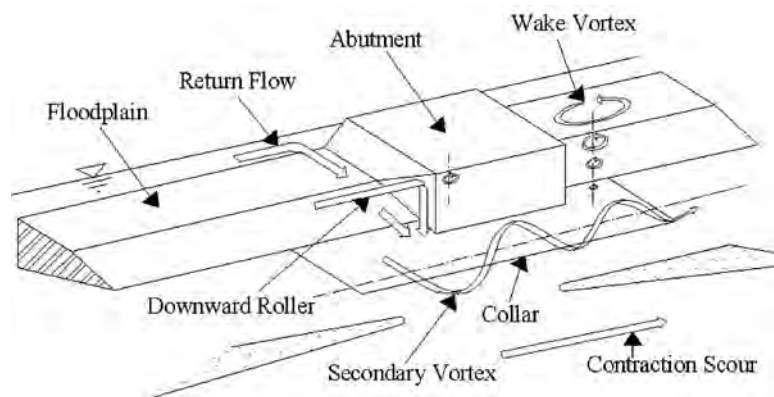


Figure 9-34. Flow patterns of a collar as a countermeasure against abutment scour in a compound channel.

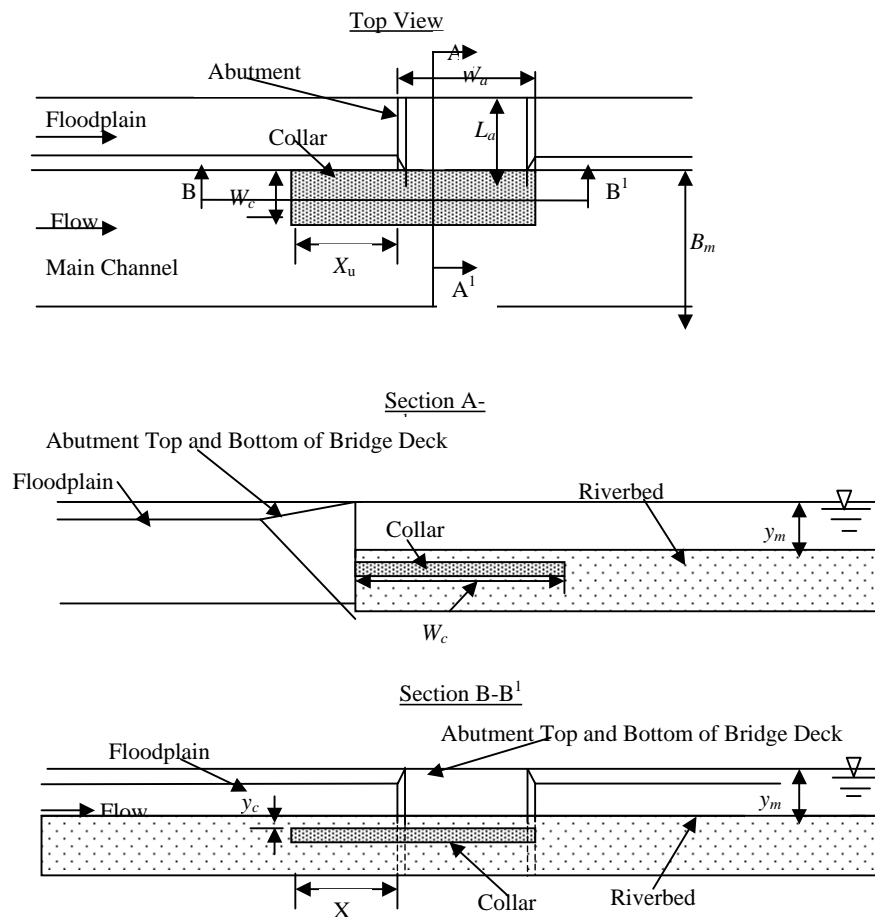


Figure 9-35. Abutment scour collar countermeasure.

conditions to determine the best configuration for a collar to be a successful countermeasure. Figure 9-35 shows the collar countermeasure.

9.5.3 Collar Results

A series of collars of different lengths and widths were attached to the bridge abutment under clear-water conditions as countermeasures against scour at the abutment. These collars were made from steel and were seated horizontally at the desired elevation. The flow depth on the floodplain, y_f was 52 mm, and the flow depth in the main channel, y_m , was 132 mm. The velocity ratio, V/V_c , was 0.9 at the center of the entire channel, as in the baseline tests. Table 9-11 gives the dimensions of each collar configuration tested, as well as the experimental results.

Figure 9-36 shows scour contours for the equilibrium condition for Test T3. It was found that the collars were able to protect the bridge abutment efficiently by isolating the return flow and the secondary vortices from the bed around the abutment that ordinarily would cause local scour. The minimum collar dimensions that eliminated local scour were

those with a width of $0.23L_a$ (L_a is the abutment length perpendicular to the flow direction) for elimination of local scour, a width of $0.8L$ for maximum reduction of scour at the edge of the collar, and a vertical location of $0.08y_m$ below the mean bed sediment elevation (y_m is the main channel flow depth). After removal of the collar, there was no scour observed under the collar around the abutment for any of the cases tested.

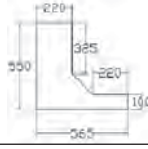
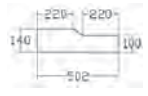
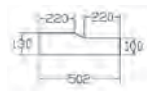
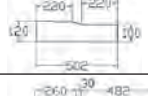
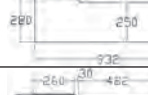
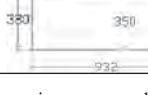
9.5.4 Discussion

Protrusion Width

Figure 9-37 shows the maximum scour depth at both the bridge abutment and the main channel edge of the collar versus the transverse collar width for all collar cases when the collar elevation was 10 mm below the initial bed level. It can be seen from Figure 9-37 that the maximum local scour depth under the main channel edge of the collar decreased from -71.0 mm to -10.0 mm as the width of the collar beyond the abutment increased from 100 mm to 350 mm.

Further examination of the experimental results shows that the maximum local scour depths at the main channel edge of

Table 9-11. Dimensions and positions of collars tested (run time = 80 hours, $y_m = 132$ mm, $y_f = 52$ mm, $Q = 0.0387 \pm 0.001$ m³/s, $V/V_c = 0.9$).

Test No.	Dimensions (mm)	Elevation	$d_{max.abut}$ (mm)	Percent reduction in time-averaged scour depth at abutment, % _{max.abut.avg}	$d_{max.col}$ (mm)
T1		Floodplain level	44.8	42.3	--
T2		Bed level	35.1	54.8	81.4
T3		10 mm below bed (Figure 9-36)	19.2	75.3	71.0
T4		20 mm below bed	20.0	74.3	78.9
T5		10 mm below bed	10.0	87.1	45.4
T6		10 mm below bed	10.0	87.1	10.0

Note: $d_{max.abut}$ = maximum scour depth at the abutment foundation; $d_{max.col}$ = maximum scour depth at the collar edge.

each of these collars had a similar magnitude as the scour depth at the same location in the baseline case with no countermeasures. Figure 9-38 shows the transverse bed profile in the bridge crossing of the baseline case and the scour profile formed by the maximum local scour depth values under the edge of the various collars of different widths. Figure 9-38 suggests that the presence of the collar did not change the strength of the vortex, but protected the abutment from scour

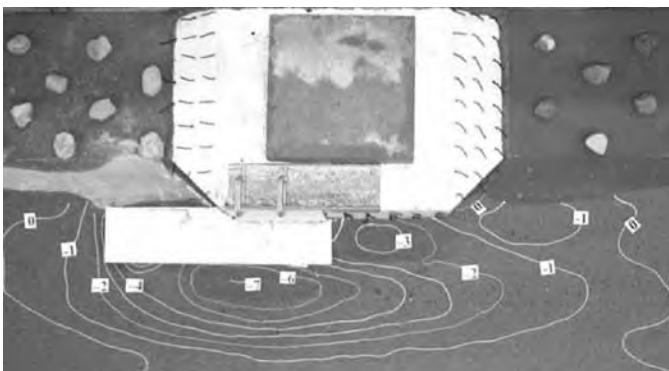


Figure 9-36. Elevation contours of Test T3 with collar at 1 cm below bed elevation (flow is from left to right).

by not allowing the scour-inducing secondary vortex to interact with the bed sediment.

Collar Elevation

To determine the optimal collar elevation, three different elevations of the collars were used in the experiments. Figure 9-39 shows the scour depth at the abutment and at the edge of the collars versus collar elevation for collars with a width of 100 mm. It is evident that a collar elevation of 10 mm below the original bed level had the least scour. This corresponds to an elevation of $1/13.2$, or $0.08y_m$, where y_m is the flow depth in the main channel. The collar should be lower than the bed in order to keep the secondary vortex above it and not interacting with the bed sediment.

Streamwise Collar Length

At the upstream edge of the collar, a shallow scour hole perpendicular to the flow was found in Tests T2 through T4. This scour hole started from the main channel bank and went transversely toward the opposite channel wall and was connected to the scour hole at the main channel edge of the collar. This scour hole remained at the collar leading edge and, therefore, did not

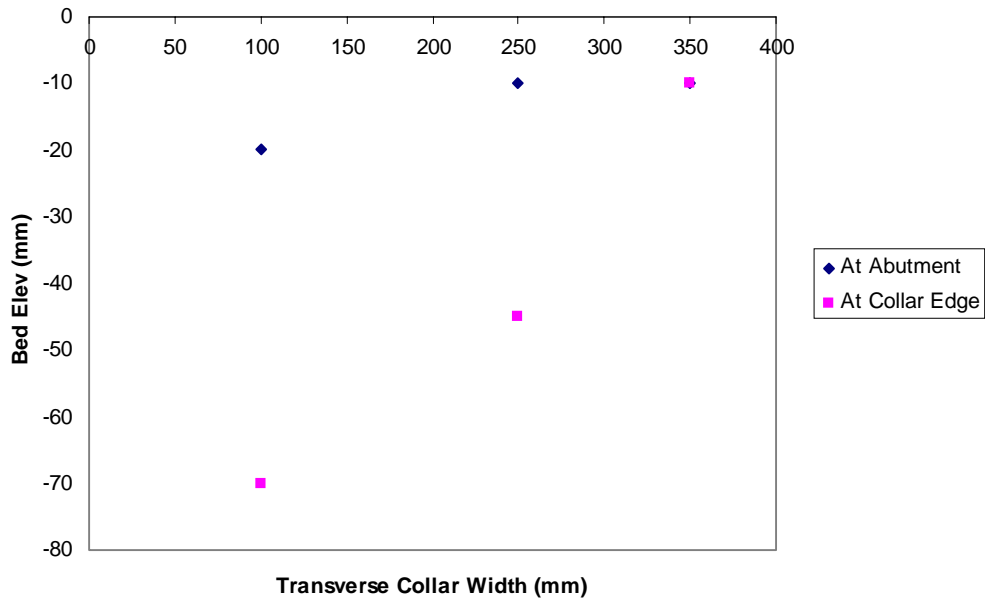


Figure 9-37. Scour at both bridge abutment and the main channel edge of the collar versus the transverse collar width for a collar elevation of 10 mm below the bed.

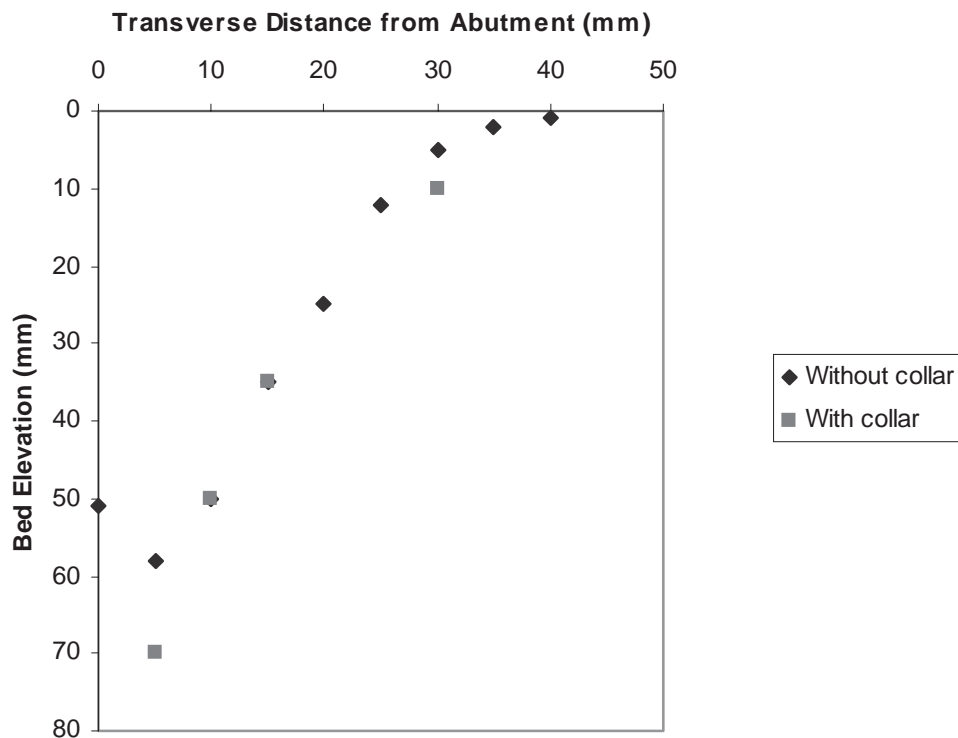


Figure 9-38. Transverse scour profile in the bridge crossing of the baseline case and the scour profile formed by the maximum local scour depths under the main channel edge of the various collars of different widths at the end of 80 hours (view is looking downstream).

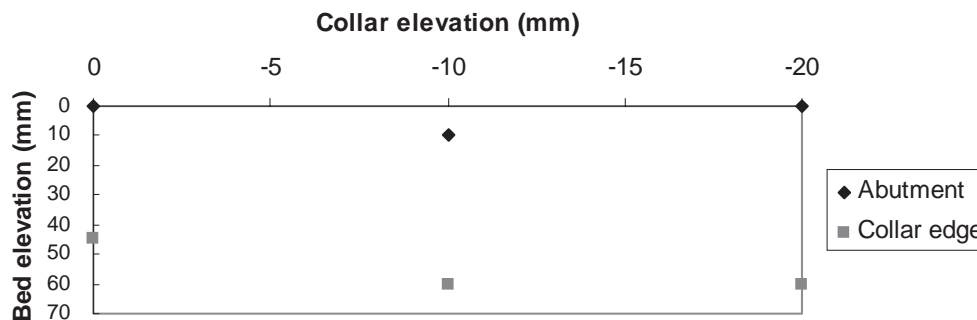


Figure 9-39. Bed elevation at the abutment and at the edge of the collars versus collar elevation (all collars had a transverse width of 10 mm from the abutment face).

threaten the abutment. In Tests T5 and T6, the upstream end of the collars was still buried in the sand at the end of the experiments and, therefore, no scour was found. The upstream end of the collar should be long enough that the scour hole won't threaten the abutment.

There was always scour downstream of the trailing edge of the collar. For Tests T3 and T4, the trailing edge of the collar ended in the middle of the bridge crossing, and scour holes of more than 19.2 mm at the abutment were found in both cases. These scour holes posed a threat to the middle of the abutment structure and may be eliminated simply by extending the trailing edge of the collar to a location that is downstream of the abutment structure, as shown in Figure 9-40. The extension of the downstream collar length may increase scour magnitude. This was observed in Tests T5 and T6, where the scour hole was more than 5 cm in Test T5 and more than 6 cm in Test T6. The scour location is not in the bridge crossing, however, and, therefore, should not correspond with a pier location.

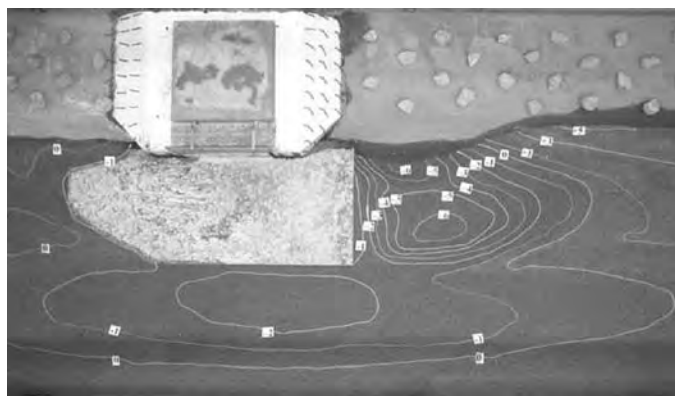


Figure 9-40. Scour contour of Test T6 with a collar attached along the abutment (collar width is 350 mm, collar elevation is 10 mm below the original bed, flow is from left to right).

Temporal Scour Variation

It was observed that, unlike the rapid scour at the upstream and downstream abutment corners in the baseline case, the scour in the first 10 hours under the main channel edge of the collar was very slow in all collar cases. Figure 9-41 shows the temporal evolution of scour under the edge of the plate in Test T3. Note the delayed scour in the first 10 hours by collars. This delayed scour constitutes another advantage of using the abutment collars.

9.5.5 Conclusions

From these clear-water experimental data, the following conclusions can be made:

- Collars were found to be effective at preventing local scour at wing-wall bridge abutments. The collars isolated the turbulent flow and vortex systems from the bed material and thereby prevented the bed underneath the collar from scouring.
- The farther the collar extended downstream of the abutment, the farther downstream the scour hole was located. As the transverse width of the collars increased, the depth of the scour hole at the edge of the collar decreased.

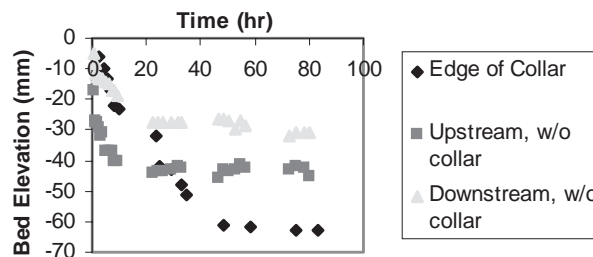


Figure 9-41. Scour depth variation under the main channel edge of the collar and for both the upstream and downstream scour holes versus time in Test T3.

The scour became insignificant as the main channel edge of the collar was extended beyond the local scour hole area measured in the baseline case without countermeasures. The trailing edge of the collar should extend to a location downstream of the abutment.

- Based on these experiments, the collar elevation should be $0.08y_m$ below the original bed level and the collar width should be at least $0.23L_a$, where L_a is the abutment length perpendicular to the flow direction.

9.6 Summary

Scour at bridge abutments can cause damage or failure of bridges and result in excessive repairs, loss of accessibility, or even death. To mitigate abutment scour, both clear-water and live-bed laboratory experiments in a compound channel were performed using parallel walls and spur dikes. In addition, collars were also tested under clear-water conditions only.

A series of experiments were performed in an open-channel flume with a compound channel for clear-water and live-bed scour conditions.

Two types of parallel walls were tested: the first type was made of a wood plate, and the second was made of piled rocks. For solid parallel walls, a series of rectangular straight plates of different lengths were used attached to the upstream end of a wing-wall abutment parallel to the flow direction. The velocity of the flow for the three cases was 0.9, 1.5, or 2.3 times the incipient motion velocity for bed sediment movement. The bed material was sand with a mean diameter of 0.8 mm and a standard deviation of 1.37. All the plates were seated at the bottom of the compound channel bank slope and were even with the abutment face.

It was found that straight plates thus situated caused the scour hole to be shifted away from the upstream corner of the abutment and to be effective as a countermeasure to

prevent scour there. As the length of the plate increased, the scour at the abutment declined. It was found that a length of $1.6L_a$, with L_a being the length of the abutment perpendicular to the flow, caused the scour to be eliminated at the abutment for a velocity ratio (V/V_c) of 0.9 (clear-water scour). Similarly, a $1.6L_a$ -long wall can eliminate the time-averaged scour depth at the abutment 100 percent for a velocity ratio of 1.5 and 70 percent for a velocity ratio of 2.3. If the upstream end of the wall is anchored below the scour depth, this countermeasure can be feasible for situations where rock is expensive.

For parallel rock walls, various values of wall length and protrusion length into the main channel were tested. It was found that a wall that does not protrude into the main channel with a length of $0.5L_a$ minimizes scour at the abutment for all three different flow velocity ratios (0.9, 1.5, and 2.3).

A series of configurations of spur dikes with varying lengths, spacings, number, and positions with respect to the abutment were tested. The most effective configuration to prevent local scour at the abutments consisted of three spur dikes composed of rock located upstream of the abutment and at the two corners.

In addition, collars at the abutment were tested. It was found that these collars were able to protect the bridge abutment efficiently by eliminating secondary vortices that ordinarily would cause local scour. The minimum collar dimensions that eliminated local scour were a flow-perpendicular width of $0.23L_a$ (L_a is the abutment length perpendicular to the flow direction) and a flow-parallel length of 0.7 times the flow-parallel abutment width. It was determined that a vertical location of $0.08y_m$ (where y_m is the main channel flow depth) below the mean bed sediment elevation gave the best results of scour reduction. In addition, the collar not only reduced scour magnitude near the abutment, but also retarded the development of the scour hole.

CHAPTER 10

Design Guidelines

10.1 Introduction

This chapter presents design guidelines for scour countermeasures for use at bridge abutments. The guidelines use the findings of the laboratory experiments discussed in Chapters 7 through 9. Additionally, the guidelines use information obtained from the survey of state DOT countermeasure practice as well as from existing literature on scour control. The guidelines are structured in terms of a simple selection process described in Section 10.1. This process identifies the countermeasure concepts that may be appropriate for addressing a scour concern, indicates possible construction options, and then provides the design relationships associated with the layout and dimensioning of the countermeasures developed in this project.

Because the project focuses on countermeasures for mitigating scour at bridge abutments, the countermeasure concepts do not address in detail countermeasure concepts for mitigating scour of channels at locations away from a bridge waterway. Instead, the guidelines identify these countermeasures and refer to current design monographs that give the pertinent design guidelines.

The design guidelines detailed in this chapter also address the set of criteria mentioned at the outset of this report:

1. Technical effectiveness (including no substantial adverse effects),
2. Constructability,
3. Durability and maintainability,
4. Aesthetics and environmental issues, and
5. Cost.

It must be stated that the guidelines can only address Criteria 2 through 5 in relative terms. Though the criteria of constructability and durability and maintainability were expressly considered when identifying the countermeasures detailed in this chapter, the present project did not dwell on the criteria of aesthetics and environmental issues or cost.

10.2 Countermeasure Selection and Construction Options

The several processes creating a scour concern for an abutment require different countermeasure concepts, and each countermeasure concept can be constructed and implemented in a variety of ways. As indicated in Table 10-1, and as discussed in Chapter 3, there are three main scour concerns:

- **General bed degradation, or overall scour**, which results from a reduction in the bed-load supply of sediment to the bridge site (i.e., degradation progressing from upstream to downstream) or a steepening of channel slope owing to head-cutting of the channel bed (i.e., degradation progressing from downstream to upstream).
- **Approach-flow scour**, which results from channel shifting or thalweg shifting.
- **Localized scour at the abutment**, which results from localized vortices.

Table 10-1 shows the corresponding countermeasure concepts for each of the three concerns, as well as construction options available for implementing the countermeasure concepts.

The steps for proceeding through the guidelines given herein are as follows:

1. Identify the process causing the scour concern.
2. Select a countermeasure concept.
3. Select a construction method for the countermeasure concept (using Criteria 1 through 5 above).
4. Design the countermeasure.
5. Review the design in terms of Criteria 1 through 5 above.

Although these steps encompass the main design considerations, the steps are not meant to be prescriptive. It is anticipated that each design office undertaking the design of a

Table 10-1. Scour concerns, countermeasure concepts, and construction options.

Abutment Scour Concern	Countermeasure Concept	Construction Option
General bed degradation	Use a bed-control structure	<ol style="list-style-type: none"> 1. Place weir across channel to maintain bed level at bridge waterway 2. Place sheet pile around abutment to maintain bed level at abutment
Channel or thalweg shift	Use a channel-control structure	<ol style="list-style-type: none"> 1. Use a channel-control structure to guide flow away from a bank 2. Use a bank-control structure to armor the bank and thereby prevent further channel shifting 3. Shift the abutment back and add a bridge span
Localized scour at abutment	Modify the flow field at the abutment	<ol style="list-style-type: none"> 1. Align approach-channel bank(s) 2. Shift the abutment back and add a bridge span 3. Add a relief bridge 4. Add a parallel wall or guidebank(s) (Ch. 9) 5. Place flow-deflection spur dike(s) or groin(s) (Ch. 9)
	Armor the abutment boundary	<ol style="list-style-type: none"> 1. Place riprap or cable-tied blocks at spill-through abutments located on floodplain (Ch. 8) 2. Place riprap, cable-tied blocks, parallel walls, or spur dikes at wing-wall abutments at main channel bank at narrow crossings (Ch. 7) 3. Armor the outflow region of lateral drains and the adjacent channel bank
	Increase the geotechnical stability of the abutment	<ol style="list-style-type: none"> 1. Place sheet pile around the abutment to retain the embankment

bridge abutment, or taking responsibility for the maintenance of the abutment, will have its own design procedure.

10.3 Channel Bed Degradation

Countermeasures to control bed degradation aim to maintain the channel bed level at the bridge waterway or around the foundations of bridge abutments and piers. If the degradation is progressing from upstream (e.g., because a dam has greatly reduced bed sediment transport in the channel):

- Place a weir across the channel at a location *close* to the downstream end of the bridge waterway or

- Place sheet-piling around the abutment.

If the degradation is progressing from downstream (usually owing to head-cutting):

- Place a low weir across the channel at a location downstream of the bridge waterway or
- Place sheet-piling around the abutment.

According to Lagasse et al. (1995) and others, channel lining with riprap and concrete has proven unsuccessful in stopping degradation. Therefore, it is normal to use a check dam or low weir. Design information on check dams and rock weirs is given by Breusers and Raudkivi (1991).

10.3.1 Low Weirs

In recent years, considerable effort has been devoted to developing low weirs that do not block fish and aquatic creatures from moving along channels. The structures typically have replicated the form and flow features of rock riffles, like small-scale rapids.

A weir is typically constructed of sheet piles, rock mound, or a combination of the two.

The rock weir concept is illustrated in Figure 10-1. The top photo shows an example, and the bottom sketch shows a conceptual drawing. Such weirs are favored by biologists because, in addition to stopping head-cutting, they resemble a natural rock riffle and enable fish and aquatic creature migration upstream or downstream. A rock weir can be constructed to halt bed degradation by head-cutting, but can enable the passage of aquatic creatures. Figure 10-2 shows an example of the combination of sheet-piling and rock weir for a small channel. In this figure, riprap is not protected with

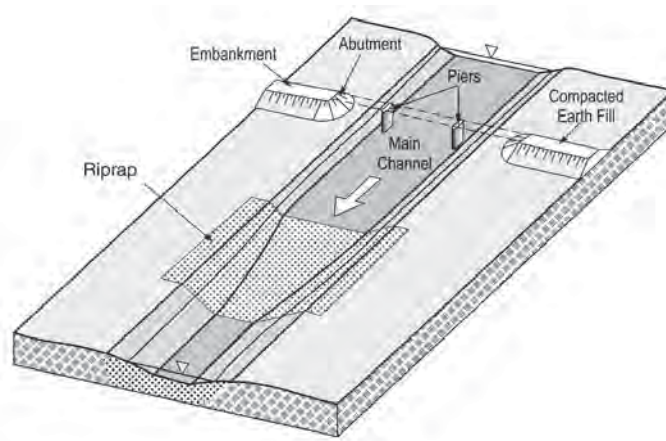
grout, so rocks can be dislodged during high flows. Figure 10-3 shows a weir built only of sheet-piling but including a fish ladder. Sheet pile weirs, though technically effective, are less favored by biologists because of their less-than-appealing appearance.

The following construction and constructability issues should be considered for rock weirs:

- A rock weir should be grouted to ensure that the rock remains in place during high flows. Although grout will crack over time, it still has a longer life than riprap. Grouting may also help protect against the effects of freeze-thaw breakdown of rock.
- The contractor should ensure that the weir's rocks are placed carefully so as not to include large protrusions that may be moved during high flows.
- For larger channels, the weir will have to be constructed with the aid of a barge (see Figure 10-1a).



(a) Example on a wide river where a barge was needed for construction



(b) Conceptual drawing on a small waterway where the rock weir was needed to arrest head-cut migration upstream toward a bridge

Figure 10-1. Rock weir concept.



Figure 10-2. A combination of sheet pile and rock weir located below a bridge to stop knickpoint migration.

The following construction and constructability issues should be considered for sheet pile weirs:

- A sheet pile weir will need scour protection along its downstream side because of flow passage over the weir.
- The channel bank adjoining the sheet pile weir will need concrete or riprap scour protection.
- The sheet piles will have to be located deep enough that they will not fail owing to scour.

10.3.2 Sheet-Piling Around Abutment

A countermeasure practice sometimes used is to place a sheet pile skirt around an abutment base. Figure 10-4 indicates the extent of sheet pile placement around a spill-through abutment. Figure 10-5 illustrates an example where the sheet pile



Figure 10-3. Use of a sheet pile weir, fitted with a fish ladder, to prevent further stream-bed degradation due to head-cutting and to enable fish to migrate upstream.

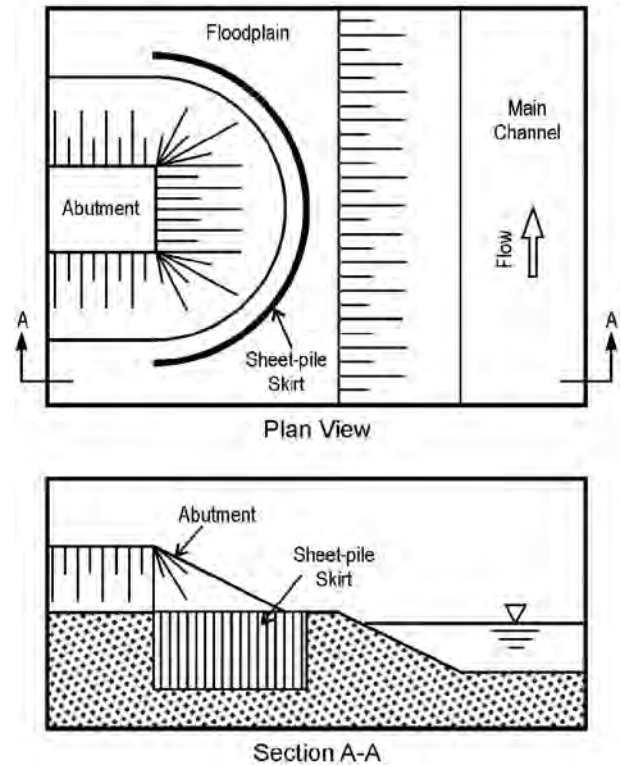


Figure 10-4. Sheet pile skirt around a spill-through abutment.

skirt prevented the possible failure of a spill-through abutment located on a floodplain. The scour condition shown is localized scour consequent to flow contraction and the local flow field generated by the abutment.

The following construction and constructability issues must be considered:

- The sheet-piling, which is not load bearing, should be placed to a depth exceeding the estimated depth of scour.



Figure 10-5. Sheet pile skirt placed to protect a spill-through abutment from collapsing into a large scour hole formed in the floodplain at the abutment.

- The sheet-piling should extend around the front and sides to the end of the bridge.
- The sheet-piling should be a short distance out from the toe of the face slope of the abutment.
- For an existing abutment, sheet-piling can be retrofitted by various means, depending on local site conditions. If access beneath the deck of a bridge is difficult for pile-driving, piles could be driven close to the sides of the deck, then piles at the central portion beneath the deck could be formed with an infill panel placed in an excavated trench, or an infill of large riprap stone could be placed.

10.4 Channel Control

The purpose of approach-channel control is to ensure that the approach flow passes directly through the bridge opening in a manner that does not expose the bridge's abutments, approach embankments, or piers to severe scour. Flow-control methods seek to guide the flow and/or to protect the banks of a channel. In terms of reducing abutment scour, it is important that channel-control countermeasures align the axis of the approach channel so as to be perpendicular to the bridge axis.

There are extensive publications concerning the design of flow-control structures and bank-protection structures. Chapter 5 provides an extensive discussion of these publications. Among the pertinent publications regarding channel-control measures are Acheson (1968), Ahmad (1951), Copeland (1983), Farsirotou et al. (1998), Grant (1948), Khan and Chaudhry (1992), Kuhnle et al. (1997, 1998, 1999), Mayerle et al. (1995), Maza Alvarez (1989), Molinas et al. (1998a, 1998b), Molls et al. (1995), Muneta and Shimizu (1994), Neill (1973), Richardson et al. (1998),

Shields et al. (1995a, 1995b, 1995c), Soliman et al. (1997), Strom (1962), Suzuki et al. (1987), Tominaga et al. (1997), United Nations Economic Commission for Asia and the Far East (1953), Wu and Lim (1993), and Zhang and Du (1997). Richardson and Simons (1984) give design recommendations based on the literature. Lagasse et al. (1995) and Richardson et al. (1991) give design guidelines for impermeable and permeable spur dikes, guide banks, and riprap stability factor design.

10.4.1 Flow Control

The options for flow control vary according to the extent to which the approach flow has to be aligned and guided through the bridge opening. In most cases, the layouts of flow-control structures have to be determined on a site-by-site basis. Sometimes, determining the layout requires investigation by means of a hydraulic laboratory model or a two-dimensional, depth-averaged numerical model.

Flow control typically requires the use of one or more of the following structures for the purpose indicated:

- **Spur dikes** are fitted to force the realignment of a channel and/or to increase flow velocities. Channel realignment may be needed when an approach channel is shifting laterally, as shown in Figure 10-6. Increased flow velocities may be needed in situations where a channel has widened, flow velocities have decreased, and the approach channel is aggrading. Channel aggradation may reduce the flow area of the bridge opening;
- **Bendway weirs or barbs** are fitted to stop lateral shifting of a channel and thereby to redirect the channel optimally through a bridge opening, as shown in Figure 10-7; and,

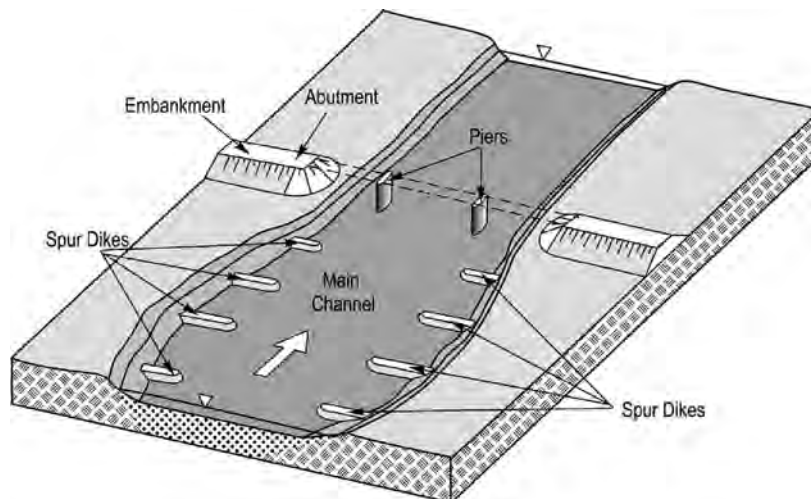


Figure 10-6. Spur dikes placed to narrow a widened approach channel and to ensure desired alignment of approach channel.

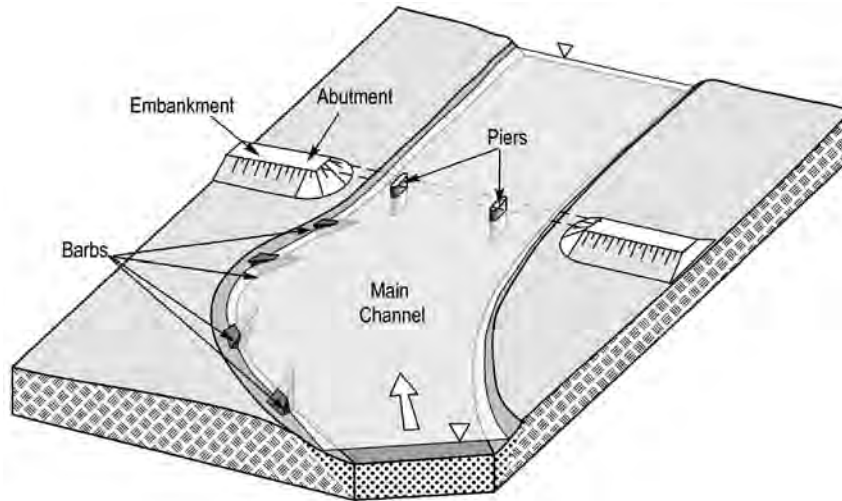


Figure 10-7. Barbs placed to stop lateral migration of an approach channel.

- **Vanes** are an alternative to spur dikes, bendway weirs, or barbs for use in improving approach channel alignment, as shown in Figure 10-8.

These flow-control structures are used in rather specific applications that often have to be tailored to fit local conditions of channel alignment and morphology, as well as bridge extent and alignment. However, because the use of guidebanks and spurs varies from one form to another (e.g., barbs, bendway weirs, and wing dams), it is useful here to mention briefly a couple of preliminary notes regarding their use.

For use of impermeable and permeable spurs, guidebanks, and riprap stability factor design to control the approach

channel to a bridge opening, the following design guidelines are useful to keep in mind:

- The flow field around a typical, straight spur causes bed scour at the spur's tip and sediment deposition (i.e., silting) close to where the spur adjoins the river/stream bank, as illustrated in Figure 10-9a. A spur is useful for defining the local path of flow thalweg (i.e., line of deepest flow), as well as providing local bank protection.
- If the spur points downstream, flow can be drawn to the river/stream bank because the scour hole is moved closer to the river/stream bank. An attracting spur is illustrated in Figure 10-9b.

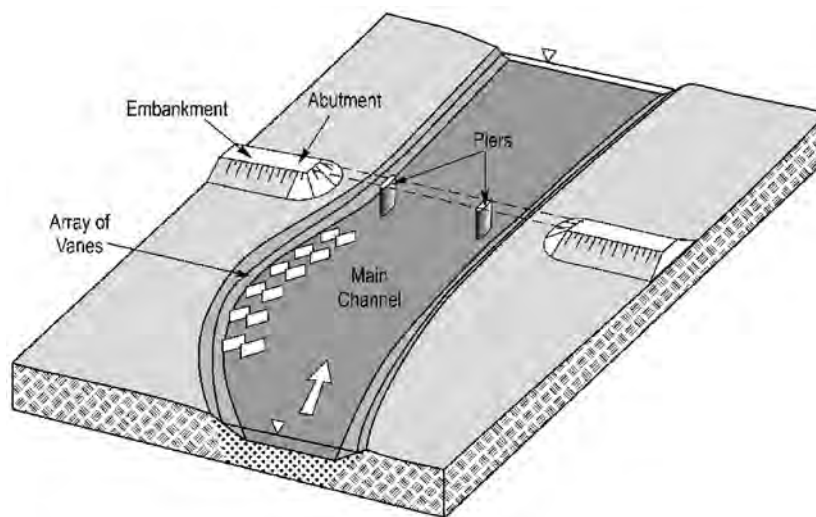


Figure 10-8. Vanes placed to stop lateral migration of an approach channel and to narrow the approach channel to match the width of the bridge opening.

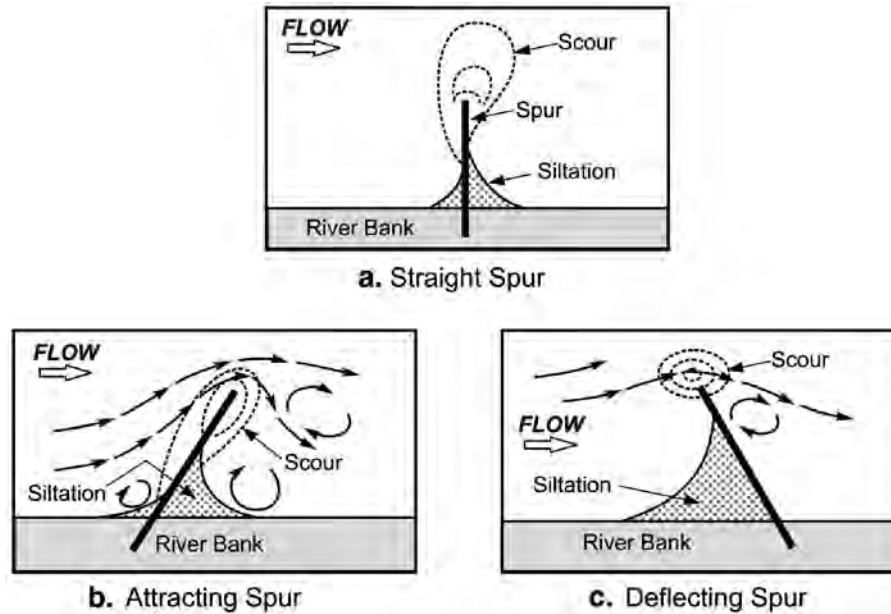


Figure 10-9. Flow, scour, and siltation features for spurs (spur dikes, groins, exposed barbs, and bendway weirs).

- If the spur points upstream, the scour hole is shifted away from the bank, and flow accordingly is deflected away from the bank. A deflecting spur is illustrated in Figure 10-9c.
- Spurs of low crest elevations (e.g., barbs or bendway weirs) are sometimes used for sites where concerns exist about excessive depth produced by a spur, spur retarding of higher flow discharges (e.g., bankfull flow), and debris accumulation on spurs. Additionally, flow passage over the submerged spurs reduces the amount of sediment deposition around the spur.
- Spurs in series are spaced so that the space between spurs just accommodates the wake eddy formed by flow around a spur, as illustrated in Figure 10-10. There is no need to space the spurs more closely. The spurs are spaced too widely if flow is drawn in toward the face of the downstream spur. Figure 10-11 shows spur dike installation along the outside bank upstream of an approach channel to a bridge.

Spurs and their variants can be built from placed rock or from timber posts driven into a stream or river bed. A great variety of sizes and construction methods have been employed in building spurs.

Vanes have been used for erosion reduction on river bends and for stopping river bend migration at a bridge waterway. Vanes are small panels placed in the riverbed at an angle of attack to the flow, which creates a vortex downstream that can be used to manage sediment and alter flow. When placed in an array, vanes deflect water current and bed sediment toward the desired orientation through a bridge waterway.

10.4.2 Bank Protection

The literature on bank protection is extensive and does not need to be elaborated on here. In general, the customary approaches for bank protection are as follows:

1. **Armor the bank.** Place a protective lining to ensure that flow does not erode the surface of the bank. Various forms of armoring are used, notably riprap, rock gabions, and concrete lining.

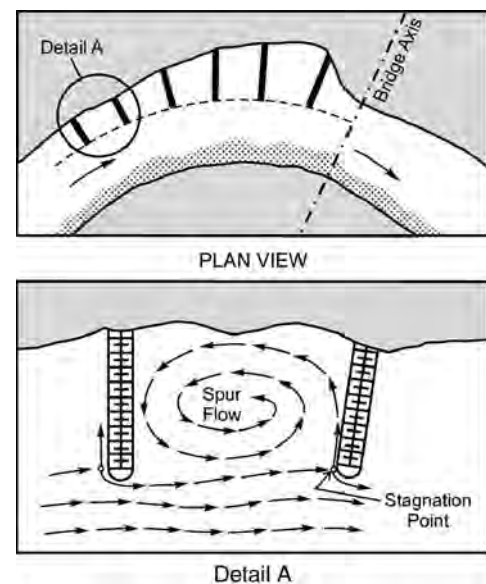


Figure 10-10. Typical spur layout along the convex bank.



Figure 10-11. Spur dike installation along the outside bank upstream of an approach channel to a bridge.

2. **Hardpoints.** Place resistant nodes along the bank to make sure that the bank holds its alignment in situations where the approach flow may otherwise tend to shift the channel laterally. The nodes, commonly called hardpoints, are usually formed from rock placed in relatively close spacing. Sometimes, hardpoints are formed from a combination of timber posts and rock. Figure 10-12 illustrates this option, and Figure 10-13 illustrates a typical application.

10.5 Design Guidelines for Localized Abutment Armoring

The construction choice between riprap, cable-tied blocks, or geobags is largely up to the designer and should be based on a life-cycle cost assessment of the structure and/or coun-

termeasure. One exception is that some designers find geobags not particularly pleasing aesthetically and may, therefore, consider geobags a temporary countermeasure.

10.5.1 Wing-Wall Abutments

Riprap

The design parameters for riprap as an abutment scour countermeasure at wing-wall abutments are riprap size and size gradation, riprap layer thickness, filter requirements, and riprap layer extent. Figure 10-14 shows the pertinent parameters.

Riprap size, d_{50} . Riprap size selection can be based on stability against shear and edge failure if the other possible modes of failure are also addressed appropriately.

Either of the following Pagan-Ortiz (1991) and Lagasse et al. (2001) equations, with appropriate factors of safety, are suitable for predicting riprap stone sizes that are resistant to shear failure at wing-wall abutments.

Pagan-Ortiz (1991):

$$d_{50} = \left(\frac{1.064U^2 y^{0.23}}{(S_s - 1)g} \right)^{0.81} \quad (10-1)$$

Lagasse et al. (2001):

$$\frac{d_{50}}{y} = \frac{K_s}{(S_s - 1)} Fr^2 \quad Fr \leq 0.8$$

$$\frac{d_{50}}{y} = \frac{K_s}{(S_s - 1)} Fr^{0.28} \quad Fr > 0.8 \quad (10-2)$$

Where:

d_{50} = median size of the riprap stones,

U = mean velocity in the contracted bridge section,

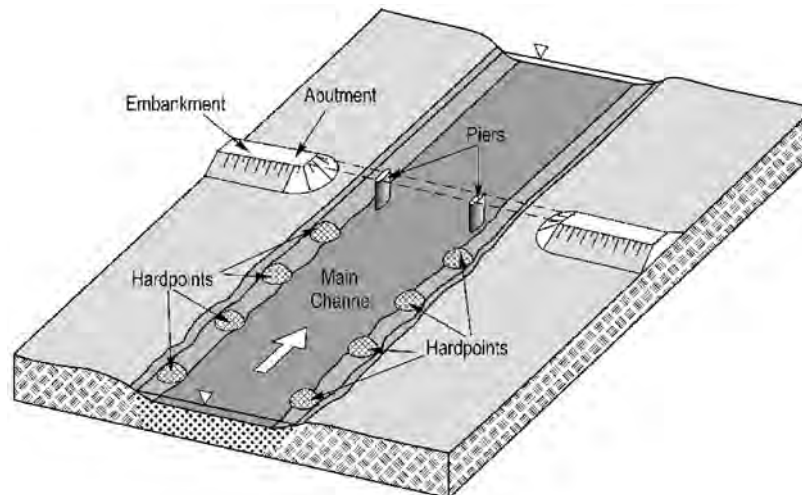


Figure 10-12. Hardpoints placed to keep an approach channel from eroding its banks.



Figure 10-13. Rock hardpoints placed along a bank approach to a bridge.

y = depth of flow in the contracted bridge section,
 Fr = Froude number in the contracted bridge section,
 S_s = specific gravity of the riprap material,
 g = gravitational acceleration, and
 K_s = shape factor.

Riprap size selection is appropriately based on stability against shear and edge failure, although consideration of the possibility of winnowing or bed-form undermining is also important in design.

Riprap layer thickness. The criterion given by Lagasse et al. (2001) (discussed in Section 5.6.3) is recommended—that is, the riprap layer thickness should be at least the larger of 1.5 times d_{50} or d_{100} .

Riprap gradation. The Brown and Clyde (1989) criteria (discussed in Section 5.6.3) for correctly grading riprap for bridge abutment protection are recommended. The criteria were shown in Table 5-7 and are shown again here in Table 10-2.

Filter Requirements. As discussed in Section 5.6.3, filters are used to prevent winnowing of bed sediment from between the riprap voids. Filters can be granular (which use the filtering effect of graded sediments) or synthetic (commonly known as geotextiles). Filters are placed beneath riprap layers to meet the following objectives:

- To prevent the groundwater seepage behind the riprap from transporting the underlying sediment through the riprap, commonly known as piping failure. The filter should be fine enough to prevent the base sediment from passing through it, but more permeable than the base sediment being protected to prevent build-up of any excess pore-water pressures.
- To prevent the high level of turbulence in front of the riprap layer from winnowing the underlying material through the riprap.

It is recommended that filters be placed beneath riprap at wing-wall abutments whenever practicable.

Riprap layer extent. Under mobile-bed conditions, riprap aprons placed at wing-wall bridge abutments are subject to undermining due to localized scour and bed-form propagation through the bridge section. Typically, the riprap apron settles (i.e., the outer edge of the riprap layer tends to settle most). If appropriately designed, the riprap layer will remain intact as it settles. The limiting condition for design is when W_{min} is zero. For this situation, the following expression was developed in Section 7.2.4:

$$W = C_1(d_{s2} - d_b + d_{50}) \quad (10-3)$$

Where:

W = apron width;

d_{s2} = scour depth (i.e., layer settlement depth) at the outer edge of the riprap;

d_b = placement (i.e., burial) depth of the riprap;

d_{50} = median size of the riprap stones; and

C_1 = 1.68 and 1.19 at the upstream and downstream corners of the riprap layer, respectively.

Equation 10-3 is recommended for determination of the lateral extent of the riprap apron. Furthermore, the apron should extend at least $1.5W$ upstream and $1.0W$ downstream from the wing-walls.

Design steps. Design steps are as follows:

1. Estimate the maximum likely scour depth, d_s .
2. Select the riprap size (using Equations 10-1 or 10-2), grading, filter, and layer extent (using Equation 10-3).
3. Sketch the abutment/countermeasure/scour hole geometry (in a cross section) that is likely to appear after scour.
4. Assess the geotechnical stability of the abutment, as shown in Figure 10-15.

Cable-Tied Blocks

The design parameters for cable-tied blocks as an abutment scour countermeasure at wing-wall abutments are block size and shape, cable design, filter requirements, and cable-tied block layer extent.

Cable-tied block aprons are subject to two observed flow-induced failure modes, as described by Parker et al. (1998). The failure modes are overturning and rolling-up of the leading edge of a cable-tied block mat (which can occur in the absence of sufficient anchoring or toeing-in of the leading edge) and uplift of the inner mat (which can occur at higher flow velocities when the leading edge is sufficiently anchored).

Block size. In order to avoid failure by uplift, the weight per unit area, ζ , of the block mattress as a whole, should be greater than the value given by the following equation, which was proposed by Parker et al. (1998):

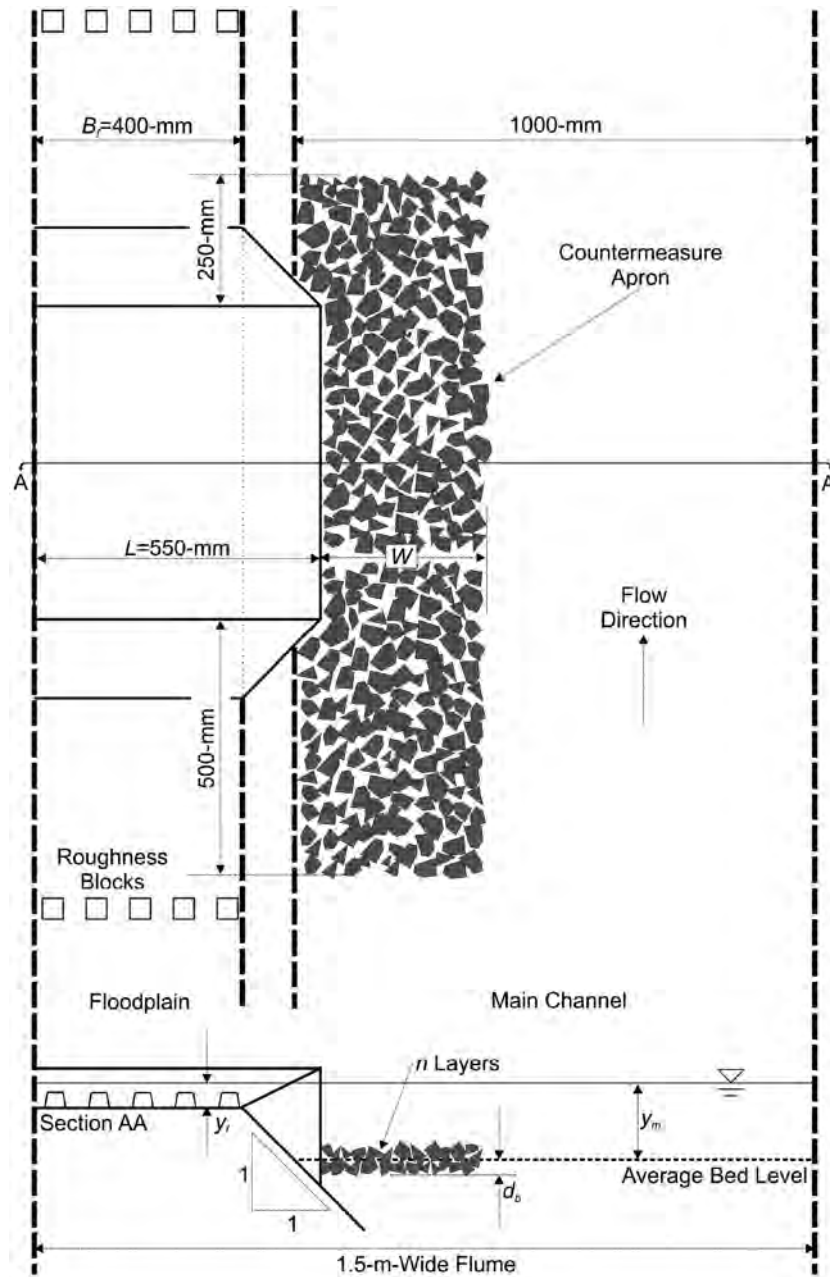


Figure 10-14. Riprap or cable-tied blocks at a wing-wall abutment.

Table 10-2. Rock riprap gradation (Brown and Clyde, 1989).

Stone Size Range	Percent of gradation smaller than the stone size range
$1.5d_{50}$ to $1.7d_{50}$	100
$1.2d_{50}$ to $1.4d_{50}$	85
$1.0d_{50}$ to $1.15d_{50}$	50
$0.4d_{50}$ to $0.6d_{50}$	15

$$\zeta = 0.2 \frac{\rho_{cb}}{\rho_{cb} - \rho} \rho U^2 \quad (10-4)$$

Where:

ρ_{cb} = block density,

ρ = fluid density, and

U = approach-flow velocity.

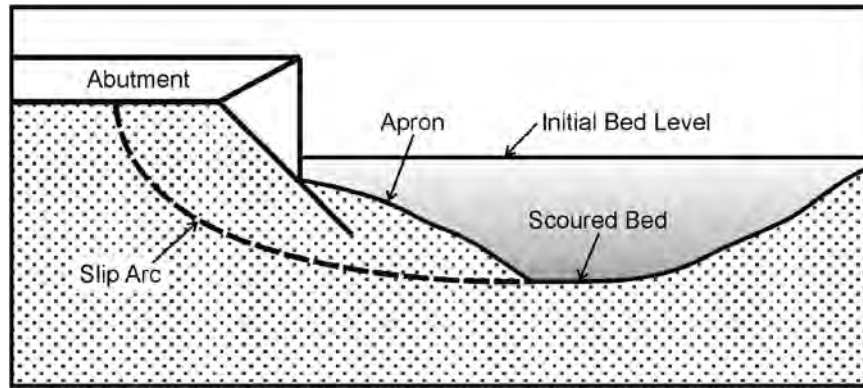


Figure 10-15. Sketch of geotechnical stability of an abutment.

The minimum required block height, H , can be calculated as follows:

$$H = \frac{\zeta}{\rho_{cb}g(1-p)} \quad (10-5)$$

Where:

p = volume fraction pore space within the mattress.

Block shape. Cable-tied blocks are typically manufactured in a truncated pyramid shape with a square base and top. Parker et al. (1998) recommend that the spacing between cable-tied block units be adequate to allow the mattress to have a sufficient degree of flexibility and that block shape not inhibit mat flexibility.

Filters. Synthetic filters are recommended for use beneath cable-tied block mats.

Cable-tied block layer extent. Under mobile-bed conditions, cable-tied block aprons placed at wing-wall bridge abutments are subject to undermining due to localized scour and bed-form propagation through the bridge section. Typically, the apron settles (i.e., the outer edge of the cable-tied block mat tends to settle most). The cable-tied block mat will remain intact as it settles. The limiting condition for design is when W_{min} is zero. For this situation, the following expression is developed in Section 7.2.4:

$$W = 1.55(d_s - d_b) \quad (10-6)$$

Where:

W = apron width,

d_s = scour depth (i.e., mat settlement depth) at the outer edge of the mat, and

d_b = placement (i.e., burial) depth of the mat.

Equation 10-6 is recommended for determination of the lateral extent of the cable-tied block apron. Furthermore, the apron should extend at least $1.5W$ upstream and $1.0W$ downstream from the wing-walls.

Edge protection. As discussed in Section 7.2.4, cable-tied block mats are stable against overturning of the leading edge when Equation 7-5 is satisfied:

$$\frac{H_b}{Y} = \frac{158}{(S_{cb} - 1)} Fr^2 \frac{n^2}{y^{0.33}} \quad (10-7)$$

Where:

S_{cb} = specific gravity of the blocks and

n = Manning coefficient.

Equation 10-7 provides a simple means of estimating block size to resist failure due to overturning and rolling-up of the leading edge. In use of Equation 10-7, care needs to be taken to ensure that the leading edge of the mat remains buried.

Design steps. Design steps are as follows:

1. Estimate the maximum likely scour depth, d_s .
2. Select the cable-tied block size (using Equations 10-4, 10-5, and 10-7), filter, and layer extent (using Equation 10-6)
3. Sketch the abutment/countermeasure/scour hole geometry (in a cross section) that is likely to appear after scour.
4. Assess the geotechnical stability of the abutment (using Figure 10-15)

Geobag Countermeasure

Guidelines are briefly presented here for the geobag layout, sizing, and post-geobag scour location as an apron around a single abutment or as a mat extending across the full bridge waterway. Each design necessarily is tailored to the site, but the following design steps should be incorporated as much as possible.

Design steps. Design steps are as follows:

1. Sizing of the geobags should be such that the thickness of an individual geobag is equivalent to or exceeds that of a riprap stone sized for the abutment site. Several methods for sizing

riprap are available (e.g., U.S. Army Corps of Engineers, 1989; Richardson and Davis, 1995; Austroads, 1994).

2. After the riprap size is calculated, the geobags can be sized with overall plan dimensions that enable convenient assembly of bags as an apron whose extent is comparable to the apron extents commonly used for riprap (e.g., Figures 7-60 and 7-62) or to an apron extent found necessary for a particular bridge site.
3. It is necessary to link (e.g., by tying) the geobags placed as an apron around an abutment. So doing enables the system of geobags to function as a moderately flexible armor cover that stays intact when the channel bed scours around the abutment.
4. The maximum slope of the geobag apron should be about 2:1 (H:V). The geobag apron should have a toe or skirt at the bottom end that extends deeper than the mattress by at least two thicknesses of geobag.
5. The region beneath, and immediately behind, the pile cap of a wing-wall abutment should be protected so as to prevent loss of embankment soil. Protection can be by means of geobags and/or riprap. Because the earthfill region of the embankment adjoining the abutment typically is poorly compacted and prone to erosion, it is important to ensure that it is protected.
6. If the aprons are linked so as to form a protective mat, the geobags should be of double layer thickness, but need not be tied together. However, it is necessary to provide toe and heel protection of the mat.

10.5.2 Spill-Through Abutments

Riprap

The design parameters for riprap as an abutment scour countermeasure at spill-through abutments are riprap size, riprap layer thickness, riprap gradation, filter requirements, riprap layer extent, and scour hole geometry. Figure 10-16 shows riprap or cable-tied blocks at a spill-through abutment.

Riprap size, d_{50} . The riprap used for the experiments undertaken for this study was selected using the following equation presented by Lagasse et al. (2001). The riprap based on Equation 10-8 was observed to be stable in all cases.

$$\frac{d_{50}}{y_f} = \frac{K_s}{(S_s - 1)} Fr^n \quad (10-8)$$

Where:

y_f = flow depth for the flood channel (i.e., adjacent to the abutment) in the contracted bridge section,

K_s = shape factor,

$Fr = U/(gy_f)^{0.5}$ = Froude number in the bridge contracted section,

U = characteristic mean velocity in the contracted section, and

S_s = specific gravity of the riprap stones.

The characteristic velocity, U , depends on the setback distance (i.e., position of the abutment toe with respect to the main channel near bank). The setback ratio (SBR) is

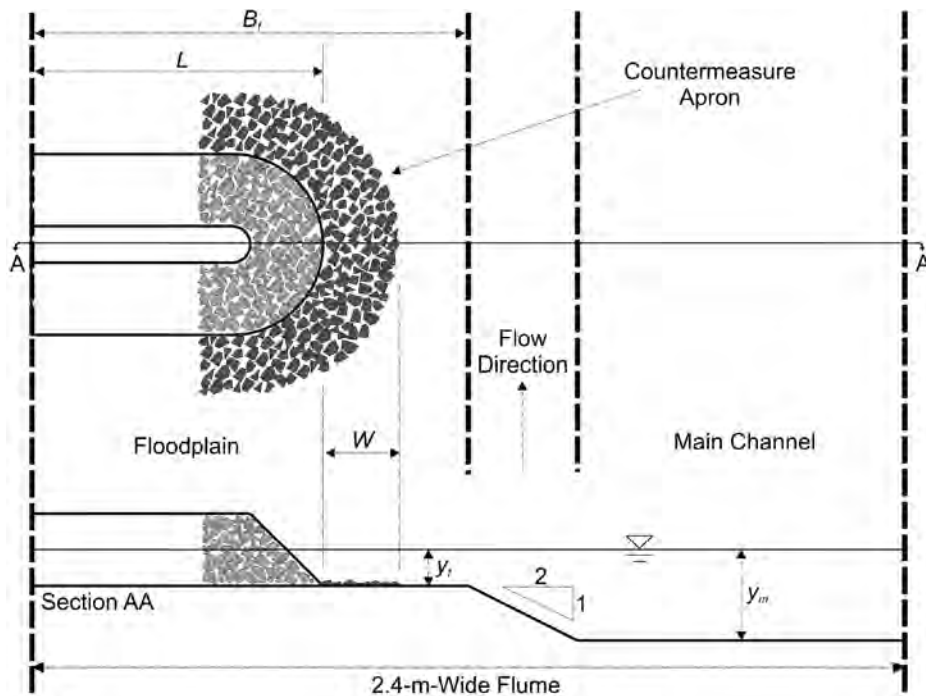


Figure 10-16. Riprap or cable-tied blocks at a spill-through abutment on a floodplain.

Table 10-3. Values of K_s and n in Equation 10-8.

Fr	K_s	n
≤ 0.8	0.89	2
> 0.8	0.61	0.1

defined as the setback distance divided by the average channel flow depth. For SBRs less than 5, U is evaluated as the total discharge divided by the total flow area of the contracted section. For SBRs greater than 5, U is evaluated as the discharge in the flood channel upstream from the bridge divided by the flow area for the flood channel in the bridge section.

For spill-through abutments, values of K_s and n are given in Table 10-3.

Riprap layer thickness. The criterion given by Lagasse et al. (2001) in Section 8.6.3 is recommended—that is, the riprap layer thickness should be at least the larger of 1.5 times d_{50} or d_{100} .

Riprap gradation. The Brown and Clyde (1989) criterion in Section 8.6.3 for correctly grading riprap for bridge abutment protection is recommended. This criterion was shown in Table 10-2.

Filter requirements. As discussed in Section 8.1.4, filters are used to prevent winnowing of bed sediment from between the riprap voids. Filters can be granular (which use the filtering effect of graded sediments) or synthetic (commonly known as geotextiles). Filters are placed beneath riprap layers to meet the following objectives:

- To prevent the groundwater seepage behind the riprap from transporting the underlying sediment through the riprap, commonly known as piping failure. The filter should be fine enough to prevent the base sediment from passing through it, but more permeable than the base sediment being protected to prevent build-up of any excess pore-water pressures.
- To prevent the high level of turbulence in front of the riprap layer from winnowing the underlying material through the riprap.

It is recommended that filters be placed beneath riprap at spill-through abutments whenever practicable.

Riprap layer extent. Based on the experimental work presented in Section 8.3.4, the minimum apron width to ensure adequate toe protection (i.e., for $W_{min} = 0$ in Figure 10-16) is

$$\frac{W}{y_f} = 0.5 \left(\frac{d_{sf}}{y_f} \right)^{1.35} \quad (10-9)$$

Where:

W = apron width and

d_{sf} = maximum scour depth measured with respect to the level of the floodplain.

Equation 10-9 is recommended for calculation of the width of riprap apron needed to adequately protect the toe of spill-through abutments. It is recommended that the protection extend around the curved portions of the abutment to the point of tangency with the plane of the embankment slopes, as was illustrated in Figure 10-14.

Scour hole geometry. As discussed in Section 8.3.4, the scour-hole geometry at a spill-through abutment featuring riprap apron protection can be described by the following set of equations:

$$d_{sf} = d_s + F(y_m - y_f) \quad (10-10)$$

Where:

d_{sf} = scour depth relative to the bed level in the flood channel;

y_m = flow depth in the main channel;

y_f = flow depth in the flood channel;

L = abutment length; and

F = a function that depends on the position of the scour hole in a compound channel, as was illustrated in Figure 10-14 and as given by

$$F = 1 - \left(1 - \frac{L}{B_f} \right)^2 \left(\frac{\alpha_c}{B_f} - 1 \right) \quad \text{when} \quad \frac{\alpha_c}{B_f} > 1$$

$$F = 0 \quad \text{when} \quad \frac{\alpha_c}{B_f} \leq 1 \quad (10-11)$$

Where:

α = position of the outer edge of the scour hole and

B_f = width of the flood channel (as was shown in Figure 10-14).

When the scour hole forms entirely in the flood channel (i.e., when $\alpha < B_f$), Equation 10-11 reduces to $d_{sf} = d_s$. When $L \geq B_f$, the scour depth forms mostly in the main channel, $F = 1$ and $d_{sf} = d_s + (y_m - y_f)$.

The position of the center of the scour hole is defined by R and $\theta = 30$ degrees; R is given as follows:

$$\frac{R}{y_f} = 4 \left(\frac{L}{y_f} \right)^{0.2} \left(1 + \frac{W}{y_f} \right)^{0.4} \quad (10-12)$$

Design steps. Design steps are as follows:

1. Estimate the maximum likely scour depth, d_{sf} , and scour hole position, R , using Equation 10-12.
2. Select riprap size with Equation 10-8 and grading, filter, and apron extent with Equation 10-9.
3. Sketch the abutment/countermeasure/scour hole geometry (in a cross section) that is likely after scour.
4. Assess the geotechnical stability of the abutment using Figure 10-15.

Cable-Tied Blocks

The design parameters for cable-tied blocks as a scour countermeasure at spill-through abutments are block size, block shape, filters, layer extent, edge protection, and scour hole geometry.

Cable-tied block aprons are subject to two observed flow-induced failure modes, as described by Parker et al. (1998). The failure modes are overturning and rolling-up of the leading edge of a cable-tied block mat (which can occur in the absence of sufficient anchoring or toeing-in of the leading edge) and uplift of the inner mat (which can occur at higher flow velocities when the leading edge is sufficiently anchored).

Block size. In order to avoid failure by uplift, the weight per unit area, ζ , of the block mattress as a whole should be greater than the value given by the following equation, which was proposed by Parker et al. (1998):

$$\zeta = 0.2 \frac{\rho_{cb}}{\rho_{cb} - \rho} \rho U^2 \quad (10-13)$$

Where:

- ρ_{cb} = block density,
- ρ = fluid density, and
- U = approach-flow velocity.

The minimum required block height, H , can be calculated from

$$H = \frac{\zeta}{\rho_{cb} g (1 - p)} \quad (10-14)$$

Where:

- p = volume fraction pore space within the mattress.

Block shape. Cable-tied blocks are typically manufactured as a truncated pyramid shape with a square base and top. Parker et al. (1998) recommend that the spacing between cable-tied block units be adequate to allow the mattress to have a sufficient degree of flexibility and that block shape not inhibit mat flexibility.

Filters. Synthetic filters are recommended for use beneath cable-tied block mats.

Layer extent. Based on the experimental work presented in Section 8.3.4, the minimum apron width to ensure adequate toe protection (i.e., for $W_{min} = 0$ in Figure 10-14) is

$$W = 1.4 d_{sf} \quad (10-15)$$

Where:

- W = apron width and
- d_{sf} = maximum scour depth measured with respect to the level of the floodplain.

Equation 10-15 is recommended for calculation of the width of cable-tied block apron needed to adequately protect

the toe of spill-through abutments. It is recommended that the protection extend around the curved portions of the abutment to the point of tangency with the plane of the embankment slopes, as was illustrated in Figure 10-14.

Edge protection. As discussed in Section 7.2.4, cable-tied block mats are stable against overturning of the leading edge when the following expression is satisfied:

$$\frac{H_b}{Y} = \frac{158}{(S_{cb} - 1)} Fr^2 \frac{n^2}{\gamma^{0.33}} \quad (10-16)$$

Where:

- S_{cb} = specific gravity of the blocks and
- n = Manning roughness coefficient.

Equation 10-16 provides a simple means of estimating block size to resist failure due to overturning and rolling-up of the leading edge. In the use of Equation 10-16, care must be taken to ensure that the leading edge of the mat remains buried.

Scour hole geometry. As discussed in Section 8.3.4, the scour-hole geometry at a spill-through abutment featuring cable-tied block apron protection can be described by the following set of equations:

$$d_{sf} = d_s + F(y_m - y_f) \quad (10-17)$$

Where:

- d_{sf} = scour depth relative to the bed level in the flood channel,
- y_m = flow depth in the main channel,
- y_f = flow depth in the flood channel,
- L = abutment length, and
- F = a function that depends on the position of the scour hole in a compound channel, as illustrated in Figure 10-14 and as given by

$$F = 1 - \left(1 - \frac{L}{B_f}\right)^2 \left(\frac{\alpha_e}{B_f} - 1\right) \quad \text{when } \frac{\alpha_e}{B_f} > 1$$

$$F = 0 \quad \text{when } \frac{\alpha_e}{B_f} \leq 1 \quad (10-18)$$

Where:

- α = position of the outer edge of the scour hole and
- B_f = width of the flood channel (as was shown in Figure 10-14).

When the scour hole forms entirely in the flood channel (i.e., $\alpha < B_f$), Equation 10-18 reduces to $d_{sf} = d_s$. When $L \geq B_f$, the scour depth forms mostly in the main channel, $F = 1$ and $d_{sf} = d_s + (y_m - y_f)$.

The position of the center of the scour hole is defined by R and $\theta = 30$ degrees (Figure 10-14); R is given by

$$\frac{R}{y_f} = \left(\frac{L}{y_f} \right)^{0.2} \left(1 + \frac{W}{y_f} \right)^{0.9} \quad (10-19)$$

Design steps. Design steps are as follows:

1. Estimate the maximum likely scour depth, d_{sf} , and scour hole position, R , using Equation 10-19.
2. Select the cable-tied block size using Equations 10-13 and 10-14, and select the filter and apron extent using Equation 10-15.
3. Sketch the abutment/countermeasure/scour hole geometry (in a cross section) that is likely after scour.
4. Assess the geotechnical stability of the abutment using Figure 10-15.

Guidance for Estimating Scour Depth, d_s

Use of Equations 10-15 and 10-17 to estimate apron extent requires knowledge of expected scour depth. A number of equations exist for prediction of localized scour depth at bridge abutments. However, the scour depth where protection is in place differs from that traditionally measured in laboratory experiments, so that existing scour equations may lead to excessively large aprons using Equations 10-15 and 10-17.

In Equation 7-6, it is shown that the settlement depth, due to bed-form propagation, at the outside edge of aprons at wing-wall abutments is given by

$$d_s = C_2 \lambda_{H-max} \quad (10-20)$$

Where:

λ_{H-max} = maximum bed-form height and

$C_2 = 1.2$ and 1.0 for the upstream and downstream corners of the riprap layer, respectively.

Equation 10-20 can be used in situations where local scour is relatively insignificant. This is often the case due to the riprap protection inhibiting scour near the abutment walls.

10.6 Design Guidelines for Localized Flow Field Modification

10.6.1 Parallel-Wall Countermeasure

The design parameters for parallel-wall scour countermeasures are the wall length, wall side angle, wall height, wall base width, wall protrusion, wall plan form, and apron. See Figure 10-17 for a sketch of the design dimensions.

Wall Length, L_w

The length of the parallel wall should be $0.5_a L_a$, where L_a is the abutment length (perpendicular to flow direction).

Wall Side Angle, θ

The maximum steepness of the side wall angle should be the angle of repose for the rock employed.

Wall Height, H_w

The height of the wall should be sufficient to have the top of the wall be above the highest flow depth that the bridge will experience.

Wall Base Width, $2H_w$

The wall should be wide enough to accommodate the wall height and the sidewall angle of the rock wall.

Wall Protrusion

The bottom of the rock wall should be even with the abutment such that no part of the wall protrudes out into the main channel.

Wall Plan Form

The wall should be parallel to the river banks. Thus, if the river section is straight, then the wall should be straight as well, but if the river section is curved, then the wall should also be curved and parallel to the river banks. See Figure 10-18 for a sketch of a curved wall.

Apron

The thickness of the apron should be at least two times the diameter of the size of rocks used for the wall. The width of the apron should be at least four times the wall height. The apron should extend the full length of the wall. At the upstream end, the apron should join the floodplain.

10.6.2 Spur Dike Countermeasure

The design parameters for spur dikes as abutment scour countermeasures are number of dikes, dike length, dike height, dike spacing, dike face angle, and dike width. See Figure 10-19 for a definition sketch.

Number of Dikes

There should be at least three dikes used: two shorter dikes at the upstream and downstream corners of the abutment and a longer dike upstream of the abutment. For wide abutments parallel to the flow, there may need to be additional short dikes, as well (see the discussion on dike spacing below).

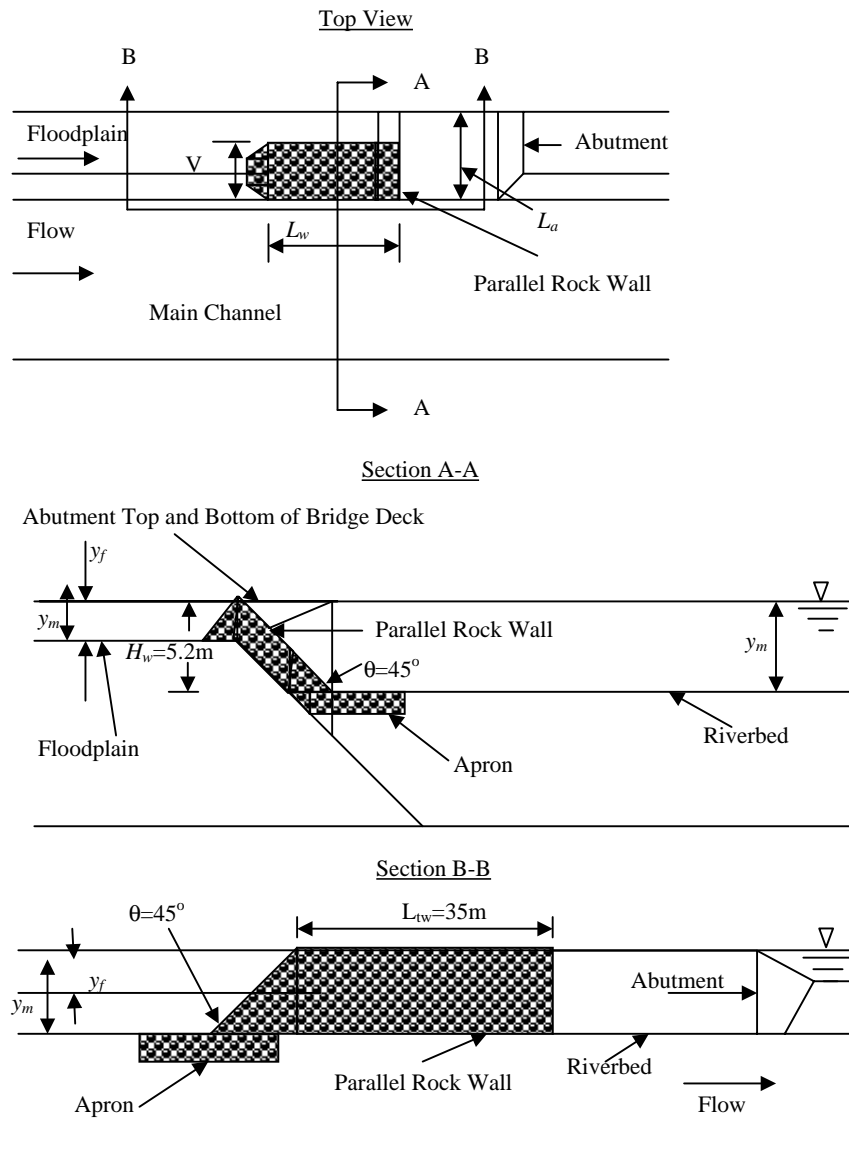


Figure 10-17. Design dimensions for parallel-wall countermeasure using piled rocks.

Dike Length

The top length of the dike (perpendicular to the flow) should be equal to the abutment length, L_a (perpendicular to the flow). For the shorter dikes, this length extends from the abutment face out into the main channel. For the longer dikes upstream of the abutment, the length is longer than L_a . The dike should extend the same distance into the river that the shorter dikes do and extend back onto the floodplain a distance far enough not to affect the river flow. The bottom dike length is determined by the angle of the wall face. Care should be taken, however, on narrower rivers not to block too much of the river width with the dikes. Therefore, the dikes should not extend farther out into the main channel than one-fourth of the river width.

Dike Height

The top elevation of the dike should be higher than the highest expected water level.

Dike Spacing

Dikes should be located at the abutment corners and extend out into the main channel. Since dike spacing should be less than the abutment length, L_a , an intermediate dike may be needed if the abutment width (parallel to flow direction) is longer than the abutment length, L_a .

Dike Face Angle

The steepness of the side wall angle should be the angle of repose for the rock employed.

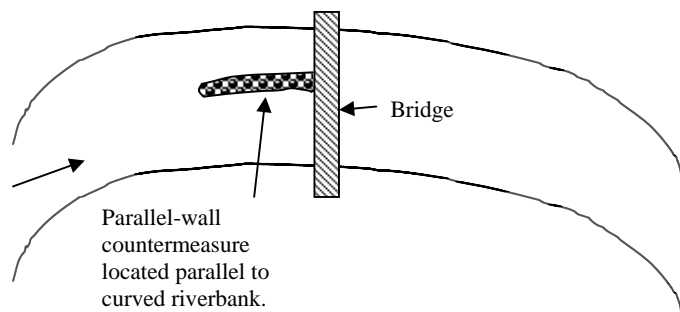


Figure 10-18. Curved parallel-wall countermeasure located on a river bend.

Dike Width

Dike width is determined by the dike face angle, which should be less than the angle of repose of the rock used to construct the dike.

10.7 Relation to Existing HEC Guidelines

The set of HEC guidelines that currently address bridge scour and stream instability countermeasures is HEC-23 (Lagasse et al., 1997), which describes design guidelines for the following countermeasures: bendway weirs/stream barbs,

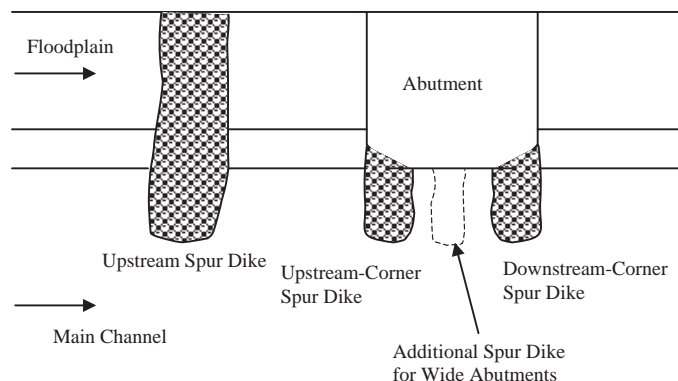


Figure 10-19. Spur dike countermeasure design.

soil cement, wire-enclosed riprap mattresses, articulated concrete block systems, articulating grout-filled mattresses, toskanes, grout- or cement-filled bags, and rock riprap at abutment and piers. These countermeasures are applicable to preventing bank erosion and therefore addressing stream instability. They are not addressed in the context of pier or abutment protection except for rock riprap. None of them address compound-channel flow, in which there is flow in the floodplain as well as in the main channel.

It is suggested, therefore, that this report be used to supplement HEC-23 and be used specifically for the design of countermeasures at abutments with compound-channel flow conditions, which is when most of the critical scouring occurs.

CHAPTER 11

Conclusions

From the literature review and laboratory studies, several key points emerge. The following sections summarize the conclusions for countermeasures involving wing-wall abutments, spill-through abutments, and flow guidance.

11.1 Wing-Wall Abutments

Experiments were performed for a wing-wall abutment located close to the main channel edge. Countermeasures tested were riprap, cable-tied blocks, geobags, parallel walls, spur dikes, and collars. In addition, two-dimensional modeling of the flow field was compared with laboratory results. Tests were also performed in a large-scale flume, and the results were compared with experimental results.

11.1.1 Riprap, Cable-Tied Blocks, and Geobags

Local scour in the general vicinity of an abutment cannot be eliminated completely by an apron of riprap or geobags, because an apron only shifts the scour region away from an abutment. The experiments show that an apron can prevent scour from developing at the abutment itself, but significant scour can occur readily near the downstream edge of the apron. A possible concern in using an apron is to ensure that shifting of scour does not imperil a nearby pier or portion of riverbank. Moreover, if the scour is likely to extend to an adjacent pier, then the abutment and pier countermeasure apron should be placed so as to protect both elements of a bridge.

The experiments show that it is necessary to protect the following regions of the river bed and banks near an abutment:

- The river bed at the abutment pile cap,
 - The riverbank immediately upstream of the abutment and a short distance downstream of the abutment,
 - The side slopes of embankment immediately behind the abutment (i.e., the standard stub for a wing-wall abutment or spill-through abutment), and
 - The area beneath and immediately behind the pile cap.
- For use of riprap or cable-tied blocks alone, the following conclusions emerged from this study:
- For the range of experimental investigation in this study, the scour at wing-wall abutments in live-bed conditions directly relates to the level of the deepest bed-form trough that propagates past the abutment (which can be predicted using existing expressions) and to any localized scour that may occur.
 - Stones on the outer edge of riprap aprons tend to settle and move away from the abutment, thereby pushing the troughs of the bed forms farther away from the abutment. Conversely, cable-tied block mats remain intact during settlement. The outer edge of the apron settles vertically, allowing the troughs of the bed forms to pass closer to the abutment face than for an equivalent riprap apron.
 - Equations 7-10 and 7-11 allow prediction of the minimum apron width remaining horizontal after erosion. Equation 7-12 allows prediction of the horizontal distance between the abutment face and the point of deepest scour. These predictions, along with prediction of apron settlement, facilitate assessment of the stability of an abutment structure.
- With regard to the specific use of geobags for wing-wall abutments, the following conclusions can be drawn:
- Geobags are a promising alternative to riprap for use as a bridge abutment scour countermeasure.
 - It is necessary to connect the geobags placed as an apron around an abutment. The initiation of the failure of geobag apron, shown in Figure 7-58, was due to the failure of an individual geobag placed in front of the abutment.

- The apron should have a perimeter toe whose lower level approximately coincides with the average elevation of dunes moving through the channel in the vicinity of the bridge.
- The geobags should be placed in a shingled manner, whereby adjoining geobags overlies joints between underlying geobags.
- It is necessary to place geobags or riprap immediately under the pile cap in order to prevent the winnowing of embankment sediment from beneath the pile cap.
- Geobags may serve as a useful alternative to a geotextile filter cloth placed beneath a riprap apron because geobags are more readily placed than an underlay cloth for blocking the winnowing of sediment from between bed-armor elements like riprap stone. However, the geobags should be placed somewhat below bed level so as not to increase riprap exposure to flow.

11.2 Spill-Through Abutments

The flowfield and the behavior of riprap and cable-tied blocks were studied. Pertinent conclusions are as follows.

11.2.1 Abutment Flow Field

The following conclusions can be drawn from the abutment flow field study:

- Velocity, vorticity strength, and normalized bed shear stress in the flow field at the end of the abutment all increase with increasing abutment length and floodplain width.
- The normalized bed shear stress on the main channel bank upstream of the abutment increases significantly as the abutment setback distance from the main channel bank decreases. The transverse component of the flow that is diverted around the abutment is strongest at the upstream end of the abutment. The smaller the setback distance is, the stronger the transverse velocity component over the top of the main channel bank is. The transverse velocity component destabilizes the bed material on the main channel bank, making the bed material susceptible to significant erosion in that region.
- Regions of high vorticity in the wake of the abutment correspond to the zone where scour is initiated. There is a strong correlation between the scour hole position and the line of strongest vorticity.
- The effect of placing a protection apron around an abutment is to inhibit the initiation of scour at the point where the vorticity is strongest. Consequently, the scour hole develops farther away from the end of the abutment, where the bed is unprotected. The vorticity strength is weaker farther away from the abutment, thereby decreasing the size of the scour hole.

- Zones of excess shear stresses are responsible for the erosion that occurs near the main channel, where the vorticity is weaker.

11.2.2 Riprap and Cable-Tied Blocks in Clear-Water Conditions

The conclusions from the spill-through abutment experimental study are as follows:

- Apron countermeasure protection at spill-through abutments does not significantly reduce the depth of local scour. Rather, the apron deflects the scour development away from the end of the abutment, preventing the developing scour hole from undermining the abutment toe.
- By increasing the apron extent, the scour hole is deflected farther away from the end of the abutment. When the scour hole forms on the floodplain, the depth of scour typically reduces as the scour hole is deflected farther away. However, for abutment and compound channel configurations where the scour hole forms close to the main channel bank, the depth of scour relative to the bed of the floodplain increases as the scour hole is deflected away from the abutment and into the main channel.
- The scour depth for spill-through abutments, situated on the floodplain of a compound channel, is given by Equation 8-13. Alternatively, the scour depth can be determined by Equation 8-19, using the abutment flow field parameters.
- Cable-tied block aprons allow scour holes to form closer to the abutment than equivalent riprap aprons. Therefore, wider cable-tied block aprons are needed to provide the same level of protection to an abutment as equivalent riprap aprons. Consequently, riprap is likely to be economically preferable to cable-tied blocks as a form of apron protection at spill-through abutments.
- The minimum apron width required to prevent undermining of the toe of the spill-through abutment is related to the depth of scour and is given by Equation 8-16.
- The extent of apron protection required to ensure that spill-through abutment fill material is stable can be determined using the design procedure given in Equation 10-15.

11.2.3 Two-Dimensional Modeling

Conclusions regarding the two-dimensional modeling using FESWMS are as follows:

- The local peak velocity on the floodplain and in the main channel was well predicted by the two-dimensional model, although the location of the local maximum was not.

- The average velocity in the channel was well predicted by the two-dimensional model. One unusual velocity observation in the particle-tracking velocimetry (PTV) measurements causes the PTV point data to deviate from the two-dimensional model results. The average velocity for the PTV floodplain data is significantly higher than that of the two-dimensional model for transects 8.18 and 8.67.
- The PTV-measured velocity in the floodplain (from 0 m to 1.6 m along the transect) is higher than that computed from the two-dimensional modeling.

11.2.4 Large-Scale Tests of Riprap Apron Performance

Relative to abutment position, the locations of deepest scour coincide reasonably well. Scour depths, though, were proportionately less for the large-scale tests.

Given the differences in geometric scale and layout of abutment for the large-scale test, this agreement is a substantial validation of the design relation developed from the smaller-scale tests presented in Section 8.1.

11.3 Flow Guidance

Three flow modification countermeasures were investigated in this project for scour reduction at wing-wall abutments located close to the main channel bank: parallel walls, spur dikes, and abutment collars.

11.3.1 Scour with No Countermeasures

In order to understand abutment scour and its mechanisms, scour without any countermeasures was explored first. Scour was studied for both clear-water and live-bed scour conditions.

11.3.2 Clear-Water Conditions

Conclusions regarding the clear-water conditions are as follows:

- As shown in Figure 9-5, five locations of scour were found in the whole scour region, provided that the roughness on the floodplain was the same as it was in the main channel and the velocity ratio between the floodplain flow and the main channel flow was relatively high. The floodplain flow tended to shoot into the main channel at a distance upstream from the upstream corner of the abutment. Under this condition, the maximum scour in the whole region was normally found in Zone B of Figure 9-5.
- The more the floodplain flow was constricted at the abutment, the deeper the scour hole would be at the upstream

corner of the abutment. When the roughness on the floodplain was increased and the velocity ratio between the floodplain and the main channel decreased, the floodplain flow moved to the corner of the abutment. As a consequence, the scour zones A, B, and E from Figure 9-5 converged into a single scour hole, and the maximum scour depth was found at the upstream corner of the abutment.

- The principal vortex systems and secondary vortex systems at the upstream corner of the abutment were stronger than the wake vortex systems at the downstream corner of the abutment. Consequently, the scour hole induced by the principal vortex systems and by the secondary vortex systems reaches equilibrium more quickly than the scour hole induced by the downstream wake vortex systems.
- Clear-water scour with no countermeasures resulted in a scour depth of 77.7 mm.

11.3.3 Live-Bed Conditions

Conclusions regarding the live-bed conditions are as follows:

- Maximum scour took place at the upstream corner of the abutment. Time-averaged scour depth at the upstream corner was less than the scour depth under critical clear-water conditions, while instantaneous scour depths were between values near zero to values nearly twice the maximum scour under clear-water flows because of the superposition of the trough of the bed forms (see Figure 9-10).
- Live-bed scour reaches equilibrium more quickly than clear-water scour.

11.3.4 Parallel-Wall Countermeasures

Conclusions regarding the parallel-wall countermeasures are as follows:

- A parallel solid wall attached at the upstream corner of the abutment parallel with the flow can be used as a countermeasure against abutment scour. The length of the solid wall should be $1.6L$ to obtain an acceptable scour reduction rate at the abutment for the conditions tried in this study.
- A parallel solid wall attached at the upstream corner of the abutment parallel with the flow may or may not be able to reduce the amplitude of the bed forms that pass through the bridge opening, depending on the changes of the flow parameters from the approaching channel after entering the bridge crossing.
- There may be significant scour at the upstream solid wall end, so no other structures should be located in this region.
- Parallel rock walls attached at the upstream of the abutment can also be used as countermeasures against scour at

the abutment. The foot of the wall should not protrude into the main channel beyond the abutment, and a top wall length of $0.5L$ will provide sufficient protection. The side slope of the rock wall should be on the order of 30 degrees, but in no case should it be steeper than about 70 percent of the rocks' angle of repose.

- Rock walls have more advantages than solid walls in terms of efficiency, stability, and cost.

11.3.5 Spur Dikes Under Clear-Water and Live-Bed Scour

Conclusions regarding the spur dikes under clear-water and live-bed conditions are as follows:

- A single spur dike made of a solid plate having the same protrusion length as, or less protrusion length than, the abutment and placed upstream of the abutment was not able to protect the abutment. The downflow and the principal vortex are very strong at the stream end of the structure. As a consequence, a huge scour hole was always found at the end of the structure, which threatened both the structure and the channel bank.
- Rock spur dikes show several advantages over rigid spur dikes and are preferred.
- Three rock spur dikes-as configured in Tests Sp-9 (Table 9-9) and Sp-13 (Table 9-10)-were considered the best configuration for protecting the abutment. This configuration can provide 100-percent protection to the abutment under the

velocity ratios of 0.9, 1.5, and 2.3. Two spur dikes at the upstream and downstream corners of the abutment were also successful at preventing scour in both clear-water and live-bed experiments.

11.3.6 Abutment Collars in Clear-Water Scour Conditions

Conclusions regarding abutment collars in clear-water conditions are as follows:

- Collars were found to be effective at preventing local scour at vertical-wall bridge abutments. The collars isolated the turbulent flow and vortex systems from the bed material and thereby prevented the bed underneath the collar from scouring.
- The farther the collar extended downstream of the abutment, the farther downstream the scour hole was located. As the transverse width of the collars increased, the depth of the scour hole at the edge of the collar decreased. The scour became insignificant as the main channel edge of the collar was extended beyond the local scour hole area measured in the baseline case without countermeasures. The trailing edge of the collar should extend to a location downstream of the abutment.
- Based on these experiments, the collar elevation should be $0.08y_m$ below the original bed level, and the collar width should be at least $0.23L$, where L is the abutment length perpendicular to the flow direction.

References

- Acheson, A. R. (1968). *River Control and Drainage in New Zealand and Some Comparisons with Overseas Practices*. Ministry of Works, New Zealand.
- Adams, M., Ketchart, K., Ruckman, A., DiMillio, A. F., Wu, J., and Satyanarayana, R. (1999). Reinforced soil for bridge support applications on low-volume roads. *Transportation Research Record 1652: Seventh International Conference on Low-Volume Roads, May 23-26, 1999, Baton Rouge, Louisiana*, Volume 1, Transportation Research Board.
- Ahmad, M. (1951). Spacing and projection of spurs for bank protection. *Civil Engineering and Public Work Review*, London, United Kingdom, March 172-174, April 256-258.
- Ahmad, M. (1953). Experiments on design and behavior of spur dikes. *Proc., Minnesota International Hydraulics Convention*, International Association of Hydraulic Research.
- Ashley, G. M. (1990). Classification of large-scale subaqueous bedforms: A new look at an old problem. *Journal of Sedimentary Petrology*, Vol. 60, No. 1.
- Atayee, A. T. (1993). Study of riprap as scour protection for spill-through abutments. *Transportation Research Record 1420: Hydrology, Hydraulics, and Water Quality*, Transportation Research Board.
- Atayee, A. T., Pagan-Ortiz, J. E., Jones, J. S., and Kilgore, R. T. (1993). Study of riprap as scour protection for bridge abutments. *Proc., Conference on Hydraulic Engineering*, Part 1, American Society of Civil Engineers.
- Austroroads (1994). *Waterway Design—A Guide to the Hydraulic Design of Bridges, Culverts and Floodways*. Sydney, Australia.
- Bertoldi, D. A., and Jones, J. S. (1994). *An Experimental Study of Scour Protection Alternatives at Bridge Piers*. Turner-Fairbank Laboratory, Federal Highway Administration.
- Biglari, B., and Sturm, T. W. (1998). Numerical modeling of flow around bridge abutments in compound channel. *Journal of Hydraulic Engineering*, Vol. 124, No. 2, American Society of Civil Engineers.
- Blench, T. (1969). *Mobile-Bed Fluviology*. University of Alberta Press, Edmonton, Alberta, Canada.
- Blodgett, J. C., and McConaughy, C. E. (1985). *Evaluation of Rock Riprap Design Practices for Protection of Channels Near Highway Structures—Phase I*. Preliminary report subject to revision, prepared by the U.S. Geological Survey in cooperation with Federal Highway Administration. [Subsequently published as *Rock Riprap Design for Protection of Stream Channels Near Highway Structures*, U.S. Geological Survey report 86-4127 (Vol. 1) and 86-4128 (Vol. 2), 1986.]
- Borghesi, S. M., Vatannia, Z., Ghodsian, M., Jalili, M. R., and Nalder, G. (2004). Discussion: Oblique rectangular sharp-crested weir. *Water Management*, Vol. 157, No. 4.
- Bradley, J. N. (1978). *Hydraulics of Bridge Waterways*. Hydraulic Design Series 1, Federal Highway Administration.
- Breusers, H. N. C., and Raudkivi, A. J. (1991). Scouring. *IAHR Hydraulic Structures Design Manual 2*, International Association of Hydraulic Research.
- Brown, S. A. (1985a). *Streambank Stabilization Measures for Highway Engineers*. Report FHWA/RD-84/100, Federal Highway Administration.
- Brown, S. A. (1985b). *Design of Spur-Type Streambank Stabilization Structures*. Report FHWA/RD-84-101, Federal Highway Administration.
- Brown, S. A., and Clyde, E. S. (1989). *Design of Riprap Revetment*. Hydraulic Engineering Circular 11, Report FHWA-IP-89-016, Federal Highway Administration.
- Burns, R. S., Fotherby, L. M., Ruff, J. F., and Carey, J. M. (1996). Design example for bridge pier scour measures using Toskanes. *Transportation Research Record 1523: Geometric and Other General Design Issues*, Transportation Research Board.
- Cardoso, A. H., and Bettess, R. (1999). Effects of time and channel geometry on scour at bridge abutments. *Journal of Hydraulic Engineering*, Vol. 125, No. 4, American Society of Civil Engineers.
- Central Board of Irrigation and Power (1989). *River Behaviour Management and Training*. Edited by C. V. J. Sharma, K. R. Saxema, and M. K. Rao, Publication 204, Vol. 1, New Delhi, India.
- Central Board of Irrigation and Power (1989). *River Behaviour Management and Training*. Edited by C. V. J. Sharma, K. R. Saxema, and M. K. Rao, Publication 204, Vol. 2, New Delhi, India.
- Cheung, K. M. (2002). *Cable-tied blocks as a countermeasure*. M.E. Thesis, Civil and Environmental Engineering Department, the University of Auckland, New Zealand.
- Chiew, Y. M. (1995). Mechanics of riprap failure at bridge piers. *Journal of Hydraulic Engineering*, Vol. 121, No. 9, American Society of Civil Engineers.
- Chiew, Y. M. (2000). Failure behavior of riprap layer at bridge piers under live-bed conditions. *Journal of Hydraulic Engineering*, Vol. 126, No. 1, American Society of Civil Engineers.
- Chitale, S. V. (1980). Radius of curved heads of guide banks. *Irrigation and Power*, Vol. 37, No. 4.
- Choi, S. U., Paik, J., and Cho, W. (2000). Hydraulic properties of concrete blocks for bed protection. Paper presented at the International Symposium on Scour of Foundations, International Society of Soil Mechanics and Geotechnical Engineering, Melbourne, Australia.
- Copeland, R. R. (1983). *Bank Protection Techniques Using Spur Dikes*. Hydraulics Laboratory, U.S. Army Waterways Experiment Station, Vicksburg, Mississippi.

- Croad, R. N. (1989). *Investigation of the Pre-Excavation of the Abutment Scour Hole at Bridge Abutments*. Report 89-A9303, Central Laboratories, Works and Development Services Corporation (NZ) Ltd., Lower Hutt, New Zealand.
- De Sousa Pinto, N. L. (1959). *Riprap Protection Against Scour Around Bridge Piers*. Masters thesis, University of Iowa, Iowa City.
- Dongol, D. M. S. (1994). *Local Scour at Bridge Abutments*. Ph.D. dissertation, Civil and Environmental Engineering Department, University of Auckland, New Zealand.
- Escarameia, M. (1995). *Channel Protection—Gabion Mattresses and Concrete Blocks*. Report SR 427, HR Wallingford, Oxfordshire, United Kingdom.
- Escarameia, M., and May, R. W. P. (1992). *Channel Protection—Turbulence Downstream of Structures*. Report SR 313, HR Wallingford, Oxfordshire, United Kingdom.
- Ettema, R. (1990). *Hydraulic Model Studies of Circulating-Water and Essential-Service-Water Pump-Intake Structures*. IHR Limited Distribution Report 173, Korea Electric Power Corporation Yong-gwang Station, Units 3 and 4.
- Ettema, R. (1992). *Enhanced Performance and Reliability of Water Intakes for Generating Stations*. Proposal of Iowa Institute of Hydraulic Research to Electric Power Research Institute.
- Ettema, R., Kirkil, G., and Muste, M. (2006). Similitude of large-scale turbulence in experiments on local scour at cylinders. *Journal of Hydraulic Engineering*, Vol. 132, No. 1, American Society of Civil Engineers.
- Eve, N. J. (1999). *Riprap Protection at Bridge Abutments*. M.E. thesis, the University of Auckland, New Zealand.
- Farabee, G. B. (1986). Fish species associated with revetted and main channel border habitats in Pool 24 of the Upper Mississippi River. *North American Journal of Fisheries Management*, Vol. 6, No. 4.
- Farraday, R. V., and Charlton, F. G. (1983). *Hydraulic Factors in Bridge Design*. Hydraulics Research Station, Wallingford, England.
- Farsiroto, E. D., Soulis, J. V., and Dermissis, V. D. (1998). Two-dimensional, multi-grid, viscous, free-surface flow calculation. *Proc., 1998 7th International Conference on Hydraulic Engineering Software*, HYDROSOFT.
- Federal Highway Administration (1995). *Evaluating Scour at Bridges*. Hydraulic Engineering Circular 18.
- Federal Highway Administration (1997). *Bridge Scour and Stream Instability Countermeasures*. Hydraulic Engineering Circular 23.
- Forchheimer, P. (1914) *Hydraulik*. Teubner, Leipzig/Berlin.
- Franco, J. J. (1982). *Summary Report: Model-Prototype Comparison Study of Dike Systems, Mississippi River*. Technical Report HL-82-11, U.S. Army Engineer Waterways Experiment Station, Vicksburg, Mississippi.
- Froehlich, D. C. (2002). *User's Manual for FESWMS Flo2DH Two-Dimensional Depth-Averaged Flow and Sediment Transport Model, Release 3*. Report FHWA-RD-03-053, Federal Highway Administration Office of Research, Development, and Technology, Turner-Fairbank Highway Research Center.
- Gadd, P. E. (1988). Sand bag slope protection: Design, construction and performance. In: *Arctic Coastal Processes and Slope Protection Design*, A. T. Chen and C. B. Leidersdorf (editors), Technical Council on Cold Regions Engineering Monograph, American Society of Civil Engineers.
- Garde, R. J., Subramanya, K., and Nambudripad, K. D. (1961). Study of scour around spur dikes. *Journal of the Hydraulics Division*, 87(HY6), American Society of Civil Engineers.
- Gill, M. A. (1972). Erosion of sand beds around spur dikes. *Journal of the Hydraulics Division*, 98(HY9) American Society of Civil Engineers.
- Grant, A. P. (1948). Channel improvements in alluvial streams. *Proc., New Zealand Institution of Engineers*, Vol. XXXIV.
- Gregorius, B. H. (1985). *Waterway Design Procedures—Guidelines*. Civil Division Publication, Ministry of Works and Development, Hamilton, New Zealand.
- Harris, J. D. (1988). Hydraulic design of bridges, Chapter I. *MTC Drainage Manual*, Drainage and Hydrology Section, Ontario Ministry of Transportation, Downsview, Ontario, Canada.
- Heibaum, M. H. (2002). Scour protection and repair by filtering geosynthetic containers. *Proc., First International Conference on Scour of Foundations (ICSF-1)*, Vol. 1.
- Heibaum, M. H. (2004). Geotechnical filters: The important link in scour protection. *Proc., 2nd International Conference on Scour of Foundations*, CD, Singapore.
- Herbich, J. B. (1967). Prevention of scour at bridge abutments. *Proc., 12th Congress of International Association of Hydraulic Research*.
- Hjorth, P. (1975). Studies of the nature of local scour. *Bulletin Series A*, No. 46, Department of Water Resources Engineering, University of Lund, Sweden.
- Hoe, D. (2001). *Cable-Tied Block Protection of Bridge Abutments*. Fourth-year project in resource engineering, Department of Civil and Resource Engineering, the University of Auckland, New Zealand.
- Hoffmans, G. J., and Verheij, H. J. (1997). *Scour Manual*. A. A. Balkema Publishers, Brookfield, Vermont.
- Hudson, K., and East, G. R. W. (1991). *Geo-Textiles*. Transit New Zealand Research Report, Wellington, New Zealand.
- Inglis, C. C. (1949). *The Behavior and Control of Rivers and Canals*. Research Publication 13, Parts I and II, Central Waterpower Irrigation and Navigation Research Station, Poona, India.
- Isbash, S. V. (1936). Construction of dams by depositing rock on running water. Translated, *Proc., 2nd Congress on Large Dams*, Vol. 5.
- Jacobs, B. K., and Kobayashi, N. (1983). *Sandbag Stability and Wave Runup on Bench Slopes*. Research Report CE-83-36, University of Delaware, Department of Civil Engineering.
- Johnson, P., Hey, R., Tessier, M., and Rosgen, D. (2001). Use of vanes for control of scour at vertical-wall abutments. *Journal of Hydraulic Engineering*, Vol. 127, No. 9, American Society of Civil Engineers.
- Jones, J. S., Bertoldi, D., and Stein, S. (1995). Alternative scour countermeasures. *Proc., 1st International Conference on Water Resources*. Part 2 (of 2), Vol. 2, American Society of Civil Engineers.
- Kandasamy, J. K. (1989). *Abutment Scour*. Ph.D. dissertation, Civil and Environmental Engineering Department, University of Auckland, New Zealand.
- Kapoor, B. S., and Keana, C. M. (1994). Experimental overview to mechanism of scour around a round nosed pier and effect of delta wing like device on scour pattern around it. *Modelling, Measurement & Control C: Energetics, Chemistry, Earth, Environmental & Biomedical Problems*, Vol. 46, No. 3, AMSE Press, Tassin-la-Demi-Lune, France.
- Karaki, S. S. (1959). *Hydraulic Model Study of Spur Dikes for Highway Bridge Openings*. Report CER59SSK36, Colorado State University, Civil Engineering Section, September.
- Karaki, S. S. (1961). Laboratory study of spur dikes for highway bridge protection. *Highway Research Board Bulletin 286*, Highway Research Board.
- Kerenyi, K., Jones, J. S., Goeden, K., Phillips, R., and Oien, P. (2005). A better design for box culverts? *Public Roads*, Vol. 69, No. 2.
- Khan, K. W., Chaudhry, M. H. (1992). Numerical modelling of flow around spur dikes. *Proc., 4 International Conference on Hydraulic Engineering Software HYDROSOFT/92*.
- Kirkil, G., Ettema, R., and Muste, M. V. (2004). Similitude of coherent turbulence structures in flume studies of bridge scour. *Proc., 2nd International Conference on Scour and Erosion*, Singapore, Vol. 1.

- Korkut, R. (2004). *Geobags as Abutment-Scour Countermeasure*. M.S. thesis, Civil and Environmental Engineering Department, University of Iowa, Iowa City.
- Kuhnle, R. A., Alonso, C. V., and Shields, F. D. (1997). Volume of scour holes associated with spur dikes. *Proc., 27th Congress of International Association of Hydraulic Research*. Part B-1.
- Kuhnle, R. A., Alonso, C. V., and Shields, F. D. (1998). Volume of scour holes for angled spur dikes. *Proc., International Water Resources Engineering Conference*. Part 2 (of 2), Vol. 2, American Society of Civil Engineers.
- Kuhnle, R. A., Alonso, C. V., and Shields, F. D. (1999). Geometry of scour holes associated with 90-degree spur dikes. *Journal of Hydraulic Engineering*, Vol. 125, No. 9, American Society of Civil Engineers.
- Kwan, T. F. (1984). *A Study of Abutment Scour*. M.E. thesis, Civil and Environmental Engineering Department, University of Auckland, New Zealand.
- Kwan, T. F. (1988). *A Study of Abutment Scour*. Department of Civil Engineering Report 451, University of Auckland.
- Lagasse, P. F., Byars, M. S., Zevenbergen, L. W., and Clopper, P. E. (1997). *Bridge Scour and Stream Instability Countermeasures*. Report FHWA HI-97-030, Hydraulic Engineering Circular 23, Federal Highway Administration.
- Lagasse, P. F., Richardson, E. V., and Zevenbergen, L. W. (1996). Design of guide banks for bridge abutment protection. *Proc., Conference on North American Water and Environment Congress & Destructive Water*. American Society of Civil Engineers.
- Lagasse, P. F., Richardson, E. V., and Zevenbergen, L. W. (1999). Design of guide banks for bridge abutment protection. In: *Stream Stability and Scour at Highway Bridges*. American Society of Civil Engineers.
- Lagasse, P. F., Schall, J. D., Johnson, F., Richardson, E. V., and Chang, F. (1995). *Stream Stability at Highway Structures*. Report FHWA IP-90-014, Hydraulic Engineering Circular 20, Federal Highway Administration.
- Lagasse, P. F., Zevenbergen, L. W., Schall, J. D., and Clopper, P. E. (2001). *Bridge Scour and Stream Instability Countermeasures*. Report FHWA NHI 01-003, Hydraulic Engineering Circular 23, Pages 2.7, 2.9, 4.6, 6.16 - 6.18, Design Guidelines 1, 9, 10.
- Lauchlan, C. S. (1999). *Pier Scour Countermeasures*. Ph.D. thesis, the University of Auckland, New Zealand.
- Laursen, E. M. (1962a). Scour at bridge crossings. In: *Transactions*, American Society of Civil Engineers, Paper 3294, Vol. 127, Part I.
- Laursen, E. M., and Flick, M. W. (1983). *Final Report, Predicting Scour at Bridges: Questions Not Fully Answered—Scour at Sill Structures*. Report ATTI-83-6, Arizona Department of Transportation.
- Lim, S. Y., and Nugroho, J. (2004). Observations on flow field around an abutment in a two-stage channel. *Proc. 2nd International Conference on Scour and Erosion*, Singapore, Vol. 1.
- Liu, M. K., Chang, F. M., and Skinner, M. M. (1961). *Effect of Bridge Construction on Scour and Backwater*. Report CER60-HKL22, Department of Civil Engineering, Colorado State University, Fort Collins, Colorado.
- Macky, G. H. (1986). *Model Testing of Bridge Abutment Scour Protection*. Report 3-86/12, Central Laboratories, Ministry of Works and Development, Lower Hutt, New Zealand.
- Martinez, E. J. (2003). *An Assessment of Two Countermeasures to Reduce Abutment Scour*. M.S. thesis, Civil and Environmental Engineering Department, University of Iowa, Iowa City.
- Mayerle, R., Toro, F. M., and Wang, S. S. Y. (1995). Verification of a three-dimensional numerical model simulation of the flow in the vicinity of spur dikes. *Journal on Hydraulic Research*, Vol. 33, No. 2.
- Maynard, S. T. (1987). *Stable Riprap Size for Open Channel Flows*. Ph.D. thesis, Department of Civil Engineering, Colorado State University.
- Maynard, S. T. (1988). *Stable Riprap Size for Open Channel Flows*. Technical Report HL-88-4, U.S. Army Engineer Waterways Experiment Station, Vicksburg, Mississippi.
- Maynard, S. T. (1993). *Flow Impingement, Snake River, Wyoming*. Technical Report HL-93-9, U.S. Army Engineer Waterways Experiment Station, Vicksburg, Mississippi.
- Maynard, S. T., Ruff, J. F., and Abt, S. R. (1989). Riprap design. *Journal of Hydraulic Engineering*, Vol. 115, No. 7, American Society of Civil Engineers.
- Maza Alvarez, J. A. (1989). Design of groynes and spur dikes. *Proc., 1989 National Conference on Hydraulic Engineering*.
- McCorquodale, J. A., Moawad, A., and McCorquodale, A. C. (1993). Cable-tied block erosion protection. *Hydraulic Engineering (1993)*, American Society of Civil Engineers conference.
- Melville, B. W. (1992). Local scour at bridge abutments. *Journal of Hydraulic Engineering*, Vol. 118, No. 4, American Society of Civil Engineers.
- Melville, B. W. (1997). Pier and abutment scour: Integrated approach. *Journal of Hydraulic Engineering*, Vol. 123, No. 2, American Society of Civil Engineers.
- Melville, B. W., and Coleman, S. E. (2000). *Bridge Scour*. Water Resources Publications.
- Miller, M. C., McCave, I. N., and Komar, P. D. (1977). Threshold of sediment motion under unidirectional currents. *Sedimentology*, Vol. 24, No. 4.
- Ministry of Works and Development (1979). *Code of Practice for the Design of Bridge Waterways*. Civil Division Publication 705/C, Ministry of Works and Development, Wellington, New Zealand.
- Molinas, A., Kheireldin, K., and Wu B. (1998a). Shear stress around vertical wall abutments. *Journal of Hydraulic Engineering*, Vol. 124, No. 8, American Society of Civil Engineers.
- Molinas, A., Reiad, N. G. Y., and Jones, S. (1998b). Effect of cohesion on abutment scour. *Proc., Conference on Water Resources Engineering*, American Society of Civil Engineers.
- Molls, T., Chaudhry, M. H., Khan, K. W. (1995). Numerical simulation of two-dimensional flow near a spur-dike. *Advances in Water Resources*, Vol. 18, No. 4.
- Morales, R. (2006). *Large-Scale Hydraulic Model of Riprap-Apron Performance at a Bridge Abutment on a Floodplain*. M.S. thesis, University of Iowa, Iowa City.
- Muneta, N., and Shimizu, Y. (1994). Numerical analysis model with spur-dike considering the vertical flow velocity distribution. *Proc., Japan Society of Civil Engineering*, Pt. 2-2.
- Neill, C. R. (1967). Mean velocity criterion for scour of coarse uniform bed material. *Proc., 12th International Association of Hydraulic Research Congress*, Vol. 3.
- Neill, C. R. (1973). *Guide to Bridge Hydraulics*. Roads and Transportation Association of Canada, University of Toronto Press.
- Neill, C. R. (1976). Scour holes in a wandering gravel river. *Proc., Symposium on Inland Waterways for Navigation, Flood Control, and Water Diversions, 3rd Annual Conference of American Society of Civil Engineers Waterways, Harbors and Coastal Engineering Division*.
- Novak, P. (1955). Study of stilling basins with special reference to their end sills. *Proc., 6th Congress of the International Association of Hydraulic Research*, Vol. 3.
- Novak, P. (1961). Influence of bed load passage on scour and turbulence downstream of a stilling basin. *Proc., 9th Congress of the International Association of Hydraulic Research*.

- Odgaard, A. J. (1988). *Construction and Evaluation of Submerged Vanes for Stream Control*. IIHR Report 321, University of Iowa, Iowa City.
- Odgaard, A. J., and Kennedy, J. F. (1982). *Analysis of Sacramento River Bend Flows, and Development of a New Method for Bank Protection*. IIHR Report 328, University of Iowa, Iowa City.
- Odgaard, A. J., and Kennedy, J. F. (1983). River-bend bank protection by submerged vanes. *Journal of Hydraulic Engineering*, Vol. 109, No. 8, American Society of Civil Engineers.
- Odgaard, A. J., and Lee, H. Y. E. (1984). *Submerged Vanes for Flow Control and Bank Protection in Streams*. IIHR Report 279, University of Iowa, Iowa City.
- Odgaard, A. J., and Mosconi, C. E. (1987). Streambank protection by submerged vanes. *Journal of Hydraulic Engineering*, Vol. 113, No. 4, American Society of Civil Engineers.
- Odgaard, A. J., and Wang, Y. (1987). Scour prevention at bridge piers. *Hydraulic Engineering, Proc., 1987 National Conference*, American Society of Civil Engineers, Hydraulics Division.
- Odgaard, A. J., and Wang, Y. (1990a). *Hydraulic-Laboratory Model Study of River Intake at Duane Arnold Energy Center*. IIHR Limited Distribution Report 177, University of Iowa, Iowa City.
- Odgaard, A. J., and Wang, Y. (1990b). *Sediment Control in Bridge Waterways*. IIHR Report 336, University of Iowa, Iowa City.
- Odgaard, A. J., and Wang, Y. (1991). Sediment management with submerged vanes. I: theory. *Journal of Hydraulic Engineering*, Vol. 117, No. 3, American Society of Civil Engineers.
- Okada, K., Muraishi, H., and Kunihiro, T. (1989). Statistical judgement about stability of protection against scour around pier. *Proc., Japan Society of Civil Engineers*, Pt. 6-10.
- Pagan-Ortiz, J. E. (1991). *Stability of Rock Riprap for Protection at the Toe of Abutments Located at the Flood Plain*, Report FHWA-RD-91-057, Federal Highway Administration.
- Parker, G., Toro-Escobar, C., and Voigt Jr., R. L. (1998). *Countermeasures to Protect Bridge Piers from Scour*, unpublished final report for NCHRP Project 24-7, Transportation Research Board.
- Parola, A. C. (1993). Stability of riprap at bridge piers. *Journal of Hydraulic Engineering*, Vol. 119, No. 10, American Society of Civil Engineers.
- Peterka, A. J. (1984). *Hydraulic Design of Stilling Basins and Energy Dissipaters*, Engineering Monograph 25, U.S. Department of the Interior Bureau of Reclamation.
- Pilarczyk, K. W. (1990). *Coastal Protection, Proc., Short Course on Coastal Protection*, Delft University of Technology, Balkema, Rotterdam, the Netherlands.
- Pilarczyk, K. (editor) (1998). *Dikes and Revetments*. A. A. Balkema (publisher), the Netherlands.
- Pilarczyk, K. W. (2000). Geomattresses in Erosion Control—An Overview of Design Criteria. In *Filters and Drainage in Geotechnical and Environmental Engineering*, A. A. Balkema, Rotterdam.
- Pzedwojski, B., Blazejewski, R. and Pilarczyk, K. W. (1995). *River Training Techniques*. A. A. Balkema, Rotterdam, the Netherlands.
- Rajaratnam, N., and Nwachukwu, B. A. (1983a). Flow near groin-like structures. *Journal of Hydraulic Engineering*, Vol. 109, No. 3, American Society of Civil Engineers.
- Raudkivi, A. J. (1998). *Loose Boundary Hydraulics*. A. A. Balkema, Rotterdam, the Netherlands.
- Ray, R. (1977). *A Laboratory Study of the Stability of Sand-Filled Nylon Bag Breakwater Structures*. U.S. Army Coastal Engineering Research Center, Vicksburg, Mississippi.
- Richardson, E. V., and Davis, S. R. (1995). *Evaluating Scour at Bridges*. Report FHWA-IP-90-017, Hydraulic Engineering Circular 18, Third Edition, Office of Technology Applications, HTA-22, Federal Highway Administration.
- Richardson, E. V., Harrison, L. J., and Davis, S. R. (1991). *Evaluating Scour at Bridges*. Report FHWA-IP-90-017, Highway Engineering Circular 18, Federal Highway Administration.
- Richardson, J. R., and Richardson, E. V. (1993a). Discussion of local scour at bridge abutments, by B.W. Melville. *Journal of Hydraulic Engineering*, Vol. 119, No. 9, American Society of Civil Engineers.
- Richardson, J. R., and Richardson, E. V. (1993b). The fallacy of local abutment scour equations. *Proc., Conference on Hydraulic Engineering*, American Society of Civil Engineers.
- Richardson, J. R., and Richardson, E. V. (1993c). Determining contraction scour. In: *Stream Stability and Scour at Highway Bridges*, American Society of Civil Engineers.
- Richardson, J. R., and Roberts, D. L. (1998). Non-structural method to reduce local pier scour. *Proc., 1998 International Water Resources Engineering Conference*, Part 1 (of 2), American Society of Civil Engineers.
- Richardson, E. V., and Simons, D. B. (1984). Use of spurs and guidebanks for highway crossings. *Transportation Research Record 950: Second Bridge Engineering Conference*, Vol. 2, Transportation Research Board.
- Richardson, E. V., Simons, D. B., and Julien, P. Y. (1990). *Highways in the River Environment: Participant Notebook*. Report FHWA/HI-90-016. Federal Highway Administration.
- Ruff, J. F., Fotherby, L. M., and Burns, R. S. (1995). Bridge pier scour protection using Toskanes. *Proc., 1st International Conference on Water Resources*, Part 2 (of 2), American Society of Civil Engineers.
- Shields, A. (1936). Applications of similarity principles and turbulence research to bed load movements. *Mitteilungen der Preuss Versuchsanstalt für Wasserbau und Schiffbau*, Berlin, Heft 26.
- Shields Jr., F. D., Cooper, C. M., and Knight, S. S. (1995a). Experiment in stream restoration. *Journal of Hydraulic Engineering*, Vol. 121, No. 6, American Society of Civil Engineers.
- Shields Jr., F. D., Cooper, C. M., and Testa III, S. (1995b). Towards greener riprap: Environmental considerations from microscale to macroscale. In: *River, Coastal and Shoreline Protection Using Riprap and Armourstone*, C. R. Thorne, S. R. Abt, F. B. J. Barends, S. T. Maynard, and K. W. Pilarczyk (editors), John Wiley, New York.
- Shields Jr., F. D., Knight, S. S., and Cooper, C. M. (1995c). Rehabilitation of watersheds with incising channels. *Water Resources Bulletin*, Vol. 31, No. 6.
- Simons, D. B., and Lewis, G. L. (1971). *Flood Protection at Bridge Crossings*. Colorado State University Civil Engineering Report CER71-72DBS-GL10. Report prepared for the Wyoming State Highway Department in conjunction with the U.S. Department of Transportation.
- Simons, D. B., and Senturk, F. (1977). *Sediment Transport Technology: Water and Sediment Dynamics*. Water Resources Publications, Littleton, Colorado.
- Smart, G. M. (1990). *Riprap Scour Protection: Practices for New Zealand Roads*. Department of Scientific and Industrial Research (DSIR) Hydrology Centre, Christchurch, Canterbury, New Zealand.
- Smith, C. D. (1984). Scour control at Outlook Bridge—A case study. *Canadian Journal of Civil Engineering*, Vol. 11, No. 4.
- Soliman, M. M., Attia, K. M., Kotb, M. M., Talaat, A. M., and Ahmed, A. F. (1997). Spur dike effects on the river Nile morphology after high Aswan dam. *Proc., Congress of the International Association of Hydraulic Research*, Part A.
- Spring, F. J. E. (1903). *River Training and Control of the Guide Bank System*. Technical Paper 153, Railway Board, Government of India, New Delhi.

- Strom, H. G. (1962). *River Improvement and Drainage in New Zealand and Australia*. State Rivers and Water Supply Commission, Victoria, Australia.
- Sturm, T. W., and Chrisochoides, A. (1998a). Abutment scour in compound channels for variable setbacks. *Proc., Conference on Water Resources Engineering*, American Society of Civil Engineers.
- Sturm, T. W., and Chrisochoides, A. (1998b). One-dimensional and two-dimensional estimates of abutment scour prediction variables. *Transportation Research Record 1647: General Design and Roadside Safety Features*, Transportation Research Board.
- Sturm, T. W., and Janjua, N. S. (1993). Bridge abutment scour in a floodplain. *Proc., Conference on Hydraulic Engineering*, American Society of Civil Engineers.
- Suzuki, K., Michiue, M., and Hinokidani, O. (1987). Local bed form around a series of spur dikes in alluvial channel. *Proc., 22nd Congress of the International Association of Hydraulic Research*.
- Terzaghi, K., and Peck, R. B. (1958). *Soil Mechanics in Engineering Practice*, 10th edition, John Wiley & Sons, New York.
- Tey, C. B. (1984). *Local Scour at Bridge Abutments*. M.E. thesis, Civil and Environmental Engineering Department, University of Auckland, New Zealand.
- Thorne, C. R., Abt, S. R., and Maynard, S. T. (1995). Prediction of near-bank velocity and scour depth in meander bends for design of riprap revetments. In: *River, Coastal and Shoreline Protection: Erosion Control Using Riprap and Armourstone*, C. R. Thorne, S. R. Abt, F. B. J. Barends, S. T. Maynard, and K. W. Pilarczyk (editors), Wiley, New York.
- Tominaga, A., Nagao, M., and Nezu, I. (1997). Flow structures and mixing processes around porous and submerged spur dikes. *Proc., 27th Congress of the International Association of Hydraulic Research*, Part B-1, International Association of Hydraulic Research.
- United Nations Economic Commission for Asia and the Far East (1953). *River Training and Bank Protection*. Flood Control Series 4, Bangkok.
- U.S. Army Corps of Engineers (1994). *Engineering and Design—Hydraulic Design of Flood Control Channels*, Report EM 1110-2-1601, U.S. Army Corps of Engineers.
- Van Ballegooy, S. (2005). *Bridge Abutment Scour Countermeasures*, Ph.D. dissertation, Department of Civil and Environmental Engineering, the University of Auckland, New Zealand.
- Vanoni, V. A. (1977) *Sedimentation Engineering*, Manuals and Reports on Engineering Practice 54, American Society of Civil Engineers.
- Van Rijn, L. C. (1984). Sediment transport, Part III: Bed forms and alluvial roughness. *Journal of Hydraulic Engineering*, Vol. 110, No. 12, American Society of Civil Engineers.
- Wong, W. H. (1982). *Scour at Bridge Abutments*. M.E. thesis, Civil and Environmental Engineering Department, University of Auckland, New Zealand.
- Wu, X., Lim, S. Y (1993). Prediction of maximum scour depth at spur dikes with adaptive neural networks. *Civil-Comp93, Part 3: Neural Networks and Combinatorial Optimization in Civil and Structural Engineering*. Civil-Comp Press, Edinburgh, United Kingdom.
- Yalin, M. S. (1992). *River Mechanics*. Pergamon Press, New York.
- Zhang, Y., and Du, X. (1997). Limited scour around spur dike and the evaluation of its depth. *Journal of Xi'an Highway Transportation University*, Vol. 17, No. 4.
-

Notation

a_{cb}	= coefficient, Equation 7-1	$d_{max,sp2,avg}$	= maximum scour depth behind the second spur dike, Table 9-9
b	= flow parallel wing-wall abutment thickness, Figure 6-9	$d_{max,sp3,avg}$	= maximum scour depth behind the third spur dike, Table 9-9
B	= upstream width of the flume, Equation 5-19	$d_{max,sp1,inst}$	= maximum instantaneous scour depth in front of the first spur dike
B_f	= floodplain width, Figure 7-3	$d_{max,sp2,inst}$	= maximum instantaneous scour depth at the second spur dike, Table 9-10
B_1	= original channel width, Equations 5-4 and 5-6 in Table 5-2	$d_{abut,avg}$	= time-averaged scour depth at the abutment, Table 9-2
B_2	= constricted channel width, Equations 5-4 and 5-6 in Table 5-2	$d_{max,ch}$	= scour depth in the channel away from the abutment, Table 9-1
C	= coefficient, Equation 5-18	$d_{max,cm,inst}$	= maximum instantaneous scour depth at the countermeasure, Table 9-4
C_s	= stability coefficient for incipient failure: 0.3 angular rock, 0.375 rounded rock, Equation 5-14	$d_{max,dn,abut}$	= scour depth at a short distance downstream of the downstream corner of the abutment, Table 9-1
C_T	= blanket thickness coefficient, given by Figure 1 in Maynard 1993, Equation 5-14	$d_{max,sp,avg}$	= maximum scour depth at the spur dike, Table 9-8
C_v	= vertical velocity distribution coefficient, Equation 5-14	$d_{max,up,abut}$	= scour depth at the upstream corner of the abutment, Table 9-1
C^*	= coefficient determined from laboratory and field testing, Equation 5-15	d_M	= tail-water depth immediately downstream of the scour hole, Equation 5-8
d	= sediment diameter, Equation 8-7	ds_A	= scour reduction at the abutment with scour countermeasure, Section 6.4.1
$d_{abut,avg}$	= time-averaged scour depth at abutment, Table 9-2	ds_{AO}	= scour depth at the abutment without scour countermeasure, Section 6.4.1
d_b	= distance between the average bed level and the bottom of the apron, Figure 7-13	d_{smax}	= maximum scour depth, Section 7.3.4
d_c	= maximum scour at the countermeasure, Table 9-3	ds_O	= equilibrium scour depth below the bed surface without countermeasures, Section 8.5.3
$d_{cm,avg}$	= time-averaged scour depth at the countermeasure, Table 9-4	d_{s1}	= vertical distance from the original top of the apron to the apron settlement near the abutment, Figure 7-13
$d_{max,abut}$	= maximum scour depth at the abutment foundation, Table 9-11	d_{s2}	= vertical distance from the top of the apron to the apron edge settlement, Figure 7-13
$d_{max,abut,inst}$	= maximum instantaneous scour depth at abutment, Table 9-4	d_{sf}	= depth of the scour hole relative to the floodplain, Figure 8-12
$d_{max,col}$	= maximum scour near the abutment collar countermeasure, Table 9-11		
$d_{max,sp1,avg}$	= maximum scour depth behind the first spur dike, Table 9-9		

d_{16}	= particle size of which 16 percent of the grains are finer, Section 7.2.1	K_{sl}	= embankment slope factor, Equations 5-B and 5-C in Table 5-5
d_{50}	= median particle size, Section 6.3.1	K_T	= turbulence adjustment factor, Equation 5-17
d_{84}	= particle size of which 84 percent of the grains are finer, Section 7.2.1	L_a	= abutment length perpendicular to flow, Equation 5-19
D	= riprap diameter, Table 5-6	L_b	= bottom length of cable-tied block, Figure 7-8
D_B	= geobag thickness, Equation 5-23	L_p	= pier length, Section 5.7; and projected width of the parallel-wall countermeasure, Figure 9-14
D_n	= design diameter of the cable-tied blocks, Equation 5-20	L_s	= apron spread length, Figure 7-28
D_R	= equivalent riprap diameter, Equation 7-17	L_{sd}	= effective length of the spur dike, Equations 5-5 and 5-7 in Table 5-2
D_s	= distance between the farthest spur dike tip at the main channel end and the abutment tip, Table 9-8; and spacing between spur dikes or the spur dike and the abutment, Table 9-9	L_{sdp}	= spur dike protrusion length, Table 9-8
D_{30}	= riprap size for which 30 percent by weight are finer, Equation 5-13	L_{spw}	= wall length, Table 9-4
D_{50}	= median grain or riprap size, Equations 5-6 in Table 5-2	L_t	= top length of cable-tied block, Figure 7-8
E	= parameter that has a value of 0.86 for loosely placed stones in flowing water and 1.2 for those that have become embedded, Equation 5-10	n	= Manning coefficient, Equation 7-5
E_v	= kinematic eddy viscosity, Section 8.4.2	N_{sc}	= dimensionless stability factor for riprap stone, Equation 5-10
f	= Lacey silt factor, Equation 5-1 in Table 5-2	N_{sd}	= number of spur dikes, Table 9-9
F_{bo}	= Blench's zero bed factor, which is a function of grain size, Equation 5-2 in Table 5-2	p_m	= volume fraction pore space within the mattress, Equation 7-2
F_n	= Froude number, Equations 5-4 and 5-5 in Table 5-2	P_b	= protrusion of the blocks above bed level, Equation 7-4
Fr	= flow Froude number, Equation 5-15	Pe	= Peclet number, Section 8.4.2
Fr_2	= Froude number in the contracted section, Equations 5-F through 5-H in Table 5-5	q	= discharge per unit width, Equations 5-2 and 5-3 in Table 5-2
h_1	= main channel bank height, Table 9-1	Q	= total discharge, Equation 5-1 in Table 5-2
H_a	= flow parallel thickness of abutment, Figure 6-3	Q_f	= lateral or floodplain flow discharge, Section 9.3.1
H_b	= minimum required block height, Equation 7-2	Q_O	= flow directly upstream of the bridge opening, Figure 8-26
H_t	= total drop in head, measured from the upstream to downstream energy grade line m , Equation 5-8	Q_T	= total flow in the compound channel upstream of the bridge crossing, Figure 8-26
H_{cb}	= height of concrete blocks, Equation 5-22	Q_{100}	= discharge in the 100 feet of stream adjacent to the abutment, Section 9.3.1
k	= function of approach conditions, Equations 5-1 through 5-5 in Table 5-2	r_a	= apron width, Figure 6-9
k_s	= roughness height, Equation 8-2	r_s	= assumed multiple of scour at a dike taken as 11.5 by Laursen, Equation 5-7 in Table 5-2
K	= function of drag coefficient (C_D) that varies between 2.5 and 5.0, Equation 5-4 in Table 5-2	r_t	= radius of the spill-through abutment toe, Equation 5-19
K_1	= side slope correction factor, Equation 5-14	R_b	= centerline radius of curvature of bend, Equation 5-14
K_d	= slope factor, Equation 5-17	R_{dmax}	= distance to the deepest point of the scour hole from the abutment end, Equation 8-9
K_h	= depth parameter, Equation 5-17	R_{50}	= median grain size of stone that makes up the grade control, weir, or check-dam, Equation 5-9
K_s	= shape factor, Equations 5-G and 5-H in Table 5-5	S_b	= parallel-wall countermeasure side slope, Table 9-5
K_S	= shape factor associated with the abutment shape, Equation 7-17	S_{cb}	= specific gravity of the blocks, Equation 7-5
		S_{fa}	= stability factor varying from 1.6 to 2.0 for abutment protection, Equation 5-C in Table 5-5

S_f	= safety factor >1, Equation 5-14	y_c	= critical depth of flow, Equation 5-9
S_n	= parallel-wall countermeasure end slope, Table 9-5	y_f	= floodplain flow depth, Figure 7-3
S_r	= the specific gravity of the riprap stones, Equation 5-11	y_m	= main channel flow depth, Figure 7-3
S_s	= specific gravity of riprap stone, Equation 5-20	y_s	= equilibrium scour depth measured from water surface, Equations 5-1 through 5-7 in Table 5-2
S_{SB}	= specific gravity of the geobag, Equation 5-23	y_2	= flow depth in contracted section, Equations 5-D, 5-G; and 5-H in Table 5-5
t	= run time, Table 9-2	Y	= flow depth in the bridge section, Equation 7-17
t_e	= experiment run time, Table 9-1	Y_0	= flow depth, Section 6.3.1
t_p	= thickness of the protection unit, Equation 5-17	z	= vertical direction, Equation 8-2
TI	= turbulent intensity at 10 percent of the water depth above the bed, Equation 5-20	$\%o_{max,abut}$	= maximum percentage of scour reduction at the abutment, Table 9-9
U	= mean flow velocity, Figure 5-34	$\%o_{max,abut,avg}$	= percentage reduction in time-averaged scour depth at abutment, Table 9-4
u_*	= shear velocity, Section 6.3.1	$\%o_{max,abut,inst}$	= percentage reduction in maximum instantaneous scour depth at abutment, Table 9-4
u_{*c}	= critical value of the shear velocity associated with bed-particle movement, Section 6.3.1	α_b	= angle of the boundary on which the geobag is placed, Equation 5-24
V	= local depth-averaged velocity, Equation 5-14; and cross-sectionally averaged velocity, Section 7.2.1	α_e	= horizontal distance from floodplain wall to opposite edge of scour hole, Section 8.1.4
V_b	= velocity at abutment end, Equation 5-B in Table 5-5; and velocity at 10 percent of the water depth above the bed, Equation 5-20	α_r	= angle of sediment repose, Section 6.3.1
V_c	= critical velocity for bed sediment movement, Figure 8-7	α_s	= main channel bank slope angle, Equation 8-8
V_{cr}	= critical threshold velocity for stone, Equation 5-11	α_x	= horizontal distance from the abutment tip to the deepest scour location in the flow direction, Figure 8-12
V_{cs}	= critical velocity for bed sediment movement, Section 5.7	α_y	= horizontal distance from the abutment tip to the deepest scour location in the transverse direction, Figure 8-12
V_r	= velocity at a level of one-rock diameter above the bed, Equation 5-A in Table 5-5	α_2	= horizontal width of the apron, including settled and unsettled portions, Figure 7-13
V_{tip}	= velocity just outside the separation zone at the end of the abutment, Table 8-4	β	= angle with the horizontal of the settled portion of apron, Figure 7-13
V_2	= mean velocity in contracted bridge section, Equations 5-D and 5-E in Table 5-5	γ_s	= unit weight of stone, Equation 5-14
V_{2-ave}	= bridge section depth-averaged flow velocities, Table 7-6	γ_w	= unit weight of water, Equation 5-14
V_{2-surf}	= upstream and bridge section surface flow velocities, Table 7-6	λ_D	= bed-form trough depth, Figure 7-14
V_0	= mean velocity, Section 6.3.1	λ_H	= bed-form trough height, Figure 7-14
W	= water surface width at upstream end of bend, Equation 5-14	λ_{H-max}	= maximum bed-form height, Equation 7-3
W_a	= apron width, Equation 5-19	λ_L	= bed-form trough length, Figure 7-14
W_{CR}	= critical block weight, Figure 5-34	λ_{L-ave}	= average bed-form length, Equation 7-3
W_{min}	= width of apron in the unsettled region, Figure 7-13	δ_c	= stability factor for current, Equation 5-17
W_o	= apron extent, Equation 8-16	Δ	= change in a quantity, Equation 8-1
x	= streamwise direction, Figure 7-3	Δ_m	= relative density of protection system, Equation 5-17
y	= transverse direction, Figure 7-3; flow depth, Equation 5-12; and average depth in uncontracted section, Equations 5-1 and 5-4 through 5-7 in Table 5-2	ζ	= weight per unit area of the mattress, Equation 5-21
		η	= stability factor, Equation 5-A in Table 5-5
		θ	= spur angle, Figure 5-5
		θ_r	= angle of repose, Equation 5-B in Table 5-5
		θ_C	= critical value of the Shields parameter for particle geobag entrainment, Equation 5-23; and angle of repose of the sediment forming the boundary, Equation 5-24

ν	= fluid kinematic viscosity, Equation 8-3	ϕ	= stability parameter, Equation 7-18
ρ_{cb}	= density of the concrete blocks, Equation 5-21	ϕ_{ai}	= downstream apron initiation angle, Equation 5-19
σ_g	= standard deviation of sediment size, Section 6.3.1	ϕ_{sl}	= slope angle, Equation 5-B in Table 5-5
τ	= bed shear stress, Equation 8-6	ϕ_{st}	= stability parameter, Equation 5-23
τ_c	= critical bed shear stress for incipient movement of bed sediment, Equation 8-7	ϕ_{cr}	= critical shear stress parameter, Equation 5-17
τ_{wc}	= critical bed shear stress on local bed slope, Equation 8-8	ϕ'	= repose angle of the bed material, Equation 8-8
		ω	= vorticity, Equation 8-1

Abbreviations and acronyms used without definitions in TRB publications:

AAAE	American Association of Airport Executives
AASHO	American Association of State Highway Officials
AASHTO	American Association of State Highway and Transportation Officials
ACI-NA	Airports Council International-North America
ACRP	Airport Cooperative Research Program
ADA	Americans with Disabilities Act
APTA	American Public Transportation Association
ASCE	American Society of Civil Engineers
ASME	American Society of Mechanical Engineers
ASTM	American Society for Testing and Materials
ATA	Air Transport Association
ATA	American Trucking Associations
CTAA	Community Transportation Association of America
CTBSSP	Commercial Truck and Bus Safety Synthesis Program
DHS	Department of Homeland Security
DOE	Department of Energy
EPA	Environmental Protection Agency
FAA	Federal Aviation Administration
FHWA	Federal Highway Administration
FMCSA	Federal Motor Carrier Safety Administration
FRA	Federal Railroad Administration
FTA	Federal Transit Administration
IEEE	Institute of Electrical and Electronics Engineers
ISTEA	Intermodal Surface Transportation Efficiency Act of 1991
ITE	Institute of Transportation Engineers
NASA	National Aeronautics and Space Administration
NASAO	National Association of State Aviation Officials
NCFRP	National Cooperative Freight Research Program
NCHRP	National Cooperative Highway Research Program
NHTSA	National Highway Traffic Safety Administration
NTSB	National Transportation Safety Board
SAE	Society of Automotive Engineers
SAFETEA-LU	Safe, Accountable, Flexible, Efficient Transportation Equity Act: A Legacy for Users (2005)
TCRP	Transit Cooperative Research Program
TEA-21	Transportation Equity Act for the 21st Century (1998)
TRB	Transportation Research Board
TSA	Transportation Security Administration
U.S.DOT	United States Department of Transportation